
ANALYTICA CHIMICA ACTA

An international journal devoted to all branches of analytical chemistry

EDITORS

HARRY L. PARDUE (West Lafayette, IN, U.S.A.)

ALAN TOWNSHEND (Hull, Great Britain)

J.T. CLERC (Berne, Switzerland)

WILLEM E. VAN DER LINDEN (Enschede, The Netherlands)

PAUL J. WORSFOLD (Plymouth, Great Britain)

Editorial Advisers

F.C. Adams, Antwerp
M. Aizawa, Yokohama
J.F. Alder, Manchester
C.M.G. van den Berg, Liverpool
A.M. Bond, Bundoora, Vic.
S.D. Brown, Newark, DE
J. Buffle, Geneva
P.R. Coulet, Lyon
S.R. Crouch, East Lansing, MI
R. Dams, Ghent
L. de Galan, Vlaardingen
M.L. Gross, Lincoln, NE
W. Heineman, Cincinnati, OH
G.M. Hieftje, Bloomington, IN
G. Horvai, Budapest
T. Imasaka, Fukuoka
D. Jagner, Gothenburg
G. Johansson, Lund
D.C. Johnson, Ames, IA
A.M.G. Macdonald, Birmingham
D.L. Massart, Brussels
P.C. Meier, Schaffhausen
M.E. Meyerhoff, Ann Arbor, MI

J.N. Miller, Loughborough
H.A. Mottola, Stillwater, OK
M.E. Munk, Tempe, AZ
M. Otto, Freiberg
D. Pérez-Bendito, Córdoba
C.F. Poole, Detroit, MI
S.C. Rutan, Richmond, VA
J. Ruzicka, Seattle, WA
A. Sanz-Medel, Oviedo
S. Sasaki, Toyohashi
T. Sawada, Tokyo
K. Schügerl, Hannover
M.R. Smyth, Dublin
M. Thompson, Toronto
G. Tölg, Dortmund
Y. Umezawa, Tokyo
E. Wang, Changchun
J. Wang, Las Cruces, NM
H.W. Werner, Eindhoven
O.S. Wolfbeis, Graz
Yu.A. Zolotov, Moscow
J. Župan, Ljubljana

ANALYTICA CHIMICA ACTA

Scope. *Analytica Chimica Acta* publishes original papers, preliminary communications and reviews dealing with every aspect of modern analytical chemistry. Reviews are normally written by invitation of the editors, who welcome suggestions for subjects. Preliminary communications of important urgent work can be printed within four months of submission, if the authors are prepared to forego proofs.

Submission of Papers

Americas

Prof. Harry L. Pardue
Department of Chemistry
1393 BRWN Bldg, Purdue University
West Lafayette, IN 47907-1393
USA
Tel: (+ 1-317) 494 5320
Fax: (+ 1-317) 496 1200

Computer Techniques

Prof. J.T. Clerc
Universität Bern
Pharmazeutisches Institut
Baltzerstrasse 5, CH-3012 Bern
Switzerland
Tel: (+ 41-31) 654171
Fax: (+ 41-31) 654198

Other Papers

Prof. Alan Townshend
Department of Chemistry
The University
Hull HU6 7RX
Great Britain

Tel: (+ 44-482) 465027
Fax: (+ 44-482) 466410

Prof. Willem E. van der Linden
Laboratory for Chemical Analysis
Department of Chemical Technology
Twente University of Technology
P.O. Box 217, 7500 AE Enschede
The Netherlands

Tel: (+ 31-53) 892629
Fax: (+ 31-53) 356024

Prof. Paul Worsfold
Dept. of Environmental Sciences
University of Plymouth
Plymouth PL4 8AA
Great Britain

Tel: (+ 44-752) 233006
Fax: (+ 44-752) 233009

Submission of an article is understood to imply that the article is original and unpublished and is not being considered for publication elsewhere. *Anal. Chim. Acta* accepts papers in English only. There are no page charges. Manuscripts should conform in layout and style to the papers published in this issue. See inside back cover for "Information for Authors".

Publication. *Analytica Chimica Acta* appears in 14 volumes in 1993. The subscription price for 1993 (Vols. 267-280) is Dfl. 4214.00 plus Dfl. 462.00 (p.p.h.) (total approx. US\$ 2672.00). *Vibrational Spectroscopy* appears in 2 volumes in 1993. The subscription price for *Vibrational Spectroscopy* (Vols. 4 and 5) is Dfl. 700.00 plus Dfl. 66.00 (p.p.h.) (total approx. US\$ 437.75). The price of a combined subscription (*Anal. Chim. Acta* and *Vib. Spectrosc.*) is Dfl. 4592.00 plus Dfl. 528.00 (p.p.h.) (total approx. US\$ 2925.75). All earlier volumes (Vols. 1-266) except Vols. 23 and 28 are available at Dfl. 259.50 (US\$ 148.25), plus Dfl. 18.00 (US\$ 10.25) p.p.h., per volume. The Dutch guilder price is definitive. The U.S. dollar price is subject to exchange-rate fluctuations and is given only as a guide. Subscriptions are accepted on a prepaid basis only, unless different terms have been previously agreed upon.

Our p.p.h. (postage, packing and handling) charge includes surface delivery of all issues, except to subscribers in the U.S.A., Canada, Australia, New Zealand, China, India, Israel, South Africa, Malaysia, Thailand, Singapore, South Korea, Taiwan, Pakistan, Hong Kong, Brazil, Argentina and Mexico, who receive all issues by air delivery (S.A.L.-Surface Air Lifted) at no extra cost. For Japan, air delivery requires 25% additional charge of the normal postage and handling charge; for all other countries airmail and S.A.L. charges are available upon request.

Subscription orders. Subscription orders can be entered only by calendar year and should be sent to: Elsevier Science Publishers B.V., Journals Department, P.O. Box 211, 1000 AE Amsterdam, The Netherlands. Tel: (+31-20) 5803 642, Telex: 18582, Telefax: (+31-20) 5803 598, to which requests for sample copies can also be sent. Claims for issues not received should be made within six months of publication of the issues. If not they cannot be honoured free of charge. Readers in the U.S.A. and Canada can contact the following address: Elsevier Science Publishing Co. Inc., Journal Information Center, 655 Avenue of the Americas, New York, NY 10010, U.S.A. Tel: (+1-212) 633 3750, Telefax: (+1-212) 633 3990, for further information, or a free sample copy of this or any other Elsevier Science Publishers journal.

Advertisements. Advertisement rates are available from the publisher on request.

Detailed "Instructions to Authors" for *Analytica Chimica Acta* was published in Volume 256, No. 2, pp. 373-376. Free reprints of the "Instructions to Authors" of *Analytica Chimica Acta* and *Vibrational Spectroscopy* are available from the Editors or from: Elsevier Science Publishers B.V., P.O. Box 330, 1000 AH Amsterdam, The Netherlands. Telefax: (+31-20) 5862 845.

US mailing notice - *Analytica Chimica Acta* (ISSN 0003-2670) is published biweekly by Elsevier Science Publishers (Molenwerf 1, Postbus 211, 1000 AE Amsterdam). Annual subscription price in the USA US\$ 2672.00 (subject to change), including air speed delivery. Second class postage paid at Jamaica, NY 11431. *USA Postmasters:* Send address changes to *Anal. Chim. Acta*, Publications Expediting, Inc., 200 Meacham Av., Elmont, NY 11003. Airfreight and mailing in the USA by Publication Expediting.

ANALYTICA CHIMICA ACTA

An international journal devoted to all branches of analytical chemistry

(Full texts are incorporated in CJELSEVIER, a file in the Chemical Journals Online database available on STN International; Abstracted, indexed in: Aluminum Abstracts; Anal. Abstr.; Biol. Abstr.; BIOSIS; Chem. Abstr.; Curr. Contents Phys. Chem. Earth Sci.; Engineered Materials Abstracts; Excerpta Medica; Index Med.; Life Sci.; Mass Spectrom. Bull.; Material Business Alerts; Metals Abstracts; Sci. Citation Index)

VOL. 276 NO. 2

CONTENTS

APRIL 30, 1993

Chromatography and Preconcentration

- Matrix independent headspace gas chromatographic analysis. The full evaporation technique
M. Markelov (Chesterland, OH, USA) and J.P. Guzowski, Jr. (Cleveland, OH, USA) 235
- Determination of blood cyanide by headspace gas chromatography with nitrogen-phosphorus detection and using a megabore capillary column
Y. Seto, N. Tsunoda, H. Ohta and T. Shinohara (Tokyo, Japan) 247
- Determination of oxidizable inorganic anions by reversed-phase ion-pair chromatography with amperometric detection
J. Xu, M. Xin (Fujian, China), T. Takeuchi and T. Miwa (Gifu, Japan) 261
- Preparation and analytical properties of a chelating resin loaded with thionalide
J. Chwastowska, W. Żmijewska and E. Sterlińska (Warsaw, Poland) 265

Flow-Injection Analysis

- Flow-injection spectrophotometric enzymatic and non-enzymatic methods for the determination of direct and total bilirubin in serum
J.M. Fernández-Romero, M.D. Luque de Castro and M. Valcárcel (Córdoba, Spain) 271
- Determination of fluphenazine hydrochloride in a flow assembly incorporating cerium(IV) arsenite as a solid-bed reactor
S. Laredo Ortiz, C. Gómez Benito and J. Martínez Calatayud (Valencia, Spain) 281

Environmental Analysis

- Determination of nitrogen in water: comparison of a continuous-flow method with on-line UV digestion with the original Kjeldahl method
H. Kroon (Rotterdam, Netherlands) 287
- Determination by pyrolysis-gas chromatography of the phenolic resin concentration in particulate matter accumulated from traffic on roads
T. Saito (Kanagawa, Japan) 295

Immobilized Enzymes

- Comparison between different inorganic supports for the immobilization of amyloglucosidase and α -amylase to be used in enzyme reactors in flow-injection systems. Part I. Hydrolysis of maltose, maltooligosaccharides and soluble starch
J. Ern eus and L. Gorton (Lund, Sweden) 303
- Comparison between different inorganic supports for the immobilization of amyloglucosidase and α -amylase to be used in enzyme reactors in flow-injection systems. Part II. Hydrolysis of glycogen
J. Ern eus and L. Gorton (Lund, Sweden) 319

Sensors

- Development of a piezoelectric immunosensor for the detection of human erythrocytes
B. K onig and M. Gr atzel (Lausanne, Switzerland) 329

(Continued overleaf)

Contents (continued)

| | |
|--|-----|
| Glucose oxidase enzyme electrode: relation between inner membrane permeability and substrate response S.P.J. Higson, M. Desai, Z. Koochaki and P.M. Vadgama (Salford, UK) | 335 |
| Enzyme-based catechol sensor based on the cyclic reaction between catechol and 1,2-benzoquinone, using L-ascorbate and tyrosinase S. Uchiyama, Y. Hasebe, H. Shimizu and H. Ishihara (Saitama, Japan) | 341 |
| Chemically modified ion-sensitive field-effect transistors: elimination of the liquid junction potential in a double sensor flow-injection analysis cell P.L.H.M. Cobben, R.J.M. Egberink, J.G. Bomer, R. Schouwenaar, Z. Brzozka, M. Bos, P. Bergveld and D.N. Reinhoudt (Enschede, Netherlands) | 347 |
| Comparative study of tripodal oxa-amides and oxa-esters as ionophores in potentiometric ion-selective electrodes for alkali and alkaline earth cations R. Kataký, D. Parker and A. Teasdale (Durham, UK) | 353 |
| <i>Electroanalytical Chemistry</i> | |
| Comparison of potentiometric stripping analysis and square-wave voltammetry with respect to the influence of Triton X-100 Š. Komorsky-Lovrić and M. Branica (Zagreb, Croatia) | 361 |
| Square-wave voltammetry of uranyl–humate complex M. Mlakar (Zagreb, Croatia) | 367 |
| Potentiometric method for the determination of adenosine-5'-triphosphate T. Katsu and K. Yamanaka (Okayama, Japan) | 373 |
| <i>Atomic Spectrometry</i> | |
| Comparative study of argon and helium plasmas in a TM ₀₁₀ cavity and a surfatron and their use for hydride generation microwave-induced plasma atomic emission spectrometry E. Bulska, J.A.C. Broekaert, P. Tschöpel and G. Tölg (Dortmund, Germany) | 377 |
| Automatic determination of reducing sugars by atomic absorption spectrometry M.C. Yebra, M. Gallego and M. Valcárcel (Córdoba, Spain) | 385 |
| <i>Spectrophotometry and Spectrofluorimetry</i> | |
| Determination of beryllium(II) on solid substrates by photothermal spectrometry after selective complexation with Chrome Azurol S E.P.C. Lai, B.D. Statham and K. Ansell (Ottawa, Canada) | 393 |
| Study of europium-sensitized fluorescence of tetracycline in a micellar solution of Triton X-100 by fluorescence and thermal lens spectrometry J. Georges and S. Ghazarian (Villeurbanne, France) | 401 |
| Determination of traces of iron by thin-layer spectroelectrochemistry Q. Xie, W. Kuang, L. Nie and S. Yao (Changsha, China) | 411 |
| Stopped-flow kinetic spectrophotometric method for the simultaneous determination of iron, titanium and vanadium J. Wang and R. He (Yantai, China) | 419 |
| <i>Chemometrics</i> | |
| Unique resolution of hidden minor peaks in multidetection chromatography by first-order differentiation and orthogonal projections Y.-z. Liang and O.M. Kvalheim (Bergen, Norway) | 425 |
| Evaluation of stability constants from multi-wavelength absorbance data: program STAR J.L. Beltrán, R. Codony and M.D. Prat (Barcelona, Spain) | 441 |
| Identification of "grey" analytical systems with incomplete information Y.-L. Xie, Y.-Z. Liang and R.-Q. Yu (Changsha, China) | 455 |
| <i>Titrimetry</i> | |
| Direct cerimetric determination of tellurium(IV) S.N. Dindi and V.V. Reddy (Visakhapatnam, India) | 465 |
| <i>Book Reviews</i> | 469 |
| <i>Author Index</i> | 473 |
| <i>Erratum</i> | 476 |

Matrix independent headspace gas chromatographic analysis. The full evaporation technique

Michael Markelov

ACS Labs, P.O. Box 306, Chesterland, OH 44026 (USA)

John P. Guzowski, Jr.

British Petroleum, Research and Environmental Center, 4440 Warrensville Center Rd., Cleveland, OH 44128 (USA)

(Received 23rd September 1992; revised manuscript received 9th December 1992)

Abstract

This paper presents the full evaporation technique (FET) as a simple methodology to overcome the matrix effects which can be experienced in headspace and direct liquid injection chromatographic analysis. The technique involves dispensing a small aliquot of sample into a headspace bottle and thermal equilibration of the sample. It was found for most cases that reproducible results independent of time and temperature are generated by heating several milligrams of the sample at temperatures above 100°C for 5–10 min. The full evaporation methodology addresses the problems associated with the analysis of analytes in unpredictably changing sample matrices including soils, biological liquids, and a multitude of chemical and petroleum streams. This is especially advantageous for samples containing salts, mineral acids, polymers, detergents and other practically non-volatile constituents. The FET analysis of standard solutions prepared in various matrices provides a very uniform detector response indicating a reduction in sensitivity towards matrix effects. The described methodology offers sensitivity comparable to that of direct liquid injection while providing the benefits associated with traditional headspace analysis.

Keywords: Gas chromatography; Blood; Food; Headspace analysis; Petrochemicals; Polymers

The chromatographic analysis of samples with unpredictable changing matrices poses an analytical challenge which has yet to be easily remedied by either headspace or direct injection techniques. The full evaporation technique (FET) was developed as a means to sidestep some of the shortcomings of both headspace and direct injection methods. If a matrix independent chromatographic method was available both calibration and analysis of these problematic samples would become quite simple.

In the full evaporation technique, a small aliquot of sample (mg amounts) is quantitatively

dispensed into a headspace bottle and left to equilibrate at an elevated temperature for a short period of time. The term 'full evaporation' applies only to the analytes, and not necessarily to the sample matrix thus the full evaporation approach can be applied to volatile and non-volatile matrices. Thermodynamically, if headspace analysis is considered to be a simple extraction procedure where the extraction solvent is a gas, small sample sizes and/or volatile sample matrices will afford the opportunity of minimizing the matrix effect especially for analytes with small partition coefficients. This is precisely the concept behind the full evaporation technique: reduce the sample size and increase the temperature thus reducing the effect of the sample matrix.

Correspondence to: M. Markelov, ACS Labs., 7276 Greenfield, Chesterland, OH 44026 (USA).

This technique has been tested with several commercial headspace instruments including a dynamic 'purge and trap' system and manual headspace injections. Tables of chemicals and conditions at which full evaporation can be performed as well as the methodology of estimating the limitations of the technique are provided. Important considerations are given to the validity of the results, stability of calibration, speed of the analysis, convenience of use, and reliability of the instrumentation. The full evaporation methodology has been incorporated into a short course [1] and presented at an ASTM meeting [2].

Matrix effects and quantification

Direct liquid injection techniques are sensitive to variations in the matrix. These matrix problems are often not as pronounced as in headspace analysis, but manifest themselves in several forms such as injection port discrimination and non-volatile analytes entering the chromatographic system.

Traditionally, there are several standardization techniques employed in the practice of headspace analysis. The following methods can be used; external standards, internal standards [3,4] standard addition, multiple headspace extraction [3,5,6] and the variable volume technique [7,8]. The last three methods can be utilized to overcome a variety of matrix related problems. For cases of truly unknown sample matrices, these techniques prove both laborious and time consuming.

Simply stated, the matrix effect is the manner in which the analytes of the sample interact with the sample matrix. If the analytes or the matrix are changed, then the matrix effect also changes. Matrix effects are most profound in polar systems. For example, acetonitrile–water mixtures represent systems where non-ideality is expected and any application of headspace analysis must be carefully verified. When the ratio of acetonitrile–water in the matrix changes, the behavior of other chemicals in solution also changes. The concentration of components in the vapor phase dramatically changes with respect to the acetonitrile concentration in the liquid. Most compo-

nents are more soluble in acetonitrile than water, thus their response in the vapor phase decreases as the concentration of acetonitrile increases because they tend to remain in solution. Therefore, unless the concentration of acetonitrile or water could be determined *before* analyzing the samples by headspace chromatography, it would not be possible to know which calibration curve to apply to that particular sample.

Direct injection analyses also requires that the proper calibration standards be prepared for accurate quantitation. Standards are generally prepared in a solution which resembles the sample matrix. This is difficult if the samples vary widely in composition or are truly unknown. Often times the sample cannot be injected directly as it contains acids or non-volatile species which would contaminate the chromatographic system.

The considerations above indicate that neither headspace nor conventional chromatography is an option for the accurate analysis of the streams with variable matrices containing non-volatile components.

THEORY

Full evaporation technique (FET)

The full evaporation technique is based on a near-complete transfer of analytes from a condensed matrix, either liquid or solid, into a confined vapor phase. Experimental logistics are similar to techniques involving gaseous standard preparation, such as for multiple headspace extraction [4,6]. The full evaporation technique does not require full evaporation of the condensed phase. It is concerned only with the conditions leading to the near complete transfer of analytes into the vapor phase.

If such a transfer is possible, it will accomplish two goals. First, non-volatile components such as salts and mineral acids will never enter and contaminate the analytical instrumentation, thus ensuring that the headspace advantage is retained. Second, the sample matrix will not affect the calibration of the analytical procedure. This creates the potential for universal standardization.

Basic headspace theory

To visualize and then minimize the matrix effect, this paper represents headspace analysis as a simple extraction process where the extraction solvent is a gas. The condition in an sealed, thermally equilibrated headspace vial can be described by the following equations [3,7,8]:

(1) Material balance

$$M_0 = C_0V_c = C_gV_g + C_cV_c \quad (1)$$

where M_0 is the total mass of analyte in the vial, C_0 is the original concentration of the analyte in the condensed phase (liquid or solid); V_c and V_g the volumes of the condensed and gaseous phases respectively; C_g and C_c the equilibrium concentrations in the gaseous and liquid phases respectively. This equation assumes that V_c does not change significantly during equilibration. This generally holds true with the exception of extreme cases when V_c is very large or very small with respect to V_g . For these cases, the changes in V_c due to thermal expansion and/or partial evaporation of the condensed phase should be taken into account.

(2) Condition of equilibrium

$$K = C_c/C_g \quad (2)$$

Henry's Law assumes that the partition coefficient, K , is independent of the concentration of the analyte. This assumption is valid only when the analyte concentrations are very small and do not change the properties of the sample matrix.

(3) Headspace sensitivity

$$C_g = C_0/(K + V_g/V_c) \quad (3)$$

This equation is the result of solving Eqns. 1 and 2 for C_g , and reflects the sensitivity of the headspace analysis. Equation 3 contains the assumptions taken for Eqns. 1 and 2 and encompasses the majority of headspace applications.

The 'matrix effect' is the variability of the partition coefficient for an analyte in different sample matrices. Equation 3 states that with increasing volumetric ratios of V_g/V_c , or when $K \ll V_g/V_c$, the effect on the analyte concentration in the vapor phase diminishes.

The effect of the partition coefficient can be essentially eliminated by equilibrating a small

amount of sample at higher temperatures. This increases V_g/V_c , thus reducing the significance of the partition coefficient. For typical headspace vials, V_g/V_c ranges between 22500 ($V_c = 1 \mu\text{l}$) to 2250 ($V_c = 10 \mu\text{l}$). These values greatly exceed partition coefficients for volatile chemicals at temperatures above 75°C. The partition coefficient of acrylonitrile in water is less than 60 at 77°C. For acrylonitrile in an organic matrix, such as its oligomers, the partition coefficient is approximately 400. For a volatile analyte in a non-volatile sample matrix (which ranges from completely aqueous to completely organic) the variation of analyte concentration in the vapor phase will be about 7%. This value is derived from Eqn. 3 with a 5- μl sample volume, V_g being 22.5 ml, and K being varied from 60 to 400. This 7% value will be the magnitude of the analytical error if the headspace analysis of an organic sample is performed using a calibration standard prepared in water, or visa versa. This error can be dramatically reduced if the matrix is fully or partially volatile, or if higher equilibration temperatures are employed.

Volatile matrices in FET. The matrix may itself be volatile, thus the small aliquot of sample dispensed into the vial may partially or completely vaporize. Equation 3 is then no longer valid because it presumes that V_c is not significantly changed by heating. Equation 4 accounts for the change in condensed phase volume from V_c to V_r upon heating. V_r is the residue volume that remains after thermal equilibration of the sample.

$$C_g = C_0/[K(V_r/V_c) + V_g/V_c] \quad (4)$$

This equation may be rewritten as:

$$C_g = (C_0V_c)/(KV_r + V_g) = M_0/(KV_r + V_g) \quad (4a)$$

Equation 4a indicates that the concentration of analyte in the vapor phase is proportional to the total mass of analyte in the vial. At small sample volumes, the gaseous volume is approximately equal to the volume of the headspace vial. Perkin-Elmer, Hewlett-Packard and Tekmar instruments utilize 22.5-ml vials. LEAP and ASIST headspace analyzers use 10- and 24-, or 42-ml vials respectively. For a non-volatile matrix, a

22.5-ml vial, and 10- μ l sample volume, Eqn. 4a becomes:

$$C_g = M_0 / (K \cdot 0.01 + 22.5) \quad (4b)$$

Equation 4b indicates that when the partition coefficient of the matrix is varied between 1 and 100, changes in the headspace response are less than 5%. This is well within repeatability requirements of most chromatographic analyses. When the matrix contains only 10% of non-volatile and variable constituents, the same 5% stability of analyte concentration in the vapor phase can be guaranteed, even when the partition coefficient is varied between 1 to 1000. The partition coefficients can even be as great as 2000 with 42-ml vials.

This stability of the full evaporation technique to matrix variations covers most of the systems that produce a response in conventional headspace analysis. However, some chemicals with a high boiling point and/or unusually strong affinity to the non-volatile portion of the matrix may exhibit very large partition coefficients. There are several ways to minimize these effects. First, reduce the sample volume or dilute the sample with a volatile solvent. This would result in the smaller residue values and subsequent reduction of the matrix effect. However, this will proportionally reduce the sensitivity of the analysis. Second, increase the equilibration temperature of the vial. This will result in reducing the partition coefficient. This reduction is usually exponential and can be approximated by the Arrhenius equation:

$$K = A \text{Exp}(B/T) \quad (4c)$$

where A and B are system constants and T is absolute temperature (K). To visualize the mutual effects of sample volume and the matrix, Eqn. 4a can be rewritten as Eqn. 4d if the total mass of an analyte in gaseous phase can be expressed as $M_g = C_g V_g$:

$$M_g/M_0 = V_g/(V_g + KV_r) = 1/[1 + K(V_r/V_g)] \quad (4d)$$

Equation 4d indicates that the ratio M_g/M_0 will not deviate from unity (or full analyte evapora-

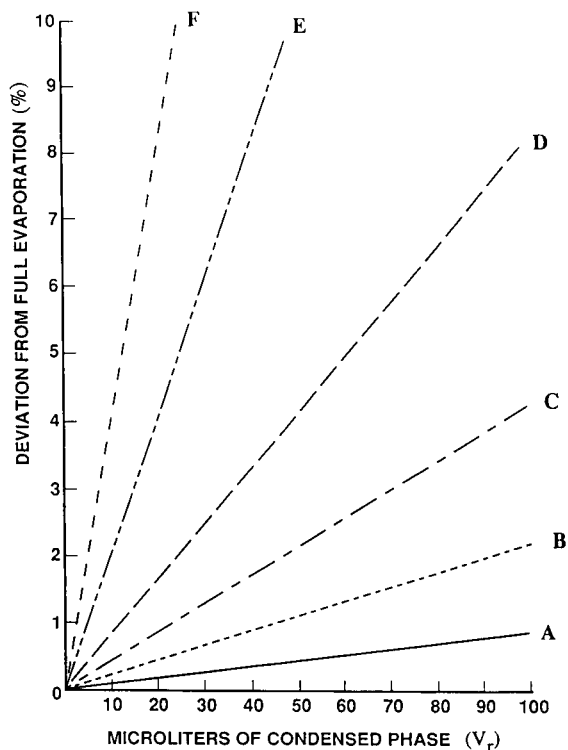


Fig. 1. The impact of sample volume on systematic errors in the full evaporation technique. For small values of the partition coefficient (K), an increase in the residual volume (V_r) reduces the accuracy of the analysis with respect to conditions leading to full evaporation ($V_r = 0$). The partition coefficients are as follows: A = 2, B = 5, C = 10, D = 20, E = 50, F = 100.

tion) by more than 10% in any analyte–matrix combinations where $KV_r < 0.1V_g$. Figure 1 illustrates the limits of insensitivity of the full evaporation technique to matrices for residue volumes up to 100 μ l and partition coefficients up to 100. For chemicals in matrices that do not exhibit chem-adsorption and which can be analyzed by headspace, partition coefficients are typically less than 100 at temperatures above 100°C. For partition coefficients less than 100 and sample sizes less than 10 μ l, the margin of error will not exceed 5%, even for non-volatile samples.

Guidelines for development of FET methods

Previous theoretical considerations indicate that the full evaporation technique should be performed using a small sample size and high equilibration temperatures. These parameters are

governed by the required sensitivity as well as the thermal lability of the analyte.

In terms of Eqn. 4, for large ratios of V_g/V_c and partial matrix evaporation, ($V_r/V_c < 1$) the matrix effect is very small. As the sample residue volume approaches 0, complete matrix evaporation is achieved which fully eliminates the effect of the matrix. The condition of complete evaporation is given by:

$$P^0 > P = nRT/V_g \quad (5)$$

where P^0 is a saturated vapor pressure of the matrix chemical; P is the pressure that would be developed by n moles of this chemical in the vial

with volume V_g (liters) at absolute temperature T (K); R is the universal gas constant, which equals 62.4 if pressures are expressed in mmHg.

To estimate the maximum amount of sample which can be added to the vial and still fulfill the criteria of full evaporation, Eqn. 5 can be rewritten as:

$$V_s(\mu\text{l}) = P^0(M_w/d)V_g/RT \quad (6)$$

where M_w and d are molecular weight and density. In the case of acetonitrile as a sample matrix, $P^0 = 758$ mmHg at 80°C . Placing these values into Eqn. 6 yields:

$$V_s = (758)(41/0.8)(22.5)/(62.4 \cdot 353) = 40 \mu\text{l}$$

TABLE 1

Maximum mass of analyte which can be evaporated in a 22.5-ml headspace vial at various temperatures

| | Maximum mass (mg) at temperatures of | | | | |
|------------------------------|--------------------------------------|-------|-------|-------|-------|
| | 40°C | 60°C | 80°C | 100°C | 120°C |
| Oxygenates | | | | | |
| Furan | 80.9 | 143.7 | 235.7 | 362.9 | 530.4 |
| Acetaldehyde | 73.0 | 123.5 | 195.9 | 296.1 | 431.6 |
| Acetone | 28.3 | 54.4 | 95.7 | 156.9 | 242.6 |
| Allyl alcohol | 4.1 | 10.4 | 23.4 | 47.3 | 87.7 |
| Water | 1.1 | 2.9 | 6.5 | 13.2 | 24.6 |
| Acetic acid | 2.4 | 5.8 | 12.5 | 24.6 | 44.4 |
| Acrolein | 31.5 | 58.3 | 99.8 | 160.1 | 244.3 |
| Acrylic acid | 0.9 | 2.4 | 5.8 | 12.6 | 25.0 |
| Nitriles | | | | | |
| Hydrogen cyanide | 39.4 | 20.8 | 37.9 | 64.1 | 102.2 |
| Acrylonitrile | 12.5 | 24.6 | 44.3 | 74.2 | 117.4 |
| Propionitrile | 6.0 | 12.8 | 24.5 | 43.3 | 71.4 |
| <i>cis</i> -Crotononitrile | 5.0 | 11.0 | 21.7 | 39.3 | 66.4 |
| <i>trans</i> -Crotononitrile | 2.9 | 6.6 | 13.6 | 25.6 | 44.8 |
| Methacrylonitrile | 10.4 | 20.8 | 37.9 | 64.1 | 102.2 |
| Benzonitrile | 0.2 | 0.7 | 1.8 | 4.1 | 8.06 |
| Acetonitrile | 8.2 | 16.5 | 30.4 | 52.0 | 83.8 |
| Aromatics | | | | | |
| Benzene | 16.4 | 33.0 | 60.3 | 101.7 | 160.7 |
| Toluene | 6.3 | 13.8 | 27.4 | 49.6 | 83.3 |
| Ethyl benzene | 2.6 | 6.4 | 13.6 | 36.4 | 46.9 |
| <i>o</i> -Xylene | 1.9 | 4.7 | 10.3 | 20.4 | 37.1 |
| <i>m</i> -Xylene | 2.3 | 5.7 | 12.3 | 23.9 | 43.0 |
| <i>p</i> -Xylene | 2.4 | 5.9 | 12.7 | 24.6 | 44.0 |
| Amines | | | | | |
| Pyridine | 4.1 | 9.5 | 19.5 | 36.6 | 63.3 |
| 2-Picoline | 2.7 | 6.7 | 14.3 | 27.7 | 49.5 |
| 3-Picoline | 1.5 | 3.9 | 8.7 | 17.5 | 32.3 |
| 4-Picoline | 1.5 | 3.7 | 8.4 | 16.8 | 31.1 |

Typical headspace autosamplers inject between 1 and 5 ml of vapors from a headspace vial, which corresponds with the sample loop volume in the instrument. In the case of full evaporation headspace, this corresponds to between 1/22nd to 5/22nd of the total vapor phase in the bottle. If 40 μ l of sample is dispensed into the headspace bottle, this approximates a sensitivity of between 2 and 10 μ l of liquid sample directly injected onto the column. [40(1/22) = 1.8 μ l, 40(5/22) = 9.1 μ l].

Two concerns must be addressed when using the full evaporation technique approach. First, it is conceivable that some chemicals of interest present at higher levels in the samples may not completely evaporate at the given temperature. Second, it is possible that some volatile matrices will develop pressures unsafe for the glass vials. Also, the vial pressure may exceed instrumental pressures and create reproducibility and/or cross-contamination problems.

The first issue can be clarified by calculating the maximum analyte mass that can be completely evaporated in 22.5-ml headspace vials at different temperatures. Rearranging Eqn. 6 yields:

$$\text{Weight (mg)} = V_s \cdot d = (P^o \cdot M_w \cdot 22.5) / RT \quad (7)$$

Table 1 compiles the results of these calculations for several groups of chemicals. It shows that, at 100°C and a sample size of 10 mg, all chemicals

will completely evaporate. The only exception is benzonitrile which is 41% evaporated. The full evaporation technique can be applied whether the chemicals are the analytes or the sample matrix.

The condition of complete evaporation can be also experimentally verified by increasing the equilibration temperature of the vial. This should not cause an increase in sensitivity if the sample has been completely vaporized. If an increase of sensitivity is experienced, then a higher equilibration temperature must be employed, or a smaller sample volume must be used.

The issue of excessive pressures is detailed by Table 2. This was constructed from an available thermodynamic data base. Table 2 represents the list of saturated vapor pressures that can be developed in the vials at reasonable headspace operating conditions. These tables serve as a guide to the development of full evaporation procedures. They demonstrate the conflict between increased sensitivity by increased sample size and the operating pressures which can be developed by the sample matrix. Table 1 shows that up to 64 mg of liquid hydrogen cyanide can be vaporized in the headspace vial at 100°C, resulting in very high sensitivity for impurities in the sample. Table 2, on the other hand, shows that this evaporation will result in 9 atm of pressure. This may lead to contamination of the instrument by sample vapors being forced back into instrumental gas lines

TABLE 2

Saturated vapor pressures for several nitriles at various temperatures

| Temperature (°C) | Vapor pressure (Torr) | | | | | | | |
|------------------|-----------------------|---------------|---------------|------------------|--------------------|-------------------|--------------|--------------|
| | Hydrogen cyanide | Acrylonitrile | Propionitrile | cis-Crotonitrile | trans-Crotonitrile | Methacrylonitrile | Benzonitrile | Acetonitrile |
| 30 | 892 | 135 | 60 | 41 | 22 | 89 | 1 | 114 |
| 40 | 1267 | 204 | 95 | 65 | 37 | 135 | 2 | 174 |
| 50 | 1761 | 299 | 145 | 101 | 59 | 199 | 4 | 257 |
| 60 | 2398 | 428 | 215 | 152 | 91 | 287 | 6 | 372 |
| 70 | 3208 | 598 | 310 | 222 | 136 | 403 | 11 | 525 |
| 80 | 4224 | 817 | 437 | 317 | 199 | 553 | 17 | 726 |
| 90 | 5482 | 1097 | 602 | 444 | 283 | 747 | 27 | 985 |
| 100 | 7024 | 1448 | 814 | 607 | 395 | 990 | 42 | 1313 |
| 110 | 8899 | 1883 | 1082 | 817 | 541 | 1292 | 62 | 1723 |
| 120 | 11160 | 2415 | 1414 | 1080 | 729 | 662 | 91 | 2229 |
| 130 | 13880 | 3058 | 1821 | 1407 | 965 | 2110 | 129 | 2846 |

as well as poor analytical data. Additionally, this is not a safe working pressure for glass vials and silicone septa. To reduce this pressure to about 1 atm, it is necessary to reduce the temperature and/or sample size to 1/10 of the maximum evaporative for hydrogen cyanide. Any increase in the amount of the sample should be accompanied by an increase of instrumental pressurization of the vial. It is desirable to keep this pressure about 1.5 times higher than the pressure developed by the sample.

It is convenient to calibrate the full evaporation instrument in terms of 'absolute amount of analyte' in the vial. Such calibration results in the reported values (RV) being expressed in nanograms. It is relatively easy to convert the reported value into a concentration unit (mg kg^{-1}) by the following calculation:

$$C = \text{RV} / (d \cdot V_s)$$

where V_s represents sample volume (μl) added to the vial, and d is density (g ml^{-1}). This approach provides the analyst with the flexibility of changing the sample size to accommodate different

levels of analyte concentrations without the need for recalibrating the instrument.

EXPERIMENTAL

The full evaporation technique utilizes currently available chromatographic equipment. The headspace sampler simply provides the thermal equilibration and accurate sampling of the vapors in the headspace bottle. The chromatograph provides the separation and detection of the analyte. The normal chromatographic detectors such as flame ionization, thermal conductivity, flame photometric, and electron capture are all available for use with this technique. System maintenance is reduced when the full evaporation technique is utilized because non-volatile species do not contaminate the chromatographic system.

The only requirement is that the sample be accurately dispensed into the vial, and then the vial must be quickly capped. There are many manufactures which can provide syringes capable of delivering small (μl) sample volumes. Cali-

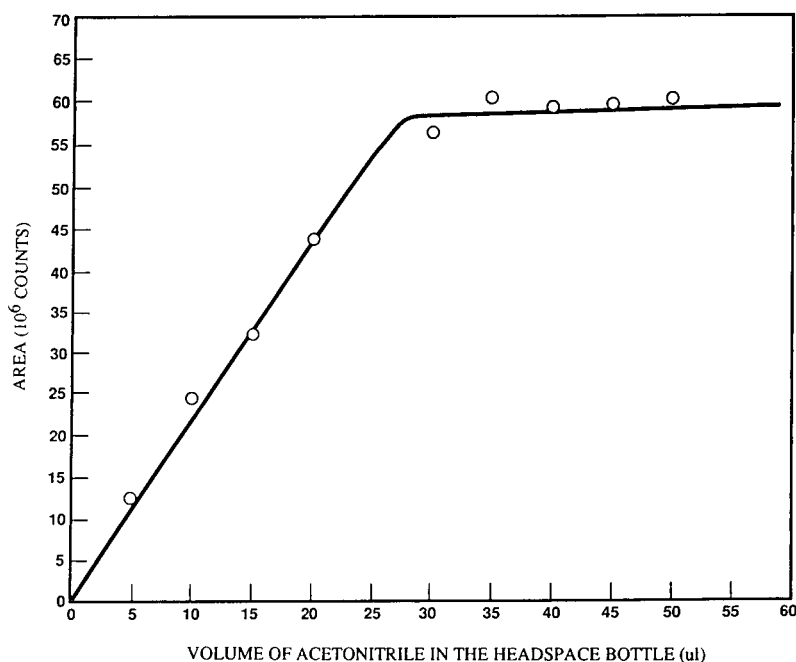


Fig. 2. Flame ionization detector response for various amounts of acetonitrile dispensed into a headspace vial. The linear working range and point of saturation for acetonitrile are illustrated. Sample was equilibrated at 100°C for 5 min prior to analysis.

brated capillaries can also be used to dispense small aliquots of the sample.

RESULTS AND DISCUSSION

Experimental verification of full evaporation technique

Pure chemicals. Figure 2 displays the response of the flame ionization detector as a function of volume (μl) of pure acetonitrile dispensed into the headspace bottle at 65°C . Above the point of about $25 \mu\text{l}$ (19 mg), there exists a saturated vapor in the bottle. This value corresponds well to theoretically predicted maximum evaporative amount of acetonitrile at this temperature. The linear portion of this graph serves as a calibration plot for this chemical. The slope of this plot (response factor) should be independent of the temperature and the matrix of the sample if conditions of full evaporation have been achieved.

Water–organic solvent mixtures. It was necessary to establish that, as the sample matrix was

changed from low to high levels of organics, or visa versa, the response of analytes would be unaffected by the matrix. Standards of the same concentrations were prepared in various sample matrices ranging from 0 to 100% organic (w/w). If the response is unaffected by sample matrix, then the response of each component should remain uniform for each matrix when analyzed by this technique. Indeed, Fig. 3 demonstrates that this is true; the response did not vary as a function of sample matrix in contrast to the case with conventional headspace analysis.

Effects of salinity. Standards solutions of ethanol, acrylonitrile and pyridine (1 ppm) were prepared in water containing various concentrations of salt (0–20%, w/w, Na_2SO_4). The solutions were analyzed using the conventional headspace approach (10 ml of sample in a 22.5-ml vial) and the full evaporation technique ($50 \mu\text{l}$ of sample in a 22.5-ml vial). Identical instrumental conditions were utilized. The results of this experiment are presented in Fig. 4 in terms of ratio of peak sizes generated from salt solutions to

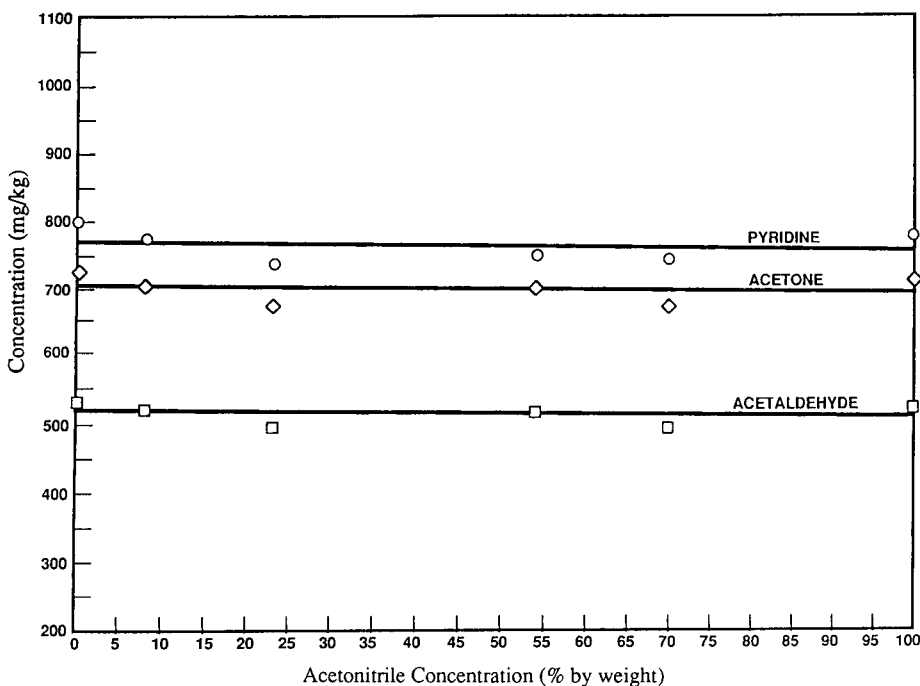


Fig. 3. Variation of detector response as a function of sample matrix for the full evaporation technique. The detector response of analytes in the vapor phase is uniform over a wide range of matrix compositions indicating that the method is matrix insensitive ($10 \mu\text{l}$ of sample at 120°C).

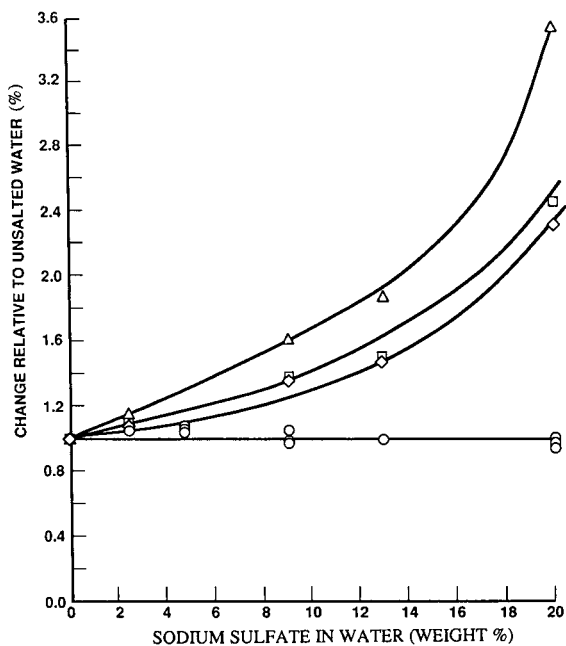


Fig. 4. The effect of salinity on the full evaporation technique and headspace analysis. The 'salting out effect' causes an increase of sensitivity in headspace analysis due to the lower solubility of analytes in the matrix as the salt content increases. Unsalted water is the reference point against which all data was ratioed. No variation was observed when sampling by the full evaporation technique indicating that the method is not sensitive to matrix effects. \diamond , Ethanol headspace (HS); \square , acrylonitrile HS; \triangle , pyridine HS; \circ , ethanol FET; \square , acrylonitrile FET; \circ , pyridine FET.

those obtained for pure water matrix. The figure shows that this ratio is close to unity for each of the chemicals for all the salt solutions studied at full evaporation conditions. The ratio deviates from unity in the headspace experiment and behaves differently for different chemicals (the salting out effect). At this point we would like to once again point out that the term 'full evaporation' refers to the evaporation of the *analytes* and *not necessarily* to the matrix. Indeed, 50 μl of water can not be completely vaporized in a 22.5-ml vial at 100°C.

Alcohol in blood. Headspace analysis is a standard method for the determination of blood alcohol levels in many countries [3]. The technique, however, is applied to the whole blood, plasma, or blood serum and involves dilution and internal standard calibration to minimize variations in blood matrices. We attempted to apply the full evaporation approach for this test using 50 μl of whole blood. The blood was drawn from volunteers, spiked with ethanol (0.08%, w/w) and dispensed into headspace vials using disposable calibrated glass capillaries. No differences in the results were observed between dispensing the blood from capillaries and simply leaving the filled capillary in the vial. The vials were equilibrated at 100°C for 5 min. Figure 5 illustrates that there were no matrix effects encountered for

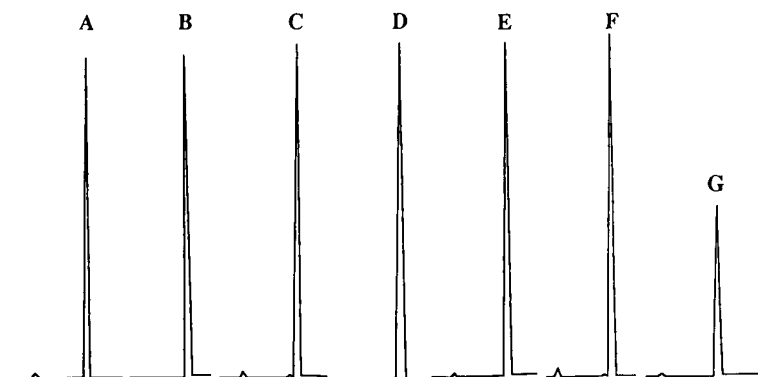


Fig. 5. Determination of blood alcohol levels using the full evaporation technique. Various samples were spiked with ethanol (wt.%) and dispensed into vials using calibrated glass capillaries. Samples were equilibrated at 100°C for 5 min prior to analysis. A = tap water, 0.08%; B = blood sample 1, 0.08%; C = serum sample 1, 0.08%; D = distilled water, 0.08%; E = blood sample 2, 0.08%; F = blood sample 3, 0.08%; G = blood sample 2, 0.04%.

TABLE 3

Various sample matrices spiked with constituents (8–10 mg kg⁻¹) and analyzed by the full evaporation technique (The detector response appears uniform for each analyte indicating matrix independence of the analytical method)

| Matrix | Detector response (10 ⁴ counts) | | | | |
|-----------------|--|---------|--------------------|------------|-------------------|
| | Ethanol | Benzene | <i>n</i> -Propanol | Isobutanol | <i>n</i> -Butanol |
| Distilled water | 1.75 | 2.51 | 2.98 | 3.17 | 3.17 |
| Urine sample 1 | 1.72 | 2.72 | 2.67 | 3.12 | 3.16 |
| Coffee sample 1 | 1.75 | 2.41 | 2.77 | 3.17 | 3.15 |
| Tap water | 1.74 | 2.38 | 2.88 | 3.19 | 3.20 |
| Urine sample 2 | 1.75 | 2.60 | 2.67 | 3.12 | 3.21 |
| Coffee sample 2 | 1.76 | 2.39 | 2.81 | 3.08 | 3.07 |
| Distilled water | 1.65 | 2.31 | 2.73 | 2.88 | 3.11 |
| Urine sample 3 | 1.88 | 2.61 | 2.73 | 3.04 | 3.34 |
| Coffee sample 3 | 1.63 | 2.37 | 2.79 | 2.91 | 3.24 |
| S.D. | 0.72 | 1.38 | 0.99 | 1.13 | 0.76 |
| Mean | 1.75 | 2.48 | 2.78 | 3.07 | 3.19 |
| R.S.D. (%) | 4 | 6 | 4 | 4 | 2 |

different blood specimens or even between blood and tap water. No oxidation of ethanol or formation of acetaldehyde was observed, as previously had been reported [9,10]. This example does not represent an alternative procedure whose development requires more rigorous testing [4], but simply presents the utility of this technique.

Foods and biological liquids. Table 3 compiles raw areas of headspace chromatographic peaks generated by several chemicals spiked into different matrices. A sample volume of 50 μ l was heated for 10 min at 100°C in 22.5-ml headspace

vials. The table shows that variations in the matrix did not result in excessive values of standard deviations (2–6%) for any of the chemicals. Contamination of the sample matrices contributed to some of the deviations in the results.

Table 4 expands the scope of the matrices and chemicals tested and presents the results in terms of total nanograms of chemicals in the sample aliquot in the headspace vial. The table shows that the near complete transfer of analytes from the matrices does occur. Indeed, at 8–10 ppm spikes and a 50- μ l sample volume, the mass of

TABLE 4

Total mass of analyte in the headspace over various matrices

[Samples were prepared with analyte concentrations of 8–10 ppm (mg kg⁻¹). 50 μ l of this standard mixture was dispensed into a headspace vial. Results indicate good recoveries for the analytes. The chromatograph was previously calibrated (in nanograms) by an independent standard]

| Matrix | Mass in the vapor phase (ng) | | | | |
|-------------------------|------------------------------|---------------|-------------------|----------|---------|
| | Ethanol | Acrylonitrile | <i>n</i> -Butanol | Pyridine | Styrene |
| Urine sample 1 | 415 | 401 | 392 | 478 | 424 |
| Distilled water | 397 | 396 | 398 | 479 | 436 |
| Milk, D3 | 408 | 394 | 386 | 466 | 445 |
| Pepsi Cola [®] | 415 | 371 | 373 | 188 | 439 |
| Chicken soup | 402 | 389 | 442 | 494 | 379 |
| Urine sample 2 | 400 | 386 | 387 | 470 | 405 |
| Tap water | 371 | 380 | 379 | 446 | 430 |
| Milk | 404 | 355 | 374 | 457 | 396 |
| Chicken soup | 393 | 403 | 437 | 486 | 413 |

the analytes should be approximately 400–500 ng ($10 \text{ ng } \mu\text{l}^{-1} \times 50 \mu\text{l} = 500 \text{ ng}$). This expectation is met by most of the experimental results listed in Table 4. The exceptions, like pyridine spiked into Pepsi Cola[®], is attributable to the chemical reaction of the matrix ($\text{pH} \approx 2$) with the basic analyte.

Conclusions

The full evaporation technique is experimentally simple, convenient, economical and safe. Experience with implementation of this technique indicates that very brief instructions are sufficient for operators of gas chromatographic equipment to become comfortable with the methodology. It is generally more convenient to dispense microliters of sample into a headspace vial at room temperature than to provide fast injection through a small opening of a hot injection port. The variety and number of calibration standards for different sample matrices can be reduced due to the universal calibration approach which is a distinct advantage of the full evaporation technique.

The full evaporation technique uses standard headspace and purge and trap autosamplers or manual syringe injections which are available in most laboratories. The chromatograph in these experiments simply provided separation and detection of the analytes while the headspace sampler provided a convenient heating and sampling strategy. Our preliminary experiments indicated that Draeger tubes as well as infrared instruments provide reasonable detection schemes when coupled with these sampling devices.

The full evaporation technique is reproducible and has a sensitivity comparable to direct liquid injections. The enhanced reproducibility of this technique can be attributed to its insensitivity to temperature fluctuations within the instrument. The sensitivity of the method depends on the amount of the sample one can place in the vial without deviating from full evaporative conditions. Sensitivity for the technique ranges between that which is expected for headspace and direct injection techniques. It is generally worse

than headspace analysis and better than direct injection.

The full evaporation technique is matrix insensitive and protects the analytical instrument from non-volatile constituents of the sample (salts, polymers, detergents, mineral acids, etc.). Some matrices are viscous or solid and can not be directly injected into a gas chromatograph. An example would be a contaminated soil. By employing the full evaporation sampling strategy, elaborate extraction procedures commonly used for direct injection are eliminated. Extensive calibrations required for headspace analysis also become obsolete.

The full evaporation methodology is theoretically sound and its applicability to a particular analysis is predictable. Indeed, experimental parameters and the expected sensitivity for a chemical can be theoretically estimated prior to the analysis. Any reference book or a data base which provides vapor pressures as a function of temperature is adequate for this calculation.

We gratefully appreciate those who helped in the testing, validation, and review of our work. Especially Lynn Wolfram, J. Grills, P. Grandsard, M. Cohen, and countless others who in one way or another made a contribution to this effort.

REFERENCES

- 1 M. Markelov, *Headspace Analysis – Theory and Practice*, Short course, ACS Labs., Chesterland, OH, 1989–1992.
- 2 M. Markelov, ASTM E-19 Meeting, Atlanta, GA, 1990.
- 3 B. Ioffe and A. Vitenberg, *Headspace Analysis and Related Methods in Gas Chromatography*, Wiley, 1984.
- 4 J. Drozd, Z. Vodakova and P. Koupil, *J. Chromatogr.*, 518 (1990) 1.
- 5 B. Kolb and P. Pospisil, *Chromatographia*, 10 (1977) 705.
- 6 C. McAuliffe, *Chem. Technol.*, 1 (1971) 46
- 7 M. Markelov, D. Mendel and L. Talanker, in *Pittsburgh Conference Abstracts*, 1983, No. 206.
- 8 M. Markelov and J. Biesenberger (Ed.), *Devolatilization of Polymers*, Hanser Publishers, 1984, Chap. 4.
- 9 B. Kolb, *Chromatographia*, 15 (1982) 587.
- 10 P. Wilkinson, J. Wagner and A. Sedman, *Anal. Chem.*, 47 (1975) 1506.

Determination of blood cyanide by headspace gas chromatography with nitrogen–phosphorus detection and using a megabore capillary column

Yasuo Seto, Noriko Tsunoda, Hikoto Ohta and Toshiaki Shinohara

National Research Institute of Police Science, 6, Sanban-cho, Chiyoda-ku, Tokyo 102 (Japan)

(Received 5th October 1992; revised manuscript received 8th December 1992)

Abstract

A method for the determination of cyanide in blood using head-space capillary gas chromatography (HS-GC) with nitrogen–phosphorus detection (NPD) was developed. The separation efficiency and sensitivity for hydrogen cyanide (HCN) were improved by using a GS-Q megabore capillary column and by injection of 500 μl of HS gas with a splitting ratio of 5. No interference or column deterioration was observed. Optimum HS conditions were found to be incubation at 50°C for 30 min in the presence of 10% phosphoric acid as an acidifying reagent. The distribution coefficient (k) was 75.7 and 158.9 for HCN and acetonitrile (CH_3CN ; candidate for internal standard), respectively. HCN showed a different vaporization behaviour to CH_3CN with respect to temperature and matrix effect. The salting-out effect was relatively small for HCN and CH_3CN . An increase in the blood content in the liquid phase resulted in a significant increase in k for HCN. The calibration graph was linear over a wide concentration range of cyanide, and the limit of determination was 1 ng ml^{-1} (R.S.D. 10%). Because a considerable amount of CH_3CN was detected in control blood, the direct calibration method could be used instead of the internal standard method using CH_3CN . The detectable amount of cyanide was significantly decreased during the preincubation of cyanide and blood at 2°C. Thiocyanate in blood showed a positive interference. Contents determined by this HS-GC method agreed closely with those obtained by the microdiffusion–spectrophotometric method for blood samples from fire victims.

Keywords: Gas chromatography; Blood; Cyanide; Headspace analysis

Cyanide is a potent and rapidly acting toxic agent which prevents the tissues from utilizing oxygen by inhibition of the terminal cellular respiratory enzyme cytochrome oxidase [1]. Cyanide is widely used in the chemical industry, e.g., in electroplating, and as a fumigant. Cyanide is also produced endogenously from sodium nitroprusside, prescribed as a hypotensive medicine [2], or from cyanogenetic glycosides [3]. In addition, hydrogen cyanide (HCN) is found in tobacco smoke [4].

In fires where nitrogen-containing polymeric materials pyrolyse or burn, HCN is released [5]. Recently, it has been reported that significant amounts of cyanide were detected in the blood of fire victims [6–11]. Although the principle causes of death in fires are heat, burns, oxygen deprivation and carbon monoxide poisoning, there is a possibility that HCN may be involved in lethality in fires. Therefore, it is important to determine cyanide concentrations in the blood of fire victims in order to elucidate the cause to death.

Many methods for the determination of cyanide have been developed. This paper is restricted to blood samples only. The determination

Correspondence to: Y. Seto, National Research Institute of Police Science, 6, Sanban-cho, Chiyoda-ku, Tokyo 102 (Japan).

of cyanide involves extraction of HCN from samples and the measurement of the extracted cyanide. Aeration [12,13], distillation [14], micro-diffusion [15,16] and headspace (HS) methods [17–20] are used for the extraction procedure. Titration [21], spectrophotometry [22], fluorimetry [23], polarography [24], ion chromatography [25] and gas chromatography (GC) [17–20,26–28] are used for quantification. GC is more suitable for qualitative and quantitative determinations than the other, non-specific methods. Flame ionization detection (FID) [29] and electron-capture detection (ECD) [18,28] are used for direct detection and after conversion to cyanogen halide, respectively. Recently, specific and sensitive flame thermionic detection (FTD) was introduced to detect HCN [26,27], and it has been applied in combination with HS-GC for blood analysis [17,19,20].

The HS-GC method is currently used for the determination of volatile substances [30,31], and can be divided into two basic categories: the equilibrium HS method and the dynamic HS (purge and trap) method. Because of the simple procedure without the need for a special instrument, the equilibrium HS method seems to be suitable for cyanide determination. However, with regard to the dynamics of HCN in HS equilibrium, no information is available.

In a previous paper [19], a method for the determination of blood cyanide using HS-GC was reported, in which Porapak QS was used as a stationary phase with FTD detection and acetonitrile (CH_3CN) as an internal standard (I.S.) [20]. However, the method suffered from poor resolution of the HCN peak and severe interference from several components present in blood samples, especially after several sample injections, requiring frequent column conditioning. This may be attributable to deterioration of this polar type of stationary phase.

This paper describes the improvement of the GC of HCN by adopting a GS-Q megabore capillary column. The behaviour of HCN and CH_3CN in HS equilibrium was investigated with regard to the effects of temperature, phase volume ratio and matrix components in order to consider the suitability of CH_3CN as an I.S. By using optimum

HS-GC conditions, a micro method for the determination of blood cyanide was developed. The disappearance of cyanide in blood samples and the conversion of thiocyanate into HCN were also examined.

EXPERIMENTAL

Reagents

Potassium cyanide, acetonitrile, sulphuric acid, ovalbumin and sodium *N*-chloro-*p*-toluenesulphonamide (Chloramine T) were purchased from Wako (Osaka), phosphoric acid (85% solution), silver nitrate and *p*-dimethylaminobenzylidene-rhodanine from Nacalai Tesque (Kyoto), Cyanoline Blue [a mixture of 1-phenyl-3-methyl-5-pyrazolone and 4,4'-bis(1-phenyl-3-methyl-5-pyrazolone) (12.5:1, w/w)] from Dojindo Labs. (Kumamoto) and standard gases (ethane, ethylene, propane, propylene, isobutane and *n*-butane, each 1% in nitrogen) and methane (100%) from GL Science (Tokyo). Other chemicals were of analytical-reagent grade. All aqueous solutions were prepared with deionized, distilled water. Outdated transfusion blood was used as control blood.

Apparatus

The instrument used was a Model 5890 A gas chromatograph (Yokogawa Hewlett-Packard, Tokyo) equipped with a flame ionization detector (FID) and nitrogen-phosphorus detector (NPD) and split injector (the FTD is called NPD in Hewlett-Packard GC instrumentation). A GS-Q capillary column (30 m \times 0.53 mm i.d.) (J&W Scientific, Folson, CA) was used. The carrier gas (helium) flow-rate was 4.7 ml min⁻¹ when the column head pressure was adjusted 5 psi. The injection port and detector were maintained at 200 and 250°C, respectively. GC control and data processing were performed by a Model 5895 A GC ChemStation.

Preparation of standard cyanide solution

A stock standard solution of cyanide (10 mg ml⁻¹) was prepared by dissolving potassium cyanide in 0.1 M NaOH solution and standardized by titration with 0.1 M silver nitrate using

p-dimethylaminobenzylidenerhodanine as an indicator [21]. This solution was stored at 4°C in the dark and used within 1 week. Dilute working standard solutions were prepared by diluting the stock standard solution with 0.1 M NaOH to obtain the desired concentrations.

Head space conditions

HS equilibrium was performed in a screw-capped septum vial (7 ml, clear borosilicate glass) (Pierce, Rockford, IL). The actual inner volume of this vial was measured to be 8.76 ml by weighing water in the vial. A 0.8-ml volume of sample solution was placed in a vial which was then sealed with a Tuf-Bond disc (thickness 0.25 mm Teflon and 2.25 mm silicone) (Pierce). The sample solution consisted of 0.5 ml of blood and 0.3 ml of water. The standard samples for the calibration consisted of 0.5 ml of control blood, 0.1 ml of a known concentration of cyanide solution and 0.2 ml of water. A 200- μ l volume of 50% phosphoric acid was introduced through the disc by using a Luer glass-tipped syringe (0.5 ml volume) (Top, Tokyo) fitted with needles (25 G \times 1", 0.50 \times 25 mm) (Terumo, Tokyo). The mixture was vortex mixed and allowed to stand at 50°C on an aluminium Reacti-Block (hole size 16.5 mm i.d. \times 5.65 cm deep) heat-controlled with a Pierce Reacti-Therm heating module. After incubation for 30 min, 0.5 ml of gaseous phase in the sealed vial was withdrawn using a Luer glass-tipped syringe (1.0 ml volume) fitted with needles (25 G \times 1") prewarmed to 50°C and immediately applied to the GC column. This volume (0.5 ml) should be low enough not to disturb HS equilibrium.

Correction for the gas pressure in the HS vial

Because of the increased pressure of the gas phase when the HS vial was warmed, part of the HS gas sampled by the syringe was lost before GC injection. This loss of gas was calculated by measuring the gas pressure in the following way. Syringes (5.0 ml volume) fitted with needles prewarmed at 50°C were injected into the HS vial and the increased volume was read after the cylinder of the syringe had been raised by the elevated pressure to reach a balance with the atmospheric pressure. This volume, designated *x*

ml, varied from 1 to 1.5 ml. When 0.5 ml of HS gas was withdrawn, the pressure in the gas syringe is assumed to be $(7.76 + x)/8.26$ atm and was returned to 1 atm immediately by losing air. Accordingly, the corrected analyte concentration in HS gas is given by multiplying the obtained GC peak area by $(7.76 + x)/8.26$.

Microdiffusion-spectrophotometric method for the determination of cyanide in blood

A 2-ml volume of 0.1 M NaOH solution and 1 ml of blood sample were added to the centre well and on one side of the outer well of a glass Conway microdiffusion cell (Shibata Scientific, Technology, Tokyo). After addition of 0.5 ml of 50% (v/v) sulphuric acid on the side opposite to the blood, the cell was rapidly closed with a glass plate coated with glycerol. Blood and acid were immediately mixed by gentle tilting and the mixture was left for 2 h at room temperature. A 1-ml volume of an alkaline solution was pipetted into a glass tube cooled in ice, and 0.2 ml of ice-cooled 0.0625% Chloramine T solution containing 0.75 M NaH₂PO₄ was added. After 2 min, 3 ml of Cyanoline Blue solution (0.27 g dissolved in 20 ml of pyridine and then 100 ml of water added) were added, and the tube was left for 40 min at room temperature. Absorbance was measured at 630 nm. The calibration graph was linear up to cyanide concentrations of at least 2 μ g ml⁻¹. The absorbance value was about 1 for cyanide of 1.0 μ g ml⁻¹ in alkaline solution. It was verified that the analytical recovery of cyanide was quantitative through the microdiffusion procedure.

Determination of cyanide concentration in gaseous phase in HS vial

After HS equilibrium, 0.5 ml of gaseous phase was withdrawn with a syringe and injected into another sealed vial containing 1 ml of 0.1 M NaOH solution and vortex mixed. The concentration of cyanide absorbed in this alkaline solution was measured by the spectrophotometric method.

RESULTS

GC separation

A polar stationary phase of the porous polymer type, Porapak Q or QS, is commonly used

for the GC separation of HCN. In this work, in order to effect the simultaneous determination of HCN and CH_3CN and to investigate their HS behaviour, GC with FID and a GS-Q capillary column was first tried. Figure 1 shows a typical gas chromatogram of the HS sample. The number of theoretical plates for the HCN peak was found to be 12400, compared with 1340 using HS-GC with a Porapak QS column [19]. The column oven temperature was programmed for the optimum separation of HCN and interfering compounds. Lower hydrocarbons (methane, methylene, ethane, propane and propylene), which were eluted earlier than HCN, and isobutane and *n*-butane, which were eluted between HCN and CH_3CN , did not interfere. Methanol was eluted just after HCN, but well separated from it. Ethanol was eluted just after CH_3CN , and separated from this peak, except when large amounts were present (Fig. 5D). Acetaldehyde, which was eluted just before HCN (Fig. 1), did not disturb the determination of HCN, even at the maximum blood concentration encountered in a case of alcohol intoxication (below $50 \mu\text{g ml}^{-1}$) [32].

To obtain maximum sensitivity and resolution for the proposed method, the GC parameters such as injection volume and splitting ratio were optimized. The injection volume was correlated with the GC peak area for injection volumes up to $200 \mu\text{l}$. Above this volume, a concave curvature of the volume–peak area response was observed. Even at a volume of $500 \mu\text{l}$, about 17% and 23% gas loss were observed for HCN and CH_3CN , respectively. This may be ascribed to leakage of injected gas from the septum purge port. The splitting ratio was inversely correlated with peak area, and correlated with resolution, expressed as the peak width at half-height. The peak resolution was not further improved at splitting ratios > 10 . Therefore, a $500\text{-}\mu\text{l}$ injection with a splitting ratio of 5 was adopted.

Headspace conditions

Constant peak areas of HCN and CH_3CN were obtained from 30 min to 3 h of incubation, as shown in Fig. 2. This result indicates that within 30 min of incubation vaporization equilibria of HCN and CH_3CN are established in the HS vial and HCN and CH_3CN are stable without

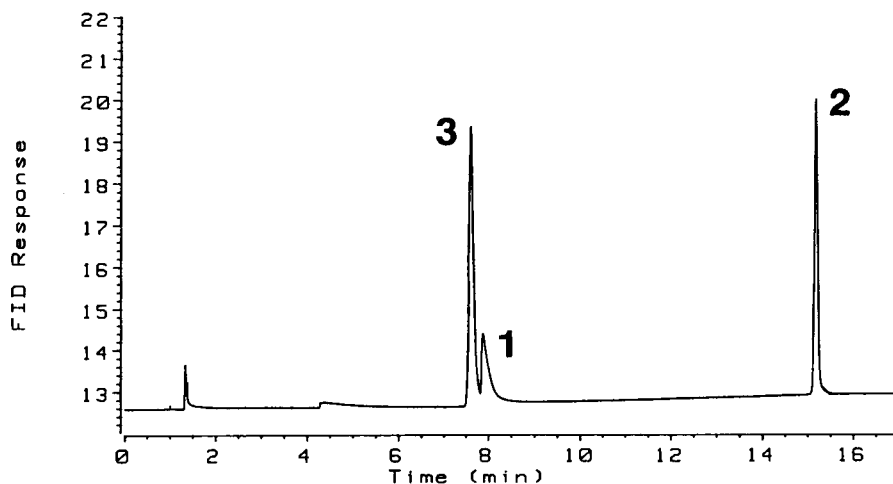


Fig. 1. Gas chromatogram of HCN and acetonitrile detected by FID. $40 \mu\text{g}$ of cyanide, $62.6 \mu\text{g}$ of acetonitrile and $50 \mu\text{g}$ of acetaldehyde were incubated in 1.0 ml of aqueous solution containing 10% phosphoric acid in an HS vial at 50°C . After 30 min, $500 \mu\text{l}$ of HS gas were injected into the system conditions: column, GS-Q ($30 \text{ m} \times 0.53 \text{ mm i.d.}$); carrier-gas (helium) flow-rate, 4.6 ml min^{-1} ; injection port and detector (FID) temperatures, 200 and 250°C , respectively; splitting ratio, 17; column oven, isothermal for 7 min at 90°C , then programmed at 5°C min^{-1} to 140°C . Peaks 1, 2 and 3 represent the elution peaks of HCN, acetonitrile and acetaldehyde, respectively.

any degradation or adsorption during the incubation.

Under the HS conditions, where 80 μg of cyanide were incubated at 50°C for 30 min, the HCN concentration in the gaseous phase was measured by the alkaline absorption–spectrophotometric procedure after gas pressure correction. The HCN concentration in the liquid phase was calculated from the remaining content subtracted from the HCN content in the gaseous phase. The distribution coefficient (k) for HCN, defined as the ratio of analyte concentration in the liquid phase to that in the gaseous phase, was found to be 75.7. The k value for CH_3CN was also determined under the same HS conditions with a CH_3CN concentration of 125 $\mu\text{g ml}^{-1}$. The gaseous CH_3CN concentration was calculated by comparison with the data for the direct GC injection of a methanolic solution. The k value for CH_3CN was found to be 158.9.

As shown in Fig. 3, raising the HS temperature resulted in a decrease in k for both HCN and

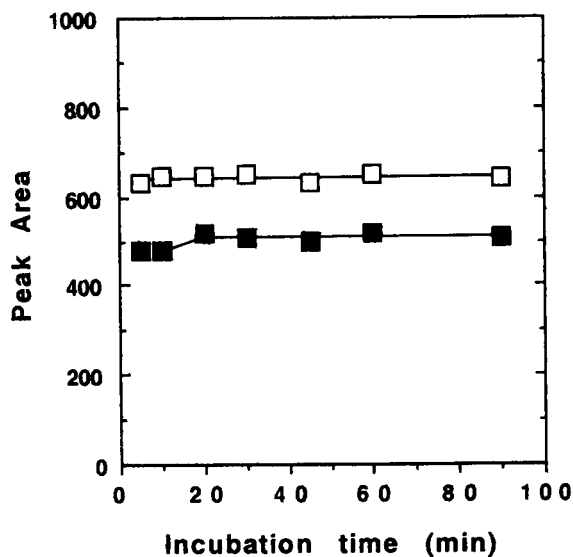


Fig. 2. Effect of incubation time on peak area of HCN and acetonitrile. 80 μg of cyanide and 31.3 μg of acetonitrile were incubated in 1.0 ml of aqueous solution containing 10% phosphoric acid in an HS vial at 50°C. After appropriate time intervals as shown, 500 μl of HS gas were injected into the GC system. GC conditions as in Fig. 1. Peak areas of (■) HCN and (□) CH_3CN were plotted against incubation time.

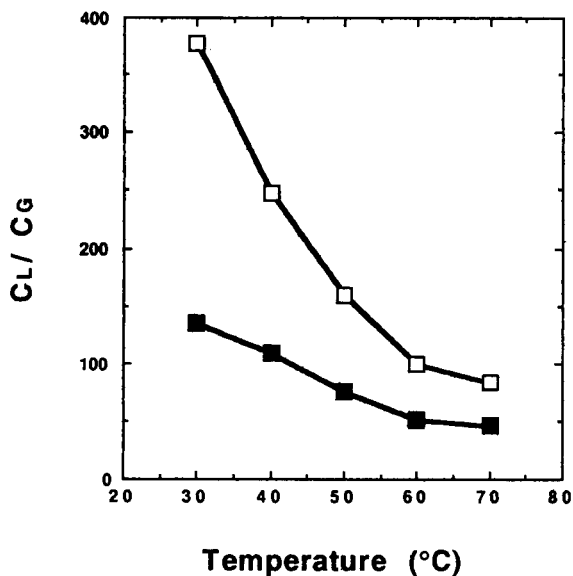


Fig. 3. Effect of temperature on distribution coefficient. 80 μg of cyanide and 125 μg of acetonitrile were incubated in 1.0 ml of aqueous solution containing 10% phosphoric acid in an HS vial at an appropriate temperature as indicated. After 30 min, 500 μl of HS gas were injected into the GC system. GC conditions as in Fig. 1. The cyanide concentration in the gaseous phase (C_G) at 50°C was determined by the alkaline absorption–spectrophotometric method. The cyanide concentration in the HS gas at other temperatures was calculated from the data at 50°C. The acetonitrile concentration in the HS gas was calculated by comparison of direct injection data for methanolic solution. The concentration in the liquid phase (C_L) was calculated as the residue subtracted from the content in the gaseous phase. Distribution coefficients, defined as C_L/C_G , of (■) HCN and (□) CH_3CN were plotted against temperature. Each point is an average of duplicate measurements.

CH_3CN , and this decrease was most marked for CH_3CN . However, at higher temperatures, the peak area showed a larger variation because of the high gas pressure. Taking the sensitivity and the error into account, an HS temperature of 50°C was adopted.

The effect of the volume ratio of gas phase to liquid phase (β) on the k value for HCN and CH_3CN was also investigated. As shown in Fig. 4, k did not alter much over a wide range of β , although the k values had the tendency to decline with increasing β value. This decrease may be due to an inaccuracy in adjusting the total liquid volume. This result indicates that the ana-

lyte concentration in the gaseous phase is dependent on the initial analyte concentration in the liquid phase.

It is known that matrix components in the liquid phase affect the HS behaviour of volatile substances. The effects of various additives on the HS behaviour were examined. Figure 5A shows the effect of acid concentration on peak area. Non-volatile phosphoric acid was chosen as an acidifying reagent, offering sufficient acidity and a homogeneous solution for blood samples without clotting. Raising the acid concentration resulted in a significant increase in the peak areas of HCN and CH_3CN . Increases of ca. 33% and 18% were observed in the presence of 10% acid in comparison with the presence of 0.1% acid. At a low acid concentration (0.01%), which is insufficient to acidify the cyanide solution, no HCN peak was observed. Inorganic salts are known to enhance the vaporization of volatile

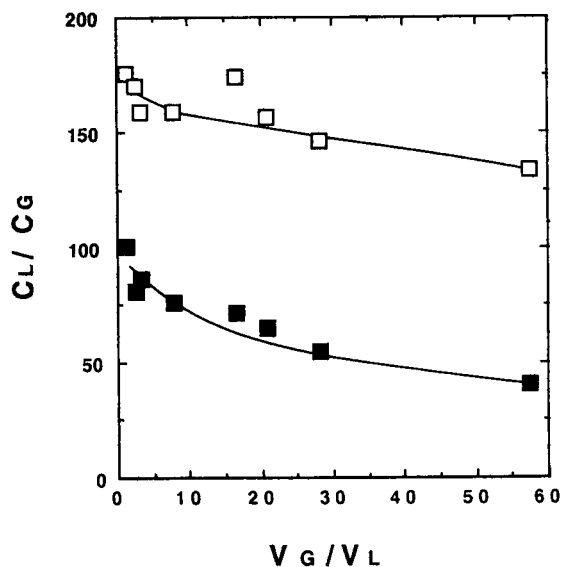


Fig. 4. Effect of phase volume ratio on distribution coefficient. 80 μg of cyanide and 125 μg of acetonitrile per ml were incubated in aqueous solution containing 10% phosphoric acid [total liquid phase volume (V_L) = 0.15, 0.3, 0.4, 0.5, 1, 2, 2.5, 4 ml] in an HS vial at 50°C. After 30 min, 500 μl of HS gas were injected into the GC system. GC conditions as in Fig. 1. Distribution coefficients of (■) HCN and (□) CH_3CN were plotted against volume ratio of gas phase to liquid phase (V_G/V_L). Each point is an average of duplicate measurements.

substances. As shown in Fig. 5B, addition of NaCl resulted in a slight increase in the GC peak areas of HCN and CH_3CN . About 21% and 16% increases were observed in the presence of 10.5% NaCl compared with the situation where NaCl is absent. This slight salting-out effect of NaCl may be due to the fact that at a phosphoric acid concentration of 10% used as an acidifying reagent sufficient salting-out already occurs and additional NaCl does not have a large effect. Blood mainly consists of proteins. As shown in Fig. 5C, over a wide range up to about 20%, ovalbumin caused almost no alteration in the HCN peak area, in contrast to a slight increase in the CH_3CN peak area (by about 10%). Ethanol was sometimes detected in post-mortem blood. As shown in Fig. 5D, there was virtually no effect of ethanol on the peak areas of HCN and CH_3CN , even at the lethal blood level (about 5 mg ml^{-1}) [33]. For ethanol concentrations over 2%, the CH_3CN peak merged with the ethanol peak, disturbing the determination of CH_3CN .

The calibration graphs for HCN detected by FID (splitting ratio 17) were linear for cyanide concentrations ranging from 1.25 to 80 $\mu\text{g ml}^{-1}$. The slopes of the linear lines were unity, indicating a constant k value irrespective of the cyanide concentration. The limit of determination was 0.2 $\mu\text{g ml}^{-1}$ when the splitting ratio was 5 [relative standard deviation (R.S.D.) 10% ($n = 6$), signal-to-noise ratio = 3.5].

Microdetermination of cyanide

NPD permits the sensitive and specific detection of nitrogen-containing compounds [34]. In the absence or presence of blood, stable peak area values were obtained from 30 min to 3 h of incubation of small amounts of cyanide (100 ng ml^{-1}). This result indicates that HS equilibrium was achieved within 30 min and that even very small amounts of cyanide were just as stable during the incubation as large amounts of cyanide (Fig. 2).

A typical gas chromatogram of the HS of HCN detected by NPD is shown in Fig. 6. Although the HCN peak showed tailing, there were no interfering peaks. This tailing was observed for large amounts of HCN injected (Fig. 1) and was not

due to overloading. From control blood, considerable amounts of CH_3CN (above 10 ng ml^{-1}) were detected with large fluctuations. Fig. 7 shows the effect of blood on peak area. An increasing blood content in the liquid phase resulted in a gradual decrease in the peak area of HCN; this decrease was about 30% in the presence of 60% blood. However, for blood concentrations above 30%, this decreased level was almost constant, indicating saturation of the suppressive effect of blood on HCN vaporization. On the other hand, addi-

tion of blood resulted in a negligible alteration of the peak area of CH_3CN .

Figure 8 shows calibration graphs for HCN in the absence and presence of blood. Without blood, good linearity was obtained for cyanide concentrations ranging from 10 ng ml^{-1} to $20 \mu\text{g ml}^{-1}$. The intra-assay R.S.D. was 6.1% ($n = 8$) for cyanide at $0.1 \mu\text{g ml}^{-1}$. The limit of determination was 1 ng ml^{-1} with a splitting ratio of 5 (R.S.D. 7% ($n = 6$), signal-to-noise ratio = 10). The sensitivity for HCN using NPD was over 100

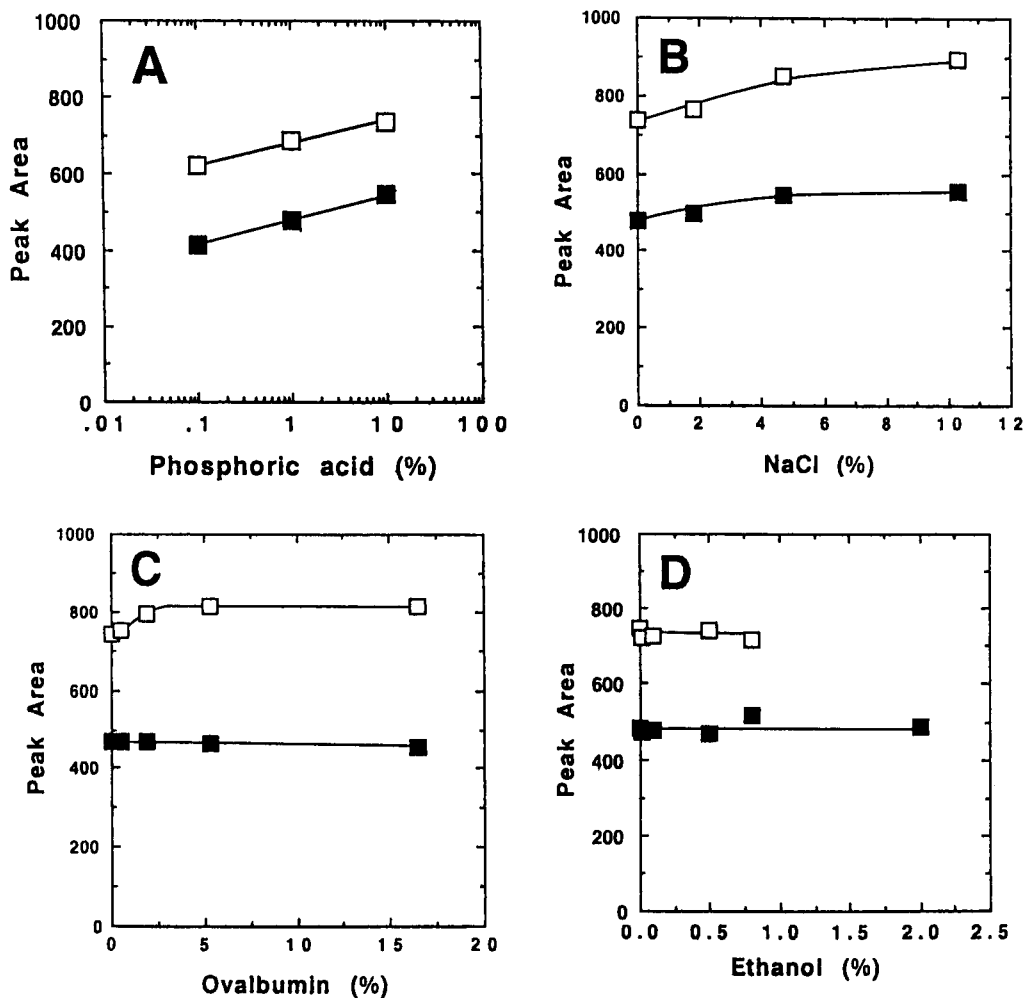


Fig. 5. Matrix effects of (A) phosphoric acid, (B) sodium chloride, (C) ovalbumin and (D) ethanol. $80 \mu\text{g}$ of cyanide and $125 \mu\text{g}$ of acetonitrile were incubated in 1.0 ml of aqueous solution containing 10% phosphoric acid and a known amount of additive in an HS vial at 50°C . After 30 min, $500 \mu\text{l}$ of HS gas were injected into the GC system. In (A) the phosphoric acid concentration was adjusted to be 0.1, 1 and 10% in the liquid phase. GC conditions as in Fig. 1. Peak areas of (■) HCN and (□) CH_3CN were plotted against concentration of additive. Each point is an average of duplicate measurements.

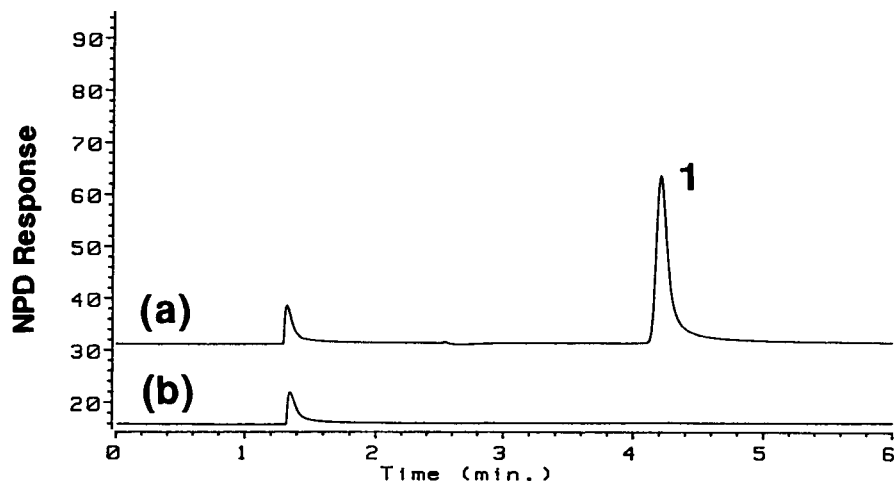


Fig. 6. Gas chromatogram of HCN detected by NPD. 500 μl of control blood were incubated in 1.0 ml of aqueous solution containing 10% phosphoric acid in (a) the presence or (b) the absence of 100 ng of cyanide in an HS vial at 50°C. After 30 min, 500 μl of HS gas were injected into the GC system. GC conditions as in Fig. 1 except for the detector (NPD), splitting ratio (3.7) and column oven, which after a 4-min isothermal period at 110°C was programmed at 10°C min^{-1} to 160°C. Peak 1 represents the elution peak of HCN.

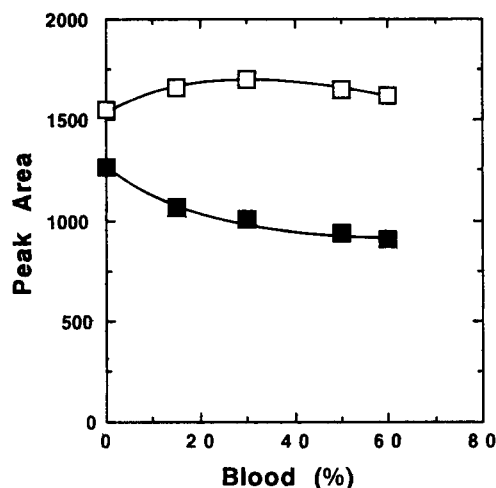


Fig. 7. Effect of blood on peak area of HCN and acetonitrile. 100 ng of cyanide and 156.6 ng of acetonitrile were incubated in 1.0 ml of aqueous solution containing 10% phosphoric acid and a known amount of control blood as indicated in an HS vial at 50°C. After 30 min, 500 μl of HS gas were injected into the GC system. GC conditions as in Fig. 6. The value of the peak area for CH_3CN was corrected by subtracting that from a blank containing the same amount of blood. Peak areas of (■) HCN and (□) corrected value of CH_3CN were plotted against blood volume. Each point is an average of duplicate measurements.

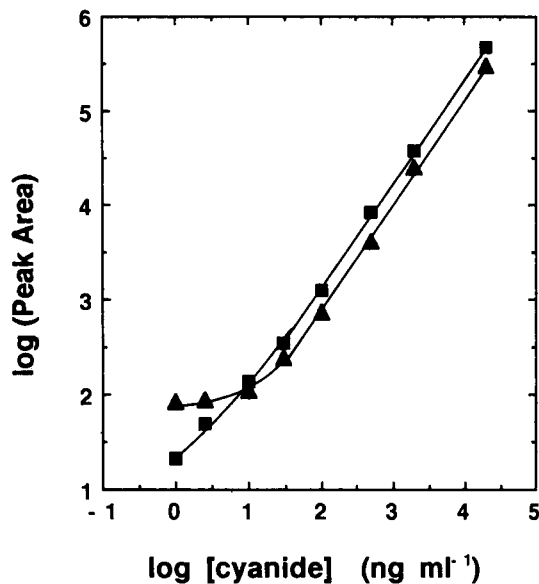


Fig. 8. Calibration graphs for cyanide detected by NPD. A known amount of cyanide was incubated in 1.0 ml of aqueous solution containing 10% phosphoric acid, (▲) with and (■) without 0.5 ml of control blood, at 50°C. After 30 min, 500 μl of HS gas were injected into the GC system. GC conditions as in Fig. 6. Peak area of HCN was plotted against cyanide concentration. Each point is an average of duplicate measurements.

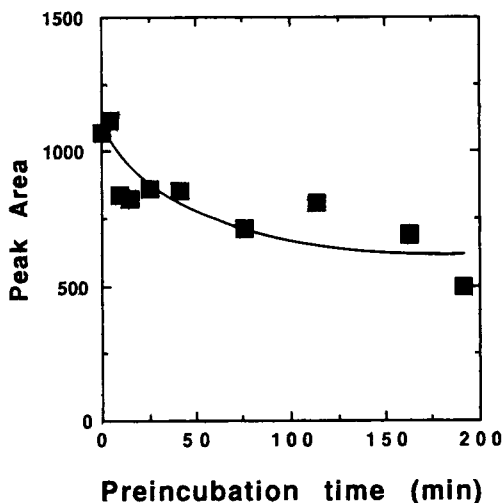


Fig. 9. Effect of preincubation time on peak area of HCN. 100 ng of cyanide were preincubated in 0.8 ml of aqueous solution containing 0.5 ml of control blood in an HS vial at 2°C for an appropriate time as indicated, and then 0.2 ml of 50% phosphoric acid was added. After 30 min, 500 μl of HS gas were injected into the GC system. GC conditions as in Fig. 6. Peak area was plotted against preincubation time.

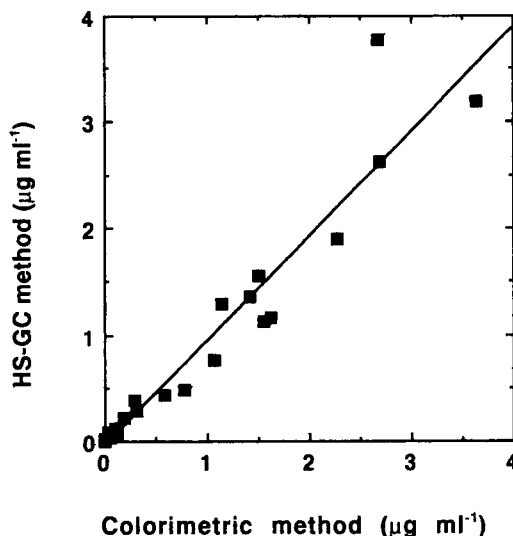


Fig. 11. Correlation of blood cyanide levels determined using the HS-GC method and the microdiffusion-spectrophotometric method. Cyanide concentrations were determined by the two methods simultaneously for blood samples from fire victims. The straight line shows the correlation line calculated by least-square regression analysis. The equation is $y = 0.983x - 0.0355$ ($r^2 = 0.917$).

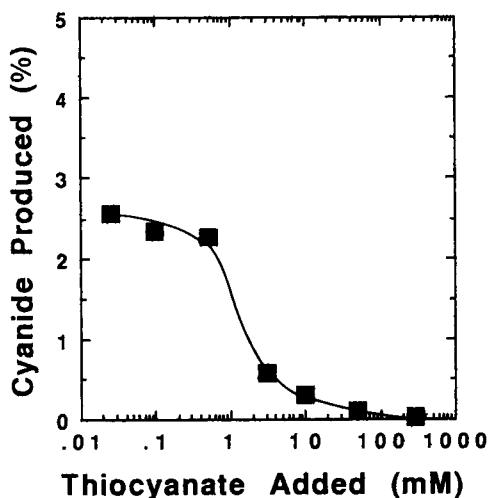


Fig. 10. Conversion of thiocyanate into HCN under acidic conditions in the presence of blood. Known amounts of thiocyanate as indicated were incubated in 1.0 ml of aqueous solution containing 10% phosphoric acid and 0.5 ml of control blood at 50°C. After 30 min, 500 μl of HS gas were injected into the GC system. GC conditions as in Fig. 6. HCN detected in HS gas was expressed as % molar conversion from thiocyanate added, and plotted against thiocyanate concentration. Each point is an average of duplicate measurements.

times that using FID. With blood, the graph was linear for cyanide concentrations ranging from 50 ng ml⁻¹ to 20 μg ml⁻¹. However, below a concentration of 50 ng ml⁻¹, the graph showed a concave curvature, owing to the presence of a background cyanide level in the control blood. The two linear lines were almost parallel for cyanide concentrations over 50 ng ml⁻¹, indicating an identical matrix effect of blood on HCN vaporization over a wide range of cyanide concentrations.

The effect of storage over a short period on the cyanide level in blood at 2°C was examined. When a large amount of cyanide (25 μg) was added to blood, the detected value gradually decreased with the time taken for the preincubation of cyanide and blood before addition of phosphoric acid; 72% of the originally added cyanide was detectable after a preincubation for 3 h. Figure 9 shows the effect of storage on a small amount of cyanide (100 ng) in blood. The detected value also gradually decreased with increasing preincubation time, and showed considerable fluctuation.

Conversion of thiocyanate into hydrogen cyanide

It is known that thiocyanate occurs in blood and is increased in the case of tobacco smoke and tobacco amblyopia [35]. Figure 10 shows the result of the conversion of thiocyanate to HCN under acidic conditions in the presence of blood at 50°C. About 2–3% of thiocyanate was converted into HCN under the HS conditions for concentrations below 1 mM thiocyanate. Above this concentration, the conversion ratio expressed as moles of HCN produced per mole of thiocyanate added was considerably decreased. A similar conversion was also observed when sulphuric acid (final concentration 5%) or acetate buffer (final concentration 0.6 M, pH 5.2) were used as an acidifying reagent. Without blood, thiocyanate did not produce HCN. At room temperature in HS equilibrium, phosphoric acid and sulphuric acid showed significant conversion, in contrast to acetate buffer, which did not show any conversion.

Comparison with microdiffusion–spectrophotometric method

Cyanide in blood has most frequently been determined spectrophotometrically after a microdiffusion procedure. Consequently, a comparison with such a method would be informative. Blood specimens from fire victims were split and analysed by the proposed HS-GC and microdiffusion–spectrophotometric methods. Figure 11 shows the good correlation between these two methods.

DISCUSSION

The GC separation of HCN was markedly improved by adopting a GS-Q capillary column instead of a Porapak QS packed column [19]. The GS-Q column is a polar gas–solid open-tubular megabore capillary column corresponding to Porapak Q, and is widely used for the determination of volatile polar substances. This capillary column showed high resolution, sensitivity and stability without any deterioration, which has been encountered in HS-GC using Porapak QS [19]. Interference with the HCN determination was not

observed, except for large amounts of acetaldehyde detected by FID.

The choices of the septum for sealing the HS vial and the injector syringe are important for obtaining reproducible analyses. A Tuf-Bond disc was selected as a sealing septum because the inert Teflon seal prevented adsorption of analytes and the silicone layer prevented gas leakage. For sampling and GC injection of HS gas, the usual gas-tight syringe or a pressure lock-type gas-tight syringe was unsuccessful because of low reproducibility. A Luer glass-tipped syringe fitted with a thin needle was adequate because of easy handling without any large hole made in the septa.

The HS-GC method appears to have advantages over other methods such as the microdiffusion–spectrophotometric method. It is simple without any complicated extraction procedure, and the overall analysis time is short, i.e., GC separation within 10 min and HS incubation for 30 min, permitting rapid processing of large numbers of samples. Column conditioning after fitting the column to the GC system takes a fairly short time (less than 1 h).

According to HS theory, in a sealed vessel, the following equation is valid:

$$C_L^0 V_L = C_L V_L + C_G V_G \quad (1)$$

where C_L^0 , C_L and C_G are the analyte concentrations in the liquid phase prior to and after HS equilibrium and that in the gaseous phase after equilibrium, respectively, and V_L and V_G are the volumes of the liquid and gaseous phases, respectively. The distribution coefficient (k) and phase ratio (β) are defined as C_L/C_G and V_G/V_L , respectively and Eqn. 1 becomes

$$C_G = C_L^0 / (k + \beta) \quad (2)$$

Accordingly, the sensitivity related to C_G is dependent on k , β and C_L^0 ; k is constant under conditions of dilute analyte concentrations, constant temperature and identical matrix. The results demonstrated that k was constant, irrespective of β (Fig. 3) and C_L^0 (Fig. 8).

The distribution coefficients of HCN and CH_3CN were obtained as 75.7 and 158.9, respectively, under HS conditions of an aqueous solution containing 10% phosphoric acid at 50°C. The

k values for HCN are reported to be 245 at 25°C in water [36] and 1/0.007 at room temperature [17]; these are compatible with the present data. The k values for HCN and CH₃CN are larger than those of benzene and toluene, and smaller than those of alcohols [30]. The large k value for HCN, giving a relatively low concentration in the gaseous phase, necessitates sensitive GC detection.

For HCN, there is no detailed report available on HS dynamics. The behaviour of HCN in HS equilibrium and the suitability of CH₃CN as an internal standard (I.S.) were studied. In HS analysis, addition of an excess of salt to the sample solution is used to provide reproducible matrix conditions and increase the sensitivity by increasing the concentration of the volatile analyte in the gaseous phase. HCN and CH₃CN did not show significant salting-out effects (Fig. 5) compared with the other volatile substances [30]. The present results demonstrate that HCN and CH₃CN show different behaviour in HS with respect to temperature (Fig. 3) and composition of the liquid phase such as NaCl (Fig. 5B), ovalbumin (Fig. 5C) and blood (Fig. 7). Therefore, the I.S. method using CH₃CN requires strict adjustment of the matrix composition. Because blood samples from fire victims do not often provide a reproducible matrix, it is difficult to prepare standards and samples in identical matrices. Moreover, a considerable amount of CH₃CN was detected in control blood, which may have resulted from contamination from the chemical laboratory or city air pollution. Taking these points into account, a direct calibration method was adopted instead of the I.S. method. The non-reproducibility of the matrix of unknown blood samples can be overcome by adopting HS conditions, where a high concentration of phosphoric acid shows sufficiently strong salting-out effect (Fig. 5A) and high concentrations of blood show a saturated suppressive effect on HCN vaporization (Fig. 7). The HS conditions of the liquid phase containing 10% phosphoric acid and 50% blood should yield relatively reproducible matrix conditions.

An important problem is the formation of cyanide from thiocyanate under acidic conditions

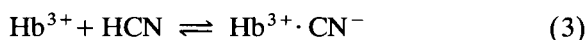
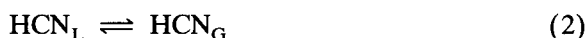
in the presence of erythrocytes [37,38], encountered through an extraction procedure in cyanide analysis. Sano et al. [23] succeeded in preventing this conversion by using an acetate buffer (pH 5.2) as an acidifying reagent. In this work (Fig. 10), a significant conversion (<3%) of thiocyanate to HCN was observed in the presence of both blood and acidifying reagents at 50°C. Therefore, in HS-GC analysis, artificial formation of cyanide is inevitable if large amounts of thiocyanate are present. It is reported that thiocyanate molar concentrations are about 100 and 30 times higher than cyanide molar concentrations for smoker and non-smoker blood, respectively [35], indicating that the blank cyanide level in control blood should reflect the artificial production from thiocyanate. In contrast, the ratio of thiocyanate to cyanide in the blood of fire victims is reported to be almost unity [6], offering no problem in forensic analysis. On the other hand, in cases of chronic cyanide intoxication, significant amounts of thiocyanate may accumulate in the blood through cyanide detoxication, offering a severe problem in clinical analysis. If desired, positive interference by thiocyanate could be avoided by adopting HS conditions where blood is incubated at room temperature in the presence of acetate buffer, or measuring cyanide by HS-GC in the adsorbed alkaline solution diffused from blood acidified with acetate buffer.

The cyanide level in blood shows larger variations. In cases of acute cyanide intoxication, 2–160 (average 29) [39], 0–35 (average 13.5 ± 12.6) [40] and 4–45 (average 22.4 ± 17.9) [41] $\mu\text{g ml}^{-1}$ have been reported and in cases of fire victims 0–6.19 (average 1.19 ± 0.81) [6], 1.47 ± 1.26 [7], 0–7.6 (average 1.33 ± 1.45) [9] and 0.17–2.2 (0.65 ± 0.36) [10] $\mu\text{g ml}^{-1}$. The lethal level of cyanide in blood can be assumed to be 3 $\mu\text{g ml}^{-1}$ [42] or 5 $\mu\text{g ml}^{-1}$ [43]. Therefore, the sensitivity of the proposed HS-GC method even using FID (0.2 $\mu\text{g ml}^{-1}$) is well below the lethal level, and this method is sufficiently sensitive for diagnostic application in cases of possible cyanide poisoning. For non-smokers, 0–294 (average 75 ± 62) [6], 0.1 [23], 39 ± 23 [35], 0–86 (average 32) [44] and 3.4 ± 2.1 [45] ng ml^{-1} have been reported, and for smokers 34–505 (180 ± 110) [6], 1.6 [23], $21 \pm$

26 [35], 0–94 (average 48) [44] and 8.6 ± 3.1 [45] ng ml^{-1} . These reported values seem to be controversial, which may be due to the different methodology used, especially for the cyanide extraction procedure, suffering from thiocyanate interference. The limit of determination of the proposed HS-GC method with NPD was at the ng ml^{-1} level. This sensitivity surpasses that of the microdiffusion–spectrophotometric method ($0.02 \mu\text{g ml}^{-1}$), and is equal to or more sensitive than fluorimetric (0.8 ng ml^{-1}) [23] and polarographic ($1 \mu\text{M}$) [24] methods.

The suitability of the proposed HS-GS method in comparison with the microdiffusion–spectrophotometric method, used mainly in Japanese forensic laboratories, were investigated (Fig. 11). A good correlation was observed between these methods for the determination of cyanide in blood samples from fire victims. Therefore, this HS-GC method should be applicable to practical analyses of forensic samples.

HCN is a volatile weak acid (b.p. = 25.7°C , $\text{p}K_a = 9.2$), and possesses three equilibria in blood: an acid–base equilibrium (Eqn. 1); vaporization equilibrium of protonated HCN (Eqn. 2); and association–dissociation equilibrium of HCN with methaemoglobin (met-Hb, Hb^{3+}), which is a non-physiological oxidized form of haemoglobin (Eqn. 3). This equilibrium markedly prefers the associated form ($K_d = 4.5 \times 10^{-6}$) [46].



It is important to consider the behaviour of cyanide in blood. Cyanide is absorbed in the bloodstream from the stomach in cases of oral ingestion of cyanide salts [1], from the lung and skin in cases of exposure to HCN gas [44] and from the decomposition process of cyanogenetic glycosides [3] and sodium nitroprusside [2]. Detoxication of cyanide is mediated mainly through an enzymatic transformation by mitochondrial rhodanase to excrete thiocyanate [47] and to a lesser extent through a reaction with cystine [48]. Most of the cyanide added to whole blood is trapped in erythrocytes [49], and met-Hb

is responsible for this cyanide-binding capacity in normal blood [45]. The haeme concentration in normal blood is assumed to be about 10 mM. If a blood met-Hb content of 1% is assumed, cyanide concentrations up to $100 \mu\text{M}$ ($2.6 \mu\text{g ml}^{-1}$) should exist in the stable bonded form. Katsumata et al. [50] reported that in cases of fire victims, significant amounts of met-Hb were produced. Our data for blood samples from fire victims (personal communication) were $10.5 \pm 9.6\%$ (0–41.7%). Therefore, cyanide at the lethal level should exist solely in a form binding met-Hb in the blood of fire victims.

In a post-mortem blood sample the alteration of blood cyanide level should be considered [24,51]. A rapid loss of detectable cyanide when added to blood was observed (Fig. 9), which is in accordance with other reports [52]. This loss is considered to be attributable to chemical reaction with serum albumin [45,49]. Therefore, precautions should be taken against rapid loss of cyanide in blood samples. In the preparation of standard solutions, an acidifying reagent should be added immediately after mixing of cyanide standard and control blood.

REFERENCES

- 1 D.A. Labianca, *J. Chem. Educ.*, 56 (1979) 788.
- 2 M. Bogusz, J. Moroz, J. Karski, J. Gierz, A. Regieli, R. Witkowska and A. Golabek, *Clin. Chem.*, 25 (1979) 60.
- 3 R.C. Clapp, F.H. Bissett, R.A. Coburn and L. Long, Jr., *Phytochemistry*, 5 (1966) 1323.
- 4 K.D. Brunemann, L. Yu and D. Hoffmann, *J. Anal. Toxicol.*, 1 (1977) 38.
- 5 W.D. Woolley, *Br. Polym. J.*, 4 (1972) 27.
- 6 R.A. Anderson and W.A. Harland, *Med. Sci. Law*, 22 (1982) 35.
- 7 M. Fukui, *Rep. Natl. Res. Inst. Police Sci. (in Japanese)*, 22 (1969) 35.
- 8 B.C. Levin, P.R. Rechani, J.L. Gurman, F. Landren, H.M. Clark, M.F. Yoklavich, J.R. Rodriguez, L. Droz, F. Mattos de Cabrera and S. Kaye, *J. Forensic Sci.*, 35 (1990) 151.
- 9 T. Shinohara, Y. Seto and N. Tsunoda, *Rep. Natl. Res. Inst. Police Sci. (in Japanese)*, 41 (1988) 168.
- 10 H.R. Wetherell, *J. Forensic Sci.*, 11 (1966) 167.
- 11 M. Yoshida, J. Adachi, T. Watabiki, Y. Tatsuno and N. Ishida, *Forensic Sci. Int.*, 52 (1991) 13.
- 12 G.E. Boxer and J.C. Richards, *Arch. Biochem.*, 30 (1951) 372.
- 13 T. Matsuoka and J. Okuda, *Eisei Kagaku*, 35 (1989) 420.

- 14 A.O. Gettler and L. Goldbaum, *Anal. Chem.*, 19 (1947) 270.
- 15 M. Feldstein and N.C. Klendskoj, *J. Lab. Clin. Med.*, 44 (1954) 166.
- 16 Y. Takekoshi, S. Kannno and S. Kawase, *Rep. Natl. Res. Inst. Police Sci.* (in Japanese), 41 (1988) 285.
- 17 R.W. Darr, T.L. Capson and F.D. Hileman, *Anal. Chem.*, 52 (1980) 1379.
- 18 C. Maseda, K. Matsubara and H. Shiono, *J. Chromatogr.*, 490 (1989) 319.
- 19 T. Shinohara and Y. Seto, *Rep. Natl. Res. Inst. Police Sci.* (in Japanese), 40 (1987) 154.
- 20 J. Zamecnik and J. Tam, *J. Anal. Toxicol.*, 11 (1987) 47.
- 21 J.A. Ryan and G.W. Culshaw, *Analyst*, 69 (1944) 370.
- 22 J. Epstein, *Anal. Chem.*, 19 (1947) 272.
- 23 A. Sano, M. Takezawa and S. Takitani, *Anal. Chim. Acta*, 225 (1989) 351.
- 24 J.O. Egekeze and F.W. Oehme, *J. Anal. Toxicol.*, 3 (1979) 119.
- 25 A.M. Bond, I.D. Heritage, G.G. Wallace and M.J. McCormick, *Anal. Chem.*, 54 (1982) 582.
- 26 M. Donike, *Z. Naturforsch., Teil B*, 28 (1973) 533.
- 27 M. Paabo, M.M. Birky and S.E. Womble, *J. Combust. Toxicol.*, 6 (1979) 99.
- 28 J.C. Valentour, V. Aggarwal and I. Sunshine, *Anal. Chem.*, 46 (1974) 924.
- 29 R.R. Claeys and H. Freund, *Environ. Sci. Technol.*, 2 (1968) 458.
- 30 B.V. Ioffe and A.G. Vitenberg (Eds.), *Head-Space Analysis and Related Methods in Gas Chromatography*, Wiley, New York, 1984.
- 31 J.D. Ramsey and R.J. Flanagan, *J. Chromatogr.*, 240 (1982) 423.
- 32 M. Kinoshita, *Jpn. J. Stud. Alcohol* (in Japanese), 9 (1974) 1.
- 33 R.N. Harger, in C.P. Stewart and A. Stolman (Eds.), *Toxicology*, Vol. II, Academic, New York, 1961, p. 85.
- 34 P.L. Patterson, *J. Chromatogr.*, 167 (1978) 381.
- 35 A.R. Pettigrew and G.S. Fell, *Clin. Chem.*, 19 (1973) 466.
- 36 W.A. Robbie, *J. Cell Comp. Physiol.*, 27 (1946) 181.
- 37 J. Chung and J.L. Wood, *J. Biol. Chem.*, 246 (1971) 555.
- 38 C.J. Vesey and J. Wilson, *J. Pharm. Pharmacol.*, 30 (1978) 20.
- 39 R. Bonnichson and A.C. Maehly, *J. Forensic Sci.*, 11 (1966) 516.
- 40 A.S. Curry, *Acta Pharmacol. Toxicol.*, 20 (1963) 291.
- 41 C.L. Winek, E. Fusia, W.D. Collon and S.P. Shanor, *Forensic Sci.*, 11 (1978) 51.
- 42 H.L. Kaplan, A.F. Grand and G.E. Hartzell, *Fire Saf. J.*, 7 (1984) 11.
- 43 A.H. Stead and A.C. Moffat, *Hum. Toxicol.*, 3 (1983) 437.
- 44 H. Chandra, B.N. Gupta, S.K. Bhargava, S.H. Clerk and P.N. Mahendra, *J. Anal. Toxicol.*, 4 (1980) 161.
- 45 P. Lundquist, H. Rosling and B. Sörbo, *Clin. Chem.*, 31 (1985) 591.
- 46 B. Chance, *J. Biol. Chem.*, 194 (1952) 483.
- 47 W.A. Himwich and J.P. Saunders, *Am. J. Physiol.*, 153 (1948) 348.
- 48 J.L. Wood and S.L. Cooley, *J. Biol. Chem.*, 218 (1956) 449.
- 49 D.E. McMillan and A.C. Svobosa, IV, *J. Pharmacol. Exp. Ther.*, 221 (1982) 37.
- 50 Y. Katsumata, M. Aoki, M. Oya, O. Suzuki and S. Yada, *J. Forensic Sci.*, 25 (1980) 546.
- 51 B. Ballantyne, *J. Forensic Sci. Soc.*, 16 (1976) 305.
- 52 B. Ballantyne, J. Bright and P. Williams, *J. Forensic Sci. Soc.*, 13 (1973) 111.

Determination of oxidizable inorganic anions by reversed-phase ion-pair chromatography with amperometric detection

Jinrui Xu and Meihua Xin

Department of Applied Chemistry, Huaqiao University, Quanzhou, Fujian (China)

Toyohide Takeuchi and Tomoo Miwa

Faculty of Engineering, Gifu University, 1-1 Yanagido, Gifu 501-11 (Japan)

(Received 10th October 1992; revised manuscript received 26th November 1992)

Abstract

Operating conditions for the determination of oxidizable inorganic anions by reversed-phase ion-pair chromatography with amperometric detection were optimized. Tetrabutylammonium hydroxide was selected as the ion-pairing agent, which was modified *in situ* on the reversed-phase stationary phase. The present system can be used to determine nitrite, thiosulphate, iodide, sulphide and thiocyanate ions, and was applied to the determination of inorganic anions in lake water.

Keywords: Amperometry; Ion chromatography; Inorganic anions; Waters

Ion exchange has been employed for the determination of inorganic anions [1–3]. Reversed-phase ion-pair chromatography (RP-IPC) has been demonstrated to be another option for the determination of inorganic anions [4–13], in which tetraalkylammonium bromide (or hydroxide) and alkylamines have been utilized as ion-pairing agents. The ion-pairing agent is modified *in situ* on the stationary phase, acting as ion-exchange sites.

In RP-IPC, direct [4,6,8,9,11,12] and indirect photometric detection methods [8,9,11,13] have been most widely used for the determination of inorganic anions. Conductimetric detection has been also used in RP-IPC [5,7,8,10] from the time ion chromatography was initiated by Small et al.

Correspondence to: T. Takeuchi, Faculty of Engineering, Gifu University, 1-1 Yanagido, Gifu 501-11 (Japan).

[1]. However, these detection methods are not selective. There have been a few papers dealing with amperometric detection for the selective and sensitive determination of inorganic anions in RP-IPC [10,14]. Oxidizable inorganic anions have been selectively determined by RP-IPC with amperometric detection and the detection limits achieved were compared with those achieved with other detection methods [10]. Postcolumn reaction with fluorimetric detection has also been employed for the selective determination of oxidizable inorganic anions [15].

This paper describes the determination of inorganic anions by RP-IPC with amperometric detection, where the ion-pairing agent is modified *in situ* on the reversed-phase stationary phase. The operating conditions were optimized for the determination of oxidizable inorganic anions such as nitrite, thiosulphate, iodate, sulphide and thio-

cyanate. The type and concentration of the ion-pairing agents and organic modifiers and the pH of the eluent were examined. The oxidizable anions mentioned above could be separated within 10 min under the optimized condition.

EXPERIMENTAL

Apparatus

A liquid chromatographic system was assembled in the laboratory from an LC-6A pump (Shimadzu, Kyoto), a Model 7125 loop injector with an injection volume of 20 μl (Rheodyne, Cotati, CA), a 150 \times 6 mm i.d. Shim-Pack CLC-C₈ (5 μm) separation column (Shimadzu), an L-ECD-6A amperometric detector (Shimadzu) with a glassy carbon indicator electrode and a silver/silver chloride (Ag/AgCl) reference electrode and a Chromatopac C-R3A data processor (Shimadzu).

Separations were carried out at room temperature ($22 \pm 2^\circ\text{C}$). The flow-rate of the eluent was 1.0 ml min^{-1} .

Reagents

The reagents used were of analytical-reagent grade, unless noted otherwise, and were used as received. Stock standard solutions of the analytes, each at a concentration of 1 mg ml^{-1} , were prepared from sodium nitrite, sodium thiosulphate pentahydrate, potassium iodide, sodium sulphide enneahydrate and sodium thiocyanate. Working standard solutions of the analytes were prepared from the stock solutions before use. Doubly distilled water was employed throughout. Eluents were filtered with 0.45- μm membrane filters and degassed in vacuo.

RESULTS AND DISCUSSION

Optimization of applied potential

The dependence of the signal intensities of the analytes on the applied voltage was examined, using a 15 + 85 mixture of methanol and 60 mM phosphate buffer solution (pH 5.5) containing 3.0 mM tetrabutylammonium hydroxide (TBAH) and

0.1 mM disodium ethylenediaminetetraacetate (EDTA) as the eluent at a flow-rate of 1.0 ml min^{-1} . It was found that the peak heights increased with increasing applied potential, and the background signal was not significant at applied potentials more negative than +1.0 V vs. Ag/AgCl. As the most favourable signal-to-noise ratio (S/N) was generally obtained at +1.0 V, the applied potential was kept at this value in subsequent experiments.

Effect of ion-pairing agent

Tetraethylammonium bromide, tetrabutylammonium bromide, TBAH and hexadecyltrimethylammonium bromide were examined as ion-pairing agents. A 10 + 90 mixture of methanol and 60 mM phosphate buffer solution (pH 5.5) containing 0.1 mM EDTA and each ion-pairing agent was employed as the eluent. TBAH was selected in the following experiment because it was superior to the other reagents in terms of background interference, resolution of the analytes, retention time and regeneration of the separation column.

Figure 1 illustrates the relationships between the capacity factors (k') of the analyte ions and the concentration of TBAH. It is seen that the capacity factors of iodide and thiocyanate increase with increasing concentration and tend to reach plateaux at higher concentrations. This result can be explained by the following two competing phenomena as discussed in the literature

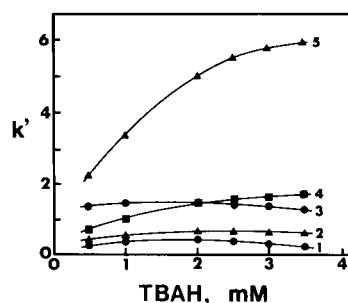


Fig. 1. Effect of concentration of TBAH. Column, 150 \times 6 mm i.d., packed with 5- μm Shim-Pack CLC-C₈; eluent, 10 + 90 mixture of methanol and 60 mM phosphate buffer solution (pH 5.5) containing 0.1 mM EDTA; flow-rate, 1.0 ml min^{-1} ; injection volume, 20 μl . Analytes: 1 = nitrite; 2 = thiosulphate; 3 = sulphide; 4 = iodide; 5 = thiocyanate.

[7]. The analyte ions are retained by TBAH adsorbed on the stationary phase in the ion-exchange mechanism. This means that the anion-exchange capacity of the stationary phase increases with increasing concentration of TBAH in the eluent. On the other hand, as hydroxide ion competes with analyte ions for the ion-exchange sites of TBAH on the stationary phase, the increase in the hydroxide ion concentration in the eluent increases the driving force for analyte ions. On the other hand, the capacity factors of nitrite, thiosulphate and sulphide are almost independent of the concentration of TBAH. Unfortunately, the reason is unknown.

Considering the resolution and analysis time, 3.0 mM TBAH was selected in subsequent experiments.

Effect of organic modifier

The effect of the methanol concentration on the capacity factor of the analyte ions is shown in Fig. 2. It is seen that the capacity factor decreases with increasing methanol concentration. This is because the amount of TBAH adsorbed on the stationary phase decreases with increasing methanol concentration. Considering the resolu-

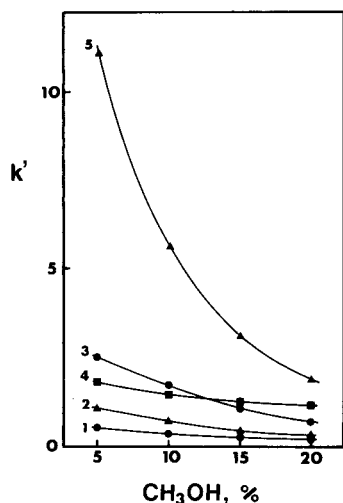


Fig. 2. Effect of methanol concentration on the capacity factor. Eluent, mixture of methanol and 60 mM phosphate buffer solution (pH 5.5) containing 3.0 mM TBAH and 0.1 mM EDTA. Other operating conditions as in Fig. 1.

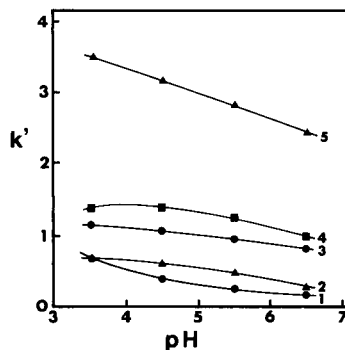


Fig. 3. Effect of pH of the eluent on the capacity factor. Eluent, 15+85 mixture of methanol and 60 mM phosphate buffer containing 3.0 mM TBAH and 0.1 mM EDTA. Other operating conditions as in Fig. 1.

tion and analysis time, 15% methanol was selected in subsequent experiments.

Effect of pH

Dissociation constants and hydrophobicity of both analytes and TBAH are affected by the pH of the eluent. In this work the pH was adjusted with 60 mM phosphate solution. Figure 3 shows the relationships between the capacity factor and the pH of the eluent. The capacity factor decreases with increasing pH. As an eluent of pH 4.5–6.5 achieved good separations, pH 5.5 was chosen in subsequent experiments.

Under the optimum conditions, nitrite, thiosulphate, iodide, sulphide and thiocyanate ions can be separated within 10 min, as demonstrated in Fig. 4, in which 6 ng of nitrite, 0.4 μg of thiosulphate, 8 ng of iodide, 4 ng of sulphide and 0.4 μg of thiocyanate were injected.

Analytical figures of merit

Calibration graphs were prepared under the conditions given in Fig. 4. The peak heights were linear up to at least 3.0, 3.5, 5.0, 50 and 60 $\mu\text{g ml}^{-1}$ for nitrite, sulphide, iodide, thiosulphate and thiocyanate, respectively, and the detection limits at $S/N = 3$ were 0.8, 1.1, 3.6, 99 and 104 ng ml^{-1} , respectively. These detection limits were better than those reported previously [10] except for thiosulphate. The relative standard deviations for ten successive determinations of 0.4 $\mu\text{g ml}^{-1}$

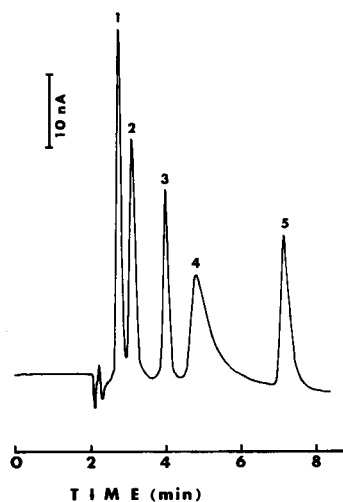


Fig. 4. Separation of oxidizable inorganic anions. Eluent, 15+85 mixture of methanol and 60 mM phosphate buffer solution (pH 5.5) containing 3.0 mM TBAH and 0.1 mM EDTA. Concentrations of analytes: $0.3 \mu\text{g ml}^{-1}$ nitrite; $20 \mu\text{g ml}^{-1}$ thiosulphate; $0.4 \mu\text{l ml}^{-1}$ iodide, $0.2 \mu\text{g ml}^{-1}$ sulphide and $20 \mu\text{g ml}^{-1}$ thiocyanate. Other operating conditions as in Fig. 1.

nitrite, sulphide and iodide were 2.4, 1.4 and 1.6%, respectively, and those for $40 \mu\text{g ml}^{-1}$ thiosulphate and thiocyanate were 2.7 and 3.7%, respectively.

Interfering anions

Interfering anions were examined for $0.4 \mu\text{g ml}^{-1}$ nitrite, sulphide and iodide and for $40 \mu\text{g ml}^{-1}$ thiosulphate and thiocyanate. The presence of a 1000-fold excess concentration of sulphate, silicate, carbonate, phosphate, bromate, nitrate, molybdate and chloride did not interfere with the analyte ions. Oxalate and bromide did not interfere up to a 500-fold excess and sulphite up to a 100-fold excess.

Determination of anions

The present system was applied to the determination of oxidizable inorganic anions in lake water, with operating conditions as in Fig. 4. The sample water was filtered with a $0.45\text{-}\mu\text{m}$ membrane filter before injection. The concentrations determined were 0.23 , 0.08 and $0.024 \mu\text{g ml}^{-1}$ (average values for three successive measurements) with recoveries of 98, 100 and 103% for nitrite, thiosulphate and sulphide, respectively. The concentrations of iodide and thiocyanate were lower than the detection limits.

REFERENCES

- 1 H. Small, T.S. Stevens and W.C. Bauman, *Anal. Chem.*, 47 (1975) 1801.
- 2 D.T. Gjerde, J.S. Fritz and G. Schmuckler, *J. Chromatogr.*, 186 (1979) 509.
- 3 R.J. Williams, *Anal. Chem.*, 55 (1983) 851.
- 4 R.N. Reeve, *J. Chromatogr.*, 177 (1979) 393.
- 5 I. Molnár, H. Knauer and D. Wilk, *J. Chromatogr.*, 201 (1980) 225.
- 6 N.E. Skelly, *Anal. Chem.*, 54 (1982) 712.
- 7 Z. Iskandarani and D.J. Pietrzyk, *Anal. Chem.*, 54 (1982) 1065.
- 8 B.B. Wheals, *J. Chromatogr.*, 262 (1983) 61.
- 9 A. Mangia and M.T. Lugari, *Anal. Chim. Acta*, 159 (1984) 349.
- 10 M. Wu, V. Pacáková, K. Štulík and G.A. Sacchetto, *J. Chromatogr.*, 439 (1988) 363.
- 11 M.C. Gennaro and P.L. Bertolo, *J. Chromatogr.*, 472 (1989) 433.
- 12 R. Steudel, G. Holdt and T. Göbel, *J. Chromatogr.*, 475 (1989) 442.
- 13 B.A. Bidlingmeyer, C.T. Santasania and F.V. Warren, Jr., *Anal. Chem.*, 59 (1987) 1843.
- 14 M. Lookabaugh and S. Krull, *J. Chromatogr.*, 452 (1988) 295.
- 15 S. Tanabe, M. Kitahara, M. Nawata and K. Kawanabe, *J. Chromatogr.*, 424 (1988) 29.

Preparation and analytical properties of a chelating resin loaded with thionalide

Jadwiga Chwastowska, Wanda Żmijewska and Elżbieta Sterlińska

Department of Analytical Chemistry, Institute of Nuclear Chemistry and Technology, ul. Dorodna 16, 03-195 Warsaw (Poland)

(Received 17th August 1992; revised manuscript received 30th October 1992)

Abstract

A sorbent was obtained by immobilization of thionalide (2-mercapto-*N*-2-naphthylacetamide) on the macroporous resin Bio-Beads SM-7 (acrylic ester polymer). Its properties (amount of the chelating agent deposited per gram of the resin, the mechanism of attaching the reagent to the resin, stability, retention capacity and sorption kinetics) were determined. The retention of 21 elements from HCl solutions, over a wide acidity range, was studied. Possible applications of the sorbent to the separation of a group of elements and individual elements are discussed.

Keywords: Sample preparation; Chelating resins; Preconcentration; Thionalide

Separation and preconcentration techniques are of great importance owing to the limited sensitivity and selectivity of modern instrumental methods of trace analysis. Recently, sorbents obtained by immobilization of chelating agents on solid supports have gained much attention. High preconcentration factors obtained with the aid of those sorbents make them very useful in the analysis of environmental samples, particularly natural waters.

This work was devoted to the preparation and examination of the analytical properties of a sorbent obtained by immobilization of thionalide (2-mercapto-*N*-2-naphthylacetamide) on the synthetic macroporous resin Bio-Beads SM-7 (acrylic ester polymer).

Thionalide reacts with a number of elements that precipitate with sulphide [1]. The reagent has been used in gravimetric analysis and in trace analysis for the separation and preconcentration

of trace elements by extraction [2–4] and coprecipitation [5,6]. As thionalide reacts with some elements in particular oxidation states, e.g., with As(III), Sb(III) and Tl(I) but not with As(V), Sb(V) and Tl(III), there is a possibility of applying this reagent to speciation analysis.

Terada and co-workers [7,8] first prepared a sorbent by immobilization of thionalide on silica gel and applied it to the preconcentration of palladium(II) [7] and arsenic(III) [8] from sea water, of antimony(III) from river and sea water [9] and of bismuth(III) from river water [10]. A sorbent with thionalide loaded on glass beads with the aid of collodion was prepared by the same group [11] and used for the preconcentration of antimony(III) from sea water.

So far no detailed studies on the sorbents obtained by immobilization of thionalide on solid supports have been carried out. In addition, the method of preparation of the hitherto obtained sorbents is tedious and time consuming and their retention capacity is low.

Recently, macroporous synthetic resins (polystyrene–divinylbenzene copolymers, acrylic ester

Correspondence to: J. Chwastowska, Department of Analytical Chemistry, Institute of Nuclear Chemistry and Technology, ul. Dorodna 16, 03-195 Warsaw (Poland).

polymers), e.g., Amberlite XAD resins, have been widely used as supports for chelating sorbents owing to their good physical properties (uniform pore size, high surface area) and high chemical resistance. In contrast to sorbents with chelating agents immobilized on silica gel, they can be readily prepared. This encouraged us to prepare a sorbent with thionalide immobilized on a macroporous resin. As information on previously obtained sorbents with thionalide was fragmentary it seemed useful also to carry out more comprehensive studies of the sorbent.

EXPERIMENTAL

Reagents and apparatus

Thionalide (puriss p.a.) was obtained from Fluka. Bio-Beads SM-7 resin (20–50 mesh) was purchased from Bio-Rad. All other reagents were of analytical-reagent grade. Doubly distilled water was used throughout.

Quantification of the elements studied was carried out with the aid of radioactive tracers (^{110m}Ag , ^{76}As , ^{198}Au , ^{115}Cd , ^{64}Cu , ^{197}Hg , ^{42}K , ^{24}Na , ^{109}Pd , ^{197}Pt and ^{122}Sb) or by atomic absorption spectrometry (AAS) (Ca, Bi, Fe, Mg, Mn, Ni, Pb, Tl).

A Swan (IPJ, Warsaw) gamma-ray spectrometer with an Ortec HP germanium detector (resolution 1.8 keV for 1332 keV, efficiency 40%) was used for activity measurements. A Pye Unicam SP-9 atomic absorption spectrometer was used for the determination of the above-mentioned elements. A Shimadzu UV-160 spectrophotometer was used for the determination of thionalide. IR studies were carried out using a Perkin-Elmer Model 577 spectrophotometer. pH measurements were carried out with the aid a Model 26 pH meter (Radiometer).

Preparation of thionalide-loaded Bio-Beads SM-7 (T-BB)

Bio-Beads SM-7 resin (20–50 mesh) was washed with several portions of ethanol and allowed to dry. About 3 g of the resin were placed in a 100-ml separating funnel and shaken with 50 ml of 0.05 M thionalide solution in ethanol. The

solution was then filtered off under reduced pressure. The sorbent was allowed to dry in air for 12 h and stored in a refrigerator.

Examination of properties of T-BB

The amount of thionalide loaded on the sorbent was determined spectrophotometrically at 331 nm, after removal from the sorbent with ethanol. The stability of the sorbent was determined by measuring the amount of thionalide on the sorbent after definite time intervals after its preparation. IR spectra of T-BB and of thionalide and Bio-Beads SM-7 were measured in the range 800–3500 cm^{-1} . The samples were ground, mixed with KBr and pelletized.

The retention capacity of T-BB was determined for Sb(III) and Pd(II) by the batch method. Sb(III) was retained from 1.0 and 0.1 M HCl solutions and Pd(II) from 1 M HCl and a solution of pH 3.

Retention of elements on T-BB

Procedure for batch experiments. A solution of the elements studied containing 1–20 μg of each element was adjusted to a suitable acidity or pH (HCl, NaOH) and transferred into a 50-ml separating funnel. The final volume of the solution was 20 ml. Then 0.1 g of the sorbent was added and the contents of the separating funnel were shaken for 30 min on a mechanical shaker. The solution was filtered off and the sorbent was washed twice with 2-ml portions of a solution of the same pH. The washings were combined with the filtrate. The amount of element retained on the sorbent was determined from the difference in the amounts in the solution before sorption and in the filtrate.

Procedure for column experiments. A glass column (0.4 mm i.d.) was filled with 0.1 g of the sorbent and conditioned with a solution of suitable acidity or pH. A sample containing 1–10 μg of the element studied in 20 ml of HCl, adjusted to a suitable acidity or pH, was passed through the column at 0.7–1.0 ml min^{-1} . The column was washed with 10 ml of a solution of the same acidity or pH. The washings were combined with the effluent. The element retained on the column was then eluted with a suitable eluent.

Effect of shaking time

The effect of shaking time was studied for As(III), Co(II), Cd(II), Pd(II) and Sb(III). Sorption of each of the elements was carried from a solution of an acidity or pH corresponding to the maximum retention of the element in question. The shaking time was varied from 1 min to 1 h. After a definite shaking time a portion of the solution was taken and the concentration of the element was measured, after which the solution was combined with the sorbent and shaking was continued.

RESULTS AND DISCUSSION

Characteristics of the sorbent

The amount of thionalide loaded on Bio-Beads SM-7 varied in the range 41–49 mg g⁻¹. The average value for seven preparations was 44 mg g⁻¹ (203 μmol g⁻¹).

The amount of thionalide loaded on Bio-Beads did not change for 32 days. After 52 days it had decreased to 88% of the initial value. After 90 days a significant decrease to 16% of the initial value was observed, but the retention of 15 μg of Sb(III) (from 1 M HCl) on the sorbent stored for 90 days was still quantitative. It can be concluded that T-BB (stored in darkness at 4°C) can be used for at least 2 months.

The IR spectra of T-BB, thionalide and the resin (Bio-Beads SM-7) are shown in Fig. 1. It can be seen that the bands in the range 3400–3000 cm⁻¹ characteristic of the NH group of thionalide (clearly visible in the spectrum of thion-

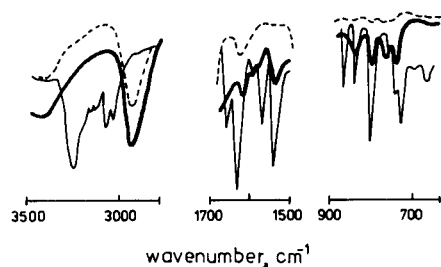


Fig. 1. IR spectra of (thin solid lines) thionalide, (dashed lines) Bio-Beads SM-7 resin and (thick solid lines) T-BB.

alide) disappear in the spectrum of T-BB. On the other hand, the bands characteristic of the chelating groups of thionalide (CO and SH in the ranges 1700–1500 and 850–800 cm⁻¹, respectively) are still present in the spectrum of the sorbent. On the basis of the IR spectra it can be concluded that thionalide molecules are attached to the support (Bio-Beads SM-7) through the nitrogen of the NH group.

The average retention capacity of T-BB for Sb(III) from 1.0 and 0.1 M HCl solution was the same, 8.85 mg (72.3 μmol) Sb(III) g⁻¹ for a sorbent containing 47.6 mg (219 μmol) thionalide g⁻¹. The retention capacity for Pd(II) from 1 M HCl was 10.5 mg (98 μmol) Pd(II) g⁻¹ for T-BB containing 42 mg (193 μmol) thionalide g⁻¹.

The values obtained for the retention capacity of T-BB are roughly by an order of magnitude higher than those reported in the literature for thionalide-loaded silica gel {4.6 μmol g⁻¹ for Sb(III) [9], 2.1 μmol g⁻¹ for Bi(III) [10] and 7.5 μmol g⁻¹ for Pd(II) [7]}.

The mole ratios of thionalide to the metal (in the sorbent) calculated on the basis of the above data were 3.03 and 1.97 for Sb(III) and Pd(II), respectively, and are very close to the theoretical values. This may indicate that all the chelating groups are accessible to the metal ions. For comparison, the mole ratio of thionalide to Pd(II) for thionalide-loaded silica gel was 3.2 [7]. It follows that the Bio-Beads SM-7 macroporous resin is more suitable than silica gel for immobilization of thionalide.

Retention of elements

The retention of elements on T-BB from HCl solutions as a function of the acidity or pH was determined by the batch method. The shaking time was 30 min. The results obtained are shown in Fig. 2.

It can be seen that some elements, e.g. Pd, Hg and Sb(III), are retained on the sorbent over a wide acidity range. Others show narrow maxima (Pb, Co, Ni). As would be expected, some elements are retained from nearly neutral (Cd, Zn, Co) or alkaline (Tl) media.

In the most suitable acidity (pH) ranges, the retention reaches 100% or nearly 100% for most

TABLE 1

Sorption of elements on T-BB and desorption under dynamic conditions ^a

| Element | Sorption | | Desorption | | |
|---------|----------|-----|--------------------------------|-------------|-----|
| | pH | % | Eluent | Volume (ml) | % |
| Ag(I) | 3 | 99 | 2 M HCl | 15 | 98 |
| Au(III) | 3 | 78 | 0.4 M thiourea in 0.1 M HCl | 25 | 97 |
| Cd(II) | 6.5 | 98 | 0.01 M HCl | 15 | 100 |
| Co(II) | 7.5 | 27 | 10 M HCl | 15 | 55 |
| Cu(II) | 3 | 100 | 1 M HCl | 15 | 98 |
| Hg(II) | 3 | 91 | 10 M HCl | 10 | 99 |
| Hg(II) | 1 | 100 | | | |
| Pd(II) | 3 | 99 | 0.4 M thiourea in 0.1 M HCl | 25 | 98 |
| Pt(IV) | 3 | 32 | 0.4 M thiourea in 0.1 M HCl | 25 | 97 |
| Sb(III) | 5 | 88 | 10 M HCl | 15 | 100 |
| Sb(III) | 0 | 100 | 10 M HCl | 15 | 100 |
| Zn(II) | 7 | 84 | 1 M HCl | 15 | 100 |

^a Column i.d., 0.4 cm; bed, 0.1 g of T-BB; flow-rate, 0.7–1.0 ml min⁻¹.

elements: Co and Zn show lower retentions (90 and 85%, respectively); the retention for Mn(II) and Tl(I) is low (40 and 50%, respectively). Arsenic(III) shows two maxima, in strongly acidic medium above 2 M (retention 100%) and in the pH range 7–9 (retention 60–70%). The retention of Bi increases sharply starting from 2 M HCl and reaches 100% at pH 1. It was not possible to study the retention of Bi at pH > 1.5 owing to hydrolysis. A similar situation occurred with Fe at pH > 4.

The data obtained for Na, K, Ca and Mg are not shown in Fig. 2. Na and K are not retained

from solutions of pH > 1, and are partly retained from solutions of higher acidities (8% at 1 M HCl). Ca and Mg are not retained over the whole acidity range examined.

The retention of some elements was also studied under dynamic conditions. Sorption of individual elements was carried out at the most suitable acidity (or pH) selected on the basis of the curves shown in Fig. 2. The results are given in the Table 1. It follows that under dynamic conditions some species [Au(III), Co(II), Pt(IV)] show lower retentions than under static conditions. For Co this phenomenon is presumably due to poor

TABLE 2

The effect of shaking time on the retention of some elements on T-BB

| Shaking time (min) | Retention (%) | | | | | | | |
|--------------------|------------------|----|----------------|----------------|--------|---------|---------|--|
| | As(III), 1 M HCl | | Cd(II), pH 6.5 | Co(II), pH 7.5 | Pd(II) | | Sb(III) | |
| | | | | 1 M HCl | pH 3 | 1 M HCl | pH 5 | |
| 1 | – | 57 | – | – | – | – | – | |
| 3 | 41 | – | – | 90 | 86 | 98 | – | |
| 5 | – | 97 | 15 | – | 91 | 99 | 83 | |
| 10 | 70 | 98 | 32 | 95 | 95 | 100 | – | |
| 20 | 90 | – | 50 | 95 | 96 | 100 | 93 | |
| 30 | 95 | 99 | 72 | 97 | 97 | 100 | 93 | |
| 60 | – | – | 87 | – | – | – | 93 | |

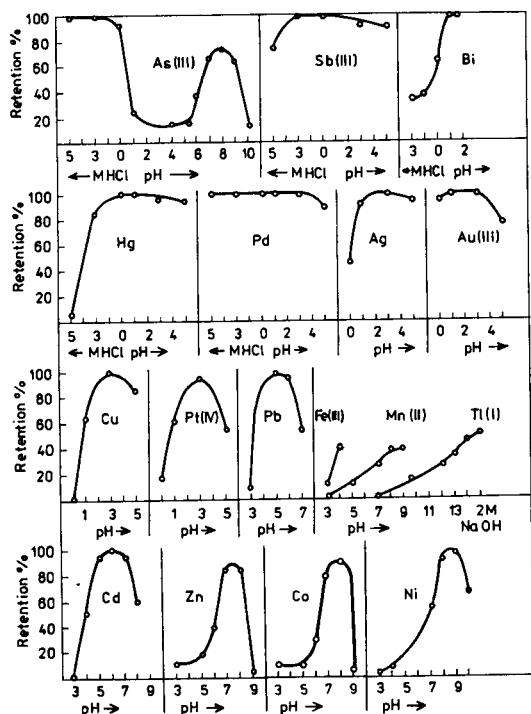


Fig. 2. Retention of elements from HCl solutions of various acidity (or pH).

reaction kinetics (see the data for Co in Table 2). Au and Pt form complexes with thionalide only when present in lower oxidation states. Therefore, if present in higher oxidation states the complexation reaction must be preceded by reduction (thionalide itself is also a reducing agent), which may not be sufficiently fast under the applied conditions.

Results of desorption studies are presented in Table 1. Most of the elements studied can be completely removed from the sorbent with the aid of HCl solutions of suitable concentration. Pd, Pt and Au cannot be removed from the column even with concentrated HCl. Therefore, a complexing agent (thiourea) was used. Even so, the volumes of the eluent necessary for complete elution of those elements are large and better eluents may be found.

The effect of shaking time on the retention of elements on T-BB is shown in Table 2. The data indicate that the time of attaining equilibrium varies with the nature of the element. For Sb(III)

(1 M HCl), Cd and Pd equilibrium is attained in few minutes, whereas for As and Co longer periods are necessary. Co does not attain equilibrium even after 60 min (typical inertia of cobalt species). For the elements that react over a wide acidity range (see Sb and Pd) the reaction rate is higher at higher acidity.

Conclusions

In contrast to the previously reported sorbents with thionalide, the sorbent described here, thionalide immobilized on Bio-Beads SM-7, can be easily prepared. The sorbent (stored in darkness at 4°C) exhibits high stability and can be used for at least 2 months.

The sorbent offers the possibility of preconcentration and separation of various elements. As(III), Sb(III) and Pd(II) can be separated from strongly acidic medium (above 1 M HCl). Ag, Au, Cu, Hg, Pd, Pt and Sb(III) can be separated from solutions of pH 2–3. Pb and Cd can be separated from neutral or slightly acidic media and Zn, Co and Ni from neutral or slightly alkaline media. Separation of individual elements can be achieved by eluting them from the sorbent with the aid of suitable eluting agents.

Alkali and alkaline earth metals are not retained on the sorbent over a wide acidity range, which is of advantage from the viewpoint of possible applications of the sorbent to the analysis of natural waters and biological materials.

The possibility of application of the sorbent to speciation analysis is under investigation.

Thanks are due to Dr. W. Skwara and Mr. J. Dudek for carrying out AAS measurements.

REFERENCES

- 1 Z. Holzbecker, L. Davis, H. Kral, L. Suchra and F. Vlacil, Handbook of Organic Reagents in Inorganic Analysis, Horwood, Chichester, 1976.
- 2 W. Żmijewska, Chem. Anal. (Warsaw), 21 (1976) 853.
- 3 Y. Kanda, Anal. Chem., 52 (1980) 1672.
- 4 N. Suzuki, J. Radioanal. Nucl. Chem., Articles, 124 (1988) 197.
- 5 W. Żmijewska, H. Polkowska-Mortenko and H. Stokowska, J. Radioanal. Nucl. Chem., Articles, 116 (1987) 243.

- 6 J.E. Portman and J.P. Riley, *Anal. Chim. Acta*, 31 (1964) 509.
- 7 K. Terada, K. Matsumoto and Y. Taniguchi, *Anal. Chim. Acta*, 147 (1983) 411.
- 8 K. Terada, K. Matsumoto and T. Inaba, *Anal. Chim. Acta*, 158 (1984) 207.
- 9 H. Fukuda, J. Tsunoda, K. Matsumoto and K. Terada, *Bunseki Kagaku*, 36 (1987) 11; *Chem. Abstr.*, 108 (1988) 26739w.
- 10 A. Haruta, K. Matsumoto and K. Terada, *Anal. Sci.*, 5 (1989) 319.
- 11 M. Matusi, K. Matsumoto and K. Terada, *Anal. Chim. Acta*, 193 (1987) 381.

Flow-injection spectrophotometric enzymatic and non-enzymatic methods for the determination of direct and total bilirubin in serum

J.M. Fernández-Romero, M.D. Luque de Castro and M. Valcárcel

Department of Analytical Chemistry, Faculty of Sciences, University of Córdoba, E-14004 Córdoba (Spain)

(Received 16th June 1992)

Abstract

Two automatic spectrophotometric methods based on the use of flow-injection analysis are proposed for the determination of total and direct (conjugated) bilirubin in serum. The first method is based on the oxidation of bilirubin catalysed by bilirubin oxidase and it uses an adaptation of reagent injection and stopped flow modes for the sequential determination of total and direct bilirubin. The second method is based on the Erlich diazotation reaction and calls for the simultaneous determination of both bilirubin forms. The enzymatic method affords linear determination ranges between 0.09 and 25.0 and between 0.14 and 13.0 μM for total and direct bilirubin, respectively. The non-enzymatic method allows the determination of total and direct bilirubin with the linear ranges 0.85–144.0 and 3.80–125.0 μM , respectively. The relative standard deviation was 3% in all instances.

Keywords: Enzymatic methods; Flow injection; UV–Visible spectrophotometry; Bilirubin; Serum

Bilirubin is a tetrapyrrolic pigment that is produced by enzymatic catabolism of haemoglobin in the reticulo-endothelial cells of liver, marrow bone and spleen. In the blood stream, it exists either as a free (unconjugated) water-soluble form, or as a conjugated, water-soluble form. Unconjugated bilirubin is transported in plasma by binding to protein, principally albumin, after which it is converted in the liver into conjugated bilirubin by conjugation with glucuronic acid. Conjugation is a prerequisite for transport to the bile and subsequent excretion in the urine and faeces [1].

The determination of bilirubin in serum is of clinical significance for the diagnosis and treatment of different organic failures, mainly to the neonatal kernicterus, biliary obstructions, liver

necrotic and haematological disfunction. Because the most important variation between direct (conjugated) and indirect forms of bilirubin can occur in obstructive hepato-biliary disease, the simultaneous determination of both forms is crucial in the diagnosis of these pathologies [2].

Since 1913, when Van den Bergh and Snapper [3] proposed the first method for the determination of bilirubin in human serum, a number of methods have been described, mainly spectrophotometric techniques with direct determination [4] or by measurement of the reaction product formed in the Erlich diazotation reaction [5,6]. Later, an interesting approach was developed with an enzymatic method [7–9] after commercialization of bilirubin oxidase (BOX, bilirubin: oxygen oxidoreductase, EC 1.3.3.5) from *Myrothecium verrucaria* [10,11]. Several methodologies have also been described for bilirubin determination with electrochemical detection (amperometric [12] and voltammetric [13]). A number of chromato-

Correspondence to: M.D. Luque de Castro, Department of Analytical Chemistry, Faculty of Sciences, University of Córdoba, E-14004 Córdoba (Spain).

graphic methods have also been developed to determine bilirubin and its conjugates [14–17].

In the last decade there have been important advances in the automation of bilirubin determination in clinical chemistry (e.g. with the introduction of dry reagents [18] and centrifugal [19] and batch [20,21] analysers). However, no flow-injection (FI) methods for the determination of bilirubin have been proposed [22–24].

Two FI approaches for the determination of total and direct bilirubin in human serum are proposed in this paper. The first method is based on an FI system for the sequential determination of total and direct bilirubin by using a reagent injection and stopped flow arrangement. The biochemical basis of the method is the oxidation of the analyte catalysed by bilirubin oxidase and spectrophotometric monitoring of the decrease in absorbance at 460 nm. Bilirubin oxidase catalyses the oxidation of conjugated bilirubin in acidic medium, but in a basic medium the oxidation of unconjugated bilirubin is also catalysed by this enzyme. Selection of a suitable pH affords the sequential determination of both fractions.

A simultaneous FI method is also proposed for determination of direct and indirect bilirubin based on their differential reactivity with Erlich's reagent and monitoring at 560 nm of the azorubin pigment formed. In acidic medium the reaction between conjugated bilirubin and the azoreagent is very fast, but it is very slow for unconjugated bilirubin and it is faster when an accelerator (caffeine–benzoic acid [25] or methanol [8,26]) is present in the medium. In this work methanol was used as an accelerator because the reaction with other accelerators requires more than one step and it would require a more complicated manifold.

EXPERIMENTAL

Reagents

All reagents were of analytical-reagent grade.

Two buffer solutions were prepared for the enzymatic method. Buffer 1 was an aqueous solution containing 2 mM sodium cholate (Sigma) and 100 mM tris(hydroxymethyl)aminomethane

(Merck), with the pH adjusted to 8.4 with 1 M HCl. Buffer 2 was an aqueous solution containing 100 mM citric acid monohydrate (Merck) with the pH adjusted to 4.5 with 1 M NaOH. A solution of bilirubin oxidase (5 UI^{-1}) was prepared by dissolving the contents of a vial (Sigma) in each buffer solution.

Three solutions were prepared for the simultaneous method: an aqueous solution containing 0.25 M HCl; a reagent (R_1) (for total bilirubin) containing 3.5 mM sulphanic acid (Sigma), 5 mM sodium nitrite (Merck) and 12% (v/v) methanol (Merck) and a reagent (R_2) (for direct bilirubin) with the same composition as R_1 but without methanol.

A standard solution of bilirubin (0.1 g l^{-1}) was prepared by dissolving bilirubin (Sigma) in 1 M NaOH. Bilirubin Lin-trol serum control (Sigma) with certified concentrations of total and direct bilirubin was diluted with a saline solution as required. Serum samples from a routine clinical laboratory were also used.

Apparatus and instruments

A Pye Unicam SP-500 spectrophotometer furnished with a Hellma 178.12 QS flow cell and equipped with a Radiometer REC 80 Servograph recorder and a Selecta 382-S recirculating thermostat, a Gilson Minipuls-2 four-channel peristaltic pump with a rate selector, a Ismatec Mini-S 840 peristaltic pump, a Rheodyne model 5041 injection valve, a laboratory-built double injection system made with two Rheodyne model 5041 injection valves and PTFE tubing of 0.5 mm i.d. were used. A Leo PC system equipped with a DAS-8PGA interface (Metrabyte) was used for collection and treatment of the absorbance–time data.

Configurations and procedures

Enzymatic method. Figure 1a shows the reagent injection FI–merging zones arrangement proposed for the sequential determination of total and direct bilirubin based on the enzymatic oxidation of the analyte. The enzyme solution (E) either injected (IV) into buffer B_1 or B_2 merged with the sample (S) at point a. The reacting sample–enzyme plug was driven through the

manifold and the peristaltic pump (P) was halted when the plug reached the flow cell. During the stop time the kinetic development of the enzymatic reaction was monitored. The pump was started again and the plug was sent to waste. The buffer was changed by switching valve SV, thus allowing direct or total bilirubin in the sample to be sequentially determined.

Non-enzymatic method. Configuration b in Fig. 1 consists of a double injection valve (IV1 and IV2) that inserted two identical volumes of sample (S) into two symmetrical channels through which an acidic solution circulated (C). Each plug was mixed with another stream containing the reagents to develop either the reaction for the direct (R_1) or the total (R_2) determination of bilirubin. Both reaction plugs reached the flow cell sequentially and a two-peak recording was obtained as a result.

RESULTS AND DISCUSSION

Types of signal and measurement

The nature of the signal obtained in each method was different, as was the degree of information about the analytical reaction they provided. Both types of signal are shown in Fig. 2. The signal obtained by using the reagent injection-merging zones manifold (Fig. 2a and b) shows a portion where the absorbance decreased as the enzymatic reaction increased. A series of signal-time data were collected. In the simultaneous method a double peak was obtained (Fig. 2c and d), in which the height of the first peak corresponds to the direct reaction and that of the second peak to the sum of both direct and indirect reactions (total) of bilirubin.

Study of variables

The variables involved in each of the approaches were studied by using the univariate method. The variables were previously grouped into physical, chemical and hydrodynamic. Tables 1 and 2 show the ranges over which each variable was studied for each method and the optimum value found.

Optimization of the enzymatic method. Increased temperatures had a positive effect on the enzymatic reaction up to 40°C; above this value the signal decreased, possibly because of denaturation of the biocatalyst.

Oxidation of the mono- and diglucuronic derivatives of bilirubin, catalysed by BOX, occurred in acidic medium [8]. All solutions were prepared in 100 mM citrate buffer for the determination of bilirubin conjugates and the influence of the pH on the enzymatic reaction was studied between 4 and 10. The best analytical response was obtained at pH 4.5. A change of pH to a basic value allowed the oxidation of unconjugated bilirubin also to be catalysed by the enzyme. In this instance all solutions were prepared

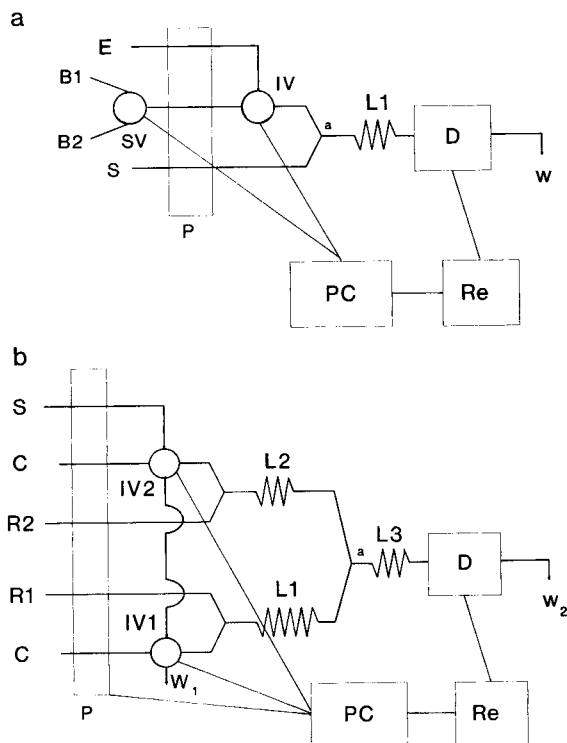


Fig. 1. Manifolds designed for the (a) sequential enzymatic and (b) simultaneous non-enzymatic determination of direct and total bilirubin. P = peristaltic pump; IV, IV1 and IV2 = injection valves; SV = selecting valve; D = detector; PC = personal computer; Re = recorder; w, w1 and w2 = waste; L1, L2 and L3 = open reactors; B1 and B2 = buffer solutions; E = enzyme solution; S = sample solution; C = acidic solution; R1 and R2 = reagent solutions; a = confluence point.

in 100 mM Tris–HCl buffer and the influence of the pH on the analytical signal was also studied. A pH 8.4 provided the highest analytical signal.

The addition of sodium cholate to solution B₁ increased the dissociation of the unconjugated bilirubin bound to proteins [9]. This influence was studied, and the best signal was obtained when 2.0 mM sodium cholate was added.

The stopped flow method required that the reaction plug reached the detector as soon as possible to avoid a decrease in sensitivity owing to dispersion. The best response was obtained with a minimum reactor length (15 cm) between the injection valve and flow cell and a flow-rate of 3.1 ml min⁻¹. The influence of the volume injected on the enzymatic reaction was studied,

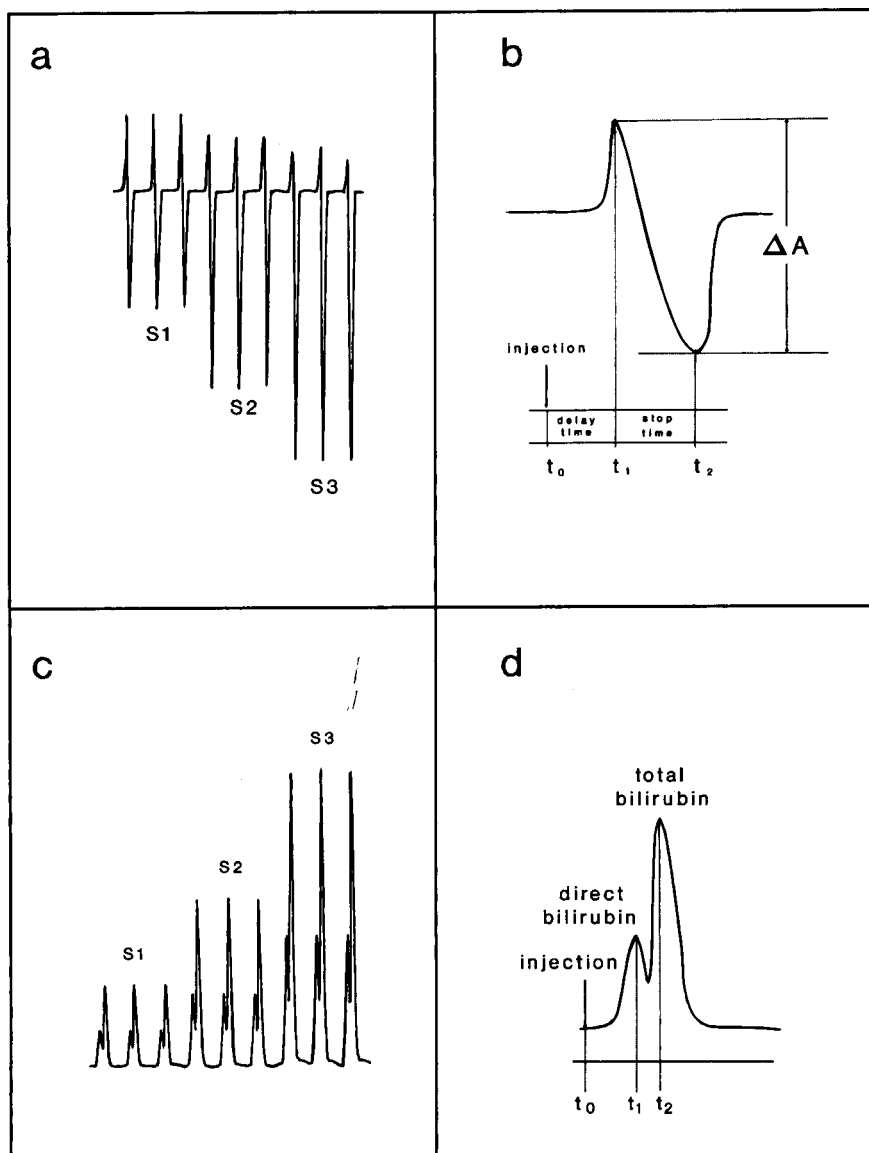


Fig. 2. Recordings obtained by using the FI manifold for the (a and b) enzymatic and (c and d) non-enzymatic determination of total and direct bilirubin. Slow (a and c) and fast (b and d) chart speeds.

TABLE 1
Range and optimum values of variables: enzymatic method

| Type | Variable | Range studied | Optimum value |
|----------|------------------------------------|---------------|---------------|
| Physical | Temperature (°C) | 20–50 | 40 |
| Chemical | [BOX] (U l^{-1}) | 0.05–1.0 | 0.2 |
| | Buffer 1 (B_1): | | |
| | [Tris-HCl] (M) | | |
| | pH | – | 0.1 |
| | [Sodium cholate] (M) | 4–10 | 8.4 |
| | | 0.5–5.0 | 2.0 |
| | Buffer 2 (B_2): | | |
| | [Citric acid] (M) | – | |
| | pH | 4–10 | 0.1 4.5 |
| FI | Flow-rate (ml min^{-1}) | 0.4–4.4 | |
| | Volume injected (μl) | 30–700 | 3.1 |
| | Delay time (s) | 5–15 | 300 |
| | Stop time (s) | 15–120 | 10 |
| | Length of open reactor (cm) | – | 90 |
| | | | 15 |

and for values above 300 μl no substantial increase in the analytical signal was found.

The influence of the delay and stop times was also studied and times of 10 and 90s, respectively, provided the highest analytical signal.

Optimization of the non-enzymatic method. Changes in the temperature of the reaction had

no influence on the analytical signal, so room temperature (20–25°C) was used.

All solutions were prepared in 0.1 M HCl according to the literature [8]. The influence on the analytical signal of sulphanic acid and sodium nitrite concentrations in the reagent solutions R_1 and R_2 was studied. The signal re-

TABLE 2
Range and optimum values of variables: non-enzymatic method

| Type | Variable | Range studied | Optimum value |
|--|-------------------------|------------------------------------|---------------|
| Physical | Temperature (°C) | 20–50 | 30 |
| Chemical | [HCl] (M) | – | 0.1 |
| | pH | 0–5 | 1.0 |
| | Reagent 1: | | |
| | [Sulphanilic acid] (mM) | 1.0–20.0 | 3.5 |
| | [Sodium nitrite] (mM) | 1.0–20.0 | 5.0 |
| | [Methanol] (%) | 0–40 | 12 |
| | Reagent 2: | | |
| | [Sulphanilic acid] (mM) | 1.0–20.0 | 3.5 |
| | [Sodium nitrite] (mM) | 1.0–20.0 | 5.0 |
| | FI | Flow-rate (ml min^{-1}) | 1.1–3.7 |
| Volume injected (VI_1) (μl) | | 30–500 | 300 |
| Volume injected (VI_2) (μl) | | 30–500 | 300 |
| Length of open reactor: | | | |
| L_1 (cm) | | 100–800 | 600 |
| L_2 (cm) | | – | 15 |
| L_3 (cm) | | 20–200 | 50 |

mained constant for concentrations above 3.5 and 5.0 mM for sulphanic acid and sodium nitrite, respectively. The effect of the methanol concentration on the acceleration of the total reaction was studied between 0 and 40% (v/v). The signal increases with increasing concentration of methanol, but the increase in the noise increased faster than the signal provided by the reaction product, so 12% (v/v) methanol was used as a compromise.

Two aspects were taken into account when studying the influence of the hydrodynamic variables: the rate of the conjugated bilirubin reaction was very fast, and it was therefore necessary that the plug injected through IV₂ reached the detector as soon as possible to avoid dispersion; and the rate of the unconjugated bilirubin reaction was slower than that of conjugated bilirubin reaction, even if the accelerator was added, and it needed a sufficient residence time for development of the reaction. A suitable L₂/L₁ ratio allowed the best residence time for each injected plug to be achieved and also an adequate separation between the maxima of the peaks they provided. Each reactor was studied separately and it was found that lengths of 600, 15 and 50 cm, respectively, provided the best analytical signal. The influence of the flow-rate was studied between 1.1 and 3.7 ml min⁻¹ in order to enhance the effect obtained with the optimum L₂/L₁ ratio. A flow-rate of 2.0 ml min⁻¹ was appropriate for the proposed aims. The influence of each of the volumes injected on the analytical signal was

also studied. Volumes over 300 μl produced a mixture of both boluses.

Features of the methods

Calibration graph and reproducibility. The calibration graphs for each method were obtained by using the optimum values of the variables studied above. Standard solutions of bilirubin Lin-trol at concentrations between 0.01 and 150 μM were injected in triplicate into the FI manifold. Table 3 summarizes the features of the methods (equation, regression coefficient, linear range and reproducibility). The linear ranges of the calibration graphs of the proposed methods are different. The enzymatic method allows for a lower determination limit for the total and direct bilirubin (0.09 and 0.14 μM, respectively) than the non-enzymatic method (0.84 and 3.80 μM, respectively). Nevertheless, the linear ranges are wider in the latter method (144 and 125 μM, respectively). These differences can be expressed by the α-coefficient (see Table 3), which is defined as the ratio between the upper limit of linear portion of the calibration graph and the determination limit. The values of α are 278 and 93 for the enzymatic method and 169 and 34 for the non-enzymatic method for the determination of total and direct bilirubin, respectively.

The reproducibility provided by both methods was studied at two concentration levels (5.0 and 15.0 μM). Similar experiments were carried out by using both methods to determine their precision: eleven samples containing two different

TABLE 3
Features of the proposed methods

| Method | FI manifold | Equation ^a | r ² | Linear range ^b | α | R.S.D. (%) ^c | |
|---------------|---|---|----------------|---------------------------|-----|-------------------------|------|
| | | | | | | Low | High |
| Enzymatic | Sequential, reagent injection- stopped flow | $\Delta A = (0.095 \pm 0.001)[B_T] + (0.06 \pm 0.01)$ | 0.9986 | 0.09–25.0 | 278 | 2.6 | 1.4 |
| | | $\Delta A = (0.082 \pm 0.001)[B_d] + (0.017 \pm 0.081)$ | 0.9978 | 0.14–13.0 | 93 | 2.8 | 1.6 |
| Non-enzymatic | Simultaneous, dual injection | $A = (0.018 \pm 5.5 \times 10^{-5})[B_T] + (0.05 \pm 0.003)$ | 0.9996 | 0.85–144.0 | 169 | 1.4 | 0.8 |
| | | $A = (0.002 \pm 2.2 \times 10^{-5})[B_d] + (0.015 \pm 0.001)$ | 0.9986 | 3.80–125.0 | 34 | 2.4 | 0.4 |

^a ΔA = absorbance increment, A = absorbance, B_T and B_d = total and direct bilirubin concentrations (μM), respectively.

^b Expressed in μM. ^c Total bilirubin: 5.0 and 15.0 μM for low and high levels, respectively; n = 11.

concentrations of bilirubin (5.0 μM low level and 15.0 μM high level, expressed as total bilirubin) were assayed in triplicate. The precision, expressed as relative standard deviation (R.S.D.) was acceptable in all instances for the two methods, the best value corresponding to the non-enzymatic method.

Sampling frequency. The sampling frequency was also very different for the proposed methods. The non-enzymatic method afforded a sampling frequency of 80 h^{-1} for the simultaneous determination of total and direct bilirubin. The enzymatic method provided a lower sampling frequency (30 h^{-1}) for the sequential determination of each fraction.

Study of interferences. The study of potential interferences was aimed at those commonly present in serum: glucose, cholesterol, urea, uric acid, creatinine, haemoglobin and albumin. The potential interferent was added to the samples at higher concentrations than are usually present in serum and the signal obtained was compared with that corresponding to samples in the absence of the foreign species. Similar results were obtained by both methods: glucose, cholesterol, urea, uric acid and creatinine do not interfere at a 100:1 (foreign species to bilirubin) weight ratio. Haemoglobin was investigated because some haemolysed serum can be present; a 50:1 ratio was tolerated. An important amount of bilirubin

TABLE 4
Determination and recovery of bilirubin in serum samples: enzymatic method

| Sample No. | Conventional method ^a | | Dilution | B_{total} found ^b | Recovery % ^c | B_{direct} found ^b | Recovery (%) ^c |
|------------|----------------------------------|----------------------------------|----------|---------------------------------------|-------------------------|--|---------------------------|
| | B_{total} ^b | B_{direct} ^b | | | | | |
| 1 | 34.3 | 28.9 | 1:100 | 0.336 | 102 | 0.294 | 100 |
| | | | | | 100 | | 102 |
| | | | | | 99 | | 101 |
| 2 | 11.6 | 7.3 | 1:100 | 0.114 | 102 | 0.061 | 94 |
| | | | | | 99 | | 102 |
| | | | | | 99 | | 98 |
| 3 | 48.4 | 24.6 | 1:100 | 0.481 | 102 | 0.242 | 103 |
| | | | | | 98 | | 97 |
| | | | | | 101 | | 104 |
| 4 | 7.5 | 3.4 | 1:100 | 0.069 | 102 | 0.346 | 97 |
| | | | | | 98 | | 97 |
| | | | | | 101 | | 100 |
| 5 | 364.8 | 310.7 | 1:1000 | 0.358 | 100 | 0.309 | 98 |
| | | | | | 103 | | 98 |
| | | | | | 97 | | 99 |
| 6 | 33.2 | 23.5 | 1:100 | 0.345 | 97 | 0.234 | 97 |
| | | | | | 104 | | 100 |
| | | | | | 101 | | 101 |
| 7 | 72.1 | 47.3 | 1:100 | 0.674 | 102 | 0.475 | 103 |
| | | | | | 103 | | 102 |
| | | | | | 102 | | 101 |
| 8 | 462.0 | 289.1 | 1:1000 | 0.463 | 97 | 0.288 | 101 |
| | | | | | 101 | | 103 |
| | | | | | 100 | | 101 |
| 9 | 35.4 | 21.4 | 1:100 | 0.349 | 103 | 0.209 | 101 |
| | | | | | 105 | | 100 |
| | | | | | 103 | | 102 |
| 10 | 59.2 | 46.2 | 1:100 | 0.595 | 102 | 0.457 | 99 |
| | | | | | 105 | | 101 |
| | | | | | 101 | | 98 |

^a AACC method [26]. ^b Bilirubin concentrations in μM . ^c Standard addition: 0.47, 0.96 and 1.92 μM .

was transported in serum bound to protein (mainly albumin), hence the potential interference of albumin was studied. There was no interference from albumin at a 10:1 ratio.

Application of the proposed methods. As a preliminary step, the total and direct concentrations of bilirubin in ten serum samples for healthy and sick individuals were determined by using the AACC standard method [26]. Both proposed methods were then applied to the determination of each fraction in these samples in two ways, namely the determination of the analyte in each sample and the study of the recovery afforded by the proposed methods after addition of three standard solutions (0.47, 0.96 and 1.92 μM , re-

spectively) to each sample. Previously all samples were diluted to fit the concentration level within the linear calibration ranges. The concentrations and recoveries are given in Tables 4 and 5. The results show excellent agreement between the two methods and also with the conventional method (recoveries between 94 and 106%).

Conclusion

Two FI methods for the determination of bilirubin and its fraction in serum have been proposed. Both methods afford excellent linear ranges of determination, precision and sampling frequency. The enzymatic method provides a lower determination limit and higher sensitivity,

TABLE 5
Determination and recovery of bilirubin in serum samples: non-enzymatic method

| Sample No. | Conventional method ^a | | Dilution | B _{total} found ^b | Recovery (%) ^c | B _{direct} found ^b | Recovery (%) ^c |
|------------|----------------------------------|----------------------------------|----------|---------------------------------------|---------------------------|--|---------------------------|
| | B _{total} ^b | B _{direct} ^b | | | | | |
| 1 | 34.3 | 28.9 | 1:5 | 6.86 | 100 | 5.76 | 103 |
| | | | | | 101 | | 100 |
| | | | | | 98 | | 99 |
| 2 | 11.6 | 7.3 | – | 10.70 | 101 | 6.58 | 97 |
| | | | | | 97 | | 96 |
| | | | | | 99 | | 99 |
| 3 | 48.4 | 24.6 | 1:5 | 9.62 | 99 | 4.93 | 101 |
| | | | | | 98 | | 99 |
| | | | | | 100 | | 101 |
| 4 | 7.5 | 3.4 | – | 7.42 | 98 | 3.50 | 105 |
| | | | | | 96 | | 106 |
| | | | | | 99 | | 104 |
| 5 | 364.8 | 310.7 | 1:50 | 7.30 | 101 | 6.23 | 99 |
| | | | | | 102 | | 102 |
| | | | | | 101 | | 101 |
| 6 | 33.2 | 23.5 | 1:5 | 6.47 | 96 | 4.72 | 100 |
| | | | | | 98 | | 99 |
| | | | | | 99 | | 98 |
| 7 | 72.1 | 47.3 | 1:5 | 9.44 | 96 | 9.39 | 103 |
| | | | | | 99 | | 101 |
| | | | | | 100 | | 100 |
| 8 | 462.0 | 289.1 | 1:50 | 9.19 | 99 | 5.81 | 103 |
| | | | | | 98 | | 104 |
| | | | | | 101 | | 102 |
| 9 | 35.4 | 21.4 | 1:5 | 7.03 | 103 | 4.28 | 99 |
| | | | | | 101 | | 96 |
| | | | | | 100 | | 98 |
| 10 | 59.2 | 46.2 | 1:5 | 11.82 | 100 | 9.18 | 101 |
| | | | | | 99 | | 100 |
| | | | | | 102 | | 98 |

^{a-c} See Table 4.

as shown by the slope of the calibration graph, and sequential determination of the two forms of bilirubin. Nevertheless, the non-enzymatic method provides the simultaneous determination of both bilirubin fractions and it does not require expensive reagents or catalysts.

The results obtained by applying these methods to serum samples agreed well with those obtained by a well established conventional method. This fact, together with the features mentioned above demonstrate that these methods can be successfully applied to routine clinical analysis.

The Dirección General de Investigación Científica y Técnica (DGICYT) is thanked for financial support (Grant No. PB90-0925). One of the authors (J.M.F.-R.) expresses his gratitude to the Junta de Andalucía for the award of a post-doctoral grant.

REFERENCES

- 1 D. Zakim and T. Boyer, *Hepatology. A Textbook of Liver Disease*, Saunders, Philadelphia, 1990, pp. 254–302.
- 2 P. Farreras and C. Rozman, *Medicina Interna*, Vol. I, Dogma Ediciones, Barcelona, 12th edn., 1992, pp. 262–269.
- 3 A.A.H. Van den Bergh and J. Snapper, *Dtsch. Arch. Klin. Med.*, 110 (1913) 540.
- 4 N. Chaimori, R.J. Henry and O.J. Golub, *Clin. Chim. Acta*, 6 (1961) 1.
- 5 S. Meites and L.K. Hogg, *Clin. Chem.*, 5 (1959) 470.
- 6 B.T. Doumas, B. Perry, E.A. Sasse and J.V. Straumfjord, *Clin. Chem.*, 19 (1973) 984.
- 7 B. Perry, B.T. Doumas, G. Buffone, M. Glick, C.N. Ou and K. Ryder, *Clin. Chem.*, 32 (1986) 329.
- 8 B.T. Doumas, B. Perry, B. Jendrzeczak and L. Davis, *Clin. Chem.*, 33 (1987) 1349.
- 9 C.J.P. Mullan and R. Langer, *Clin. Chem.*, 33 (1987) 1822.
- 10 S. Murao and N. Tanaka, *Agric. Biol. Chem.*, 45 (1981) 2383.
- 11 S. Murao and N. Tanaka, *Agric. Biol. Chem.*, 46 (1982) 2499.
- 12 J. Wang and M. Ozsoz, *Electroanalysis*, 2 (1990) 647.
- 13 J. Saar and C. Yarnitzky, *Isr. J. Chem.*, 23 (1983) 249.
- 14 E. Polz-Schaerffenberg and J.L. Barnes, *Clin. Chem.*, 31 (1985) 1923.
- 15 M.E. Goldfinch and G.A. Maguire, *Ann. Clin. Biochem.*, 25 (1988) 73.
- 16 S.P. Harrison and I.M. Barlow, *Clin. Chem.*, 35 (1989) 1980.
- 17 M. Prezelj, *Clin. Chem.*, 34 (1988) 176.
- 18 P. Meisel, D. Jaehring and M. Meisel, *Clin. Chim. Acta*, 166 (1987) 61.
- 19 J. Rothuizen, K.P.M. Heirwegh and A.M. Van Kouwen, *J. Chromatogr.*, 71 (1986) 19.
- 20 W. Spivak and W. Yuey, *Biochem. J.*, 15 (1986) 101.
- 21 Y. Adachi, H. Innfusa, M. Yamashita, A. Kambe, K. Yamazaki, Y. Sawada and T. Yamamoto, *Clin. Chem.*, 34 (1988) 385.
- 22 P. Linares, M.D. Luque de Castro and M. Valcárcel, *Rev. Anal. Chem.*, 8 (1985) 229.
- 23 J. Ruzicka and E.H. Hansen, *Flow Injection Analysis*, Wiley, New York, 2nd edn., 1988.
- 24 R.D. Schmid and W. Kunnecke, *J. Biotechnol.*, 14 (1990) 3.
- 25 L. Jendrassik and P. Gróf, *Biochem. Z.*, 297 (1938) 82.
- 26 W.R. Faulker and S. Meites (Eds.), *Selected Methods for the Small Clinical Chemistry Laboratory*, Vol. 9, American Association for Clinical Chemistry, Washington, DC, 1982, pp. 119–124.

Determination of fluphenazine hydrochloride in a flow assembly incorporating cerium(IV) arsenite as a solid-bed reactor

S. Laredo Ortiz and C. Gómez Benito

Departamento de Química, Colegio Universitario CEU, Moncada, Valencia (Spain)

J. Martínez Calatayud

Departamento de Química Analítica, Universidad de Valencia, 46100 Burjasot, Valencia (Spain)

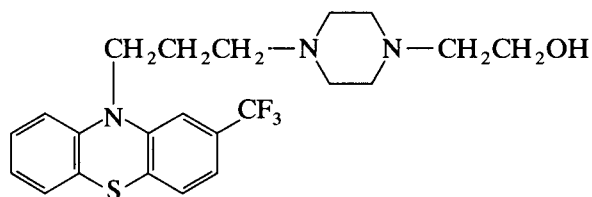
(Received 10th August 1992; revised manuscript received 19th October 1992)

Abstract

Cerium(IV) arsenite is used as a strong oxidizing solid-bed reactor in an unsegmented flow assembly. The solid was synthesized as homogeneous size particles with the suitable physico-chemical properties to resist the continuous-flow with good reactivity. The resulting manifold is proposed for the analytical determination of fluphenazine in pharmaceutical preparations by means of the fluorimetric monitoring of the oxidized drug. A linear calibration graph is obtained over the range 0.05–100 ppm of fluphenazine hydrochloride.

Keywords: Fluorimetry; Flow system; Cerium; Fluphenazine

Fluphenazine hydrochloride or 4-{3-[2-(trifluoromethyl)-10*H*-phenothiazin-10-yl] propyl}-1-piperazine ethanol dihydrochloride, is a white odourless crystalline powder used in pharmaceutical preparations. It has similar properties and uses like chlorpromazine hydrochloride but it has greater tranquilising and anti-emetic actions and less sedative effects. It also has longer duration of action [1]



Correspondence to: J. Martínez Calatayud, Departamento de Química Analítica, Facultad de Química, Universidad de Valencia, C/. Doctor Moliner 50, 46100 Burjasot (Valencia) (Spain).

The determination of fluphenazine is achieved by different procedures: by color complex formation with palladium chloride [2], fluorimetry with the aid of sulphuric acid [3] or upon oxidation with potassium permanganate [4] or hydrogen peroxide [5], ion-exchange column chromatography [6] and gas-liquid chromatography [7]. Titrimetric procedures are also widely used, like visual titration with perchloric acid in glacial acetic acid solution and crystal violet as indicator [4] or with a photometric titration on the basis of the oxidation with ceric sulphate [8].

The recommended titration procedures in pharmacopoeial monographs of three different phenothiazines have been recently reconsidered in an interlaboratory statistical evaluation [9].

The use of solid or immobilized reagents as bed-reactors is an interesting trend in continuous-flow methodologies like flow-injection analysis (FIA) [10,11]. The importance of this trend

can be ascribed to the advantages it offers over the dissolved reagents, basically increased sensitivity and injection rate, resulting from the inherently lower sample dispersion [12]. On the other hand, it is important to point out the different applications offered, e.g., sample [13] or reagent [14] pre-treatment, sample-conversion reactions [15,16] and integrated reaction–detection devices [17,18]. The approaches to the preparation of reagent beds and the physico-chemical mechanisms used to immobilize a given reagent, are usually dictated by its nature and by the analytical purpose of the immobilization. One approach is “natural” immobilization; the other broad category involves the physical or chemical immobilization of the reagent on a solid support [19].

This article is dealing with a bed-reactor based on “natural immobilization”. The proposed reactor is a PTFE tubing filled with cerium(IV) arsenite. The reaction of sodium arsenite with Ce(IV) ions produces a dark red solid with the suitable physical characteristics for continuous flow and good chemical reactivity [20]. The solid-bed reactor is inserted in the sample loop of a single-channel FIA manifold for the spectrophotometric determination of fluphenazine.

EXPERIMENTAL

Reagents, apparatus and procedures

Aqueous solution of fluphenazine (Guinama, pure grade) in de-ionized water, sucrose (Probus, pure grade), lactose (Poulenc Freres, pure grade) and bexamethasone (Guinama, pure grade). The solid bed reactor was prepared with cerium(IV) arsenite prepared in this laboratory from sodium arsenite (Panreac), nitric acid (Probus), and $\text{Ce}(\text{NH}_4)_2(\text{NO}_3)_6$ (Merck), all analytical reagent grade. Other reagents used were obtained from different manufacturers and were all analytical grade.

Flow-injection assembly

Figure 1 shows the continuous-flow manifold. The sample injector (Model 5041) was from Rheodyne, and a Gilson Minipuls 2 pump was used. The determination of fluphenazine was car-

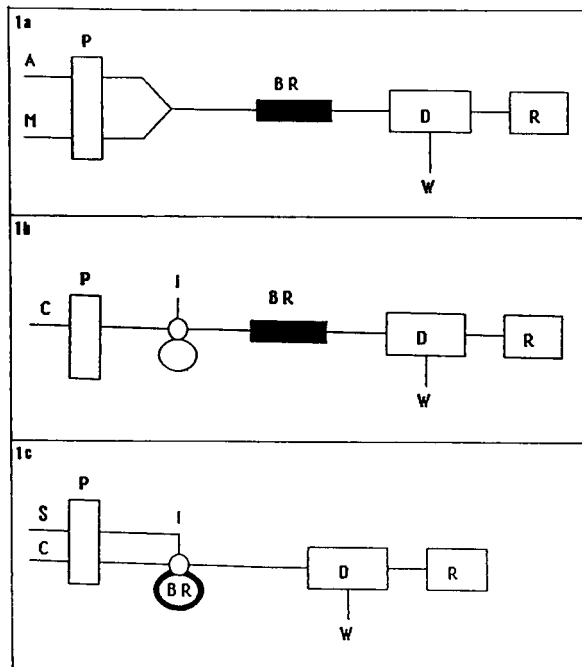


Fig. 1. Flow-injection assemblies. (a) Manifold for preliminary experiments. (b and c) Assemblies for the drug determination. A = analyte solution; M = acidic or basic solution; C = carrier; S = sample; P = peristaltic pump; BR = bed-reagent; D = detector; R = recorder; W = waste.

ried out by means of a Model FR-520 fluorimeter (Shimadzu) at wavelengths of 352 nm for excitation and 410 nm for emission. PTFE tube coils in the flow-injection assembly were 0.8 and 1.5 mm i.d. for carrier and reactor-bed, respectively.

Procedures

Preparation of the bed-reactor: the solid was prepared as formerly published [20]: 6.635 g of sodium arsenite was dissolved in 500 ml of distilled water and the pH was potentiometrically adjusted to 1.25 with 2 M nitric acid. From a burette Ce(IV) solution was slowly added which was previously prepared by dissolving 6.871 g of $\text{Ce}(\text{NH}_4)_2(\text{NO}_3)_6$ in 250 ml of water. The gelatinous precipitate obtained was left for 24 h in contact with the resulting solution, filtered, washed with distilled water and air-dried. A dark-red, hard solid of heterogeneous size particles was obtained. When the solid was still hot it was introduced into 1 M nitric acid at room tempera-

ture, filtered and dried again. The suitable size for the reactor was selected by sieving over the 150–200 μm range. The dry solid was stored (dark glass bottle) to be used. The bed reactor was prepared by filling a 1.5 mm i.d. PTFE tubing using a tiny funnel.

RESULTS AND DISCUSSION

The procedure is based on the oxidation of fluphenazine by Ce(IV) and fluorimetric monitoring of the transient oxidation product. The development of a fluorescent transient product is in accordance with the proposed two oxidation stages, typical of *N*-substituted phenothiacines [21–23]. The first stage, resulting simply from the loss of an electron from the parent compound, produces the corresponding cation free radical and the second stage is a further 1-electron oxidation of the free radical. The chronopotentiograms of these compounds also show a definite but rather attenuated third wave which evidently

corresponds to further oxidation. This third reaction probably involves oxidation of side chains.

Preliminary studies under continuous-flow conditions

Preliminary experiments for fluphenazine oxidation were carried out by merging an aqueous solution of 20.0 ppm fluphenazine with an acidic or basic stream, both at 2.89 ml min^{-1} ; the resulting mixture flows through the bed-reactor, $15 \text{ cm} \times 1.5 \text{ mm i.d.}$ (assembly a in Fig. 1). Tested acids were perchloric, hydrochloric, nitric, sulphuric, acetic and phosphoric, all 0.5 M. The emission spectra were recorded in the continuous flow assembly. The results showed the highest emitted light for acetic and phosphoric acid media. The phosphoric medium was further studied by varying the acid concentration over the range 0.05–1.00 M. Results are depicted in Fig. 2 and as it can be observed, lower phosphoric concentrations resulted in higher emitted light. Other tested media were distilled water, sodium hydroxide and ammonium ions; the response was 50%

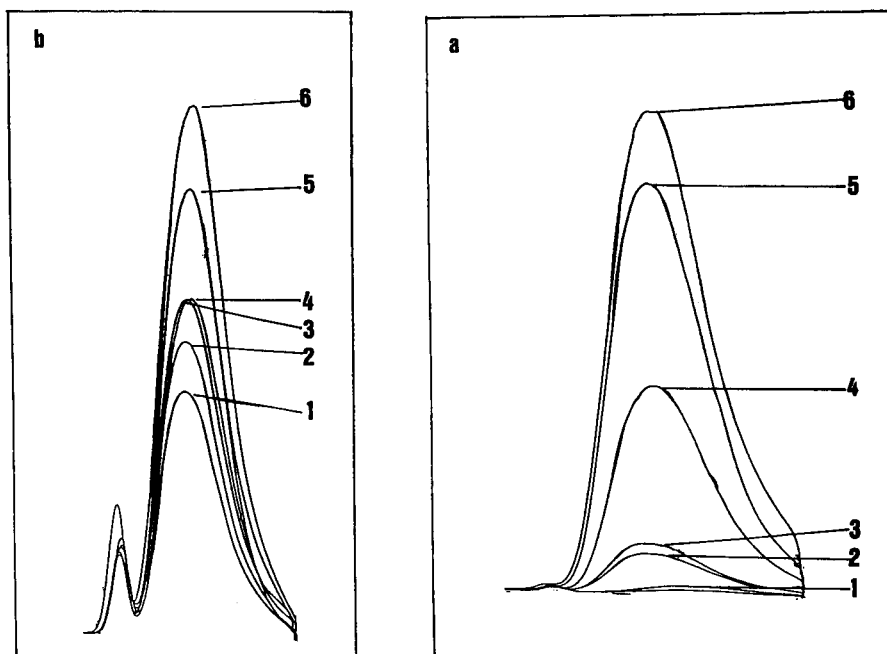


Fig. 2. Emission spectra of the fluphenazine in different acidic media. (a) Different acidic media (all 0.50 M) 1 = Sulphuric; 2 = perchloric; 3 = hydrochloride; 4 = nitric; 5 = phosphoric; 6 = acetic. (b) Different phosphoric concentrations (in M): 1, 1.00; 2, 0.50; 3, 0.25; 4, 0.10; 5, 0.05; 6, 0.01.

of that obtained with the 0.05 M phosphoric acid, which was therefore selected for further work. The optimum wavelengths for fluorescence were 352.0 and 410.0 nm for excitation and emission, respectively.

The influence of acidity was tested in a flow-injection assembly in which the bed reactor was located between the injection valve and the detector flow-cell and the optimum was close to pH 4. Different buffer solutions (potassium phthalate–sodium hydroxide, citric acid–sodium hydroxide, acetic acid–potassium hydroxide, phosphoric acid–sodium phosphate and tartaric acid–sodium hydroxide) were studied by maintaining the pH in the close vicinity of 4 and varying the buffer amount in order to test the influence of ionic strength on the fluorescence response. Because no significant variations were observed and slight acidity was obtained by adding phosphoric acid dropwise, this was selected as the most simple solution pretreatment.

The influence of temperature was studied with the aid of the same manifold by introducing the bed-reactor into a water bath. A temperature increase to 80°C resulted in a slightly lower output, probably due to a higher reaction rate which means the disappearance of the fluorescent transient free radical. Room temperature was selected for further studies.

The configuration of the flow assembly is an important matter and it was tested by changing the placement of the bed-reactor in the injection valve–detector line to the sample loop, see Fig. 1b and c. Best transient outputs were observed in the assembly type 1c maybe due to a more complete sample–solid reagent contact and minor sample dispersion in the way to the detector flow-cell.

The bed reactor configuration (internal diameter and particle size) was a critical parameter due to several reasons, e.g., the dependence of the sample dispersion on the diameter or the pressure required with small particles. The set of peaks from several series lead us to select an internal diameter of 1.5 mm and particle size over the 200–250 μm range.

The chemical parameters (acidity and temperature) were reoptimized using the adopted FIA

TABLE 1
Optimization of FIA parameters

| Parameter | Studied range | Selected value |
|--|---------------|----------------|
| Valve–detector distance (cm) | 12–84 | 32 |
| Column length (cm) | 5–24 | 18 |
| Flow-rate ratio (sample and carrier) ^a | 0.2–2.3 | 0.7 |
| Contact time (s) | 0–120 | 60 |
| Particle size (μm) | 100–350 | 200–250 |

^a Studied flow-rate ranges for each channel (in ml min^{-1}) from 0.5 to 6.5. The optimum ratio was obtained for values of 2.4 and 1.7 for sample and carrier streams, respectively.

assembly by means of the univariate method and on the basis of the previously reported results. The acidity content of the carrier solution (distilled water as sample solvent) was tested with phosphoric acid with the highest response corresponding to 0.01 M phosphoric acid. Additionally the stability of base-line was clearly improved.

The optimization of the FIA parameters injection valve–detector distance, column length, flow-rate (carrier and sample), sample–solid reagent contact time and particle size, was carried out in the reported order and by means of the univariate method. A sequential optimization method was used by finely re-optimizing the most relevant parameters (contact time and column length) on the basis of the optimum selected values. Table 1 depicts the studied range for any tested parameter and the selected value. The most influential parameters were the length of the packed-bed reactor and the flow-rates (ratio) of sample and carrier streams.

Analytical application

The study of the analytical figures of merit for the continuous flow procedure was carried out to establish the linear range, reproducibility, detection limit, sample throughput and life time of the solid-bed reactor.

The calibration graph was linear over the range 0.05–100 ppm of fluphenazine and could be described by the equation $Y = 13.33 + 46.02X$ (where Y is the fluorescence intensity and X the concentration of fluphenazine in ppm).

To test the stability or durability of the column a complementary experiment was carried out by

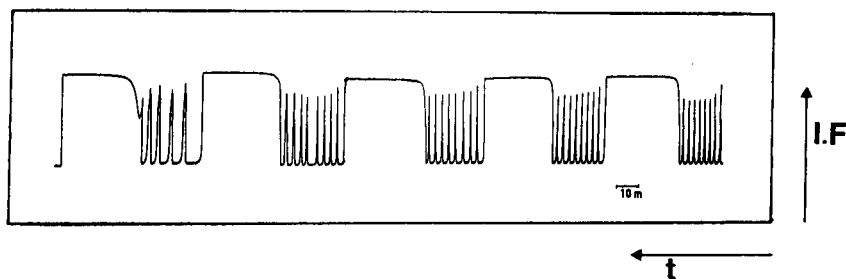


Fig. 3. Lifetime of the column. 30 min of continuous flow of analyte solution alternated with sets of 8 injections (for details see text).

passing a solution containing 20.0 ppm of fluphenazine as a carrier stream by means of the assembly c in Fig. 1 and continuous monitoring for 30-min periods. A set of 8 aliquots containing 20.0 ppm of fluphenazine were injected between two continuous monitoring periods. Total monitoring time was 150 min. As can be observed in Fig. 3, mean values of fluorescence intensity during the periods in which fluphenazine solution was passing continuously were 70.30, 69.6, 69.2, 70.5 and 71.5. Average values of peak-height were 55.38, 55.04, 56.27, 55.85 and 56.30. Bearing in mind the flow-rate of the continuously passing fluphenazine solution and its concentration, the total amount of drug forced through the bed-reactor was 71.7 mg, which is equivalent to 23 000 injections.

The tolerance of the method to foreign compounds which can be found in typical pharmaceutical samples containing fluphenazine was investigated by using solutions containing 10.0 ppm of the drug and adding various concentrations of the interfering compounds. The results obtained for various interfering compounds were as follows (concentration in ppm and relative error in %): sucrose 160, 3.2; lactose 75, 2.8; and bexamethasone saturated aqueous solution 5.7.

The fluphenazine content of Celesemine capsules and Celesemine syrup (both from Schering Plough) was determined. Five capsules were powdered by grinding them in an agate mortar and pestle. Aliquots of the powdered tablets were transferred to a beaker and shaken with distilled water. Aliquots of the syrup sample were diluted with distilled water up to 1:5 and directly injected into the FIA manifold. Up to 15 repetitive

injections were performed with the soluble extract from each aliquot. Five different preparations were analyzed and the results compared with those supplied by the manufacturer. Celesemine capsules: manufacturer 0.250 mg, found 0.245 mg (relative error 1.9%). Celesemine syrup: manufacturer 0.250 mg ml⁻¹, found 0.243 mg ml⁻¹ (relative error 2.8%).

Conclusions

A fluorimetric-FIA procedure is proposed for the determination of fluphenazine with application in control analysis of pharmaceutical formulations. The method is based on the reaction with solid cerium(IV) arsenite. The preparation of the column is quick and easy and the durability of the reactor allows the processing of a high number of samples.

REFERENCES

- 1 Martindale, *The Extra Pharmacopoeia*, The Pharmaceutical Press, London, 27th edn., 1978, p. 1538.
- 2 J.A. Ryan, *J. Pharm. Sci.*, 48 (1959) 240.
- 3 T.J. Mellinger and C.E. Keeler, *Anal. Chem.*, 35 (1963) 554.
- 4 K. Florey (Ed.), *Analytical Profile of Drug Substances*, Vol. 2, Academic Press, New York, 1978.
- 5 J.B. Rangland and V.J. Kinross-Wright, *Anal. Chem.*, 36 (1964) 1356.
- 6 J.W. Steele, *Can. Pharm. J. Sci. Sect.*, 97 (1964) 91.
- 7 M.W. Anders and G.J. Mannering, *J. Chromatogr.*, 7 (1962) 258.
- 8 S.P. Agarwal and M.I. Blake, *J. Pharm. Sci.*, 48 (1969) 1011.
- 9 J.O. De Beer, B.M.J. Spielberg, J. Hoogmartens, I. Samson, D.L. Massart and M. Moors, *Analyst*, 117 (1992) 933.

- 10 J. Ruzicka and A. Aindal, *Anal. Chim. Acta*, 216 (1989) 243.
- 11 H.A. Mottola, *Quim. Anal.*, 8 (1989) 119.
- 12 J. Martínez Calatayud and J.V. Garcia Mateo, *Analyst*, 116 (1991) 327.
- 13 E.A. Novikov, L.K. Shpigun and Yu.A. Zolotov, *Anal. Chim. Acta*, 230 (1990) 157.
- 14 R.C. Schothorst, O.D. Schmitz and G. Den Boef, *Anal. Chim. Acta*, 179 (1986) 299.
- 15 J. Martínez Calatayud, C. Gómez Benito and D. Gaspar Gimenez, *J. Pharm. Biomed. Anal.*, 8 (1990) 667.
- 16 J. Martínez Calatayud and C. Gómez Benito, *Anal. Chim. Acta*, 231 (1990) 259.
- 17 A. Martínez, M.C. Moreno and C. Camara, *Anal. Chem.*, 58 (1986) 1877.
- 18 M.A. Shakir and A.T. Faizullah, *Analyst*, 114 (1989) 951.
- 19 J. Garcia Mateo and J. Martínez Calatayud, *Chem. Anal.*, in press.
- 20 J.V. Garcia Mateo and J. Martínez Calatayud, *Anal. Chim. Acta*, 264 (1992) 283.
- 21 G. Duchinski, *Pharmazie*, 13 (1958) 478.
- 22 G.J. Patriarche, *Mikrochim. Acta*, 84 (1970) 950.
- 23 G. Clarke, in K. Florey (Ed.), *Analytical Profile of Drug Substances*, Vol. 9, Academic Press, New York, 1990, p. 284.

Determination of nitrogen in water: comparison of a continuous-flow method with on-line UV digestion with the original Kjeldahl method

Hennie Kroon

Environmental Laboratory, Zuiveringsschap Hollandse Eilanden en Waarden (ZHEW), Bonn en Meeswerf 205, 3087 EH Rotterdam (Netherlands)

(Received 14th September 1992; revised manuscript received 22nd December 1992)

Abstract

An automated continuous-flow method with on-line UV digestion for the determination of total nitrogen in waste water and surface water is described. The method is based on the digestion of nitrogen by potassium peroxodisulphate catalysed by UV radiation and detected as nitrite (reaction with sulfanilamide and α -naphthylethylenediamine dihydrochloride). This method was compared with the conventional Kjeldahl method based on the Dutch NEN 6481 standard. No significant differences were found between the two methods for surface and waste waters. The proposed method is suitable for waste water samples with a high nitrate content whereas the Kjeldahl method is not suitable for this type of samples. Further advantages of the proposed method are its fast response, less pollution, safer operation, and the need for fewer laboratory staff and less space.

Keywords: Flow system; UV-Visible spectrophotometry; Kjeldahl method; Nitrogen; Waters

When determining nitrogen in surface and waste waters, normally a separate digestion and measuring procedure is used. In The Netherlands, when a permit is required to discharge waste water, the company will often be referred to the NEN 6481 standard. This method prescribes the determination of the total concentration of ammonia nitrogen and organic bound nitrogen according to the Kjeldahl method. The organic bound nitrogen is digested with a mixture of concentrated sulphuric acid and potassium sulphate with selenium as catalyst. In the continuous-flow method proposed here, the organic and inorganic nitrogen is converted into nitrate by potassium peroxodisulphate promoted by UV ra-

diation and, after reduction to nitrite, is measured spectrophotometrically. Several workers have reported continuous-flow systems for the determination of total nitrogen in water, especially in soil extracts. Kutscha-Lissberg and Prillinger [1] and Houba et al. [2] used a combination of photooxidation and the action of potassium peroxodisulphate which has a high oxidation potential. They did not compare their method with the conventional Kjeldahl method but with a manual method (Devarda's alloy- H_2O_2) which is particularly aimed at the analysis of soil extracts in 0.01 M $CaCl_2$. Based on Houba et al.'s method, the continuous-flow system was made available by Skalar. This system was adapted to the determination of total nitrogen in waste water.

The objective of this work was to make a comparison between the proposed UV method and the conventional Kjeldahl method according

Correspondence to: H. Kroon, Environmental Laboratory, Zuiveringsschap Hollandse Eilanden en Waarden (ZHEW), Bonn en Meeswerf 205, 3087 EH Rotterdam (Netherlands).

to the NEN 6481 standard for surface and waste waters. Known N-containing substances such as hexamethylenetetramine (HMTA), glutamic acid and nicotinic acid and a large number of samples of surface waters, influents and effluents from different sewage treatment plants were investigated.

EXPERIMENTAL

Instrumentation

The continuous-flow system was a Skalar system and consisted of an SA 1000 sampler, SA 5101 pump module, SA 461 nitrate module, SA 5550 UV digester, SA 6000/6010 single-channel spectrophotometer and SA 8601 one-channel data

system with SAN^{plus} software. A schematic diagram is shown in Fig. 1.

Principle of determination

The sample is mixed with potassium peroxydisulphate as oxidizing agent and disodium tetraborate buffer solution. Under the influence of UV radiation the organic and inorganic nitrogen compounds are digested and converted into nitrate. The nitrate formed is reduced to nitrite with copper-activated cadmium. Nitrite will react in an acidic medium with sulphanilamide and α -naphthylethylenediamine dihydrochloride to form a coloured diazo compound. The absorption is measured at 540 nm with a spectrophotometer and the absorbance is related to the total amount of nitrogen in the sample. When the result is

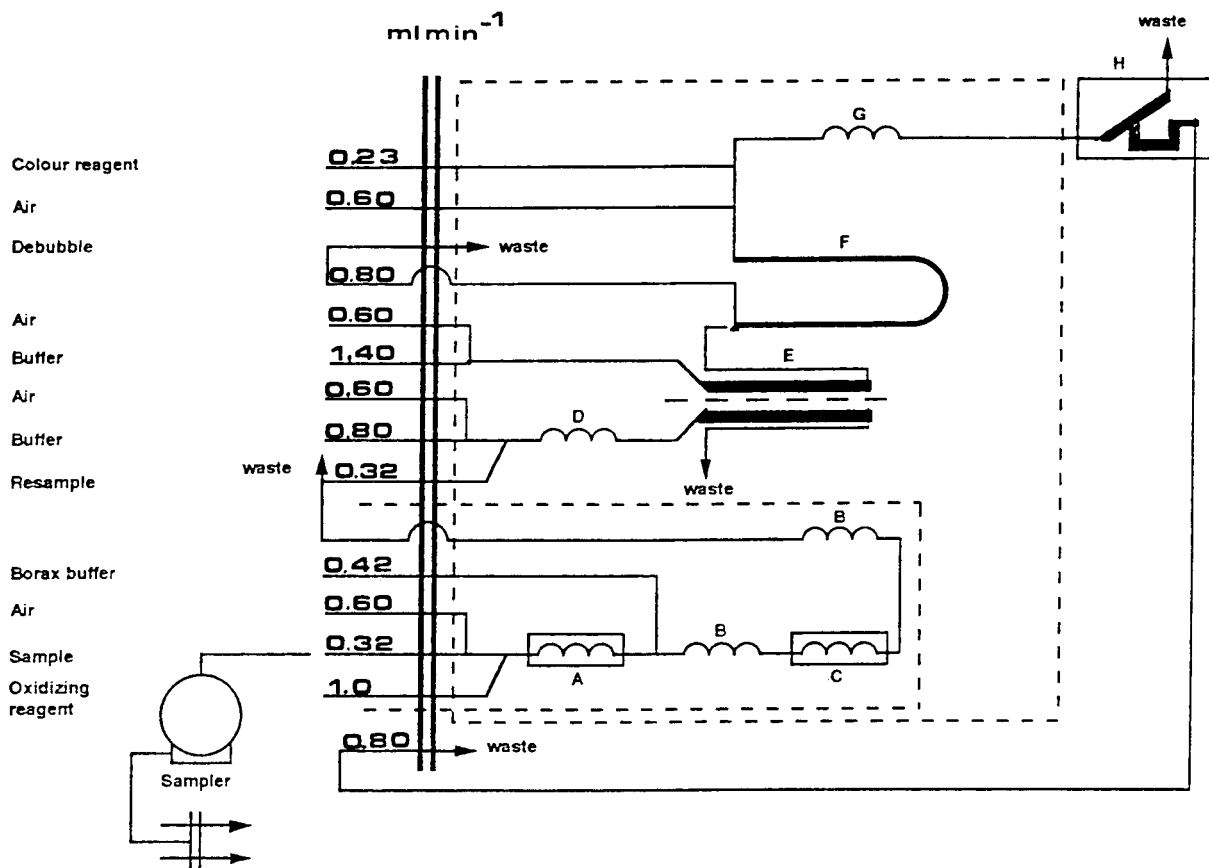


Fig. 1. Schematic diagram of continuous-flow system. A = Heated mixing coil, 50 turns; B = mixing coil, 10 turns; C = UV digester with 30-turn coil and UV lamp; D = mixing coil, 10 turns; E = dialyser; F = cadmium column; G = mixing coil, 20 turns; H = spectrophotometer with 30-mm flow cell and interference filter (540 nm).

compared with that given by the Kjeldahl method, the amount of nitrate + nitrite has to be subtracted from the total amount of nitrogen. The concentration of NO_x (sum of nitrate and nitrite) was determined according to the NEN 6652 standard.

Reagents

Analytical-reagent grade chemicals (Merck) and deionized water were used in all experiments.

Oxidizing agent. Potassium peroxodisulphate, 49 g l^{-1} .

Buffer solution for digestion. Dissolve 38 g of disodium tetraborate in 800 ml of water. Add 30 ml of 2.5 M sodium hydroxide, solution and dilute to 1000 ml with water.

Buffer solution for reducing NO_3 to NO_2 . Dissolve 25 g of ammonium chloride in 800 ml of water and adjust the pH to 8.2 with concentrated ammonia solution. Dilute to 1000 ml with water, add 1 ml of 30% Brij-35, solution and mix.

Colour reagent. Dissolve completely 10.0 g of sulphanilamide in 600 ml of water containing 150 ml of concentrated phosphoric acid. Add 0.5 g of α -naphthylethylenediamine dihydrochloride, dilute to 1000 ml with water and mix. Store in a brown bottle.

KNO_3 stock standard solution. Calibration of the analyser was done by using a 1000 mg l^{-1} nitrate-N stock standard solution, prepared by dissolving 7.221 g l^{-1} KNO_3 in water. Working standard solutions were prepared from this stock standard solution by dilution.

Other N-containing standards. Different N-containing compounds were tested to calculate the efficiency of the UV reactor. The starting point was always a 1000 mg l^{-1} N stock solution. The compounds analysed were ammonium sulphate, glutamic acid, HMTA, urea and nicotinic acid.

Sample preparation

In principle, the samples can be introduced into the system without preparation. For this comparison the samples were homogenized with an Ultra-Turrax. Also, conservation of the samples was effected by adding concentrated sulphuric acid up to a maximum of 1%.

RESULTS AND DISCUSSION

UV irradiation at mainly 254 nm catalyses the decomposition of peroxodisulphate to reactive components such as O_2 and hydroxyl radicals [3]. These components will support the oxidation of the organic compounds. The efficiency of the UV-peroxodisulphate digestion is influenced by different parameters such as pH, concentration of the oxidizing agent and the reaction time [4–6]. The optimum pH in the UV reactor was 9 [7]. For reduction of the nitrate by cadmium, the optimum pH should also be between 8 and 9. The production of protons by the oxidation reaction was neutralized by the sodium tetraborate buffer and sodium hydroxide. The CO_2 liberated from the oxidation of organic compounds was converted into carbonate.

A long reaction time with peroxodisulphate was chosen in the first stage, to achieve the optimum effect of the oxidation prior to introducing the solution into the UV reactor. In the first instance 49 g l^{-1} $\text{K}_2\text{S}_2\text{O}_8$ was used and also the oxidation step was effected with heating at 70°C .

Determination of different N-containing compounds

The results for different N-containing compounds are given in Table 1. These compounds were measured in the range $0\text{--}30 \text{ mg l}^{-1}$ N. The relative standard deviation (R.S.D.) for the UV method varied from 1.5 to 5%. For this reason, the samples were analysed a minimum of three times over 3 or 4 days. At levels of 2 mg l^{-1} N the

TABLE 1

Recoveries of nitrogen compounds using the Kjeldahl and the UV method

| Compound | Recovery (%) | |
|----------------|-----------------|-----------|
| | Kjeldahl method | UV method |
| Urea | 95–100 | 85–100 |
| HMTA | 93 | 90 |
| Glutamic acid | 90 | 100 |
| Nicotinic acid | 53–75 | 100 |

R.S.D. varied from 5 to 10%. In addition to the standard solutions, a number of real samples were analysed during the test period.

Surface water

A number of surface water samples with concentrations between 3 and 10 mg l⁻¹ Kjeldahl nitrogen were analysed using both methods. The relationship between the results of the Kjeldahl method (x) and the UV method (y) could be expressed by the straight line $y = 1.0794x - 0.20987$ ($n = 16$, regression coefficient $r = 0.989$, standard error of slope = 0.043 and standard error of intercept = 0.215).

Standard additions of ammonium sulphate were made to a normal surface water sample from an area controlled by the ZHEW. The results obtained by the two methods are given in Table 2.

The degree of agreement between the methods can be calculated with Student's t -test. This calculation is made to determine whether the methods deliver the same average results with a reliability of 95%. By comparing squared standard deviations (S.D.s), the F -test shows whether both methods are of similar precision. This is a

prerequisite for comparing results. For Student's t -test, the value 0 expresses that within 95% reliability (two-tail test) there is no reason to assume that the UV method differs significantly from the Kjeldahl method. For the F -test, + or - expresses that the variance of the analytical methods will be significantly more or less accurate, respectively, by testing within 95% reliability (one-tail test).

The conclusion is that the UV method does not differ significantly from the Kjeldahl method. The results are ambiguous; they do not show whether the UV method is more or less accurate than the Kjeldahl method.

Sewage water

To compare the UV method for analyses of nitrogen in sewage waste (mainly domestic waste), it was decided to divide the samples into two categories: (1) untreated sewage, influent for treatment plant, $\text{NO}_x < 5 \text{ mg l}^{-1} \text{ N}$ and Kjeldahl nitrogen (N-Kj) $> 10 \text{ mg l}^{-1} \text{ N}$; and (2) treated sewage, effluent from treatment plant, $\text{NO}_x > 5 \text{ mg l}^{-1} \text{ N}$ and N-Kj $< 10 \text{ mg l}^{-1} \text{ N}$.

The relationship between the results of the Kjeldahl method (x) and the UV method (y) for

TABLE 2
Results of standard additions to surface water

| Sample | Parameter | Nitrogen content (mg l ⁻¹) | | Comparison of UV vs. Kjeldahl methods ^a | |
|--|-------------------------|--|-----------|--|-----------|
| | | Kjeldahl method | UV method | Student's t -test | F -test |
| Surface water | \bar{X}_{mean} | 2.55 | 2.55 | 0 | + |
| | S.D. | 0.21 | 0.10 | | |
| | R.S.D. (%) | 8.2 | 3.9 | | |
| | n | 11 | 10 | | |
| Surface water + addition of 1 mg l ⁻¹ N | \bar{X}_{mean} | 3.33 | 3.45 | 0 | - |
| | S.D. | 0.06 | 0.13 | | |
| | R.S.D. (%) | 1.9 | 3.8 | | |
| | n | 12 | 10 | | |
| Surface water + addition of 3 mg l ⁻¹ N | \bar{X}_{mean} | 5.53 | 5.23 | 0 | + |
| | S.D. | 0.28 | 0.07 | | |
| | R.S.D. (%) | 5.0 | 1.8 | | |
| | n | 12 | 10 | | |

^a For explanation of symbols, see text.

TABLE 3

Results of additions to (un)treated sewage water ^a

| Sewage water | Parameter | Nitrogen content (mg l ⁻¹) | | Comparison of UV vs. Kjeldahl methods ^b | |
|---|-------------------|--|-----------|--|----------------|
| | | Kjeldahl method | UV method | Student's <i>t</i> -test | <i>F</i> -test |
| Influent | X_{mean} | 31.44 | 31.97 | | |
| | S.D. | 1.32 | 0.34 | 0 | + |
| | R.S.D. (%) | 4.2 | 1.1 | | |
| Influent + 10 mg l ⁻¹ NH ₄ -N | X_{mean} | 40.39 ^c | 41.99 | | |
| | S.D. | 0.36 | 0.44 | + | 0 |
| | R.S.D. (%) | 0.9 | 1.1 | | |
| Influent + 20 mg l ⁻¹ NH ₄ -N | X_{mean} | 49.83 | 52.06 | | |
| | S.D. | 0.45 | 0.27 | + | 0 |
| | R.S.D. (%) | 0.9 | 0.5 | | |
| Influent + 10 mg l ⁻¹ HMTA-N | X_{mean} | 41.21 | 42.27 | | |
| | S.D. | 0.86 | 0.46 | 0 | + |
| | R.S.D. (%) | 2.1 | 1.1 | | |
| Influent + 20 mg l ⁻¹ HMTA-N | X_{mean} | 49.36 | 53.23 | | |
| | S.D. | 1.15 | 0.62 | + | + |
| | R.S.D. (%) | 2.3 | 1.2 | | |
| Effluent | X_{mean} | 8.59 | 10.61 | | |
| | S.D. | 0.28 | 0.58 | + | - |
| | R.S.D. (%) | 3.3 | 5.4 | | |
| Effluent + 5 mg l ⁻¹ NH ₄ -N | x_{mean} | 13.91 | 16.32 | | |
| | S.D. | 0.30 | 0.64 | + | - |
| | R.S.D. (%) | 2.2 | 3.9 | | |
| Effluent + 10 mg l ⁻¹ NH ₄ -N | X_{mean} | 18.64 | 21.22 | | |
| | S.D. | 0.37 | 0.85 | + | - |
| | R.S.D. (%) | 2.0 | 4.0 | | |
| Effluent + 5 mg l ⁻¹ HMTA-N | X_{mean} | 13.05 | 15.82 | | |
| | S.D. | 0.46 | 0.99 | + | - |
| | R.S.D. (%) | 3.5 | 6.3 | | |
| Effluent + 10 mg l ⁻¹ HMTA-N | X_{mean} | 18.52 | 21.42 | | |
| | S.D. | 0.48 | 0.76 | + | 0 |
| | R.S.D. (%) | 2.6 | 3.6 | | |

^a For all samples $n = 9$ except where indicated otherwise.^b For explanation of symbols, see text.^c $n = 7$.

the influents can be expressed by the straight line $y = 0.903x + 4.09$ ($n = 27$, $r = 0.979$, standard error of slope = 0.038 and standard error of intercept = 2.479) and that for the effluents by $y = 1.01x + 0.727$ ($n = 20$, $r = 0.87$, standard error of slope = 0.129 and standard error of intercept = 1.021).

Further studies were done through additions of ammonium and HMTA to waste waters of type 1 and 2.

Influents

A "common" influent was measured on subsequent days with and without addition of ammonium and HMTA. Table 3 shows that the results of the Kjeldahl method are on average lower than those given by the UV method. Student's t -test and the F -test were performed on the readouts and the results are given in Table 3.

From investigations done in similar laboratories, the R.S.D. for the Kjeldahl method was found to be 4%. The conclusion was that the UV

method used for influents does not differ significantly from the Kjeldahl method. From the F -test it can be deduced that the UV method delivers results at least as reliable as those given by the Kjeldahl method.

Effluents

In the area controlled by the ZHEW, the treatment plants in general do have effluents with Kjeldahl values $< 10 \text{ mg l}^{-1} \text{ N}$ and nitrate values $> 10 \text{ mg l}^{-1} \text{ N}$. From Table 3 it became clear that the UV method delivers significant higher results than the Kjeldahl method. The cause of these significantly higher results can be explained as the result of the high nitrate contents of these samples (ca. $20 \text{ mg l}^{-1} \text{ N}$).

Interference by NO_x in the analysis of effluents

To prove this interference, the following experiment was done. An influent was diluted to the Kjeldahl value of an effluent; the nitrate content was 0.1 mg l^{-1} . Different concentrations

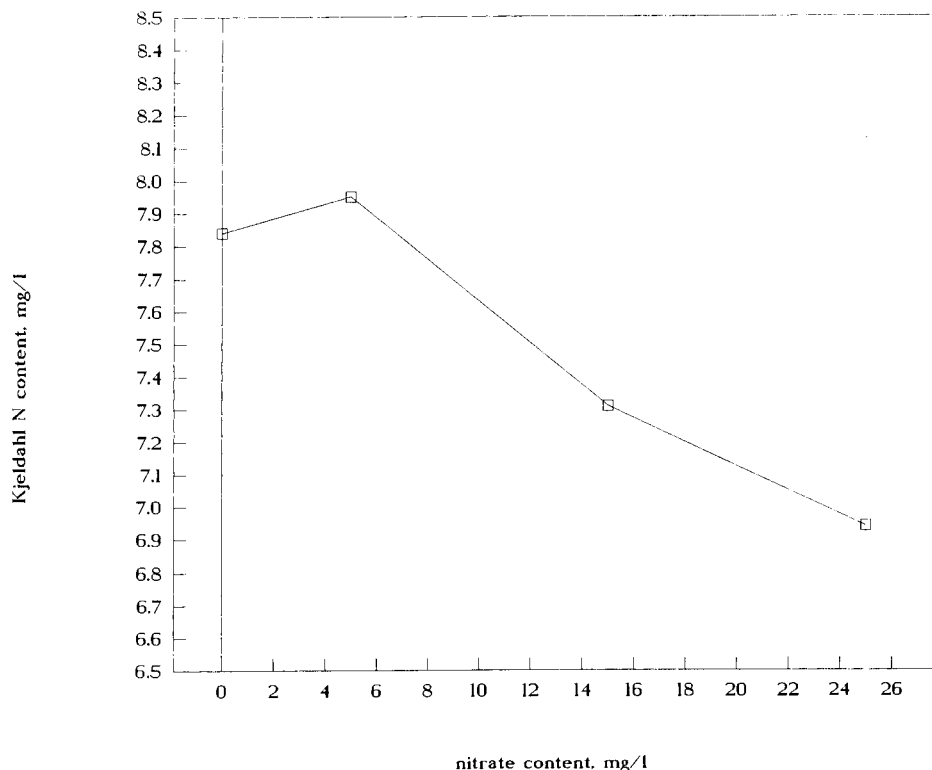


Fig. 2. Effect of nitrate on the N content of treated sewage water measured with the Kjeldahl method.

of nitrate were added to the sample. The results are shown in Fig. 2, and demonstrate that nitrate suppresses the Kjeldahl N value systematically. The R.S.D. for the different samples varied from 1.6 to 5%. The samples were analysed five times during one run.

Advantages of the UV method

A general comparison of the UV method with the Kjeldahl method shows a number of advantages for the former. The Kjeldahl method needs digestion prior to measurement, which is time consuming. The UV method includes digestion in the analytical system. The digestion time in the flow system can be neglected. The delay time compared with a flow system for nitrate only is increased. The Kjeldahl method produces a lot of chemical waste with high concentrations of sodium hydroxide and sodium and potassium sulphate and low concentrations of the catalyst selenium.

Of course, savings depend on the number of samples handled, but for control laboratories in the field of sewage treatment, considerable savings of labour time can be made for this determination, especially as the laborious digestion step can be omitted. On the other hand, extra analyses of nitrate should be carried out.

Conclusions

From this comparison between the Kjeldahl method (NEN 6481) and a continuous-flow UV

method with on-line digestion, it can be concluded that the proposed UV method is a good alternative to the Kjeldahl method. No significant differences in the results were found for analyses of surface and sewage waters (influent of treatment plants). The UV method generally reports more precise results (lower S.D.). For treated waste water with relatively high nitrate contents, as in biologically treated sewage, the Kjeldahl method is less suitable because of suppression of the nitrogen content. The UV method offers several advantages over the Kjeldahl method, viz., rapid results, less pollution, safer conditions and savings of laboratory space and staff time.

The author thanks Reina Roest and Coby de Deugd for carrying out the analyses and Bram Neele for making the analysis system available.

REFERENCES

- 1 P. Kutscha-Lissberg and F. Prillinger, *Plant Soil*, 64 (1982) 63.
- 2 V.J.G. Houba, I. Novozamsky, J. Uittenbogaard and J.J. van der Lee, *Landwirtsch. Forsch.*, 40 (1987) 295.
- 3 D.A. House, *Chem. Rev.*, 62 (1962) 188.
- 4 F.A.J. Armstrong, P.M. Williams and J.D.H. Strickland, *Nature*, 211 (1966) 481.
- 5 B.K. Afghan, P.D. Goulden and J.F. Ryan. *Adv. Autom. Anal.*, 2 (1970) 291.
- 6 L. Gustafsson, *Talanta*, 31 (1984) 979.
- 7 S. Hinkamp and G. Schwedt, *Z. Wasser Abwasser Forsch.*, 24 (1991) 60.

Determination by pyrolysis–gas chromatography of the phenolic resin concentration in particulate matter accumulated from traffic on roads

Takashi Saito

Department of Chemical Technology, Kanagawa Institute of Technology, 1030, Shimoogino, Atsugi, Kanagawa 243-02 (Japan)

(Received 20th August 1992; revised manuscript received 4th November 1992)

Abstract

A simple and rapid method for determining the phenolic resin concentration in particulate matter accumulated on roads due to traffic was investigated. The phenolic resin concentration may provide an indirect estimate of the concentration of asbestos because both compounds originate from brake friction materials of automobiles. After extracting the particulate matter with tetrahydrofuran, the extract was analysed with a gas chromatograph to which a Curie-point pyrolyser was attached. The phenolic resin concentrations in the particulate matter were measured by determining the amount of phenol generated by pyrolysis of the polymer. An estimate of the asbestos concentration can then be obtained based on the known contents of phenolic resin and asbestos in brake friction materials of automobiles. It was estimated that the asbestos particle concentration originating from brake friction materials of automobiles was in the range of 0.753–2.19 mg g⁻¹ for particulate matter accumulated on roads in Tokyo.

Keywords: Gas chromatography; Asbestos; Brake friction materials; Phenolic resins; Pyrolysis; Road particulate matter

Because of its excellent heat insulation properties, toughness and resistance against shock, asbestos is widely utilized. Materials for structures take about 78% of the total consumption of asbestos in Japan [1] and about 6.8% has been used in friction materials of brakes and clutches for automobiles. However, asbestos is potentially carcinogenic to humans. In recent years, asbestos pollution in the indoor atmosphere of buildings, gymnasiums and houses has become an environmental problem. According to the results of the measurement of asbestos concentrations in the

atmosphere, however, it has been shown that, although not of great concern yet, higher concentrations of asbestos are detected in the outdoor atmosphere, particularly along roads [2–6], than in indoor atmospheres. This arises because the brake linings and/or disc pads and clutch disc pads wear during automobile use, releasing the asbestos present. The performance evaluation of brake linings and the wear behaviour of asbestos in brake friction materials on drum brake systems of automobiles have been reported [7–10], and the observation of the decomposition products for their materials by electron microscopy has been carried out [11–13]. Further, levels of exposure to asbestos during brake maintenance have been measured [14].

Correspondence to: T. Saito, Department of Chemical Technology, Kanagawa Institute of Technology, 1030, Shimoogino, Atsugi, Kanagawa 243-02 (Japan).

Recently, the demand for disc brakes for automobiles has increased owing to their excellent brake efficiency and heat dissipation, and the transition from conventional drum brakes to the use of disc brakes is advancing rapidly. Asbestos particles from disc brake pads are easily released into the atmosphere because they are not an enclosed system like drum brakes. Accordingly, it is considered that the contribution of asbestos pollution along roads from disc brake pads is significant.

For a quick overview of the asbestos pollution from traffic, the asbestos concentration in particulate matter accumulated on roads may give an indication because the accumulated particulate matter on roads can be easily collected over a wide area in a short time compared with the particulate matter suspended in ambient air. For the determination of asbestos concentration in suspended particles in the atmosphere, the method of counting the number of asbestos fibres by means of an optical microscope has been widely used. For samples of particulate matter accumulated on roads, however, it is difficult to count with accuracy the number of asbestos fibres because of the many co-existing materials (such as asphalt and rubber particles, oily compounds, condensates of automobile exhaust gases and dust). No report on the determination of the asbestos concentration in the particulate matter originating from traffic accumulated on roads could be found. Although an attempt was made previously to determine the asbestos particles present in the particulate matter on roads [15], no details of the method of determination were reported.

Brake friction materials such as disc brake pads include asbestos fibres, phenolic resin, organic fillers (cashew, gum), inorganic fillers (BaSO_4 , CaCO_3 , graphite, MoS_2), metals (Fe, Cu, Al, Zn), oxides (Al_2O_3 , SiO_2 , MgO) and lubricant oil. Phenolic resin is used as the binder for the brake friction materials. In this work, the phenolic resin concentration was determined from the amount of pyrolysates produced by the pyrolysis of particulate matter using pyrolysis–gas chromatography (Py–GC). Further, asbestos concentrations can be obtained indirectly, rapidly

and approximately from the concentration of phenolic resin based on the known contents of phenolic resin and asbestos in brake friction materials.

EXPERIMENTAL

Reagents

Tetrahydrofuran (THF), phenol, *o*- and *p*-cresol, 2,4- and 2,6-xyleneol, benzene, toluene and xylene were of analytical reagent grade from Wako.

Phenolic resin

Generally, phenolic resin, that possess a structure of the novolak type are utilized as binders for brake friction materials. The novolak-type phenolic resins used in this study were Plyphen J-363, J-375 and 5510, BA-5097, Varcum TD-2003 and TD-2033 (Dainippon Ink and Chemicals), which are widely used in Japan. The contents of formaldehyde in the powder phenolic resin were 0.5–1.2 (mean 0.9) mol mol⁻¹ phenol. The content of hexamethylenetetramine used as a curing agent was 10% (w/w). These phenolic resins were cured at 150°C and used in the experiments.

Apparatus and Py–GC conditions

A Model JHP-2 Curie-point pyrolyser (Japan Analytical Industry) for the pyrolysis of particulate matter extracts was used, and was coupled directly to a Model GC-8APF gas chromatograph (Shimadzu). The pyrolysis temperature and time were 670°C and 5 s, respectively. The pyrolysates were analysed using a gas chromatograph equipped with a Model CBP5-M25-025 silica capillary column [5% (w/w) phenylmethylsilicone, 25 m × 0.2 mm i.d.] (Shimadzu) and a flame ionization detector. The temperatures of the separation column and detection and injection ports were 70–140 (programmed at 4°C min⁻¹), 220 and 220°C, respectively. The carrier gas was helium at a flow-rate of 0.67 ml min⁻¹.

Analytical procedure

After drying the sample of particulate matter in a desiccator, coarse particles were removed

using a 40-mesh sieve. A 3-g amount of this particulate matter was placed in a 30 ml Erlenmeyer flask and 10 ml of tetrahydrofuran (THF) were added. Thereafter, extraction was carried out for 10 min in an ultrasonic wave generator (Bransonic B-321; Branson) at 150 W, followed by centrifugal separation at 300 rpm; the extract was collected, then another 10 ml of THF were added to the residue and extraction was carried out in a similar manner. The two extracts were combined and then evaporated to dryness under reduced pressure. The residue was dissolved by adding 2 ml of THF and the solution obtained was used for the Py-GC analysis. A 40- μ l volume of this sample was taken with a microsyringe and coated on a metal sheet (Pyrofoil) with a Curie point of 670°C. After air drying, Py-GC analysis was carried out.

The amount of phenol monomer produced was determined. The concentration of phenolic resin in a particulate matter sample was then calculated using a calibration graph that shows the

correlation between the amount of phenolic resin and the amount of phenol monomer produced. Based on the average content of phenolic resin, the concentration of brake friction materials was calculated and finally the asbestos concentration was calculated based on the average asbestos content in the brake friction materials.

RESULTS AND DISCUSSION

Pyrogram of phenolic resin

Figure 1 shows the pyrogram of Plyophen J-375 novolak phenolic resin which was pyrolysed at 670°C for 5 s. When the pyrolysis of the phenolic resin was carried out, phenol, which is the main component, was obtained. Further, as the novolak phenolic resin possesses a structure in which HCHO is coupled to the *ortho* and *para* positions of the phenol, *o*- and *p*-cresol monomers were also obtained as products. The other phenol derivatives such as 2,4- and 2,6-xyleneol monomers

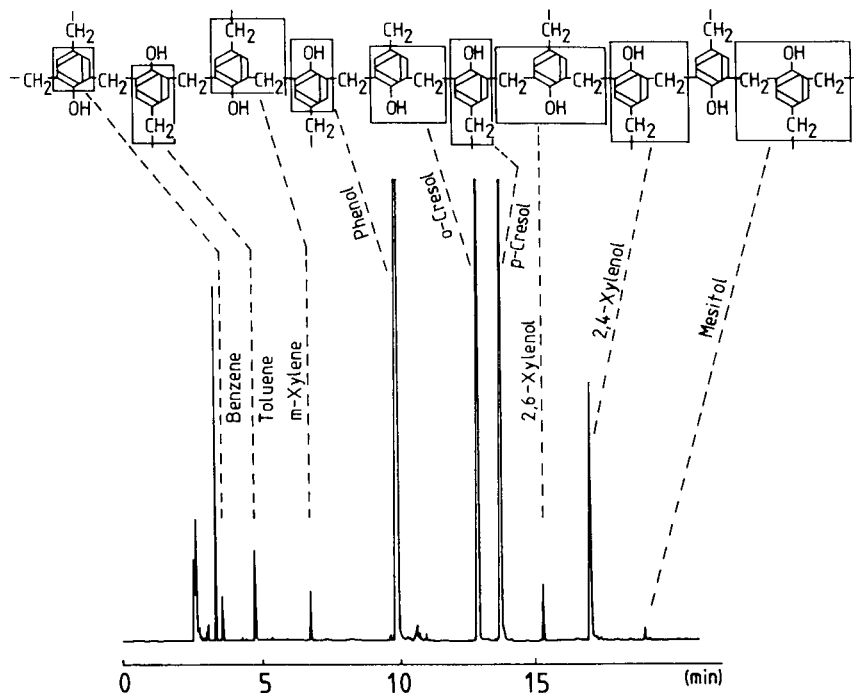


Fig. 1. Typical pyrogram of novolak phenolic resin.

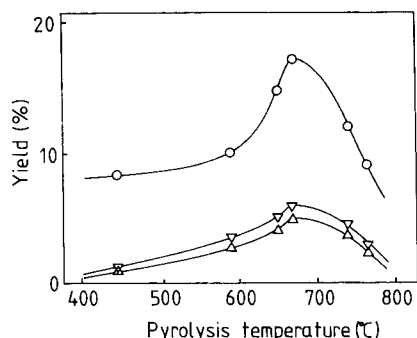


Fig. 2. Relationship between the pyrolysis temperature and the yield of characteristic pyrolysates of phenolic resin. \circ = Phenol; ∇ = *p*-cresol; \triangle = *o*-cresol.

were produced in small amounts, and also low-molecular-weight hydrocarbons such as benzene, toluene and xylene were detected.

Yields of pyrolysates versus pyrolysis temperature

Figure 2 shows the relationship between the pyrolysis temperature and the yields of fragments for the novolak-type phenolic resin (Plyophen J-375). A high yield was obtained near 670°C for the pyrolysates of both phenol and *o*- and *p*-cresol. A similar tendency was also seen for other phenolic resins. At a pyrolysis temperature lower than 670°C, the yields of pyrolysates decreased because the pyrolysis of the phenolic resin became incomplete. However, when the temperature exceeded 670°C, the yields also tended to decrease rapidly. This is assumed to be due to

breaking of C–C and C=C bonds and pyrolysis to benzene and other low-molecular-weight hydrocarbons.

Yields of pyrolysates versus pyrolysis time

The effect of pyrolysis time of the phenolic resin (Plyophen J-375) on the yield of phenol and *o*- and *p*-cresol was examined. When the pyrolysis time was 2 s and shorter, the yield of the phenol monomer was low and the reproducibility of the yield was not very good. By setting the pyrolysis time at 3 s or longer, it was observed that the yields of all the pyrolysates were constant.

Extraction recovery

The extraction recovery of the phenolic resin in particulate matter using THF was determined. Material with particle sizes of $\leq 420 \mu\text{m}$ that accumulated on roads was extracted by ultrasonic treatments using 10 ml of THF for 10 min. After the extract had been recovered, another 10 ml of THF were added to the residue, and the ultrasonic extraction was repeated. This operation was repeated once more. The respective extracts were then analysed by Py–GC and the concentrations of phenolic resin was measured. Table 1 shows the extraction recovery of the phenolic resin. By repeating the ultrasonic extraction, the concentration of phenolic resin in the extracts decreased, and it was found that the phenolic resin was hardly detected in the third extract.

TABLE 1

Extraction recovery of phenolic resin in particulate matter

| Sample | Concentration of phenolic resin ($\mu\text{g g}^{-1}$) | | | Recovery (%) | |
|--------|--|-------|-------|--------------|-----------------|
| | Run 1 | Run 2 | Run 3 | $1/(1+2+3)$ | $(1+2)/(1+2+3)$ |
| A | 200.0 | 31.0 | 0 | 86.5 | 100.0 |
| B | 196.0 | 35.8 | 0 | 84.6 | 100.0 |
| C | 212.0 | 30.2 | 0 | 87.5 | 100.0 |
| D | 315.0 | 53.5 | 0 | 85.5 | 100.0 |
| E | 325.0 | 41.3 | 0 | 88.7 | 100.0 |
| F | 409.0 | 68.8 | 31.9 | 80.2 | 93.7 |
| G | 403.0 | 73.9 | 9.2 | 82.9 | 98.1 |
| H | 431.0 | 81.0 | 0 | 84.2 | 100.0 |
| I | 493.0 | 79.1 | 8.4 | 84.9 | 98.5 |
| | | | | Av. 85.0 | 98.9 |

The percentage recovery in each extraction referred to the total amount of phenolic resin recovered by three extractions was determined. With only one extraction, the recovery of the phenolic resin in particulate matter samples was 80.2–88.7% (average 85.0%) and therefore the recovery was incomplete. By repeating the extraction twice, the average total recovery became 98.9%. Moreover, the particulate matter residue after three extractions with THF was dried, wrapped with Pyrofoil (670°C) and analysed directly by Py-GC. As a result, it was confirmed that the detected amounts of the pyrolysates such as phenol and *o*- and *p*-cresol were negligible. Accordingly, in this method, it was decided to carry out two ultrasonic extractions using THF.

Amounts of pyrolysates produced from phenolic resin

For six kinds of phenolic resins for brake friction materials, the pyrolysis of the resin samples was carried out at 670°C and the yields of the components obtained were measured.

Figure 3 shows a comparison of the yields from the various phenolic resins. Slight differences were observed in the yield of the respective components. The yields of phenol and *o*- and *p*-cresols were 12–17, 4–6 and 3–6%, respectively. As an index compound for the phenolic resin in the particulate matter originating from brake fric-

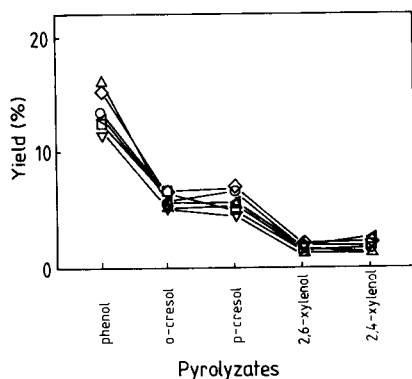


Fig. 3. Yields of pyrolysates from phenolic resins. ○ = Plyophen J-363; △ = Plyophen J-375; ◇ = Varcum TD-2003; ◁ = Varcum TD-2033; □ = Plyophen BA-5097; ▽ = Plyophen BA-5510.

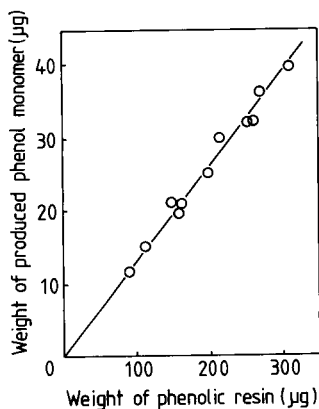


Fig. 4. Relationship between the amounts of phenolic resin and the amounts of phenol monomer produced.

tion materials phenol can be used because it is obtained in high yield. The relationship between the produced amounts of phenol and the amount of phenolic resin was investigated. The same amount of the different kinds of phenolic resins was taken, and pyrolysis was carried out under the same conditions. The mean values of the amounts of phenol produced for the same sample weight were calculated. The linear relationship between the amounts of phenolic resin pyrolysed (90–3300 µg) and the amounts of monomer produced is shown in Fig. 4. The concentration of phenolic resin can be calculated by the equation.

$$C_{\text{phenol}} = 0.116C_{\text{resin}}$$

where C_{phenol} is the amount of phenol produced (µg) and C_{resin} is the amount of phenolic resin pyrolysed (µg). The mean, the relative standard deviation and the repeatability, r , for the yield of phenol monomer obtained by pyrolysis of phenolic resin were 102 ± 8.70 µg, 8.6% and 24.4, respectively, from five repeated measurements with 0.880 mg of phenolic resin (Plyophen J-363) under the same conditions. Although the concentration of phenolic resin in dust on road cannot be assessed with high accuracy owing to the use of various types of phenolic resins, it will be possible to estimate the concentration of phenolic resin roughly and quickly from the amounts of phenol produced by the pyrolysis of particulate matter samples.

For the determination of phenolic resin, the effect of other compounds that co-exist with brake friction materials in particulate matter was investigated. The pyrolysis of asphalt materials, tyre tread rubber and engine oil was carried out using Py-GC under the same conditions. As a result, although many unknown components in the pyrograms were detected, no products that possessed the same retention time as that of phenol were observed. Therefore, interference from co-existing compounds can be neglected.

Contents of phenolic resin and asbestos in brake friction materials

Resin-mould type disc brake pads have been widely used in a popular class of cars on the market in Japan. The contents of the phenolic resins in commercially available disc brake pads, which were supplied by the Nihon Brake Industry and Hitachi Seisakusyo, was measured by the proposed method. The contents of the phenolic resin and other additives in commercial brake friction materials are given in Table 2. The average value of the phenolic resin content was $8.16 \pm 1.10\%$ (w/w) [15]. As about 6–12% (w/w) of the phenolic resin is generally included in a brake disc pad [16,17], it can be concluded that the

content of phenolic resin obtained in this experiment is a valid value.

Regarding the content of asbestos in the disc brake pads, it is known that its content is usually in the range 20–40% or 30% (w/w) on average [16–19]. It was assumed that the typical composition of commercial brake friction materials in the popular class of cars and that of the brake friction material particles in particulate matter which was emitted from automobiles and accumulated on roads are similar, i.e., ca. 30%. Accordingly, after determining the phenolic resin concentration in particulate matter samples, the concentrations of abraded brake friction materials and asbestos particles can be indirectly and approximately estimated using the equation

$$C_{\text{asbestos}} = 0.30C_{\text{resin}}/0.0816$$

where C_{asbestos} is the asbestos concentration in particulate matter (mg g^{-1}) and C_{resin} is the phenolic resin concentration (mg g^{-1}).

Applications

The contents of asbestos particles in particulate matter collected at the intersection of national highway Route 246 and the loop line No. 8 road (Tokyo) and at the entrance of Shin-

TABLE 2
Composition of commercial disc brake pads in a popular class of cars

| Proposed method [% (w/w)] | | Literature [% (w/w)] | | | | | | | | |
|--------------------------------|---|----------------------|-------|---------|------|-------|------------|-------|------|-------|
| Pyrolysates as an index | Run 1 | Run 2 | Run 3 | Average | | [16] | [17] | [19] | [18] | [14] |
| <i>Phenolic resin (binder)</i> | | | | | | | | | | |
| Phenol | A ^a | 8.06 | 8.32 | 8.04 | 8.14 | 8.13 | 8.16 | 6–12 | 6–12 | |
| | B ^a | 6.60 | 6.48 | 6.65 | 6.58 | | | | | |
| | C ^a | 10.02 | 9.33 | 9.59 | 9.65 | | | | | |
| o-Cresol | A ^a | 8.66 | 8.59 | 8.32 | 8.52 | 8.18 | ± 1.10 | | | |
| | B ^a | 6.55 | 6.70 | 7.60 | 6.95 | | | | | |
| | C ^a | 9.31 | 8.46 | 9.49 | 9.08 | | | | | |
| <i>Asbestos fibres</i> | | | | | | | | | | |
| Friction control agent | (Organic fillers (cashew, gum)) | | | | | 20–40 | 20–40 | 20–50 | 30 | 10–30 |
| | (Inorganic fillers (BaSO ₄ , CaCO ₃ , Sb ₂ O ₃)) | | | | | 5–10 | 5–10 | 10–20 | | |
| | (Inorganic fillers (graphite, MoS ₂ , Sb ₂ S ₃)) | | | | | 10–30 | 15–20 | | | |
| | (Metals (Fe, Cu, Al, Zn)) | | | | | 5–20 | | < 20 | | |
| | (Oxides (Al ₂ O ₃ , SiO ₂ , MgO)) | | | | | 5–20 | 5–20 | 10–30 | | |
| | | | | | < 5 | 1– 5 | | | | |

^a A, B and C are commercial disc brake pads in a popular class of cars.

TABLE 3

Concentrations of phenolic resin, brake friction materials and asbestos particles in particulate matter accumulated on roads in Tokyo and Kanagawa

| Sampling location | Concentration (mg g ⁻¹) | | | | | |
|--|-------------------------------------|---------|--------------------------|---------|----------|---------|
| | Phenolic resin | Average | Brake friction materials | Average | Asbestos | Average |
| National highway Route 246 | | | | | | |
| Shibuya station | 0.483 | | 5.92 | | 1.78 | |
| Kamiizumi town | 0.312 | | 3.82 | | 1.15 | |
| Setatamagawa | 0.595 | 0.433 | 7.29 | 5.42 | 2.19 | 1.63 |
| Sangenchaya rump | 0.397 | | 4.87 | | 1.46 | |
| Kamiyama | 0.424 | | 5.20 | | 1.56 | |
| Loop line No. 8 road | | | | | | |
| Tanihara | 0.251 | | 3.08 | | 0.924 | |
| Kamitakaido | 0.466 | 0.322 | 5.71 | 3.95 | 1.71 | 1.18 |
| Youga rump | 0.205 | | 2.51 | | 0.753 | |
| Denenchoufu | 0.366 | | 4.49 | | 1.35 | |
| Distance from entrance of Shinmorobuchi tunnel | | | | | | |
| 0 m (entrance) | 0.176 | | 2.16 | | 0.647 | |
| 8 m | 0.193 | | 2.36 | | 0.708 | |
| 15 m | 0.0461 | | 0.565 | | 0.170 | |
| 50 m | 0 | | 0 | | 0 | |

morobuchi tunnel on national highway Route 246 and its circumference (Kanagawa) in July 1990 were measured.

Table 3 shows the estimated concentration of asbestos particles in the particulate matter contributed by traffic. It was estimated that the asbestos particle concentration on the Route 246 road originating from brake friction materials was in the range 1.15–2.19 mg g⁻¹; on average, it was 1.63 mg g⁻¹, i.e., 0.163% (w/w). The estimated asbestos concentration in the particulate matter accumulated on loop line No. 8 road was 0.753–1.71 mg g⁻¹; on average, it was 1.18 mg g⁻¹ [0.118% (w/w)]. The estimated contents of asbestos at distances of 0, 8 and 15 m from the entrance of the tunnel in the direction perpendicular to the highway were 0.647, 0.708 and 0.170 mg g⁻¹, respectively. At distances ≥ 50 m from the entrance of the tunnel, no phenolic resin was detected.

It should be noted that when the asbestos included in brake friction materials wears physically by applying brakes and is released, most of the particles have sizes smaller than a few hundred nanometres. It is known that the amount of

asbestos with a long fibre shape, which are highly dangerous, is ca. 1% in released asbestos particles [10,13,20]. Therefore, it was assumed that the concentration of long asbestos fibres in the particulate matter accumulated on roads in Tokyo are in the range 7.5×10^{-4} – 2.2×10^{-3} (w/w).

REFERENCES

- 1 T. Kurihara, Kougai To Taisaku, 25 (1989) 971.
- 2 T. Nagoya, Kotsuzai Shigen, No. 80 (1989) 222.
- 3 K. Kimura, Roudou No Kagaku, 42 (1987) 4.
- 4 N. Kohyama and K. Morinaga, Kagaku Asahi, No. 6 (1987) 116.
- 5 J. Alste, D. Watson and J. Bagg, Atmos. Environ., 10 (1978) 583.
- 6 G.J. Jacko, R.T. DuCharme and J.H. Somers, Automob. Eng. (London), 81 (1973) 38.
- 7 M.H. Weintraub, A.E. Anderson and R.L. Gealer, Polym. Sci. Technol., 513 (1974) 623.
- 8 M.H. Weintraub, A.E. Anderson and R.L. Gealer, Am. Chem. Soc., Div. Org. Coat. Plast. Chem. Pap., 34 (1974) 389.
- 9 K. Tanaka, S. Ueda and N. Noguchi, Wear, 23 (1973) 349.
- 10 M.G. Jacko, R.T. DuCharme and J.H. Somers, SAE (Soc. Automat. Eng.) Tech. Pap., No. 730548 (1973).

- 11 A.N. Rohl, A.M. Langer, R. Klimentidis, M.S. Wolff and I.J. Selikoff, *Proc. R. Soc. Med.*, 70 (1977) 32.
- 12 J.R. Lynch, *J. Air Pollut. Control Assoc.*, 18 (1968) 824.
- 13 A.E. Anderson, R.L. Gealer, R.C. McCune and J.W. Sprys, *SAE (Soc. Automat. Eng.) Tech. Pap.*, No. 730549 (1973).
- 14 T. Kauppinen and K. Korhonen, *Am. Ind. Hyg. Assoc. J.*, 48 (1987) 499.
- 15 T. Saito, *Anal. Sci.*, 7 (1991) 901.
- 16 T. Shinbo, *Jidousya Gijyutsu*, 40 (1986) 1041.
- 17 K. Nakamura and T. Yoshimura, *Jidousya Gijyutsu*, 35 (1981) 639.
- 18 U. Knecht, H.J. Elliehausen, W. Judas and H.J. Weitowitz, *Int. J. Environ. Anal. Chem.*, 28 (1987) 227.
- 19 T. Mibe, *Jidousya Gijyutsu*, 44 (1990) 68.
- 20 A.D. Jones and R.W. Gale, *Ann. Occup. Hyg.*, 25 (1982) 39.

Comparison between different inorganic supports for the immobilization of amyloglucosidase and α -amylase to be used in enzyme reactors in flow-injection systems

Part I. Hydrolysis of maltose, maltooligosaccharides and soluble starch

Jenny Emnéus and Lo Gorton

Department of Analytical Chemistry, University of Lund, P.O. Box 124, S-221 00 Lund (Sweden)

(Received 11th August 1992)

Abstract

Amyloglucosidase was immobilized on twelve different inorganic supports by silanization with aminopropyltriethoxysilane followed by glutaraldehyde activation. Two of the supports were alumina based and were also functionalized with polyethylenimine (PEI) followed by glutaraldehyde activation. The different enzyme immobilized supports were packed in identical reactors (30 μ l) and compared with respect to optimum pore size, surface area, immobilization efficiency and enzyme activity for three substrates: soluble starch, maltooligosaccharides and maltose. A comparison of five silanized controlled-pore glasses (CPG) with different pore sizes resulted in the highest immobilization efficiency on the support with a pore size of 170 Å and a surface area of 150 m² g⁻¹. A comparison of all the silanized enzyme supports again gave the highest immobilization efficiency on 170 Å CPG, but the highest enzyme activity was obtained on a new support, Micropil A, with a pore size of 300 Å and a surface area of 100–150 m² g⁻¹. The functionalization of the alumina supports with aminopropyltriethoxysilane proved to be superior to that with PEI.

Keywords: Enzymatic methods; Flow injection; Amyloglucosidase; Enzyme reactors; Maltooligosaccharides; Maltose; Starch

Work in this and other laboratories has been focused on the development of flow-injection (FI) systems and post-column liquid chromatographic systems using immobilized enzyme reactors (IM-ERs) for the identification and determination of starch polymers [1–8]. In the course of this development, a number of problems were encountered, mainly that of starch itself. Starch is the general name for large α -D-glucose-containing polymers which, depending on the biological ori-

gin and age of the plant, vary in size, shape, molecular weight, degree of branching, amylose to amylopectin ratio and the content of lipids and proteins [9]. The ultimate aim is to develop a fast FI system that can determine starch regardless of the criteria mentioned above. As the glucose monomers (C₆H₁₀O₅)_n, constituting the building blocks of the starch polymer, are the sole standardizable chemical components available in starch, the determination of the total content of glucose can be a quantitative measure of the amount of starch in starch material. It is therefore essential to achieve on-line 100% degradation of the original starch molecule to glucose.

Correspondence to: J. Emnéus, Department of Analytical Chemistry, University of Lund, P.O. Box 124, S-221 00 Lund (Sweden).

In some previous studies, two different starch-hydrolysing enzymes were used, a thermostable α -amylase (Termamyl), which hydrolyses starch to smaller fractions consisting of α -limit dextrins, maltooligosaccharides and maltose, and amyloglucosidase (AMG), which hydrolyses the remaining fractions to glucose. It was found that the completion of the hydrolysis depended on the origin of the starch. Native potato starch was totally hydrolysed to glucose, but native starch from wheat, corn and rice was not [5,7]. According to the literature this can be due to the varying contents of lipids and proteins of starch from different origins [9–13]. Amylose–lipid complex formation is reported to prevent the access of the enzyme to the starch molecule or to cause the enzyme not to recognize the starch molecule in the complexed configuration. Evidently this will result in incomplete degradation of the starch molecule. Potato starch contains a much smaller amount of lipids than the other starch types, which could explain why a complete degradation of this type of starch is obtained. An increase in temperature or a tenfold increase in the α -amylase concentration has been reported to increase the degree of hydrolysis of lipid-containing starch [10,11]. A strong increase in the degree of hydrolysis of native wheat, corn and rice starch when the residence time in the α -amylase reactor was prolonged has been reported [7]. The time for analysis was, however, extremely long (> 60 min) owing to the long residence time and the large AMG reactor used in comparison with what is commonly used in FI.

In order to achieve shorter times of analysis, the need for highly efficient enzyme reactors is a major goal. The efficiency of a packed-bed reactor will be dependent on a number of factors. A high enzyme loading on the support should be realized, retaining a high activity of the bound enzyme. To achieve these goals the choice of the enzyme support and immobilization chemistry should be optimized. This work was aimed at finding a new and better support material and an optimum pore size for the immobilization of AMG. Two of the alumina-based supports, Biotage and Micropil C, were additionally functionalized with a procedure reported to be superior

using polyethyleneimine (PEI) [14–16], and were compared with their corresponding silanized counterparts to see whether the AMG reactors showed an improved behaviour.

EXPERIMENTAL

Enzymes and enzyme reactors

Amyloglucosidase (AMG) reactors. Twelve different support materials were used: controlled-pore glass, CPG-10 (Serva, Heidelberg, Germany), particle size 37–74 μm , pore size 117 Å (Cat. No. 44722) and surface area 210 $\text{m}^2 \text{g}^{-1}$ (support 1), pore size 170 Å (Cat. No. 44732) and surface area 150 $\text{m}^2 \text{g}^{-1}$ (support 2), pore size 230 Å (Cat. No. 44742) and surface area 110 $\text{m}^2 \text{g}^{-1}$ (support 3), pore size 500 Å (Cat. No. 44762) and surface area 50 $\text{m}^2 \text{g}^{-1}$ (support 4) and pore size 729 Å (Cat. No. 44772) and surface area 36 $\text{m}^2 \text{g}^{-1}$ (support 5); Micropil A (Microporous Materials, Braunston, UK, Art. No. SP4/100), particle size 7–20 μm , pore size 300 Å and surface area 100–150 $\text{m}^2 \text{g}^{-1}$ (support 6); Micropil C (Microporous Materials, Art. No. SP3/22), particle size 5–40 μm , pore size 130 Å and surface area 100 $\text{m}^2 \text{g}^{-1}$ (support 7); Uncoated Neutral Unisphere-PBD Alumina (Biotage, Charlottesville, VA, USA, Lot. No. PP77), particle size 8 μm , pore size 250 Å and surface area 50 $\text{m}^2 \text{g}^{-1}$ (support 8); Lichrospher (Merck, Darmstadt, Germany, Art. No. 9313), particle size 10 μm , pore size 1000 Å and surface area 5 $\text{m}^2 \text{g}^{-1}$ (support 9); Kromasil (Eka Nobel, Surte, Sweden, Lot. No. AT 0002), particle size 16 μm , pore size 100 Å and surface area 340 $\text{m}^2 \text{g}^{-1}$ (support 10); hydroxyapatite (Pentax, Asahi Optical, Tokyo, Lot. No. IAF 1823), particle size 10 μm (support 11); and hydroxyapatite (Pentax, Lot. No. KBH 2514), particle size 20 μm (support 12). All supports were activated with glutaraldehyde according to a previously reported procedure [17–19] modified as described below.

The supports were first treated with concentrated nitric acid (except the two hydroxyapatite supports as they were totally dissolved in nitric acid) for 2 h, after which they were thoroughly washed with highly purified water (Millipore, Milli-RO4) and dried at 190°C in a furnace oven

for 6 h. The twelve supports were then silanized by refluxing in a boiling water-bath with 10% 3-aminopropyltriethoxysilane (Janssen Chimica) in dry toluene for 40 min, after which they were thoroughly washed with toluene and acetone over a G3 or G4 filter, depending on the particle size of the support, and dried in a furnace oven at 115°C overnight. The silanized supports were activated at reduced pressure and 4°C with 2.5% glutaraldehyde in 0.1 M phosphate buffer (pH 7) for 30 min. Prior to dilution of commercial 25% glutaraldehyde solution (Sigma), it was shaken with activated carbon and centrifuged to remove polymeric material. The clear supernatant was then used. The Schiff bases produced were then reduced by adding 7 mg of sodium cyanoborohydride (NaCNBH₃) (Janssen Chimica) to 100 mg of support and the reaction was allowed to proceed for another 90 min. The activated supports were thoroughly washed with highly purified water over a G3 or G4 filter.

A 500-mg amount of Biotage or Micropil C was added to 3.0 ml of a 10% solution of polyethylenimine (PEI) (Sigma) in phosphate buffer (pH 10) and allowed to react at reduced pressure for 10 min and then at atmospheric pressure over 2 days at room temperature. The supports were then thoroughly washed over a G4 or G5 filter with 10 mM phosphate buffer (pH 7.4). The PEI-functionalized supports were then activated at reduced pressure and 4°C with 2.5% glutaraldehyde as above in 0.1 M phosphate buffer (pH 7) for 30 min. The Schiff bases produced were then reduced as above with NaCNBH₃ and the reaction was allowed to continue for 90 min. The activated supports were thoroughly washed with highly purified water over a G4 filter.

An aliquot of 700 mg of amyloglucosidase (AMG) (EC 3.2.1.3) from *Aspergillus niger*, 100 IU mg⁻¹ (Merck), was dissolved in 14 ml of 0.1 M phosphate buffer (pH 7), resulting in a solution containing 46 mg AMG ml⁻¹. The solution was kept at 4°C before being added to the aminopropyl-functionalized and glutaraldehyde-activated supports.

A 1-ml volume of the prepared AMG solution and 200 μl of 0.1 M phosphate buffer (pH 7) were added to 100 mg of each of the twelve

glutaraldehyde-activated supports and allowed to react at 4°C and reduced pressure for 30 min. The Schiff bases produced between the enzyme and supports were reduced as above with NaCNBH₃ and the reaction was continued for 90 min. The enzyme supports were washed with 0.1 M acetate buffer (pH 4.5). The coupling yields were measured spectrophotometrically as the protein content of the supernatant at 280 nm before and after immobilization and were as follows: for support 1, 35%; 2, 59%; 3, 46%; 4, 39%; 5, 30%; 6, 57%; 7, 24%; 8, 33%; 9, 32%; 10, 25%; 11, 30% and 12, 11%.

A 350-mg amount of AMG (EC 3.2.1.3) from *Aspergillus niger*, 100 IU mg⁻¹ (Merck), was dissolved in 7 ml of 0.1 M phosphate buffer (pH 7) resulting in a solution containing 46 mg AMG ml⁻¹. The solution was kept at 4°C before being added to the PEI-functionalized support.

A 2.5 ml volume of the prepared AMG solution was added to each of the Biotage and Micropil C PEI-functionalized and glutaraldehyde-activated supports and the coupling was performed as described above. The coupling yields were 18 and 30% for Micropil C and Biotage, respectively, measured as above.

The fourteen different immobilized enzyme supports were then packed into identical reactors (30 μl, 10 mm × 2 mm i.d.) and stored in 0.1 M acetate buffer (pH 4.5) and 4°C. A BET nitrogen adsorption analysis was done on both the unmodified and enzyme-modified Kromasil and Micropil A supports with single-point surface area measurements (Flowsorb II 2300).

Glucose dehydrogenase (GDH)–mutarotase (MUT) reactor. A 4.56-mg (1012-U) amount of glucose dehydrogenase (GDH) (EC 1.1.1.47) from *Bacillus megaterium*, 220 U mg⁻¹ (Merck), 0.35 mg (1750 U) of mutarotase (MUT) (EC 5.1.3.3) from porcine kidney (Sigma) and a few mg of nicotinamide adenine dinucleotide (NAD⁺) (Merck), were dissolved in 0.1 M phosphate buffer (pH 7). The enzyme solution (1 ml) was added to 150 mg of aminopropylsilanized and glutaraldehyde-activated CPG-10 of particle size 37–74 μm and pore size 500 Å according to a previously described procedure [17]. The immobilized enzyme support was packed into a 240-μl reactor

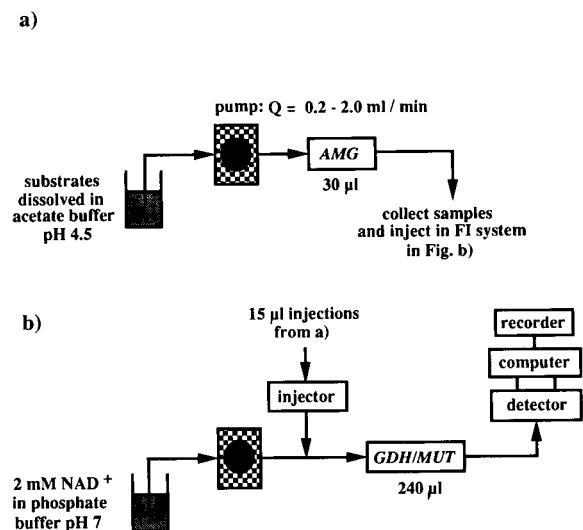


Fig. 1. Flow systems (a) for steady-state operational mode of the AMG reactors and (b) for FI determination of the glucose in the effluent from the AMG reactors in (a).

(7.6 cm \times 2 mm i.d.) and stored at 4°C in 0.1 M phosphate buffer (pH 7) also containing 0.5 M NaCl.

Analytical system

The various parts of the system used for investigating the performance of the fourteen reactors are depicted in Fig. 1a and b. In the steady-state set-up in Fig. 1a, a Model 2150 LC pump (LKB, Bromma, Sweden) was continuously pumping substrate dissolved in 0.1 M acetate buffer (pH 4.5) through each of the fourteen AMG reactors, one at a time. Seven different flow-rates between 0.2 and 2.0 ml min⁻¹ were investigated. For each flow-rate and reactor, samples of the effluents were collected and injected into the FI system, as shown in Fig. 1b, to examine the amount of glucose produced in the AMG reactors. Before injection, the effluents were diluted appropriately so that the concentration of glucose produced in the AMG reactors would fall within the linear range of the glucose-determining system in Fig. 1b. At a constant flow-rate of 1.0 ml min⁻¹, another Model 2150 LC pump was continuously pumping a solution of 0.1 M phosphate buffer (pH 7), also containing 2 mM NAD⁺, through the GDH-MUT reactor in the FI system in Fig. 1b.

Before start-up the phosphate buffer was degassed for 10 min under reduced pressure to prevent the appearance of microbubbles in the flow system. The samples collected from the effluents of the different AMG reactors were injected from a 15- μ l injection loop into the flow stream with a pneumatically operated injection valve (Cheminert Type SVA, Kemila, Stockholm, Sweden). PTFE tubing of 0.5 mm i.d., with Altex screw couplings, connected the various parts of the flow system. All buffers were prepared from ultrapure water and chemicals of analytical-reagent grade. Model 2151 variable-wavelength flow-through detector (LKB) was used for monitoring the NADH produced from the GDH-MUT reactor at 340 nm.

Solutions of D-glucose (BDH), 50 mM maltose (Sigma) 50 mM maltooligosaccharide mixture (PF, Pfanstiehl Laboratories, Waukegan, IL) and 50 mM soluble starch (Zulkowsky, Merck) were prepared by dissolving appropriate amounts in 0.1 M acetate buffer (pH 4.5). All concentrations were calculated in terms of the amount of glucose units contained, where every glucose unit in the maltooligosaccharide and starch solutions was given a mean molecular weight of 162.14. Kathon CG (50 μ l l⁻¹) containing 1.125% methylchloroisothiazolinone and 0.375% methylisothiazolinone was added to the acetate buffer to prevent bacterial growth in the system.

RESULTS AND DISCUSSION

There is no general rule on how to immobilize enzymes and an empirical approach is always required. Each enzyme is unique in its characteristics and this will influence which immobilization procedure should be chosen for a particular enzyme. The type of linkage, the support material and the method of immobilization may have pronounced effects, on the substrate binding constant and the maximum rate of reaction, and also on the pH optimum and sensitivity towards changes in ionic strength. The Michaelis-Menten constant, K_M , may thus be altered by more than one order of magnitude as compared with the soluble enzyme [20]. The enzyme, enzyme sub-

strate(s), and enzyme support therefore have to be considered independently of each other in terms of physio-chemical properties before immobilization.

CPG is a macroporous high-silica glass and is one of the most widely used supports today. Its silanol groups provide a mildly reactive surface for introducing different functionalities. This is true also for other silica-based supports and for ceramic- and metal oxide-based supports. Functionalization with a silane derivative, reacting with the oxide or hydroxide groups on glass, silica, ceramics or metal oxide supports, is a common procedure [21,22]. Aminopropylsilanized CPG has so far proved to be the most successful functionalized support for further activation and binding of the enzyme(s) [23].

The aminopropyl-functionalized support can be activated through several different procedures such as glutaraldehyde, isothiocyanate, carbodiimide, triazine, azide and bromoacetate coupling [22]. The most commonly used method is, however, glutaraldehyde coupling [17,21], because of its simplicity and applicability to most enzymes with good results. A carbonyl residue is introduced which is prone to subsequent reaction with the nucleophilic amino acid groups on the enzyme. For both activation of the functionalized support and binding to the enzyme, a Schiff base is formed [24].

The functionalization of the support with PEI has been reported to improve the performance of several immobilized enzymes, including AMG [14–16]. The reason for this is believed to be an increased amount of introduced amine groups on the support surface, which, followed by activation with glutaraldehyde, results in a larger number of aldehyde groups that can react with the amine groups of enzymes.

As the condensation reactions above are acid catalysed, the optimum pH will be a compromise between the preferred acidic catalytic conditions, that is, the pK_a of the amino acid residue and the stability of the enzyme at different pH values. The formation of the Schiff base is a reversible reaction, which can be suppressed by reducing the imine form ($-N=C\langle$) to the amine form ($-NH-CH\langle$) with a weak reducing agent such as

sodium cyanoborohydride ($NaCNBH_3$). As $NaCNBH_3$ is a weak reducing agent it does not reduce aldehydes or ketones at neutral pH, which otherwise would be damaging to the immobilized enzyme [18,19]. Additionally, the imine formed is itself a reactive species and is prone to further reaction with a new nucleophilic agent such as water, which may result in an unsuccessful activation of the functionalized material and/or the release of the immobilized enzyme from the support.

In earlier reports, the support mainly studied was CPG, functionalized and activated with aminopropyltriethoxysilane and glutaraldehyde, respectively. The objective was therefore to compare different materials and find a more suitable material for the immobilization. To be able to compare different supports, in a first investigation the same immobilization chemistry was chosen for all immobilizations, which thus includes only the twelve silanized and glutaraldehyde-activated supports.

Influence of surface area and pore size on immobilization efficiency

A high specific surface area makes a high enzyme loading possible and can be achieved by using small particle and pore sizes. In addition, small dimensions result in small additional band broadening effects, but will cause increased pressure drops over the IMER as it will be proportional to the square of the particle diameter [25]. An inhomogeneous packing and an inhomogeneous support material will also give rise to large band broadening but can be avoided by using a more balanced density type of slurry technique [26] or a support with more homogeneous particles in size and/or shape. The pores have to be large enough that the enzyme can enter the porous material in the actual immobilization procedure and large enough for the substrate(s) to reach all enzyme sites within the porous material. The conclusion to be drawn is that the smallest possible pore diameter should be used in order to compound as much enzyme as possible into each unit volume as well as making sure that the substrate(s) has access to the enzyme within the pore structure.

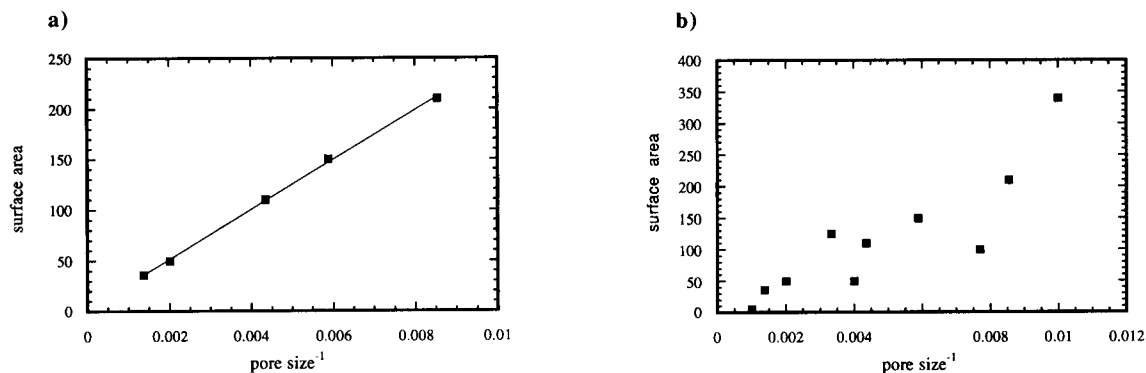


Fig. 2. Plots of surface area (m² g⁻¹ support) versus inverse of pore size (Å⁻¹). (a) CPG supports; (b) all ten supports.

Among the ten supports investigated there are five CPG materials differing only in their pore sizes. This means that it can be assumed that there are no great differences in surface structure or surface chemistry so that no microenvironmental effects will influence how the binding of the enzyme is affected by the pore sizes and surface areas of the supports. The following discussion is therefore divided into two parts. First, a separate investigation of CPG was done to evaluate the strict influences of pore size and surface area. Second, all supports are included in the investigation to evaluate the influence of the differences of the microenvironment of the various supports.

In Table 1, the physical parameters and the kinetic data for soluble starch, maltooligosaccharides and maltose of ten investigated supports immobilized with AMG are listed. Hydroxyap-

atite (particle size 10 and 20 μm) could not be included in the investigation as the packing of these supports caused problems imposed by very large back pressures. It appears that some chemical reaction has changed the supports by making them aggregate and clog when packing. This apparently happened during either the functionalization, activation and/or immobilization reaction, as there were no problems when packing these materials into reactors prior to chemical modification.

In Fig. 2a, a plot of surface area versus the inverse of pore size for CPG results in a linear increase in surface area with decrease in pore size, as expected [21,27]. One would therefore expect an increase in the amount of immobilized AMG with increasing surface area. However, as shown in Fig. 3, where the immobilization effi-

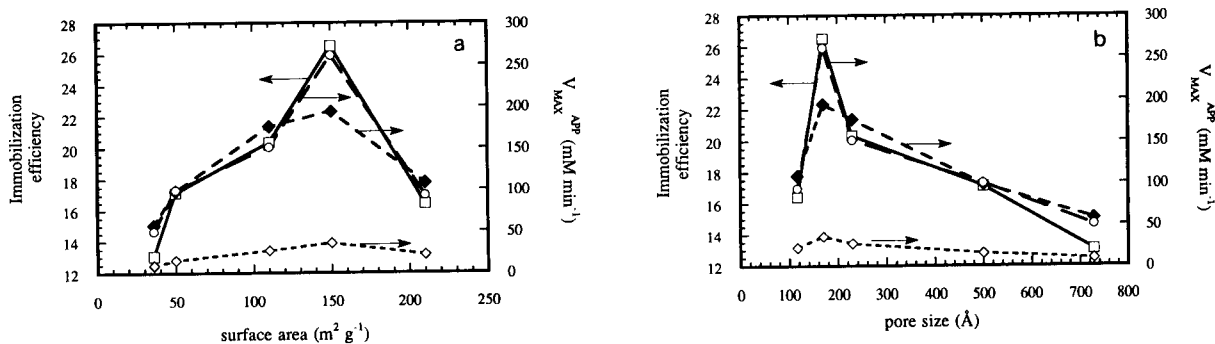


Fig. 3. (a) Immobilization efficiencies in mg of AMG per 100 mg of CPG (left ordinate) (□) and V_{\max}^{app} for (♦) soluble starch, (○) maltooligosaccharides and (◇) maltose in mM min⁻¹ (right ordinate) plotted versus the surface area of the supports (m² g⁻¹). (b) Immobilization efficiencies in mg of AMG per 100 mg of CPG (left ordinate) (□) and V_{\max}^{app} for (♦) soluble starch, (○) maltooligosaccharides and (◇) maltose in mM min⁻¹ (right ordinate) plotted versus the pore size of the supports (Å).

ciency (left ordinate) is plotted versus (a) surface area and (b) pore size, an immobilization optimum is obtained for a surface area of $150 \text{ m}^2 \text{ g}^{-1}$ and a pore size of 170 \AA . This optimum can be explained by the combined effects of a large surface area for binding of the enzyme and an optimum pore size for the enzyme to enter in the immobilization reaction. The pore size of 117 \AA is apparently too small for the enzyme to enter, but its external surface is still larger than the total surface area of the support with a pore size of 729 \AA , which is illustrated by a better immobilization efficiency on the former material (see

also Table 1). If the size of the enzyme is not known, but its approximate molecular weight is available, it is possible to find the average pore diameter in which the enzyme should fit, provided that it is assumed that the protein is globular. According to the manufacturer of CPG, a mean particle diameter of 117 \AA excludes globular proteins with molecular weights higher than about 150 000 [27]. The molecular weight of the AMG used in this work is reported by Merck to be 97 000, which would make a pore size of 117 \AA large enough to be used. Purification experiments with AMG on a Mono Q ion-exchange resin gave

TABLE 1

Physical parameters for all supports studied and kinetic parameters for immobilized AMG on the various supports using soluble starch, maltooligosaccharides and maltose as substrates

| Substrate | Reactor No. | Support | Pore size (\AA) | Surface area ($\text{m}^2 \text{ g}^{-1}$) | AMG per 100 mg support (mg) | K_{ps}^{app} (min^{-1}) | $V_{\text{max}}^{\text{app}}$ (mM min^{-1}) | K_M^{app} (mM) | Necessary reactor volume to obtain 99% conversion (μl) |
|-----------------------|-------------|-------------|----------------------------|--|-----------------------------|---|--|-------------------------|---|
| Soluble starch | 1 | CPG | 117 | 210 | 16.4 | 2.64 | 108.0 | 40.8 | 523 |
| | 2 | CPG | 170 | 150 | 26.5 | 4.98 | 193.8 | 38.9 | 277 |
| | 3 | CPG | 230 | 110 | 20.3 | 4.38 | 175.8 | 40.2 | 315 |
| | 4 | CPG | 500 | 50 | 17.1 | 2.22 | 98.4 | 44.4 | 622 |
| | 5 | CPG | 729 | 36 | 13.1 | 1.32 | 57.6 | 43.7 | 1047 |
| | 6 | Micropil A | 300 | 100–150 | 24.3 | 10.32 | 401.4 | 38.9 | 134 |
| | 7 | Micropil C | 130 | 100 | 11.0 | 1.68 | 74.4 | 44.4 | 822 |
| | 8 | Biotage | 250 | 50 | 14.4 | 3.72 | 142.2 | 38.3 | 371 |
| | 9 | Lichrospher | 1000 | 5 | 14.3 | 1.80 | 76.2 | 42.3 | 768 |
| | 10 | Kromasil | 100 | 340 | 11.0 | 0.42 | 20.4 | 47.9 | 3289 |
| Maltooligosaccharides | 1 | CPG | 117 | 210 | 16.4 | 2.22 | 93.0 | 41.7 | 622 |
| | 2 | CPG | 170 | 150 | 26.5 | 6.13 | 261.0 | 42.6 | 225 |
| | 3 | CPG | 230 | 110 | 20.3 | 3.90 | 151.2 | 38.7 | 354 |
| | 4 | CPG | 500 | 50 | 17.1 | 2.28 | 99.6 | 43.8 | 606 |
| | 5 | CPG | 729 | 36 | 13.1 | 1.08 | 49.8 | 46.2 | 1279 |
| | 6 | Micropil A | 300 | 100–150 | 24.3 | 8.16 | 329.4 | 40.4 | 169 |
| | 7 | Micropil C | 130 | 100 | 11.0 | 4.92 | 180.6 | 36.7 | 281 |
| | 8 | Biotage | 250 | 50 | 14.4 | 6.72 | 242.4 | 36.1 | 206 |
| | 9 | Lichrospher | 1000 | 5 | 14.3 | 3.12 | 127.2 | 40.7 | 443 |
| | 10 | Kromasil | 100 | 340 | 11.0 | 0.72 | 33.6 | 46.8 | 1919 |
| Maltose | 1 | CPG | 117 | 210 | 16.4 | 0.46 | 21.6 | 46.9 | 1495 |
| | 2 | CPG | 170 | 150 | 26.5 | 0.78 | 35.4 | 45.1 | 886 |
| | 3 | CPG | 230 | 110 | 20.3 | 0.57 | 26.4 | 46.3 | 1212 |
| | 4 | CPG | 500 | 50 | 17.1 | 0.30 | 15.0 | 47.8 | 2303 |
| | 5 | CPG | 729 | 36 | 13.1 | 0.18 | 9.0 | 48.6 | 3838 |
| | 6 | Micropil A | 300 | 100–150 | 24.3 | 1.08 | 46.8 | 43.3 | 640 |
| | 7 | Micropil C | 130 | 100 | 11.0 | 0.30 | 14.4 | 47.7 | 2303 |
| | 8 | Biotage | 250 | 50 | 14.4 | 0.42 | 19.8 | 47.1 | 1645 |
| | 9 | Lichrospher | 1000 | 5 | 14.3 | 0.21 | 10.2 | 48.2 | 3289 |
| | 10 | Kromasil | 100 | 340 | 11.0 | 0.06 | 3.0 | 49.1 | 11513 |

four different fractions eluting with AMG activity, implying an oligomeric structure of AMG. In electrophoretic experiments with AMG, Paszynski et al. [28] found one main band with a molecular weight of 70 000 and three additional bands with molecular weights of 136 000, 209 000 and 263 000. The size suggested in that report would be excluded by a pore size of 117 Å, but large enough to fit in a pore size of 170 Å, which according to the manufacturer excludes globular proteins with molecular weights higher than about 400 000 [27].

Additionally, Artyomova et al. [29] found that a pore size 5–10 times larger than the protein globules possesses the maximum capacity and, hence, the maximum accessible surface for enzyme penetration and their chemical grafting, which again suggests that 170 Å is a more appropriate pore size of the CPG material to use. Weetall [21] found an optimum pore size of 300 Å for an immobilized AMG based on activity measurements. According to Stratilová et al. [30], the enzymatic pattern and kinetics both for high- and low-molecular-weight substrates was greatly influenced by the size of the pore. Regardless of whether the enzyme has a monomeric or oligomeric structure, the discussion above indicates, together with the present results shown in Fig. 3b and Table 1, that a pore size of 117 Å excludes the enzyme, and that the combined effects of a sufficiently large pore size and a large surface area result in a high enzyme loading.

On comparing all ten supports, the picture becomes more complicated. In Fig. 2b, the surface areas for all supports are plotted against the inverse of the corresponding pore sizes and illustrate fairly well a linear increase in surface area with decreasing pore size. The deviation from a strict linearity is probably due to the structural variations in both the shape of the particles and the pore structure between the different types of supports. The geometric aspects of pore structure are often simplified to the assumption that pores are in general an assembly of non-intersecting cylindrical capillaries. This is, however, an assumption that demands a pore uniformity that is far from reality. The pores in porous materials can be described by two mathematical models, namely corpuscular and spongy systems [25]. In corpuscular systems, the pores consist of the interstices between discrete particles of a solid material, where the pore structure depends on the shape of the particles and their mutual arrangement. The sizes of the pores are controlled by the size of the particles and their packing density. Most amorphous xerogels belong to this type. In spongy systems, the pores consist of channels, hollows or cavities in the solid matter, interconnected by narrow passages. Porous glasses such as CPG belong to this latter type. In addition to these two main types, mixed systems can also be observed. It can be assumed that a better correlation between surface area and pore size in Fig. 2b would be expected for different pore sizes within

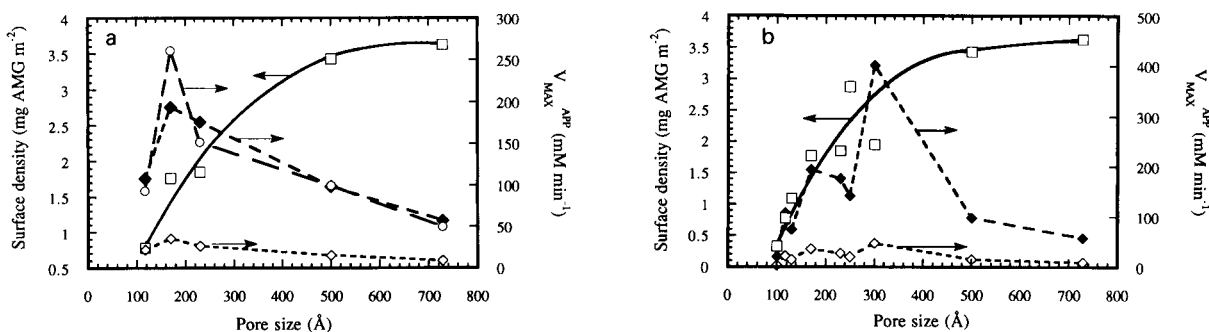


Fig. 4. (a) Enzyme surface density in mg AMG m^{-2} for CPG (left ordinate) (\square) and $V_{\text{max}}^{\text{app}}$ for (\blacklozenge) soluble starch, (\circ) maltooligosaccharides and (\diamond) maltose in mM min^{-1} (right ordinate) plotted versus the pore sizes of CPG (Å). (b) Enzyme surface density in mg AMG m^{-2} for all supports (left ordinate) (\square) and $V_{\text{max}}^{\text{app}}$ for (\blacklozenge) soluble starch and (\diamond) maltose in mM min^{-1} (right ordinate) plotted versus the pore size (Å).

the same type of material, as seen for CPG in Fig. 2a.

When comparing the immobilization efficiency for all supports, the pore size and structure are again important. An investigation of the surface of two of the materials was undertaken using a BET nitrogen adsorption technique. Kromasil and Micropil A were investigated both for the unmodified silica surfaces and after modification of the surfaces with immobilized AMG. According to the manufacturers, the surface areas of Kromasil and Micropil A are 340 and 100–150 $\text{m}^2 \text{g}^{-1}$, respectively. According to the results of the BET analysis, the surface area of Kromasil was 265 $\text{m}^2 \text{g}^{-1}$ and that of Micropil A 140 $\text{m}^2 \text{g}^{-1}$, indicating that the values given by the manufacturers are not fully reliable. The surface areas after immobilization were calculated to be 208 and 90 $\text{m}^2 \text{g}^{-1}$ for Kromasil and Micropil A, respectively. From Table 1 it can thus be seen that 11 mg of AMG apparently cover 5.7 m^2 per 100 mg of the Kromasil surface and for Micropil A 24 mg of AMG cover only 5.0 m^2 per 100 mg of the surface. The most likely reason for these results is that the pore entries of the Kromasil pores are clogged by immobilized AMG so that the unmodified surface inside the pores is not detected by a BET nitrogen adsorption, thus giving a false value for the modified surface. Another interesting result is that only about 36% of the Micropil A surface seems to be modified, indicating that a large portion of the interior of the particles is not accessible to AMG.

In Fig. 4, the enzyme surface density in mg AMG m^{-2} (left ordinate) for (a) CPG and (b) all supports is plotted against the pore size. It can be seen that as the pore size increases the enzyme surface density increases until a steady state is reached for a pore size of about 500 Å. This indicates that as the pore size increases, a larger portion of the surface is utilized until a surface coverage equal to a monolayer of about 3.5 mg AMG m^{-2} is reached. In Fig. 5, the immobilization efficiency (left ordinate) is plotted against surface area, showing the complexity of the binding of the enzyme to different types of supports (see also Table 1). It would be expected that the much larger surface area of Kromasil with a pore

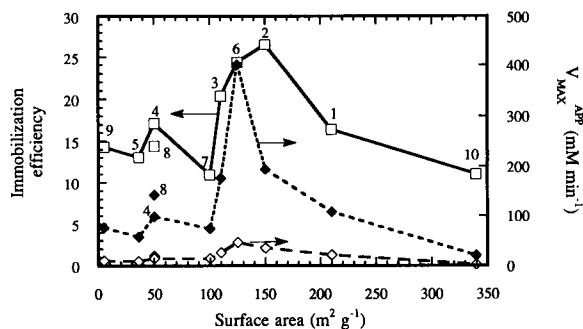


Fig. 5. Immobilization efficiencies in mg of AMG per 100 mg of all supports (\square) and V_{\max}^{app} for (\blacklozenge) soluble starch and (\diamond) maltose in mM min^{-1} (right ordinate) plotted versus the surface areas of all supports ($\text{m}^2 \text{g}^{-1}$).

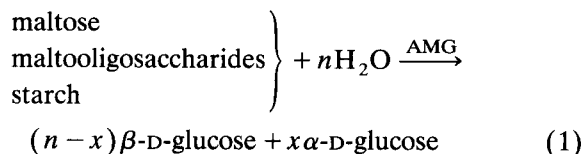
size of 100 Å (No. 10) compared with CPG with a pore size of 117 Å (No. 1) would result in a better immobilization efficiency at the external surface of the former. The high surface area of Kromasil is, however, a result of a very high porosity, making the external surface virtually negligible. On comparing Biotage with a pore size of 250 Å (No. 8) with CPG with a pore size of 500 Å (No. 4), Biotage has a lower immobilization efficiency even though the surface areas are the same. This might be explained by either an unsuccessful silanization procedure or by some microenvironmental property such as the type of pore structure of the material. The pore structure could be incompatible with allowing the enzyme to diffuse into the pores. Additionally, Biotage is an alumina-based support and CPG is a silica-based support, which could chemically influence the binding properties of the enzyme.

As can be seen, the highest immobilization efficiency is obtained for CPG with a pore size of 170 Å (No. 2) followed by Micropil A with a pore size of 300 Å (No. 6), which is apparently due to the combined effects of pore size and surface area. The reason why the immobilization efficiency on Micropil C with a pore size of 130 Å (No. 7) is so much lower than those on Micropil A (No. 6) and CPG with a pore size of 117 Å (No. 1) might again be explained by the inability of the enzyme to enter the pores and its lower surface area, and also the fact that Micropil C is an alumina-based support whereas Micropil A and CPG are silica-based supports. The conclusion to

be drawn from this discussion is that a high immobilization efficiency can be reached with the proper combination of pore size and surface area and by considering the structure and composition of the support material.

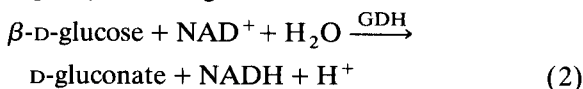
Enzyme kinetics

The enzymatic reactions discussed here refer to the hydrolysis of maltose, maltooligosaccharides and soluble starch to glucose by AMG according to the following reaction (see Fig. 1a):

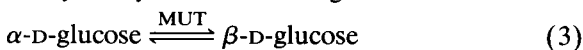


The α -1,4-linkages of the saccharides are attacked from the non-reducing ends of the substrate molecules, cleaving off one β -D-glucose unit at a time. When a branching point in the α -1,6-position is reached it will be hydrolysed if the next linkage is in the α -1,4-position. The α -1,6-linkages are, however, hydrolysed at a lower rate than the α -1,4-linkages and smaller molecules are hydrolysed at a lower rate than that of larger molecules [31]. This means that in the course of starch hydrolysis, the kinetic rate constant decreases as the substrate molecule decreases in molecular size, eventually reaching the kinetic rate constant of the reaction for the hydrolysis of maltotriose and maltose, respectively.

The β -D-glucose formed in reaction 1 is then oxidized in the presence of an excess amount of NAD^+ in an IMER in the FI system containing a co-immobilized GDH and MUT reactor seen in Fig. 1b, according to the reaction

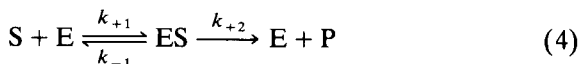


As GDH is only active on the β -form of glucose, the α -D-glucose also formed in reaction 1 needs to be converted into its corresponding β -form catalysed by MUT according to the reaction



The NADH produced in reaction 2 will be proportional to the amount of glucose produced in the different AMG reactors.

The simplest enzyme-catalysed reaction obeying the Michaelis–Menten model is that in which only one substrate participates in the reaction:



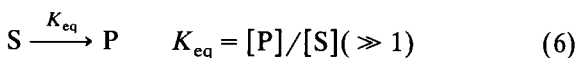
The rate equation according to Michaelis–Menten is

$$-\partial[\text{S}]/\partial t = V_{\max}[\text{S}]/(K_M + [\text{S}]) \quad (5)$$

where $K_M = [(k_{-1} + k_{+2})/k_{+1}]$ is the Michaelis–Menten constant and V_{\max} is the maximum reaction rate at a particular enzyme concentration.

Enzyme-catalysed reactions with one substrate binding site per enzyme and the formation of a single intermediate complex are very rare. However, Eqn. 5 may be a valid approximation for more complex kinetic schemes under certain conditions [32,33].

If the equilibrium constant, K_{eq} , strongly favours the product side:



integration of the rate Eqn. 5 yields an expression which relates the fractional conversion of the substrate ($X = ([\text{S}_0] - [\text{S}])/[\text{S}_0]$) to the time elapsed, t :

$$-\ln(1 - X) = V_{\max}t/K_M - [\text{S}_0]X/K_M \quad (7)$$

This expression can be used to describe the conversion in a packed-bed reactor provided that the residence time distribution is narrow, i.e. a small reactor with low dispersion, and the reaction time (t) is taken as the mean residence time (τ). Immobilization of an enzyme may, owing to mass transfer limitations and microenvironmental effects [33], alter its kinetic properties, which leads to the treatment based on apparent properties as seen below.

Rearranging Eqn. 7 results in an expression given by the equation

$$X[\text{S}_0] = K_M^{\text{app}} \ln(1 - X) + V_{\max}^{\text{app}}\tau \quad (8)$$

On varying the residence time by changing the volumetric flow-rate (Q) and keeping $[\text{S}_0]$ constant or varying $[\text{S}_0]$ and keeping the residence time constant, the kinetic parameters can be de-

terminated by plotting $X[S_0]$ versus $\ln(1 - X)$ or τ , giving K_M^{app} or $V_{\text{max}}^{\text{app}}$ from the respective slopes.

In Eqn. 7, the fractional conversion varies with the initial substrate concentration $[S_0]$. If, however, $[S_0] \ll K_M$, the last term in Eqn. 7 can be neglected, giving the pseudo-first-order approximation

$$-\ln(1 - X) = V_{\text{max}}^{\text{app}} \tau / K_M^{\text{app}} \quad (9)$$

The ratio $V_{\text{max}}^{\text{app}} / K_M^{\text{app}}$ can be defined as the pseudo-first-order rate coefficient, $K_{\text{ps}}^{\text{app}}$, for an enzyme-catalysed reaction in a packed-bed reactor. If the residence time is varied by changing the volumetric flow-rate (Q), the fractional conversion (X) can be calculated. A linear relationship is expected when $-\ln(1 - X)$ is plotted against the residence time (τ) and $K_{\text{ps}}^{\text{app}}$ can then be obtained from the slope.

This approximation is valid in a small packed-bed reactor as it is assumed that the mass transfer limitation results in a much lower substrate concentration in the immediate proximity of the enzyme than in the bulk flow. Equation 9 can also be used to predict the necessary reactor volume to obtain the desired conversion [32].

In this work, the kinetic parameters were evaluated to be able to compare the behaviour of AMG on the ten different supports. In order to do so correctly, the influence of mass transfer limitations should be minimized [34]. The comparison between the reactors was performed by using small AMG reactors (30 μl) at steady state in the flow set-up shown in Fig. 1a and then analysing the glucose content of the effluent in

the FI mode in a second set-up with the GDH-MUT reactor shown in Fig. 1b. The argument for working with small reactors at steady state was to minimize mass transfer limitations, avoiding the influence of the difference in dispersion behaviour of the different support materials and the difference in dispersion behaviour between different substrates if small sample volumes were to pass the AMG reactor directly into the GDH-MUT reactor in an FI set-up consisting of both reactors. Maltose and maltooligosaccharides are small molecules compared with starch and therefore have large diffusion coefficients. Additionally, starch samples will have large molecular weight distributions and consequently also large diffusion coefficient distributions, which will contribute to the dispersion of the sample plug injected in a flow system [5,7].

To calculate the kinetic parameters it was first necessary to determine whether the 30- μl reactors were controlled by kinetics or mass transfer resistances. It has been shown that if a linear relationship is obtained when $-\ln(1 - X)$ is plotted against the inverse of the flow-rate, Q^{-1} , or versus the inverse of the square of the flow-rate, $Q^{-1/2}$, the reactor is controlled either by kinetics or diffusion, respectively [7,34–37]. A function of the fractional conversion $-\ln(1 - X)$ was plotted against Q^{-1} and $Q^{-1/2}$, respectively as depicted for maltose in Fig. 6a and b. The linear relationship in Fig. 6a proves the reactions to be kinetically controlled whereas Fig. 6b shows a deviation from linearity, meaning that mass transfer resistances can virtually be neglected. The same was

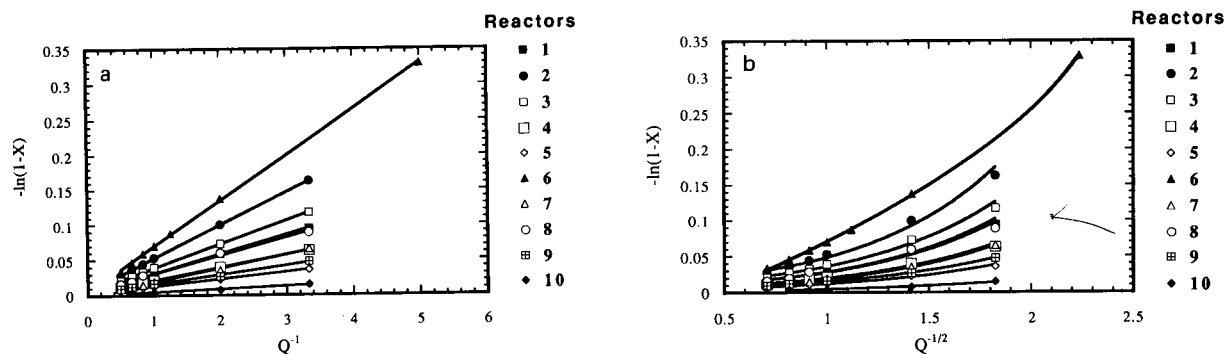


Fig. 6. Fractional conversion, $-\ln(1 - X)$, for maltose plotted versus (a) the inverse of the flow-rate, Q^{-1} , and (b) the inverse of the square of the flow-rate, $Q^{-1/2}$, for all supports. The numbers indicate the numbers of the reactors in Table 1.

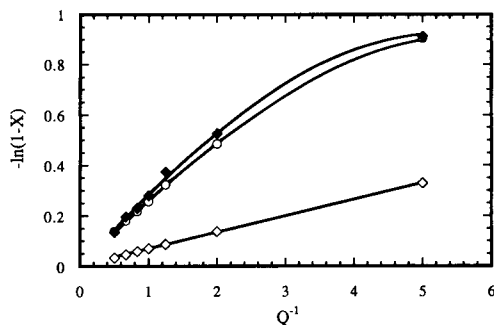


Fig. 7. Fractional conversion, $-\ln(1-X)$, for (\blacklozenge) soluble starch, (\circ) maltooligosaccharides and (\diamond) maltose plotted versus the inverse of the flow-rate, Q^{-1} , for Micropil A as support.

shown to be true when using starch and maltooligosaccharides as substrates for all reactors except that containing Micropil A. Here a negative deviation from linearity is observed for both starch and maltooligosaccharides, as shown in Fig. 7. If there were mass transfer limitations, the deviation would be expected to be positive as the fractional conversion would increase more as the internal mass transfer limitations will be smaller at the lower flow-rates. For all substrates and all flow-rates investigated, the highest conversion efficiencies were obtained with the Micropil A reactor. At the lowest flow-rate in Fig. 7 where the deviation is significant, the fractional conversion approaches 60% for both starch and maltooligosaccharides. As both starch and maltooligosaccharides are converted into increasingly smaller molecules hydrolysed at an increasingly lower rate by the enzyme [31], the negative deviation at a high conversion efficiency could be due to increasingly larger amounts of small molecules produced, causing slower enzyme kinetics. This is also illustrated in Fig. 7 by the lack of deviation from linearity for maltose, which is hydrolysed to glucose at a constant rate.

In Table 1, the kinetic parameters for all reactors calculated according to Eqns. 8 and 9 are shown. For the Micropil A reactor, the kinetic parameters were calculated from the linear parts of the curves. The K_{ps}^{app} values obtained define the mean reaction rate in units of min^{-1} with which the enzyme cleaves α -1,4-linkages (and α -

1,6-linkages) in the substrate molecules. V_{max}^{app} defines the maximum concentration of linkages cleaved per minute in units of mM min^{-1} . Initially for starch and maltooligosaccharides this means that one glucose molecule is produced each time the enzyme cleaves a linkage. For maltose, on the other hand, one cleavage produces two glucose molecules. As the kinetic parameters describe the cleavage of linkages and not the amount of glucose produced, the values for maltose will be twice too large, as the conversion is used in the calculations. The K_{ps}^{app} and V_{max}^{app} values obtained for maltose from Eqns. 8 and 9 have therefore been divided by two. The K_M^{app} values merely describe the systems and remain unchanged ($K_M^{app} = V_{max}^{app}/K_{ps}^{app}$). In the literature it is reported that the linkages in starch are hydrolysed three to eight times the rate of maltose and twice the rate of maltotriose. The higher maltooligosaccharides are hydrolysed at similar rates to amylopectin and soluble starch [31]. It can be seen from Table 1 that the K_{ps}^{app} values obtained for maltose are on average 5–10 times lower than those for both starch and maltooligosaccharides, which is in agreement with what would be expected for the enzyme in solution.

It is well known that V_{max} increases with increasing enzyme concentration for soluble enzymes. To illustrate whether there is a similar trend for immobilized AMG, the V_{max}^{app} values for soluble starch, maltooligosaccharides and maltose (right ordinate) were plotted on the same graph as the immobilization efficiencies (left ordinate) for the different CPG supports versus (a) surface area and (b) pore size in Fig. 3. For the same reasons as above, it is important that this should first be done for different pore sizes of the same type of support material. It can be seen that for all three substrates the V_{max}^{app} values follow similar trends to the immobilization efficiencies, reaching an optimum surface area at $150 \text{ m}^2 \text{ g}^{-1}$ and a pore size of 170 \AA . However, on plotting the V_{max}^{app} values (right ordinate) and the enzyme surface densities (left ordinate) on the same graph versus the pore size for the CPG supports (Fig. 4a), the highest reaction rates are not obtained for the optimum enzyme surface density. A plausible

reason could be that the substrates simply do not diffuse all the way into the porous matrix where most of the enzyme is situated. This would, however, contradict the results obtained earlier (see Figs. 6a, 6b and 7) and the similar behaviour of all three substrates which differ greatly in molecular size (see Fig. 3a and b). One could argue that the time needed for the substrate to diffuse all the way into the pores is much too long compared with the reaction rate of the enzyme at the exterior of the support matrix. Another interesting speculation might be to compare the pore sizes of the support materials in this work with those of the cavities in reversed micelles used for enzymes in organic solvents [38]. In these systems the enzyme is entrapped in a water cavity, which, surrounded by a shell of surfactant molecules, separates the enzyme from the surrounding organic solvent. The size of the inner cavity becomes larger as the amount of water in the system increases. For a variety of enzymes an exceptionally high enzyme activity compared with that in aqueous solutions has been observed when the inner cavity of the reversed micelles corresponds almost exactly to the size of the enzyme. This so-called superactivity was explained by a hypothesis that the relatively high rigidity of the surfactant shell may function as an absorber of excessive fluctuations of the enzyme usually destroying the catalytic conformation in water. The optimum pore size of 170 Å observed in Fig. 4a for the three substrates could indicate a similar function as an absorber of fluctuation imposed on the enzyme. This would mean that a certain pore size gives the enzyme the necessary space to fold and act on the substrate.

In Fig. 5, the V_{\max}^{app} values (left ordinate) for soluble starch and maltose of all ten supports are similar to the above plotted on the same diagram as the immobilization efficiencies (right ordinate) versus surface area. It can be seen that the V_{\max}^{app} values and the immobilization efficiencies for maltose and starch do not follow the same trends as for the CPG supports alone. The highest V_{\max}^{app} is obtained for Micropil A of 300 Å (No. 6), despite the fact that CPG of 170 Å (No. 2) has a higher immobilization efficiency. Biotage, which has the same surface area as CPG of 500 Å, has a

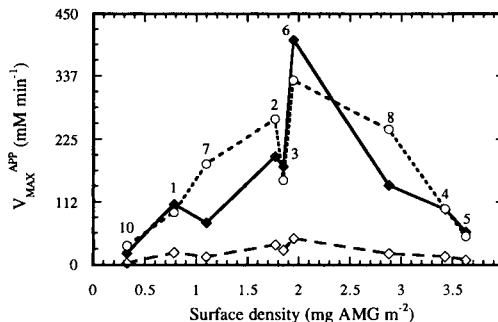


Fig. 8. For all supports, V_{\max}^{app} plotted in mM min^{-1} versus the enzyme surface density in mg AMG m^{-2} support. (\blacklozenge) Soluble starch; (\circ) maltooligosaccharides; (\diamond) maltose. The numbers indicate the numbers of the reactors in Table 1.

lower immobilization efficiency, but yet a more efficient hydrolysis of all three substrates (see also Table 1). The trend is similar for the maltooligosaccharide substrate (not shown) with the highest V_{\max}^{app} value also obtained for the Micropil A support. In Fig. 8, the V_{\max}^{app} values are plotted versus the enzyme surface densities and it is clearly seen that there seems to be an optimum pore size around 300 Å, which again indicates that a high enzyme surface density is not necessarily equivalent to a high reaction rate. One of the conclusions that can be drawn is that it is not only the amount of enzyme bound to the support that determines the enzyme kinetics, but also how the enzyme is affected by the pore size, pore structure and the microenvironmental characteristics of a particular support material. The $K_{\text{ps}}^{\text{app}}$ values follow the same pattern as the V_{\max}^{app} values, with the Micropil A support having the highest rate coefficient for all three substrates. In Table 1, the necessary reactor volumes for 99% conversion at a flow-rate of 0.3 ml min^{-1} calculated from Eqn. 9 are given and it can be seen that a substantial decrease in the reactor volume can be made by choosing Micropil A as the support material compared with the ordinarily used CPG material even if the 170 Å preparation is used. In previous work with immobilized AMG [1,2,5–7] CPG with a pore size of 729 Å was used. This is obviously not a suitable material, as shown in this investigation. An additional beneficial property of the Micropil A support is that the

particles are spherical, in contrast to all CPG materials, leading to much improved packing and flow characteristics. The K_M^{app} values in Table 1 are constants that are independent of the reactor size and therefore also of the enzyme concentration in the reactor. They should be seen as constants describing the different immobilized systems which can be used to evaluate new immobilizations when the same support material, substrate and enzyme are used.

PEI functionalization

In all the immobilizations above, the amino-propyl functionalization was performed followed by glutaraldehyde activation. Often it is necessary to change the immobilization chemistry either in the functionalization and/or activation step of the support in order to improve the efficiency of packed-bed reactors. There is, however, no rule as to which method should be used for enzymes in general and consequently an empirical investigation is necessary.

PEI functionalization is a strictly electrostatic attraction between an ionized support surface and the ionized imine group of the polymer. This electrostatic attraction is best achieved at high pH values where the imine part of PEI and the surface groups on the support are highly ionized. It is well known that silica-based supports start to dissolve under alkaline conditions [25,29,39]. As most of the supports available to us are silica based, we were left with two alumina-based supports, Micropil C and Biotage, which are stable at high pH. In fact, silica-based supports are common supports when PEI functionalization is involved, but it has been found necessary to aluminate the support surfaces prior to adding PEI so that dissolution of the silica-based backbone could be prevented [14–16]. Even though Micropil C was found to be an unsuitable support for AMG immobilization, it would still be interesting to see whether PEI functionalization could improve its qualities. Biotage was found to be one of the better of the investigated supports for AMG im-

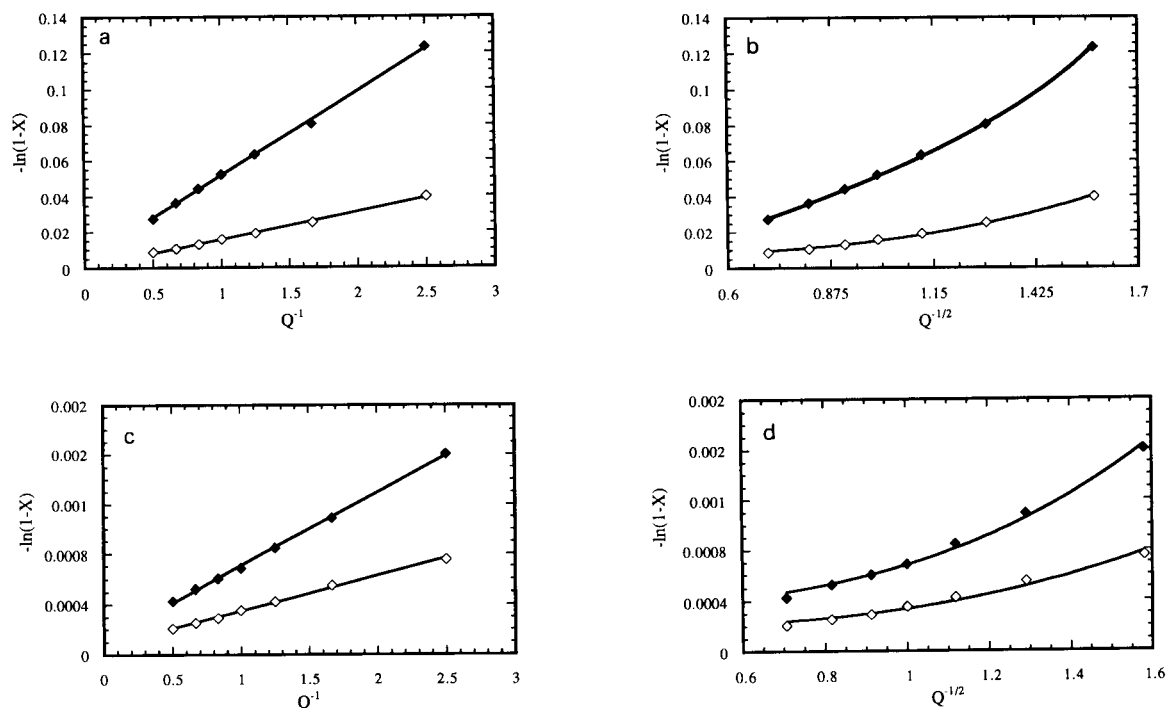


Fig. 9. Fractional conversion, $-\ln(1-X)$, for (◆) soluble starch and (◇) maltose plotted versus the inverse of the flow-rate, Q^{-1} , for (a) Biotage-PEI and (c) Micropil C-PEI, and versus the square of the inverse of the flow-rate, $Q^{-1/2}$, for (b) Biotage-PEI and (d) Micropil C-PEI.

TABLE 2

Immobilization efficiencies and K_{ps}^{app} values for PEI-functionalized Biotage and Micropil C using soluble starch, maltooligosaccharides and maltose as substrates

| Substrate | Support | AMG per 100 mg support (mg) | K_{ps}^{app} (min^{-1}) |
|----------------------------|----------------|-----------------------------------|---|
| Soluble starch | Micropil C-PEI | 8.1 | 0.019 |
| | Biotage-PEI | 13.8 | 1.566 |
| Maltooligo- saccharides | Micropil C-PEI | 8.1 | 0.020 |
| | Biotage-PEI | 13.8 | 6.120 |
| Maltose | Micropil C-PEI | 8.1 | 0.005 |
| | Biotage-PEI | 13.8 | 0.258 |

mobilization and an improved performance with the aid of PEI would be welcome.

Whether the PEI-functionalized reactors are controlled by diffusion or kinetics for the three substrates can be deduced from Fig. 9. A function of the fractional conversion, $-\ln(1 - X)$, for soluble starch and maltose is plotted against the inverse of the volumetric flow-rate, Q^{-1} , and also against the inverse of the square of the volumetric flow-rate, $Q^{-1/2}$ [7,34–37]. The linear relationships obtained in Fig. 9a and c indicate that the reactors are kinetically controlled. The deviation from linearity in Fig. 9b and d depict that there are no diffusional resistances in the reactors. Similar results were obtained for maltooligosaccharides (not shown) and for the three substrates on the corresponding silanized supports. The apparent reaction rate constants, K_{ps}^{app} , were calculated as above according to Eqn. 9. In Table 2, the immobilization efficiencies and the K_{ps}^{app} values for Micropil C and Biotage functionalized with PEI are listed. It can be seen for Biotage-PEI that the immobilization efficiency is slightly lower than that for the corresponding silanized support, but not significantly so (see Table 1). The K_{ps}^{app} values for all three substrates on Biotage-PEI have, however, decreased significantly compared with the silanized support. This decrease in reaction rates cannot be explained by diffusional resistance on the polymeric structure, as Fig. 9b and d show a non-linear relationship. The explanation can be, on the other hand, that the substrates are sterically hindered by the large

polymeric structure of PEI (MW \approx 50 000). This would mean that the substrate never reaches the enzyme sites inside the matrix and so kinetically this enzyme does not take part in the reaction and consequently would not be reflected in plots such as those in Fig. 9b and d.

Both the immobilization efficiency of AMG and the activity for all three substrates on Micropil C-PEI are lower than those on the corresponding silanized supports and the decrease is much more significant than for the Biotage support, as seen in Tables 1 and 2. There is no obvious explanation for this unexpected behaviour with PEI, except that the functionalization procedure might have been unsuccessful or that the materials were simply not compatible with the procedure. The conclusion is that an improved performance with PEI functionalization on these two investigated supports was not obtained here.

Financial support from Stärkelsen (Kristianstad, Sweden), the Swedish National Board for Technical Development (STU) and the Swedish Natural Science Research Council (NFR) is gratefully acknowledged. The authors thank Biotage, Microporous Materials, Pentax and Eka Nobel for their generous gifts of enzyme supports. Elena Domínguez is thanked for very fruitful discussions and Gunilla Nilsson for performing the immobilization on the PEI-functionalized supports.

REFERENCES

- 1 J. Emnéus, R. Appelqvist, G. Marko-Varga, L. Gorton and G. Johansson, *Anal. Chim. Acta*, 180 (1986) 3.
- 2 R. Appelqvist, G. Marko-Varga, L. Gorton and G. Johansson, in J.-L. Aucouturier, J.-S. Cauhapé, M. Destriau, P. Hagenmuller, C. Lucat, F. Ménil, J. Portier and J. Salardenne (Eds.), *Proceedings of the 2nd International Meeting on Sensors*, Imprimerie Biscaye, Bordeaux, 1986, p. 603.
- 3 L.A. Larew, D.A.J. Mead and D.C. Johnson, *Anal. Chim. Acta*, 204 (1988) 43.
- 4 L.A. Larew and D.C. Johnson, *Anal. Chem.*, 60 (1988) 1867.
- 5 J. Emnéus and L. Gorton, *Anal. Chim. Acta*, 234 (1990) 97.

- 6 J. Emnéus and L. Gorton, *Anal. Chem.*, 62 (1990) 263.
- 7 L. Gorton, E. Csöregi, E. Domínguez, J. Emnéus, G. Jönsson-Pettersson, G. Marko-Varga and B. Persson, *Anal. Chim. Acta*, 250 (1991) 203.
- 8 F. Ortega, *Anal. Chim. Acta*, 257 (1992) 79.
- 9 K. Svegmarm, Stärkelse—Struktur och Realogi. En Litteratursammomställning, SIK-Rapport, No. 547, SIK, Göteborg, 1987.
- 10 J. Holm, I. Björck, S. Ostrowska, A. Eliasson, N. Asp, K. Larsson and I. Lundquist, *Starch/Stärke*, 35 (1983) 294.
- 11 K. Ghiasi, E. Varriano-Marston and R.C. Hosoney, *Cereal Chem.*, 59 (1981) 86.
- 12 J. Holm, I. Björck, N. Asp, L. Sjöberg and I. Lundquist, *J. Cereal Sci.*, 3 (1985) 193.
- 13 P. van Twisk, *Stärke*, 22 (1970) 228.
- 14 R. Bahulekar, N.R. Ayyangar and S. Ponrathnam, *Enzyme Microb. Technol.*, 13 (1991) 858.
- 15 R. Janzen, K.K. Unger, W. Müller and M.T.W. Hearn, *J. Chromatogr.*, 522 (1990) 77.
- 16 B.P. Wasserman, D. Burk and B.S. Jacobson, *Enzyme Microb. Technol.*, 4 (1982) 107.
- 17 H.H. Weetall and R.A. Messing, in M.L. Hair (Ed.), *The Chemistry of Biosurfaces*, Vol. 2, Dekker, New York, 1972, Chap. 12.
- 18 R.T. Lee and Y.C. Lee, *Biochemistry*, 19 (1980) 156.
- 19 N. Jentoft and D.G. Dearborn, *J. Biol. Chem.*, 254 (1979) 4349.
- 20 L. Goldstein, Y. Levin and E. Katchalski, *Biochemistry*, 3 (1964) 1913.
- 21 H.H. Weetall, *Methods Enzymol.*, 4 (1976) 134.
- 22 G. Gübitz, in R.W. Frei and K. Zech (Eds.), *Selective Sample Handling and Detection in High-Performance Liquid Chromatography*, *J. Chromatogr. Library*, Vol. 39, Part A, Elsevier, Amsterdam, 1988, p. 145.
- 23 J. Ruz, F. Lázaro and M.D. Luque de Castro, *J. Autom. Chem.*, 10 (1988) 15.
- 24 E.E. Snell and S.J. Di Mari, in P.D. Boyer (Ed.), *The Enzymes*, Vol. 2, Academic Press, New York, 1970, p. 335.
- 25 K.K. Unger, *Porous Silica*, *J. Chromatogr. Library*, Vol. 16, Elsevier, Amsterdam, 1979, p. 12.
- 26 G. Marko-Varga, E. Domínguez, B. Hahn-Hägerdal and L. Gorton, *J. Chromatogr.*, 506 (1990) 423.
- 27 CPG, Information Sheet, SIK, Göteborg, 1990.
- 28 A. Paszynski, I. Miedziak, J. Lobarzewski, J. Kochmanska and J. Trojanowski, *FEBS Lett.*, 149 (1982) 63.
- 29 A.A. Artyomova, O.I. Voroshilova, Y.S. Nikitin and T.D. Khoklova, *Adv. Colloid Interface Sci.*, 25 (1986) 235.
- 30 E. Stratilová, M. Capka and L. Rexová-Benková, *Biocatalysis*, 2 (1989) 317.
- 31 N.K. Matheson and B.V. McCleary, in G.O. Aspinall (Ed.), *The Polysaccharides*, Vol. 3, Academic Press, New York, 1985, p. 70.
- 32 G. Johansson, L. Ögren and B. Olsson, *Anal. Chim. Acta*, 145 (1983) 71.
- 33 P.W. Carr and L.D. Bowers, in P.J. Elving and J.D. Wineforder (Eds.), *Immobilized Enzymes in Analytical and Clinical Chemistry, Fundamentals and Applications*, Wiley, New York, 1980.
- 34 H. Huck, A. Schelter-Graf and H.-L. Schmidt, *Bioelectrochem. Bioenerg.*, 13 (1984) 199.
- 35 H. Huck, *Bioelectrochem. Bioenerg.*, 21 (1989) 99.
- 36 C. Horváth and J. Engasser, *Biotechnol. Bioeng.*, 16 (1974) 909.
- 37 R.S. Schifreen, D.A. Hanna, L.D. Bowers and P.W. Carr, *Anal. Chem.*, 49 (1977) 1929.
- 38 K. Martinek, N.L. Klyachko, A.V. Kabanov, Y.L. Khmel-nitsky and A.V. Levashov, *Biochim. Biophys. Acta*, 981 (1989) 161.
- 39 G. Marko-Varga, *Anal. Chem.*, 61 (1989) 831.

Comparison between different inorganic supports for the immobilization of amyloglucosidase and α -amylase to be used in enzyme reactors in flow-injection systems

Part II. Hydrolysis of glycogen

Jenny Emnéus and Lo Gorton

Department of Analytical Chemistry, University of Lund, P.O. Box 124, S-221 00 Lund (Sweden)

(Received 11th August 1992)

Abstract

Amyloglucosidase (AMG) was immobilized on four different inorganic supports, two controlled-pore glasses (CPG, 170 and 729 Å), one ceramic silica support (Micropil A) and one alumina-based surface porous support (Biotage), by silanization followed by glutaraldehyde activation. The alumina-based support, Biotage, was also used for immobilization with polyethylenimine functionalization followed by glutaraldehyde activation. A thermostable α -amylase, Termamyl, was immobilized on three different supports, CPG of 1489 Å, Biotage and Micropil A, by silanization and glutaraldehyde activation. The different immobilized supports were packed into identical reactors (30 μ l). The AMG supports were investigated regarding immobilization efficiency and the optimum pore size necessary for the entry of a high-molecular-weight substrate (glycogen) so that optimum activity could be obtained. The highest immobilization efficiency was obtained on CPG of 170 Å, but the highest activity was obtained on CPG of 729 Å. The three Termamyl supports were compared and the highest immobilization efficiency was obtained on Micropil A, but the highest enzyme activity was obtained on CPG of 1489 Å followed by Biotage.

Keywords: Enzymatic methods; Flow injection; Amylase; Amyloglucosidase; Enzyme reactors; Glycogen

Several attempts have been made to develop accurate and rapid qualitative and quantitative starch determination systems [1–8]. It was found to be necessary to use two starch-hydrolysing enzymes, namely a heat stable α -amylase (Termamyl) and amyloglucosidase (AMG), to obtain the most efficient hydrolysis [2,5–7]. The complex formation between amylose and lipids and the presence of surface-bound starch proteins are believed to be the main reasons why the total breakdown of native starch from different

origins into its glucose constituents has not been entirely successful [9–13]. The conclusions drawn through the years have therefore stressed the necessity for more efficient starch-hydrolysing enzyme reactors.

The efficiency of a packed-bed reactor will be dependent on a high enzyme loading with a high retained activity of the bound enzyme. To achieve these goals an optimization should be made considering the choice of enzyme support and immobilization chemistry. In an earlier investigation [5] in which Termamyl was immobilized on controlled-pore glass (CPG) supports with different pore sizes, an optimum average pore size of 1489 Å was found when using glycogen as substrate.

Correspondence to: J. Emnéus, Department of Analytical Chemistry, University of Lund, P.O. Box 124, S-221 00 Lund (Sweden).

The combined effects of using two reactors, one containing Termamyl (CPG, 1489 Å) and the other AMG (CPG, 729 Å) were successful in the total hydrolysis of glycogen and native potato starch, but was unsuccessful in hydrolysing native starch of wheat, corn and rice [5]. In Part I of this investigation, a thorough discussion on the relationship between reaction rates of AMG for lower molecular mass substrates and pore size, surface area and immobilization efficiency on five different pore sizes of CPG and additionally five new supports was presented. Additionally, polyethylenimine (PEI) functionalization was performed followed by glutaraldehyde activation of two alumina-based supports. It was found for CPG that the combined effects of a large surface area of $150 \text{ m}^2 \text{ g}^{-1}$ and an optimum pore size of 170 Å gave the best immobilization efficiency and the most efficient hydrolysis of maltose, maltooligosaccharides and soluble starch. When the supports were compared, the most efficient hydrolysis was obtained on a ceramic support, Micropil A, 300 Å, with a surface area of $100\text{--}150 \text{ m}^2 \text{ g}^{-1}$ in spite of the fact that the highest immobilization efficiency was obtained on CPG, 170 Å. The conclusions drawn were that an optimum pore size is important both for the actual immobilization of the enzyme and for the action of the enzyme on its substrates and as the importance of microenvironmental effects such as the pore structure of the support material and surface chemistry. The three substrates all differed in their molecular weights and, as expected, their rate of reaction with AMG increased with the increasing chain length of the substrates [14].

As the highest molecular weight substrate, soluble starch, is a partially hydrolysed starch (MW ≈ 5000), it cannot be considered to be a true starch [15]. The aim of this work, as stated above, was to analyse native starch of different origins. This made it necessary to hydrolyse efficiently the large starch granules to lower molecular weight fractions with Termamyl before letting AMG act to complete the hydrolysis to glucose. The three substrates behaved similarly with AMG on all supports and the reactions were found to be kinetically controlled for all three substrates, meaning that there were no limiting diffusional

resistances. Two questions that should be asked are how small the molecular weight fractions must be when eluting from the Termamyl reactor in order to be completely hydrolysed by the AMG reactor and how a larger and more branched substrate like glycogen would behave with immobilized AMG on these supports. Evidently these questions require the AMG reactor to be optimized in terms of substrate size and, for the Termamyl reactor, for more suitable support material with an appropriate pore size to be found, as was done for AMG in Part I. In this work, some of the AMG reactors that were used in Part I were evaluated with glycogen as the enzyme substrate. Based on the results obtained from the investigated AMG reactors, Termamyl was immobilized on three different supports and evaluated with glycogen as the enzyme substrate.

EXPERIMENTAL

Enzymes and enzyme reactors

Amyloglucosidase (AMG) reactors. Four different support materials were activated with glutaraldehyde according to a previously described procedure [16–18] modified as described below: controlled pore glass, CPG-10 (Serva, Heidelberg, Germany), particle size $37\text{--}74 \mu\text{m}$, pore size 170 Å (Cat. No. 44732) and surface area $150 \text{ m}^2 \text{ g}^{-1}$ and pore size 729 Å (Cat. No. 44772) and surface area $36 \text{ m}^2 \text{ g}^{-1}$; Micropil A (Microporous Materials, Braunston, UK, Art. No. SP4/100), particle size $7\text{--}20 \mu\text{m}$, pore size 300 Å and surface area $100\text{--}150 \text{ m}^2 \text{ g}^{-1}$; and Uncoated Neutral Unisphere-PBD Alumina (Biotage, Charlottesville, VA, USA, Lot. No. PP77), particle size $8 \mu\text{m}$, pore size 250 Å and surface area $50 \text{ m}^2 \text{ g}^{-1}$. The supports were first treated with concentrated nitric acid for 2 h, after which they were thoroughly washed with highly purified water (Millipore, Millie-RO4) and dried at 190°C in a furnace oven for 6 h. The four supports were then silanized by refluxing in a boiling water-bath with 10% 3-aminopropyltriethoxysilane (Janssen Chimica) in dry toluene for 40 min, after which they were washed thoroughly with toluene and acetone over a G3 or G4 filter, depending on the

particle size of the support, and dried in a furnace oven at 115°C overnight. The silanized supports were activated at reduced pressure and 4°C with 2.5% glutaraldehyde (Sigma), in 0.1 M phosphate buffer (pH 7.0) for 30 min. Prior to dilution of commercial 25% glutaraldehyde solution (Sigma), it was shaken with activated carbon and centrifuged to remove polymeric material. The clear supernatant was then used. The Schiff bases produced were then reduced by adding 7 mg of sodium cyanoborohydride (NaCNBH_3) (Janssen, Chimica) to 100 mg of support and the reaction was allowed to proceed another 90 min. The activated supports were thoroughly washed with highly purified water over a G3 or G4 filter.

A 500-mg amount of Biotage was added to 3 ml of a 10% solution of polyethylenimine (PEI) (Sigma) in phosphate buffer (pH 10) and allowed to react at reduced pressure for 10 min and then at atmospheric pressure over 2 days at room temperature. The support was then thoroughly washed over a G4 filter with 10 mM phosphate buffer (pH 7.4). The PEI-functionalized support was then activated as above with 2.5% glutaraldehyde (Sigma) at reduced pressure and 4°C in 0.1 M phosphate buffer (pH 7.0) for 30 min. The Schiff bases produced were reduced with NaCNBH_3 as described previously.

A 700-mg amount of AMG (EC 3.2.1.3) from *Aspergillus niger*, 100 IU mg^{-1} (Merck), was dissolved in 14 ml of 0.1 M phosphate buffer (pH 7.0), resulting in a solution containing 46 mg AMG ml^{-1} . The solution was kept at 4°C during all immobilization experiments. A 1-ml volume of the prepared AMG solution and 200 μl of 0.1 M phosphate buffer (pH 7.0) were added to 100 mg of each of the four silanized and glutaraldehyde-activated supports and allowed to react at 4°C and reduced pressure for 30 min. A 2.5-ml volume of the prepared AMG solution was added to the Biotage–PEI-functionalized and glutaraldehyde-activated support and the coupling was performed as described above. The Schiff bases produced between the enzyme and activated supports were reduced with NaCNBH_3 and the reaction was continued for 90 min. The enzyme supports were washed with 1 M NaCl in 0.1 M acetate buffer (pH 4.5).

α -Amylase (Termamyl) reactors. A 2.5-ml volume of the thermostable α -amylase Termamyl 300 L (EC 3.2.1.1) from *Bacillus licheniformis* (part of the FiberZyme kit, product No. 7367503; Novo Biolabs, Bagsvaerd, Denmark) was passed through PD 10 GPC columns (Pharmacia LKB Biotechnology, Uppsala, Sweden, Art. No. 17-0851-01) to remove interfering compounds and was collected as 7 ml of enzyme in 0.05 M citrate buffer (pH 7.0) which was kept at 4°C.

A 500-mg amount of each three supports [CPG-10 (Serva), particle size 75–125 μm , pore size 1489 Å (Cat. No. 44791), and Uncoated Neutral Unisphere-PBD Alumina and Micropil A as above], silanized and glutaraldehyde activated as described above, were each added to 2 ml of the above-prepared Termamyl solution. The coupling was done as described for the AMG reactors except that the final washing of the enzyme supports was done with 1 M NaCl in 0.1 M acetate buffer (pH 6.0).

Coupling yields were measured spectrophotometrically as the protein content of the supernatant at 280 nm before and after immobilization. The eight different immobilized enzyme preparations were then packed into identical reactors (30 μl , 10 mm \times 2 mm i.d.) and stored at 4°C in 0.1 M acetate buffer (pH 4.5) for AMG-modified supports or 0.05 M acetate buffer (pH 6.0) for Termamyl-modified supports.

Sweep electron micrographes were taken of the three unmodified supports with an ISI 100A scanning electron microscope (SEM).

Glucose dehydrogenase (GDH–mutarotase reactor MUT). A 4.56-mg (1012-U) amount of glucose dehydrogenase (GDH) (EC 1.1.1.47) from *Bacillus megaterium*, 220 U mg^{-1} (Merck), 0.35 mg (1750 U) of mutarotase (MUT) (EC 5.1.3.3) from porcine kidney (Sigma) and a few mg of nicotinamide adenine dinucleotide, oxidized form, (NAD^+) (Merck), were dissolved in 0.1 M phosphate buffer (pH 7.0). The enzyme solution (1 ml) was added to 150 mg of aminopropylsilanized and glutaraldehyde-activated CPG-10, particle size 37–74 μm , pore size 500 Å, according to a previously described procedure [16]. The immobilized enzyme support was packed into a 240- μl reactor (7.6 cm \times 2 mm i.d.) and stored at 4°C in 0.1 M

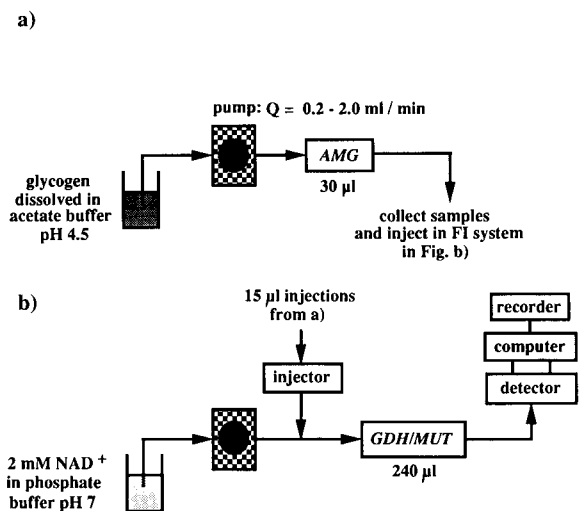


Fig. 1. Flow systems (a) for steady-state operational mode of the AMG reactors and (b) for FI determination of the glucose in the effluent from the AMG reactors in (a).

phosphate buffer (pH 7.0) also containing 2 mM NAD^+ .

Analytical system

The various parts of the systems used for investigating the performance of the five AMG reactors and the three Termamyl reactors are depicted in Figs. 1 and 2. In the steady-state set-ups in Figs. 1a and 2a, a Model 2150 LC pump (LKB, Bromma, Sweden) was continuously pumping substrate dissolved in either 0.1 M acetate buffer (pH 4.5) (AMG) or 0.05 M acetate buffer at (pH 6) (Termamyl) through each of the five AMG or the three Termamyl reactors, respectively, one at a time. Flow-rates between 0.2 and 2.0 ml min^{-1} were investigated. For each flow-rate and reactor, samples of the effluent were collected and injected into the flow-injection (FI) system as shown in Fig. 1b for AMG effluents and into the FI system in Fig. 2b for Termamyl effluents, to examine the amount of glucose produced either by AMG itself or by the combination of Termamyl and AMG. Before injection the effluents were, if necessary, diluted so that the final concentration of glucose produced would fall within the linear range of the glucose-determining systems in Figs. 1b and 2b. In Fig.

1b, another Model 2150 LC pump was used at a constant flow-rate of 1.0 ml min^{-1} , continuously pumping a solution of 0.1 M phosphate buffer (pH 7.0), also containing 2 mM NAD^+ , through the GDH–MUT reactor in the FI system.

In Fig. 2b, two Model 2150 LC pumps, denoted pumps 1 and 2, are included. Pump 1 was used with a constant flow-rate of 0.5 ml min^{-1} , continuously pumping 0.1 M acetate buffer (pH 4.5) through the Micropil A-immobilized AMG reactor which at a merging point met a second flow, pump 2, pumping at a constant flow-rate of 0.5 ml min^{-1} 0.2 M phosphate buffer (pH 7.3) also containing 4 mM NAD^+ , resulting in a total flow-rate through the GDH–MUT reactor of 1.0 ml min^{-1} and with the pH adjusted to about 7. Before start-up the buffers were degassed for 10 min under reduced pressure to prevent the appearance of microbubbles in the flow systems.

The samples collected from the effluents of the different AMG and Termamyl reactors were injected from a 15- μl injection loop into the flow streams with a pneumatically operated injection valve (Cheminert Type SVA, Kemila, Stockholm, Sweden). PTFE tubing, 0.5 mm i.d., with Altex screw couplings connected the various parts of

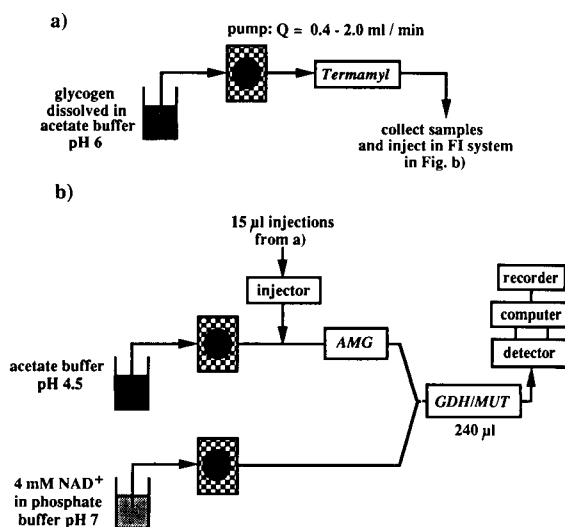


Fig. 2. Flow systems (a) for steady-state operational mode of the Termamyl reactors and (b) for FI determination of the glucose in the effluent from the Termamyl reactors in (a).

the flow system. All buffers were prepared from ultrapure water (Millipore, Milli-RO4) and chemicals of analytical-reagent grade. A Model 2151 flow-through variable-wavelength detector (LKB) monitored the NADH produced from the GDH-MUT reactor at 340 nm.

Solutions of D-glucose (BDH), and 50 mM glycogen from *Mytilus edulis* (Sigma), were prepared by dissolving appropriate amounts in either 0.1 M acetate buffer (pH 4.5) (AMG investigation) or at pH 6.0 (Termamyl investigation). All concentrations were calculated in terms of the amount of glucose units contained, where every glucose unit in the glycogen solution was given a mean molecular weight of 162.14. Kathon CG (50 $\mu\text{l l}^{-1}$) containing 1.125% methylchloroisothiazolinone and 0.375% methylisothiazolinone was added to all the buffers to prevent bacterial growth in the systems.

All investigation were performed, if not stated otherwise, by continuously pumping substrate solution at steady state through the AMG or Termamyl reactors as shown in Figs. 1a and 2a. The amount of hydrolytic products produced in the respective reactors were determined by injecting aliquots of the collected eluents into the FI systems shown in Figs. 1b and 2b.

RESULTS AND DISCUSSION

In many instances in this paper, reference will be made to Part I of the investigation and readers

are asked to consult both the theory and some of the figures in Part I.

AMG reactors

In Part I, the hydrolysis of relatively low molecular weight substrates by AMG was investigated. The maltooligosaccharide substrate is a mixture of oligosaccharides with a degree of polymerization (DP) between 2 and 8 and the largest substrate, soluble starch, is prepared from native potato starch, which, according to the manufacturer, has been hydrolysed to an average molecular weight of about 5000 [15]. In nature, starch exists as semicrystalline granules shown to be difficult for AMG to hydrolyse [10,19]. The native starch granules normally first need to be prehydrolysed by α -amylase so that products are released which AMG is able to attack. The question that arises here is how efficient the AMG reactor must be to be able to break down totally the products eluting from a Termamyl reactor. This question can, however, be posed the other way around, i.e., how efficient a Termamyl reactor must be for the AMG reactor to succeed in the complete hydrolysis of native starch to glucose. In Part I, the importance of the pores of a support being large enough for the enzyme to enter was discussed. It is obviously equally important for the substrate to be able to enter and gain access to the enzyme within the pores. In order to answer the questions posed above, a larger and more difficult substrate than was used in Part I needs to be investigated. Glycogen was previously

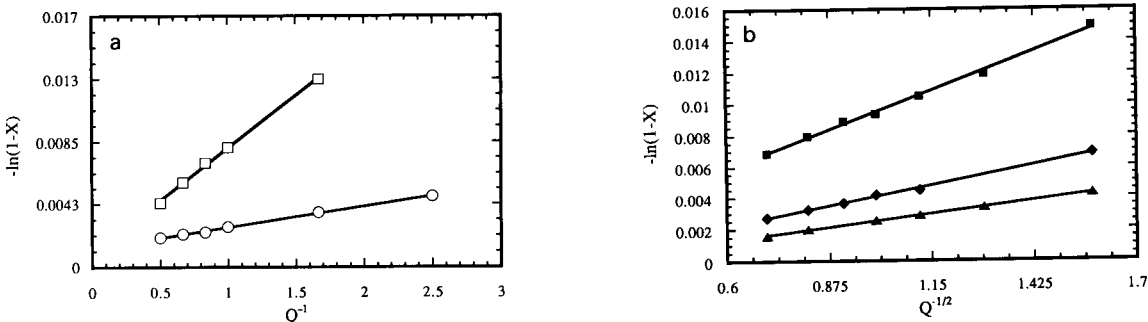


Fig. 3. Fractional conversion, $-\ln(1 - X)$, for glycogen plotted versus (a) the inverse of the flow rate, Q^{-1} for (○) CPG, 170 Å, and (□) CPG, 729 Å, and (b) the inverse of the square of the flow-rate, $Q^{-1/2}$ for (■) silanized Biotage, (▲) Biotage-PEI and (◆) Micropil A.

found to be a good test substrate for starch-hydrolysing enzymes [5]. It is a more highly branched starch-type polymer and does not exist as granules in nature, which makes it easier to solubilize and therefore easier to handle [20,21]. The reactors chosen for the following investigation were selected both according to excellence in Part I, namely the CPG, 170 Å, and the Micropil A, 300 Å, reactors, and according to structure, namely CPG, 729 Å with large pores, and Biotage with a surface porous structure, as discussed below.

Whether the AMG reactors are controlled by diffusion or kinetics for glycogen can be deduced from Fig. 3. A function of the fractional conversion, $-\ln(1-X)$, where X denotes the fractional conversion for glycogen, is plotted against the inverse of the volumetric flow-rate, Q^{-1} , and also against the inverse of the square of the volumetric flow-rate, $Q^{-1/2}$ (see theory in Part I) [7,22–25]. From Fig. 3a, the linear relationships obtained for the CPG, 729 and 170 Å, supports ($r = 0.99907$ and 0.99884) indicate that these are controlled by kinetics, whereas the linear relationships obtained in Fig. 3b for the Micropil A ($r = 0.99848$), silanized Biotage ($r = 0.99822$) and Biotage-PEI reactors ($r = 0.99966$) indicate that these reactors are controlled by diffusion. The apparent reaction rate constants, K_{ps}^{app} , can be calculated from the slopes of the graphs shown in Fig. 4, where the abscissa is exchanged for the residence time in the reactors, τ ($\tau = \text{reactor size} \times Q^{-1}$). If one refers to the theory in Part I, it is

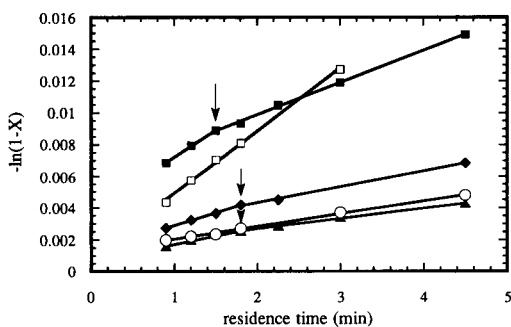


Fig. 4. Fractional conversion, $-\ln(1-X)$, for glycogen plotted versus the residence time in the reactors for (○) CPG, 170 Å, (□) CPG, 729 Å, (■) silanized Biotage, (◆) Micropil A and (▲) Biotage-PEI. The arrows indicate a change in the reaction rate.

TABLE 1

Physical and kinetic parameters for immobilized AMG on five different supports using glycogen as substrate

| Support | Pore size (Å) | Surface area (m ² g ⁻¹) | AMG per 100 mg ⁻¹ support (mg) | K_{ps}^{app} (min ⁻¹) |
|-------------|---------------|--|---|-------------------------------------|
| CPG | 170 | 150 | 26.5 | 0.048 |
| CPG | 729 | 36 | 13.1 | 0.234 |
| Micropil A | 300 | 100–150 | 24.3 | 0.066 |
| Biotage | 250 | 50 | 14.4 | 0.132 |
| Biotage-PEI | 250 | 50 | 11.0 | 0.042 |

apparent that the kinetic parameters of an immobilized enzyme cannot be calculated in this way for diffusion-controlled reactors [26]. This can be seen in Fig. 4 as a change in direction of the slopes at a break point (arrows) for the two Biotage supports and the Micropil A support. As the aim is to make a comparative study between the different enzyme supports, the K_{ps}^{app} values listed in Table 1 should just be regarded as average and tentative values. It can be seen in Table 1 that all five supports have much lower K_{ps}^{app} values for glycogen than for the low molecular mass substrates investigated in Table 1 in Part I, which verifies that glycogen is a more difficult substrate for AMG to hydrolyse. The highest K_{ps}^{app} value for glycogen with AMG is obtained for the CPG, 729 Å, support in spite of a much lower immobilization efficiency compared with the CPG, 170 Å, and Micropil A, 300 Å, supports. The reaction rate constant obtained for AMG on the CPG, 729 Å, support with low molecular weight substrates was found much lower than for the CPG, 170 Å, Micropil A, 300 Å, and silanized Biotage supports in Part I. For these supports, the low molecular weight substrates all had access to the enzyme sites within the pores of the supports (no diffusional resistance), and the activity was partly governed by the immobilization efficiency and by other factors discussed in Part I.

The high K_{ps}^{app} obtained on the CPG, 729 Å, support is apparently due to free access of glycogen (no diffusional resistance) to the enzyme sites inside the pores, which is also supported by the steeper slope obtained for this reactor compared with those of the other reactors shown in Fig. 4.

Despite the fact that the CPG, 170 Å, support has the highest immobilization efficiency and no apparent diffusional resistances (see Fig. 3a and Table 1), the K_{ps}^{app} value obtained is lower than those for both the CPG, 729 Å, and silanized Biotage supports. Glycogen has an average molecular weight of more than 10^9 and is probably so large that it is totally excluded from the 170 Å pores of CPG, which according to the manufacturer excludes globular proteins with molecular weights higher than about 400 000 [27]. The enzyme within the porous structure does apparently not take part in the reaction, meaning that the substrate is only converted to a small extent on the surface of the support, which would give a kinetically controlled reaction and a low K_{ps}^{app} value. The Micropil A and the two Biotage reactors are diffusion controlled, meaning that the reaction rate is limited by the fact that glycogen first has to diffuse to the enzyme sites before it can be converted, which results in overall lower K_{ps}^{app} values. Normally, a positive deviation from linearity is expected and not a negative deviation, as seen in Fig. 4 for the Micropil A and the two Biotage reactors. The fractional conversion will be relatively larger at long residence times as a more efficient internal mass transfer will be the result. The change in the slopes at the break points (see arrows in Fig. 4) for the two Biotage and the Micropil A supports represents a change from a faster to a slower reaction rate. This is probably a similar phenomenon to that seen for the conversion of soluble starch and maltooligosaccharides on the Micropil A support in Part I. There, a high fractional conversion of soluble starch was obtained at long residence times, which resulted in the production of large amounts of low molecular weight molecules, which were converted at a slower reaction rate [14], indicated by a negative deviation of the slope. In this case, the large glycogen molecule is probably first broken down to smaller molecules at the surface which then diffuse into the pores resulting in an overall slower reaction rate.

It seems curious that the K_{ps}^{app} value obtained for glycogen is twice as high on the silanized Biotage as on the Micropil A support, whereas the pores of the former are smaller and the

immobilization efficiency is almost half of that on Micropil A (see Table 1). The experimental results might be understood by comparing the sweep electron micrographs of the supports shown in Fig. 5. The Biotage particles have, as reported, an average pore size of 250 Å. Additionally, and in contrast to the CPG supports (Fig. 5b) and the Micropil A support (Fig. 5c), Biotage has a narrow particle size distribution (Unisphere) and, as seen in Fig. 5a, also a surface porous structure. The surface porosity will result in a higher enzyme density at the surface and better access for the large glycogen molecule to reach the enzyme. Additionally, the small particle size and the fact that a unispheric property gives a better packing profile result in a larger total amount of enzyme support packed into the reactor.

In Fig. 6, FI peaks are depicted in order of decreasing peak area for the five different 30- μ l AMG reactors, placed one at a time in front of the GDH–MUT reactor in the FI set-up in Fig. 2b. As the same substrate solution is used in all experiments and the reactors have equal size, the differences in dispersion in this FI system are mainly caused by two parameters: the apparent reaction rate, which is partly governed by the amount of enzyme in the reactor and the accessibility of the substrate for this enzyme, and the packing profile of the support material. The dispersion behaviour in the reactors is illustrated by the height and shape of the FI peaks. AMG immobilized on CPG, 729 Å, constitutes the most efficient reactor, resulting in the largest peak area, but the dispersion in this reactor is large, seen as a low broad peak in Fig. 6a. This is because a good packing profile is difficult to obtain owing to the shape of the CPG particles seen in Fig. 5b, and because the substrate has access to the inside of the matrix of the porous material. As mentioned above, the packing profile of the monospheric Biotage particles is good and consequently the dispersion behaviour is improved in this reactor, which is seen as a higher and less broad peak in Fig. 6b. The accessibility of the substrate to the enzyme is, however, limited by the small interior pores of Biotage, which evidently also results in a smaller contribution to dispersion but also to a lower conversion and

hence a smaller peak area. The peaks in Fig. 6c, d, and e for the Micropil A, the CPG, 170 Å, and the Biotage–PEI reactors all have small areas and small dispersions. This is evidently because the substrate is more or less excluded from the

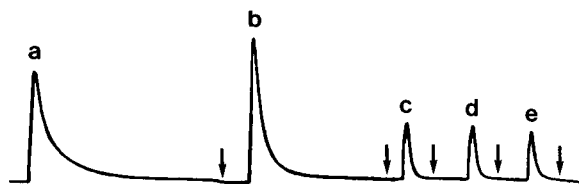


Fig. 6. FI peaks from 15- μ l injections of the steady-state effluents of hydrolysed glycogen from the AMG reactors in Fig. 1a into the FI system in Fig. 1b. (a) CPG, 1489 Å; (b) silanized Biotage; (c) Micropil A; (d) CPG, 170 Å; (e) Biotage–PEI. Arrows indicate end of peak.

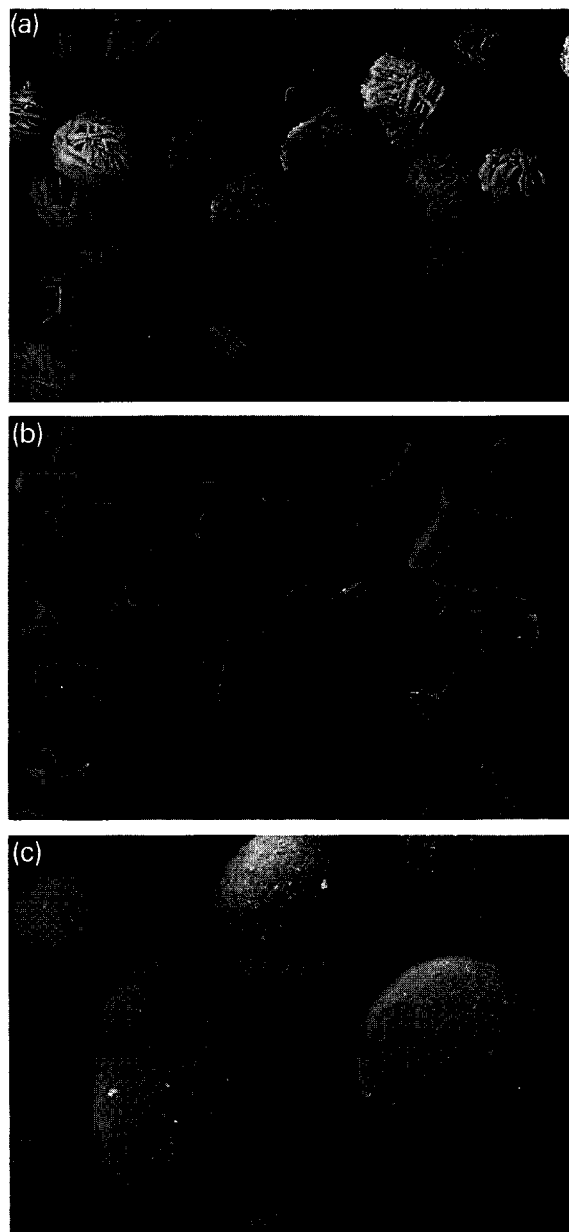


Fig. 5. Sweep electron micrographs of (a) Biotage, $\times 1770$, (b) CPG, 1489 Å, $\times 59$, and (c) Micropil A, $\times 1770$.

pores of these supports and as a consequence is hydrolysed mainly at the surface, after which it is eluted with the dead volume.

The conclusion to be drawn from these results is that the conversion of glycogen with AMG is not very high even for the most efficient reactors. The K_{ps}^{app} values obtained for these supports are given in Table 1 and are much lower than for low molecular weight substrates such as soluble starch (see Table 1 in Part I). It was also shown that a high immobilization efficiency has no effect if the substrate cannot enter the pores where most of the enzyme is situated. Either a support with a sufficiently large pore size or a surface porous structure is necessary to prevent total exclusion of high molecular weight substrates such as glycogen and probably also native starch.

Termamyl reactors

It has been reported that AMG hydrolyses the α -1,4-linkages in starch three to eight times the rate of maltose and twice the rate of maltotriose [14]. The hydrolytic rate for higher maltooligosaccharides is similar to that for amylopectin and soluble starch, which is in agreement with the results obtained in Part I and with the literature [14]. It is therefore obvious that the Termamyl reactor should hydrolyse native starch and glycogen into products having molecular weights of the same order of magnitude as for soluble starch for the AMG reactor to be most efficient. To succeed in this, the support material for Termamyl immobilization must either be surface porous or the pores of the support must be large enough that the substrate can reach the enzyme within the porous matrix. In an earlier study, Termamyl

was immobilized on CPG supports of different pore sizes ranging from 700 to 3000 Å and the average pore size of 1489 Å was found to give the most efficient hydrolysis [5]. In this work, Termamyl was immobilized on CPG, 1489 Å, Biotage and Micropil A to compare the effects on this enzyme of a surface porous support (Biotage), a support with an appropriate pore size (CPG, 1489 Å) and a support with a possible high immobilization efficiency (Micropil A).

An AMG reactor was included in the FI set-up in Fig. 2b because α -limit dextrans, maltooligosaccharides and maltose produced from the Termamyl reactors are not converted by the GDH-MUT FI system in Fig. 1b. The choice of the support for immobilization of AMG, contained in the AMG reactor in Fig. 2b, was Micropil A, because it was found to be highly efficient for soluble starch (see Part I). This reactor was hence used throughout all the Termamyl experiments. The conversion of glycogen obtained is thus the result of a combined effect of Termamyl and AMG and from the above results with AMG alone it can be deduced that an efficient Termamyl reactor will result in an efficient AMG reactor or vice versa. Evidently this means that if the kinetic parameters are calculated as before they can solely be used as a comparative measure between the three systems. When plotting $-\ln(1-X)$ versus Q^{-1} or $Q^{-1/2}$ [7,22–25], kinetic control was observed for both the Biotage and CPG, 1489 Å, combined systems. For the Micropil A combined system, both plots showed deviations from linearity, which should be interpreted as a borderline case where the system is limited by both kinetics and diffusion.

In Table 2, the apparent reaction rate constants, K_{ps}^{app} , and the immobilization efficiencies for the three Termamyl reactors are given. As can be seen, the highest immobilization efficiency is obtained on Micropil A but the K_{ps}^{app} values for the Biotage and CPG, 1489 Å, systems are both approximately three times higher than those for the Micropil A system. These results again verify the need for substrate access by either a surface porous support or a support with a large pore size. From Tables 1 and 2, it is apparent that the total hydrolytic rate for glycogen has increased

TABLE 2

Physical and kinetic parameters for immobilized Termamyl reactors in combination with AMG immobilized on Micropil A for three different supports using glycogen as substrate

| Support | Pore size (Å) | Surface area (m ² g ⁻¹) | Immobilization efficiency on Termamyl (%) | K_{ps}^{app} (min ⁻¹) |
|------------|---------------|--|---|-------------------------------------|
| Biotage | 250 | 50 | 72 | 0.566 |
| CPG | 1489 | | 70 | 0.629 |
| Micropil A | 300 | 100–150 | 98 | 0.191 |

about 3–10 times by the combined effect of one of the Termamyl reactors and the Micropil A AMG reactor as compared with the Micropil A AMG reactor alone. The K_{ps}^{app} values now obtained are higher than or of the same order of magnitude as those obtained for maltose with AMG alone (see Table 1 in Part I).

The reactor size used throughout this investigation was small (30 μ l). In the final FI system for starch determination, the reactors will be designed to obtain maximum hydrolysis, which necessitates an increase in size of both the AMG and Termamyl reactors. With the investigation performed here and in Part I, a new and better support, Micropil A, to immobilize AMG has been found, which should make it possible to decrease the size of the previously used 700- μ l reactor, using CPG, 729 Å, substantially for hydrolysis of low-molecular-weight substrates. The Micropil A support has additionally a smaller particle size and a smooth and round structure compared with the larger and rougher structure of the normally used CPG support (see Fig. 5b and c). It is hoped that these properties will improve the packing profile of the reactor and lead to a decrease in the otherwise large dispersion. Biotage has been shown to be a possible candidate for Termamyl immobilization, whereas CPG, 1489 Å, proved to be the most efficient support (see Table 2). The surface porous structure of Biotage and the overall better dispersion behaviour might prove valuable when dealing with native starches. One problem may arise, however, owing to a high back-pressure in a large, well packed Biotage reactor. It remains to be seen

how large the Termamyl reactor will have to be and if it will succeed in hydrolysing native starch from different origins to something equivalent to soluble starch so that AMG can complete the hydrolysis to glucose.

Financial support from Stärkelsen (Kristianstad, Sweden), the Swedish Board for Technical Development (STU) and the Swedish Natural Science Research Council (NFR) is gratefully acknowledged. The authors thank Biotage and Microporous Materials for their generous gifts of enzyme supports. Elena Domínguez is thanked for very fruitful discussions and Gunilla Nilsson for helping with the Termamyl immobilizations.

REFERENCES

- 1 J. Emnéus, R. Appleqvist, G. Marko-Varga, L. Gorton and G. Johansson, *Anal. Chim. Acta*, 180 (1986) 3.
- 2 R. Appelqvist, G. Marko-Varga, L. Gorton and G. Johansson, in J.-L. Aucounturier, J.-S. Cauhapé, M. Destriau, P. Hagenmuller, C. Lucat, F. Ménil, J. Portier and J. Salardenne (Eds.), *Proceedings of the 2nd International Meeting on Sensors*, Imprimerie Biscaye, Bordeaux, 1986, p. 603.
- 3 L.A. Larew, D.A.J. Mead and D.C. Johnson, *Anal. Chim. Acta*, 204 (1988) 43.
- 4 L.A. Larew and D.C. Johnson, *Anal. Chem.*, 60 (1988) 1867.
- 5 J. Emnéus and L. Gorton, *Anal. Chim. Acta*, 234 (1990) 97.
- 6 J. Emnéus and L. Gorton, *Anal. Chem.*, 62 (1990) 263.
- 7 L. Gorton, E. Csöregi, E. Domínguez, J. Emnéus, G. Jönsson-Pettersson, G. Marko-Varga and B. Persson, *Anal. Chim. Acta*, 250 (1991) 203.
- 8 F. Ortega, *Anal. Chim. Acta*, 257 (1992) 79.
- 9 P. van Twisk, *Stärke*, 22 (1970) 228.
- 10 K. Svegmarmark, *Stärkels—Struktur och Reologi. En Litteratursammanställning SIK-Rapport*, No. 547, SIK, Göteborg, 1987.
- 11 J. Hohm, I. Björck, N. Asp, L. Sjöberg and I. Lundquist, *J. Cereal Sci.*, 3 (1985) 193.
- 12 K. Ghiasi, E. Varriano-Marston and R.C. Hosenev, *Cereal Chem.*, 59 (1981) 86.
- 13 J. Holm, I. Björck, S. Ostrowska, A. Eliasson, N. Asp, K. Larsson and I. Lundquist, *Starch/Stärke*, 35 (1983) 294.
- 14 N.K. Matheson and B.V. McCleary, in G.O. Aspinall (Ed.), *The Polysaccharides*, Vol. 3, Academic Press, New York, 1985, p. 70.
- 15 K. Zulkowsky, *Ber. Dtsch. Chem. Ges.*, 18 (1880) 1395.
- 16 H.H. Weetall and R.A. Messing, in M.L. Hair (Ed.), *The Chemistry of Biosurfaces*, Vol. 2, Dekker, New York, 1972, Chap. 12.
- 17 R.T. Lee and Y.C. Lee, *Biochemistry*, 19 (1980) 156.
- 18 N. Jentoft and D.G. Dearborn, *J. Biol. Chem.*, 254 (1979) 4349.
- 19 A. Guilbot and C. Mercier, in G.O. Aspinall (Ed.), *The Polysaccharides*, Vol. 3, Academic Press, New York, 1985, p. 209.
- 20 R. Geddes, in G.O. Aspinall (Ed.), *The Polysaccharides*, Vol. 3, Academic Press, New York, 1985, p. 283.
- 21 D.J. Manners, *Carbohydr. Res.*, 16 (1991) 37.
- 22 C. Horváth and J. Engasser, *Biotechnol. Bioeng.*, 16 (1974) 909.
- 23 R.S. Schifreen, D.A. Hanna, L.D. Bowers and P.W. Carr, *Anal. Chem.*, 49 (1977) 1929.
- 24 H. Huck, A. Schelter-Graf and H.-L. Schmidt, *Bioelectrochem. Bioenerg.*, 13 (1984) 199.
- 25 H. Huck, *Bioelectrochem. Bioenerg.*, 21 (1989) 99.
- 26 G. Johansson, L. Ögren and B. Olsson, *Anal. Chim. Acta*, 145 (1983) 71.
- 27 CPG, Information Sheet, SIK, Göteborg, 1990.

Development of a piezoelectric immunosensor for the detection of human erythrocytes

Bernd König and Michael Grätzel

Institut de Chimie Physique, Ecole Polytechnique Fédérale de Lausanne, CH-1015 Lausanne (Switzerland)

(Received 19th August 1992)

Abstract

A reusable piezoelectric immunosensor was developed for the detection of purified human erythrocytes and erythrocytes in whole human blood. Three different methods for immobilization of anti-glycophorin A antibody to the gold electrode were tested. Coating the electrode with polyethylenimine gave the best results in terms of stability, sensitivity and reproducibility. The other two methods, coating the electrode with γ -aminopropyltriethoxysilane and protein A, gave inferior results. Applying an anti-glycophorin A antibody layer via polyethylenimine immobilization on a 10-MHz AT-cut crystal resulted in a linear frequency change for 1×10^3 – 5×10^4 cells ml^{-1} .

Keywords: Biosensors; Piezoelectric sensors; Antibodies; Blood; Erythrocytes; Immunosensors

A biosensor is generally defined as a device that utilizes a biological sensing element connected to a transducing system leading to the output of an electronic signal. The height of this signal is usually proportional to the concentration of the substance. The general philosophy behind biosensor technology is real-time output, high analyte sensitivity and specificity, simplicity of use and cost effectiveness [1–3]. Therefore, biosensors are being developed for a wide range of applications such as in the food industry, for environmental monitoring and processing, in biotechnology and in clinical diagnostics [4].

The biological sensing element can be an enzyme, a biological receptor molecule, a whole organism such as an environmentally sensitive bacterium or antibodies. Direct enzyme biosensors convert a substrate into products that can make contact with the transducer, either directly

or through a mediator such as ferrocene [5]. Receptor-based biosensors detect the analyte by changes in the electrical or optical fields due to receptor–analyte (antigen) interaction. The first biosensor of this type, based on the nicotinic cholinergic receptor detecting ng ml^{-1} amounts of cholinergic ligands, was reported by Taylor et al. [6].

Antibody-based biosensors detect the antigen concentration either by indirect competitive and displacement reactions similar to immunoassays, or by direct changes in transducer output [7]. An example of the latter type of system is the piezoelectric (PZ) crystal detector for assays both in the gas phase and in solution. PZ devices consist of an oscillating quartz crystal containing an adsorbent on its surface that selectively interacts with the analyte. Adsorption of the analyte (antigen) increases the mass of the crystal and decreases proportionally the resonance frequency of oscillation. This frequency-to-mass relationship is described by the equation of Sauerbrey [8]:

$$\Delta F = -2.3 \times 10^6 F^2 \Delta M / A$$

Correspondence to: B. König, Institut de Chimie Physique, Ecole Polytechnique Fédérale de Lausanne, CH-1015 Lausanne (Switzerland).

where ΔF is the change in resonance frequency of the coated crystal, F is the resonance frequency of the crystal, ΔM is the mass increase and A is the area of the coated crystal. The detection limit of this technique is about 10^{-12} g. In 1964 King [9] reported for the first time the use of a PZ crystal as an analytical detector. Since then, work with these detectors has focused mainly on the use of inorganic and organic coatings for gaseous environmental pollutants (for a recent review, see [10]). Since biologically active molecules, such as enzymes and antibodies, have recently become available in large amounts, a new class of PZ biosensors has been developed, the piezoimmunosensor. This system offers many of the properties desired for an ideal immunosensor such as sensitivity, specificity, stability and simplicity.

In this paper, we report the development of a PZ immunosensor for human red blood cells. The strong complexation between the gold electrode and anti-glycophorin A antibody was exploited to construct a reusable immunosensor. The sensor was applied to pure human erythrocytes and whole human blood. The sensitivity, long-term stability and reusability of three different immobilization methods were also reported.

EXPERIMENTAL

Materials

Anti-glycophorin A antibody was obtained from Flow Laboratories (Allschwil, Switzerland). Human whole blood and erythrocytes were from the Zentrallaboratorium Blutspendedienst of the Swiss Red Cross (Berne, Switzerland). Polyethylenimine and γ -aminopropyltriethoxysilane were purchased from Aldrich (Buchs, Switzerland). All other reagents and solvents were of analytical-reagent grade or better (Fluka, Buchs, Switzerland).

Equipment

The PZ crystals (Microcrystal, Grenchen, Switzerland) used in this work were AT-cut with a basic resonance frequency of 10 MHz. The crystal consists of a 14×5 mm quartz wafer which

is placed between 8×2 mm gold electrodes. An identical (uncoated) crystal was used as reference to correct for temperature and humidity fluctuations. The crystal frequency was monitored with a universal counter (Hewlett-Packard).

Immobilization procedures

Three different methods of immobilization were employed, as follows.

Immobilization via a thin polyethylenimine (PEI) layer. A methanol solution (5 ml) containing 2% polyethylenimine was spread on the electrode of the crystal for 30 s. After air drying, the crystal was washed three times with methanol to remove unbound material. The crystal was then immersed in an aqueous 2.5% glutaraldehyde solution (pH 7) for 30 min and washed with water. Subsequently, 5 μ l of a 4 mg ml⁻¹ antibody solution was placed on each side of the crystal for 1 h. Unreacted aldehyde groups were blocked by immersing the crystal in a solution of 0.1 M glycine in 20 mM phosphate-buffered saline (pH 7). The crystal was subsequently rinsed with phosphate-buffered saline and distilled water and dried in air.

Immobilization via a thin silane layer. The crystal was dipped in a 5% solution of γ -aminopropyltriethoxysilane (APTES) in dry benzene for 2 h at room temperature. After vacuum drying at 70°C, the crystal was washed several times with acetone and incubated for 2 h in 2.5% glutaraldehyde (pH 7). Following washing with distilled water, 5 μ l of a 4 mg ml⁻¹ antibody solution were spread on both sides of the crystal. After drying for 45 min, the crystal was washed with phosphate-buffered saline and distilled water and subsequently air dried.

Immobilization via protein A-gold. The PZ crystal was dipped for 30 min in 1.2 M NaOH, then washed with distilled water and placed for 10 min in 1.2 M HCl. Following washing with distilled water and ethanol, the crystal was dried at 70°C. Then 5 μ l of a protein A solution (1 mg ml⁻¹, pH 7) were added to the electrodes on both sides of the crystal. After drying, the coated crystal was washed with distilled water and 5 μ l of a 4 mg ml⁻¹ antibody solution were spread over both gold electrode surfaces, dried, washed with phos-

phate-buffered saline and then washed with distilled water and dried again.

Measurement procedures

ΔF_1 , the frequency difference between the coated crystal and the reference crystal, was determined first. The coated crystal was subsequently dipped for several minutes in 1 ml of a solution of human red blood cells in phosphate-buffered saline (pH 7) or human whole blood containing different concentrations of cells. After rinsing with phosphate-buffered saline and air drying, the coated crystal was placed in the test chamber and a new frequency difference was measured (ΔF_2). The shift in the frequency difference ($\Delta F = \Delta F_2 - \Delta F_1$) was related to the amount of cells adsorbed on the crystal.

RESULTS

Comparison of the three different immobilization methods showed that the best results for pure human erythrocytes with regard to sensitivity, reusability and stability were obtained with the polyethylenimine method (Table 1). The crystal precoated with a thin layer of polyethylenimine could be reused five times without a detectable decrease in sensitivity over a period of 15 days (data not shown) and additionally it provided the most reproducible results. As can be seen from Fig. 1, a plot of frequency change versus number of pure human erythrocytes for this method is linear from 1×10^3 to 5×10^4 cells. Additional studies comparing the frequency change of pure human erythrocytes and human whole blood showed a 10% increased signal for

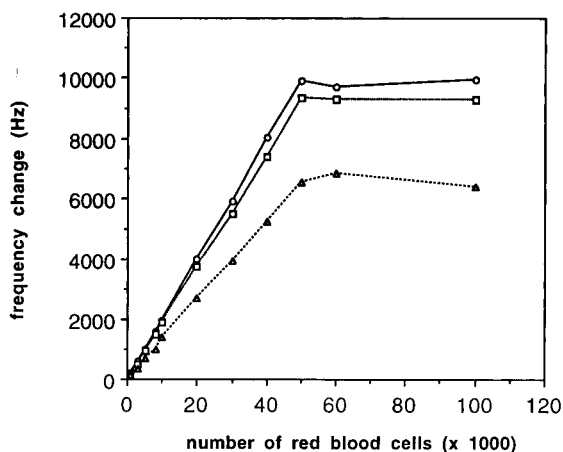


Fig. 1. Comparison of three different immobilization procedures and relationship between the concentration of human erythrocytes and the frequency change of the anti-glycophorin A antibody-coated crystal: \circ = immobilization via polyethylenimine; \square = immobilization via γ -aminopropyltriethoxysilane; \triangle = immobilization via protein A. The points represent the average of ten experiments.

whole blood, indicating that only a small amount of unspecific material contained in the whole blood sample adhered to the electrode surface (Fig. 2). Imaging the electrodes with stained blood

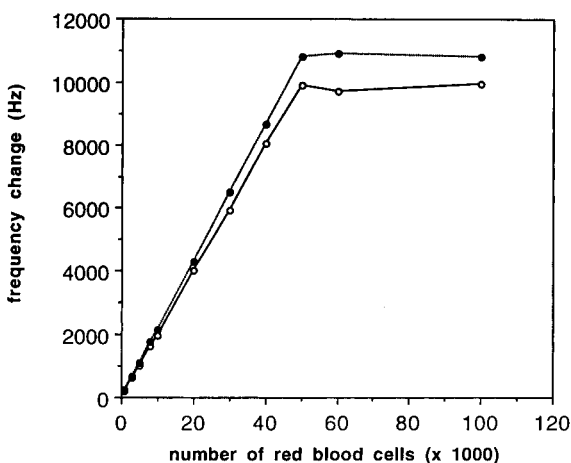


Fig. 2. Comparison of frequency changes with increasing concentrations of (\circ) pure human erythrocytes and (\bullet) erythrocytes in whole human blood (polyethylenimine immobilization procedure). With whole human blood a 10% increased frequency change is observed owing to unspecific binding of other blood cells, mainly platelets. The points represent the average of ten experiments.

TABLE 1

Frequency changes (ΔF) with three different immobilization procedures (average of ten experiments)

| Immobilization method | ΔF | |
|--------------------------------------|--------------------|-------------------|
| | Human erythrocytes | Whole human blood |
| Polyethylenimine | 9860 \pm 11 | 10848 \pm 39 |
| γ -Aminopropyltriethoxysilane | 9322 \pm 18 | 11442 \pm 32 |
| Protein A | 6612 \pm 192 | 10024 \pm 46 |

cells indicated that about 95% of the unspecifically bound cells are platelets (data not shown).

Immobilization via APTES led to inferior sensor performance, the sensitivity and reusability (only four times) of the detection system being slightly decreased. Although linear from 1×10^3 to 5×10^4 cells, a 23% increased signal for whole blood compared with pure erythrocytes was observed, indicating enhanced interaction with interfering agents.

Sensors prepared by immobilization via protein A gave the most unfavourable results. The smallest frequency changes and the highest interference from unspecifically bound material (52%) contained in whole human blood were observed (Table 1). Also, the crystal could be used for only one assay because it could not withstand the regeneration step. When the crystal was immersed in a solution containing 8 M urea, partial desorption of the immobilized antibody occurred. Other dissociating agents such as 0.2 M glycine-HCl (pH 2.8) and 0.2 M ethanolamine (pH 8) did not totally remove the adsorbed cells.

The crystal surface coated with 4 mg ml^{-1} of antibody solution was considered optimum. Up to 4 mg ml^{-1} , the sensitivity of the crystal increased with increase in the antibody concentration used for immobilization. Above this concentration, the frequency change was no longer dependent on the antibody concentration (data not shown).

Another important factor affecting the sensitivity of the PZ detecting system is the time of incubation of the antibody-coated crystal with antigen. In order to optimize this parameter the crystal was exposed to a solution of 1×10^4 erythrocytes ml^{-1} for different periods. The results showed that an incubation time of 10 min gave optimum sensitivity. Prolonged exposure for up to 3 h did not improve the observed frequency change (Fig. 3). Therefore, in all subsequent experiments, a 10-min incubation time was used.

DISCUSSION

This study demonstrates the successful application of piezoelectric immunosensor technology to detect pure human erythrocytes in the range

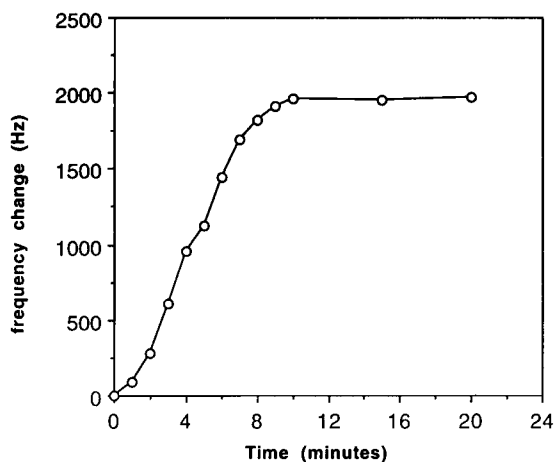


Fig. 3. Correlation between human erythrocytes and anti-glycophorin A antibody reaction time resonance frequency shift (ΔF) for cell concentrations of 1×10^4 cells ml^{-1} . Each point represents the average of five experiments.

1×10^3 – 5×10^4 cells. Erythrocyte levels in whole human blood were also determined.

Of the three different immobilization procedures employed, attachment of the antibody to a polyethylenimine-coated electrode surface gave the best results with regard to stability, sensitivity, and reproducibility. This agrees with earlier observations by Prusak-Sochaczewski et al. [11]. Additionally, this method seems to be superior in specificity to the two other immobilization procedures because it resulted in the lowest response to other blood cells.

This contrasts with results published by Plomer et al. [12], who obtained optimum results with the protein A–gold immobilization method. In our hands, however, this method gave the most unfavourable sensor performance. A possible explanation for the reduced sensitivity and stability observed with this immobilization technique could be that the strength of the protein–protein interaction in the gas phase is dramatically reduced, and that during the different washing and drying steps the protein A–antibody interaction was destroyed, resulting in a reduced sensitivity of the piezoelectric device. As a consequence, the advantage of the geometric orientation via the Fc part of the antibody is lost. Moreover, protein A-derivatized electrodes exhibit enhanced unспе-

cific interaction with non-erythrocytic cells contained in whole blood, owing to the non-homogeneous electrode surface exposing both its hydrophilic and hydrophobic parts. The APTES method showed nearly the same sensitivity and reproducibility as the polyethylenimine method. However, the amount of unspecifically bound human blood cells, mainly platelets, was slightly increased, perhaps owing to the more polar surface.

The results demonstrate that a piezoelectric crystal coated with polyethylenimine and anti-glycophorin A antibody can be applied for the determination of pure human erythrocytes and erythrocytes in whole human blood. The coating process with the polymer is simple and reproducible. However, from the plots of frequency change versus cell concentration one can estimate 5×10^4 erythrocytes as the maximum number of cells bound to the electrode area. Comparing this number with the theoretical maximum possible number of erythrocytes (2.7×10^5 for an area of $1.6 \times 10^7 \mu\text{m}^2$ and a diameter of $7.7 \mu\text{m}$ for the erythrocytes) showed that only 20% of the immobilized antibodies are active. Therefore, better methods for antibody immobilization and regeneration have to be developed to improve the

sensitivity, stability and reproducibility of the piezoelectric immunoassays.

The authors thank S. Dalla-Piazza (Asulab, Neuchâtel) for his help.

REFERENCES

- 1 C.R. Lowe, *Biosensors*, 1 (1985) 3.
- 2 A.P.F. Turner, *Sensor Actuators*, 17 (1989) 433.
- 3 R.F. Taylor, in D.L. Wise (Ed.), *Bioinstrumentation: Research, Developments and Applications*, Butterworths, Boston, 1990, p. 355.
- 4 C. Kösslinger, S. Drost, F. Aberl, H. Wolf, S. Koch and P. Woias, *Biosensors Bioelectr.*, 7 (1992) 397.
- 5 M.F. Cardosi and A.P.F. Turner, in A.P.F. Turner, I. Karube and G.S. Wilson (Eds.), *Biosensors: Fundamentals and Applications*, Oxford University Press, London, 1987.
- 6 R.F. Taylor, I.G. Marenchic and E.J. Cook, *Anal. Chim. Acta*, 213 (1988) 131.
- 7 I. Karube and M. Suzuki, *Biosensors*, 2 (1986) 343.
- 8 G.Z. Sauerbrey, *Z. Phys.*, 155 (1959) 206.
- 9 W.H. King, *Anal. Chem.*, 36 (1964) 1735.
- 10 G.G. Guilbault and J. Jordan, *CRC Crit. Rev. Anal. Chem.*, 19 (1988) 1.
- 11 E. Prusak-Sochaczewski, J.H.T. Luong and G.G. Guilbault, *Enzyme Microb. Technol.*, 12 (1990) 173.
- 12 M. Plomer, G.G. Guilbault and B. Hock, *Enzyme Microb. Technol.*, 14 (1992) 230.

Glucose oxidase enzyme electrode: relation between inner membrane permeability and substrate response

Séamus P.J. Higson, Mohamed Desai, Zahra Koochaki and Pankaj M. Vadgama

Department of Medicine (Section of Clinical Biochemistry), University of Manchester, Hope Hospital, Eccles Old Road, Salford M6 8HD (UK)

(Received 9th June 1992; revised manuscript received 4th November 1992)

Abstract

Permeability coefficients, P ($\text{cm}^2 \text{s}^{-1}$), for H_2O_2 and O_2 across microporous polycarbonate membranes of varying pore radii together with similar membranes coated with an organosilane have been determined, using a classical diffusion chamber. A correlation has been attempted between the permeability of such membranes with their performance when used as inner membranes of glucose oxidase electrodes.

Organosilane coated polycarbonate membranes were found to impart extended linearity ranges ($> 40 \text{ mM}$) to glucose enzyme electrodes. The $\text{O}_2/\text{glucose}$ permeability coefficient (P) ratio of such inner membranes was found to be critical in determining sensor performance. It is proposed that for the oxidase based electrodes used, extensions in linearity were due to the cumulative effect of two phenomena. Firstly the relative augmentation of O_2 returning into the enzyme layer following the oxidation of H_2O_2 helps free the sensor from the effects of low ambient pO_2 levels. Secondly inner membrane barriers offering increased diffusional resistances towards H_2O_2 maintain linear diffusion of H_2O_2 to the working electrode at higher substrate concentrations.

Keywords: Enzymatic methods; Glucose oxidase electrode; Membrane permeability

Enzyme electrodes permit direct measurement of intermediary metabolites with relative simplicity [1]. Oxidase enzyme-based electrodes using the amperometric detection of H_2O_2 have been the most extensively studied types of system, most notably for glucose [2]. This sensor utilizes the catalytic oxidation of glucose with the coincident reduction of O_2 to H_2O_2 , the latter being oxidised at anodic potentials at the working electrode (Fig. 1).

For the classical arrangement, O_2 is an absolute requirement, and a low oxygen concentration can prove rate limiting for the enzyme reaction, rendering the device susceptible to O_2 variation

in the bulk sample at low ambient pO_2 and high glucose levels, as well as imposing a restricted linearity well below the enzyme Michaelis constant K_m . Stabilisation of oxygen requirements has been attempted using artificial mediators [3] but membrane technology can also allow performance optimisation [1]. Thus substrate diffusion limiting membranes have been used [4] to reduce access of glucose to the enzyme laminate, so reducing the local glucose concentration in the enzyme microenvironment to below the enzyme K_m and extending practical limits. Specific tailoring of the external covering membrane has been achieved using membranes that have a high O_2 permeability relative to glucose, which further reduces the chances of background O_2 limitation. Such membranes include organosilane [4], polyurethane [5] and lipid impregnated barriers [6].

Correspondence to: S.P.J. Higson, Department of Medicine (Section of Clinical Biochemistry), University of Manchester, Hope Hospital, Eccles Old Road, Salford M6 8HD (UK).

Inner membrane effects involving an intersecting membrane between the enzyme layer and the working electrode have not been studied however. Although the enzyme reaction consumes O_2 , it must be recalled that some O_2 is regenerated at the working electrode due to the oxidation of H_2O_2 (Fig. 1). This is free to diffuse to the bulk analyte solution, or to the enzyme laminate. The permeability of O_2 across the inner membrane would therefore be expected to be a further variable in determining the local pO_2 within the enzyme layer.

This paper reports the characterisation and correlations of O_2 and H_2O_2 transport across inner polycarbonate microporous membranes of enzyme electrodes to the enzyme kinetics and linearity ranges for glucose analysis.

EXPERIMENTAL

Reagents

Disodium hydrogenphosphate, sodium benzoate, sodium chloride, EDTA, hydrogen peroxide, 1,1,1-trichloroethane, potassium iodide, sodium thiocyanate, and sulphuric acid (AnalaR grade) and methyl trichloroethane (general purpose reagent) were purchased (from BDH, Poole) and used without further purification. Glucose oxidase from *Asperigillus niger* (75% protein, 150 000 units g^{-1} solid) and bovine serum albumin (Fraction V) were purchased from Sigma (Poole).

A buffer (pH 7.4) consisting of 5.28×10^{-2} M Na_2HPO_4 , 1.3×10^{-2} M NaH_2PO_4 , 5.1×10^{-3} M $NaCl$, 1.16×10^{-2} M EDTA and 6.24×10^{-3} M C_6H_5COONa was prepared in distilled water. This solution was used for all electrode and diffusional studies.

Apparatus

An electrode assembly designed for O_2 detection (Rank Brothers, Bottisham) was adapted as previously described for H_2O_2 detection [4,5], the working electrode (anode) being polarized here at +650 mV (vs. Ag/AgCl). The electrode cell comprised a central 2 mm diameter platinum disc as the working electrode (anode) with an outer 12 mm diameter, 1 mm wide silver ring (Ag/AgCl) as a combined reference and counter electrode. The diffusion chamber apparatus and the purpose built voltage polarization source and potentiostat were constructed by the chemistry workshops (University of Newcastle). An $x-t$ chart recorder (Lloyd Instruments, Fareham) was used to record the amperometric responses of the electrode assembly from the potentiostat current follower. A blood gas analyzer (Instrumentation Lab IL1802, Hope Hospital, Clinical Biochemistry Laboratory) was used for the determination of pO_2 within buffer aliquots.

A classical diffusion chamber was used for the measurement of solute permeability, as previously described [5,7]. The apparatus comprised two stirred 170-ml compartments separated by the membrane of interest held by stainless steel discs and rubber O-rings.

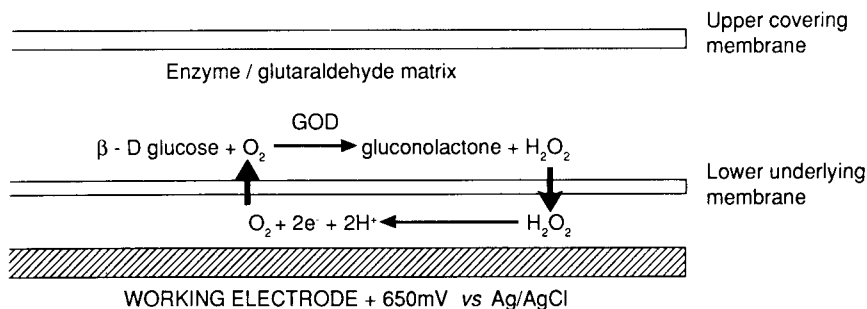


Fig. 1. Schematic diagram of a glucose oxidase enzyme electrode.

Membranes

Polycarbonate membranes with designated pore radii ranging from 0.01 to 0.6 μm were purchased from the Poretics Co. (Pleasanton, CA). Organosilane coated membranes were prepared as follows.

A 5 cm diameter membrane was immersed in a 2% aqueous solution of methyl trichlorosilane for 30 s. The membrane was then extracted and placed between two glass slides under finger pressure for 30 s to expel excess silane solution. The slides were gently prised apart and allowed to dry for around 5 min till a homogeneous white film was seen to form. The membrane was washed in a jet of distilled water for approximately 30 min to remove excess or non adhered silane. All membranes were stored in buffer prior to use.

Enzyme laminates

Glucose oxidase (GOD, 2560 units ml^{-1}) and bovine serum albumin (BSA, 0.1 g ml^{-1}) were dissolved in buffer solution. 6 μl of GOD-BSA solution and 3 μl of glutaraldehyde (5%, v/v) were mixed rapidly and placed on a 1- cm^2 portion of the polycarbonate membrane to be used as the inner membrane. A further 1- cm^2 portion of the polycarbonate membrane was then placed on the enzyme and glass slides were used to compress the enzyme laminate under finger pressure for 5 min. The resulting crosslinked enzyme layer was placed over the working electrode prior to final enzyme electrode assembly and fixation by an O-ring.

Determination of permeability coefficients

Permeability coefficients were calculated using the expression derived by Sun et al. [7]. pO_2 was assayed anaerobically in syringe aspirated chamber samples using a blood gas analyzer. H_2O_2 was determined amperometrically using the Rank electrode polarized at +650 mV vs. Ag/AgCl. Amperometric calibrations for H_2O_2 were correlated with titimetric determinations with acidified potassium iodide [8]. This method of determination was employed because stabilizers present in proprietary preparations have been shown not to influence the determination of H_2O_2 .

RESULTS AND DISCUSSION

Conventional glucose oxidase enzyme electrodes comprise an enzyme laminate made up of inner and outer membranes together encapsulating an immobilized enzyme layer. The diffusion of substrate and O_2 to the enzyme matrix catalyses the production of H_2O_2 which is then free to diffuse either through the lower membrane to the working electrode where it is oxidized to generate an amperometric signal, Fig. 1, or to the bulk solution. The problem of O_2 limitation on the reaction has been previously addressed by us, using generic external membranes [4]. The oxidation of H_2O_2 at the anodic working electrode generates more O_2 , augmenting pO_2 levels close to the electrode surface. It is therefore, likely that the porosity of inner membrane will be a critical factor in determining the pO_2 levels within the active enzyme matrix.

Inner membrane porosity was varied using polycarbonate membranes with pore radii 0.05, 0.04, 0.03 and 0.01 μm respectively. The resulting calibration graphs are shown in Fig 2. Responses are seen to fall with decreasing nominal pore radius, as would be expected [4], due to the increased diffusional resistance offered to H_2O_2 . However a small increase of linearity is suggested

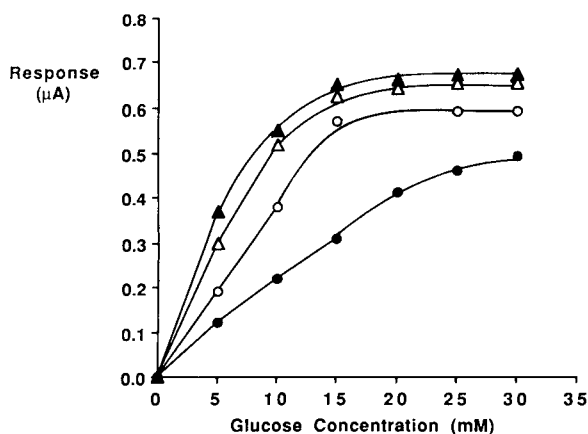


Fig. 2. Glucose electrode calibration using external 0.01 μm pore radii polycarbonate membranes with inner polycarbonate membranes of (●) 0.01, (○) 0.03, (△) 0.04 and (▲) 0.05 μm pore radii. Correlation coefficients (r^2): (●) 0.946, (△) 0.789, (○) 0.846, (▲) 0.756.

for the lowest responding system, (as shown by the r^2 values, Fig 2). The lower porosity membranes will offer increased diffusional resistances for both H_2O_2 transfer to the working electrode and returning O_2 . An increased diffusional resistances towards H_2O_2 over O_2 (due to its slightly larger size), might cause relative enhancement of pO_2 levels within the enzyme microenvironment, explaining some of the effect on the linear range.

This effect was studied further by increasing the diffusional distance between the working electrode and the enzyme matrix. A series of enzyme electrodes was constructed all with $0.01 \mu\text{m}$ pore radii external covering polycarbonate membranes and up to 4 inner $0.6 \mu\text{m}$ pore radii polycarbonate inner membranes; each membrane

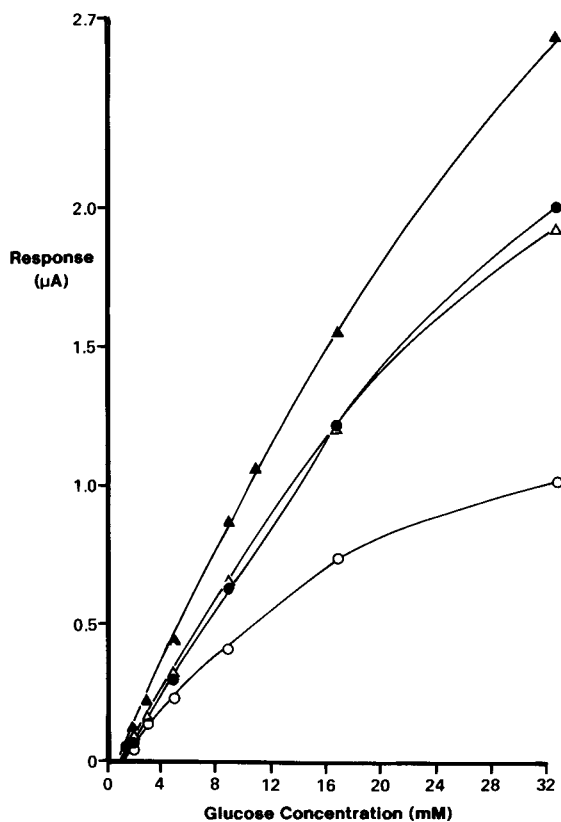


Fig. 3. Glucose electrode calibration using external $0.01 \mu\text{m}$ pore radii polycarbonate membranes with (▲) 1, (●) 2, (△) 3, (○) 4, multiple inner polycarbonate membranes of $0.6 \mu\text{m}$ pore radii. Correlation coefficients (r^2): (▲) 0.986, (●) 0.986, (△) 0.982, (○) 0.980.

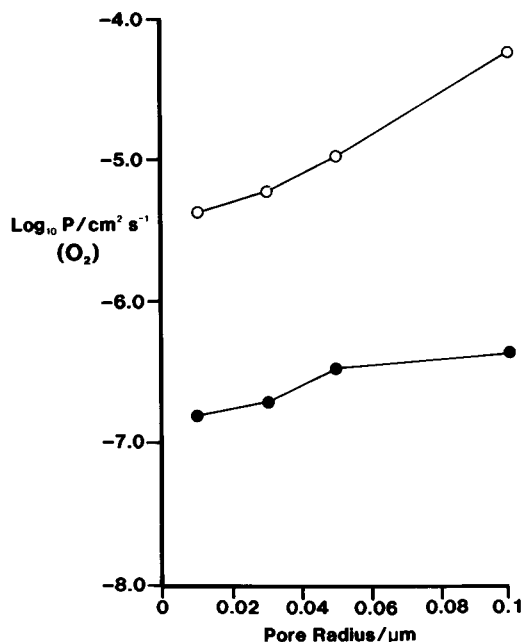


Fig. 4. Relationship of permeability coefficients for O_2 with membrane pore radius, for uncoated (○) and organosilane coated (●) polycarbonate membranes.

had a nominal thickness of $10 \mu\text{m}$ [9]. Calibration graphs for these sensors (Fig. 3), show as expected that as the diffusional distance to the working electrode increases, glucose responses diminish. However the least sensitive electrode shows the greatest departure from linear behaviour (as seen by the r^2 values, Fig 3). Again a direct correlation is seen between the diffusional resistance offered to O_2 returning from the working electrode to the enzyme layer and the electrode performance. It should be noted that increased diffusional resistance to O_2 will lower pO_2 values in the enzyme matrix which might be expected to influence enzymatic behaviour, however an increased diffusional resistance to H_2O_2 should have no effect on electrode linearity.

Organosilane coatings of polycarbonate membranes [4], and of microporous polyurethane covering membranes [5], have previously been used to manipulate the O_2 /substrate permeability coefficient, P , ratios. In these studies, microporous polycarbonates membranes coated with methyl trichlorosilane were used instead as underlying

membranes in the enzyme laminate. In addition, permeability coefficients of H_2O_2 and O_2 were determined using diffusion chambers to allow correlations to be made with electrode performance. Figures 4 and 5 show permeability coefficients of O_2 and H_2O_2 which are seen to be lower for organosilane coated membranes than uncoated polycarbonate membranes; in addition P values for O_2 and H_2O_2 were found to decrease as the pore radii of uncoated and organosilane coated polycarbonate membranes were decreased. This confirms that the organosilane coating decreases the available pore area, so presenting increased diffusional resistance to any solute.

O_2 transfer is less affected than H_2O_2 transfer as the pore radius is decreased, and when a silane coating is utilised (Fig. 6). When a calibration graph is obtained for a glucose electrode using a silanised 0.03 or 0.01 μm inner membrane (Fig. 7), the sensitivity is less than that for the non-silanised counterpart. More importantly, however, linearity is markedly increased to at least 40

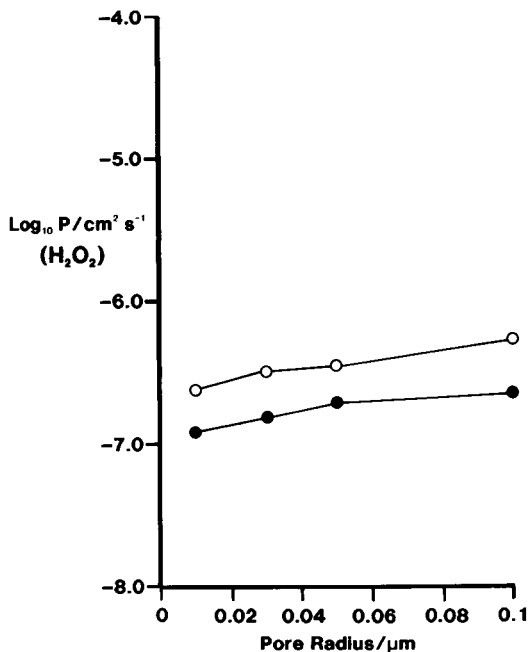


Fig. 5. Relationship of permeability coefficients for H_2O_2 with membrane pore radius, for uncoated (○) and organosilane coated (●) polycarbonate membranes.

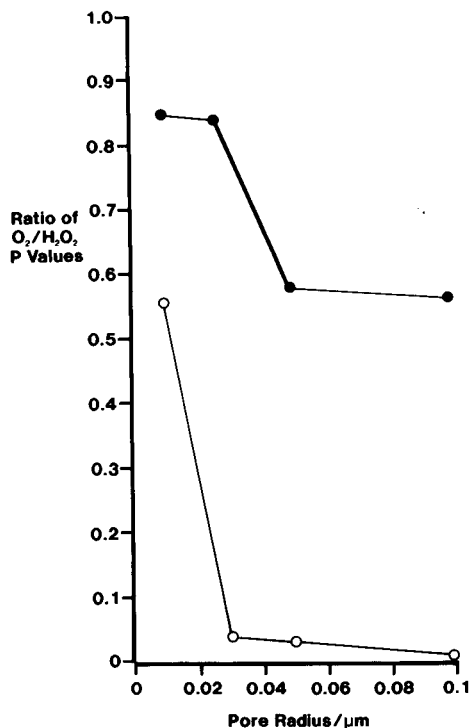


Fig. 6. Relationship of $\text{O}_2/\text{H}_2\text{O}_2$ P ratio with membrane pore radius for uncoated (○) and organosilane coated (●) polycarbonate membranes.

mM glucose when a silanised membrane is used as an inner membrane.

It is clear that a silane treated inner membrane has a more potent effect for increasing linearity range than barrier layers without silane. This is probably a cumulative effect of two phenomena. Fig. 6 shows that the $\text{O}_2/\text{glucose}$ P ratio is crucial in determining the sensor performance. Firstly a high O_2 permeability of such a membrane at least relative to H_2O_2 , will increase the steady state $p\text{O}_2$ within the enzyme layer, freeing the enzyme from the limitations imposed by low ambient $p\text{O}_2$ levels. Secondly increased diffusional resistance towards H_2O_2 across inner membranes progressively raise the diffusional gradient for H_2O_2 from the enzyme layer to the working electrode, (in this case the diffusional distance remains constant). This clearly has the effect of linearising sensor responses to higher glucose concentrations by enabling a *linear* diffu-

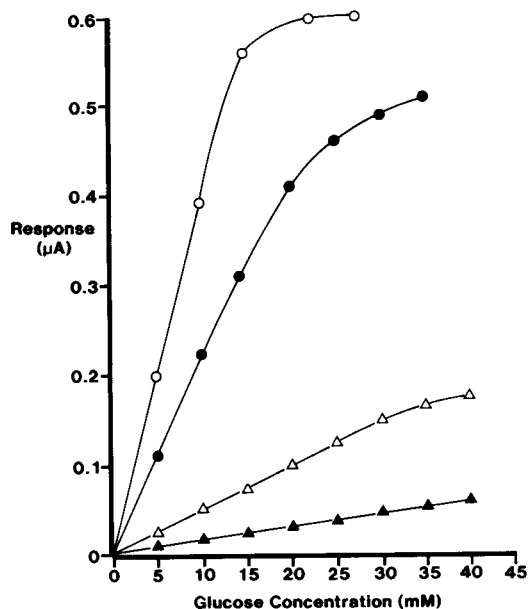


Fig. 7. Glucose electrode calibration using external $0.01 \mu\text{m}$ pore radii polycarbonate membranes. Inner membranes: uncoated (\circ) 0.03 , (\bullet) 0.01 pore radii membranes; organosilane coated (Δ) 0.03 , (\blacktriangle) $0.01 \mu\text{m}$ pore radii polycarbonate membranes. Correlation coefficients (r^2): (\circ) 0.846 , (\bullet) 0.946 , (Δ) 0.966 , (\blacktriangle) 0.988 . For (\blacktriangle), regression equation: Response (μA) = $0.0132 + 0.0151$ (glucose conc. in mM). S.D. slope = 6.3×10^{-5} , standard error = 2.2×10^{-5} . S.D. intercept = 1.5×10^{-3} , standard error = 5.3×10^{-4} .

sion of H_2O_2 to be maintained to the working electrode proportional to H_2O_2 production within the immobilised enzyme matrix.

Conclusions

Inner membrane permeability effects may generically influence the linearity of response of oxidase based enzyme electrodes. The raising of $\text{O}_2/\text{H}_2\text{O}_2$ P ratios causes a relative augmentation of pO_2 levels within the local enzyme mi-

croenvironment. Polycarbonate membranes of decreasing pore radii progressively show higher $\text{O}_2/\text{H}_2\text{O}_2$ P ratios associated with extended linearity ranges, although with diminished sensitivity. Organosilane coated membranes exhibit higher $\text{O}_2/\text{H}_2\text{O}_2$ P ratios than non-silanised membranes with consequent extensions in linearity range and decrease in sensitivity.

These observations may be partially explained by an relative augmentation of pO_2 levels caused by a relative facilitated return of O_2 from the working electrode to the enzyme together with a lineraising of H_2O_2 diffusion from the enzyme to the working electrode by the inclusion of inner membranes offering increased diffusional resistance to H_2O_2 .

The authors would like to thank the Science and Engineering Research Council (UK) for financial support for SPJH and ZK.

REFERENCES

- 1 P. Vadgama, *J. Membr. Sci.*, 50 (1990) 141.
- 2 A.P.F. Turner, I. Karube and G.S. Wilson, *Biosensors. Fundamentals and Applications*, Oxford University Press, Oxford, 1987.
- 3 A.E.G. Cass, G. Davis, G.D. Francis, H.A.O. Hill, W.J. Aston, I.J. Higgins, E.V. Plotkin, L.D.L. Scott and A.P.F. Turner, *Anal. Chem.*, 56 (1984) 667.
- 4 W.H. Mullen, F.H. Keedy, S.J. Churchouse and P. Vadgama, *Anal. Chim. Acta*, 183 (1986) 59.
- 5 S. Churchouse, W. Mullen, C. Battersby and P. Vadgama, *Biosensors*, 2 (1986) 325.
- 6 L.X. Tang, Z.B. Koochaki and P. Vadgama, *Anal. Chim. Acta*, 232 (1990) 357.
- 7 Y. Sun, S. Furusaki, A. Yamauchi and K. Ichimura, *Biotechnol. Bioeng.*, 34 (1989) 55.
- 8 A.I. Vogel, *A Textbook of Quantitative Inorganic Analysis*, Longman, London, 3rd edn., 1978, p. 363.
- 9 Poretics catalog, Livermore, CA, 1992.

Enzyme-based catechol sensor based on the cyclic reaction between catechol and 1,2-benzoquinone, using L-ascorbate and tyrosinase

Shunichi Uchiyama, Yasushi Hasebe, Hiroya Shimizu and Hideki Ishihara

Department of Environmental Engineering, Saitama Institute of Technology, 1690 Fusaiji, Okabe, Saitama 369-02 (Japan)

(Received 29th September 1992; revised manuscript received 7th December 1992)

Abstract

A cyclic reaction between catechol and 1,2-benzoquinone takes place by combining the tyrosinase reaction and the chemical reduction of 1,2-benzoquinone to catechol by L-ascorbic acid. Catechol is oxidized by the dissolved oxygen catalysed by the enzyme and its consumption is not compensated for by the chemical regeneration of catechol from 1,2-benzoquinone. The dissolved oxygen thus continues to decrease during the cyclic reaction and consequently the decrease in the reduction current of oxygen is amplified. The amplification factor of 1×10^{-6} M catechol at 0.01 M L-ascorbate and pH 7.0 was found to be 300 when enzyme activity was 20 U ml^{-1} and the reaction time was 10 min. The calibration graph for catechol obtained with a potato tissue membrane electrode was moved in parallel to a lower concentration range and the detection limit was found to be 5×10^{-8} M (amplification factor 400) when buffer solution of pH 7.0 containing 0.01 M L-ascorbic acid was used.

Keywords: Enzymatic methods; Biosensors; Amplification; Catechol; Enzyme electrodes

Recently, amplification of responses has received much attention in biosensors research and recycling of the substrate [1,2] and mediator [3–5] have been reported to enhance the responses of substrates. In biosensor systems, the oxygen electrode has been widely used to measure substrates which are oxidized by oxygen catalysed by an oxidase enzyme, and a number of biosensors employing an oxygen electrode and oxidase enzyme have been successfully fabricated. In the oxidase enzymatic reaction, the substrate is oxidized and an oxidized compound is produced. If this oxidized compound is reconverted into the original compound by chemical reduction with an appro-

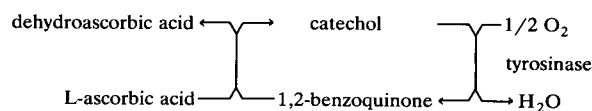
priate reducing agent, a cyclic reaction between the substrate and oxidized product may proceed.

Recently, it has been found that the cyclic reaction between the reduced and oxidized forms of vitamin C takes place by combining the ascorbate oxidase reaction and the chemical reduction of the oxidized form of vitamin C by dithiothreitol [6]. By using this cyclic reaction, the current response of the oxygen electrode can be amplified [7].

A variety of plant tissues have a high tyrosinase activity and tyrosinase in beet [8] and banana [9] tissues have been utilized to fabricate tyrosine and dopamine sensors with detection limits of about 10^{-5} M. Tyrosinase has a broad specificity for *o*-diphenol compounds and catalyses the oxidation of catechol to 1,2-benzoquinone. Schiller et al. [10] suggested that 1,2-

Correspondence to: S. Uchiyama, Department of Environmental Engineering, Saitama Institute of Technology, 1690 Fusaiji, Okabe, Saitama 369-02 (Japan).

benzoquinone is reduced to catechol by hexacyanoferrate(II) ion in the potentiometric method for phenol, although a cyclic reaction system was not described [10]. Hence, a chemically amplified catechol response might be observed by combining the tyrosinase reaction and a reducing agent. L-Ascorbic acid is well known as an effective reducing agent and 1,2-benzoquinone would be reduced to catechol and may drive the reaction in the opposite direction to that of enzymatic oxidation of catechol. By comparing the two reactions, it can be seen that the oxygen consumed in the enzymatic reaction is not compensated for by the chemical reduction. Therefore, if L-ascorbic acid does not affect the enzyme activity of tyrosinase, a cyclic reaction should take place and the consumption of the dissolved oxygen will continue until its concentration becomes zero. This cyclic reaction can be described by the following cyclic reaction scheme:



This scheme suggests that the enzymatic current response of catechol is amplified when L-ascorbic acid is present in the solution containing tyrosinase and, moreover, the unstable 1,2-benzoquinone can be determined in addition to catechol. Consequently, this cyclic reaction system has a unique feature that permits the total determination of catechol and 1,2-benzoquinone when the sample solution contains both species.

Catechol sensors based on an immobilized catechol monooxygenase [11] and spinach [12] leaves have been reported, but 1,2-benzoquinone could not be detected and the detection limits were at the 10^{-5} M level. It can be expected that the sensitivity of the catechol sensor would be increased by combining the tyrosinase reaction and chemical reduction. In this work, the amplification of the current response of catechol in this cycle was evaluated and a potato tissue electrode [13] was fabricated for the observation of the amplified biosensor response of catechol. The effects of pH, concentration of L-ascorbic acid and enzyme activity on the amplification factors are also described.

EXPERIMENTAL

A 1-mg amount of tyrosinase (EC 1.14.18.1) (Sigma, from mushroom, 1000 U mg^{-1}) was added to 50 ml of sample solution. The reducing agents [L-ascorbic acid, potassium hexacyanoferrate(II) and nicotinamide adenine dinucleotide disodium salt (NADH)] and catechol were of analytical-reagent grade. All experiments were done at room temperature.

The concentration of dissolved oxygen in the sample solution was monitored with a Clark-type oxygen electrode (Denki Kagaku Keiki) with a gold working electrode and a gas-permeable membrane. The electrode potential of the working electrode was maintained by a potentiostat (Nikko Keisoku NPOT 2501) at -0.7 V vs. an Ag/AgCl counter electrode and the reduction current of oxygen was recorded with a one-pen recorder (Nippon Denshi Kagaku, Unicorder U-228).

The potato tissue electrode was fabricated by placing a round, thin, potato tissue membrane (0.2 mm thick, 5 mm diameter) on the surface of the oxygen gas-permeable membrane of the oxygen electrode and this tissue was covered with a dialysis membrane.

Sample solutions (50 ml) were prepared by dissolving L-ascorbic acid in buffer solutions and were stirred by a magnetic stirrer throughout the experiment. After the background current of the dissolved oxygen in buffer solution had reached a steady-state value (about $0.8\text{--}1.2 \mu\text{A}$), catechol was added to this solution and the response current was recorded.

RESULTS AND DISCUSSION

According to the enzyme reaction, the colour of the catechol solution containing the enzyme changed from colourless to red-yellow (absorption maxima 400 nm) and this colour was completely extinguished again within 1 min when $1 \times 10^{-3} \text{ M}$ L-ascorbic acid was added. This result suggests that the enzymatic reaction product of catechol, 1,2-benzoquinone, is returned to original catechol via chemical reduction.

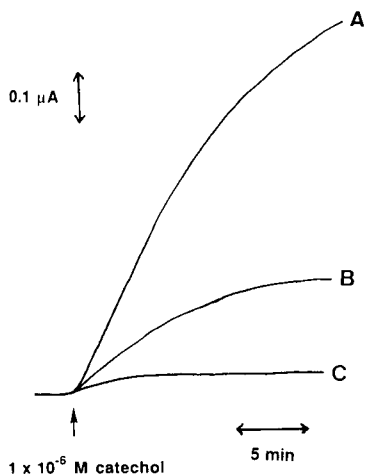


Fig. 1. Typical current responses of 1×10^{-6} M catechol enzyme solution containing reducing agents at pH 7.0: (A) 1×10^{-2} M L-ascorbic acid; (B) 1×10^{-2} M hexacyanoferrate(II) ion; (C) 1×10^{-2} M NADH. Enzyme activity = 20 U ml^{-1} .

The cyclic reaction of catechol results in a continuing decrease in the oxygen current, but the current response of catechol in the presence of enzyme without reducing agents reaches a limiting value because the catechol is depleted according to the advance of the enzymatic reaction and the dissolved oxygen is gradually resupplied from air. The limiting response current value of 1×10^{-4} M catechol was found to be 160 nA and the slope of the calibration graph corresponded to $1.6 \text{ nA } \mu\text{mol}^{-1}$. Therefore, the am-

plification factor of the current response was calculated from the ratio of this slope obtained without reducing agent and that obtained with reducing agent.

The typical current responses of catechol obtained in the presence of the enzyme solution with each reducing agent are shown in Fig. 1. These results indicate that L-ascorbic acid gave the largest current response among these reducing agents, and the amplification factors of 1×10^{-6} M catechol by L-ascorbic acid, hexacyanoferrate(II) ion and NADH were found to be 300, 89 and 25, respectively. The amplification of these current responses supports the assumption that a cyclic reaction of catechol takes place. The oxygen concentration continues to decrease nearly to zero because the cyclic reaction does not stop and a very long reaction time is needed until the current reaches a steady-state level after the sample addition. Therefore, 10 min were chosen as the reaction time for amplification. For L-ascorbic acid, the reproducibility of five response current values at 10 min was about 5% (relative standard deviation).

The amplified current response is pH dependent because the enzyme activity of tyrosinase is decreased in acidic and alkaline media. However, with L-ascorbic acid, no significant variation of the current response was observed in the pH range 5.5–8.5, and pH 7.0 was chosen throughout the experiment for maximum response. The amplified current increased with increase in the

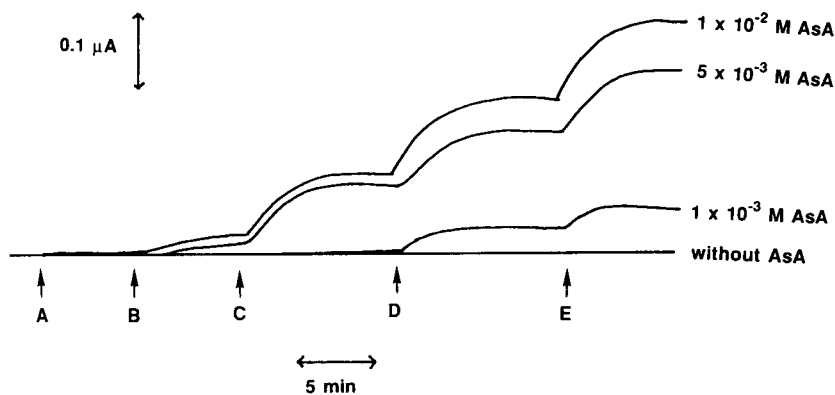


Fig. 2. Amplified and non-amplified tissue electrode responses obtained by the successive addition of catechol at each L-ascorbic acid concentration. Sample concentration: (A) 1×10^{-7} ; (B) 1×10^{-6} ; (C) 5×10^{-6} ; (D) 1×10^{-5} ; (E) 2×10^{-5} M.

amount of enzyme; 1 mg of enzyme (the enzyme activity of the sample solution is 200 U ml^{-1}) was chosen for further experiments.

The amplified and non-amplified potato tissue membrane electrode responses obtained by the successive addition of catechol are shown in Fig. 2. These results indicate that the current responses are significantly amplified by using an L-ascorbic acid sample solution and the response reaches the steady-state value in a few minutes. The relative standard deviation of the amplified responses of $1 \times 10^{-6} \text{ M}$ catechol was found to be 5% ($n = 5$). The amplification factors obtained with the enzyme solutions were much larger than those obtained with a potato tissue electrode. This difference is caused by the higher enzyme activity of the enzyme solution than that of the potato tissue.

The effect of the concentration of L-ascorbic acid on the amplified response of catechol after a reaction time of 10 min is shown in Fig. 3. The current responses increased on increasing the concentration of L-ascorbic acid but approached a constant value. When $1 \times 10^{-6} \text{ M}$ catechol was added to the enzyme solution containing $1 \times 10^{-3} \text{ M}$ L-ascorbic acid, the amplification factor obtained was 250 at a 10-min reaction time and the detection limit was $5 \times 10^{-9} \text{ M}$. The amplifica-

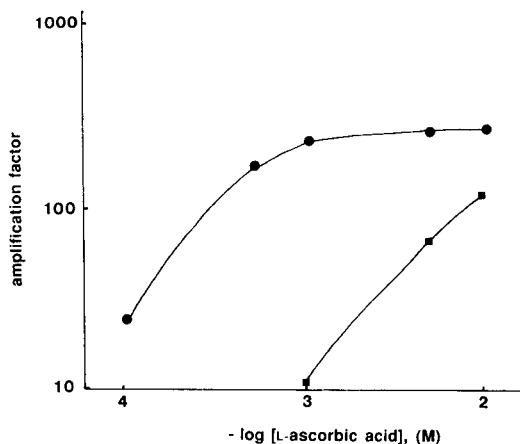


Fig. 3. Effect of the concentration of L-ascorbic acid on the amplification factor for $1 \times 10^{-6} \text{ M}$ catechol. (●) Enzyme solution at 10-min reaction time; (■) tissue electrode.

tion factors obtained with the potato tissue electrode at each concentration of L-ascorbic acid are also shown in Fig. 3.

The amplified and non-amplified calibration graphs for catechol obtained with the potato tissue electrode are shown in Fig. 4. These results indicate that the dynamic range obtained with $1 \times 10^{-2} \text{ M}$ L-ascorbic acid is shifted towards lower concentrations (5×10^{-8} – $2 \times 10^{-5} \text{ M}$) compared with the range (2×10^{-5} – $5 \times 10^{-4} \text{ M}$)

TABLE 1
Amperometric results obtained for the determination of catechol

| [Reducing agent] (M) | [Catechol] (M) | Enzyme solution | | Tissue electrode | |
|------------------------------|--------------------|-----------------|-----------------|---------------------------|-----------------|
| | | Current (nA) | AF ^a | Current (nA) ^b | AF ^a |
| $1 \times 10^{-2} \text{ c}$ | 1×10^{-7} | – | – | 5 | 200 |
| | 1×10^{-6} | 480 | 300 | 30 | 120 |
| | 5×10^{-6} | – | – | 105 | 84 |
| | 1×10^{-5} | – | – | 200 | 80 |
| $5 \times 10^{-3} \text{ c}$ | 1×10^{-6} | – | – | 18 | 72 |
| | 5×10^{-6} | – | – | 82 | 66 |
| | 1×10^{-5} | – | – | 160 | 64 |
| | 1×10^{-6} | 400 | 250 | 4 | 16 |
| $1 \times 10^{-3} \text{ c}$ | 1×10^{-5} | – | – | 30 | 12 |
| | 2×10^{-5} | – | – | 60 | 12 |
| | 1×10^{-4} | – | – | 300 | 12 |
| | 1×10^{-6} | 40 | 25 | – | – |
| 0 | 1×10^{-4} | 160 | 1 | 25 | 1 |
| $1 \times 10^{-2} \text{ d}$ | 1×10^{-6} | 142 | 89 | – | – |
| $1 \times 10^{-2} \text{ e}$ | 1×10^{-6} | 40 | 25 | – | – |

^a AF = amplification factor. ^b Mean values of five results. ^c L-Ascorbic acid. ^d Hexacyanoferrate(II) ion. ^e NADH.

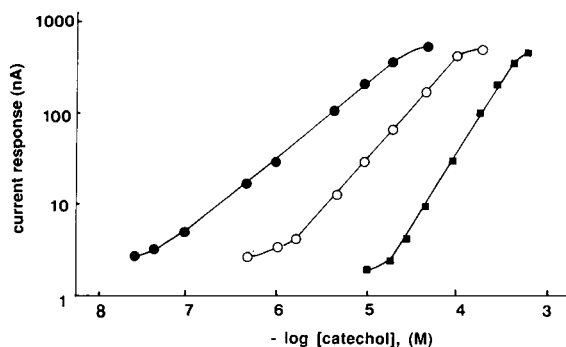


Fig. 4. Comparison of the calibration graphs for catechol obtained in buffer solution (pH 7.0) with and without L-ascorbic acid. L-Ascorbic acid concentration: ■ = 0; ○ = 1×10^{-3} ; ● = 1×10^{-2} M.

obtained using a buffer solution without L-ascorbic acid, and the detection limit was decreased by more than two decades from 1×10^{-5} to 3×10^{-8} M. The reason why the sensitivity of the potato tissue membrane electrode is lower than that obtained by the free enzyme solution is that the enzyme activity of the tissue membrane is lower than that of the free enzyme solution. The sensitivity should be increased by using an immobilized tyrosinase membrane with higher activity than that of the potato tissue membrane. The amperometric results obtained by the present methods are summarized in Table 1.

The potato tissue membrane electrode retained its enzyme activity for 3 days, but the current response of catechol was decreased to 70% after 4 days. Therefore, it is necessary to fabricate an artificially immobilized enzyme membrane electrode with high stability in order to obtain a more stable sensor.

From these results, it can be seen that the slope of the graph is decreased and the linear range becomes wider with increase in the concentration of L-ascorbic acid. This indicates that the cycling rate of the substrate increases with a decrease in the concentration of substrate when the enzyme activity and L-ascorbic acid concentration are constant. Therefore, this cyclic reaction scheme is very effective for the detection of

low concentrations of the substrate because the amplification factor is increased according to the decrease in the concentration of the substrate.

When the reactants of L-ascorbic acid are contained in a real sample solution, the current response would interfere with these reactants because the concentration of L-ascorbic acid in an enzyme solution is decreased. However, this serious problem could be avoided by the dissolution of large amounts of L-ascorbic acid in an enzyme solution and if large amounts of reactants that consume L-ascorbic acid exist, these reactants can be eliminated in advance by the addition of L-ascorbic acid to the real sample solutions prior to the measurement.

Tyrosinase catalyses not only catechol but also tyrosine, and catecholamines such as dopamine and adrenaline. The amplified current responses of these compounds would be obtained in addition to catechol and the chemical amplification of tyrosine and catecholamines will be reported in a later paper.

REFERENCES

- 1 T. Yao, H. Yamamoto and T. Wasa, *Anal. Chim. Acta*, 236 (1990) 437.
- 2 A. Wang and M.A. Arnold, *Anal. Chem.*, 64 (1992) 1051.
- 3 P. Seegopaul and G.A. Rechnitz, *Anal. Chem.*, 56 (1984) 852.
- 4 F. Mizutani, S. Yabuki and M. Asai, *Biosensors Bioelectron.*, 6 (1991) 305.
- 5 F. Schubert, J. Lutter and F. Scheller, *Anal. Chim. Acta*, 243 (1991) 17.
- 6 S. Uchiyama, *Talanta*, 39 (1992) 1289.
- 7 S. Uchiyama, Y. Hasebe and S. Suzuki, *Electroanalysis*, in press.
- 8 U. Wallenberger and F.W. Scheller, *Biotechnol. Lett.*, 5 (1983) 239.
- 9 J.S. Sidwell and G.A. Rechnitz, *Biotechnol. Lett.*, 7 (1985) 419.
- 10 J.G. Schiller, A.K. Chen and C.C. Liu, *Anal. Biochem.*, 85 (1978) 25.
- 11 H.Y. Neujahr, *Biotechnol. Bioeng.*, 22 (1980) 913.
- 12 S. Uchiyama, M. Tamata, Y. Tohoku and S. Suzuki, *Anal. Chim. Acta*, 208 (1988) 287.
- 13 F. Schubert, R. Renneberg, F.W. Scheller and L. Kirstein, *Anal. Chem.*, 56 (1984) 1677.

Chemically modified ion-sensitive field-effect transistors: elimination of the liquid junction potential in a double sensor flow-injection analysis cell

Peter L.H.M. Cobben^{1,2}, Richard J.M. Egberink¹, Johan G. Bomer², Robert Schouwenaar¹, Zbigniew Brzozka¹, Martinus Bos³, Piet Bergveld² and David N. Reinhoudt¹

University of Twente, P.O. Box 217, 7500 AE Enschede (Netherlands)

(Received 23rd October 1992; revised manuscript received 6th January 1993)

Abstract

A flow-through cell was designed that can be used for flow-injection analysis with two chemically modified ion-sensitive field-effect transistors (CHEMFETs) in close proximity. This offers the possibility of a differential measurement without influence of the liquid junction potential. The differential signal of a potassium- and a sodium-selective CHEMFET responded in a Nernstian manner and selectively towards potassium in an excess (fixed) concentration of sodium. A highly lead-selective CHEMFET was used in the same flow cell in combination with a potassium-selective CHEMFET.

Keywords: Flow injection; Ion selective electrodes; Sensors; Ion-sensitive field effect transistors; Lead; Potassium

Selective chemical recognition of ionic species by neutral receptor molecules is the important feature in chemical sensors and field-effect transistors (FETs) are very attractive transducers of this chemical recognition because of their fast response time and in situ impedance transformation. The attachment of a polymeric membrane in which the receptor molecule is embedded to the gate oxide chemically modifies the FET into a selective potentiometric sensor for several ions (CHEMFET). The proposed new architecture of the CHEMFET [1] offers several advantages. First, the membrane can be chemically [2,3] anchored to the surface of the gate oxide. Further,

the influence of CO₂ on the CHEMFET response can be eliminated by the introduction of an intermediate buffered hydrogel layer [4,5]. Moreover, this hydrogel stabilizes the potential developed in the sensing membrane. The incorporation of calixarene-based receptor molecules in the membrane of such a CHEMFET has led to accurate sensors for the selective detection of potassium [1], sodium [6] and several heavy metal ions [7] in aqueous solution.

The relatively high drift rate of the ion-sensitive field-effect transistor (ISFET) can be circumvented when CHEMFETs are used in flow systems [8,9]. Several workers have reported the application of multiple ion sensors or arrays of ion sensors [10–12]. This paper, however, describes the use of two CHEMFETs in a differential arrangement where one CHEMFET functions as a reference for the other. Moreover, the flow-through cell, in which these are used, is

Correspondence to: D.N. Reinhoudt, Laboratory of Organic Chemistry, University of Twente, P.O. Box 217, 7500 AE Enschede (Netherlands).

¹ Laboratory of Organic Chemistry.

² Laboratory of Bio-Informatics.

³ Laboratory of Chemical Analysis.

constructed in such a way that the two CHEMFETs are positioned in such close proximity that the sample plug will cover both of them simultaneously. This effectively eliminates the interference of the liquid junction potential between the sample and the carrier solution from the differential measurements. Earlier designs [9] served as a basis for this cell, because of the easy interchangeability of the CHEMFETs. The first experimental results of measurements with potassium- or lead-selective CHEMFETs (with a sodium- or potassium-selective reference CHEMFET, respectively) in this cell design are presented.

EXPERIMENTAL

Chemicals

Ethylene glycol dimethacrylate (EGDMA) (Merck-Schuchardt), 2-hydroxyethyl methacrylate (HEMA) (Merck-Schuchardt) and 2,2-dimethoxy-2-phenylacetophenone (Janssen Chimica) were used. Poly(vinylpyrrolidone) (PVP) with

an average molecular weight of 360 000 (Janssen Chimica) and poly(vinyl chloride) (PVC) of high molecular weight (Janssen Chimica) were used. Valinomycin, sodium ionophore III, bis(1-butylpentyl) adipate (BBPA), bis(2-ethylhexyl) sebacate (DOS), 2-nitrophenyl octyl ether (*o*-NPOE) and potassium tetrakis(4-chlorophenyl)borate (KTCPB) were obtained from Fluka. The synthesis of the lead-sensitive tetrathioamidecalix[4] arene (**1**; see Fig. 4) was described previously [7]. Tetrahydrofuran (THF) was freshly distilled from sodium-benzophenone ketyl before use. The alkali metal salts used were of analytical-reagent grade (Merck-Schuchardt) and solutions were prepared with doubly distilled, deionized water.

CHEMFET

The ISFETs were fabricated as described previously [2], but because of the new flow cells [9] the detailed structure of the ISFET was changed. The external dimensions were enlarged from 1.2 × 3.0 mm to 3.0 × 5.0 mm and the number of contact pads was reduced from three to two by

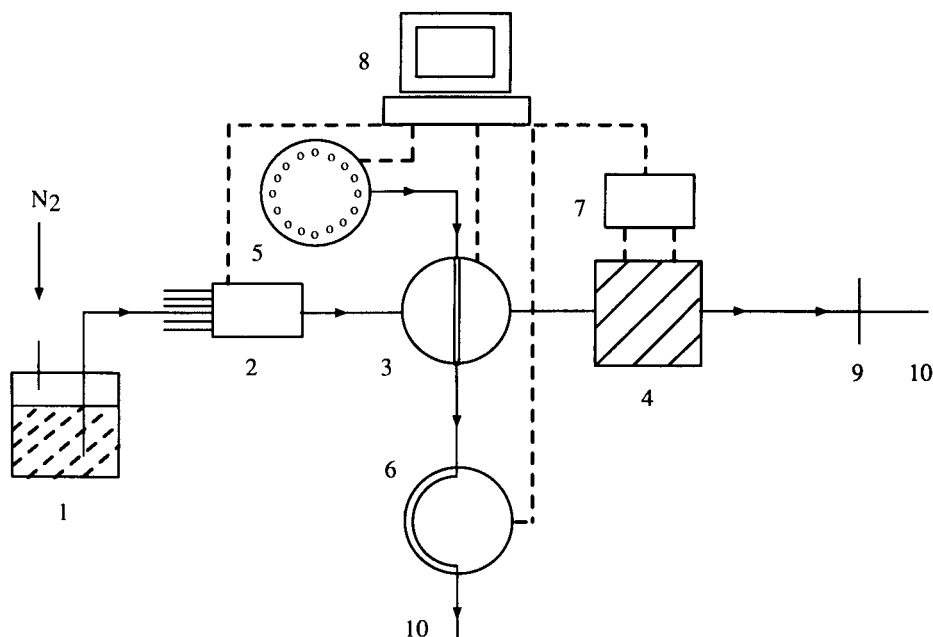


Fig. 1. Schematic diagram of the flow-injection system: 1 = carrier solution; 2 = six-way valve; 3 = injection valve; 4 = flow cell; 5 = autosampler; 6 = peristaltic pump; 7 = ISFET amplifier; 8 = Apple IIGS computer; 9 = saturated calomel (pseudo)reference electrode; 10 = waste.

connecting the source and the bulk internally. The size of the contact pads is 1.0×1.25 mm. Such an ISFET can be used in flow cells without traditional wire bonding and encapsulation with epoxy resin [9].

A hydrogel [4] was applied on the gate oxide of the ISFET by photopolymerization of a mixture of EGDMA, HEMA, PVP, water and photoinitiator in a ratio of 0.4:100:10:40:4 (w/w). The hydrogel was anchored chemically to the gate oxide via surface silylation [4] and had dimensions of $800 \times 15 \times 15$ μm .

The whole device was soaked in a 100 mM solution metal chloride for 1 h and subsequently the excess of solution was removed with a tissue. The potassium-sensitive membranes were made by dissolving a 10% mixture of valinomycin (2–3 wt.%), KTCPB (50–60 mol% with respect to valinomycin), DOS (65 wt.%) and PVC (32 wt.%) in THF. The sodium-sensitive membranes were made by dissolving a 10% mixture of *N,N,N',N'*-tetracyclohexyl-1,2-phenylenedioxydiacetamide (sodium ionophore III) (1–2 wt.%), KTCPB (50–60 mol% with respect to sodium ionophore III), BBPA (65 wt.%), and PVC (33 wt.%) in THF. The lead-sensitive membranes were made by dissolving a 10% mixture of the calix[4]arene **1** (2 wt.%), KTCPB (0.8 wt.%), *o*-NPOE (64.8 wt.%) and PVC (32.4 wt.%) in THF. A droplet of the membrane solution was applied to the poly-HEMA-covered ISFETs and the solvent was allowed to evaporate overnight. The response of the modified ISFETs was measured with a source and drain follower-type ISFET amplifier (Electro Medical Instrumentation, Enschede, Netherlands) in a constant drain-current mode ($I_d = 100$ μA), with a constant drain-source potential ($V_{ds} = 0.5$ V) [13]. The differential signal from two ISFET amplifiers was recorded with an Apple IIGS computer with the use of a 12-bit analogue-to-digital converter (DIGILOG, Enschede, Netherlands).

Double sensor flow-through cell

General. The flow-injection analysis (FIA) system has been reported previously [9] and was used with minor adjustments (Fig. 1). The carrier solution (1) is propelled through the double sen-

sor flow cell by nitrogen pressure. The PTFE tubing supplying the carrier solution was of 0.8 mm i.d. The sample (V_i) of 220 μl is injected with a rotary valve (3) (Rheodyne Model 5020) into the carrier solution. In order to minimize the dispersion of the sample the distance between the injection valve and the detector [8] was as short as possible and the connector of the injection valve was mounted directly on the cell (4). The flow cell was equipped with two CHEMFETs which are measured differentially with respect to a saturated calomel electrode (9) [8,14] which is placed downstream, near the waste (10). Thus, one of the CHEMFETs functions as the reference of the other CHEMFET.

In one series of experiments the potassium-selective CHEMFET was measured with respect to the sodium-selective CHEMFET. In these experiments the concentrations of potassium used were 0.01, 0.1 and 10 mM in 100 mM NaCl. The flow-rate was 1.3 ml min^{-1} . In other experiments a potassium-selective CHEMFET functioned as a reference for the lead-selective CHEMFET. The concentrations of lead used were 0.01, 0.1 and 1 mM in 100 mM KCl. All aqueous solutions were buffered [1×10^{-3} M $\text{Mg}(\text{OAc})_2\text{-HCl}$, pH 4]. The flow-rate was 1.1 ml min^{-1} . Corrections for the activity of the salts were calculated by the extended Debye-Hückel approximation given by Meier [15].

Automation of the FIA set-up. The FIA system consisted of an autosampler (5), a peristaltic pump (6), a six-way valve (2) to select different carrier streams, an injection valve (3) and the double sensor flow-through detector (4). The operation of this system was fully automated with an Apple IIGS computer (8) equipped with a 12-bit ADC and parallel and serial interface cards to control the FIA molecules. A schematic diagram of the set-up is given in Fig. 1.

The program to control the FIA equipment and to register the signal from the detector and its amplifier (7) was written in the computer language FORTH [16–18], which is very suitable for this type of real-time programming. A full measurement cycle consists of the choice of a sample via the autosampler, pumping of the sample into the rotary injection valve, injection of the

sample into the carrier stream and registration of the ISFET amplifier signal via the ADC. Processing of the acquired data was performed in a Lotus spread sheet program.

Construction. The cell consists of three Perspex blocks, A (two) and B (Fig. 2). Part A is a Perspex block (1) ($24 \times 24 \times 20$ mm) equipped with two pairs resilient hooks (3) for the electrical contact. These hooks, via a spring, press at the surface of the contact pads of the CHEMFET (4), whose reverse side is on the Perspex surface.

In this way the gate of the CHEMFET is positioned in the centre of the Perspex block which is marked with a cross engraved in the Perspex [9]. Part B of the cell is a rectangular Perspex block (2) ($85 \times 24 \times 10$ mm) in which a Z-shaped flow channel of 0.5 mm i.d. is drilled. Each of the wedges of the Z reaches the exterior of the rectangular block. At those two points the gate of a CHEMFET is positioned via block A. In this way a Z-type flow cell is formed without a dead volume in the cell. Consequently, the volume of solution between the two CHEMFETs is

very small ($3 \mu\text{l}$). The cell is sealed by gently pushing block A to B with a lever. The inherent plasticity of the PVC membrane ensures a water-tight closure of the cell.

RESULTS AND DISCUSSION

An electrochemical cell without any liquid junction is possible when in the experimental set-up the reference electrode is replaced with a second ion-selective electrode, selective towards an ion other than the primary ion [19,20]. Analogously, if two CHEMFETs in an FIA experiment are in contact with the same sample, the possible liquid junction potential will have no influence on the differential signal. In this experimental set-up one of the CHEMFETs is the reference of the other. This can only function is one of the CHEMFETs is a reference FET or is selective towards only one type of ion of which the activity is constant in all samples. The latter situation was

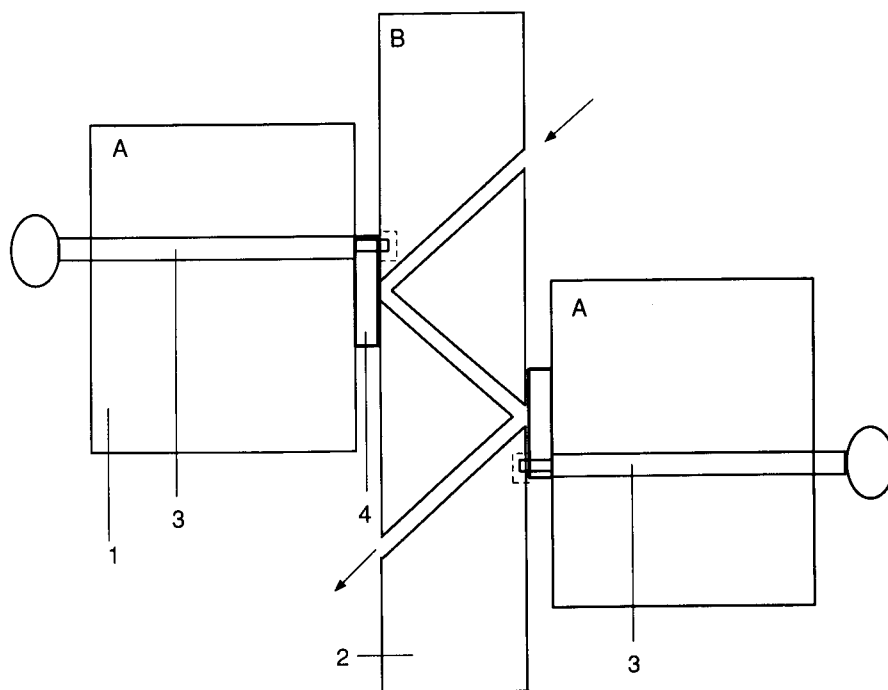


Fig. 2. Detailed structure (side view) of the double sensor flow-through cell: 1,2 = Perspex; 3 = contact wire (hook); 4 = CHEMFET.

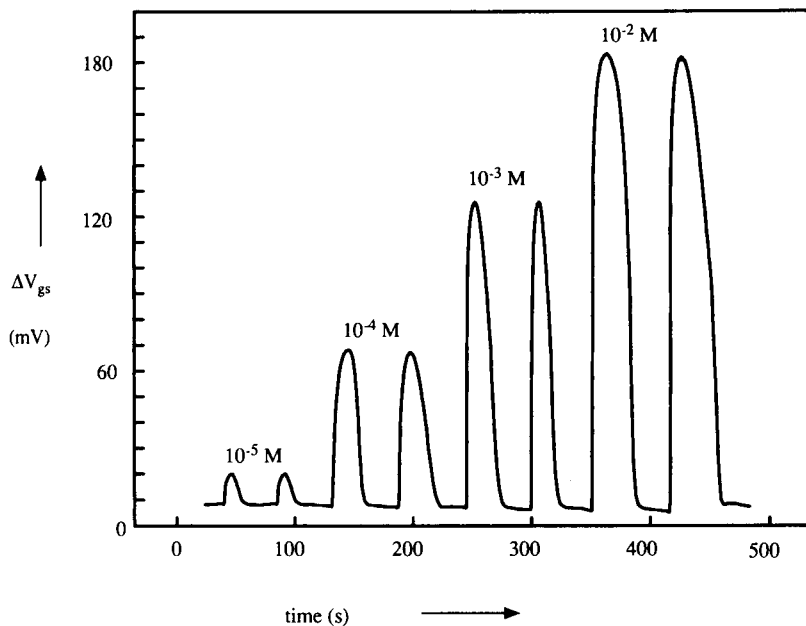


Fig. 3. Response of K^+ CHEMFET in the flow cell. Sodium reference CHEMFET. Carrier, 100 mM NaCl; injection, 1×10^{-5} – 1×10^{-2} M KCl + 100 mM NaCl; $V_i = 220 \mu\text{l}$; $Q = 1.3 \text{ ml min}^{-1}$.

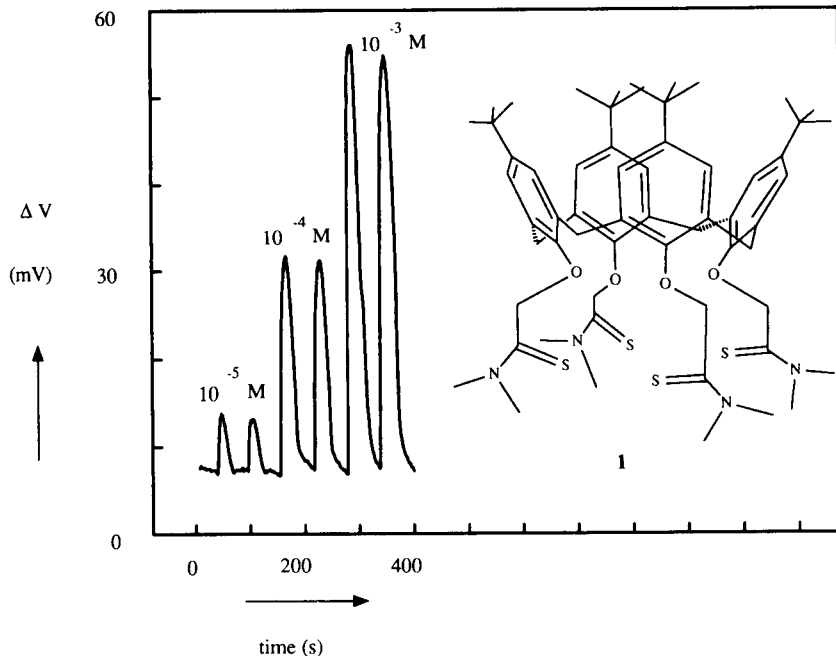


Fig. 4. Response of Pb^{2+} CHEMFET in the flow cell. Potassium reference CHEMFET. Carrier, 100 mM KCl; injection, 1×10^{-5} – 1×10^{-3} M $PbCl_2$ + 100 mM KCl; $V_i = 220 \mu\text{l}$; $Q = 1.1 \text{ ml min}^{-1}$. The structure of the highly lead-selective tetra-thioamidecalix[4]arene (1) is shown.

tested experimentally in the new double sensor flow-through cell. In previous work only the experimental results of a potassium-selective CHEMFET in a V-type flow cell in combination with a saturated calomel reference electrode were reported [9]. Therefore, in the first experiment a combination of a sodium- and a potassium-selective CHEMFET was measured in the above-described flow-through cell. The sodium-selective CHEMFET consisted of a PVC–BBPA membrane with the ionophore *N,N,N',N'*-tetracyclohexyl-1,2-phenylenedioxydiacetamide. The potassium-selective CHEMFET was identical with those used before. The concentration of sodium was fixed at 0.1 mol l^{-1} . Thus, the sodium-selective CHEMFET functions as the reference FET of the potassium-selective CHEMFET.

The concentration of potassium was varied in the sample from 1×10^{-5} to $1 \times 10^{-2} \text{ mol l}^{-1}$. At a flow-rate (Q) of 1.3 ml min^{-1} a calibration run was performed with such a double sensor flow cell. The differential signal of the two CHEMFETs responded selectively and Nernstian (57 mV per decade) to the various potassium concentrations (Fig. 3). These results indicate that under the experimental conditions used, the double sensor flow-through cell and the flow-through cell and the flow-through cell described previously [9] are identical with respect to the performance of the CHEMFET.

For the detection of lead in the double sensor flow-through cell, a potassium- and a lead-selective CHEMFET were tested experimentally. The potassium-selective CHEMFET is based again on valinomycin as the ionophore. Tetrathioamide-calix[4]arene (**1**) is the ionophore in the lead selective CHEMFET. The concentration of potassium was fixed at 0.1 M .

The concentration of lead was varied in the sample from 1×10^{-5} to $1 \times 10^{-3} \text{ M}$. At a flow-rate (Q) of 1.1 ml min^{-1} a calibration run was performed with this double sensor flow cell. The differential signal of the two CHEMFETs responded selectively and in a Nernstian manner (ca. 25 mV per decade) to the various lead concentrations (Fig. 4).

The authors thank the Netherlands Technology Foundation (STW), Technical Science Branch of the Netherlands Organization for Advanced and Pure Research (NWO), for the financial support.

REFERENCES

- 1 D.N. Reinhoudt and E.J.R. Sudhölter, *Adv. Mater.*, **2** (1990) 23.
- 2 P.D. van der Wal, M. Skowronska-Ptasinska, A. van den Berg, P. Bergveld, E.J.R. Sudhölter and D.N. Reinhoudt, *Anal. Chim. Acta*, **231** (1990) 41.
- 3 D.J. Harrison, A. Teclemariam and L. Cunningham, *Anal. Chem.*, **61** (1989) 246.
- 4 E.J.R. Sudhölter, P.D. van der Wal, M. Skowronska-Ptasinska, A. van den Berg, P. Bergveld and D.N. Reinhoudt, *Anal. Chim. Acta*, **230** (1990) 59.
- 5 H.H. van den Vlekkert, C. Francis, A. Grisel and N.F. de Rooij, *Analyst*, **113** (1988) 1029.
- 6 J.A.J. Brunink, J.R. Haak, J.G. Bomer, D.N. Reinhoudt, M.A. McKervey and S.J. Harris, *Anal. Chim. Acta*, **254** (1991) 75.
- 7 P.L.H.M. Cobben, R.J.M. Egberink, J.G. Bomer, P. Bergveld, W. Verboom and D.N. Reinhoudt, *J. Am. Chem. Soc.*, **114** (1992) 10573.
- 8 P.D. van der Wal, E.J.R. Sudhölter and D.N. Reinhoudt, *Anal. Chim. Acta*, **245** (1991) 159.
- 9 P.L.H.M. Cobben, R.J.M. Egberink, J.G. Bomer, E.J.R. Sudhölter, P. Bergveld and D.N. Reinhoudt, *Anal. Chim. Acta*, **248** (1991) 307.
- 10 A.U. Ramsing, J. Janata, J. Ruzicka and M. Levy, *Anal. Chim. Acta*, **118** (1980) 45.
- 11 A. Sibbald, P.D. Whalley and A.K. Covington, *Anal. Chim. Acta*, **159** (1984) 47.
- 12 B.H. van der Schoot, H.H. van den Vlekkert, N.F. de Rooij, A. van den Berg and A. Grisel, *Proc. 3rd Int. Meeting Chemical Sensors*, Cleveland, OH, 1990, p. 40.
- 13 P. Bergveld, *Sensors Actuators*, **1** (1981) 17.
- 14 P. Bergveld, A. van den Berg, P.D. van der Wal, M. Skowronska-Ptasinska, E.J.R. Sudhölter and D.N. Reinhoudt, *Sensors Actuators*, **18** (1989) 307.
- 15 P.C. Meier, *Anal. Chim. Acta*, **136** (1982) 363.
- 16 A. Winfield, *The Complete FORTH*, Sigma Technical Press, Cheshire, 1983.
- 17 L. Brodie, *Starting FORTH*, Prentice-Hall, Englewood Cliffs, NJ, 1981.
- 18 E. Flögel, *FORTH*, Kluwer, Deventer, 1985.
- 19 G. Biedermann, J. Lagrange and P. Lagrange, *Chem. Scr.*, **5** (1974) 153.
- 20 E. Bottari and M.R. Festa, *Analyst*, **114** (1989) 1623.

Comparative study of tripodal oxa-amides and oxa-esters as ionophores in potentiometric ion-selective electrodes for alkali and alkaline earth cations

Ritu Katakya, David Parker and Andrew Teasdale

Department of Chemistry, University of Durham, South Road, Durham DH1 3LE (UK)

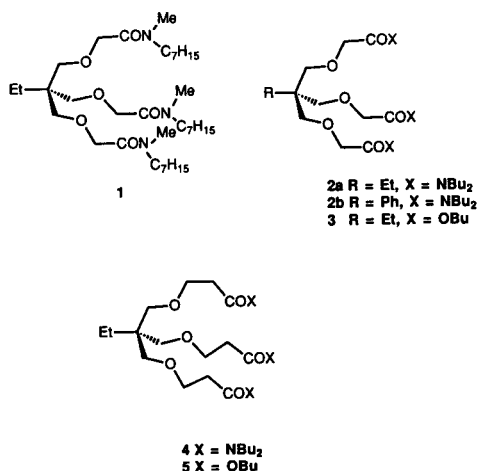
(Received 23rd July 1992; revised manuscript received 19th October 1992)

Abstract

Two sets of oxa-amide and oxa-ester tripodal ligands have been prepared and evaluated as ionophores in PVC membrane electrodes for the analysis of Li^+ , Na^+ , K^+ , Ca^{2+} and Mg^{2+} ions. The effects of the nature of the plasticiser bis(butylpentyl)adipate (BBPA) vs. *o*-nitrophenyl octyl ether (oNPOE), the structure of the ionophore, the pH and the ionic strength of the analyte solution on the electrode response were studied. The oxa-amides gave a superior performance (slope, limits of detection) than the oxa-esters particularly at higher ionic strengths, although super-Nernstian responses were observed with the more charge-dense ions in the presence of chloride and/or with the less polar plasticiser BBPA. Intracellular measurements of sodium concentration could be effected with a sensor based on bis(*N,N',N''*-tributyl)-4,4',4''-propylidinitris(3-oxabutanamide) and oNPOE for which $-\log K_{\text{Na,K}}^{\text{POT}} = 2.64$ and $-\log K_{\text{Na,Mg}}^{\text{POT}} = 3.0$, while bis(*N,N',N''*-tributyl)-2,2',2''-phenylmethylidinitris(3-oxabutanamide) and oNPOE functioned as an effective calcium sensor with high selectivity over magnesium ($-\log K_{\text{Ca,Mg}} = 4.8$).

Keywords: Ion selective electrodes; Potentiometry; Calcium; Sodium; Magnesium

There is considerable interest in devising new potentiometric ion-selective electrodes for the measurement of intracellular or extracellular concentrations of cations [1–4]. For intracellular sodium measurements, for example, high discrimination over potassium and magnesium is required. The ionophore *N,N',N''*-triheptyl-*N,N',N''*-trimethyl-4,4',4''-propylidinitris(3-oxabutanamide) (**1** or ETH 227), has been used widely as a sodium ionophore. Using this acyclic tripodal ligand as a basic structure, we have undertaken a study of the variation of ionophore structure on the properties of potentiometric ion-selective



Correspondence to: D. Parker, Department of Chemistry, University of Durham, South Road, Durham DH1 3LE (UK).

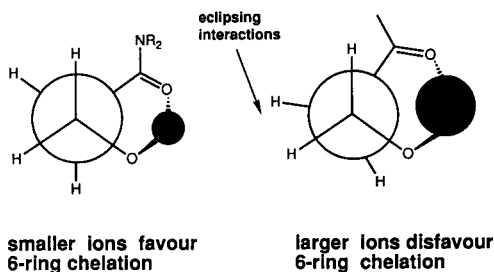


Fig. 1. Tendency of 6-ring chelate complexes to favour binding of smaller cations.

electrodes for Periodic Group Ia and IIa cations. Compounds **2** to **5** have been prepared allowing a comparison both of carbobutoxy versus dibutylamide as a σ donor, and of chelate ring size in the shorter chain ligands **2** and **4** versus the extended ionophores **3** and **5**. It was expected that the more polar amide donors might enhance discrimination in favour of the more charge dense cations (e.g., Na^+ over K^+ , Mg^{2+} over K^+), and that the extended ionophores which generate a 6-ring chelate when cooperatively binding the ether oxygen (Fig. 1) might exhibit some selectivity for the smaller ions over the large ions. In related work with macrocyclic ligands, six-ring chelate structures enhance discrimination in favour of Li over Na and Mg over Ca [5,6]. Additionally the nature of the plasticiser was varied from the more polar *o*-nitrophenyl octylether (oNPOE) to bis(butylpentyl)adipate (BBPA) which has a much lower dielectric constant and should favour the transport of ions with lower charge density.

EXPERIMENTAL

Ionophore synthesis

Bis(N,N',N''-tributyl)-4,4',4''-propylidintris(3-oxabutanamide) (2a)

To a solution of 2-ethyl-2-(hydroxymethyl)-1,3-propanediol (100 mg, 0.75 mmol) in dry tetrahydrofuran (40 cm³) was added sequentially sodium hydride (120 mg, 5 mmol) and *N,N*-dibutyl-2-bromoethanamide (1.25 g, 5 mmol) and the mixture heated to reflux for 48 h. After

removal of solvent under reduced pressure the residue was purified by chromatography on neutral alumina [elutant, hexane–ethyl acetate (2:1, v/v)] to yield a colourless oil, R_F 0.60 [Al_2O_3 ; ethyl acetate–hexane (2:1)], (280 mg, 59%). δ_{H} (ppm) (CDCl_3) 0.93 (21H, t + t + t, $\text{CH}_3\text{CH}_2\text{CH}_2 + \text{CH}_3\text{CH}_2$) 1.32–1.51 (26H, mult., CH_2C), 3.22 (12H, t + t, CH_2N), 3.46 (6H, s, CH_2O), 4.11 (6H, s, CH_2O). δ_{C} (CDCl_3) 7.69 (CH_3), 13.81 (CH_3), 20.12 (CH_2C), 22.95 (CH_2C), 29.61, 30.98 (CH_2C), 43.33 (quaternary C), 45.34, 46.53 (CH_2N), 70.68, 72.02 (CH_2O), 168.73 (CO). m/e (d.c.i., NH_3) 643 ($\text{M}^+ + 1$, 63%), 642 (M^+ , 100%), 471 (11%), 172 (13%). ν_{max} (Nujol) 1647 cm⁻¹ (s, amide CO).

Bis(N,N',N''-tributyl)-2,2',2''-phenylmethyldintris(3-oxabutanamide) (2b)

To a solution of 2-phenyl-2-(hydroxymethyl)-1,3-propanediol (500 mg, 2.75 mmol) in dry tetrahydrofuran (50 cm³) was added sequentially sodium hydride (181 mg, 8.25 mmol) and *N,N*-dibutyl-2-chloroethanamide (1.71 g, 8.32 mmol) and the mixture was heated to reflux for 72 h. After cooling and filtering, solvent was removed under reduced pressure and volatiles distilled on a Kugelrohr apparatus. The residue was purified by chromatography on neutral alumina [elutant, hexane–ethyl acetate (5:1, v/v)] to yield a colourless oil ($R_F = 0.34$) (894 mg, 47%). δ_{H} (CDCl_3) 0.87 (18H, t + t, Me), 1.07–1.49 (24H, mult., CH_2C) 3.01–3.27 (12H, dt, CH_2N), 3.89 (6H, s, CH_2O) 4.09 (6H, s, CH_2O), 7.15–7.53 (5H, mult., arom. H). δ_{C} (ppm) (CDCl_3) 13.75 (Me), 19.95, 20.14, 29.59, 30.83 (CH_2C) 45.28, 46.37 (CH_2N), 48.27 (quaternary C), 70.73, 73.39 (CH_2O) 126.28, 127.20, 127.93, 141.27 (arom. C), 168.54 (carbonyl). ν_{max} (thin film) 1647 cm⁻¹ (CO). m/e (d.c.i.) 690 ($\text{M}^+ + 1$, 100%), 188 (20%), 172 (40%).

Tributyl-4,4',4''-propylidintris-(3-oxabutanate) (3)

This was prepared by transesterification from the related triethyl ester reported previously [3]. A solution of triethyl-4,4',4''-propylidintris-(3-oxabutanate) was dissolved in *n*-butanol (150 cm³) and *p*-toluene sulphonic acid (0.2 g) added and the mixture heated to reflux for 18 h through

molecular sieves (4 Å). Solvent was removed under reduced pressure, the residue dissolved in dichloromethane (50 cm³), washed with aqueous hydrogen carbonate solution (3 × 20 cm³), dried (K₂CO₃) and solvent evaporated to leave a residue which was purified by chromatography on neutral alumina, *R_F* 0.71 [hexane–ethyl acetate (4:1, v/v)], (135 mg, 48%). δ_H (ppm) 0.86 (12H, t + t, CH₃C), 1.29–1.59 (14H, mult., CH₂C). 3.42 (6H, s, CH₂O), 4.00 (6H, s, CH₂O), 4.06 (6H, t, CH₂O). δ_c (CDCl₃) 7.56 (CH₃C), 13.65 (CH₃); 19.07, 22.84, 30.59 (CH₂C), 43.42 (quaternary C); 64.49, 68.94, 72.18 (CH₂O), 170.81 (CO). *m/e* (NH₃ c.i.), 477 (M⁺ + 1, 29%)N, 494 (M⁺ + 18, 100%), 275 (23%), 213 (32%), 199 (16%), ν_{max} (Nujol) 1735 cm⁻¹ (CO).

Bis(N,N',N''-tributyl)-5,5',5''-propylidintris-(4-oxa-pentanamide) (4)

This was prepared from the acid chloride of the related acid 5,5',5''-propylidintris-(4-oxa-pentanoic acid), which had been prepared according to Ref. 7. δ_H (ppm) (CDCl₃) 0.78 (3H, t, CH₃C), 0.94 (18H, t + t, CH₃C), 1.28–1.52 (26H, mult., CH₂C) 2.54 (6H, t, CH₂CO), 3.26 (18H, mult., CH₂O + CH₂N), 3.68 (6H, t, CH₂O). δ_c (CDCl₃) 7.62 (CH₃C), 13.73 (CH₃); 19.96, 22.97, 29.8, 31.1 (CH₂C); 33.51 (CH₂CO), 42.94 (quaternary C), 45.60, 47.71 (CH₂N), 68.11, 71.45 (CH₂O), 170.60 (CO). *m/e* (c.i.), 684 (M⁺, 29%), 200 (24%), 184 (92%). ν_{max} (film) 1643 cm⁻¹ (CO), 1110 cm⁻¹ (CO).

Tributyl-5,5',5''-propylidintris(4-oxa-pentanoate) (5)

This was prepared by butanolysis (*n*-butanol, dry HCl) of the related trinitrile which was synthesised according to Ref. 7. δ_H (ppm) (CDCl₃)

0.79 (3H, t, CH₃CH₂), 0.94 (9H, t, CH₃), 1.21–1.34 (14H, mult., CH₂C), 2.53 (6H, t, CH₂CO) 3.25 (6H, s, CH₂O), 3.64 (6H, t, CH₂O), 4.09 (6H, t, CH₂O). δ_c (CDCl₃) 7.49 (CH₃), 13.59 (CH₃C); 19.01, 22.74, 30.56 (CH₂C); 35.10 (CH₂CO), 42.94 (quaternary C), 64.13, 66.69, 71.01 (CH₂O); 171.69 (CO). ν_{max} (film) 1743 cm⁻¹ (CO). *m/e* (d.c.i., NH₃) 536 (M⁺ + 18, 48%), 519 (M⁺ + 1, 100%), 303 (35%), 227 (53%) 159 (48%), 129 (48%).

Reagents and chemicals

Salts of lithium, sodium, potassium, magnesium and zinc were dried at 50°C. Calcium chloride solution (BDH, AnalaR, 1 mol dm⁻³) was used. All standard solutions were prepared in de-ionised water. The materials for the electroactive membranes were high relative molecular mass poly(vinyl chloride) (PVC), *o*-nitrophenyl octyl ether (oNPOE); bis(1-butylpentyl) adipate (BBPA) and potassium tetrakis(*p*-chlorophenyl) borate (KTpClPB), all obtained from Fluka. Tetrahydrofuran (THF) was of spectroscopic grade, distilled from sodium benzophenone ketyl.

Membrane preparation

The membranes were prepared from a mixture composed of 1.3% ionophore, 65.4% plasticiser, 32.8% PVC and 0.5% KTpClPB dissolved in 10 cm³ of THF. The membranes were cast according to published procedures [8].

Calibration and selectivity measurements

A Philips IS (561) electrode body was used to mount the electroactive membrane. The inner

TABLE 1

Selectivity coefficients of calcium electrodes evaluated by the fixed interference method (Expressed as $-\log K_{Ca,M}^{POT}$ in the presence of an 0.1 mol dm⁻³ solution of interferent)

| Ion | Electrodes | | | | | |
|------------------|--------------|--------------|-------------|-------------|-------------|-------------|
| | 2a and oNPOE | 2b and oNPOE | 2a and BBPA | 3 and oNPOE | 4 and oNPOE | 5 and oNPOE |
| Mg ²⁺ | 3.1 | 4.8 | 3.3 | 3.4 | 1.5 | 3.8 |
| K ⁺ | 3.5 | 3.2 | 2.7 | 0.1 | 2.1 | 0.1 |
| Na ⁺ | 3.5 | 2.3 | 2.8 | 0.1 | 1.2 | 0.1 |

filling solution was a 1.0 mmol dm⁻³ solution of the analyte. Calibrations and selectivity measurements were performed by a constant dilution technique described previously [5]. Figs 2–7 are calibration graphs of the electrodes with 1.0 mmol dm⁻³ solutions of the appropriate electrolyte as inner filling solution and conditioning solution, in 0.1 mol dm⁻³ analyte diluted continuously with MQ water. The selectivity coefficient numbers are obtained by the fixed interference method, the electrodes being introduced in a solution of 1.0 mol dm⁻³ analyte and 0.1 mol dm⁻³ interferent diluted continuously with 0.1 mol dm⁻³ interferent. Selectivity coefficients for calcium and sodium electrodes are shown in Tables 1 and 2. All measurements were at 37°C.

RESULTS AND DISCUSSION

Amide ionophores 2a, 2b and 4

The ionophore 1 (ETH 227) was originally reported as a sensor for sodium, and although it shows strong interference from calcium ($-\log K_{\text{Na,Ca}}^{\text{POT}} = 0.54$) its selectivity over potassium and magnesium is quite good ($-\log K_{\text{Na,K}}^{\text{POT}} = 2.36$, $-\log K_{\text{Na,Mg}}^{\text{POT}} = 3.0$ (selectivities were measured by the separate solutions method) [3]. When the related ionophore 2a was examined as a sodium sensor with oNPOE as plasticiser, it showed a good limit of detection and slope in the absence of interferences (limit of detection 10^{-6.0} mol dm⁻³, slope 60.5 mV per decade [37°C]). Interference from calcium was severe (in the presence of an 0.1 mol dm⁻³ solution of calcium the response to sodium was poor with a slope of less than 5 mV per decade), although selectivity over

potassium was improved ($-\log K_{\text{Na,K}}^{\text{POT}} = 2.63$). With the less polar plasticiser BBPA, the response to sodium was super-Nernstian for concentrations less than 10⁻³ mol dm⁻³.

When 2a was examined as a calcium sensor, with oNPOE, good selectivities were observed over sodium, potassium and magnesium ($-\log K_{\text{Ca,Na}}^{\text{POT}} = 3.5$, $-\log K_{\text{Ca,K}}^{\text{POT}} = 3.5$, $-\log K_{\text{Ca,Mg}}^{\text{POT}} = 3.1$) with a Nernstian slope and a moderate limit of detection (10^{-3.9} mol dm⁻³). Using BBPA, the limit of detection improved marginally, and although selectivity over Na⁺ was reduced ($-\log K_{\text{Ca,Na}}^{\text{POT}} = 2.8$), it was improved over magnesium ($-\log K_{\text{Ca,Mg}}^{\text{POT}} = 3.3$) (Fig. 3 and Tables 1 and 2).

The behaviour of the electrode with 2a and oNPOE was also studied with respect to lithium and magnesium (Fig. 2). With lithium a super-Nernstian response was observed at less than 10⁻³ mol dm⁻³, while with magnesium the response was Nernstian down to 10^{-4.4} mol dm⁻³ but there was severe interference from sodium, potassium or calcium (less than 8mV per decade slopes).

2b was examined for use in a sensor for Ca²⁺, Mg²⁺ and Na⁺ with oNPOE as plasticiser. In a calcium electrode it behaved in a Nernstian manner down to 10⁻⁴ mol dm⁻³ with a slope of 25 mV per decade. In a background of 0.1 mol dm⁻³ Mg²⁺, the electrode's performance improved giving a slope of 29 mV per decade (the limit of detection was 10^{-5.8} mol dm⁻³) and an excellent selectivity coefficient of $-\log K_{\text{Ca,Mg}}^{\text{POT}} = 4.8$. Selectivities over K⁺ and Na⁺ were also good; $-\log K_{\text{Ca,Mg}}^{\text{POT}} = 3.2$ and $-\log K_{\text{Ca,Na}}^{\text{POT}} = 2.3$, respectively (Table 1). The ionophore was very poor as a Mg²⁺ sensor with a slope of only 5 mV up to 10⁻² mol dm⁻³ dilution. It was rather surpris-

TABLE 2

Selectivity coefficient of sodium electrodes by a fixed interference method (Expressed as $-\log K_{\text{Na,M}}^{\text{POT}}$ in the presence of an 0.1 mol dm⁻³ solution of interferent)

| Ion | Electrode | | | | |
|------------------|-----------|--------------|-------------|-------------|-------------|
| | ETH 227 | 2a and oNPOE | 3 and oNPOE | 4 and oNPOE | 5 and oNPOE |
| K ⁺ | 2.36 | 2.63 | 0.1 | 1.5 | 0.2 |
| Ca ²⁺ | 0.54 | 0.1 | 3.1 | 0 | 0.8 |
| Mg ²⁺ | 3.0 | 3.0 | 3.0 | 0 | - |

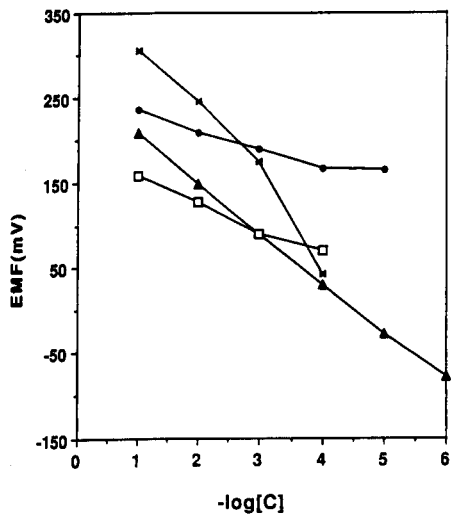


Fig. 2. Response of electrode based on 2a/oNPOE/KTpClB/PVC (with 1.0 mmol dm^{-3} appropriate inner filling solutions, conditioned in corresponding analyte solution) for different cations (37°C). Key to symbols: \times = LiCl; \blacktriangle = NaCl; \square = CaCl₂; \bullet = MgCl₂.

ingly poor as an Na^+ sensor as well, with a 50 mV per decade slope and a limit of detection of $10^{-2} \text{ mol dm}^{-3}$, 2.0 (Fig. 7).

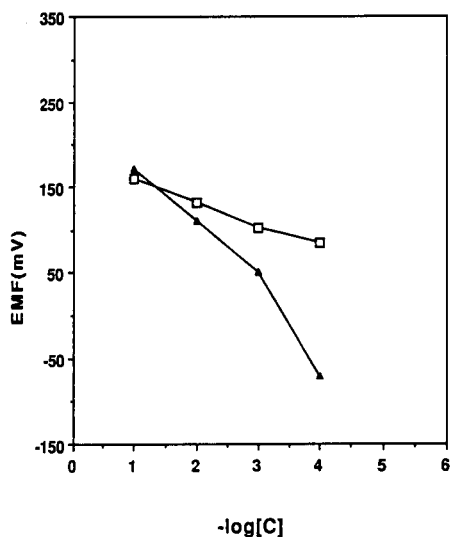


Fig. 3. Response of electrode based on 2a/BBPA/KTpClB/PVC (with 1.0 mmol dm^{-3} appropriate filling solutions, conditioned in corresponding analyte solution) for different cations (37°C). Key to symbols: \blacktriangle = NaCl; \square = CaCl₂.

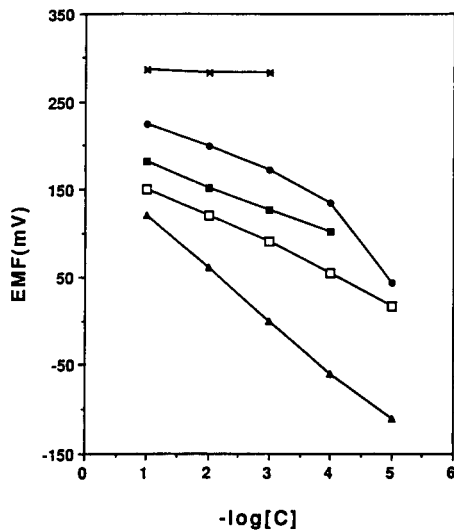


Fig. 4. Response of electrode based on 4/oNPOE/KTpClB/PVC (with 1.0 mmol dm^{-3} appropriate filling solutions, conditioned in corresponding analyte solution) for different cations (37°C). (The response to potassium ions was very similar to that shown for sodium and is omitted for clarity.) Key to symbols: \times = LiCl; \blacksquare = Ca(NO₃)₂; \square = CaCl₂; \bullet = MgCl₂; \blacktriangle = NaCl.

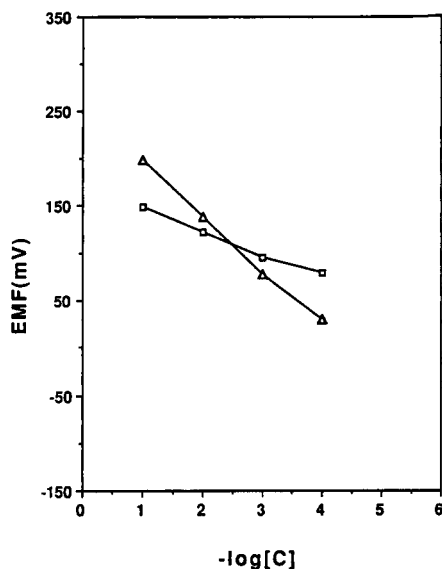


Fig. 5. Response of electrode based on 3 and oNPOE/KTpClB/PVC (with 1.0 mmol dm^{-3} appropriate filling solutions, conditioned in corresponding analyte solution) for different cations (37°C). Key to symbols: \triangle = NaCl/KCl; \square = CaCl₂.

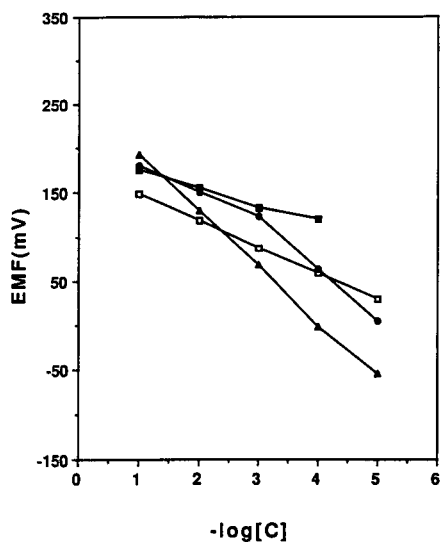


Fig. 6. Response of electrode based on 5/oNPOE/KTpCIB/PVC (with 1.0 mol dm^{-3} appropriate filling solutions, conditioned in corresponding analyte solution) for different cations (37°C). Key to symbols: ▲ = NaCl; ● = CaCl₂; □ = Ca(NO₃)₂; ■ = MgCl₂.

The extended amide **4**, differs from **2a** only in respect of the chelate ring size formed on cooperative binding of the ether oxygen and the amide (carbonyl (5-ring vs. 5-ring chelate: Fig. 1). It may also be anticipated that the 1:1 binding constant may be lower for the extended amide. Ion-selective electrodes were constructed using **4** and oN-

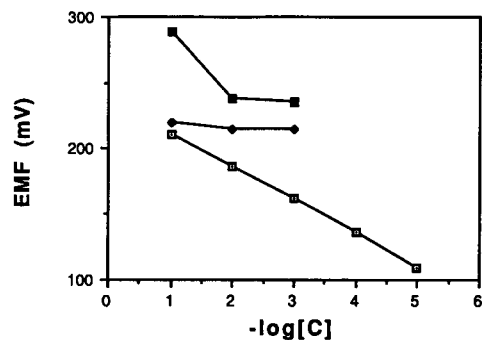


Fig. 7. Response of electrode based on 2b/oNPOE/KTpCIB/PVC (with 1.0 mol dm^{-3} appropriate filling solutions, conditioned in corresponding analyte solution) for different cations (37°C). Key to symbols: □ = CaCl₂; ■ = NaCl; ◆ = MgCl₂.

POE and the response to both potassium and lithium was very poor. Sodium responded in a Nernstian manner with a limit of detection of $10^{-4.3} \text{ mol dm}^{-3}$, but there was severe interference from calcium (slopes less than 5.0 mV per decade change in concentration) and selectivity over potassium was reduced compared to **2** ($-\log K_{\text{Na,K}}^{\text{POT}} = 1.5$). When studied as a calcium electrode, the response was dependent on the nature of the counterion. With calcium chloride as analyte, the response was Nernstian down to $10^{-3} \text{ mol dm}^{-3}$, but on further dilution evidence of a super-Nernstian response appeared with a response slope of 36 mV per decade at $10^{-4} \text{ mol dm}^{-3}$. This behaviour was not observed with nitrate: with Ca(NO₃)₂ a limit of detection of $10^{-3.3} \text{ mol dm}^{-3}$ was found with a response slope of 30 mV per decade. The selectivity for calcium over Mg²⁺, Na⁺ and K⁺ was reduced compared to the unextended amide **2** ($-\log K_{\text{Ca,Na}}^{\text{POT}} = 1.2$, $-\log K_{\text{Ca,K}}^{\text{POT}} = 2.1$, $-\log K_{\text{Ca,Mg}}^{\text{POT}} = 1.5$).

The behaviour of this electrode with respect to magnesium was examined and revealed a super-Nernstian response (for chloride solutions) at greater than $10^{-3} \text{ mol dm}^{-3}$ (Fig. 4). Interference from calcium was severe ($< 5.0 \text{ mV}$ per decade change in concentration), as expected, and sodium also interfered strongly ($-\log K_{\text{Mg,Na}}^{\text{POT}} = 0.5$).

Ester ionophores **3** and **1**

The introduction of ester groups was expected to favour binding of the less-polar ions albeit with lower overall binding constants. Electrodes based on **3** with oNPOE as plasticiser showed nearly identical responses to Na⁺ and K⁺ ions with Nernstian slopes and limits of detection of $10^{-3.5}$ and $10^{-3.7} \text{ mol dm}^{-3}$, respectively (Fig. 5). Severe mutual interference was therefore observed (e.g. $-\log K_{\text{Na,K}}^{\text{POT}} = 0.1$), although selectivity for sodium over calcium was good ($-\log K_{\text{Na,Ca}}^{\text{POT}} = 3.1$). When examined as a calcium sensor, severe sodium interference was obviously found, although good selectivity over magnesium was noted ($-\log K_{\text{Ca,Mg}}^{\text{POT}} = 3.4$).

With the extended ester, **5**, and oNPOE as plasticiser, the response to sodium was Nernstian with a limit of detection of $10^{-4.3} \text{ mol dm}^{-3}$.

Interference from potassium was severe (< 10 mV per decade) and the selectivity over calcium had also reduced considerably compared to **3** ($-\log K_{\text{Na,Ca}}^{\text{POT}} = 0.8$). Examination of the response to calcium revealed a super-Nernstian response above 10^{-3} mol dm $^{-3}$: in more concentrated solutions a response slope of 25 mV per decade was noted increasing to 35 mV per decade. This behaviour was not shown with nitrate as the counter ion. Interference from sodium was severe, as expected, and good selectivity over magnesium was maintained ($-\log K_{\text{Ca,Mg}}^{\text{POT}} = 3.8$) (Tables 1 and 2, Fig. 6).

Origin of super-Nernstian behaviour

In certain cases (noted above) with both doubly and singly charged ions, a super-Nernstian response was evident. For the doubly charged ions as chloride salts (e.g., Mg $^{2+}$ with **4** and oNPOE and **5** and oNPOE) this may be attributed to the formation of [LM–Cl] $^{+}$ species, according to:



where L is the ionophore. At higher ionic strength (favouring stabilisation of more charge dense species) the equilibrium in Eqn. 2 will be towards dissociation of the chloride. As the solution is diluted, if formation of LMCl $^{+}$ is increasingly favoured, the slope of the electrode will tend towards 61.5 mV per decade. With the less nucleophilic nitrate anion this LMX interaction is much less favoured. This sort of behaviour has been reported previously, for example with magnesium complexes of bis-crown ethers [9] and in the response of cadmium ions with some thio-amides [10]. For the singly charged cations which exhibit a super-Nernstian response, then the origin of the deviation must be different. A possible explanation is that the aquated species [ML· $n\text{H}_2\text{O}$] $^{+}$ may be in equilibrium with the neutral conjugate base [ML·($n-1$)H $_2$ O(OH)] so that the effective charge is less than unity. This equilibrium will favour the uncharged species in solutions of low ionic strength, consistent with the observed super-Nernstian deviation at concentrations less

than 10^{-3} dm $^{-3}$ analyte, and in the absence of a background of interferent ions.

Conclusions

The electrode based on **2** and oNPOE may be well-suited to the detection of intracellular sodium, where the relative concentration of interferent ions leads to a requirement for good Na $^{+}$ /K $^{+}$ and Na $^{+}$ /Mg $^{2+}$ selectivity (intracellular background: 200 mM K $^{+}$, 2.0 mM Mg $^{2+}$, < 0.01 mM Ca $^{2+}$; log Na ca. – 2.5). It may offer some improvement over ETH 227 in respect of its slightly enhanced Na $^{+}$ /K $^{+}$ selectivity.

The sensors based on **2b** and oNPOE and **2a** and oNPOE both function as useful calcium electrodes measuring calcium concentrations in the 10^{-3} – 10^{-6} mol dm $^{-3}$ range with good selectivities over magnesium. The former sensor exhibits the better selectivity over Mg (log $K_{\text{Ca,Mg}} = -4.8$), while the latter shows better selectivity over sodium (log $K_{\text{Ca,Na}} = -3.5$) (Tables 1 and 2).

The other electrodes behave less well in terms of their selectivities and slopes. It is possible that their relatively poor behaviour may be related to a relatively weak 1:1 L–M formation constant which may be associated (for the ester ionophores) with the weak σ -donor ability of ester carbonyl oxygens and with the lack of convergent functionality (i.e., a lack of focussed oxygen and amide lone pairs) in the molecular structure of these conformationally flexible acyclic ionophores. In order to enhance binding strength, and possibly increase cation selectivity, ionophores based on a more rigid framework with more ‘convergent’ ion pairs are required (without of course losing fast kinetics of cation exchange to maintain good response times). Further work is in progress with these features in mind.

We thank the SERC for support (AT).

REFERENCES

- 1 D. Ammann, P. Anker, E. Metzger, U. Oesch and W. Simon, in M. Kessler, J. Höper and D.K. Harrison, (Eds.) Ion Measurement in Physiology and Medicine, Springer Verlag, Berlin, Heidelberg, New York, 1985, p. 102.

- 2 P. Anker, H.-B. Jenny, U. Wuthier, R. Asper, D. Ammann and W. Simon, *Clin. Chem.*, (1983) 1508.
- 3 M. Guggi, M. Oehme, E. Pretsch and W. Simon, *Helv. Chim. Acta*, 59 (1976) 2417; R.A. Steiner, M. Oehme, D. Ammann and W. Simon, *Anal. Chem.*, 51 (1979) 351.
- 4 J.A.J. Brunink, J.R. Haak, J.G. Boner, D.N. Reinhoudt, M.A. McKervey and S.J. Harris, *Anal. Chim. Acta*, 254 (1991) 75; M. Telting-Diaz, D. Diamond, M.R. Smyth, E.M. Seward and A.M. McKervey, *Electroanalysis*, 3 (1991) 371.
- 5 R. Kataký, P.E. Nicholson and D. Parker, *J. Chem. Soc., Perkin Trans. II*, (1990) 321.
- 6 R.D. Hancock, *Pure Appl. Chem.*, 58 (1986) 1445.
- 7 I. Dayan, J. Libman, A. Shanzer, C.E. Felder and S. Lifson, *J. Am. Chem. Soc.*, 113 (1991) 3431.
- 8 A. Craggs, G.J. Moody and J.D.R. Thomas, *J. Chem. Educ.*, 51 (1974) 541.
- 9 N.G. Lukyanenko, N.Y. Nazarova, O.S. Karpinchik and O.T. Melnik, *Zh. Anal. Khim.*, 43 (1988) 1745.
- 10 J.K. Schneider, P. Hofstetter, E. Pretsch, D. Ammann and W. Simon, *Helv Chim. Acta*, 63 (1980) 217.

Comparison of potentiometric stripping analysis and square-wave voltammetry with respect to the influence of Triton X-100

Šebojka Komorsky-Lovrić and Marko Branica

Centre for Marine Research Zagreb, Rudjer Bošković Institute, P.O.B. 1016, 41001 Zagreb (Croatia)

(Received 30th July 1992)

Abstract

Potentiometric stripping analysis (PSA) is less sensitive to the presence of electroinactive surface-active substances than anodic stripping square-wave voltammetry (ASSWV). Influences of the non-ionic detergent Triton X-100 on the responses of Tl^+ , Pb^{2+} , Cu^{2+} , Cd^{2+} , $Bi(III)$ and $In(III)$ obtained by direct and derivative PSA, square-wave voltammetry, d.c. polarography and ASSWV are compared.

Keywords: Potentiometry; Stripping voltammetry; Surfactants; Triton X-100

Potentiometric stripping analysis (PSA) is a well established method for the determination of trace metals [1–5]. The principle of PSA is that metal ions are first reduced at a constant potential to form either amalgams or metal films at the electrode surface and then stripped by a chemical oxidant present in the solution. During the reoxidation of the accumulated metals, the potential of the working electrode increases in a stepwise manner, the time duration of each step being proportional to the concentration of the given metal in the sample solution. The time–potential curve may be recorded either directly [1] or in derivative [2,4] or differential [6] modes. The theory of the PSA in all three modes is well developed [7]. The method can employ different types of working electrodes: hanging mercury drop [1], mercury film-covered rotating disc [2,8], bare glassy carbon disc [9] or a set of mercury-covered

carbon fibre microelectrodes [10]. The measurements are performed under hydrodynamic conditions [2,4,5,10] or in unstirred solutions [1,11]. Several oxidizing agents, such as oxygen, $Hg(II)$, $Fe(III)$, acidic permanganate, $Ce(IV)$ or dichromate, can be used, depending on the choice of the working electrode [2,7,9]. The PSA can be applied to a variety of matrices, such as samples of groundwaters [5], sea water [12–14], whole blood [15,16], urine [17] and acid digests of biological material [8,17], because it exhibits low sensitivity to the presence of electroactive organic matter and oxidizing agents (e.g. dissolved oxygen and organic nitro compounds) [6,8,13,15] and, to a certain extent, of surface-active substances [10,18], especially when the working electrode is modified by a layer of Nafion [19].

In this work, the influences of the non-ionic detergent Triton X-100, as a model of electroinactive surface-active substances, on the responses of PSA and square-wave voltammetry [20] were compared. The surface properties of Triton X-100 [21–23] and its influence on the charge transfer of several metal ions [24–29] are well known.

Correspondence to: Š. Komorsky-Lovrić, Centre for Marine Research Zagreb, Rudjer Bošković Institute, P.O.B. 1016, 41001 Zagreb (Croatia).

EXPERIMENTAL

Chemicals were of analytical-reagent grade: TlNO_3 , $\text{Pb}(\text{NO}_3)_2$, $\text{Cu}(\text{NO}_3)_2 \cdot 3\text{H}_2\text{O}$, $\text{CdSO}_4 \cdot (8/3)\text{H}_2\text{O}$, Bi_2O_3 , $\text{Hg}(\text{NO}_3)_2$, concentrated HClO_4 (70%), concentrated HCl (37%) (all from Merck), $\text{InCl}_3 \cdot 4\text{H}_2\text{O}$ (Fluka), NaClO_4 (Kemika) and Triton X-100 (Rohm and Haas). Solutions were prepared in doubly distilled water. Stock solutions of Bi(III) and In(III) were prepared in concentrated HClO_4 and HCl , respectively. Mercury for the working electrode was purified by washing with 10% HNO_3 and by double distillation under reduced pressure.

The measurements were performed with an Autolab multimode polarograph with an IME module (Eco Chemie, Utrecht, Netherlands) which were connected to an AT 286-16 personal computer, a P60 printer (NEC) and a Model 303 A static mercury drop electrode (SMDE) with a Model 305 stirrer (both from Princeton Applied Research). A platinum wire was used as a counter electrode and an $\text{Ag}/\text{AgCl}/4\text{ M NaCl}$ electrode as the reference electrode.

Potentiometric stripping measurements were performed in both the direct (PSA) and the derivative (dPSA) modes. The acronym dPSA is used in this paper to distinguish derivative PSA from differential PSA (usual acronym DPSA [6]). During the accumulation of amalgams and throughout the dPSA measurements, the solutions were stirred with a magnetic rod. PSA measurements were performed in unstirred solutions, as recommended [11]. The mercury drop is not the most suitable electrode for dPSA [2], but it permits the repetitive measurements of the influence of Triton X-100 because of the renewal of its surface. D.c. polarographic (DCP), the square-wave voltammetric (SWV) and anodic stripping square-wave voltammetric (ASSWV) measurements were performed in the usual manner. The solutions were deaerated with extra-pure nitrogen for 20 min prior to the measurements; a nitrogen blanket was maintained thereafter.

The concentrations of all metal ions were $2 \cdot 10^{-5}\text{ M}$. The supporting electrolytes were 0.5 M NaClO_4 (pH 2, adjusted with HClO_4) (for Tl^+ , Pb^{2+} , Cu^{2+} and Cd^{2+}), 1 M HClO_4 + 0.01 M

HCl [for Bi(III)] and 0.5 M HCl [for In(III)]. To each solution $2 \cdot 10^{-5}\text{ M Hg(II)}$ was added.

RESULTS AND DISCUSSION

PSA and ASSWV are similar in that both are preceded by an amalgam accumulation period, but they differ in the reoxidation step and, consequently, in the nature of the response. The characteristic of the ASSWV response is the maximum in the current vs. potential relationship (i_p). The response in PSA is the potential vs. time curve characterized by the so-called [7] elapsed or stripping time, τ . In its derivative mode (dPSA), the characteristic value is the maximum of the first derivative of τ with respect to the potential, $(d\tau/dE)_{\text{max}}$. Electroinactive, surface-active substances (SAS), such as Triton X-100, can influence the responses of both PSA and ASSWV significantly. These dependences are shown in Figs. 1–6 for Tl^+ , Pb^{2+} , Cu^{2+} , Cd^{2+} , Bi(III) and In(III), respectively. The relative responses of these ions, each divided by the respective re-

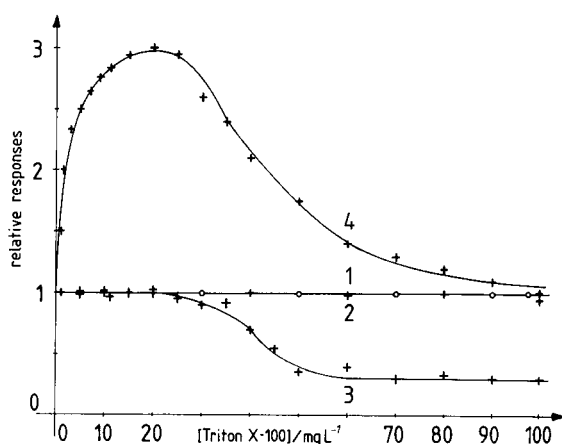


Fig. 1. Dependences of relative responses of Tl^+ on Triton X-100 concentration: (1) SWV; (2) DCP; (3) ASSWV; (4) dPSA. The responses are expressed relative to the respective responses in the solution without Triton X-100. $2 \times 10^{-5}\text{ M Tl}^+ + 2 \times 10^{-5}\text{ M Hg}^{2+}$ in 0.5 M NaClO_4 (pH 2, HClO_4). $f_{\text{sw}} = 100\text{ Hz}$; $E_{\text{sw}} = 30\text{ mV}$ (1,3); $dE = 2.4\text{ mV}$ (1–3); $t_d = 1\text{ s}$ (2); $E_{\text{acc}} = -0.85\text{ V}$ (3,4); $t_{\text{acc}} = 20\text{ s}$ (3) and 60 s (4); $t_{\text{eq}} = 5\text{ s}$ (3).

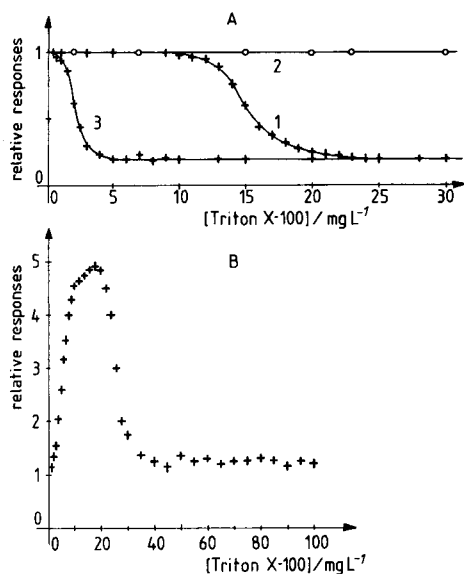


Fig. 2. Dependences of relative responses of Pb^{2+} on Triton X-100 concentration: (A) (1) SWV; (2) DCP; (3) ASSWV; (B) dPSA. $E_{acc} = -0.7$ V (3) and -0.8 V (B); $t_{acc} = 5$ s (3) and 30 s (B). All other data as in Fig. 1.

sponse in the solution without Triton X-100, are reported.

The influences of Triton X-100 on the relative responses of PSA and dPSA are very similar, so only the latter are reported. The difference in the dPSA and PSA measurements is in the stirring of the solution during the reoxidation step. The

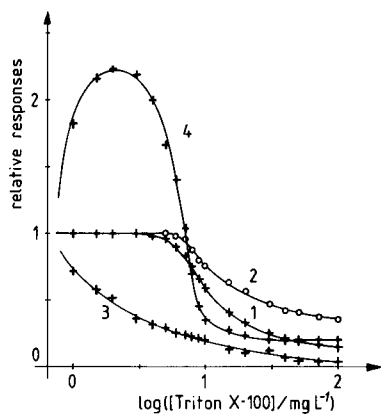


Fig. 3. Dependences of relative responses of Cu^{2+} on the logarithm of Triton X-100 concentration: (1) SWV; (2) DCP; (3) ASSWV; (4) dPSA. $E_{acc} = -0.2$ V (3) and -0.35 V (4); $t_{acc} = 5$ s (3) and 30 s (4). All other data as in Fig. 1.

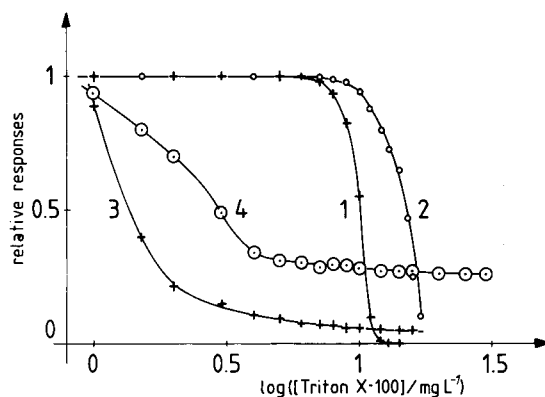


Fig. 4. Dependences of relative responses of Cd^{2+} on the logarithm of Triton X-100 concentration: (1) SWV; (2) DCP; (3) ASSWV; (4) dPSA. $E_{acc} = -0.8$ V (3,4); $t_{acc} = 5$ s (3) and 30 s (4). All other data as in Fig. 1.

similarity of their relative responses suggests that Triton X-100 mainly affects the accumulation of amalgams. This was confirmed by comparing the relative responses of ASSWV and SWV. SWV is a direct voltammetric technique, suitable for measuring metal ions in relatively higher concentrations [20]. If this condition is satisfied, SWV appears to be superior to both dPSA and ASSWV because the working electrode is exposed to the influence of SAS for a much shorter time. Finally, to investigate briefly whether Triton X-100 influences the charge transfer of a particular metal ion, or simply blocks the active electrode surface area, DCP measurements were per-

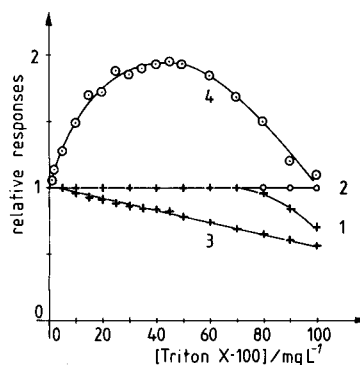


Fig. 5. Dependences of relative responses of $Bi(III)$ on Triton X-100 concentration: (1) SWV; (2) DCP; (3) ASSWV; (4) dPSA. 1 M $HClO_4$ + 0.01 M HCl . $E_{sw} = 15$ mV (1,3); $E_{acc} = -0.25$ V (3,4); $t_{acc} = 30$ s (3,4). All other data as in Fig. (1).

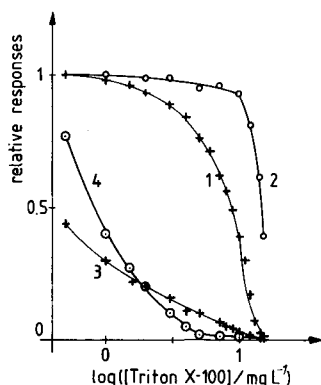


Fig. 6. Dependences of relative responses of In(III) on the logarithm of Triton X-100 concentration: (1) SWV; (2) DCP; (3) ASSWV; (4) dPSA. 0.5 M HCl; $E_{sw} = 15$ mV (1,3); $E_{acc} = -0.8$ V (3,4); $t_{acc} = 30$ s (3) and 120 s (4). All other data as in Fig. 1.

formed. The relative responses reported are the ratios between the DPC limiting currents.

Results for Tl^+ ions are shown in Fig. 1. The DPC and the SWV responses (line 1,2) are not affected by adsorption of Triton X-100 over the whole concentration range investigated. The other characteristics of these responses, namely the half-wave potential ($E_{1/2}$) and Tomeš criterion ($E_{3/4} - E_{1/4}$) in DCP or the peak potential (E_p) and peak width at half-height ($\Delta E_{p/2}$) in SWV, are also independent of the Triton X-100 concentration. This is in agreement with the well known insensitivity of $Tl^+/Tl(Hg)$ charge transfer to the presence of SAS [27,30–32]. However, the responses in ASSWV are depressed in the presence of more than 20 mg l^{-1} Triton X-100 (curve 3), but E_p and $\Delta E_{p/2}$ do not change, indicating a reversible charge transfer. In equilibrium, at potentials more negative than -0.3 V vs. SCE [22], the electrode surface is fully covered by a monolayer of adsorbed Triton X-100 molecules ($\Gamma_{max} = 3 \times 10^{-10} \text{ mol cm}^{-2}$ [23]) if its concentration is higher than 1 mg l^{-1} [28]. When this concentration exceeds 20 mg l^{-1} , the structure at the surface becomes more complex [28], including the formation of a second layer, semimicelles and similar associates of adsorbed Triton X-100 molecules [22,23]. This structure, formed during the accumulation period, probably blocks the electrode surface, hindering the reduction of Tl^+ ,

but the charge transfer at the free surface, which remains in pores of the structure, remains fast and reversible.

The results for dPSA (and PSA) exhibit a maximum for a Triton X-100 concentration of 20 mg l^{-1} (curve 4). In the range of monolayer coverage, the relative responses increase up to three times, but more complex surface structures cause a gradual decrease back to the original value. This enhancement is probably caused by slower reoxidation. The monolayer seems to be transparent for Tl^+ , but less penetrable for mercury ions [27,28], which inhibits the reoxidation of the amalgam. When the accumulation of the amalgam becomes hindered by the complex surface structure, the influence of the slow reoxidation is compensated for by the lower amalgam concentration [18] and relative responses decrease. This hypothesis is confirmed by the change in the potentials of the dPSA maxima (E_{max}) and by the fact that the effect does not depend on the stirring of the solutions during the reoxidation step. E_{max} changes from -0.49 V in the pure electrolyte to -0.51 V in the presence of 20 mg l^{-1} Triton X-100, and back to -0.48 V in solutions with the highest Triton X-100 concentration. The cathodic shift of E_{max} indicates a lower concentration of Tl^+ ions at the electrode surface, which may be caused by the slower reoxidation. The subsequent anodic shift of E_{max} is an indication of the decreased concentration of thallium amalgam. The influence of stirring becomes negligible if the diffusion of mercury ions through the film of the adsorbed Triton X-100 becomes the rate-determining step of the reoxidation process [24].

Similar dPSA responses are obtained with Pb^{2+} , Cu^{2+} and $Bi(III)$ (Figs. 2, 3 and 5), but not with Cd^{2+} and $In(III)$ (Figs. 4 and 6). In addition, each of these ions exhibits specific relationships between voltammetric response and Triton X-100 concentration.

The fast and reversible redox reaction of lead ions at pH 2 ($k_s = 2 \text{ cm s}^{-1}$) becomes irreversible under the influence of Triton X-100 [27]. Depressions of both the SWV and the ASSWV relative responses are followed by significant changes in E_p and $\Delta E_{p/2}$, which indicates a decrease in the

standard reaction rate constant (Fig. 2A, curves 1 and 3). In SWV, $-0.33 \geq E_p$ (V) ≥ -0.41 and $69 \leq \Delta E_{p/2}$ (mV) ≤ 160 ; in ASSWV, $-0.40 \leq E_p$ (V) ≤ -0.35 and $70 \leq \Delta E_{p/2}$ (mV) ≤ 95 . The same applies to the Tomeš criterion and $E_{1/2}$ in DCP, but the limiting current does not decrease (curve 2), indicating no change in the diffusion constant and no blocking effect for a short adsorption time. However, the dPSA responses are significantly enhanced if the Triton X-100 concentration is lower than 40 mg l^{-1} (Fig. 2B).

The reduction of Cu^{2+} from the acidic perchlorate medium is not fast ($k_s = 4 \times 10^{-3} \text{ cm s}^{-1}$), but becomes totally irreversible in the presence of Triton X-100 ($k_s = 10^{-8} \text{ cm s}^{-1}$ and $\alpha = 0.59$) [27,33]. This is the cause of large decreases in the SWV and ASSWV responses, as shown in Fig. 3. The other criteria of reversibility (E_p , $\Delta E_{p/2}$, $E_{1/2}$ and Tomeš criterion) change accordingly. In addition, the surfactant blocks the electrode surface or hinders the diffusion of copper ions, also depressing the DCP limiting currents (curve 2). Again, the dPSA method is superior to ASSWV below 10 mg l^{-1} of Triton X-100 (compare curves 3 and 4 in Fig. 3).

The influence of Triton X-100 on the redox reaction of Cd^{2+} is very similar, as shown in Fig. 4. Its standard reaction rate constant decreases from 2.5 to $10^{-5} \text{ cm s}^{-1}$ (with $\alpha = 0.4$) [27,28]. However, no enhancement of the dPSA responses is observed. No explanation for this fact can be given. It is possible that the amalgam activity is heavily depressed at very low Triton X-100 concentrations. In contrast to the experiments with copper, the dPSA E_{max} of cadmium ions changes from -0.59 V in pure electrolyte to -0.55 V (for 1 mg l^{-1} Triton X-100) and -0.53 V (2 mg l^{-1}) and -0.52 V (6 mg l^{-1}) and finally -0.50 V for 30 mg l^{-1} Triton X-100. The change in E_p in ASSWV is similar, from -0.595 V (for less than 1 mg l^{-1} Triton X-100) to -0.55 V (for 2 mg l^{-1}) and -0.52 V for 4 mg l^{-1} . It is curious that, whereas $E_{1/2}$ in DCP changes by 20 mV in the cathodic direction between 14 and 17 mg l^{-1} Triton X-100, the peak potential in SWV changes in the opposite direction from -0.525 V (for less than 10 mg l^{-1} Triton X-100) to -0.45 V for 15 mg l^{-1} , but the peak widths at half-height be-

come wider, as expected for irreversible redox reaction: 68 (for $< 10 \text{ mg l}^{-1}$) $\leq \Delta E_{p/2}$ (mV) ≤ 127 (for 12 mg l^{-1} Triton X-100). A similar effect was observed in the experiment with In(III).

The reduction rate of trivalent metal ions depends on the rate of dehydration of intermediate lower valency ions that occurs at the electrode surface [30,34]. This rate is very low in concentrated perchloric acid [34], but increases significantly in the presence of inorganic anions which are surface-active and form complexes with trivalent ions, such as halides and pseudohalides [30,35,36]. However, the redox reactions accelerated in that manner are very sensitive to the influence of surface-active substances which act in three ways: by a competition with halide ions for the electrode surface and by blocking and electrostatic effects [24,27,34]. If the SAS is neutral molecule, such as Triton X-100, the electrostatic effect is negligible [27]. The competition with halides depends on the potential of the mercury drop at which the redox reaction of a particular metal ion occurs, as can be seen from the results of voltammetric and stripping potentiometric measurements of Bi(III) and In(III) ions which are shown in Figs. 5 and 6.

The reduction of Bi(III) in $1 \text{ M HClO}_4 + 0.01 \text{ M HCl}$ occurs at a positively charged mercury drop electrode ($E_{1/2} = 0.04 \text{ V}$). The choice of electrolyte ensures a reversible redox reaction in the absence of Triton X-100 [34]. At this concentration of HCl and this electrode potential, the adsorption of chloride ions is strong, but Triton X-100 is very weakly adsorbed [22,23,27–29]. Hence the competition effect is negligible and there is no influence of Triton X-100 on the rate of reduction of Bi(III). This is confirmed by the indicators of reversibility (E_p , $\Delta E_{p/2}$, $E_{1/2}$ and Tomeš criterion), all of which are independent of Triton X-100 concentration. Changes in the ASSWV and dPSA relative responses can be explained by the blocking effect and by the influence of the adsorbed film on the diffusion of mercury ions and on the amount of accumulated amalgam (Fig. 5).

In 0.5 M HCl , the reduction of In(III) occurs at a potential at which the mercury drop electrode bears almost no charge ($E_{1/2} = -0.59 \text{ V}$).

The rate of this reduction is essentially dependent on the surface activity of chloride ions [35,36], but at such a negative potential the adsorption of Cl^- is very weak and submitted to the competitive action of Triton X-100. For this reason, all the investigated voltammetric and polarographic responses are heavily depressed at very low concentrations of Triton X-100 (Fig. 6). The responses of dPSA are also decreased whereas the potentials of maxima change anodically ($-0.55 \leq E_{\text{max}} \text{ (V)} \leq -0.50$, for 5 mg l^{-1} Triton X-100) because of smaller activity of accumulated amalgam.

These results indicate that accumulation of amalgams is the critical step in both ASSWV and dPSA techniques. This step may be greatly influenced by surface-active substances. The film of SAS formed during the accumulation period may decrease the rate of the subsequent reoxidation. However, the slow reoxidation increases the dPSA response, but decreases the ASSWV response. This is why dPSA appears superior to ASSWV for most of the investigated metal ions. In this paper only the SMDE with a renewable surface is considered. Long-term influences of traces of SAS on thin mercury film-covered disc electrodes is another problem that requires consideration [19].

This work was supported by the Ministry of Science, Technology and Informatics of the Republic of Croatia in the frame of the EUREKA-ELANI 37/12 (EUROMAR) project.

REFERENCES

- 1 D. Jagner and A. Graneli, *Anal. Chim. Acta*, 83 (1976) 19.
- 2 D. Jagner and K. Aren, *Anal. Chim. Acta*, 100 (1978) 375.
- 3 D. Jagner, *Anal. Chim. Acta*, 50 (1978) 1924.
- 4 A. Graneli, D. Jagner and M. Josefson, *Anal. Chim. Acta*, 52 (1980) 2220.
- 5 A. Hu, R.E. Dessy and A. Graneli, *Anal. Chim. Acta*, 55 (1983) 320.
- 6 L. Kryger, *Anal. Chim. Acta*, 120 (1980) 19.
- 7 Y. Xia, T. Chou and J. Mo, *Anal. Chim. Acta*, 222 (1989) 263.
- 8 L.G. Danielsson, D. Jagner, M. Josefson and S. Westerlund, *Anal. Chim. Acta*, 127 (1981) 147.
- 9 C. Labar, R. Müller and L. Lamberts, *Electrochim. Acta*, 36 (1991) 2103.
- 10 H. Huiliang, C. Hua, D. Jagner and L. Renman, *Anal. Chim. Acta*, 193 (1987) 61.
- 11 C. Labar and L. Lamberts, *Anal. Chim. Acta*, 132 (1981) 23.
- 12 D. Jagner and K. Aren, *Anal. Chim. Acta*, 107 (1979) 29.
- 13 D. Jagner, M. Josefson and S. Westerlund, *Anal. Chim. Acta*, 129 (1981) 153.
- 14 H. Eskilsson and D. Jagner, *Anal. Chim. Acta*, 138 (1982) 27.
- 15 L. Almestrand, D. Jagner and L. Renman, *Anal. Chim. Acta*, 193 (1987) 71.
- 16 L. Almestrand, M. Betti, C. Hua, D. Jagner and L. Renman, *Anal. Chim. Acta*, 209 (1988) 339.
- 17 D. Jagner and K. Aren, *Anal. Chim. Acta*, 141 (1982) 157.
- 18 T.M. Florence, *Anal. Proc.*, 20 (1983) 552.
- 19 M. Huiliang, D. Jagner and L. Renman, *Anal. Chim. Acta*, 207 (1988) 17.
- 20 J. Osteryoung and J.J. O'Dea, in A.J. Bard (Ed.), *Electroanalytical Chemistry*, Vol. 14, Dekker, New York, 1986, p. 209.
- 21 A. Ray and G. Nemethy, *J. Am. Chem. Soc.*, 93 (1971) 6787.
- 22 R.G. Barradas and F.M. Kimmerle, *J. Electroanal. Chem.*, 11 (1966) 128, 163.
- 23 R. Guidelli and M.R. Moncelli, *J. Electroanal. Chem.*, 89 (1978) 261.
- 24 R.W. Schmid and C.N. Reilley, *J. Am. Chem. Soc.*, 80 (1958) 2087.
- 25 P.L. Brezonik, P.A. Brauner and W. Stumm, *Water Res.*, 10 (1976) 605.
- 26 N. Gundersen and E. Jacobsen, *Anal. Chim. Acta*, 45 (1969) 346.
- 27 R. Guidelli and M.L. Foresti, *J. Electroanal. Chem.*, 77 (1977) 73.
- 28 Z. Kozarac, S. Nikolić, I. Ružić and B. Čosović, *J. Electroanal. Chem.*, 137 (1982) 279.
- 29 M. Plavšić and B. Čosović, *Water Res.*, 23 (1989) 1545.
- 30 J. Heyrovsky, *Discuss. Faraday Soc.*, 1 (1947) 212.
- 31 R. Tamamushi and T. Yamanaka, *Bull. Chem. Soc. Jpn.*, 28 (1955) 673.
- 32 H. Imai and S. Chaki, *Bull. Chem. Soc. Jpn.*, 29 (1956) 498.
- 33 I.M. Kolthoff and Y. Okinaka, *J. Am. Chem. Soc.*, 81 (1959) 2296.
- 34 B. Lovreček, M. Metikoš-Huković and I. Mekjavić, in A.J. Bard (Ed.), *Encyclopedia of Electrochemistry of the Elements*, Vol. IX, Part B, Dekker, New York, 1986, p. 69.
- 35 R.E. Visco, *J. Electroanal. Chem.*, 10 (1965) 82.
- 36 L. Pospišil and R. De Levie, *J. Electroanal. Chem.*, 25 (1970) 245.

Square-wave voltammetry of uranyl–humate complex

Marina Mlakar

Centre for Marine Research, Rudjer Bošković Institute, P.O.B. 1016, 41001 Zagreb (Croatia)

(Received 30th July 1992; revised manuscript received 26th November 1992)

Abstract

Square-wave voltammetric measurements were applied to the identification and determination of the uranyl–humate complex in 0.55 mol l^{-1} NaCl solution and in artificial and natural sea water. The sensitivity of the square-wave voltammetric response can be enhanced by the accumulation of the complex because of its strong adsorption at the electrode surface. The detection limit for the uranyl–humate complex after an accumulation period of 10 min at a potential of 0.0 V vs. a sodium chloride-saturated Ag/AgCl electrode was found to be $(5.0 \pm 0.2) \times 10^{-9} \text{ mol l}^{-1}$ and the maximum surface concentration of the adsorbed reactant was $\Gamma_s = (7.1 \pm 0.1) \times 10^{-11} \text{ mol cm}^{-2}$. The mechanism of the electrode reaction was established. The interferences of various cations and surface-active substances were studied.

Keywords: Voltammetry; Humic substances; Sea water; Uranium; Waters

Humic materials are mixtures of various high-molecular-weight organic compounds. They are composed of three operationally distinct fractions: fulvic acid, humic acid and humin. Their structure is built up of different proteins, polysaccharides, phenols and aliphatic hydrocarbon chains bound to the polyaromatic skeleton through oxygen bridges of various functional groups. These functional groups are mostly carboxyl and phenolic hydroxyl acidic groups and they are involved in binding of metal ions. During that reaction, protons are released [1,2]. Functional groups can also contain phosphorus, nitrogen or sulphur atoms and, therefore, they possess a specific affinity for various metal ions.

Interactions of metal ions with humic materials are also studied indirectly via various model systems. Most frequently EDTA [3], nitrilotriacetic acid [4], salicylic acid [5,6], phthalic acid [5],

amino acids [7,8], etc., are used. From polyfunctional model systems, based on randomly positioned functional groups and aromatic rings, it is deduced that phthalate- and salicylate-type sites are predominant active chelating sites for most metal ions, including uranium.

Because of the great importance of uranium as a nuclear fuel [9], its presence in natural sea water and the exceptionally fast loading process of uranium on hydrogen-loaded humic acid [10], voltammetric studies of the uranyl–humate complex were performed. Square-wave voltammetry was found to be the most convenient electrochemical technique for such studies. The results were compared with those obtained by voltammetric measurements with model ligands, salicylic and phthalic acid [5].

EXPERIMENTAL

Voltammetric measurements were performed in an EA 875-20 conventional electroanalytical

Correspondence to: M. Mlakar, Centre for Marine Research, Rudjer Bošković Institute, P.O.B. 1016, 41001 Zagreb (Croatia).

cell (50 ml) with a corresponding universal cap (Metrohm, Herisau, Switzerland). The working electrode was a hanging mercury drop electrode (HMDE), the reference electrode was a silver/silver chloride (Ag/AgCl) electrode with saturated NaCl and the counter electrode was a platinum wire. Prior to the measurements the solutions were deaerated with extra-pure nitrogen for 20 min. Stirring of the solutions during the accumulation was performed with a "turbo" stirrer constructed in the laboratory, with a speed of 4000 rotations min^{-1} .

Square-wave voltammetric measurements were performed with a PAR 384B polarographic analyzer (Princeton Applied Research) connected to a Hewlett-Packard Model 9816S technical computer, a Model 82906A printer and a Model 7475 A plotter. The system was controlled by a software program [11].

Square-wave forward-backward voltammograms were recorded with a BAS 100A electrochemical analyser (Bioanalytical Systems) connected to a Model DMP-40 video monitor, keyboard and digital plotter (Houston Instruments).

pH measurements were performed with an Orion Research pH meter and EA 920 expandable ion analyzer.

The supporting electrolytes used were 0.55 mol l^{-1} NaCl and artificial sea water prepared from salts in the following amounts [12]: 23.926 g kg^{-1} NaCl, 4.008 g kg^{-1} Na_2SO_4 , 0.667 g kg^{-1} KCl, 0.196 g kg^{-1} NaHCO_3 , 0.098 g kg^{-1} KBr, 0.026 g kg^{-1} H_3BO_3 , 0.003 g kg^{-1} NaF, 1 mol l^{-1} $\text{MgCl}_2 \cdot 6\text{H}_2\text{O}$, 1 mol l^{-1} $\text{CaCl}_2 \cdot 2\text{H}_2\text{O}$ and 0.1 mol l^{-1} $\text{SrCl}_2 \cdot 6\text{H}_2\text{O}$. Natural sea water samples were taken from Sibenik area in the middle region of the Adriatic sea.

A stock standard solution of uranyl perchlorate was prepared from uranyl nitrate and standardized gravimetrically [13].

A stock standard solution of humic acid (sodium salt) was prepared by dissolving the appropriate amount of analytical-reagent grade material (EGA Chemie) in doubly distilled water. According to the specification of EGA Chemie, humic acid was obtained by extraction from peat as a sodium salt. The molecular weight distribution was determined in EAWAG Laboratories

(Switzerland) using Sephadex G-25 (fine) as MW = 5000 and a low-molecular-weight fraction of MW = 1000. Elemental analysis gave C 38.33, H 4.18, N 0.60, S 0.90, Cl 0.1, Na 8, O 41% (by difference). The contents of metals were determined by x-ray fluorescence spectroscopy as Cu 16, Cr 135, Fe 15 582, Ti 1475, Zn 14, Pb 6 and Ca 6547 mg kg^{-1} . Humic acid is of terrestrial origin as the C/N ratio is very high (63.88).

The pH of the solutions was adjusted with hydrochloric acid and/or sodium hydroxide solution.

Square-wave voltammetric measurements were performed in the potential range between 0.0 and -0.7 V vs. Ag/AgCl.

RESULTS AND DISCUSSION

The uranyl ion, UO_2^{2+} , in 0.55 mol l^{-1} NaCl in the pH range 2–5 is reduced to the UO_2^+ ion at a potential of -0.185 V vs. Ag/AgCl. At higher pH values the reduction peak decreases markedly and a second peak appears at -0.50 V, which corresponds to the reduction of uranyl hydroxide. In artificial and natural sea water samples at pH 3.5, approximately the same voltammograms were obtained $\{E_{\text{p[U(VI)]-U(V)}} = -0.200 \text{ V}\}$.

Square-wave voltammograms of humic acid (10^{-3} g l^{-1}) in the pH range 2–9 in 0.55 mol l^{-1} NaCl and sea water solutions (artificial and natural) did not show any response. By accumulation at a potential of 0.0 V vs. Ag/AgCl, humic acid adsorbs and a capacitive peak at about -0.6 V in pH range 2–9 appears. On addition of uranyl ion (1.2×10^{-6} mol l^{-1}) in a chloride solution of humic acid (1.0×10^{-3} g l^{-1}) a reduction peak at -0.330 V appeared (pH = 4.1). The uranyl-humate complex reduction peak potential and current changed with variation of pH.

From the dependence to the square-wave reduction peak on the pH of the solution, in 0.55 mol l^{-1} NaCl and artificial and natural sea water, it is evident that there is only a slight difference (Fig. 1). The maximum current in NaCl is obtained at pH 4.1 (Fig. 1, curve 1), which is in good agreement with the results obtained in square-wave voltammetric measurements with salicylic

acid as a ligand [5]. In artificial and natural sea water the maximum current was recorded at pH 4.5 (Fig. 1, curve 2). The peak potential shifts in the negative direction with increasing pH in the range 2–5. In that pH range the dependences between the peak potential and pH of the solution are linear, with a slope of 1.1 mV per decade unit (d.u.) in 0.55 mol l^{-1} NaCl, 1.3 mV d.u. $^{-1}$ in artificial sea water and 1.34 mV d.u. $^{-1}$ in natural sea water.

In the presence of different concentrations of humic acid (1×10^{-4} to $2 \times 10^{-3} \text{ g l}^{-1}$) the dependence of the uranyl–humate complex reduction peak on humic acid concentration in NaCl (Fig. 2, curve 1), artificial sea water (curve 2) and natural sea water (curve 3) was examined. The pH of the solution was kept constant (4.1 and 4.5, respectively), and also the concentration of uranyl ion ($1.2 \times 10^{-6} \text{ mol l}^{-1}$). In the examined concentration range of humic acid (1×10^{-4} – $2 \times 10^{-3} \text{ g l}^{-1}$), it is evident that the reduction current depends linearly on the humic acid concentration in all three electrolytes, but with different slopes. The reason for such behaviour is probably that the uranyl ion in NaCl is surrounded only by chloride ions and water molecules, whereas in the artificial and natural sea water in the coordination sphere of the uranyl ion in addition to water molecules, also chloride, fluoride, hydrogencarbonate, borate and sulphate ions are present. Therefore, the complexation of uranyl ion in the

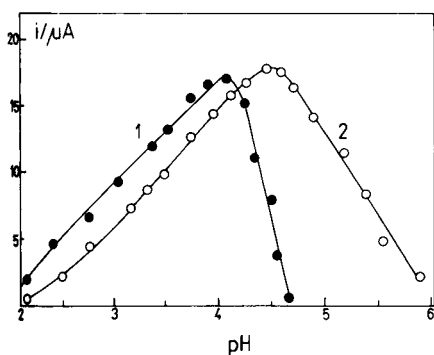


Fig. 1. Dependence of SWV peak current on pH of the solution in (1) 0.55 mol l^{-1} NaCl and (2) artificial sea water in the presence of $1.2 \times 10^{-6} \text{ mol l}^{-1} \text{ UO}_2^{2+}$ and 10^{-3} g l^{-1} humic acid; $f = 100 \text{ s}^{-1}$; $a = 70 \text{ mV}$.

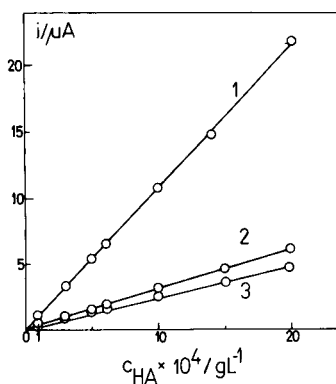


Fig. 2. Dependence of SWV peak current on humic acid concentration in the presence of $1.2 \times 10^{-6} \text{ mol l}^{-1} \text{ UO}_2^{2+}$ in (1) 0.55 mol l^{-1} NaCl (pH 4.1) and (2) artificial sea water (pH 4.5); $f = 100 \text{ s}^{-1}$; $a = 70 \text{ mV}$.

artificial and natural sea water proceeds more slowly because it is necessary to add more ligand molecules to achieve the same concentration of the uranyl–humate complex as in NaCl alone. In other words, the substitution of the ligands from the coordination sphere of uranyl ion is occurring only when higher concentrations of humic acid are present in the electrolyte solution. Further, in natural sea water samples some organic, surface-active substances can be present, so the complexation of the uranyl ion with the humic acid would be even slower. The uranyl–humate reduction peak potential shifts to more negative values with increase in the humic acid concentration in all electrolytes. The dependence is linear with slopes of 4 and 3.8 mV d.u. $^{-1}$, respectively.

It was established that the uranyl–humate complex adsorbs at the electrode surface and by accumulation of the complex at a certain potential the detection of lower uranyl ion concentrations is possible. The sensitivity of the square-wave voltammetric response can be markedly increased if the solution is stirred during the accumulation period. The forced mass transfer enhances the concentration of the adsorbed complex and permits the determination of uranyl ion at low concentration levels present in natural sea water samples (ca. $10^{-8} \text{ mol l}^{-1}$).

Measurements with lower uranyl ion concentrations were performed in 0.55 mol l^{-1} NaCl as there was no great difference in the results ob-

tained with artificial sea water or UV-irradiated natural sea water. It was established that the optimum accumulation potential is 0.0 V vs. Ag/AgCl. The concentration of humic acid ($1 \times 10^{-3} \text{ g l}^{-1}$) and pH of the electrolyte solutions (4.1) were kept constant like other square-wave parameters (frequency = 100 Hz, amplitude = 70 mV). The measurements were performed with four different concentrations of uranyl ion (1.2×10^{-8} , 6.0×10^{-8} , 1.2×10^{-7} and $6.0 \times 10^{-7} \text{ mol l}^{-1}$) and the dependence of the square-wave reduction peak current on the accumulation time is presented in Fig. 3. The dependence is linear at a uranyl ion concentration of $1.2 \times 10^{-8} \text{ mol l}^{-1}$ for accumulation times between 1 and 10 min. With a concentration of $6 \times 10^{-8} \text{ mol l}^{-1} \text{ UO}_2^{2+}$, saturation of the electrode surface takes place after an accumulation time of about 5 min. With higher uranyl ion concentrations the reduction current reaches a plateau after shorter accumulation periods. When the uranyl ion concentration in the solution is $6 \times 10^{-7} \text{ mol l}^{-1}$ saturation of the electrode is reached almost immediately. With increasing accumulation time the reduction peak potential of the uranyl–humate complex shifts in the negative direction owing to the formation of a thicker adsorbed layer of the complex molecules. Therefore, the reduction process of the uranyl–humate complex, that is, the electron transfer

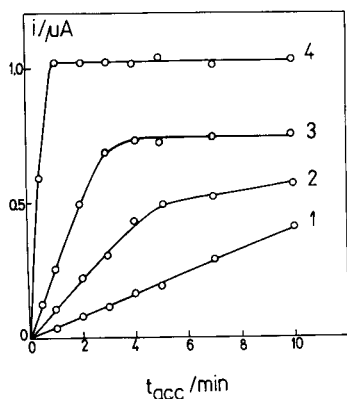


Fig. 3. Dependence of SWV peak current on the accumulation time in $0.55 \text{ mol l}^{-1} \text{ NaCl}$ in the presence of $1.0 \times 10^{-3} \text{ g l}^{-1}$ humic acid and (1) 1.2×10^{-8} , (2) 6.0×10^{-8} , (3) 1.2×10^{-7} and (4) $6.0 \times 10^{-7} \text{ mol l}^{-1} \text{ UO}_2^{2+}$; pH = 4.1; $E_{\text{acc}} = 0.0 \text{ V}$; $f = 100 \text{ s}^{-1}$; $a = 70 \text{ mV}$.

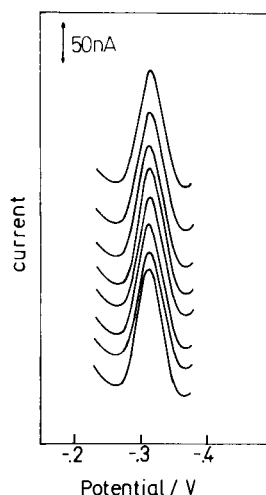


Fig. 4. Repetitive square-wave voltammograms of $10^{-8} \text{ mol l}^{-1} \text{ UO}_2^{2+}$ in $0.55 \text{ mol l}^{-1} \text{ NaCl}$; $t_{\text{acc}} = 5 \text{ min}$; $E_{\text{acc}} = 0.0 \text{ V}$; $f = 100 \text{ s}^{-1}$; $a = 70 \text{ mV}$.

through the adsorption layer, becomes more difficult. The adsorptive accumulation of the uranyl–humate complex results in reproducible stripping peak currents. Eight successive measurements of $1.2 \times 10^{-8} \text{ mol l}^{-1} \text{ UO}_2^{2+}$ with $1 \times 10^{-3} \text{ g l}^{-1}$ of humic acid in NaCl yielded a mean peak current of 158 nA and a relative standard deviation of 2.8% (Fig. 4).

The detection limit in NaCl with an accumulation time of 10 minutes at a potential of 0.0 V vs. Ag/AgCl was found to be $(5.0 \pm 0.2) \times 10^{-9} \text{ mol l}^{-1}$ uranyl ion.

Mechanism of reduction process

To elucidate the mechanism of the reduction of the uranyl–humate complex, square-wave (SW) measurements were performed and analysed. Figure 5 shows a square-wave voltammogram of the uranyl–humate complex, which is resolved in the forward and backward (reverse) current [14]. The recorded square-wave peaks are characteristic of an irreversible reduction process.

Theoretical analysis of the influenced of adsorption of the reactant on the square-wave voltammograms of a totally irreversible redox reactions [15] has shown that the peak width at half-height satisfies the relationship $\Delta E_{p/2} \text{ (mV)}$

$= (63.5 \pm 0.5)/\alpha n$, where n is the number of simultaneously transferred electrons and α is the average transfer coefficient. The obtained peak width at half-height of the uranyl–humate complex is 160 mV, which corresponds to $\alpha = 0.393 \pm 0.004$, taking into the account that the reduction process of the uranyl–humate complex is a one-electron reduction. Further, it is established that the peak width at half-height remains constant with change in the SW amplitude, which is characteristic of totally irreversible redox processes.

The dependence of the reduction peak current of the uranyl–humate complex on the SW amplitude shows that the initial slope is $(\Delta i_p/\Delta a)_{a \leq 10} = 2.5 \mu\text{A V}^{-1}$ (Fig. 6). According to the equation

$$i_p = (5 \pm 1) \times 10^2 q \alpha n^2 F a f \Delta E \Gamma \quad (1)$$

the amount of the adsorbed reactant can be calculated from the slope i_p/a , using the values $\alpha = 0.393$, $n = 1$ and $q = 0.0325 \text{ cm}^2$ [15]. The dependence of the complex reduction peak current on the uranyl ion concentration without accumulation is linear up to a concentration of $8 \times 10^{-7} \text{ mol l}^{-1}$ and saturation of the electrode surface is reached at $1.2 \times 10^{-6} \text{ mol l}^{-1} \text{ UO}_2^{2+}$. The limiting current of the square-wave voltammetric reduction peak of the uranyl–humate complex is equal to $8.80 \mu\text{A}$. Using the value $k' = 0.025$, the maximum concentration of the adsorbed uranyl–

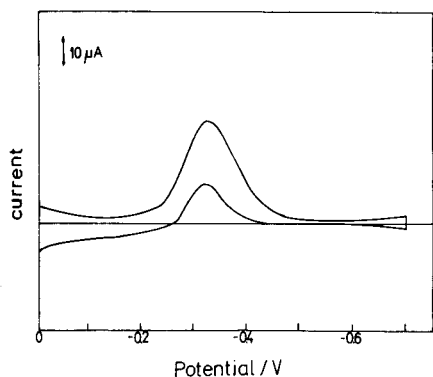


Fig. 5. Square-wave forward–backward voltammogram of $1.2 \times 10^{-6} \text{ mol l}^{-1} \text{ UO}_2^{2+}$ and 10^{-3} g l^{-1} humic acid in $0.55 \text{ mol l}^{-1} \text{ NaCl}$; pH = 4.1; $f = 100 \text{ s}^{-1}$; $a = 70 \text{ mV}$.

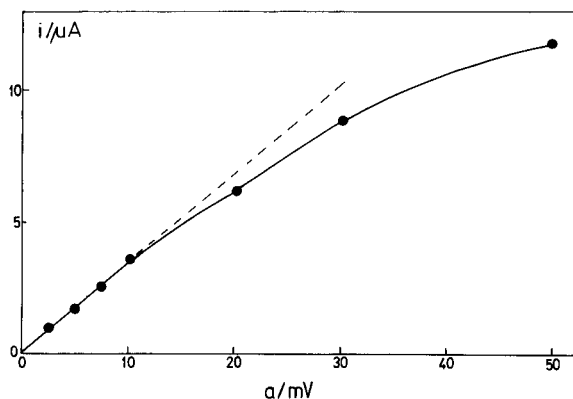


Fig. 6. Dependence of SWV peak current on SW amplitude in $0.55 \text{ mol l}^{-1} \text{ NaCl}$ in the presence of $1.2 \times 10^{-6} \text{ mol l}^{-1} \text{ UO}_2^{2+}$ and 10^{-3} g l^{-1} humic acid at pH 4.1; $f = 100 \text{ s}^{-1}$.

humate complex was calculated by Eqn. 1 to be $\Gamma_s = (7.1 \pm 0.1) \times 10^{-11} \text{ mol cm}^{-2}$.

Further, according to theoretical studies of totally irreversible redox reactions in square-wave voltammetry [16,17], the analytical sensitivity increases with increasing SW amplitude, because the peak width at half height does not change. The peak width at half-height is a very important parameter for assessing the reversibility of an electrode process. For totally irreversible redox reactions $\Delta E_{p/2}$ does not depend on SW amplitude. Such a behaviour was also established for the uranyl–humate complex.

Very important and precise information about the electrode reaction mechanism arises from the dependences of the reduction current on the SW frequency. There is a linear relationship between the reduction peak current of the uranyl–humate complex and the square-root of SW frequency, characterizes a totally irreversible redox reaction with reactant adsorption, regardless of the product adsorption. The dependence of the SW peak potential on the logarithm of the SW frequency is also a straight line with a slope $\Delta E_p/\Delta \log f = 148 \text{ mV}$. According to theoretical calculations [17] for the totally irreversible redox reactions, the dependence $\Delta E_p/\Delta \log f = -2.303 RT/\alpha nF = -59/\alpha n$. From this equation a transfer coefficient of $\alpha = 0.398$ is calculated. This value is in good agreement with the value $\alpha = 0.393$

calculated from the dependence of the SW peak current on the SW amplitude.

Interferences

Interferences from cations and surface-active substances present in natural sea water samples were examined. Most of the investigated cations did not cause serious interferences. The effects of organic surfactants that are likely to interfere because of competition for the sites at the electrode surface were evaluated. The addition of 100 $\mu\text{g l}^{-1}$ of gelatine caused a 10% depression of the uranyl–humate ($10^{-8} \text{ mol l}^{-1} \text{ UO}_2^{2+}$) reduction peak. The reduction peak height of the uranyl–humate complex decreased by ca. 25% after the addition of 250 $\mu\text{g l}^{-1}$ of Triton X-100. Therefore, the destruction of organic surface-active substances by UV irradiation is recommended when analysing natural sea water samples.

Conclusions

Uranyl ion forms a complex with humic acid in 0.55 mol l^{-1} NaCl and artificial and natural sea water. Its behaviour in all electrolytes is very similar. The maximum concentration of the uranyl–humate complex is detected at pH 4.1 in NaCl and at pH = 4.5 in artificial and natural sea water. It is adsorbed at the electrode surface and reduced irreversibly with reactant adsorption at a potential of ca. -0.33 V , depending on the pH of the solution. The detection limit for the uranyl–humate complex in 0.55 mol l^{-1} NaCl, with an accumulation time of 10 min at 0.0 V vs. Ag/AgCl, was found to be $(5.0 \pm 0.2) \times 10^{-9} \text{ mol l}^{-1}$. The maximum surface concentration of the adsorbed uranyl–humate complex was evaluated as $\Gamma_s = (7.1 \pm 0.1) \times 10^{-11} \text{ mol cm}^{-2}$.

Financial support from the Ministry of Science, Technology and Informatics of the Republic of Croatia is gratefully acknowledged.

REFERENCES

- 1 M. Schnitzer and S.U. Khan, *Humic Substances in the Environment*, Dekker, New York, 1972.
- 2 E.M. Perdu, *Chemical Modeling in Aqueous Systems* (ACS Symposium Series, No. 93), American Chemical Society, Washington, DC, 1979, pp. 99–114.
- 3 T.M. Florence and G.E. Batley, *Talanta*, 23 (1976) 179.
- 4 W. Stumm and D.A. Brauner, in J.P. Riley and G. Skirrow (Eds.), *Chemical Oceanography*, Vol. 1, Academic, London, 2nd edn., p. 173.
- 5 M. Mlakar and M. Branica, *Croat. Chem. Acta*, 60 (1987) 325.
- 6 D.V. Jahagirdar and D.D. Khanolkar, *J. Inorg. Nucl. Chem.*, 35 (1973) 921.
- 7 P.V. Selvaraj and M. Santappa, *J. Inorg. Nucl. Chem.*, 39 (1977) 119.
- 8 K.S. Rajan and A.E. Martell, *J. Inorg. Nucl. Chem.*, 26 (1964) 789.
- 9 M.F. Duret, *The Contribution of Nuclear Power to World Energy Supply 1975 to 2020*, Report to World Energy Conference, Ottawa, Canada, 1978.
- 10 K. Wagener and D. Heltkamp, *Thalassia Jugosl.*, 16 (1980) 185.
- 11 I. Pizeta and M. Branica, *J. Electroanal. Chem.*, 250 (1988) 293.
- 12 R.A. Horne, *Marine Chemistry*, Wiley, New York, 1969, p. 140.
- 13 C.Y. Rodden, *Analytical Chemistry of the Manhattan Project*, McGraw-Hill, New York, 1960, p. 46.
- 14 J.J. O'Dea, J. Osteryoung and R.A. Osteryoung, *Anal. Chem.*, 53 (1981) 203.
- 15 M. Lovric, S. Komorsky-Lovric and R. Murray, *Electrochim. Acta*, 33 (1988) 739.
- 16 M. Lovric and M. Branica, *J. Electroanal. Chem.*, 248 (1987) 239.
- 17 M. Lovric and S. Komorsky-Lovric, *J. Electroanal. Chem.*, 248 (1988) 239.

Potentiometric method for the determination of adenosine-5'-triphosphate

Takashi Katsu and Koji Yamanaka

Faculty of Pharmaceutical Sciences, Okayama University, Tsushima, Okayama 700 (Japan)

(Received 21st August 1992; revised manuscript received 8th October 1992)

Abstract

A potentiometric method for the determination of adenosine-5'-triphosphate (ATP) concentrations using a choline-sensitive membrane electrode and choline kinase enzyme is described. The choline electrode was constructed from a poly(vinyl chloride)-based membrane containing sodium tetrakis[3,5-bis(2-methoxyhexafluoro-2-propyl)phenyl]borate as an ion exchanger and 2-fluoro-2'-nitrodiphenyl ether as a membrane solvent. Choline reacted quantitatively with ATP to produce the electrode-insensitive choline phosphate and, therefore, the concentration of ATP could be determined by the measurement of choline consumed by the enzymatic reaction. ATP down to 10 μ M could be detected. This method was used successfully to determine the intracellular ATP content of human red blood cells.

Keywords: Enzymatic methods; Ion selective electrodes; Potentiometry; Blood; Adenosine-5'-triphosphate; Enzyme electrodes

Over the past few years, the concentrations of various biologically and clinically important substances have been successfully determined by using combinations of ion-selective electrodes and enzymes [1–4]. The use of an ion-selective electrode in biochemical analysis is attractive because the electrode enables a reaction process to be monitored without any associated sample colour or turbidity problems. For example, the amino acids L-tyrosine and L-phenylalanine have been determined specifically by detecting the tyramine and phenethylamine formed as a result of the enzymatic reactions of these amino acids with decarboxylases, using the corresponding amine-sensitive electrodes [2]. Another example is the determination of inorganic phosphate, based on the detection of salicylate formed by the enzy-

matic hydrolysis of *o*-carboxyphenyl phosphate by alkaline phosphatase in the presence of phosphate ions. The phosphate ions competitively inhibited the formation of salicylate and, therefore, the phosphate concentrations were determined by measuring changes in the rate of salicylate formation, using a salicylate-sensitive electrode [4].

In this study, a choline-sensitive membrane electrode and choline kinase enzyme were used to determine adenosine-5'-triphosphate (ATP) concentrations. The method is based on measuring the decrease in the concentration of choline resulting from its consumption during the enzyme-catalysed reaction of choline with ATP. Hitherto, two approaches to the potentiometric determination of ATP have been described. One involved the use of bacterial H⁺-ATPase and a pH-sensitive field-effect transistor. The ATP concentration was determined from the pH change resulting from the release of orthophosphate

Correspondence to: T. Katsu, Faculty of Pharmaceutical Sciences, Okayama University, Tsushima, Okayama 700 (Japan).

when ATP reacted with H^+ -ATPase [5]. The other involved the use of a neutral carrier, 15-hexadecyl-1,4,7,10,13-pentaazacyclohexadecane, to construct an ion-selective electrode that responded directly to ATP [6]. In this study, an assay method based on a different principle was developed, with which ATP concentrations can be measured very sensitively and selectively.

EXPERIMENTAL

A choline-sensitive membrane electrode was constructed using a poly(vinyl chloride) (PVC) membrane, as described previously [1–4]. The components were 0.5 mg of sodium tetrakis[3,5-bis(2-methoxyhexafluoro-2-propyl)phenyl]borate (NaHFPB) (Dojindo Labs.), which was chosen for its high lipophilicity [7], 60 μ l of 2-fluoro-2'-nitrodiphenyl ether (FNDPE) (Dojindo Labs.) and 30 mg of PVC (degree of polymerization 1020) (Nacalai Tesque). The materials were dissolved in tetrahydrofuran, poured into a flat Petri dish (30 mm diameter) and the solvent was allowed to evaporate at room temperature. The resulting membrane was cut and stuck to a PVC tube (4 mm o.d., 3 mm i.d.) using tetrahydrofuran as an adhesive. The electrochemical cell arrangement was Ag, AgCl/10 mM choline chloride (internal solution)/sensor membrane/sample solution/1 M NH_4NO_3 (salt bridge)/10 mM KCl/Ag, AgCl. The electromotive force between the silver/silver chloride electrodes was measured with an appropriate field-effect transistor operational amplifier (input resistance $> 10^{12} \Omega$) and recorded. The selectivity coefficients of the electrode were evaluated by the separate solution method using the respective chloride salts at 10 mM [1,2] and the detection limit was defined as the intersection point of the extrapolated linear regions of the calibration graph [2–4].

The procedure used to determine the intracellular ATP content of human red blood cells was as follows. Peripheral blood, drawn into ethylenediaminetetraacetic acid disodium salt ($EDTA \cdot 2Na$), was washed twice with 150 mM NaCl–5 mM 4-(2-hydroxyethyl)-1-piperazineethanesulphonic acid–NaOH (pH 7.4) and the intact cells were

harvested by aspiration from under a buffy coat [8]. The intracellular ATP was released from the cells by bursting the cell pellet osmotically by adding an equal volume of water; the resulting suspension is hereafter called the haemolysate. The haemolysate (10 μ l) was diluted twentyfold with an assay solution (190 μ l) that consisted of 0.4 international units (IU) choline kinase–100 μ M choline chloride–100 mM tris(hydroxymethylamino)methane (Tris)–HCl (pH 8.5)–20 mM $MgCl_2$ and the final volume used for the assay was 200 μ l. It should be emphasized that this electrode system, including the reference electrode [9], is compact and, therefore, assay solution volumes as small as 200 μ l can be used. The enzyme reaction is known to be fastest at pH 8.5 and enhanced by the presence of 20 mM $MgCl_2$ [10,11]. A 1 IU amount of choline kinase is defined as the amount required to convert 1 μ mol of choline into choline phosphate during the reaction with ATP per minute at pH 8.5 and 25°C. The mixture was incubated for 10 min at 25°C, then the concentration of choline was measured using the choline-sensitive electrode and converted into ATP concentration using a calibration graph.

The commercially available choline kinase from *Saccharomyces cerevisiae* (Sigma) used contained small amounts of impurities to which the choline electrode responded, so the enzyme was purified by dialysis prior to use. The disodium salt of ATP (Sigma, product number A-5394) was used for calibration. All other chemicals were of analytical-reagent grade unless stated otherwise.

RESULTS AND DISCUSSION

Using NaHFPB as an ion exchanger, the effect of membrane solvents was first examined. The membrane solvents tested were FNDPE, *o*-nitrophenyl phenyl ether, *o*-nitrophenyl *n*-octyl ether, di(*n*-octyl) phthalate, di(2-ethylhexyl) sebacate, di(*n*-octyl) phenylphosphonate, tris(2-ethylhexyl) phosphate and tricresyl phosphate. Of these, FNDPE and *o*-nitrophenyl phenyl ether afforded almost the same response characteristics, whereas other membrane solvents were less

effective and yielded higher detection limits for choline. A combination of NaHFPB and FNDPE was used and Fig. 1a shows the calibration graph for this electrode in 100 mM Tris-HCl (pH 8.5)–20 mM MgCl₂. The slope in the linear range was 58 mV per decade and the detection limit was 4 μM. The response time was less than 10 s when the concentration of choline was changed from 10 to 100 μM. The selectivity coefficient, $\log k_{\text{choline}, X}^{\text{pot}}$, was -4.9 for Mg²⁺, -4.8 for Ca²⁺, -3.6 for Na⁺, -2.6 for K⁺, -2.0 for CH₃NH₃⁺ and 0.9 for (CH₃)₄N⁺.

This choline-sensitive electrode was used for the determination of ATP concentrations; a typical trace of the response to ATP is shown in Fig. 2. The initial concentration of choline was 100 μM and when 1 μl of ATP aqueous solution (final concentration 25 μM) was added at the time indicated by the first arrow to a solution (200 μl) containing 100 μM choline chloride–0.4 IU choline kinase–100 mM Tris-HCl (pH 8.5)–20 mM MgCl₂, a rapid decrease in the electrical potential was observed and the final potential level reached corresponded to 75 μM choline. The same amount of ATP was further added at the times indicated by the second and third arrows and the relationship between ATP concentration and electrical potential was examined. As shown in Fig. 1b, the ATP concentration could

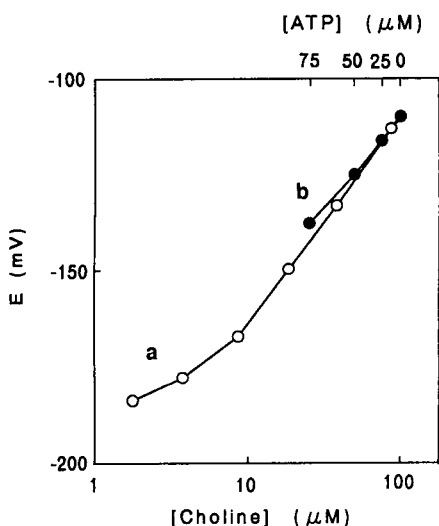


Fig. 1. Calibration graphs for the determination of (a) choline and (b) ATP.

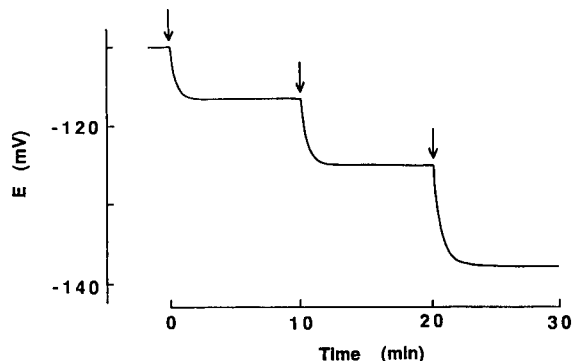


Fig. 2. Response to ATP. At the times indicated by the arrows, 25 μM of ATP was added.

easily be determined by a potentiometric measurement using the choline electrode. Addition of 1 mM adenosine-5'-diphosphate (ADP) or adenosine-5'-monophosphate (AMP) to the assay mixture had no effect on the electrode response. Therefore, this assay method was highly selective for ATP. In view of the dynamic range of the electrode, the detection limit for ATP was about 10 μM under the present conditions. It should be mentioned, however, that lowering the initial concentration of choline can decrease the detection limit of ATP to ca. 2–3 μM.

This method was used to determine the ATP levels in human red blood cells, as the choline electrode suffered no serious interference from K⁺, Na⁺ and other cations present in intracellular fluids. The electrical potential of the assay mixture containing the haemolysate was measured as described under Experimental and was -118 mV, which corresponded to 30 μM of ATP from the calibration graph shown in Fig. 1b. As the volume of red blood cells occupied half of the haemolysate and had been diluted twentyfold, the intracellular ATP concentration was calculated to be 1.2 mM, which agrees well with the results of previous studies [12,13].

These results demonstrate that the combination of a choline-sensitive electrode and choline kinase enzyme provides a practical assay system for the determination of ATP concentrations.

This work was supported by a Grant-in-Aid from the Shimadzu Science Foundation and a

Grant-in-Aid for Scientific Research from the Ministry of Education, Science and Culture of Japan.

REFERENCES

- 1 T. Katsu, M. Kuroko, T. Hirota and Y. Fujita, *Anal. Chim. Acta*, 217 (1989) 193.
- 2 T. Katsu, T. Kayamoto and Y. Fujita, *Anal. Chim. Acta*, 239 (1990) 23.
- 3 T. Katsu and T. Kayamoto, *Anal. Chim. Acta*, 254 (1991) 95.
- 4 T. Katsu and T. Kayamoto, *Anal. Chim. Acta*, 265 (1992) 1.
- 5 M. Gotoh, E. Tamiya, I. Karube and Y. Kagawa, *Anal. Chim. Acta*, 187 (1986) 287.
- 6 Y. Umezawa, M. Kataoka, W. Takami, E. Kimura, T. Koike and H. Nada, *Anal. Chem.*, 60 (1988) 2392.
- 7 G.H. Zhang, T. Imato, Y. Asano, T. Sonoda, H. Kobayashi and N. Ishibashi, *Anal. Chem.*, 62 (1990) 1644.
- 8 T. Katsu, K. Sanchika, H. Okazaki, T. Kondo, T. Kayamoto and Y. Fujita, *Chem. Pharm. Bull.*, 39 (1991) 1651.
- 9 T. Katsu, H. Kobayashi and Y. Fujita, *Biochim. Biophys. Acta*, 860 (1986) 608.
- 10 J. Wittenberg and A. Kornberg, *J. Biol. Chem.*, 202 (1953) 431.
- 11 M.A. Brostrom and E.T. Browning, *J. Biol. Chem.*, 248 (1973) 2364.
- 12 M. Nakao, T. Nakao, S. Yamazoe and H. Yoshikawa, *J. Biochem.*, 49 (1961) 487.
- 13 C. Feo and N. Mohandas, *Nature*, 265 (1977) 166.

Comparative study of argon and helium plasmas in a TM_{010} cavity and a surfatron and their use for hydride generation microwave-induced plasma atomic emission spectrometry

E. Bulska ¹

Laboratorium für Reinststoffanalytik, Max-Planck-Institut für Metallforschung, Stuttgart, Postfach 12 26 52, 4600 Dortmund 1 (Germany)

J.A.C. Broekaert

Universität Dortmund, Fachbereich Chemie, Postfach 50 05 00, 4600 Dortmund 50 (Germany)

P. Tschöpel and G. Tölg

Laboratorium für Reinststoffanalytik, Max-Planck-Institut für Metallforschung, Stuttgart, Postfach 12 26 52, 4600 Dortmund 1 (Germany)

(Received 28th May 1992; revised manuscript received 21st December 1992)

Abstract

Argon and helium microwave-induced plasmas (MIPs) operated in a TM_{010} Beenakker resonator and in a surfatron were investigated for the determination of hydride-forming elements. The MIPs in both devices were optimized with elemental mercury vapour. The analytical figures of merit were determined for As, Sb and Se in the case of hydride generation followed by trapping in a hot graphite furnace and subsequent evaporation of the analyte into the plasma. The long-term stability of the plasmas obtained in both devices was found to be very good. With the surfatron the absolute detection limits for the determination of As, Sb and Se (0.1–0.2 ng) were half those with the TM_{010} cavity.

Keywords: Atomic emission spectrometry; Flow system; Antimony; Arsenic; Hydride generation; Microwave-induced plasmas; Selenium; Surfatron

Correspondence to: P. Tschöpel, Laboratorium für Reinststoff-analytik, Max-Planck-Institut für Metallforschung, Stuttgart, Postfach 12 26 52, 4600 Dortmund 1 (Germany).

¹ On leave from Department of Chemistry, University of Warsaw, 02-093 Warsaw (Poland).

Argon or helium microwave-induced plasmas (MIPs) are commonly used as radiation sources for atomic emission spectrometry [1]. MIPs operated at powers less than 200 W can be obtained

with small-sized instrumentation and hence are less expensive than the other plasmas (e.g., direct current plasma at 500 W or inductively coupled plasma (ICP) at 1–5 kW).

The equipment for the generation of MIPs includes a microwave generator, a resonant cavity and a quartz plasma torch [2]. The analytical capabilities of the MIPs depend strongly on the cavities used [3,4]. Therefore, cavity design has often been an object of investigation. Up to 1976 in most cavities argon plasmas (Ar MIP) could be maintained at atmospheric or reduced pressure whereas the more energetic helium plasma (He MIP) could only be sustained at reduced pressure [5–8].

In 1976, Beenakker [9] introduced a TM_{010} cavity with which Ar and He MIPs can be generated at atmospheric pressure. A further advantage offered by the Beenakker TM_{010} cavity is the ability to view axially into the capillary, which permits better observation of the radiation emitted. The MIP in the Beenakker cavity has found many applications. It is used as a detector for gas chromatography [10–13], as a radiation source for atomic emission spectrometry (AES) with pneumatic nebulization [14] or electrothermal evaporation of solutions (for a review, see [15]) and for the analysis of samples introduced directly in the gaseous form [16]. Similarly to the ICP, it also has found use as an ion source for mass spectrometry (see, e.g., [17]).

For operating a low-power MIP at atmospheric pressure with both Ar and He, also the so-called surfatron is very powerful. Here surface wave propagation is used to produce an MIP [18–20]. The MIP generated in a surfatron seems to be easier to operate and to tune than that in a Beenakker cavity and it has been used successfully for many analytical purposes (see, e.g., [21,22]).

For the investigation and comparison of the plasma properties (configuration, stability and emission intensity profiles) of the MIPs in both devices, elemental mercury vapour was introduced into the plasma discharge region with the carrier gas. Additionally, it was the aim of this work to compare the figures of merit of different plasma forms sustained in a Beenakker cavity

with that in a surfatron for both Ar and He MIPs. Various methods of sample introduction were used in combination with MIPs generated in the TM_{010} cavity. A critical comparison of different introduction systems for the determination of As, Sb and Se by hydride generation was described previously [23]. Here, sample introduction by hydride generation with in situ trapping into the graphite furnace was used, followed by evaporation into the plasma, in combination with the TM_{010} cavity and the surfatron so as to compare their figures of merit for very sensitive determinations.

EXPERIMENTAL

Instrumentation

Spectrometer. This consisted of a 0.5-m Ebert monochromator (Jarrell-Ash); grating, constant, 1/2242 mm; width, 54 mm; wavelength range, 200–450 nm; reciprocal linear dispersion, 0.8 mm nm^{-1} ; slit widths, 30 μm ; photomultiplier, EMI 9781A; and potentiometric recorder, Beckman, Type 610000.

Microwave generator. An EMS-Microtron Mark III, Type EMS 6000, was used, with a frequency of 2.45 GHz and a maximum forward power of 200 W.

Cavity. A cylindrical TM_{010} cavity of 93.7 mm i.d. [24] and a special mounting chuck for the capillary [for the three-filament MIP (3-F-MIP)], as described by Kollotzek et al. [25], and a surfatron, as described by Selby and Hieftje [26], were used. Suprasil quartz tubes (Heraeus, Quarzschmelze, Germany) of 2.0 mm o.d. and 1.0 mm i.d. were used for the one-filament MIP (1-F-MIP) in a TM_{010} cavity and Suprasil tubes of 6.0 mm o.d. and 4.0 mm i.d. were used for the 3-F-MIP in a TM_{010} cavity and for all plasma forms obtained in the surfatron.

As the He MIP was not easy to ignite in either the TM_{010} cavity or in the surfatron, the gas lines of the set-up were rearranged so as to allow Ar to be mixed with He. The plasma was then ignited with Ar and after ignition He was added while the Ar flow was gradually reduced to zero so that a pure He plasma remained.

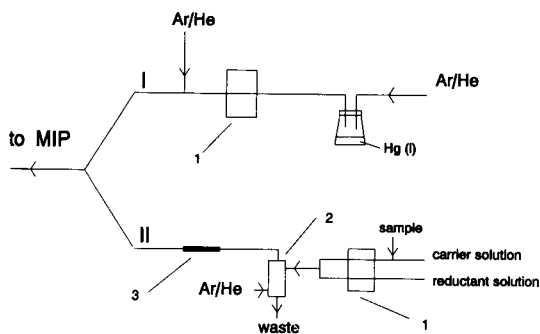


Fig. 1. Analyte introduction system for (A) Hg and (B) As, Sb and Se into MIPs. 1 = Peristaltic pump; 2 = gas-liquid separator; 3 = graphite furnace.

Analyte introduction

The sample introduction systems are shown schematically in Fig. 1. The Hg introduction was used for the investigation of the plasma stability and of the radial intensity distributions. Therefore, a flask containing elemental mercury at room temperature was flushed continuously with Ar. For the studies with As, Sb and Se hydrides, in situ trapping on to the inner wall of the graphite tube and subsequent electrothermal evaporation were used. Detailed information on the trapping conditions and introduction cycles is given in [23].

Line intensity measurements

For alignment of the monochromator on the analyte lines of Hg, Se, Sb and As, the electrodeless discharge lamps of the respective elements were used. The emission lines used for the measurements were Hg I 253.6 nm, Se I 203.9 nm, Sb I 217.6 nm and As I 228.8 nm, as they were found to give optimum signal-to-background ratios in the MIP [23]. The peak heights of their signals were selected as analytical signals.

RESULTS AND DISCUSSION

Argon plasma

TM_{010} cavity

1-F-MIP. In the TM_{010} resonator and with a gas flow-rate of 20–30 l h⁻¹ and a microwave power of 30–150 W, an Ar MIP with the shape of

a single filament located exactly along the axis of the quartz capillary (1-F-MIP) can be obtained. To obtain a stable plasma filament, it was found that the capillary should have an i.d. of no more than 2 mm [22], otherwise the filament jumps around and becomes attached to the wall.

For a capillary of 1 mm i.d., the plasma can be easily ignited and in addition its long-term stability is very good. It was not found necessary to cool the cavity, except at higher power levels (above 120 W). Here air cooling should be applied so as to prevent the discharge tube from melting. An increase in microwave power causes both the analyte line emission and the background intensity to increase. The highest signal-to-background ratio (SBR) for the Hg I 253.6-nm line was obtained at a forward power of 50 W. It must also be taken into account that at a power > 50 W the plasma discharge extends out of the cavity and an increasing leakage of microwave radiation was detected.

3-F-MIP. A three-filament MIP (3-F-MIP) has been described by Kollotzek et al. [25] and was found to be a stable and effective radiation source for the analysis of gaseous samples. It was found to be superior to the 1-F-MIP with respect to the detection limits and to the linear dynamic range. Here, the same set-up was used to compare its analytical performance with that of a surfatron. In contrast to the 1-F-MIP, the 3-F-MIP required exact tuning of the cavity and precise positioning of the capillary in the cavity so as to be able to ignite the plasma and to obtain stably positioned plasma filaments. However, once the system had been tuned for a particular forward power, it was easy to ignite the MIP and to sustain a stable discharge.

In the studies performed with the 3-F-MIP, a quartz capillary of 6.0 mm o.d. and 4.0 mm i.d. was used. The microwave forward power and the gas flow-rate required in order to obtain the different types of plasmas were determined (Table 1). The plasma gas flow-rate and the forward power affect both the intensity of the analytical lines and the stability of the plasma. Within the power range 50–150 W and the gas flow-rate range 15–50 l h⁻¹ an optimization could be made. The radial intensity profiles of the Hg 253.6-nm

TABLE 1

Working parameters for different types of Ar MIPs

| Parameter | TM ₀₁₀ (3-F) | Surfatron | | |
|------------------------------------|----------------------------|-----------|-----|-----|
| | | 1-F | 2-F | 3-F |
| Forward power (W) | 90 | 50 | 105 | 150 |
| Minimum reflected power (W) | 0 | 2.5 | 4 | 4 |
| Gas flow-rate (l h ⁻¹) | 25 | 25 | 35 | 35 |

line and for the background signal at different forward powers were investigated (Fig. 2). At a forward power of 90 W (with a reflected power of 0 W) and an Ar flow-rate of 25 l h⁻¹, maximum SBR ratios for the Hg I 253.6-nm line were obtained. The region for the maximum SBR ratio was found to lie between two adjacent filaments and 1.5 mm outside of the centre of the tube. Indeed, the maximum emission intensity was found when selecting the centre of one of the filaments as the observation zone, but also the background intensity was found to be maximum in this region. As the optimum position of the observation zone can differ slightly from one element to another [25], multi-element determinations can be performed only under compromise conditions. However, for Se, Sb and As the optimum locations in the emission intensity profiles were found to coincide.

After optimizing the working conditions for As, Sb and Se, their detection limits (based on a 3 σ concept) were as given in Table 2. The relative standard deviations of the intensities at a concentration level of 3 ng ranged from 1.8 to 2.5% ($n = 5$). The data in Table 2 show that the detection limits for As, Sb and Se with the 3-F-

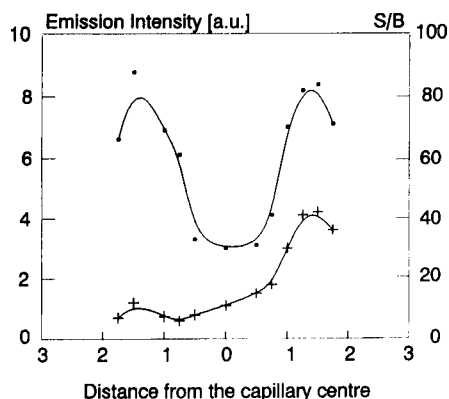


Fig. 2. Radial intensity distribution of the Hg I 253.6-nm line. 3-F-MIP in a Beenakker cavity; Ar flow-rate, 30 l h⁻¹; forward power, 90 W; reflected power, < 1 W. ■ = Emission intensity; + = SBR.

MIP were a factor of 4.25, 3.4 and 4.8, respectively, lower than in those with the 1-F-MIP.

Surfatron

The surfatron [18–20] is composed of two cylinders of appropriate shape and symmetry and enables the field to extend through a gap. With the wide range of operating conditions in a capillary of 6 mm o.d. and 4 mm i.d. (e.g., gas flow-rate, forward power and capillary position), different forms of Ar MIPs can be obtained. Mainly three stable plasma forms were found, namely one-, two- and three-filament MIPs (Table 1). The stability areas for these discharge configurations are given in Fig. 3. It is important to note that in a surfatron the plasma stabilized only at ca. 2–5 min after the ignition of the plasma. After that time, the reflected power could be easily tuned to a minimum (3–10 W). In all instances the re-

TABLE 2

Comparison of the absolute detection limit (ng) for As, Sb and Se with Ar and He MIPs using hydride generation and in situ trapping in the graphite furnace^a

| Element | TM ₀₁₀ | | | Surfatron | | |
|---------|--|--|---|--|---|---|
| | 1-F, 50 W, 20 l h ⁻¹ , Ar | 3-F, 90 W, 30 l h ⁻¹ , Ar | 1-F, 130 W, 20 l h ⁻¹ , He | 1-F, 50 W, 25 l h ⁻¹ , Ar | 3-F, 150 W, 35 l h ⁻¹ , Ar | 1-F, 170 W, 20 l h ⁻¹ , He |
| As | 1.7 | 0.40 | 0.26 | 1.5 | 0.18 | 0.08 |
| Sb | 1.3 | 0.35 | 0.17 | 0.75 | 0.17 | 0.12 |
| Se | 1.2 | 0.25 | 0.23 | 1.2 | 0.15 | 0.14 |

^a Sample volume used for preconcentration: 1 ml.

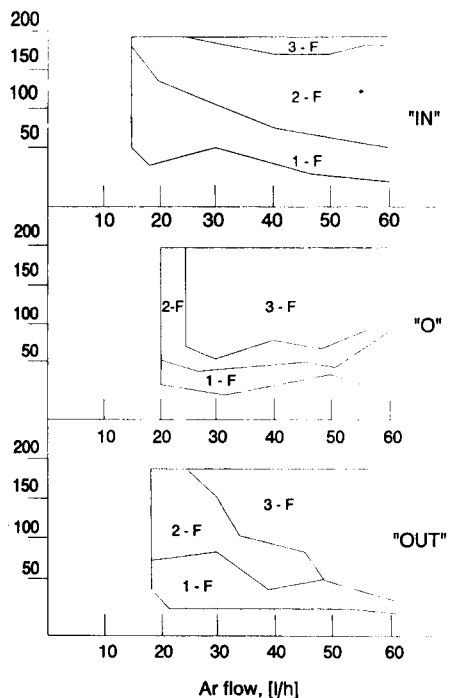


Fig. 3. Stability diagram for different forms of Ar MIPs in the surfatron. Suprasil quartz tube, 6 mm o.d., 4 mm i.d. Positions: "IN" = capillary inside the surfatron; "O" = end of the capillary at front plate of the surfatron; "OUT" = capillary extends from the surfatron.

flected power depended on the position of the inner and outer cylinder of the surfatron. It was adjusted so as to obtain a minimum reflected power after the plasma had stabilized. Generally,

more filaments appear in the discharge tube on increasing the gas flow-rate or the power. It was also found that the stability area of the different forms of the plasma depends on the position of the capillary in the surfatron.

When the capillary was withdrawn to behind the front plate (position "IN"), mostly 1-F and 2-F plasmas were obtained within a wide range of operating conditions. Indeed, the 1-F plasma could be operated at a very low power, namely at 25 W at a gas flow-rate of 40–50 l h⁻¹ or even at 15 W at a gas flow-rate of 60 l h⁻¹. At gas flow-rates below 60 l h⁻¹ a higher power was required so as to prevent the plasma from instabilities and extinction. With the capillary position "IN", the 3-F plasma appears only at a high power (175–200 W). However, under these conditions the MIP is unstable. The filaments in the capillary easily changed their positions and the plasma rotated on the tube wall. Additionally, when the power used was above 170 W, the external surface of the cylinder became very hot after 10–15 min of operation.

When the end of the capillary was situated exactly at the front plate (position "O") or about 5–10 mm out of it (position "OUT"), a stable 3-F plasma could be operated within a power range of about 40–200 W, depending on the gas flow-rate (30–60 l h⁻¹). In contrast with the position "IN", the 1-F plasma was stable only within a small range of forward power, whereas the gas flow-rate could be varied widely. In all instances

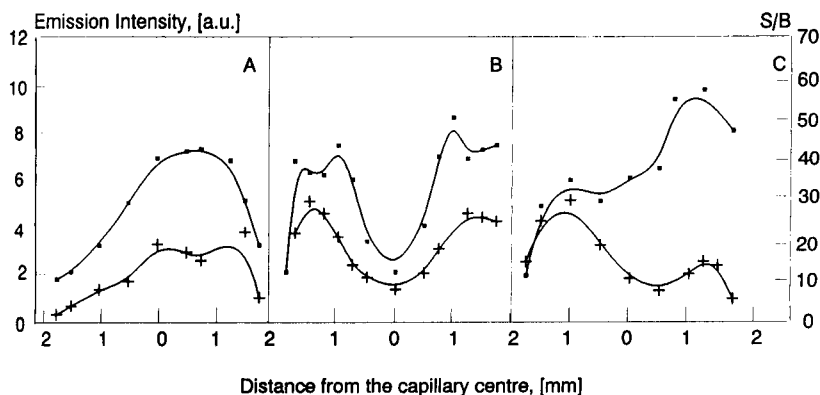


Fig. 4. Radial intensity distribution of Hg I 253.6-nm line for Ar MIP in a surfatron. (A) 1-F, (B) 2-F and (C) 3-F discharges. Forward power and gas flow-rate as in Table 1. ■ = Emission intensity (I_e); + = SBR.

the reflected power depended very sensitively on the tuning of the surfatron, and could be matched to a minimum of 5–10 W (depending on the forward power applied). It also could be observed that the reflected power strongly influences the emission intensity of the Hg line. With a forward power of 50 W, the maximum signal was obtained when the reflected power was adjusted to below 4 W, whereas the signal decreased to 50% at a reflected power of 10 W. Additionally, when the reflected power increased above 10 W, the stability of the discharge decreased and the MIP was easily extinguished. Also the reproducibility of the signals decreased at a higher reflected power level.

The advantage of the surfatron over the Beenakker cavity is that different plasma configurations can be obtained with the same cavity without a need for special modification. The radial distributions of the Hg 253.6-nm line intensities with axial observation were investigated for the different plasma forms (Fig. 4). The emission intensity profiles for the particular plasma forms (1-F, 2-F and 3-F) obtained with the surfatron in general are very similar to those of the Beenakker cavity (see Fig. 2, and data from [25]). It can be seen from the intensity profiles for the Hg line (Fig. 4) that the signal decreased uniformly with increasing distance from the plasma filament. As the same trend was also found for the background intensity, the SBR were maximum somewhere out of the centre of the filament. It can be expected that for other elements the optimum position of observation will be similar. Therefore, the optimum conditions found for Hg were also used for the determination of As, Sb and Se.

With a surfatron, the dependence of the line and background intensities on the Ar flow-rate is as shown in Fig. 5. As the gas flow-rate increased, the signal subsequently increased. In general, this trend is similar for the different plasma forms; however, the optimum Ar flow-rate is larger for the 2-F and 3-F plasmas (35 l h^{-1}) than for the 1-F plasma (25 l h^{-1}).

For the Hg I 253.7-nm line (Fig. 6), the dependence of the emission intensity on the forward power in different plasma configurations can be compared. The 3-F plasma gave the best line-to-

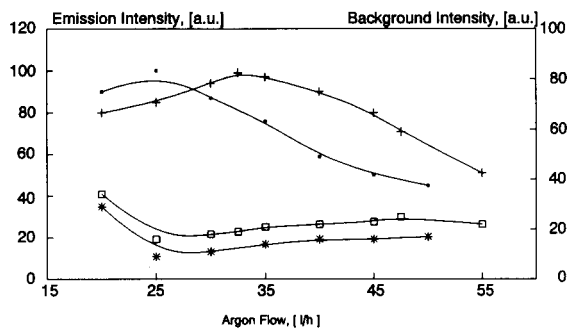


Fig. 5. Influence of gas flow-rate on the emission intensity of the Hg I 253.6-nm line for Ar 1-F-, 2-F- and 3-F-MIPs with a surfatron. I_e = emission intensity (\blacksquare = 1-F; $+$ = 2- and 3-F); I_B = background intensity ($*$ = 1-F; \square = 2- and 3-F).

background intensity ratio of the Hg I 253.7-nm line in the power range 120–150 W. The reflected power was below 3 W and only with the forward power above 150 W did the reflected power slightly increase and the intensity of the Hg I 253.7-nm line decrease.

Helium plasma

TM_{010} and surfatron

When using He as the plasma gas for both the TM_{010} cavity and the surfatron, a diffuse or a monofilament discharge was obtained depending on the i.d. of the capillary. In both instances, however, a higher forward power (120–190 W) was required so as to obtain a stable discharge and the reflected power could not be reduced to

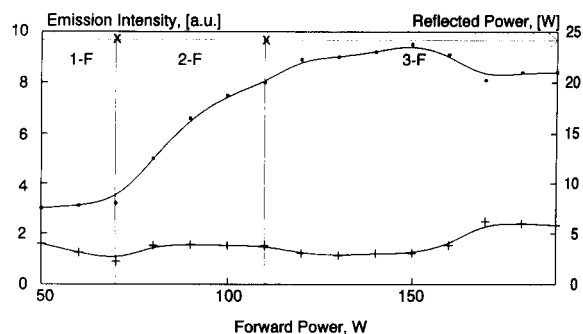


Fig. 6. Dependence of (\blacksquare) the emission intensity (I_e) of the Hg I 253.6-nm line and ($+$) the reflected power on the forward power measured for the surfatron. Gas flow-rate, 35 l h^{-1} .

less than 10–15 W. As was pointed out by Abdilahi and Snook [27], a higher thermal conductivity has the consequence that the He discharge consumes more energy and therefore it requires a higher power than Ar to sustain a plasma.

With a quartz-capillary of 1–2 mm i.d., the He plasmas in both instances had a monofilament form, being similar to the Ar 1-F-MIP. At a gas flow-rate of 10–25 l h⁻¹ a stable He 1-F-MIP was obtained. When the capillary i.d. was larger than 2 mm, (e.g., 2–4 mm), a diffuse He plasma was formed in both instances. However, with a capillary i.d. below 3 mm, the stability of the plasma was better than that of the plasma generated in a larger tube.

Detection limits for As, Sb, Se

First, the intensities of the As, Sb and Se emission signals were compared for Ar and He MIPs sustained in a surfatron. Under the optimum plasma conditions, the signals of the He plasma in all instances were found to be about a factor of 1.5–2 higher than those of an Ar plasma. However, it should be noted that the optimum forward power for the He plasma was higher than that for the Ar plasma. The background intensities of the Ar MIPs were lower than those of the He MIPs. The absolute detection limits for As, Sb and Se with hydride generation using hot trapping in a graphite furnace (for details of the working conditions, see [23]) and an MIP obtained in the surfatron were found to be about half those obtained with the Beenakker resonator (Table 2). The improvement in the detection limits was most pronounced for Sb. No difference in the linear dynamic range (three orders of magnitude) for As, Sb and Se could be found between the Ar and He MIPs in the surfatron. However, in this study on hydride generation coupled to MIP – AES, with both Ar and He as the plasma gas the Beenakker cavity shows poorer linearity (maximum two orders of magnitude) than the surfatron.

Conclusions

This comparison of the Beenakker cavity and the surfatron has shown that the detection limits

of the latter for As, Sb and Se are a factor of 1.6–2.2 lower. For the surfatron also a wide range of operating conditions exists with which stable plasmas with different configurations can be produced. Of the configurations obtained, the Ar 3-F-MIP was found to be superior to the others.

The long-term stability of the plasmas in the both cavities under optimum conditions was found to be very good. However, with the surfatron the plasma needs some time to stabilize after ignition, whereas with the Beenakker cavity no time for stabilization was required.

With both cavities the He MIP requires a higher power level in order to obtain a stable discharge. The results for the determination of As, Sb and Se with a He MIP showed that an improvement with respect to the signal-to-background ratio and power of detection in some instances can be obtained.

E. Bulska thanks the Max-Planck Gesellschaft (Munich) for the grant of a Research Fellowship.

REFERENCES

- 1 J.A.C. Broekaert, *Anal. Chim. Acta*, 196 (1987) 1.
- 2 S.R. Goode and K.W. Boughman, *Appl. Spectrosc.*, 38 (1984) 755.
- 3 J.P. Matousek, B.J. Orr and M. Selby, *Prog. Anal. At. Spectrosc.*, 7 (1984) 275.
- 4 K.A. Forbes, E.E. Reszke, P.C. Uden and R.M. Barnes, *J. Anal. At. Spectrom.*, 6 (1991) 57.
- 5 F.C. Fehsenfeld, E.M. Evenson and H.P. Broida, *Rev. Sci. Instrum.*, 36 (1965) 294.
- 6 H.P. Broida and M.W. Chapman, *Anal. Chem.*, 30 (1958) 2049.
- 7 C.A. Bache and D.J. Lisk, *Anal. Chem.*, 40 (1968) 2224.
- 8 A.J. McCormack, S.C. Tong and W.D. Cooke, *Anal. Chem.*, 37 (1965) 1470.
- 9 C.I.M. Beenakker, *Spectrochim. Acta, Part B*, 31 (1976) 483.
- 10 C.I.M. Beenakker, *Spectrochim. Acta, Part B*, 32 (1977) 173.
- 11 B.D. Quimby, P.C. Uden and R.M. Barnes, *Anal. Chem.*, 50 (1978) 2112.
- 12 B.D. Quimby, M.F. Delaney, P.C. Uden and R.M. Barnes, *Anal. Chem.*, 51 (1979) 875.
- 13 E. Bulska, D.C. Baxter and W. Frech, *Anal. Chim. Acta*, 249 (1991) 545.
- 14 C.I.M. Beenakker, B. Bosman and P.W.J.M. Boumans, *Spectrochim. Acta, Part B*, 33 (1978) 373.

- 15 H. Matusiewicz, *Spectrochim. Acta Rev.*, 13 (1990) 47.
- 16 K. Tanabe, K. Matsumoto, H. Haraguchi and K. Fuwa, *Anal. Chem.*, 52 (1986) 2361.
- 17 K. Eberhardt, G. Buchert, G. Herrmann and N. Trautmann, *Spectrochim. Acta, Part B*, 47 (1992) 89.
- 18 J. Hubert, M. Moisan and A. Richard, *Spectrochim. Acta, Part B*, 33 (1979) 1.
- 19 M.H. Abdallah, S. Coulombe, J.M. Mermet and J. Hubert, *Spectrochim. Acta, Part B*, 37 (1982) 583.
- 20 P.S. Moussounda, P. Ranson and J.M. Mermet, *Spectrochim. Acta, Part B*, 40 (1985) 641.
- 21 L.J. Galante, M. Selby and G.M. Hieftje, *Appl. Spectrosc.*, 42 (1988) 559.
- 22 U. Richts, J.A.C. Broekaert, P. Tschöpel and G. Tölg, *Talanta*, 38 (1991) 863.
- 23 E. Bulska, J.A.C. Broekaert, P. Tschöpel and G. Tölg, *Anal. Chim. Acta*, 271 (1993) 171.
- 24 J.P.J. Van Dalen, P.A. De Lezenne Coulander and L. de Galan, *Spectrochim. Acta, Part B*, 33 (1978) 545.
- 25 D. Kollotzek, P. Tschöpel and G. Tölg, *Spectrochim. Acta, Part B*, 39 (1984) 625.
- 26 M. Selby and G.M. Hieftje, *Spectrochim. Acta, Part B*, 42 (1987) 285.
- 27 M.M. Abdillahi and R.D. Snook, *Analyst*, 111 (1986) 265.

Automatic determination of reducing sugars by atomic absorption spectrometry

M.C. Yebra¹, M. Gallego and M. Valcárcel

Department of Analytical Chemistry, Faculty of Sciences, University of Córdoba, 14004 Córdoba (Spain)

(Received 9th July 1992; revised manuscript received 20th November 1992)

Abstract

A continuous precipitation system for the indirect determination of reducing sugars in various types of wine based on the classical reaction with Fehling's solutions is reported. Copper(I) oxide is precipitated by injecting the Fehling's solutions into the wine carrier, which is directly aspirated. This allows reducing sugars to be determined in the range 10–110 $\mu\text{g ml}^{-1}$ with a relative standard deviation of 2.7% at 50 $\mu\text{g glucose ml}^{-1}$ ($n = 11$). The proposed method requires no sample pretreatment. The results obtained in the analysis of six white and red wines were critically compared with those provided by the standard manual method.

Keywords: Atomic absorption spectrometry; Flow injection; Sugars; Wines

Grape juice and wine naturally contain various hexoses and pentoses that make up the so-called "reducing sugars". Fermented wines preserve small amounts of the hexoses, glucose and fructose and some unfermentable pentoses. Incompletely fermented wines, however, contain higher concentrations of both hexoses, but substantially more of the slower fermenting fructose. The average ratio of glucose to fructose in the residual sugar of wine is typically 0.58:1, but varies over wide ranges [1,2]. The oxidation of reducing sugars in the presence of an alkali is used for their detection and determination by using Fehling's, Nylander's or Benedict's solutions. Fehling's reaction is the foundation of the official method for

the determination of reducing sugars in wines, which involves quantifying copper by direct weighing of copper(I) oxide, determination of dissolved copper, by titration with different reagent, etc. [3].

Some analyses for reducing sugars in wines involve spectrophotometric detection [4,5] and enzymatic assays [6]: enzymes allow glucose and fructose in wine to be determined separately [7,8]; however, the use of dissolved enzymes increases analytical costs. Liquid chromatography (LC) in conjunction with an enzyme reactor and an electrochemical detector has also been used for the determination of glucose and ethanol in wine [9].

The need for oenological laboratories to determine reducing sugars during wine making and in the final product has propitiated marketing of autoanalysers for this purpose [10], most of which are expensive. In this context, flow-injection analysis (FIA) can be implemented with fairly inexpensive instrumentation [11,12]. Three automatic flow-injection methods allow the determination of reducing sugars in wine (0.1–7.0 g l^{-1} ex-

Correspondence to: M. Valcárcel, Department of Analytical Chemistry, Faculty of Sciences, University of Córdoba, 14004 Córdoba (Spain).

¹ Permanent address: Department of Analytical Chemistry, Nutrition and Bromatology, Faculty of Chemistry, University of Santiago de Compostela, Santiago de Compostela (Spain).

pressed as glucose) by a classical reaction and spectrophotometric detection [13]. Glucose in wine has also been determined by using an enzyme reactor [14] and a fibre-optic glucose biosensor [15].

A continuous precipitation system coupled to an atomic absorption spectrometer has been used to implement various methodologies, including indirect determinations of both organic and inorganic anions and preconcentration of traces of metals [16–18].

This paper reports on the use of a continuous precipitation system for the indirect determination of reducing sugars in wines by atomic absorption spectrometry. The method is based on the classical reaction of reducing sugars with Fehling's solutions. The officially recommended procedure was adapted to a reversed flow-injection mode and the analyte concentration was directly related to the absorbance decrease in Fehling's solutions, containing copper(II) ions, by the precipitation of copper(I) oxide (Cu_2O). The proposed automatic method allows the direct determination of reduced copper with no need for subsequent weighing of copper(I) oxide or titration of dissolved copper. The method is simple, sensitive, rapid and inexpensive.

EXPERIMENTAL

Apparatus

A Perkin-Elmer 380 atomic absorption spectrometer furnished with a copper hollow-cathode lamp was used. The instrument was set at 324.7 nm and the air-acetylene flame was adjusted according to standard recommendations. The spectrometer output was connected to a Radiometer REC-80 Servograph recorder. The flow system consisted of a Gilson Minipuls-2 peristaltic pump, fitted with PVC tubing, two Rheodyne (Models 5041 and 5301) four-way or switching valves and PTFE tubing (0.5 mm i.d.) for the coils. A Scientific System 05-105 column fitted with a removable screen-type stainless-steel filter (pore size 0.5 μm , chamber inner volume 580 μl , filtration area 3 cm^2), originally designed as a cleaning device for LC, was employed for filtra-

tion purposes. A thermostated silicone-oil bath was also used.

Reagents

A 1000 mg l^{-1} glucose (Sigma) standard solution was prepared in distilled water. Fehling's A solution was prepared by dissolving 0.40 g of $\text{CuSO}_4 \cdot 5\text{H}_2\text{O}$ (Merck) in 0.5 l of distilled water (200 $\mu\text{g Cu}^{2+} \text{ ml}^{-1}$). Fehling's B solution was prepared by dissolving 50 g of potassium sodium tartrate and 50 g of potassium hydroxide pellets (Merck) in 0.5 l of water [10% (w/v) in both reagents]. For treatment of the wines, a roughly saturated solution of $\text{Pb}(\text{OAc})_2 \cdot 3\text{H}_2\text{O}$ (Merck) was prepared by dissolving 50 g of the salt in 100 ml of hot water. Sodium oxalate (Merck) was also used.

Procedures

Manual method. The sample pretreatment used to clear the wines and the standard method for determination of reducing sugars were done according to the AOAC's recommendations [3]. A volume of 100 ml of wine was placed in a glass vessel and evaporated to one third of its volume (for ethanol evaporation). Once cool, 5 ml of $\text{Pb}(\text{OAc})_2 \cdot 3\text{H}_2\text{O}$ saturated solution were added (for decolorization of the wine) and the mixture was shaken and allowed to stand for 10 min. The precipitated formed was filtered through folded paper and excess of lead was removed with 2 g of sodium oxalate (0.4 g per ml of lead acetate), followed by a second filtration and dilution to 100 ml in a volumetric flask. For the determination of reducing sugars, 30 ml of Fehling's A solution (34.65 g of $\text{CuSO}_4 \cdot 5\text{H}_2\text{O}$ in 500 ml of distilled water) and 30 ml of Fehling's B solution (173 g of potassium sodium tartrate and 125 g of potassium hydroxide in 500 ml of distilled water) were placed in a 500-ml beaker and 60 ml of distilled water and 25 ml of pretreated sample were added. The beaker was then covered with a watch-glass and heated to boiling and then for a further 3 min. The hot solution was immediately filtered through an asbestos mat in a porcelain gooch crucible with suction. The Cu_2O precipitate was thoroughly washed with water at 60°C, then with 10 ml of ethanol and finally with 10 ml of diethyl

ether, after which it was dried in an oven at 100°C for 30 min, cooled and weighed.

FI method. The continuous-flow manifold used is shown in Fig. 1. Fehling's A and B solutions were mixed in the flow system prior to injection. The standards and dilute wine samples, containing between 10 and 110 $\mu\text{g ml}^{-1}$ of reducing sugars (expressed as glucose) at pH 4.6–8.2 (adjusted with dilute potassium hydroxide solution), were continuously pumped into the system while the carrier solution (Fehling's A and B) was injected into the sample stream. First, Fehling's reagent was injected into a distilled water blank and a positive peak due to copper(II) was obtained. Then, Fehling's solutions were injected into the sample stream and a smaller, positive peak was obtained due to the decrease in concentration of copper(II) owing to Cu_2O precipitate formed in the redox reaction involved [reduction of copper(II)]. The difference between the two peaks yielded the amount of precipitated copper, which was proportional to the reducing sugar concentration in the sample. The mixing coil for Fehling's reagent, the loop of the injection valve and the precipitation coil were all heated at 95°C. Exactly 50 s after injection, the sample–reagent plug was halted in the precipitation coil for 10 min. As the concentration of Fehling's A solution (copper) required fell outside the linear range of the atomic absorption spectrometer, a water stream was inserted to effect dilution of the cation prior to the nebulizer. The filter was washed in an ultrasonic bath with 2 M hydrochloric acid for 1 min after a day's use (*viz.*, 100–200 samples).

RESULTS AND DISCUSSION

The criteria used to optimize the automatic determination of reducing sugars were manifold simplicity, minimum sample pretreatment and maximum response function (difference between the sample and blank signals). All these rely heavily on two key features: the need to decolorize the wines and the effect of ethanol. In fact, the AOAC method [3] involves the evaporation of the ethanol and decolorization of the wine.

Optimization of chemical variables

The precipitating reagents (Fehling's A and B solutions) must be mixed immediately prior to injection, as illustrated in Fig. 1. Chemical parameters were varied while keeping the FI variables constant. Initial experiments were done by stopping the flow 50 s after injection of the reactants into the sample stream for 15 min in order to allow complete precipitation. First, the optimum composition of Fehling's B solution was studied; for a constant concentration of potassium sodium tartrate of 10% (w/v), the potassium hydroxide concentration could be varied between 4 and 20% (w/v). Likewise, for a potassium hydroxide concentration of 10% (w/v), a potassium sodium tartrate concentration of 4–10% (w/v) could be used. Fehling's B solution was prepared with 10% (w/v) of both reagents. Experiments done with a commercially available Fehling's B solution (Panreac, Spain) provided poor results because their sodium hydroxide to potassium sodium tartrate weight ratio was 1:4, *i.e.*, lower than that determined in the prelimi-

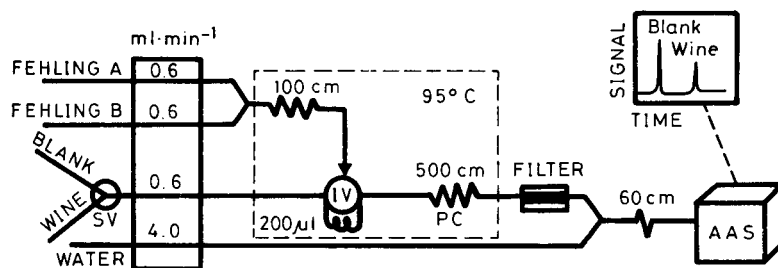


Fig. 1. Scheme of the continuous precipitation system used for the indirect determination of reducing sugars in wine samples. IV, injection valve; SV, switching valve; PC, precipitation coil; AAS, atomic absorption spectrometer.

nary study, so a laboratory prepared Fehling's B solution was adopted. The concentration of copper in Fehling's A solution was varied between 50 and 200 $\mu\text{g ml}^{-1}$. The analytical signal increased with increase in the concentration of copper; however, concentrations above 200 $\mu\text{g ml}^{-1}$ required a high flow-rate of the diluting water stream in order to prevent the blank signal from falling outside the linear range (up to 0.400 absorbance for copper) of the instrument, which resulted in smaller differences between the blank and sample signals through dilution. A concentration of Fehling's A solution of 200 $\mu\text{g ml}^{-1}$ was chosen for further experiments. The effect of sample pH was studied in the range 2.0–10.0. The absorbance versus pH graph for 50 $\mu\text{g ml}^{-1}$ glucose was plateau-shaped over the pH range 4.6–8.2. A glucose pH of 5.4 obtained directly with no adjustment was therefore chosen.

The influence of the ethanol concentration on the solubility of copper(I) oxide was also studied because the proposed automatic method was to be applied to wine samples with different ethanol contents. The ethanol was added to the glucose solution. As can be seen in Fig. 2, the absorbance remained virtually constant up to 1.0% (v/v), then decreased dramatically with increasing ethanol content up to 4%, above which it remained constant.

As in the manual Fehling's method, temperature had a decisive influence on the precipitation of copper(I) oxide. Its effect was studied in the

range 25–100°C. Increasing temperature resulting in sharply increasing absorbance differences. As can be observed in Fig. 1, the mixing coil for Fehling's solutions, the loop of the injection valve and the precipitation coil were all heated at 95°C in a silicone-oil bath, as higher temperatures resulted in the formation of bubbles that disturbed the analytical signal.

Optimization of the flow precipitation system

The flow variables studied were the sample volume, length of the precipitation coil and time of halting of the plug (residence time of sample and reagents).

The effect of the injection volume on the peak height and shape at a constant ratio of sample flow-rate (0.6 ml min^{-1}) to water dilution flow-rate (4.0 ml min^{-1}) of 0.15 and constant glucose concentration (50 $\mu\text{g ml}^{-1}$) was studied by stopping the flow 15 min after injection in order to complete the precipitation reaction. The absorbance increased as the amount of Fehling's solutions injected into the distilled water (blank) or the sample increased between 50 and 200 μl . However, injection volumes higher than 200 μl could not be used because the blank signals fell outside the linear range of the detector. The injection volume could be increased, which would be equivalent to increasing the concentration of Fehling's A solution, by decreasing the sample flow-rate to 0.1–0.3 ml min^{-1} while keeping constant that of the diluting stream at 4 ml min^{-1} , so the atomic signal would decrease before measurement. However, at low sample flow-rates the pressure is inadequate to sweep the precipitate formed to the filter so, after a few injections, the precipitation coil is contaminated with precipitate that adheres to its inner walls and requires removal between samples. Alternatively, copper can be determined under non-optimum conditions in order to be able to use higher concentrations of the metal in the flow system so as to favour precipitation of copper(I) oxide. However, this results in diminished differences between blank and signal samples. We therefore made a compromise and chose an injection volume of 200 μl , a sample flow-rate of 0.6 ml min^{-1} and a water dilution stream flow-rate of 4.0 ml min^{-1} (to

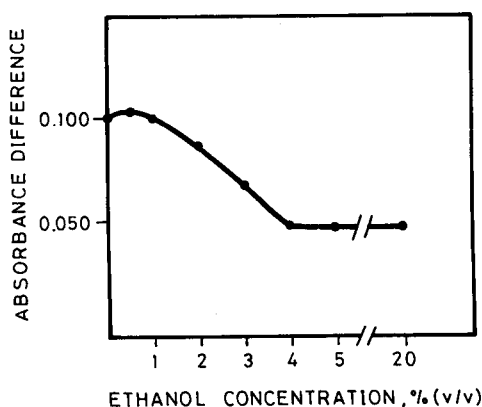


Fig. 2. Influence of ethanol concentration in the sample on the solubility of copper(I) oxide. Sample 50 $\mu\text{g glucose ml}^{-1}$.

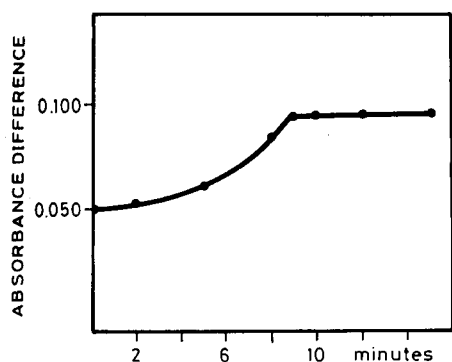


Fig. 3. Influence of residence time of the sample in the precipitation coil. Sample, $50 \mu\text{g glucose ml}^{-1}$.

dilute the copper solution prior to the nebulizer). Under these conditions, blank absorbances ranged between 0.300 and 0.350.

The influence of the length of the precipitation coil was investigated between 100 and 1000 cm (0.5 mm i.d.). Short reactor coils (less than 400 cm) resulted in short residence times of the plug for the reaction to be complete. A coil length of 500 cm was therefore chosen. The residence time was therefore crucial in order to ensure completion of the precipitation reaction. As can be seen in Fig. 3, not stopping the plug of sample and reagents in the precipitation coil resulted in short residence times (100 s) and hence in inefficient mixing and an incomplete reaction, so some cation remained unprecipitated and yielded a response at the atomic absorption detector. For a minimum residence time of 9 min precipitation was virtually complete within the plug and there was hardly any free cation, so the minimum response was obtained on passage of the filtered plug through the detector. Halting the plug for 10 min exactly 50 s after injection was sufficient for the precipitation reaction to be complete (Fig. 3); this time was therefore chosen as optimum. The blank signal obtained was the same whether or not the pump was stopped, so the blank plug need not be halted.

Calibration of the system

The calibration graph obtained under the optimum conditions stated in Fig. 1 and as described under Procedure was linear over the range 10–110

$\mu\text{g glucose ml}^{-1}$. The representative equation was absorbance difference = $0.007 + 1.77 \times 10^{-3} C$, with C in $\mu\text{g ml}^{-1}$ ($n = 7$). The detection limit ($7.0 \mu\text{g ml}^{-1}$) was calculated as three times the standard deviation of the peak height for 30 injections of the water blank. The precision of the automatic method obtained for eleven samples containing $50 \mu\text{g glucose ml}^{-1}$ was 2.7%, expressed as relative standard deviation. The sample throughput, taking into account that the pump was stopped for 10 min after injection of Fehling's solutions, was rather low (ca. five samples h^{-1}), but much higher than that of the manual method.

Analysis of wines

The proposed method was applied to the determination of reducing sugars in various types of Spanish white, red and rosé wines. The results obtained were compared with those given by the AOAC method [3] based on Fehling's reaction and direct weighing of copper(I) oxide (see Experimental) using the Hammond table to calculate the glucose content [3]. Unlike in the manual method, the samples required no pretreatment or decolorization with $\text{Pb}(\text{OAc})_2$, as the automatic method involves the indirect determination of reducing sugars by the difference between signals provided between injected copper and excess of copper remaining in the filtrate, so manipulation of the precipitate was not required, nor need it be obtained in an absolutely pure form. For continuous analysis of wines containing ca. 2 g l^{-1} of reducing sugars, different aliquots of the sample solution (0.25–1.0 ml) were diluted to 25 ml and their pH was adjusted to 4.6–8.2 with dilute potassium hydroxide solution.

In order to check that decolorization was unnecessary, wines clarified with $\text{Pb}(\text{OAc})_2$ and containing no alcohol were also analysed by using the proposed method. The results obtained with and without pretreatment were consistent. Therefore, after dilution, samples were propelled directly into the flow system with no other treatment.

The ethanol contents in the analysed wines ranged between 11.0 and 15.0%; on dilution (0.25–1.0 ml to 25 ml), they were reduced to 0.1–0.6%, i.e. within the tolerated range (Fig. 2).

Although the wines contained some copper, which was ultimately the species determined in the indirect analysis of these samples, it did not interfere as its content in the diluted samples ($\leq 10 \text{ ng ml}^{-1}$) was below the detection limit checked experimentally.

The results obtained for six wines are listed in Table 1. The FIA results were always higher than their manual counterparts, probably because the substantial manipulations involved in the manual method gave rise to analyte losses or because the manual results were the averages of only two determinations (the manual method is too slow for expedient processing of more than two samples at once).

Finally, in order to test the reliability of the proposed method, the recovery of glucose added to wines samples was determined by making two standard additions (625 or 1250 μg) to each wine sample, prior to dilution to 25 ml. Table 2 gives the results obtained; the recovery was close to 100% in all instances.

Conclusions

The proposed method offers several advantages over its manual counterpart. It is more sensitive. Although this is not too significant as regards the type of sample (wines contain abundant reducing sugars and are readily available), it is interesting as it allows samples to be diluted to the extent required to avoid any interference

TABLE 1

Comparison of the results obtained by the automatic and batch methods in the determination of reducing sugars in wines

| Wines | Source | Ethanol (%, v/v) | Concentration (g l^{-1}) | |
|-----------|-----------|---------------------|-------------------------------------|----------------------------------|
| | | | Batch method | Automatic method ^a |
| White (1) | Montilla | 14.5 | 1.79; 1.65 | 1.90 ± 0.10 |
| White (2) | Moriles | 15.0 | 1.64; 1.36 | 1.75 ± 0.10 |
| Rosé (3) | Penedés | 11.0 | 2.38; 2.24 | 2.63 ± 0.16 |
| Red (4) | La Rioja | 12.0 | 2.01; 1.84 | 2.03 ± 0.07 |
| Red (5) | La Mancha | 11.5 | 2.12; 1.84 | 2.05 ± 0.09 |
| Red (6) | Córdoba | 13.0 | 2.35; 2.21 | 2.42 ± 0.21 |

^a Average of five individual determinations \pm standard deviation.

TABLE 2

Recoveries of reducing sugars added to wine samples obtained by using the proposed method

| Wines ^a | Aliquot (ml) | Found (μg) | Added (μg) | Recovery | |
|--------------------|-----------------|----------------------------|----------------------------|---------------|-------|
| | | | | μg | % |
| White (1) | 0.25 | 475 | 625 | 1088 | 98.9 |
| | 0.25 | 475 | 1250 | 1789 | 103.7 |
| White (2) | 0.25 | 437 | 625 | 1037 | 97.6 |
| | 0.25 | 437 | 1250 | 1706 | 101.1 |
| Rosé (3) | 0.25 | 657 | 625 | 1223 | 95.4 |
| | 0.25 | 657 | 1250 | 1946 | 102.0 |
| Red (4) | 0.25 | 507 | 625 | 1165 | 102.9 |
| | 0.25 | 507 | 1250 | 1859 | 105.8 |
| Red (5) | 0.25 | 512 | 625 | 1129 | 99.3 |
| | 0.25 | 512 | 1250 | 1863 | 105.7 |
| Red (6) | 0.25 | 605 | 625 | 1188 | 96.6 |
| | 0.25 | 605 | 1250 | 2011 | 108.4 |

^a See Table 1.

from ethanol, which need not be evaporated. Sample processing is much simpler, which results in increased precision and a higher sampling frequency (the manual method requires ca. 1.5 h per analysis). However, the sampling frequency of the proposed method is modest (12 min per analysis) because the flow must be halted for 10 min. This can be partly overcome at the expense of sensitivity (a ca. 50% loss) if the pump is not stopped and analyses are performed sequentially (see Fig. 3). In this way, the sampling frequency can be increased (ca. 3 min per analysis).

The CICYT is acknowledged for financial support (Grant No. PB90-0925). The Xunta of Galicia is also acknowledged for funding M.C. Yebra (D.O.G. 13-1-92).

REFERENCES

- 1 J. Ribéreau-Gayon, E. Peynaud, P. Sudraud and P. Ribéreau-Gayon, *Sciences et Techniques du Vin. Tome 1: Analyse et Contrôle des Vins*, Dunod, Paris, 1976, Chap. 8.
- 2 H.D. Belitz and W. Grosch, *Food Chemistry*, Springer, Berlin, 1987, pp. 217 and 664.
- 3 *Official Methods of Analysis of the Association of Official Analytical Chemists*, AOAC, Washington, DC, 12th edn., 1975, pp. 195, 1015.
- 4 A. Parenthoen, *Ann. Falsif. Expert. Chim.*, 65 (1972) 279.

- 5 F. Green, C.A. Clausen and T.L. Highley, *Anal. Biochem.*, 182 (1989) 197.
- 6 A. Lay, *Weinberg Keller*, 24 (1977) 369.
- 7 I. Miwa, M. Saito, J. Okuda, M. Ishihara and S. Tejima, *Eisei Kagaku*, 30 (1984) 238.
- 8 G. Henninger and L. Mascaro, *J. Assoc. Off. Anal. Chem.*, 68 (1985) 1021.
- 9 G. Schwedt, *Labor Praxis*, 12 (1988) 1324.
- 10 R. Sawyer and E.J. Dixon, *Analyst*, 93 (1968) 669.
- 11 J. Ruzicka and E. Hansen, *Flow Injection Analysis*, Wiley, New York, 2nd ed., 1988.
- 12 M. Valcárcel and M.D. Luque de Castro, *Flow Injection Analysis. Principles and Applications*, Horwood, Chichester, 1987.
- 13 A. Maquieira, M.D. Luque de Castro and M. Valcárcel, *Analyst*, 112 (1987) 1569.
- 14 J. Ruz, A. Ríos, M.D. Luque de Castro and M. Valcárcel, *Anal. Chim. Acta*, 211 (1988) 281.
- 15 B.A.A. Dremel, B.P.H. Schaffar and R.D. Schmid, *Anal. Chim. Acta*, 225 (1989) 293.
- 16 M. Valcárcel and M. Gallego, *Trends Anal. Chem.*, 8 (1988) 34.
- 17 M. Valcárcel and M. Gallego, in J.L. Burguera (Ed.), *Flow Injection Atomic Spectroscopy*, Dekker, New York, 1989, Chap. 5.
- 18 M. Valcárcel, M. Gallego and R. Montero, *J. Pharm. Biomed. Anal.*, 8 (1990) 655.

Determination of beryllium(II) on solid substrates by photothermal spectrometry after selective complexation with Chrome Azurol S

Edward P.C. Lai, Brian D. Statham and Kathleen Ansell

Centre for Analytical and Environmental Chemistry, Ottawa-Carleton Chemistry Institute, Department of Chemistry, Carleton University, Ottawa, Ontario K1S 5B6 (Canada)

(Received 15th September 1992; revised manuscript received 2nd November 1992)

Abstract

Chrome Azurol S (CAS) has been used as a chromogenic reagent in the design of specific reagent strips for the determination by photothermal spectrometry (PTS) of beryllium(II) in aqueous samples collected on a membrane filter. This reagent must be carefully formulated for compatibility, stability, reaction speed, sensitivity and freedom from interferences. A linear relationship existed between PTS signal amplitude and Be(II) concentration for the concentration range of 0.1–15 $\mu\text{g g}^{-1}$. The potential of this method for long-term sample storage is important in practical applications where the samples cannot be analyzed for Be(II) immediately after their collection on membrane filters in the field.

Keywords: UV-Visible spectrophotometry; Beryllium; Chrome Azurol S; Complexation; Photothermal spectrometry

Beryllium (Be) is a light metal of Group IIA with a natural abundance of approximately 6 ppm in the Earth's crust [1]. It is found in many forms, such as BeO, BeH₂, and water soluble salts such as BeF₂, BeCl₂, Be₄O(CH₃COO)₆ and BeSO₄. Although the metal is difficult to work with due to its high melting point (2800.7 K) and stiffness, it does have several uses. It has been used as a moderator in reactors of the atomic energy industries and as a compact fuel element for rockets [2]. Owing to its high heat resistance and thermal conductivity, Be is used as a material in heat sinks. It is also used in many copper and nickel alloys where it augments the stiffness and electri-

cal conductivity of the alloys. Since Be is highly transparent to x-rays, it is used as a window material for x-ray tubes. As well, it has excellent neutron scattering properties and is used in radiation detectors, neutron monochromators and lasers. Lastly, BeO is an excellent insulator and is used as a substrate for transistors, silicon chips, coil cores and laser tubes.

Beryllium is very toxic, and must be handled with great care. It is particularly hazardous in the form of a dust which may be inhaled, either as the metal itself or as one of the compounds [1]. Continual inhalation of the dust produces chronic pulmonary beryllium disease (CBD), also called berylliosis. This disease leads to granular lesions in the lungs. Exposure to high doses of Be or its water soluble salts, as an aerosol for example, may also lead to an acute condition resembling a chemical pneumonia. In particular, the limits for

Correspondence to: E.P.C. Lai, Centre for Analytical and Environmental Chemistry, Ottawa-Carleton Chemistry Institute, Department of Chemistry, Carleton University, Ottawa, Ontario K1S 5B6 (Canada).

acute inhalation toxicity in humans is 0.1–0.5 mg Be/m³ for BeSO₄. Long term skin contact with Be and its compounds may cause skin sensitization and contact dermatitis. However, they are rarely absorbed via the gastrointestinal tract.

Owing to its high commercial value and toxicity, it is important to be able to detect low concentrations of Be(II) in aqueous media in order to identify the source. Traditionally, this has required that relatively large water samples be taken back to a lab for analysis by such methods as atomic absorption spectroscopy (AAS) [3,4]. This method involves atomizing the aqueous sample using a flame or a graphite furnace, and detecting the absorption of light by Be atoms at an analytical wavelength of 234.9 nm. This method has been reported to have a limit of detection for Be(II) from 1.5 μg kg⁻¹ to 0.1 μg g⁻¹. While these are quite good detection limits, the method does have some disadvantages. Firstly, AAS is a laboratory and equipment-intensive method which requires the transport of samples from the field to a lab. Thus there is a great possibility of sample contamination and/or deterioration due to improper storage, preparation, etc. Secondly, there is the question of time and cost.

A more economical method for Be(II) analysis is the spot test. This involves adding a drop of the sample solution to a solid substrate and applying a reagent on top of the analyte. Depending on the chemical nature of the reagent, one then observes a colour change or some other optical phenomena. Traditionally, such a spot test would use filter paper to contain morin which indicated the presence of Be(II) down to 0.25 μg [5]. The reagent produced a yellow-green fluorescence under UV light, with only Zr⁴⁺ as a positive interference. While the detection limit is good, this test is only semi-quantitative and cannot determine the analyte concentration precisely due to background fluorescence and light scattering. Hence, it is desirable to develop a novel spot test for Be(II) whereby a small volume of water sample may be quantitatively analyzed in situ or easily stored on a reagent strip for later analysis.

Considerable interest in specific reagent strips or dipsticks has recently developed in the analytical chemistry community since they represent the

ultimate in ease of field sampling for environmental analysis. These are flexible strips which have been sensitized with reagents, buffers and masking agents to function, in most cases, without auxiliary reagents over the entire pH range. For the most part, tests with these strips are complete in seconds. Initially, the change of color of a lead acetate tape provided the quantification of hydrogen sulfide at sub-ppm concentration levels in a gas sample to optimize refinery operation [6]. Diabetic patients with renal failure have long used test strips for self blood glucose monitoring [7]. The first dipstick to accurately measure alcohol levels in urine, saliva and plasma has gone on sale to clinical laboratories since last Fall [8]. Lately, a spot test has been designed to test human blood samples for hypoglycemia [9]. This simple test uses No. 3 Whatman filter papers soaked in 0.3% benzoic acid. A drop of blood is collected on each paper and the samples are developed with 2.5% trichloroacetic acid. Nowadays, EM Quants[®] ion specific test strips are commercially available for a wide range of inorganic cations (excluding Be(II)) and anions, as well as for ascorbic acid, formaldehyde and tartaric acid.

A major thrust in our research program has been to develop a Be(II)-selective reagent strip. It is based on spectrophotometric determination of inorganic ions which is a much researched method. Typically, the ion of interest must be complexed with a ligand which acts as a chromophore, making the analyte visible to the spectrometer. Many such ligands have been studied as chromophores for the determination of Be(II), and one of the most selective is Chrome Azurol S (CAS) [10], whose molecular structure is shown in Fig. 1. CAS is the sodium salt of 3''-sulfo-2'',6''-dichloro-3,3'-dimethyl-4-hydroxyfuchson-5,5'-dicarboxylic acid. It is also known as solochrome brilliant blue B, polytrop blue R [11], and alberon [12]. CAS forms several complexes with Be(II) depending on the pH of the reaction medium. In general, Be(II) and CAS form a 1:1 complex at pH 3–5 [12]. As mentioned above, morin can be used in a spot test on filter paper substrate to detect Be(II) in solution [5]. It is therefore logical to expect that CAS may also be used in a spot

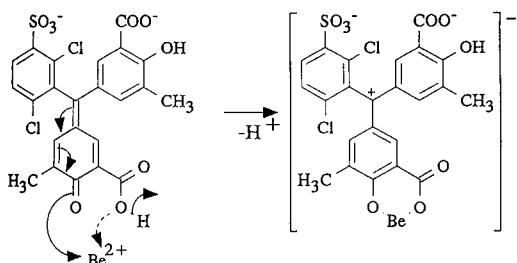


Fig. 1. Formation of Be–CAS complex.

test on a solid substrate. However, unlike the Be–morin complex, the Be–CAS complex does not fluoresce. It is normally measured in solution using an absorption spectrophotometer which, unfortunately, does not work well with samples on a solid substrate. Thus it is necessary to use another method which can measure the absorbance, directly or indirectly, of a spot on a solid substrate. One such method is photothermal spectrometry (PTS) with acoustic detection, which is a powerful non-destructive technique first applied to solid samples in the early 1970s. The photothermal effect is generated by an intense light source, usually a laser. After passing through a modulator, the laser light is absorbed by the chromophore in the sample matrix. Thus the sample is optically excited, in an enclosed gas-tight cell. Subsequent molecular collision results in a transfer of relaxation energy to translational or kinetic energy in the surrounding gas [13]. If the incident radiation is modulated at a rate that is slow compared to the rate of heat transfer, the optical modulation will result in a coherent modulation of the temperature above the sample. This then produces a pressure fluctuation in the surrounding gas at the optical modulation frequency. These pressure fluctuations are sound waves, which are in turn detected by a microphone and amplified into a measurable electrical signal. Placement of the reagent strip in the PTS cell allows for ready analysis, without further processing of the sample. Determination of the colors produced in the reagent by the analyte can be attained with high detection sensitivity and good quantitative accuracy.

EXPERIMENTAL

Reagents

All chemicals used were of analytical grade. All solutions were prepared with 18-M Ω cm deionized distilled water from a Milli-Q water system (Millipore, Bedford, MD). Reagent A (ligand chromophore) was prepared by dissolving 0.2084 g of chrome azurol S (K&K Labs., Cleveland, OH) in 1000 ml of water to give 3.44×10^{-4} M. Reagent B (buffer) was obtained by dissolving 6.8369 g of sodium acetate (Anachemia, Montreal) and 5.75 ml of glacial acetic acid (Anachemia, Montreal) in 1000 ml of water to give 5.02×10^{-2} M and 1.04×10^{-1} M, respectively. Then the CAS reagent (buffered chromophore) was formulated by mixing 350 ml of reagent A with 30 ml of reagent B. The Be(II) stock solution (analyte) was prepared by dissolving 9.823 g of $\text{BeSO}_4 \cdot 4\text{H}_2\text{O}$ (Fisher Scientific, Fair Lawn, NJ) in 500 ml of water to give 1000 ppm. Working standards were readily prepared by serial dilution of this stock solution. No. 1 Whatman filter papers (Whatman Labsales, Hillsboro, OR) and 0.45- μm Durapore membrane filters (Millipore) were used as the solid substrate without further modification.

Reagent strip preparation

Samples were prepared by first spotting a circle of solid substrate with 10 μl of CAS reagent, drying the spot in air, then applying 10–20 μl of Be(II) solution, and drying again. The sampling procedure was next reversed, with 10 μl of Be(II) solution applied to the substrate, air dried, and reacted with 20 μl of CAS reagent applied on top. This was done on microscopic glass disks, Whatman filter papers and 0.45- μm Millipore membrane filters as substrates. In order to establish a standard calibration curve, Be(II) solutions were prepared to give several concentrations of 0.1–15 ppm. Each concentration was run at least 3 times, including a blank which contained no Be(II).

Instrumentation

The UV–visible absorption spectra of the CAS reagent and the Be–CAS complex in aqueous

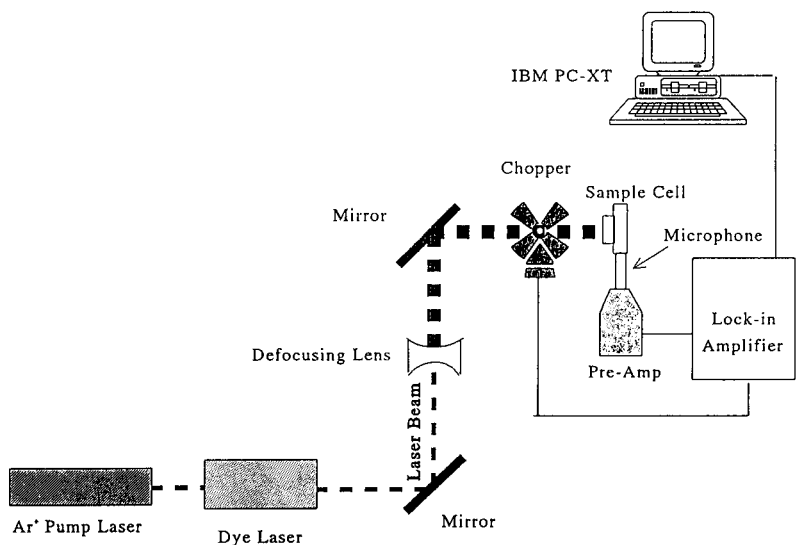


Fig. 2. Experimental set-up for PTS measurements.

solution were measured between 250 nm and 750 nm on a Perkin-Elmer Lambda 4B spectrophotometer (Perkin-Elmer, Nepean).

A schematic diagram of the experimental set-up for photothermal measurements is shown in Fig. 2. An Ar⁺-pumped dye laser ($\lambda = 579$ nm) operated at a selected modulation frequency served as the excitation light source. A defocusing lens was used to expand the laser beam so as to fill the whole sample (see Fig. 3). Attempts were made to find a laser power setting (ca. 30 mW) which gave consistent signals. Measurements were taken at octave filter settings of 31.5 Hz, 63 Hz, 125 Hz, and 250 Hz in order to cover the range of modulation frequencies employed, from 26 Hz to 375 Hz. For each chopper frequency, both the PTS signal amplitude and its phase lag were recorded. In addition to reagent strip samples, measurements were taken of blank

solid substrate as well as a highly-absorbing reference (blackened glass disk). The blank values were subtracted from the sample values, and the highly-absorbing reference data were used to normalize the subtraction results. Depth profiling data analysis was conducted by plotting graphs of phase lag ($\Delta\theta$) vs. square root modulation frequency ($\omega^{1/2}$).

RESULTS AND DISCUSSION

The UV-visible spectra of the CAS reagent and the Be-CAS complex in aqueous solution are shown in Figs. 4 and 5, respectively. The maximum absorption wavelengths (483 nm and

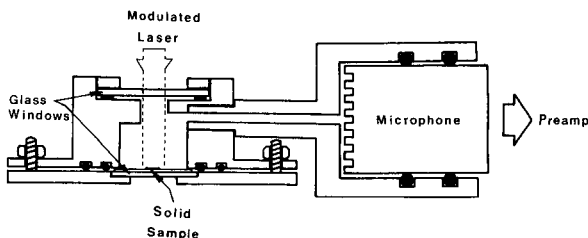


Fig. 3. Sample cell for photothermal spectrometry.

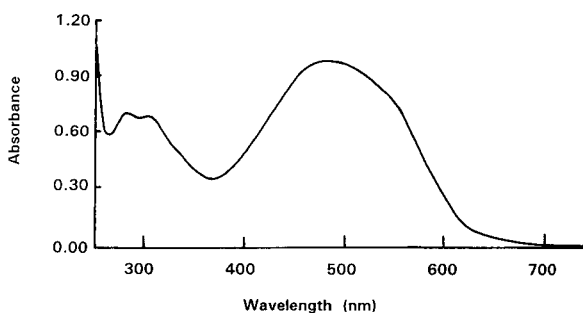


Fig. 4. UV-Visible absorption spectrum of CAS reagent.

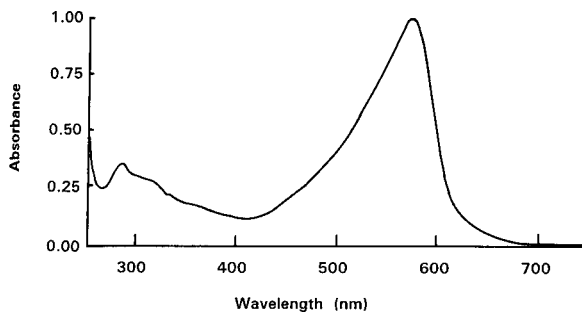


Fig. 5. UV-Visible absorption spectrum of Be-CAS complex produced from 5 ppm Be(II) in aqueous solution.

579 nm) are comparable to the literature values. According to the colour change, it appears that a charge transfer within the chromophore takes place. While the exact configuration of the 1:1 complex is unclear, it is proposed that the colour change is initiated by the transfer of positive charge to the central carbon of the triphenylmethane skeleton as shown in Fig. 1. This is supported by the fact that the colour change is from red to blue, indicating a lower-energy transition. A similar bonding arrangement occurs between another triphenylmethane chelate, aluminon, and aluminum [14]. As this distinct red-blue shift occurs only for the 1:1 stoichiometry, it is important to maintain pH in the region 3–5 from the analytical sensitivity point of view. Suggested buffers include pyridine-nitrate (pH 5.0), formate (pH 4.85), phthalate (pH 4.75), citrate (pH 4.75), hexamethylenetetramine-HCl (pH 5), and acetate (pH 5.0) [11,15–17]. At low Be(II) concentrations, it had been found that pyridine and acetate buffers interfered the least. Detection limits using CAS had been reported to be 3.2 ppm, 0.67 ppm, and 0.14 ppm using acetic acid-sodium acetate buffers [10,17,18]. For these reasons, an acetic acid-sodium acetate buffer was employed for this work.

Initially there was a problem of signal variation when the Be(II) solution was placed over the CAS reagent strip. As the Be-CAS complex was formed in a 1:1 ratio only if the pH was maintained between 3 and 5, the buffer became critical. If the acetic acid were to evaporate from the CAS reagent upon drying the buffered chromophore, the change in pH would cause the

subsequent complex formation to no longer have a 1:1 ratio with the corresponding optical absorption characteristics. When the order of application was reversed, i.e., CAS reagent over Be(II) sample spot, the resultant signals were much more consistent, implying that the buffered CAS reagent was able to react with the Be(II) to form the expected complex product. Interestingly, this is also the order of reagent application used in the morin spot test [5].

Various solid substrates (i.e., microscopic glass disks, Whatman filter papers and Millipore membrane filters) were tested to see if they produced different signals from possible surface chemistry effects. The results revealed that the 0.45- μm Millipore membrane filters provided the best signal-to-noise ratio.

PTS can be used to measure several different properties of a solid sample. A modulation frequency study may serve to indicate the optimum modulation frequency for the measurement of a particular sample type. Tam [13] found that the PTS signal intensity, V , varied as f^{-1} for low frequencies (≤ 1000 Hz) and as $f^{-3/2}$ for higher frequencies. Unfortunately at very low and specific frequencies, f^{-1} noise and power line noise may become significant, respectively. Thus, a plot of V versus f^{-1} will indicate the optimum frequency for the best signal-to-noise ratio obtainable from a particular PTS system. Our results indicated that the best modulation frequency was 45 Hz.

With all the above parameters optimized, PTS measurements were subsequently conducted to create a standard calibration curve of signal amplitude versus concentration (as in a Beer's law plot). A detection limit of $0.1 \mu\text{g g}^{-1}$ was obtained from three times the standard deviation of the blank divided by the slope of the curve in the linear dynamic range. This value is comparable to or better than those for other spectroscopic determinations of Be(II) using CAS as a reagent in solution [10,17,18]. A change in slope was observed at Be(II) concentrations higher than $15 \mu\text{g g}^{-1}$; it might be due to the penetration of Be(II) into the pores of the membrane filter.

While CAS is a highly selective reagent for the determination of Be(II), there are several known

interferents. These include Al^{3+} , Cu^{2+} , Fe^{3+} , Ni^{2+} , Th^{4+} , and Zr^{4+} [10,19]. Most of these interferences may be masked with EDTA, or with EDTA plus thiosulfate [18,20]. Only Zr^{4+} is incompletely masked with EDTA, especially if $[\text{Zr}^{4+}] \geq 100 \times [\text{Be}^{2+}]$. With careful control and standard additions, however, this should not be a big problem.

PTS can also give such sophisticated information as depth profiling and thermal information. The principle of depth profiling is quite simple. By varying the modulation frequency (ω in rad s^{-1}), one varies the amount of time that the sample is illuminated by the laser light and hence varies the thermal diffusion length or the depth at which the resultant heat energy can escape successfully from the sample. Thus the PTS signal amplitude varies with the modulation frequency. In addition, the corresponding phase lag ($\Delta\theta$ in rad) is also dependant on the modulation frequency. Theoretically, the phase lag varies as the square root of the modulation frequency [21]:

$$\Delta\theta = d \left(\frac{\omega}{2\alpha} \right)^{1/2} + \beta \quad (1)$$

where β is a phase lag caused by instrumental characteristics. From Eq. 1 it is clear that a plot of $\Delta\theta$ versus $\omega^{1/2}$ should be linear, and that one should be able to determine the solid sample thickness (d in m) if the thermal diffusivity (α in $\text{m}^2 \text{s}^{-1}$) is known. A depth profiling study was carried out in hopes of discerning information about the formation of the Be–CAS complex on the substrate surface. Unfortunately, the Be–CAS film formed on a membrane filter substrate was morphologically heterogeneous. Thus the value of α varied through the sample thickness, making Eqn. 1 imprecise to apply. When $\Delta\theta$ was plotted versus $\omega^{1/2}$, the data points showed great scattering, which rendered any calculated result an estimation at best. From these plots, the gradient, $d/(2\alpha)^{1/2}$, was ca. 9.1×10^{-5} for CAS only and ca. 8.6×10^{-4} for Be(II) only. As no thermal data for CAS or Be–CAS could be found in the literature, calculations could only be done for the Be(II) plot. Assuming an α value of $0.692 \text{ cm}^2 \text{ s}^{-1}$ for beryllium [22], the use of Eqn. 1 gave a spot thickness (d) of $10 \mu\text{m}$ which is a fairly

reasonable value. Hence, one may visualize that the sample spot was located at the surface of the membrane filter, to a depth governed largely by the permeability of Be(II).

Conclusions

The present spot test for Be(II) on a membrane filter represents our first milestone towards the development of specific reagent strips for use in on-site environmental sampling and determination of different metal ions and organic contaminants. The most critical component of this technique is sample preparation. In the design of specific reagent strips, reagents must be carefully formulated for stability, compatibility, reaction speed, sensitivity and freedom from interferences. Chrome azurol S has been evaluated as a sensitive reagent for the determination of Be(II) by photothermal spectrometry. Best results were obtained by placing the Be(II) sample on the membrane filter substrate and placing the CAS reagent over top.

There are several possible places of improvement in this method. Firstly, the laser power output was less than ideal as the operating wavelength (579 nm) was not the optimum wavelength for the laser dye used (Rhodamine 590 chloride). Future considerations will include many other reagents which had previously been used to determine Be(II) spectrometrically. These reagents include aluminon, beryllon, eriochrome cyanin R, acetylacetone, and fast sulphon black F. This last reagent, fast sulphon black F, was reported to give good results in the range 0.01 to $7 \mu\text{g g}^{-1}$ Be(II) at pH 11 to 11.2 [23]. Naturally any change in the chromogenic reagent used will require a change in the operating laser wavelength. Fortunately, the current PTS system lends itself favourably to this.

As the complexation of CAS and Be(II) is highly pH dependent, Be–CAS complexes of different Be to CAS ratios may be formed during the drying step. The early problems experienced with signal variation in this work was related to the loss of one buffer component by volatilization. Several other buffers have been suggested for use with CAS, with hexamethylenetetramine–HCl being the most recent [16]. As many of these

buffers are less volatile than the acetic acid buffer employed in the present work, they are less susceptible to loss and will hence preserve the appropriate pH upon sample application for 1:1 complex formation. This would allow emplacement of the buffered chromophore on the substrate first, thus getting closer to the hope for a new type of specific reagent strip for environmental Be(II) testing in the field. Although the long term stability of the filter paper samples has yet to be determined, the potential of this method for long-term sample storage is clearly of great importance for practical applications where the samples need not be analyzed for Be(II) immediately after their collection in the field.

REFERENCES

- 1 H.R. Zorn, T.W. Stiefel, J. Beuers and R. Schlegelmilch in H.G. Seiler and H. Sigel (Eds.), *Handbook on Toxicity of Inorganic Compounds*, Marcel Dekker, New York, 1988, p. 105–114.
- 2 F.A. Patty, *Industrial Hygiene and Toxicology*, Vol. II, Interscience, New York, 1962, pp. 1010–1020.
- 3 S. Terashima, *Geostandards Newsletter*, 7 (1983) 295.
- 4 W.F. Schmidt and F. Dietl, *Fresenius' Z. Anal. Chem.*, 329 (1988) 853.
- 5 *Reagents and Reactions for Qualitative Inorganic Analysis, Fifth Report*, International Union of Pure and Applied Chemistry, Analytical Chemistry Division, Commission on Analytical Reactions, London, 1964, p. 17.
- 6 P.J. Moore, *Am. Lab.*, May (1991) 56.
- 7 R. Henry, *Clin. Diag. Today*, 2 (1991) 25.
- 8 R. Sutherland, *Clin. Diag. Today*, 2 (1991) 23.
- 9 M. Johnstone, *Clin. Diag. Today*, 2 (1992) 15.
- 10 P. Pakalns, *Anal. Chim. Acta*, 31 (1964) 570.
- 11 L. Silverman and M.E. Shideler, *Anal. Chem.*, 31 (1959) 153.
- 12 A.V. Novoselova and L.R. Batsanova, *Analytical Chemistry of Beryllium*, Israel Program for Scientific Translation, Jerusalem, 1968, p. 67.
- 13 A.C. Tam, *Rev. Mod. Phys.*, 58 (1986) 381.
- 14 H. Onishi, *Photometric Determination of Traces of Metals*, Vol. 3, Part IIA, Wiley, Toronto, 4th edn., 1986.
- 15 L. Sommer and V. Kubáň, *Anal. Chim. Acta*, 44 (1969) 333.
- 16 H. Nishida, *Bunseki Kagaku*, 39 (1990) 805.
- 17 N.B. Hansen, *Mikrochim. Acta [Wien]*, 2 (1982) 133.
- 18 J. Valero, *Quim. Anal. (Barcelona)*, 9 (1990) 181.
- 19 L. Kutsera, H.S. Ghaziaskar and E.P.C. Lai, *Anal. Lett.*, 25 (1992) 2289.
- 20 T. Mochizuki and R. Kuroda, *Fresenius' Z. Anal. Chem.*, 309 (1981) 363.
- 21 M.J. Adams and G.F. Kirkbright, *Analyst*, 102 (1977) 678.
- 22 Y.S. Touloukian, R.W. Powell, C.Y. Ho and M.C. Nicolaou (Eds.), *Thermal Diffusivity, Thermophysical Properties of Matter*, Vol. 10, IFI/Plenum, New York, 1973.
- 23 A.M. Cabrera and T.S. West, *Anal. Chem.*, 35 (1964) 311.

Study of europium-sensitized fluorescence of tetracycline in a micellar solution of Triton X-100 by fluorescence and thermal lens spectrometry

J. Georges and S. Ghazarian

Laboratoire des Sciences Analytiques, Université Claude Bernard–Lyon I, F-69622 Villeurbanne Cedex (France)

(Received 5th October 1992; revised manuscript received 25th November 1992)

Abstract

Europium fluorescence sensitized by tetracycline, via the formation of an organic chelate, was used for the sensitive detection of tetracycline. The efficiency of the intramolecular energy transfer and of the resulting ion luminescence was studied by fluorescence and thermal lens spectrometry. The sensitivity of the method depends on the pH and the concentration of the emitting ion and it is increased by the addition of Triton X-100 to the aqueous solution. The fluorescence enhancement obtained in the micellar medium is correlated with an increase in the fluorescence lifetime of europium emission. Detection limits for tetracycline are 1.0×10^{-8} and 3×10^{-9} M in the absence and presence of Triton X-100, respectively.

Keywords: Fluorimetry; Europium; Tetracycline; Thermal lens

Tetracycline is part of a family of antibiotics whose antibacterial action is due to their ability to bind divalent cations in aqueous solution [1]. An extensive literature is available on the fluorescence of these compounds. Although tetracyclines are only weakly fluorescent themselves, increased fluorescence is obtained by the formation of highly fluorescent complexes with di- or trivalent cations [2]. Complexes with divalent cations have been studied and used to probe metal binding sites on biological membranes [3]. Organic chelates with trivalent lanthanide ions, especially those of europium, samarium and terbium with β -diketones, have been used to improve the sensitivity for the luminescence detection of the lanthanides themselves [4]. Strong fluorescence, specific of the ion, occurs when the

ion is excited as a consequence of non-radiative energy transfer from the absorbing ligand to the cation, followed by radiative emission from the latter.

Conversely, intramolecular energy transfer from the ligand to the lanthanide ion may be used to enhance the fluorescence of the ligand [5]. Such a detection method has been applied in liquid chromatography and flow-injection analysis [6–8]. The low intensity and broad emission band of the uncomplexed ligand are changed to a strong intensity and narrow emission band characteristic of the ion.

The purpose of this work was to study the efficiency of the intramolecular energy transfer from tetracycline to europium ions by fluorescence and thermal lens spectrometry. Effects of pH, europium concentration and non-ionic Triton X-100 were investigated in order to improve the fluorescence detection of tetracycline in aqueous solutions.

Correspondence to: J. Georges, Laboratoire des Sciences Analytiques, Université Claude Bernard–Lyon I, F-69622 Villeurbanne Cedex (France).

EXPERIMENTAL

Reagents

Tetracycline hydrochloride and Triton X-100R-S were obtained from Sigma and used without further purification. The non-ionic surfactant was used in its hydrogenated form to reduce UV absorption. The required amount of surfactant (generally 1%, w/w) was added to the test solution by weighing. Europium chloride was purchased from Fluka.

The structure of tetracycline is shown in Fig. 1. The molecule contains three distinct acid groups: the tricarbonylmethane group (ring A), the ammonium cation (ring A) and the phenolic diketone group (ring BCD) [9]. The macroscopic p*K* values are well known and have been reported to be 3.30, 7.68 and 9.69. However, there is a lack of agreement concerning the assignment of the dissociation constants to the respective functional groups [10,11]. If the lowest p*K* is generally attributed to the tricarbonylmethane group of ring A, there is some uncertainty about the assignment of the other two p*K* values [9–13].

Methods

In order to prevent any electrolyte effect on the fluorescence intensity, the pH was adjusted and continuously varied in the range 7–9 with the same buffer solution: 50 ml of 0.1 M tris(hydroxymethyl)aminomethane (Tris) together with a sufficient volume of 0.1 M HCl to give the required pH.

Stock standard solutions of tetracycline (1×10^{-3} M) were prepared by weighing the appropriate amount of tetracycline hydrochloride into a volumetric flask. Working standard solutions of

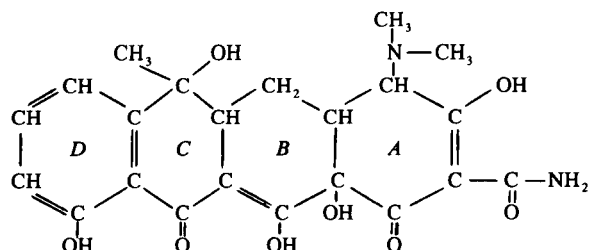


Fig. 1. Structure of tetracycline.

1×10^{-5} and 1×10^{-7} M were then prepared daily by successive dilution of the stock standard solution. Calibration graphs and detection limits were obtained using the peak emission wavelength of the europium ion (613 nm) at the peak excitation wavelength of the europium–tetracycline chelate (390 nm). All measurements were corrected for background fluorescence of the blank. Memory effects of europium adsorbed on the walls of glass vessels were problematic, especially in measurements where the europium concentration was varied while the tetracycline concentration was kept constant. For this reason, stock and sample solutions were prepared in plastic rather than glass containers. Also, fluorescence cuvettes were cleaned with dilute nitric acid in an ultrasonic bath.

Apparatus

The absorption spectra were recorded on a Beckman M25 UV–visible spectrophotometer. Steady-state fluorescence measurements were obtained on a Jobin-Yvon JY3 spectrofluorimeter with a 1-cm quartz cell, equipped with 10-nm slits for both excitation and emission. pH measurements were performed with a digital readout pH meter (Solea-Tacussel) and a TC 200 glass and reference unitubular electrode (Solea-Tacussel).

Thermal lens and time-resolved fluorescence measurements were made with the same laser-based experimental set-up (Fig. 2) [14]. The pulsed laser was a nitrogen-pumped dye laser (Jobin-Yvon, LA04 and Spectrolas 3). The experiments were carried out at 390 nm with 1×10^{-3} M 4,4'-bis(2-butyloctyloxy)-*p*-quaterphenyl (BBQ) in ethanol–toluene (60 + 40, v/v) at a repetition rate of 15 Hz. The sample cell was a 1-cm four-window fluorescence cell (Hellma 111-QS). After the cell, the excitation beam was blocked by a band-pass interference filter. The thermal lens effect was probed colinearly with a helium–neon laser. The thermal lens signal was detected through a 1-mm pinhole with a PIN silicon photodiode. The fluorescence was detected at right-angles to the laser beams. Europium emission was focused on the entrance of a monochromator and then detected by a photomultiplier tube (R928, Hamamatsu) operating at 1000 V.

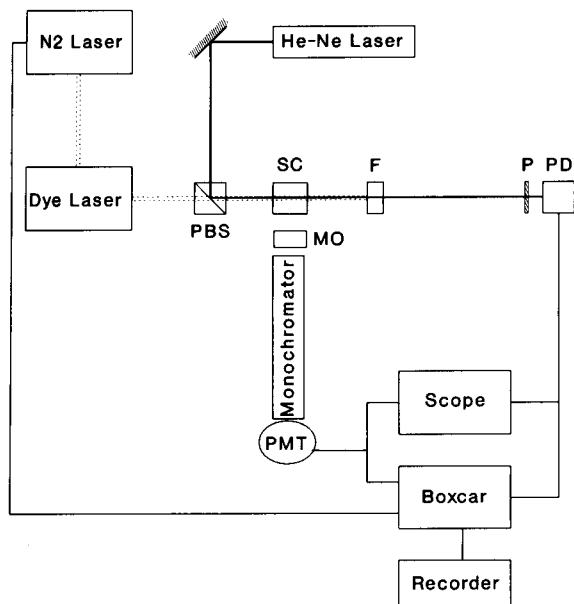


Fig. 2. Experimental set-up for thermal lens and time-resolved fluorescence measurements. PBS = polarizing beamsplitter; SC = sample cell; MO = microscope objective; PMT = photomultiplier; F = interference filter; P = pinhole; PD = photodiode.

The photodiode (thermal lens signal) and the photomultiplier (fluorescence signal) outputs, converted into a voltage with a $6.8\text{-k}\Omega$ terminator, were amplified with an a.c.-coupled preamplifier which has a rise time of about $0.2\ \mu\text{s}$ with a $10\times$ gain. Under these conditions, the rise time for the fluorescence signal was that of the preamplifier. Both signals were monitored with an oscilloscope and fed into a fast gated integrator and boxcar averager (Model SR 250, Stanford). The thermal lens signal was sampled at its maximum value, i.e., in the range $100\text{--}400\ \mu\text{s}$ after the laser pulse.

RESULTS AND DISCUSSION

Absorption and fluorescence spectra

The complexation of tetracycline by Eu^{3+} ions is demonstrated in Fig. 3. In the presence of europium, the absorption band of tetracycline is red shifted and the peak absorbance is maximum when the concentration of Eu^{3+} equals that of

tetracycline. On addition of Triton X-100, the absorption band remains unchanged except for a slight increase in peak absorbance. At higher pH (8.5), the absorption spectrum of free tetracycline moves slightly to longer wavelength whereas that of the chelate remains unchanged.

Fluorescence enhancement of tetracycline is shown in Fig. 4. On addition of europium ions, the broad emission band of tetracycline is replaced with the much narrower emission band characteristic of the lanthanide ion with a peak intensity much greater than that of the uncomplexed tetracycline. The emission spectrum of Eu^{3+} consists of several bands corresponding to the ${}^5D_0 \rightarrow {}^7F_n$ transitions, the most intense being the ${}^5D_0 \rightarrow {}^7F_1$ transition at 590 nm and the ${}^5D_0 \rightarrow {}^7F_2$ transition at 613 nm. As lanthanide ions have very low molar absorptivities (ϵ for Eu^{3+} is $2.90\ \text{l mol}^{-1}\ \text{cm}^{-1}$ at 394.3 nm), luminescence of the ion following direct excitation of the ion itself is very weak. The strong emission originates from an intra-chelate energy transfer, where the ligand absorbs the excitation radiation and transfers is

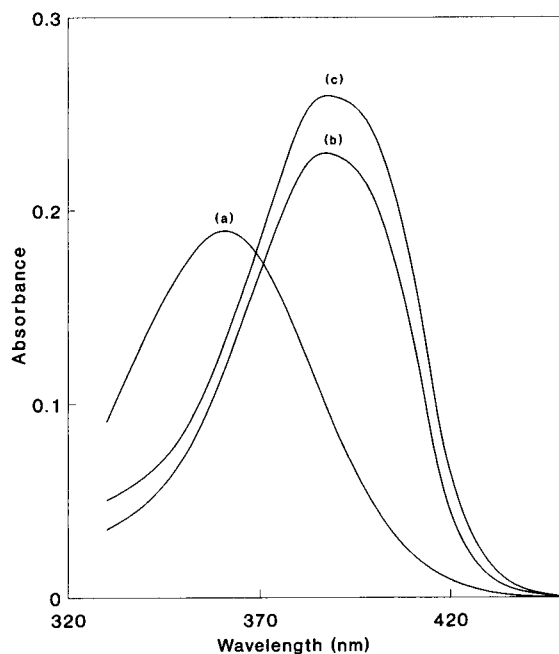


Fig. 3. Absorption spectra of (a) $1 \times 10^{-5}\ \text{M}$ tetracycline, and $1 + 1\ \text{Eu}^{3+}$ -tetracycline chelate in Tris-HCl buffer (pH 7.5) (b) without and (c) with Triton X-100.

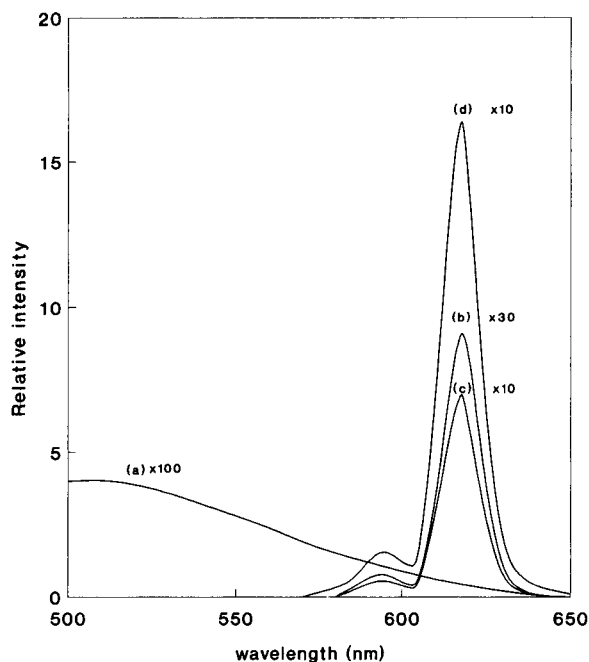


Fig. 4. Fluorescence spectra of (a) 2.5×10^{-6} M free tetracycline, (b) 2.5×10^{-6} M tetracycline + 3×10^{-6} M Eu^{3+} , (c) 2.5×10^{-6} M tetracycline + 3×10^{-6} M Eu^{3+} + 1% Triton X-100 and (d) 2.5×10^{-6} M tetracycline + 4×10^{-5} M Eu^{3+} + 1% Triton X-100. The spectra were recorded with different gains as indicated on the curves.

energy to the emitting ion. In the presence of non-ionic micelles, fluorescence enhancement is still greater and increases further on addition of an excess of europium ions.

Influence of pH

Tetracycline (TC) has several possible metal-binding sites, depending on the pH, and reflecting changes in the sensitized europium fluorescence. The conformation of Eu-TC chelates can be compared with that of Gd-TC chelates as studied by NMR spectrometry [13]. Below pH 7, the conformation of the complex is the same for both forms of tetracycline before and after the first dissociation constant. The metal is in the vicinity of the A and B rings, probably bound to the amide and ketone oxygen atoms. Above the second pK value, the metal lies close to the BC ring junction at the β -diketone site. Other workers [5] have shown that the fluorescence intensity

for Eu-TC chelates in water was maximum at pH 9, but the solution became cloudy above pH 8. Such a problem did not occur with the buffer used in this work.

The pH dependence of europium fluorescence, in the absence and in the presence of Triton X-100, is shown in Fig. 5. The shape of the curves depends slightly on the relative concentrations of both tetracycline and europium ions. In the absence of surfactant, the curve agrees with that reported when the $[\text{Eu}]/[\text{TC}]$ ratio is 1 [5], with a fluorescence maximum above pH 8. In the presence of Triton X-100, with an excess of europium ions in order to achieve the best fluorescence enhancement, the shape of the curve is not precise and only indicative owing to slow complex formation and/or solubilization inside the micelles. Also, the surfactant may induce a slight change in the acid-base equilibrium of tetracycline. These facts contribute to less reproducible results especially in experiments where the pH was varied. These effects and the resulting uncertainty were reduced when the method was then

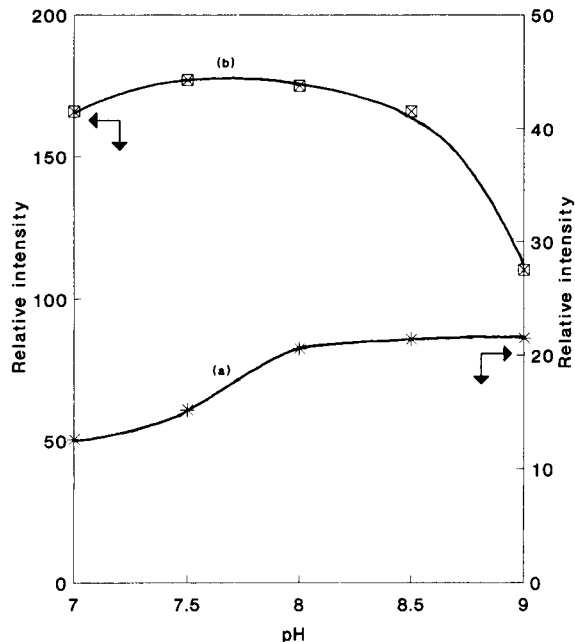


Fig. 5. Influence of pH on the fluorescence of europium at 613 nm for 2×10^{-6} M tetracycline + 4×10^{-5} M Eu^{3+} chelate solution (a) without and (b) with 1% Triton X-100.

applied to the determination of tetracycline owing to the constant pH value and more reproducible operating conditions. The greatest fluorescence intensity occurs over the pH range 7–8.5 in the presence of Triton X-100 compared with pH 8–9 in the absence of surfactant. The overall fluorescence enhancement, expressed as the ratio of europium fluorescence to free tetracycline fluorescence, depends on the pH, with values of 40 and 85 at pH 8.5 and 7.5, respectively. This difference does not result from a lower europium fluorescence intensity at pH 8.5 but rather from a greater fluorescence of tetracycline at this pH. As shown in Fig. 5, the enhancement effect of Triton X-100 varies between 5 at pH 9 and 12.5 at pH 7.

Influence of Eu^{3+} concentration

Another important parameter in the application of the method to the measurement of tetracycline is the concentration of the enhancing ion. In the absence of micelles (Fig. 6), the sensitized europium fluorescence is maximum when the

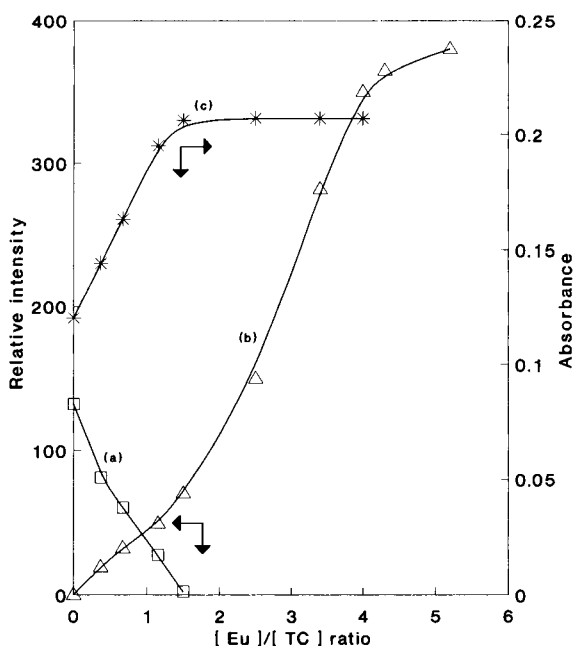


Fig. 7. Influence of Eu^{3+} concentration in 1×10^{-5} M tetracycline solution containing 1% Triton X-100 on (a) the fluorescence of free tetracycline at 510 nm, (b) sensitized europium fluorescence at 613 nm and (c) chelate absorbance at 390 nm. Different scales on the vertical axis for (a) and (b).

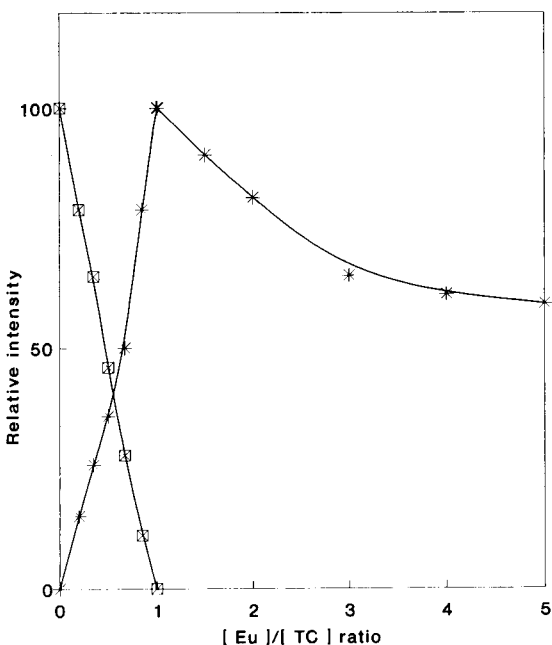


Fig. 6. Influence of Eu^{3+} concentration in 3.6×10^{-6} M tetracycline solution (without surfactant) on (\square) the fluorescence of free tetracycline at 510 nm and ($*$) sensitized europium fluorescence at 613 nm. Different scales on the vertical axis.

concentration of europium equals that of tetracycline. Simultaneously, the fluorescence of free tetracycline decreases and is zero when the $[\text{Eu}]/[\text{TC}]$ ratio is 1. At higher europium concentrations, the fluorescence of europium decreases, indicating a quenching effect of free Eu^{3+} ions. In the presence of Triton X-100 micelles, the europium fluorescence continues to increase well after the stoichiometry of the chelate as defined by the curves showing the variations of the absorbance of the chelate and the fluorescence of free tetracycline, respectively (Fig. 7). Maximum europium fluorescence is reached for an Eu/TC ratio of about 6 and 20 when the concentration of tetracycline is 1×10^{-5} M (Fig. 7) and 1×10^{-6} M (Fig. 8), respectively.

The increase in europium fluorescence while the absorbance of the chelate remains constant and the fluorescence of free tetracycline is zero may be explained as follows. The results obtained in pure water show that an excess of Eu^{3+} ions

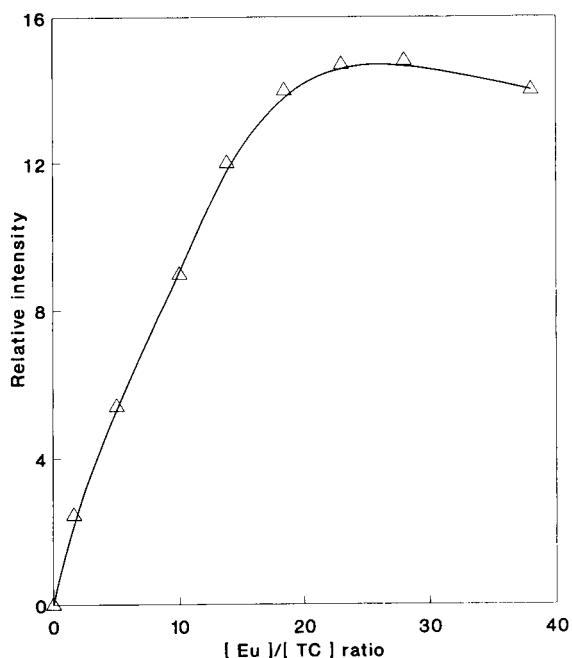


Fig. 8. Influence of Eu^{3+} concentration in 1×10^{-6} M tetracycline solution on sensitized europium fluorescence at 613 nm in the presence of Triton X-100.

produces a quenching effect, as observed previously [5]. In contrast, in the presence of Triton X-100 micelles, this quenching effect is changed

into an enhancement effect. As the absorption spectrum does not change, a new chelate is not formed when the europium concentration increases. Not only do the micelles protect the chelate against collisions with free europium ions in the aqueous phase, but also the micellar microenvironment would favour energy transfer between the chelate and free ions. This diffusion-controlled energy transfer is not very efficient in a homogeneous solvent, but may be greatly enhanced by using organized media such as micellar or cyclodextrin solutions [15]. Similarly to a co-fluorescence effect [16], europium fluorescence would result both from chelated europium excited intramolecularly and free europium excited by intermolecular energy transfer from the chelate.

Influence of Triton X-100 on fluorescence lifetime

The fluorescence lifetime of tripositive lanthanide ions ranges from $1 \mu\text{s}$ to over than 2 ms, depending on the emitting ion and on the medium. Morin et al. [17] have shown that the fluorescence enhancement observed for Eu^{3+} - β -diketone chelates on addition of Triton X-100 in water is directly related to an increase in the lifetime of lanthanide emission. The fluorescence

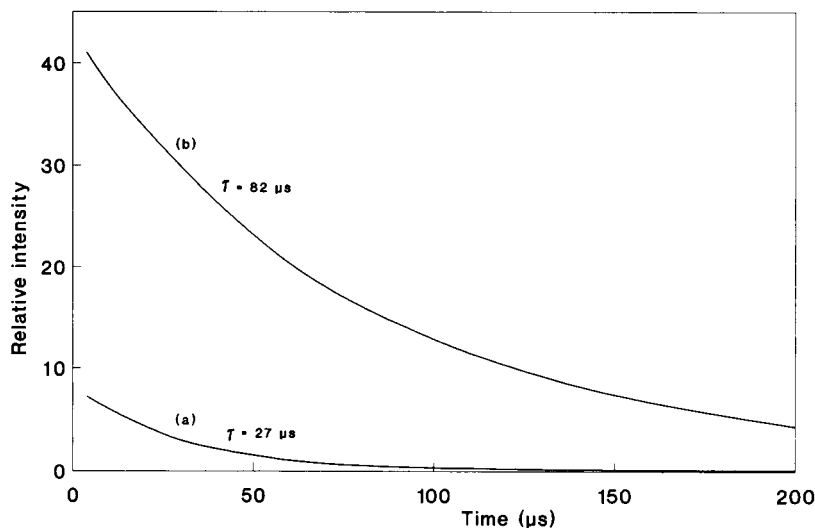


Fig. 9. Fluorescence decay curves for sensitized europium fluorescence in Tris-HCl buffer (a) without and (b) with 1% Triton X-100.

decay curve following instantaneous pulse excitation is described by the equations

$$I_t = I_0 e^{-kt} \quad (1)$$

or

$$\ln I_t = \ln I_0 - t/\tau \quad (2)$$

where I_0 and I_t are the fluorescence intensities at times zero and t , respectively, and τ is the fluorescence lifetime defined as the reciprocal of the rate constant k . The decay curves (Fig. 9), corresponding to the Eu–TC chelate in the absence and in the presence of Triton X-100, were recorded with the experimental set-up described in Fig. 2. In both instances, the plot of $\ln I_t$ versus t was straight line giving τ values of 27 and 82 μs without and with surfactant, respectively. Although the second value is low compared with the $> 900 \mu\text{s}$ obtained with β -diketone chelates in the same medium [17], the increase in fluorescence lifetime indicates a protecting effect of the micelles against non-radiative deactivation of Eu^{3+} ions and accounts for the enhancement of sensitized europium fluorescence.

Overall fluorescence quantum yield

The overall efficiency of energy transfer and europium luminescence was determined by thermal lens spectrometry (TLS). TLS is a sensitive laser-based technique in which absorbance is measured indirectly as a thermal effect resulting from non-radiative decay of the excited states after absorption of light [18–20]. Following excitation of free or chelated tetracycline, several deactivation pathways are possible. The energy absorbed may be dissipated as radiative energy (luminescence of free tetracycline and/or of chelated europium) and as thermal energy (vibrational relaxation and internal conversion of tetracycline, energy transfer from tetracycline to europium and non-radiative relaxation of europium). TLS allows the direct observation of radiationless deactivation processes and is therefore complementary to fluorescence measurements. Provided that photochemical reactions are absent, the energy absorbed equals the sum of the luminescence energy and the thermal energy. In

practice, the thermal lens signal of the unknown sample is compared with that of a reference absorber at the same wavelength and with equal absorbances [21]. The TLS signal is expressed as the ratio of the sample signal to the reference signal:

$$Q_{\text{th}} = \frac{A^r S}{AS^r} = 1 - \frac{\bar{\nu}_f}{\nu_a} Q_f \quad (3)$$

where A and S are the absorbance and the TLS signal, respectively, the superscript r referring to the reference absorber, Q_f is the fluorescence quantum yield, ν_a is the absorption level of free or chelated tetracycline, i.e., the laser absorption frequency, and $\bar{\nu}_f$ is the average fluorescence frequency of the main transition and corresponds approximately to the emitting level of europium ions (5D_0) [22]. The experimental values of Q_{th} relative to $\text{K}_3\text{Fe}(\text{CN})_6$ as the reference absorber ($= 1.00$) are tetracycline $= 1.00 \pm 0.02$ and Eu–TC chelate $= 1.00 \pm 0.02$ without Triton X-100 and 0.96 ± 0.02 with Triton X-100 (the excitation wavelength was the same as for the fluorescence measurements, i.e., 390 nm). With ν_a and $\bar{\nu}_f$ equal to $25\,640 \text{ cm}^{-1}$ and $16\,300 \text{ cm}^{-1}$, respectively, the value of Q_{th} obtained for the chelate in the presence of Triton X-100 leads to a fluorescence quantum yield of about 0.06. As expected, the fluorescence quantum yields of free tetracycline and of the chelate in the absence of surfactant are still much smaller and are less than the experimental error of the technique.

Calibration graphs and detection limits

The validity of the method for the fluorimetric determination of tetracycline and the influence of Triton X-100 are discussed with respect to the calibration graphs and the detection limits. In the absence of surfactant, linearity extends over three orders of magnitude from the limit of detection ($1.0 \times 10^{-8} \text{ M}$) upto to $1 \times 10^{-5} \text{ M}$. In the presence of Triton X-100, the graph is shifted upward owing to a better sensitivity of europium luminescence (Fig. 10). Although linearity is obtained over less than three orders of magnitude, it extends to lower concentrations, giving a detection

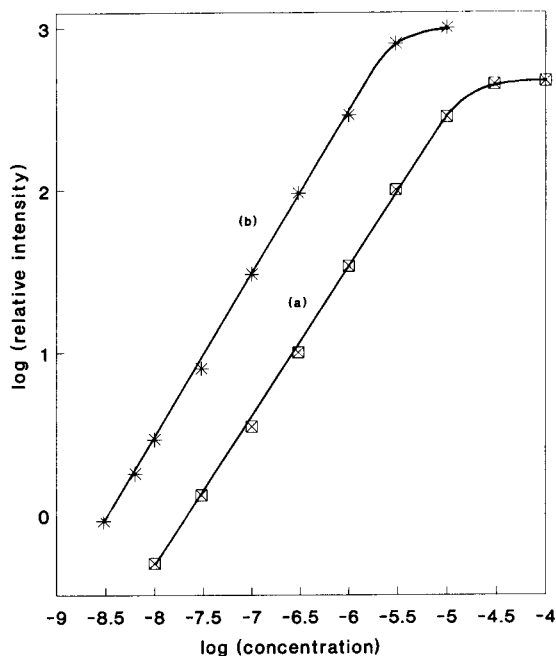


Fig. 10. Calibration graphs for tetracycline detected by sensitized europium fluorescence (a) without surfactant, $[\text{Eu}^{3+}] = 1 \times 10^{-4}$ M, and (b) with 1% Triton X-100, $[\text{Eu}^{3+}] = 2 \times 10^{-5}$ M.

limit of 3×10^{-9} M. It is noted that our detection limits were determined from the band emission of Eu^{3+} taking a peak height to peak-to-peak background noise equal to 2, i.e., ten times the r.m.s. noise, which is less favourable than the usual 3σ for a steady-state signal. The europium concentration was kept constant and was taken as low as possible in order to achieve a compromise between the background noise, the linearity range and the detection limit. Whereas the slope of the calibration graph is 1.03 in the presence of Triton X-100, it is significantly lower (0.92) in the absence of surfactant. This difference, which corresponds to an increase in the enhancement effect of Triton X-100 with increasing tetracycline concentration, reflects the greater quenching effect of free Eu^{3+} ions when the concentration of tetracycline increases. The curvature of both

graphs may originate from an inner filter effect due to high absorbance values of the solutions in this range and/or saturation of the fluorescence signal. In the presence of surfactant, the curvature arises at lower tetracycline concentrations because the $[\text{Eu}]/[\text{TC}]$ ratio is no longer high enough to give maximum fluorescence (see Figs. 7 and 8).

Further experiments are in progress in order to improve the sensitivity of the method. This may be achieved by using solutions (co-solvent, buffer, surfactant, synergistic agent, etc.) that increase the efficiency of intramolecular energy transfer from the ligand to the ion and/or the fluorescence lifetime of the sensitized europium ion.

REFERENCES

- 1 A. Albert and C.W. Rees, *Nature*, 177 (1956) 433.
- 2 O.S. Wolbeis, in S.G. Schulman (Ed.), *Molecular Luminescence Spectroscopy. Methods and Applications: Part I*, Vol. 77, Wiley-Interscience, New York, 1985, Chap. 3.
- 3 A.H. Caswell and J.D. Hutchison, *Biochem. Biophys. Res. Commun.*, 42 (1971) 43 and 43 (1971) 625.
- 4 J. Georges, *Spectrochim. Acta Rev.*, 14 (1991) 337, and references cited therein.
- 5 L.M. Hirschy, E.V. Dose and J.D. Winefordner, *Anal. Chim. Acta*, 147 (1983) 311.
- 6 E.E. Dibella, J.B. Weissman, M.J. Joseph, J.R. Schultz and T.J. Wenzel, *J. Chromatogr.*, 328 (1985) 101.
- 7 T.J. Wenzel and L.M. Collette, *J. Chromatogr.*, 436 (1988) 299.
- 8 T.J. Wenzel, L.M. Collette, D.T. Dahlen, S.M. Hendrickson and L.W. Yarmaloff, *J. Chromatogr.*, 433 (1988) 149.
- 9 C.R. Stephens, K. Murai, K.J. Brunings and R.B. Woodward, *J. Am. Chem. Soc.*, 78 (1956) 4155.
- 10 N.E. Rigler, S.P. Bag, D.E. Leyden, J.L. Sudmeier and C.N. Reilly, *Anal. Chem.*, 37 (1965) 872.
- 11 M.K. Mathew and P. Balaram, *J. Inorg. Biochem.*, 13 (1980) 339.
- 12 G.L. Asleson and C.W. Frank, *J. Am. Chem. Soc.*, 98 (1976) 4745.
- 13 M. Celotti and G.V. Fazakerley, *J. Chem. Soc., Perkin Trans. 2*, (1977) 1319.
- 14 J. Georges and J.M. Mermet, *Spectrochim. Acta, Part A*, in press.
- 15 M. Almgren, F. Grieser and J.K. Thomas, *J. Am. Chem. Soc.*, 101 (1979) 2021.
- 16 Y.-Y. Xu, I.A. Hemmila and T.N.-E. Lövgren, *Analyst*, 117 (1992) 1061.

- 17 M. Morin, R. Bador and H. Déchaud, *Anal. Chim. Acta*, 219 (1989) 67.
- 18 H.L. Fang and R.L. Swofford, in D.S. Kliger (Ed.), *Ultra-sensitive Laser Spectroscopy*, Academic, New York, 1983, p.176.
- 19 J.M. Harris and N.J. Dovichi, *Anal. Chem.*, 52 (1980) 695A.
- 20 J. Georges and J.M. Mermet, *Analisis*, 16 (1988) 203.
- 21 J. Georges, *Spectrochim. Acta Rev.*, 15 (1993) 39.
- 22 W.T. Carnall, P.R. Fields and K. Rajnak, *J. Chem. Phys.*, 49 (1968) 4450.

Determination of traces of iron by thin-layer spectroelectrochemistry

Qingji Xie, Weidong Kuang, Lihua Nie and Shouzhao Yao

Department of Chemistry and Chemical Engineering, Hunan University, Changsha 410082 (China)

(Received 8th February 1992; revised manuscript received 16th September 1992)

Abstract

The complex of iron with Chrome Azurol S (CAS) was studied using a long path-length thin-layer spectroelectrochemical cell with dual working electrodes. A method for the determination of traces of iron is proposed, based on the variation in the absorbance between the oxidized and reduced state of the complex (ΔA). ΔA was proportional to iron concentration over the range 0–3 $\mu\text{g ml}^{-1}$. Compared with the conventional spectrophotometric determination of iron using CAS, the selectivity was improved because the analytical signal here depended on both the spectral and the electrochemical behaviour of the tested species. Iron was determined in water samples by this method. A concept characterizing the sensitivity of the spectroelectrochemical signals is also presented.

Keywords: UV–Visible spectrophotometry; Voltammetry; Iron; Spectroelectrochemistry; Waters

Spectroelectrochemistry (SEC) has been widely used in the investigation of the kinetics and mechanisms of electrode reactions and the measurement of electrochemical parameters [1,2]. However, there are fewer reports on quantitative analysis, probably because the traditional optically transparent electrode (OTE) has low optical sensitivity. Tyson and West [3–5] developed a long path-length spectroelectrochemical cell with an optical sensitivity equivalent to that in conventional spectrophotometry. They also initiated quantitative analysis by spectroelectrochemistry based on the UV absorption of the complexes formed between the investigated metal ions in solution and the OH^- ions on the surface of a platinum electrode. However, this method showed poor selectivity because of the strong overlapping of the spectra of these complexes and was not used for analyses of practical samples.

Correspondence to: Shouzhao Yao, Department of Chemistry and Chemical Engineering, Hunan University, Changsha 410082 (China).

In this paper, a spectroelectroanalytical method is proposed and its selectivity is discussed in detail. Traces of iron were determined based on this method using Chrome Azurol S (CAS). A concept demonstrating the sensitivity of the spectroelectrochemical signals is also presented.

THEORY

For an electrode reaction $\text{O} + ne \rightleftharpoons \text{R}$, a variation in absorbance (ΔA) will be recorded for a long path-length thin-layer spectroelectrochemical cell immediately with a single potential step from the potential at which the oxidized state is the only species present to that at which the reduced state is the only species present. According to the Lambert–Beer law,

$$\Delta A = A_{\text{R}} - A_{\text{O}} = \epsilon_{\text{R}} C_{\text{R}} l - \epsilon_{\text{O}} C_{\text{O}} l = (\epsilon_{\text{R}} - \epsilon_{\text{O}}) Cl \quad (1)$$

where ϵ_{O} and ϵ_{R} are the molar absorptivity of the oxidized and reduced species, respectively,

C_O and C_R the concentration of the electroactive species which only exist in the oxidized and the reduced form, respectively, after a potential-step perturbation, C is the total concentration investigated and l is the light path length.

For an electrode reaction $R \rightleftharpoons O + ne$, we can similarly obtain

$$\Delta A = A_O - A_R = \epsilon_O C_O l - \epsilon_R C_R l = (\epsilon_O - \epsilon_R) C l \quad (2)$$

It is obvious that ΔA varies linearly to C according to these equations. If ΔA is taken as the analytical signal, an analytical method can be established. It can also be found that the analytical sensitivity can be enhanced only when the absorptivity of the product, reduced (as in Eqn. 1) or oxidized (as in Eqn. 2) species by electrochemical methods, is greater than that of the reactant being determined, otherwise the analytical sensitivity will be decreased. Hence it is easy to adjust the analytical sensitivity for the spectroelectroanalytical method presented here.

The selectivity of traditional polarography can be improved by adjusting the potential so as to avoid side electrode reactions. If two ions have polarographic waves that differ by 100 mV, they are considered not to interfere with each other. Also, spectrophotometry presents a certain selectivity because the tested species usually has its particular spectrum and selective chromogenic reagents have been widely used. However, the analytical selectivity may be further improved by combining the two methods, i.e., in a spectroelectroanalytical method, because only those species that not only have the same spectra but also show the same electrochemical behaviour as the tested species will interfere, otherwise interference signals do not exist or are not recorded. In our view, this method can be applied for quantitative analysis for metal ions, organic and biological species etc.

This method is also useful for the determination of the oxidized and reduced species in samples. The analytical signal here can be expressed as follows:

$$\Delta A = \epsilon_O C^O l + \epsilon_R C^R l - \epsilon_R C l = (\epsilon_O - \epsilon_R) C^O l \quad (3)$$

for an electrode reaction $O + ne \rightleftharpoons R$ and

$$\Delta A = \epsilon_R C^R l + \epsilon_O C^O l - \epsilon_O C l = (\epsilon_R - \epsilon_O) C^R l \quad (4)$$

for an electrode reaction $R \rightleftharpoons O + ne$, where C^O and C^R are the concentration of the oxidized and reduced species existing in the sample respectively. Knowing ϵ_O , ϵ_R , l and C , C^O and C^R can easily be determined. In this work, based on the color development reaction between Fe^{3+} and CAS [6] and the electrode reaction of this complex, traces of iron were determined.

As is well known, the spectroelectrochemical signal from a long path-length cell is more sensitive than that from an OTE. However, it seems that there is no quantitative demonstration of this sensitivity. Hence an attempt is made to propose a concept to characterize the sensitivity of the spectroelectrochemical signal (S_{SEC}), i.e., the molar absorbance/potential ratio. It is defined as follows:

$$S_{SEC} = \frac{\Delta A}{C \Delta E} = \frac{A_{10} - A_{0.1}}{C(E_{10} - E_{0.1})} \text{A.U. l mol}^{-1} \text{mV}^{-1} \quad (5)$$

where A_{10} , E_{10} and $A_{0.1}$, $E_{0.1}$ are the absorbance and the potential when $[O]/[R] = 10$ and 0.1 , respectively, C is the total concentration of the tested species, $\Delta A = A_{10} - A_{0.1}$ and $\Delta E = E_{10} - E_{0.1}$.

According to the following equation [1]:

$$\begin{aligned} E &= E^{0'} + \frac{2.303RT}{nF} \log \left(\frac{[O]}{[R]} \right) \\ &= E^{0'} + \frac{2.303RT}{nF} \log \left(\frac{A - A_R}{A_O - A} \right) \end{aligned} \quad (6)$$

where A_O and A_R are the absorbance when the oxidized or reduced state is the only species present, respectively, and A is the absorbance when the oxidized and the reduced state co-exist. Hence we have

$$E_{10} = E^{0'} + \frac{2.303RT}{nF} \log 10 = E^{0'} + \frac{2.303RT}{nF} \quad (7)$$

$$E_{0.1} = E^{0'} + \frac{2.303RT}{nF} \log 0.1 = E^{0'} - \frac{2.303RT}{nF} \quad (8)$$

$$\frac{A_{10} - A_R}{A_O - A_{10}} = 10 \quad (9)$$

$$\frac{A_{0.1} - A_R}{A_O - A_{0.1}} = 0.1 \quad (10)$$

Then we have

$$S_{\text{SEC}} = \frac{1.776 \times 10^{-4} nF \epsilon l}{RT} = \frac{1.776 \times 10^{-4} nF}{RT} \left(\frac{A_O - A_R}{C} \right) \times \text{A.U. l mol}^{-1} \text{ mV}^{-1} \quad (11)$$

Hence S_{SEC} is related to the constant of the spectroelectrochemical cell and the optical absorption behaviour of the tested species. However, it does not depend on the tested concentration.

Molar absorbance/potential ratios obtained from the present experiments and the literature are given in Table 1. They varied with different species and different cells. However, if $\text{Fe}(\text{CN})_6^{3-}/\text{Fe}(\text{CN})_6^{4-}$ is taken as a reference system, the enhancement of the spectroelectrochemical sensitivity of the long path-length thin-layer cell is demonstrated by this concept, as their S_{SEC} values are much larger than that of an OTE cell.

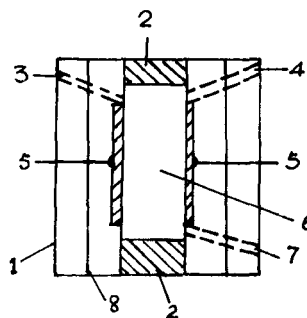


Fig. 1. Vertical section of long path-length thin-layer spectroelectrochemical cell with dual working electrodes. 1 = PTFE plates; 2 = thin polyethylene spacers; 3 = hole for the counter electrode; 4 = hole for the reference electrode; 5 = dual working electrodes; 6 = thin-layer solution; 7 = solution inlet; 8 = light windows.

EXPERIMENTAL

Fabrication of the spectroelectrochemical cell

The spectroelectrochemical cell was fabricated as described [7,8] with some improvements, and is shown in Fig. 1. The cell body was made from PTFE. The dimensions were $1.1 \times 1.1 \times 3$ cm, i.e., nearly the same as for a 1-cm cell in conventional spectrophotometry. The light path length was ca. 0.7 cm and the width of the thin-layer solution was ca. $250 \mu\text{m}$ measured by an optical microscope. The tested solution was injected into the thin-layer space confined by the dual working electrodes and two light windows. The cell was positioned and fixed in the optical path of the spectrophotometer and the light beam was passed

TABLE 1

Molar absorbance/potential ratios

| Cell type ^a | Optical path length (mm) | Species tested | Wavelength monitored (nm) | S_{SEC} (A.U. l mol ⁻¹ mV ⁻¹) | Ref. |
|------------------------|--------------------------|--|---------------------------|---|------|
| A | 9.0 | $\text{Fe}(\text{CN})_6^{3-}/\text{Fe}(\text{CN})_6^{4-}$ | 420 | 6.34 ± 0.01 | 7 |
| | 9.0 | Methylene Blue | 666 | 594 ± 4 | 7 |
| | 9.0 | $\text{Cu}(\text{NH}_3)_4^{2+}/\text{Cu}(\text{NH}_3)_2^+$ | 600 | 0.416 ± 0.001 | 7 |
| | 16.2 | $\text{Fe}(\text{CN})_6^{3-}/\text{Fe}(\text{CN})_6^{4-}$ | 420 | 10.8 | 8 |
| B | 0.24 | $\text{Fe}(\text{CN})_6^{3-}/\text{Fe}(\text{CN})_6^{4-}$ | 420 | 0.400 | 9 |
| | 0.145 | <i>o</i> -Tolidine | 438 | 9.03 | 10 |

^a A = long path-length thin-layer cells; B = normal OTE cells.

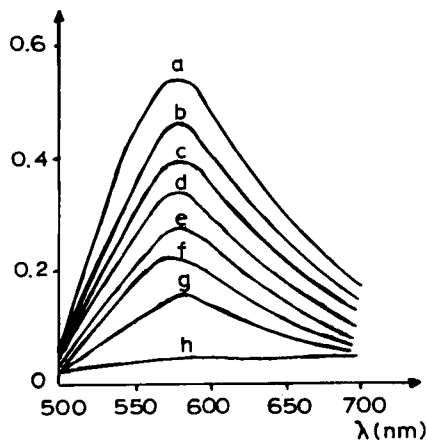


Fig. 2. Thin-layer spectra at different potentials for $1 \mu\text{g ml}^{-1}$ Fe^{3+} + 0.5 mM CAS in 0.02 M acetic acid–0.1 M sodium acetate buffer. Potential (mV): (a) 350, 450; (b) 180; (c) 130; (d) 105; (e) 90; (f) 65; (g) 40; (h) –150, –200.

over the dual working electrode surfaces at grazing incidence.

Instrumentation and reagents

Spectroelectrochemical experiments were carried out with a Model 751G UV–visible spectrophotometer (Shanghai Analytical Instruments

Factory) or Hitachi 557 double-wavelength/double-beam spectrophotometer and a CSH-2 double-electrode potentiostat (Sanming Electronic Factory). The cyclic voltammetric (CV) experiment was carried out with an XJP-821 (B) polarograph (Jiangshu Electroanalytical Instrument Factory). All potentials were measured with respect to an Ag/AgCl, saturated KCl reference electrode and read out from a PHS-3C ion analyser (Shanghai Leici Analytical Instrument Factory) which was precalibrated using a standard electrical cell. A platinum wire was used as the counter electrode and glassy carbon was used as the dual working electrode.

All chemicals were of at least analytical-reagent grade. All solutions were prepared with doubly distilled water. The experiments were done at room temperature.

Procedures

The tested solutions were injected into the spectroelectrochemical cells carefully in order to avoid gas bubbles. The cell was positioned in the optical path. Each of the electrodes was connected to the corresponding pole of the potentiostat. The wavelength and the potential step amplitude were set and optical signals were recorded in situ.

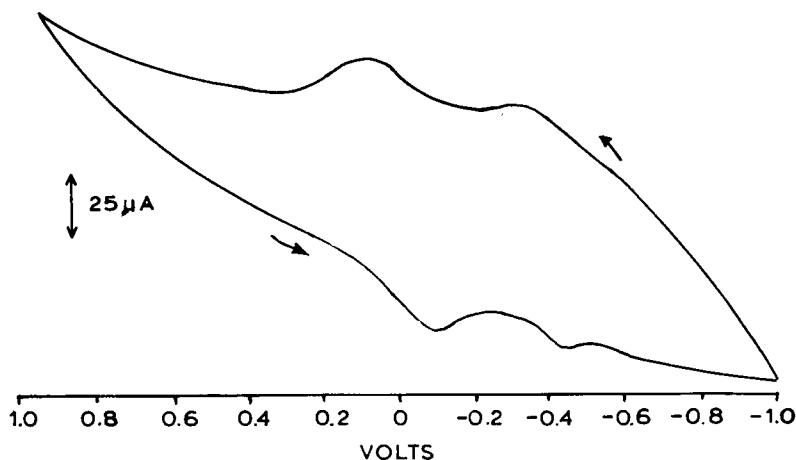


Fig. 3. Thin-layer cyclic voltammetric trace for 0.2 mM Fe^{3+} + 1 mM CAS in 0.02 M acetic acid–0.1 M sodium acetate buffer. Scan rate, 100 mV s^{-1} .

RESULTS AND DISCUSSION

Investigation by CV and SEC

Thin-layer absorption spectra at different potentials are shown in Fig. 2. The absorption maximum of the complex of Fe^{3+} with CAS is 575 nm, while the complex of Fe^{2+} with CAS does not absorb in the visible region, which agrees with the reported data [11]. Moreover, the absorption maximum of CAS alone was measured to be ca. 452 nm, which agrees well with the published value [6].

According to Eqn. 6, we can obtain $E^{0'}$ and n from the intercept and slope of the E vs. $\log[(A - A_R)/(A_O - A)]$ plot after measuring E , A_O , A_R and A at 575 nm. Results of three determinations were $E^{0'} = 91, 92$ and 91 mV and $n = 0.88, 0.93$ and 0.89 .

The results of thin-layer derivative cyclic voltabsorptometry, as shown in Fig. 4, show that two pairs of peaks were observed at 575 nm but only one pair of peaks at 480 nm. As is known, the complex of Fe^{3+} with CAS hardly absorbs at 480 nm but CAS absorbs more strongly at 480 nm than at 575 nm. Hence the peaks at 140 and 40 mV are due to the oxidation and reduction of the complex of iron with CAS, respectively, and these two peaks disappear at 480 nm; the peaks at -350 and -380 mV are due to the oxidation and reduction of CAS, respectively, and they become stronger at 480 nm than at 575 nm.

The results from the thin-layer CV experiment are shown in Fig. 3. In spite of the distortion due to the iR drop of the response from the thin-layer solution, two pairs of potential peaks can easily be found that are located at 0.1, -0.12 V and $-0.27, -0.43$ V. Considering the conclusions drawn from spectroelectrochemistry, it is readily concluded that the former pair of peaks is due to the oxidation and reduction of the complex of iron with CAS and the latter corresponds to the oxidation and reduction of CAS co-existing in the solution.

Potential step amplitude in the process of analysis

Based the spectroelectrochemical properties of the complex of iron with CAS, ΔA between 300 and -200 mV was taken as the analytical signal here. The time to reach a steady absorbance after a single potential step is about 5 min when the width of thin layer is about $300 \mu\text{m}$. Because of the dual working electrodes and therefore a large electrode surface area/solution volume ratio, it is certain that faster exhaustive electrolysis will be achieved with the present cell than that with only one working electrode, and this was verified experimentally.

Effects of the pH and the amount of CAS

pH is an important factor affecting the colour development reaction. In this work, in order to

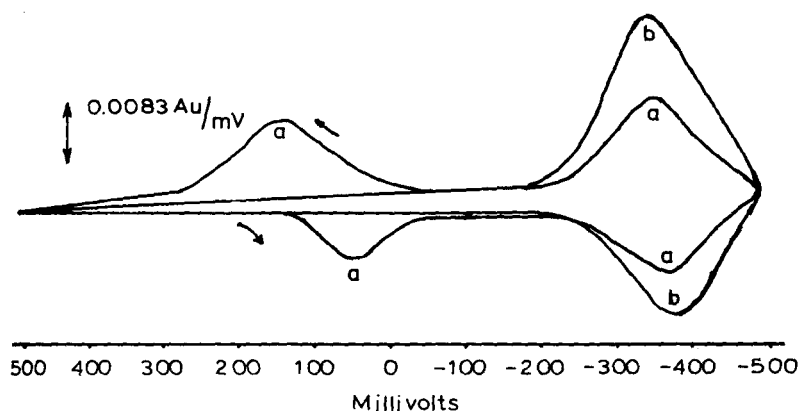


Fig. 4. Thin-layer derivative cyclic voltabsorptometric trace for $3.3 \mu\text{g ml}^{-1} \text{Fe}^{3+} + 0.5 \text{ mM CAS}$ in $0.02 \text{ M acetic acid} - 0.1 \text{ M sodium acetate}$ buffer. Observation wavelength: (a) 575 and (b) 480 nm. Potential scan rate, 1.5 mV s^{-1} .

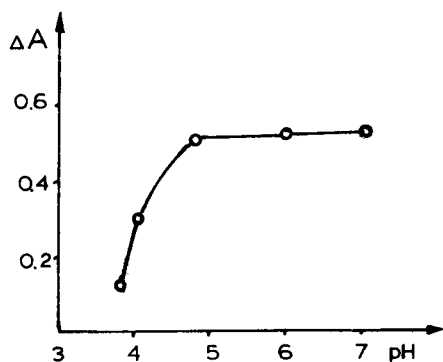


Fig. 5. Effect of pH for $1 \mu\text{g ml}^{-1} \text{Fe}^{3+} + 0.5 \text{ mM CAS}$ in acetic acid–sodium acetate buffer.

investigate the acidity effect and find the optimum concentration of acetic acid and sodium acetate, several supporting electrolytes of various pH were prepared from these components. Then ΔA values when the tested solutions contained $1 \mu\text{g ml}^{-1}$ iron, 0.5 mM CAS and one of these supporting electrolytes were measured. The results showed that the ΔA vs. pH plot (Fig. 5) had two parts. In the first, at $\text{pH} < 4.8$, ΔA increased abruptly with increasing pH. In the second, ΔA had a steady value with increasing pH from 4.8 to 7.0, but experiments proved that a precipitate formed in the solution at $\text{pH} > 6.0$. These results agree with those in [11]. A buffer solution of $0.02 \text{ M acetic acid} - 0.1 \text{ M sodium acetate}$ ($\text{pH} 5.3$) was chosen in this work, as in [11].

The amount of chromogenic reagent is also an important factor in spectrophotometry. Investigation of the effect of the concentration of CAS (Fig. 6) showed that ΔA increased rapidly with increasing concentration of CAS and eventually reached a steady value at CAS concentrations

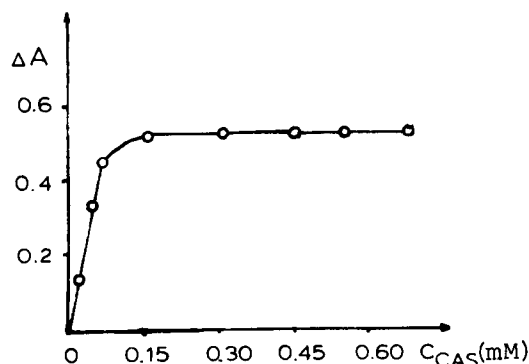


Fig. 6. Effect of the amount of CAS for $1 \mu\text{g ml}^{-1} \text{Fe}^{3+}$ plus different amounts of CAS in $0.02 \text{ M acetic acid} - 0.1 \text{ M sodium acetate}$ buffer.

$> 0.15 \text{ mM}$. The concentration of CAS was selected as 0.5 mM in subsequent work.

Calibration, reproducibility and interferences

The linear calibration graph of ΔA versus iron concentration, C_{Fe} ($\mu\text{g ml}^{-1}$), is described by the equation

$$\Delta A = 0.013 + 0.510C_{\text{Fe}} \quad (r = 0.998, n = 8) \quad (12)$$

where ΔA was measured in the test solution under the chosen conditions. The relative standard deviation for ten complete repetitive determinations of $1 \mu\text{g ml}^{-1}$ of iron was 1.0% .

The effects of other ions on the determination of iron were investigated. No significant interferences in the determination of $1 \mu\text{g ml}^{-1}$ of iron were caused by the following anions and cations (in $\mu\text{g ml}^{-1}$): Zn^{2+} (1000), Ca^{2+} (500), Ni^{2+} (1000), Cd^{2+} (100), Pb^{2+} (600), Mg^{2+} (1000), Be^{2+} (1), Al^{3+} (1), Cu^{2+} (20), NH_4^+ (1000), $\text{S}_2\text{O}_3^{2-}$

TABLE 2

Results of determination of iron in water samples ($\mu\text{g ml}^{-1}$)^a

| Sample | Iron concentration | Found by expt. | Added | Found | Recovery (%) |
|--|--------------------------------|---------------------|-------|-------|--------------|
| Tap water | 0.266 ± 0.018 ^b | 0.264, 0.252, 0.271 | 1.00 | 0.972 | 97.2 |
| Spring water from Yuelu mountain | 0.338 ± 0.013 ^b | 0.336, 0.347, 0.343 | 1.00 | 0.963 | 96.3 |
| Synthetic sample | 1.20 | 1.23, 1.17, 1.18 | 1.00 | 0.990 | 99.0 |

^a Average of three determinations. ^b Obtained by 1,10-phenanthroline spectrophotometry, mean \pm standard deviation ($n = 3$).

(100), F^- (80) and PO_4^{3-} (10). As in conventional spectrophotometry, Al^{3+} ($1 \mu g ml^{-1}$), Be^{2+} ($1 \mu g ml^{-1}$) and Cu^{2+} ($20 \mu g ml^{-1}$) interfere strongly to the determination of $1 \mu g ml^{-1}$ of iron using CAS, so the present technique is more selective, as discussed earlier.

Determination of iron in practical samples

A test solution was prepared by taking different water samples and then adding a supporting electrolyte and CAS. ΔA was then measured and the concentration of iron in samples was calculated using Eqn. 2. Iron was also determined by the 1,10-phenanthroline spectrophotometric method [12] with 4-cm cells. The results of the two methods were in good agreement (Table 2). It can be concluded that the proposed method can be applied for the determination of iron in natural waters and tap water.

The authors record their thanks for financial assistance from the National Education Commission and the Natural Science Funds of the People's Republic of China in support of this work.

REFERENCES

- 1 T. Kuwana and N. Winograd, in A.J. Bard (Ed.), *Electroanalytical Chemistry*, Vol. 7, Dekker, New York, 1974, p. 1.
- 2 W.R. Heineman, F.M. Hawkridge and H.N. Blount in A.J. Bard (Ed.), *Electroanalytical Chemistry*, Vol. 13, Dekker, New York, 1983, p. 1.
- 3 J.F. Tyson and T.S. West, *Talanta*, 26 (1979) 117.
- 4 J.F. Tyson and T.S. West, *Talanta*, 27 (1980) 335.
- 5 J.F. Tyson, *Talanta*, 33 (1986) 51.
- 6 F.J. Langmyhr and K.S. Klausen, *Anal. Chim. Acta*, 29 (1963) 149.
- 7 Q.-J. Xie, Thesis for Master's Degree, Hunan University, Changsha, 1990.
- 8 J. Zak, M.D. Porter and T. Kuwana, *Anal. Chem.*, 55 (1983) 2219.
- 9 S.-H. Song, G.-J. Chong and S.-J. Dong, *Fengxi Huaxue*, 15 (1987) 461.
- 10 D.A. Scherson, S. Sarangapani and F.L. Urbach, *Anal. Chem.*, 57 (1985) 1501.
- 11 Education and Research Institute of Analytical Chemistry, Department of Chemistry, Huangzhou University, Handbook of Analytical Chemistry, Vol. 3, Publishing House of Chemical Industry, Beijing, 1983, p. 480.
- 12 Z. Marzenko, *Spectrophotometric Determination of Elements*, Horwood, Chichester, 1976, Chap. 27.

Stopped-flow kinetic spectrophotometric method for the simultaneous determination of iron, titanium and vanadium

Jianhua Wang and Ronghuan He

Chemistry Department, Yantai Normal College, Yantai (China)

(Received 21st July 1992; revised manuscript received 1st November 1992)

Abstract

A kinetic method for the simultaneous determination of iron, titanium and vanadium is proposed based on their inductive effects on the chromium(VI)–iodide–starch reaction in weakly acidic medium. The reaction was monitored with the stopped-flow spectrophotometric technique. The calibration graphs are linear in the ranges 0–2.2, 0–3.1 and 0–1.8 $\mu\text{g ml}^{-1}$ for Fe(II), Ti(III) and V(IV), respectively, and the detection limits are 0.012, 0.020 and 0.018 $\mu\text{g ml}^{-1}$, respectively. It was found that 100–1000 times higher concentrations of Co^{2+} , Ni^{2+} , Zr^{4+} , Mn^{2+} , Cd^{2+} , Cu^{2+} , Pb^{2+} and trivalent rare earths ions do not interfere with the determination. The method was applied to the determination of Fe, Ti and V in an aluminium alloy and a synthetic sample.

Keywords: Kinetic methods; UV–Visible spectrophotometry; Alloys; Iron; Titanium; Vanadium

The determination of trace amounts of iron, titanium and vanadium is important in metallurgy and environmental analytical chemistry, and there is a growing need for procedures with high sensitivity and selectivity. Among the various procedures, spectrophotometric methods are mostly used in practice [1–3]. The determination of iron has also been carried out recently by flow-injection analysis [4], titanium by indirect polarographic analysis [5] and vanadium by flow-injection analysis with atomic absorption spectrometric detection [6]. In addition, the determination of iron, titanium and vanadium had also been performed by potentiometry [7], total reflection XRF analysis [8] and a thermometric method [9].

Kinetic procedures are generally accepted as having the advantage of high sensitivity. They

have been used successfully for the determination of iron, titanium and vanadium [4,10,11], but serious interferences limited the application of kinetic methods in systems catalysed or induced by more than one species [12]. Therefore, they can only be used for relatively pure materials, or suitable separation procedures must be introduced.

In this work, the kinetics of Fe(II)-, Ti(III)- and V(IV)-induced chromium(VI)–iodide–starch redox reaction systems were investigated with a stopped-flow spectrophotometric technique, and a procedure for the simultaneous determination of iron, titanium and vanadium is proposed.

EXPERIMENTAL

Reagents and solutions

All solutions were prepared with analytical-reagent grade chemicals and redistilled water.

Correspondence to: Jianhua Wang, Chemistry Department, Yantai Normal College, Yantai (China).

A stock standard iron(II) solution containing $125 \mu\text{g ml}^{-1}$ of iron(II) was obtained by dissolving 0.0875 g of $(\text{NH}_4)_2\text{Fe}(\text{SO}_4)_2 \cdot 6\text{H}_2\text{O}$ in water, adjusting the pH to 2.1 and diluting to 100 ml. This solution must be prepared fortnightly.

A stock standard solution containing $150 \mu\text{g ml}^{-1}$ of titanium(III) was prepared by dissolving 0.050 g of TiO_2 in the mixture of 2.5 g $(\text{NH}_4)_2\text{SO}_4$ and 5 ml of H_2SO_4 (1 + 1), reducing Ti(IV) to Ti(III) with Jones reductor prepared according to the literature [13], adjusting the pH to 2.1 and diluting to 200 ml. This solution can be used for 48 h.

A stock standard solution containing $100 \mu\text{g ml}^{-1}$ of vanadium(IV) was prepared by dissolving 0.0178 g of V_2O_5 in 5 ml of 2 mol l^{-1} HCl, reducing the V(V) to V(IV) with Jones reductor, adjusting the pH to 2.1 and diluting to 100 ml. This solution was stable for 170 h.

Working standard solutions of different concentrations were obtained by dilution of the stock standard solutions.

Other solutions prepared were $4.2 \times 10^{-3} \text{ mol l}^{-1}$ chromium(VI) (pH 2.1) and $3.6 \times 10^{-2} \text{ mol l}^{-1}$ potassium iodide (pH 2.1), the latter prepared daily. The carrier solution was redistilled water acidified with dilute HCl to pH 2.1 (containing 0.1% of starch).

Apparatus and procedure

The reaction was followed at 590 nm on a Beijing Optical Instruments Factory (BOIF) (Beijing) WFZ 900D₄ spectrophotometer, which was equipped with a $10\text{-}\mu\text{l}$ flow cell and a device for thermostatic control of the cell, connected to a Syntone (Beijing) Model FIA-2400 analyser with two peristaltic pumps of ten channels and a sixteen-way injection valve, which was controlled by a computer. The sample solutions were introduced via the valve with a sample loop of $40 \mu\text{l}$. The flow manifold is shown in Fig. 1. The inner diameter of the PTFE tubing was 0.5 mm and the lengths of the mixing coils were $L_1 = 300 \text{ mm}$ and $L_2 = 150 \text{ mm}$. The flow-rate of the carrier solution was 3.8 ml min^{-1} and those of Cr(VI) and iodide solutions were both 3.2 ml min^{-1} . The temperature was controlled with a Syntone FIA-

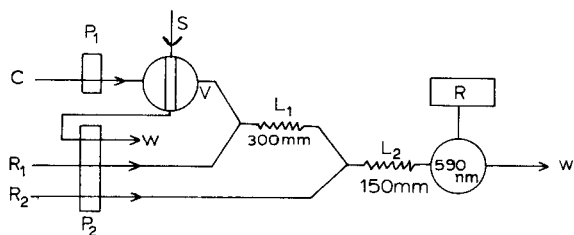


Fig. 1. The manifold used in the determination. P_1 , P_2 = peristaltic pumps; V = 16-way injection valve; L_1 , L_2 = mixing coils; R = controlling and recording system; C = carrier; S = sample; W = waste; $R_1 = 3.6 \times 10^{-2} \text{ mol l}^{-1}$ KI solution; $R_2 = 4.2 \times 10^{-3} \text{ mol l}^{-1}$ Cr(VI) solution.

TO1 thermostat and pH was measured on a PXS-5 pH meter.

The sample solution was transported by a carrier solution consisting of starch dissolved in redistilled water. This stream was mixed first with the solution of potassium iodide inside coil L_1 and then with chromium(VI) solution in coil L_2 before entering the flow cell through the thermostat. The rate of formation of the coloured product was measured at 590 nm with respect to a reagent blank. The absorbances were measured and stored in the computer, and were evaluated automatically during the analysis. Measurements were made 5, 10 and 20 s after the injection of the sample solution.

Principles of the determination

Given the following kinetically prohibited reaction:



suppose that I_1 , I_2 and I_3 are the inductors of the reaction. The induced reactions have certain induction factors, and it is assumed that there are no interactions between inductors or between intermediates. The concentration of the product, P, arising from each induced reaction after a given time t should, under fixed conditions and provided that the reagent is not exhausted ($t \ll t_\infty$), be proportional to the concentration of the corresponding inductor, i.e.

$$[P_1] = k_1[I_1], [P_2] = k_2[I_2] \text{ and } [P_3] = k_3[I_3]$$

where each factor k_i is a function of the inductive rate constant, the concentration of reagent (Ox or Re) and temperature. $[I_i]$ is the analytical

concentration of an inductor which remains unchanged during the analysis.

In a reaction system simultaneously induced by I_1 , I_2 and I_3 the absorbance (A) at a certain wavelength by the complex formed between the product of the induced reaction and a colour reagent can be expressed as:

$$\begin{aligned} A &= k_{10}[P_1] + k_{20}[P_2] + k_{30}[P_3] \\ &= k_{10}k_1[I_1] + k_{20}k_2[I_2] + k_{30}k_3[I_3] \\ &= K_1[I_1] + K_2[I_2] + K_3[I_3] \end{aligned}$$

At certain times t_1 , t_2 and t_3 , the absorbances should be

$$A_{t_1} = K_{11}[I_1] + K_{12}[I_2] + K_{13}[I_3]$$

$$A_{t_2} = K_{21}[I_1] + K_{22}[I_2] + K_{23}[I_3]$$

$$A_{t_3} = K_{31}[I_1] + K_{32}[I_2] + K_{33}[I_3]$$

The conditional parameters K_{11} , K_{12} , K_{13} , K_{21} , K_{22} , K_{23} , K_{31} , K_{32} and K_{33} can be determined in the reaction systems induced only by I_1 , I_2 or I_3 with the aid of graphs of absorbance

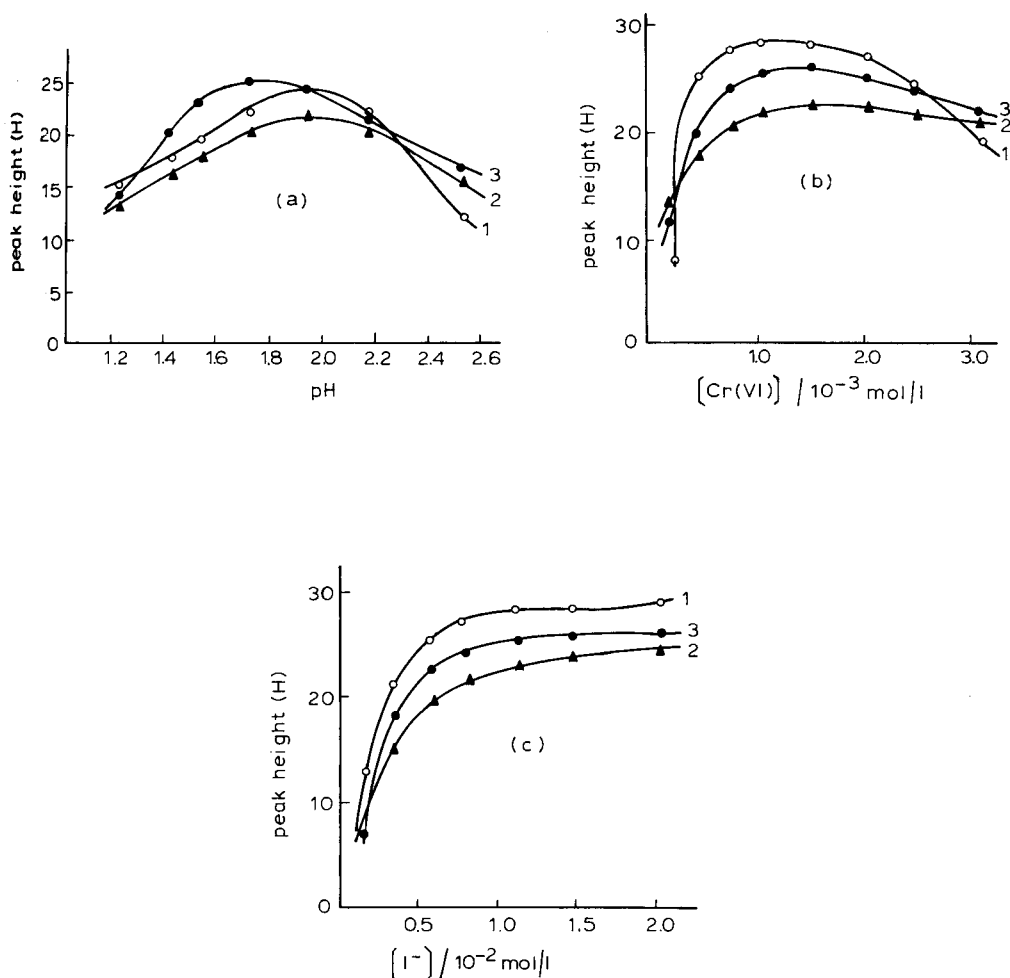


Fig. 2. Influence of variables on the determination ($t = 20$ s). (a) Influence of pH: $[Cr(VI)] = 1.5 \times 10^{-3} \text{ mol l}^{-1}$, $[I^-] = 1.2 \times 10^{-2} \text{ mol l}^{-1}$. (1) $[Fe(II)] = 0.6 \mu\text{g ml}^{-1}$; (2) $[Ti(III)] = 0.6 \mu\text{g ml}^{-1}$; (3) $[V(IV)] = 0.6 \mu\text{g ml}^{-1}$. (b) Influence of $[Cr(VI)]$: $[I^-] = 1.2 \times 10^{-2} \text{ mol l}^{-1}$, pH = 2.1. (1) $[Fe(II)] = 0.6 \mu\text{g ml}^{-1}$; (2) $[Ti(III)] = 0.6 \mu\text{g ml}^{-1}$; (3) $[V(IV)] = 0.6 \mu\text{g ml}^{-1}$. (c) Influence of $[I^-]$: $[Cr(VI)] = 1.5 \times 10^{-3} \text{ mol l}^{-1}$, pH = 2.1. (1) $[Fe(II)] = 0.6 \mu\text{g ml}^{-1}$; (2) $[Ti(III)] = 0.6 \mu\text{g ml}^{-1}$; (3) $[V(IV)] = 0.6 \mu\text{g ml}^{-1}$;

versus inductor concentration at times t_1 , t_2 and t_3 , and the concentrations of the inductors in the sample can then be calculated by solving the above equations.

In this work, the stop times were chosen as 5, 10 and 20 s, and the absorbances were represented by relative peak heights.

RESULTS AND DISCUSSION

Influence of acidity

Determinations were made in different acidic media, such as HNO_3 , H_2SO_4 , HCl , H_3PO_4 and HClO_4 . The results indicate that the highest sensitivity can be obtained in HCl medium. Figure 2a shows that the concentration of HCl had a significant influence on the chromium(VI)–iodide reaction. It is obvious that the peak heights of the reaction systems reach maxima in the pH ranges 1.6–2.2, 1.6–2.6 and 1.4–2.2, for the Fe(II)-, Ti(III)- and V(IV)-induced reactions, respectively. The results also show that the rates of induced and non-induced reactions both increased rapidly at $\text{pH} < 1.8$, resulting in a poorer reproducibility; $\text{pH} = 2.1$ was chosen for the analysis.

Influence of reagent concentrations

The effect of chromium(VI) and iodide concentrations on the relative peak heights are shown in Fig. 2b and c, respectively. It can easily be seen that they have a considerable effect on the determination. Initially, increasing the chromium(IV) concentration resulted in a significant increase in relative peak heights and the sensitivity was improved, but a plateau was reached and the peak heights remained unchanged for concentration ranges of $[\text{Cr(VI)}] = 0.5 \times 10^{-3}$ – 2.0×10^{-3} , 1.0×10^{-3} – 3.0×10^{-3} and 0.75×10^{-3} – 2.5×10^{-3} mol l^{-1} for Fe(II), Ti(III) and V(IV), respectively. $[\text{Cr(VI)}] = 1.5 \times 10^{-3}$ mol l^{-1} was chosen for the determination. On the other hand, the relative peak height increased continuously with increasing the iodide concentration, but the reproducibility deteriorated at $[\text{I}^-] > 1.8 \times 10^{-2}$ mol l^{-1} . The concentration chosen was $[\text{I}^-] = 1.2 \times 10^{-2}$ mol l^{-1} .

Influence of temperature and stop time

It is known that the sensitivity of iodine–starch complex procedures depends strongly on temperature [14]. The results indicate that higher sensitivity could be obtained with an increase in temperature in the range 15–50°C, but the complex tended to be unstable at higher temperatures, resulting in poor reproducibility, and the complex decomposed above 80°C. A temperature of $25 \pm 0.1^\circ\text{C}$ was chosen for the determination.

The sensitivity of the determination increased with time in the range of 0–50 s and it remained unchanged or decreased slightly after 50 s. Stop times of 5, 10 and 20 s were chosen only with a view to increasing the sampling rate.

Calibrations and interferences

Different amounts of iron(II), titanium(III) and vanadium(IV) standard solutions were introduced into the reaction systems under the optimum conditions and the relative peak heights were measured at times of 5, 10 and 20 s. The following linear relationships were obtained between relative peak heights (H) and iron(II), titanium(III) and vanadium(IV) concentrations:

$$\begin{aligned} H_{\text{Fe}}(5) &= 23.4658[\text{Fe}] - 6.487, r = 0.9991 \\ H_{\text{Fe}}(10) &= 41.1785[\text{Fe}] - 4.7865, r = 0.9998 \\ H_{\text{Fe}}(20) &= 48.3578[\text{Fe}] - 1.3586, r = 0.9988 \\ H_{\text{Ti}}(5) &= 18.4553[\text{Ti}] - 2.4346, r = 0.9989 \\ H_{\text{Ti}}(10) &= 29.6456[\text{Ti}] - 1.8576, r = 0.9999 \\ H_{\text{Ti}}(20) &= 36.3556[\text{Ti}] - 0.4834, r = 0.9997 \\ H_{\text{V}}(5) &= 21.3874[\text{V}] - 5.8763, r = 0.9989 \\ H_{\text{V}}(10) &= 38.9587[\text{V}] - 4.2536, r = 0.9998 \\ H_{\text{V}}(20) &= 45.2785[\text{V}] - 3.1257, r = 0.9998 \end{aligned}$$

Linear calibration graphs were obtained for 0–2.2 $\mu\text{g ml}^{-1}$ Fe(II), 0–3.1 $\mu\text{g ml}^{-1}$ Ti(III) and 0–1.8 $\mu\text{g ml}^{-1}$ V(IV), and the working equations were derived as

$$\begin{aligned} H(5) &= 23.4658[\text{Fe}] + 18.4553[\text{Ti}] \\ &\quad + 21.3874[\text{V}] - 14.7869 \\ H(10) &= 41.1785[\text{Fe}] + 29.6456[\text{Ti}] \\ &\quad + 38.9587[\text{V}] - 10.8977 \\ H(20) &= 48.3578[\text{Fe}] + 36.3556[\text{Ti}] \\ &\quad + 45.2785[\text{V}] - 4.9677 \end{aligned}$$

TABLE 1

Influence of foreign ions on the determination of $1.0 \mu\text{g ml}^{-1}$ Fe(II), Ti(III), and V(IV)

| Ion | Tolerance ratio ^a | Ion | Tolerance ratio ^a | Ion | Tolerance ratio ^a |
|---------|------------------------------|---------|------------------------------|--------|------------------------------|
| Al(III) | 1000 | Mn(II) | 200 | Sn(II) | 25 |
| As(III) | 10 | Mo(VI) | 50 | Th(IV) | 500 |
| Cd(II) | 300 | Ni(II) | 300 | Ti(IV) | 250 |
| Co(II) | 300 | Pb(II) | 50 | U(IV) | 1 |
| Cu(II) | 100 | Re(III) | 300 | W(VI) | 300 |
| Fe(III) | 20 | Sb(III) | 1 | Zr(IV) | 100 |

^a w/w for 5% error.

It is obvious that there is a term in each working equations due to the intercept of the calibration graph. This term must be taken into account, otherwise there will be large errors in the determinations.

A mixture of $1.0 \mu\text{g ml}^{-1}$ Fe(II), $1.0 \mu\text{g ml}^{-1}$ Ti(III) and $1.0 \mu\text{g ml}^{-1}$ V(IV) was analysed six times, and the recoveries were 93.7–107.9, 93.2–108.4 and 92.6–106.3% for iron, titanium and vanadium, respectively. The detection limits, calculated as three times the standard deviation of the blank, were $0.012 \mu\text{g ml}^{-1}$ Fe, $0.020 \mu\text{g ml}^{-1}$ Ti and $0.018 \mu\text{g ml}^{-1}$ V. The results also showed that there were no interactions between Fe(II), Ti(III), V(IV) and the intermediates.

The influence of foreign ions on the determination was studied. In each instance, an appropriate amount of a foreign ion was added to standard Fe(II), Ti(III) and V(IV) solutions and the recommended procedure was applied. The

ions in Table 1 can be tolerated up to the indicated amounts within an error of $\pm 5\%$.

Application of the method

A 0.200-g amount of aluminium alloy was dissolved in 10 ml of a mixture of H_2O_2 (30%) and 6 mol l^{-1} HCl (1 + 10) and the solution was heated to boiling for about 30 min, then reduced with Jones reductor, the pH was adjusted to 2.1 and the solution was diluted to 200 ml.

Another solution was prepared containing a mixture of FeCl_3 , TiO_2 and V_2O_5 . It was treated similarly to that above and diluted to 1000 ml.

The amounts of Fe(II), Ti(III), and V(IV) were determined with the proposed procedure and also by atomic absorption spectrometry (AAS). The results are summarized in Table 2. It can be seen that the results of the two methods agreed well.

REFERENCES

- 1 N. Zhou, Y. Gu and X. Yao, *Talanta*, 36 (1989) 855.
- 2 D.L. Chang and X.L. Zeng, *Fenxi Huaxue*, 17 (1989) 520.
- 3 S.P. Arga and J.L. Malla, *J. Indian Chem. Soc.*, 64 (1987) 777.
- 4 T.D. Yerian, T.P. Hadjiioannou and G.D. Christian, *Talanta*, 33 (1986) 547.
- 5 Y. Castrillejo, R. Pardo and E. Barrado, *Electroanalysis*, 1 (1989) 181.
- 6 B. Patel, S.J. Haswell and R. Grzeskowiak, *J. Anal. At. Spectrom.*, 4 (1989) 195.
- 7 S. Yang and H. Tong, *Huaxue Xuebao*, 45 (1987) 711.
- 8 C.T. Yap and K.V.R. Gunawardena, *Appl. Spectrosc.*, 43 (1989) 702.

TABLE 2

Determination of iron, titanium and vanadium in an aluminium alloy and a synthetic sample

| Sample | Fe(II) content ^a ($\mu\text{g ml}^{-1}$) | | Ti(III) content ^a ($\mu\text{g ml}^{-1}$) | | V(IV) content ^a ($\mu\text{g ml}^{-1}$) | |
|------------------|---|-------|--|-------|--|-------|
| | Suggested method (R.S.D., %) | AAS | Suggested method (R.S.D., %) | AAS | Suggested method (R.S.D., %) | AAS |
| Aluminium alloy | 1.256 (3.8) | 1.217 | 0.987 (4.1) | 1.033 | 0.465 (4.4) | 0.449 |
| Synthetic sample | 0.735 (4.1) | 0.714 | 2.432 (2.9) | 2.403 | 1.845 (3.2) | 1.904 |

^a Mean of six determinations

- 9 R.M. Marce, M. Calull, J. Torres and F. Borrull, *Analyst*, 113 (1988) 505.
- 10 Y. Zhu and J. Shao, *Fenxi Huaxue*, 15 (1987) 865.
- 11 F. Lazaro, M.D. Luque de Castro and M. Valcarcel, *Anal. Lett.*, 18 (1985) 1209.
- 12 A. Moreno, M. Silva, P. Perez-Bendito and M. Valcarcel, *Anal. Chim. Acta*, 157 (1984) 333.
- 13 A.T. Faizullah and A. Townshend, *Anal. Chim. Acta*, 167 (1985) 225.
- 14 G.L. Hatch, *Anal. Chem.*, 54 (1982) 2002.

Unique resolution of hidden minor peaks in multidetection chromatography by first-order differentiation and orthogonal projections

Yi-zeng Liang¹ and Olav M. Kvalheim

Department of Chemistry, University of Bergen, N-5007 Bergen (Norway)

(Received 4th November 1992; revised manuscript received 8th December 1992)

Abstract

A new method for unique resolution of multiwavelength chromatograms with a minor analyte completely overlapped by a major one in time direction and with no selective wavelength regions for any of the analytes is derived in this paper. An orthogonal projection is first utilized to obtain the chromatographic profile of the minor analyte. Differentiation of the two-way data matrix in the time direction is subsequently performed to determine the retention time of the chromatographic peak maximum of the major analyte. Based upon these two pieces of information, two approaches for estimating spectra and chromatographic profiles of the pure analytes are developed. A direct approach, which assumes local symmetry in the proximity of the chromatographic peak maximum of the major analyte, and an optimization approach using the estimated peak maximum of the major analyte as objective function.

Keywords: Chromatography; Derivative chromatography; Minor peak detection; Multidetection; Peak detection method

Detection and resolution of a minor chromatographic peak completely hidden under a major one represent a task of major practical significance in analytical chemistry. One way to deal with the problem is to use spectroscopic detectors that are able to produce selective regions even for very similar compounds. Selective information can readily be detected by using latent-projective graphs/datascope [1] or eigenstructure tracking analysis [2] as implemented in the heuristic evolving latent projections (HELP) method. If both analytes possess selective spectral regions, the pooled elution profile for each analyte can be

obtained by local principal component analysis at these wavelengths and the spectra of the pure analytes subsequently extracted by means of a least-squares procedure [1].

In the absence of spectral selectivity, only detection of the retention time intervals for elution of the minor and major analyte seems feasible with available approaches [1,3]. However, since selective chromatographic regions usually exist for the major analyte at the start and/or end of elution, the spectrum of the major analyte can be obtained by principal component analysis of these local regions. Making the assumption that the major analyte has at least one spectral maximum that is not coinciding with the maxima of the unknown spectrum of the minor analyte, the elution profile of the minor analyte can be obtained by using an approach developed by Milano et al. [4]. The first-order derivative of the absorbance

Correspondence to: O.M. Kvalheim, Department of Chemistry, University of Bergen, N-5007 Bergen (Norway).

¹ On leave from Department of Chemistry and Chemical Engineering, Hunan University, Changsha (China).

with respect to wavelength, dA/dw , is by definition zero for an analyte at the wavelengths corresponding to local maxima in the absorbances for that analyte. Thus, the elution profile of the minor analyte can, at least in principle, be obtained in the time direction from the first-order derivative in the spectral direction at the local spectral maxima for the major analyte.

The approach developed by Milano et al. [4] has certain drawbacks. According to Fell et al. [5], the method suffers from lack of sensitivity, except for sharp peaks whose spectral maxima are close to the observation wavelengths. For this reason, we propose that the chromatographic profile of the minor analyte is estimated by use of orthogonal projections as developed by Lorber [6]. The contributions of the major analyte to the mixture spectra are removed by projecting on the spectrum of the major analyte. The relative chromatographic profile of the minor analyte is thus obtained. The procedure is based upon the observation that a chromatographic profile of a resolved analyte maps a straight line in multivariate wavelength space [1]. There is a one-to-one correspondence between the concentrations mapped by the elution profile and their positions on this straight line. A key observation used in the derivation of the chromatographic profile of the minor analyte is that any projection of the points on this straight line onto another straight line conserves the mutual relations between the concentrations.

Unfortunately, as the spectrum is unknown for the minor analyte, the chromatographic profile of the major analyte cannot be obtained neither by projections nor by the derivative procedure of Milano et al. [4]. In principle, the background correction procedure developed by Karstang and Kvalheim [7] could be used to locate the positions of the absorbance maxima of the minor analyte. The spectrum of an unknown analyte is modelled by using positivity constraints to refine the residual spectrum. Differentiation of the mixture spectra then provides the chromatographic profile of the major analyte at the absorption maxima for the minor analyte. However, this approach cannot be recommended for cases with similar spectra and with the concentration of the major ana-

lyte being more than an order of magnitude larger than that of the minor one.

It appears that only the spectrum of the major analyte and the chromatographic profile of the minor analyte can be obtained, and that we are facing a least-squares problem with no unique solution. There is, however, one characteristic of chromatographic elution that has so far been overlooked in the analysis, namely, that every eluting analyte provides a peak with one and only one maximum. With this information at hand, we shall proceed to find a unique solution to the problem.

The aim of the present work is thus to develop reliable methods especially addressing the resolution of a minor peak completely overlapped by a major one in chromatograms acquired on multi-detector instruments. The outline of the work is as follows. First, necessary and sufficient assumptions for resolution in the case discussed above are given. Second, the absorbance matrix is differentiated in time and wavelength direction and some important properties of the derivative matrices are developed. Third, orthogonal projections are used to estimate the chromatographic profile of the minor analyte. Fourth, the derivative absorbance matrix obtained in the time direction is utilized to locate the maximum on the chromatographic profile of the major analyte. This information together with the characteristics of chromatographic elution, i.e., one maximum for each peak, is utilized to derive two approaches for estimating spectra and chromatographic profiles of the pure analytes. The performance of the developed methods is illustrated on simulated data.

THEORY

Assumptions

In the case where a minor analyte is completely overlapped by a major one in the chromatographic direction, and the spectra of the major and minor analyte overlap completely in the sense that no selective regions exist in the spectral direction, unique resolution can only be accomplished if certain assumptions are fulfilled.

First, the spectra must either be shifted or have slightly different shape. Furthermore, although the elution profile of the minor analyte is assumed completely overlapped by the major one, some selective chromatographic regions must exist in the beginning and/or end of elution for the major analyte from which the pure spectrum of the major analyte can be extracted. A final assumption is that the chromatographic peak max-

ima of the minor and major analyte do not coincide.

First-order two-way differentiation

Data from hyphenated chromatographic instruments are collected in time and wavelength direction. Let matrix A with N rows and M columns be the two-way data array of spectral intensities [absorbances in liquid chromatography

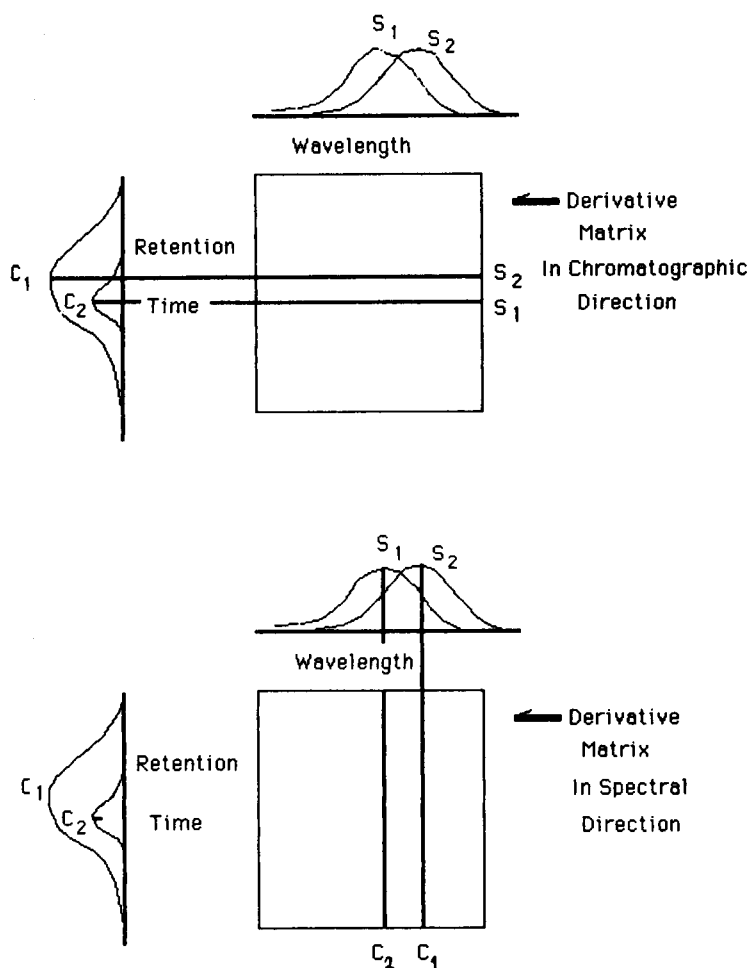


Fig. 1. The upper part of the illustration shows that the first-order derivative matrix in the time direction contains the pure spectra of the minor and major analyte at the retention times corresponding to peak maximum of the major and minor analyte, respectively. Similarly, the lower part illustrates that the first-order derivative matrix in the wavelength direction contains the pure chromatographic profiles of the minor and major analyte at the wavelengths corresponding to maximum absorbance of the major and minor analyte, respectively.

with diode array detection (LC-DAD)]. Retention time is defining the rows and wavelength the columns in the matrix. Neglecting the error term, the matrix \mathbf{A} for a mixture of two analytes can be decomposed as a sum of two bilinear matrices, one for each analyte

$$\mathbf{A} = \mathbf{c}_1 \mathbf{s}_1^T + \mathbf{c}_2 \mathbf{s}_2^T \quad (1)$$

In Eqn. 1, $\{c_i; i = 1, 2\}$ and $\{s_i^T; i = 1, 2\}$ are the (presently unknown) chromatographic and spectral profiles, respectively, of the two analytes. Transposition T is used to symbolize a row vector as opposed to a column vector.

Assuming both w and t to be continuous, the element $a(t, w)$ of the data matrix \mathbf{A} at time t and wavelength w can be written as

$$a(t, w) = c_1(t)s_1(w) + c_2(t)s_2(w) \quad (2)$$

Thus, every element in \mathbf{A} can be described by the functions $\{c_i(t); i = 1, 2\}$ and $\{s_i(w); i = 1, 2\}$. Equation 2 describes the bilinearity of the matrix \mathbf{A} . Furthermore, Eqn. 2 shows that the absorbance matrix can be differentiated in either time or wavelength direction:

$$\begin{aligned} da(t, w)/dt &= s_1(w) dc_1(t)/dt \\ &+ s_2(w) dc_2(t)/dt \end{aligned} \quad (3a)$$

$$\begin{aligned} da(t, w)/dw &= c_1(t) ds_1(w)/dw \\ &+ c_2(t) ds_2(w)/dw \end{aligned} \quad (3b)$$

The derivatives may be expressed in vectorial form:

$$\begin{aligned} d\mathbf{a}_i^T(t)/dt &= \mathbf{s}_1^T dc_1(t)/dt + \mathbf{s}_2^T dc_2(t)/dt \\ (i = 1, 2, \dots, N-1) \end{aligned} \quad (4a)$$

$$\begin{aligned} d\mathbf{a}_j(w)dw &= \mathbf{c}_1 ds_1(w)/dw + \mathbf{c}_2 ds_2(w)/dw \\ (j = 1, 2, \dots, M-1) \end{aligned} \quad (4b)$$

Here $\{d\mathbf{a}_i^T(t)/dt; i = 1, 2, \dots, N-1\}$ are the row vectors in the derivative matrix $d\mathbf{A}/dt$ obtained by differentiation in chromatographic (time) direction, while $\{d\mathbf{a}_j(w)/dw; j = 1, 2, \dots, M-1\}$ represents the column vectors for the derivative matrix $d\mathbf{A}/dw$ obtained by differentiation in the spectral (wavelength) direction.

The derivative function has a very attractive feature: it becomes zero when the original function has a maximum. This fact means that the

local chemical rank (number of analytes contributing in a specific wavelength or retention time region) in the two derivative matrices drops from two to one at the maxima. If the sampling rate in chromatographic direction and the digital spectral resolution is high it should be possible to locate the maxima directly by evaluating the local rank of the two derivative matrix by means of eigenstructure tracking analysis (ETA) [2]. By ETA, the evolving number of analytes in time and wavelength directions is revealed by moving a window of size $2 \times M$ and $N \times 2$, respectively, through the derivative matrices obtained by Eqns. 4a and 4b, starting from the first wavelength and retention time. The chromatographic profiles $\{c_i; i = 1, 2\}$ and spectra $\{s_i^T; i = 1, 2\}$ of two overlapping analytes might thus be found directly from the two derivative matrices by locating the maxima on the chromatographic and spectral profiles of the analyte. This is illustrated in Fig. 1.

As discussed in the introduction, the pure spectrum s_1 of the major analyte can easily be extracted by principal component analysis of the selective chromatographic regions for the major analyte [1]. Thus, Eqn. 4b offers a possibility for directly determining the chromatographic profile of the minor analyte since, at the spectral maxima of the major analyte, Eqn. 4b shows that the derivative in the spectral direction is proportional to the chromatogram of the minor analyte, i.e., $d\mathbf{a}_j(w)/dw = c_2 ds_2(w)/dw$. However, we shall develop another approach for this task in the next section.

Chromatographic profile of the minor analyte

The chromatographic profile of the minor analyte can be estimated by utilizing the orthogonal projection technique introduced by Lorber [6]. Neglecting the error term, the mixture spectrum \mathbf{a}_i^T at the i th retention time in the matrix \mathbf{A} can be expressed by

$$\mathbf{a}_i^T = c_{i1} \mathbf{s}_1^T + c_{i2} \mathbf{s}_2^T \quad (i = 1, 2, \dots, N) \quad (5)$$

The coefficients $\{c_{ij}; i = 1, 2, \dots, N; j = 1, 2\}$ are the (presently unknown) values of the chromatographic profiles of the two analytes. As shown in Ref. 1, the pure spectrum of the major analyte \mathbf{s}_1^T can be obtained by means of the HELP method.

With this information at hand, the chromatographic profile of the minor analyte can be obtained by using the projection technique introduced by Lorber [6]. An orthogonal projection matrix is constructed by using the pure spectrum \mathbf{s}_1^T of the major analyte:

$$\mathbf{P}_1 = \mathbf{I} - \mathbf{s}_1 \mathbf{s}_1^T / (\mathbf{s}_1^T \mathbf{s}_1) \quad (6)$$

In Eqn. 6, \mathbf{I} is the identity matrix with dimension $M \times M$. The orthogonal projection matrix \mathbf{P}_1 can be used to obtain a new vector which is orthogonal to \mathbf{s}_1 and proportional to the chromatographic profile of the second (minor) analyte. Application of the projection matrix \mathbf{P}_1 (Eqn. 6) on the mixture spectrum at retention time i (Eqn. 5) gives

$$\begin{aligned} \mathbf{a}_i^T \mathbf{P}_1 &= (c_{i1} \mathbf{s}_1^T + c_{i2} \mathbf{s}_2^T) [\mathbf{I} - \mathbf{s}_1 \mathbf{s}_1^T / (\mathbf{s}_1^T \mathbf{s}_1)] \\ &= c_{i2} [\mathbf{s}_2^T - (\mathbf{s}_2^T \mathbf{s}_1) / (\mathbf{s}_1^T \mathbf{s}_1) \mathbf{s}_1^T] \\ &= c_{i2} (\mathbf{s}_2^T - \beta \mathbf{s}_1^T) \end{aligned} \quad (7)$$

The scalar β in Eqn. 7 is defined as the ratio $(\mathbf{s}_2^T \mathbf{s}_1) / (\mathbf{s}_1^T \mathbf{s}_1)$. Equation 7 shows that the contribution of the major analyte to the mixture spectrum at retention time i is deleted by the projection. The procedure can be repeated for all the mixture spectra $\{\mathbf{a}_i^T; i = 1, 2, \dots, N\}$. In this way, we obtain a chromatographic profile which is proportional to the profile of the minor analyte. The profile proportional to \mathbf{c}_2 is obtained simply by calculating the norm of the row vectors $\{\mathbf{a}_i^T \mathbf{P}_1; i = 1, 2, \dots, N\}$ obtained by Eqn. 7 and rearranging:

$$c_{i2} = \|\mathbf{a}_i^T \mathbf{P}_1\| / \|(\mathbf{s}_2 - \beta \mathbf{s}_1)\| \quad (i = 1, 2, \dots, N) \quad (8)$$

Defining $d_i = \|\mathbf{a}_i^T \mathbf{P}_1\|$ and $\mu = \|(\mathbf{s}_2 - \beta \mathbf{s}_1)\|$ and rewriting Eqn. 8 in vectorial form, we obtain

$$\mathbf{c}_2 = \mu^{-1} \mathbf{d} \quad (9)$$

Here $\mathbf{d} = (d_1, d_2, \dots, d_N)^T$ and $\mathbf{c}_2 = (c_{12}, c_{22}, \dots, c_{N2})^T$.

Retention time for peak maximum of the major analyte

With the spectrum of the major analyte and the chromatographic profile of the minor analyte

at hand, Eqn. 4a shows that if the chromatographic peak maximum of the major analyte can be located, the spectrum of the minor analyte can be derived. The chromatographic profile of the major analyte can subsequently be estimated by simple least squares (Eqn. 12 below).

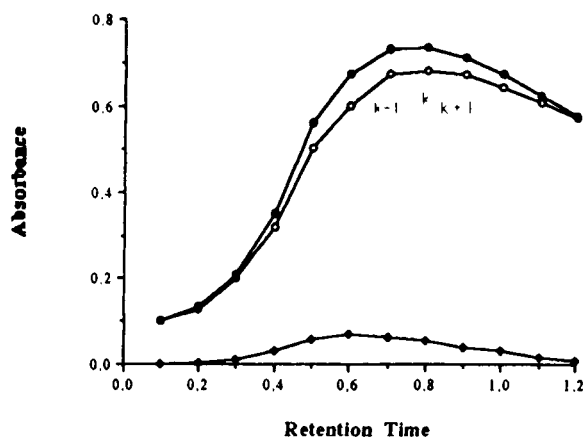
The estimation of the chromatographic peak maximum of the major analyte can be done without making any further assumptions than those discussed at the beginning of the Theory section. The positivity constraint on the pure spectra of the two analytes shows that the sign of the elements of the vectors in the derivative matrix in chromatographic direction is completely determined by the sign of $dc_1(t)/dt$ and $dc_2(t)/dt$. From the relative chromatographic profile for the minor analyte, obtained by orthogonal projections, one knows already the sign of $dc_2(t)/dt$ and thus the second term in Eqn. 4a for every retention time $(1, 2, \dots, N-1)$. Furthermore, in case of a minor chromatographic peak completely overlapped by a major one, there are only two possible overlapping modes: either the chromatographic peak maximum of the minor analyte appears before the chromatographic peak maximum of the major analyte, or the other way round. For both possibilities, the retention time corresponding to the chromatographic peak maximum for the major analyte can be determined. We shall examine in detail the case where the maximum of the minor peak appears before the maximum of the major peak.

In the proximity of the chromatographic peak maximum of the major analyte, the contribution of the minor analyte to Eqn. 4a is negative in the case where the maximum of the minor peak appears before the maximum of the major one. This is obvious since the concentration of the minor analyte is decreasing in this region. After the retention time corresponding to peak maximum of the major analyte, the first-order derivative mixture spectrum $d\mathbf{a}_i^T(t)/dt$ becomes negative at every wavelength, since after peak maximum the concentration of the major analyte is decreasing and thus its contributions to the derivative mixture spectrum becomes negative at all wavelengths. Before peak maximum, however, the contribution from the first term in Eqn. 4a, i.e.,

$s_1^T dc_1(t)/dt$, is positive at all wavelengths. Accordingly, before peak maximum of the major analyte, the derivative mixture spectrum will be positive in some part since the first term represents the major analyte. Thus, the retention time at which the derivative mixture spectrum obtained in chromatographic direction changes from positive or partially positive to negative, repre-

sents the chromatographic peak maximum of the major analyte. The situation is illustrated in Fig. 2. This piece of information is crucial for successful resolution in case of complete chromatographic overlap and no spectral selectivity.


With the retention time of chromatographic peak maximum for the major analyte at hand the present problem can be solved. Both approaches



$$a_{k-1}^T = d a_{k-1}^T(t) / dt = s_1^T \frac{dc_1(t)}{dt} + s_2^T \frac{d(t)}{dt}$$

$$= s_1^T \frac{c_{1,k} - c_{1,k-1}}{t_k - t_{k-1}} + s_2^T \frac{c_{2,k} - c_{2,k-1}}{t_k - t_{k-1}}$$

↓
↓
 positive negative



$$a_k^T = d a_k^T(t) / dt = s_1^T \frac{dc_1(t)}{dt} + s_2^T \frac{d(t)}{dt}$$

$$= s_1^T \frac{c_{1,k+1} - c_{1,k}}{t_{k+1} - t_k} + s_2^T \frac{c_{2,k+1} - c_{2,k}}{t_{k+1} - t_k}$$

↓
↓
 negative negative

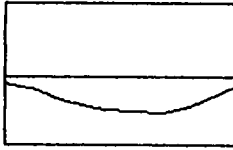


Fig. 2. Upper part shows parts of the resolved elution profile for a minor analyte, a major overlapping analyte and the observed elution profile of both analytes (before resolution). The retention time k corresponds to the chromatographic peak maximum of the major analyte. The two nearest neighbouring retention times are denoted $k-1$ and $k+1$. The derivatives obtained in the time direction (using Eqn. 4a) for the retention time intervals $[k-1, k]$ and $[k, k+1]$ are shown together with a display illustrating the change in the derivatives from partial positive to negative at all wavelengths after passing the retention time of peak maximum for the major analyte.

developed below for estimating the chromatographic and spectral profiles of the pure analytes are based on this information. If the chromatographic sampling rate is not extremely high, interpolation techniques [8] may be used to accurately determine the peak maximum of the major analyte. Interpolation is performed upon the original two-way data matrix, i.e., before differentiation. A 5-point Lagrange interpolation was used in our examples to insert some values around the peak maximum of the major analyte estimated from the two-way derivative matrix.

Resolution by estimating the spectrum of minor analyte

Knowing the retention time for the peak maximum of the major analyte, and the chromatographic profile of the minor, differentiation of the chromatographic profile of the minor analyte and insertion into Eqn. 4a, should provide an estimate of the spectrum of the minor analyte at the retention time of peak maximum for the major analyte. A more reliable estimate of the spectrum of the minor analyte is obtained by using symmetry constraints on the chromatographic peak of the major analyte.

The nearest neighbour (times $k - 1$ and $k + 1$ in Fig. 2) at each side of the retention time k corresponding to chromatographic peak maximum for the major analyte is of prime importance in the further development. If the chromatographic peak of the major analyte is symmetric in the proximity of maximum, the spectrum of the minor analyte can be obtained directly from the derivative matrix. Symmetry of the major peak just around maximum means that the derivatives in time direction calculated for the retention time intervals $[k - 1, k]$ and $[k, k + 1]$ obey the following relation:

$$\begin{aligned} & (c_{k,1} - c_{k-1,1}) / (t_k - t_{k-1}) \\ & = - (c_{k+1,1} - c_{k,1}) / (t_{k+1} - t_k) \end{aligned} \quad (10)$$

Thus, the spectrum s_2 of the minor analyte can be obtained by inserting Eqn. 10 in Eqn. 4a for

$[k - 1, k]$ and $[k, k + 1]$, combining and rearranging:

$$\begin{aligned} s_2^T &= [\mathbf{d}\mathbf{a}_{k-1}^T(t)/dt + \mathbf{d}\mathbf{a}_k^T(t)/dt] \\ & \quad / [(c_{k,2} - c_{k-1,2}) / (t_k - t_{k-1}) \\ & \quad + (c_{k+1,2} - c_{k,2}) / (t_{k+1} - t_k)] \end{aligned} \quad (11)$$

Note that the derivation of Eqn. 11 does not require symmetry of the chromatographic peak of the major analyte in the whole elution region. It is sufficient that local symmetry exists for the major peak just around maximum. For a non-symmetric chromatographic peak, the interpolation technique may be helpful to approximate symmetry just around the peak maximum for the major analyte.

With both s_2^T and s_1^T available, the chromatographic profiles for the two analytes can be estimated by a least-squares procedure,

$$\mathbf{C} = \mathbf{A}\mathbf{S}(\mathbf{S}^T\mathbf{S})^{-1} \quad (12)$$

In Eqn. 12, the matrices \mathbf{C} (dimension $N \times 2$) and \mathbf{S} (dimension $M \times 2$) contain the chromatographic profiles $\{c_1, c_2\}$ and spectral profiles $\{s_1, s_2\}$, respectively. Note that Eqn. 12 provides a second estimate of the chromatographic profile of the minor analyte which can be compared with the estimate obtained by orthogonal projections (Eqns. 7-9).

If the scalar denominator in Eqn. 11 is very small, the estimate of s_2 will inevitably be contaminated by noise. In this case, the target transformation technique developed by Malinowski and Howery [9] can be used to reduce random noise. If the concentration of the minor analyte is not too small, iterative target transformation factor analysis as developed by Vandeginste et al. [10] may be used to refine the chromatographic profiles of the analytes. In this case, least-squares can be used to recalculate the spectrum of the minor analyte, i.e., by using Eqn. 17 below, and thus provide a check on the consistency of the results.

Resolution by estimating the chromatographic profile of the major analyte

An alternative road to resolution is to estimate the chromatographic profile of the major analyte.

This can be carried out by optimization using the already estimated chromatographic peak maximum of the major analyte as objective function.

Every column of the original data matrix is a linear combination of the chromatographic profiles of the two pure analytes. The major analyte

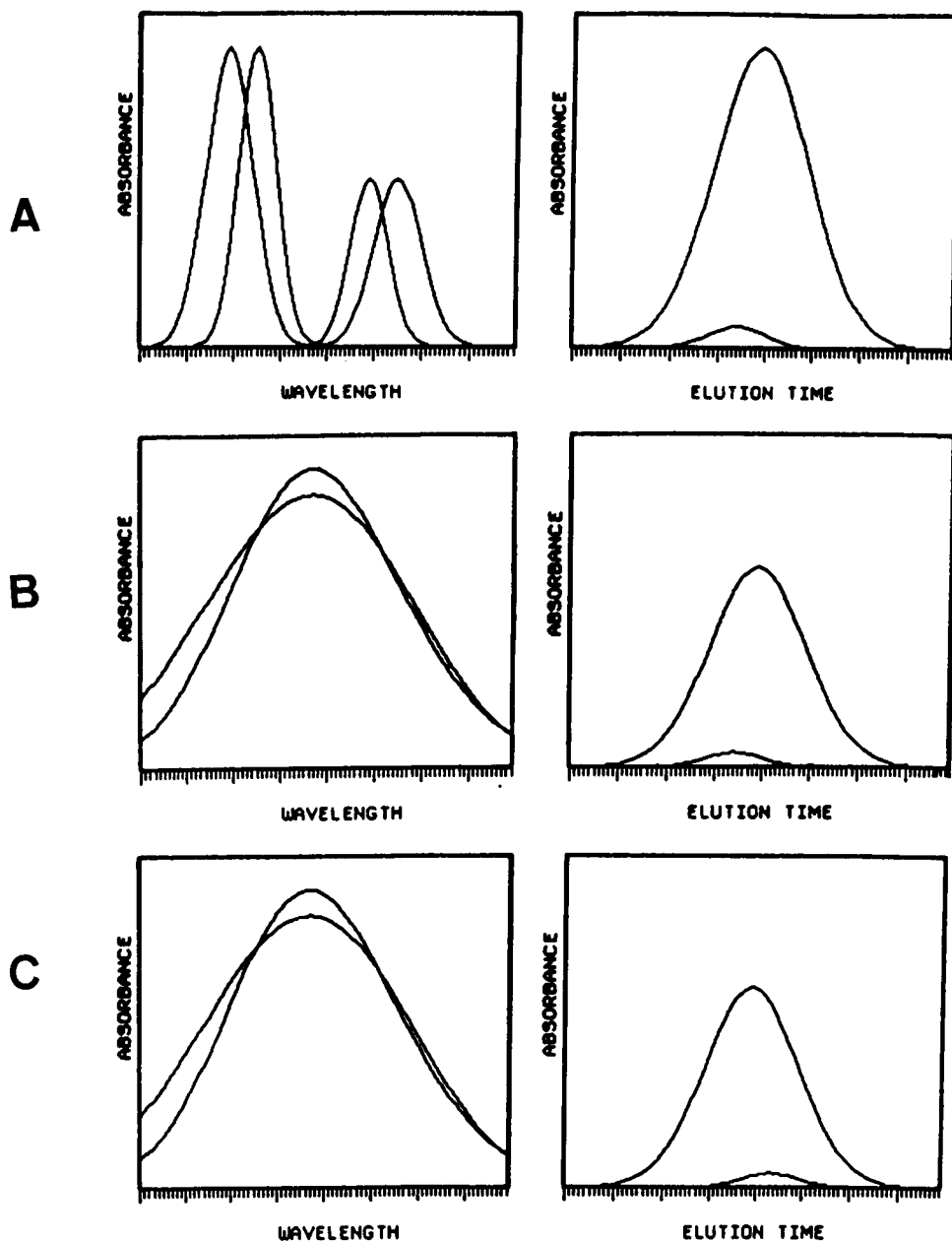


Fig. 3. Three simulated mixtures of two analytes acquired on a chromatograph with multiwavelength detector. In all cases the minor analyte is completely overlapped in the time direction. Case A differs from cases B and C by the presence of selective wavelength regions. The mixtures B and C are composed of the same analytes in the same relative concentrations, but with a shift towards later elution times for mixture C compared to B.

at wavelength j is thus the difference between the chromatographic profile of the mixture and the chromatographic profile of the minor analyte:

$$\begin{aligned} s_{1j}c_1 &= a_j - bd \\ &= s_{1j}c_1 + s_{2j}c_2 - b\mu c_2 \quad (j = 1, 2, \dots, M) \end{aligned} \quad (13)$$

Equation 13 holds if and only if b is chosen as s_{2j}/μ . The relative chromatographic profile \mathbf{d} of the minor analyte is already estimated by orthogonal projections (Eqns. 7-9) so that by Eqn. 13 the resolution problem is changed into a one-dimensional optimization search problem: find the coefficient b that provides the chromatographic profile of the major analyte. The already estimated retention time for chromatographic peak maximum of the major analyte is used as objective function. The multiplication of \mathbf{c}_1 with the absorbance s_{1j} of the major analyte at wavelength j (see Eqn. 13) does not change the position of the peak maximum. Thus, the performance of the different choices of b can be assessed with respect to the deviation they produce from the already established peak maximum of the major analyte.

In order to avoid unfortunate choices of the wavelength j and thus b , the marker-object projection technique [11] is used to define a new chromatographic profile representing all the mixtures. The marker-object projection technique as used here additionally reduces the influence from random noise. The estimated spectrum of the major analyte is used as a "marker object" and the chromatographic profile at each retention time is projected on this spectrum:

$$\begin{aligned} \mathbf{a}_i^T \mathbf{s}_1 &= (c_{i1} \mathbf{s}_1^T + c_{i2} \mathbf{s}_2^T) \mathbf{s}_1 \\ &= c_{i1} \mathbf{s}_1^T \mathbf{s}_1 + c_{i2} \mathbf{s}_2^T \mathbf{s}_1 = r_1 c_{i1} + r_2 c_{i2} \end{aligned} \quad (i = 1, 2, \dots, N) \quad (14)$$

The scalars r_1 and r_2 are defined as the projections of the pure spectra \mathbf{s}_1 and \mathbf{s}_2 on the "marker"-spectrum \mathbf{s}_1 , i.e., $\{r_i = \mathbf{s}_i^T \mathbf{s}_1; i = 1, 2\}$. The projection defined by Eqn. 14 is performed for all the mixture spectra $\{\mathbf{a}_i^T; i = 1, 2, \dots, N\}$. In this way, a chromatographic profile is obtained that is a linear combination of the chromato-

graphic profiles of the two analytes, but where the part of the minor analyte's spectrum orthogonal to the spectrum of the major analyte is removed. Collecting the projections in a vector \mathbf{m} gives

$$\mathbf{m} = r_1 \mathbf{c}_1 + r_2 \mathbf{c}_2 \quad (15)$$

and

$$\mathbf{m} - b\mathbf{d} = r_1 \mathbf{c}_1 + r_2 \mathbf{c}_2 - b\mu \mathbf{c}_2 \quad (16)$$

Optimization with the chromatographic peak maximum of the major analyte as objective function, provides the chromatographic profile of the major analyte for $b = r_2/\mu$. The converged value of the parameter b using Eqn. 16 for the optimization differs from the value obtained by use of Eqn. 13 due to the use of the marker projection to reduce the contribution of the minor analyte. With estimates of \mathbf{c}_1 and \mathbf{c}_2 available, the pure spectra for the two analytes can subsequently be obtained by a least-squares calculation

$$\mathbf{S}^T = (\mathbf{C}^T \mathbf{C})^{-1} \mathbf{C}^T \mathbf{A} \quad (17)$$

The main advantage of this approach compared to the previous one is that the estimates do not suffer from contamination of random noise. Thus, refinement by use of the target transformation technique is no longer necessary. If slightly different estimates of the chromatographic profile of the major analyte provide the maximum for the major analyte at the same retention time, the average profile is taken as the final result. Therefore interpolation [8] is useful also in this method to narrow the region around the peak maximum of the major analyte.

EXPERIMENTAL

The method has been implemented in VAX FORTRAN as a part of the heuristic evolving latent projections (HELP) program [1]. The implementation is running on a VAXstation 2000. Three different simulated two-way mixture data with the minor peak completely overlapped by the major chromatographic peak were created, denoted by the letters a-c in Fig. 3. The concentration of minor analyte is in all cases 7% of the

major one. The data were generated with random noise of standard deviation of 0.0001 which is comparable to that commonly observed in real LC-DAD data.

RESULTS AND DISCUSSION

Figure 3 shows three simulated mixtures of two analytes. Figure 3, right side, shows that all systems contain a minor analyte that is completely overlapped by a major one in the time direction. Systems B and C are mixtures of the same analytes as observed from the spectra (Fig. 3, left side) in the same proportions (Fig. 3, right side). The chromatographic conditions are different, however, as the minor analyte is shifted towards later retention times for system C compared to B. Actually, the two systems are similar around the retention time corresponding to peak maximum of the major analyte and thus we shall only resolve system B. First, however, we resolve system A.

Resolution of systems with selective spectral regions

There is a major difference between system A and systems B and C. Thus, Fig. 3 (left side) suggests that mixture A has selective spectral regions for both analytes, while the spectra of the two analytes in systems B and C overlap completely. Although this observation can only be done after the system has been resolved, selectivity in either the spectral or chromatographic domain can easily be revealed by means of procedures developed in the heuristic evolving latent projections (HELP) method [1]. Figure 4 shows the latent-projective graphs mapping the evolution in chromatographic direction (left side) and spectral direction (right side) on the two major principal analytes for mixture A in Fig. 3. The evolution implied by the latent-projective graph in chromatographic direction suggests the presence of a minor chromatographic peak being completely overlapped by a major one. This follows from the fact that there is only one straight-line segment in the latent-projective graph (Fig.

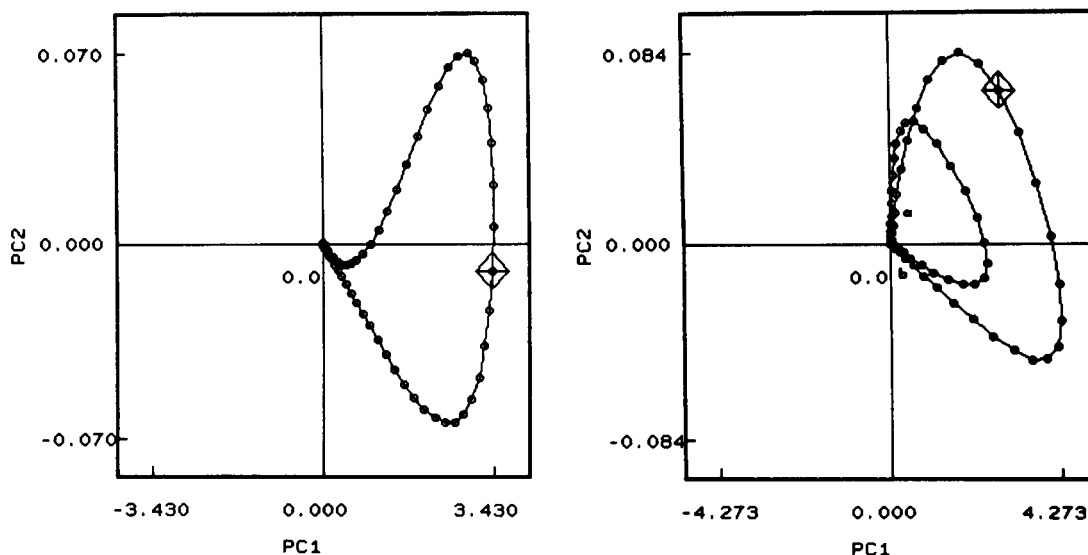


Fig. 4. Latent-projective graphs in time (left side) and wavelength (right side) domain for mixture A. The graphs are obtained by principal components analysis of the two-way data. In the time domain (left side) the chromatographic elution is described. Each point corresponds to the spectrum at a particular retention time. The continuous character of the graph reflects the continuous nature of the chromatographic profile. The first and last spectra projects in origin indicating the start and end of elution. In the spectral domain (right side), each point describes the chromatographic profile at a particular wavelength. Straight-line segments pointing towards origin are indicative of selective regions.

4, left side) mapping the chromatographic profile of the major analyte at the beginning and end of elution. The straight line segment represents the chromatographic retention time regions where the major analyte elutes alone. This follows from the

fact that only the concentration changes for a single eluting analyte, while the spectrum remains the same. Thus, the chromatographic profile of a pure analyte maps a line in multivariate space. The straight-line segment in Fig. 4 (left side) is a

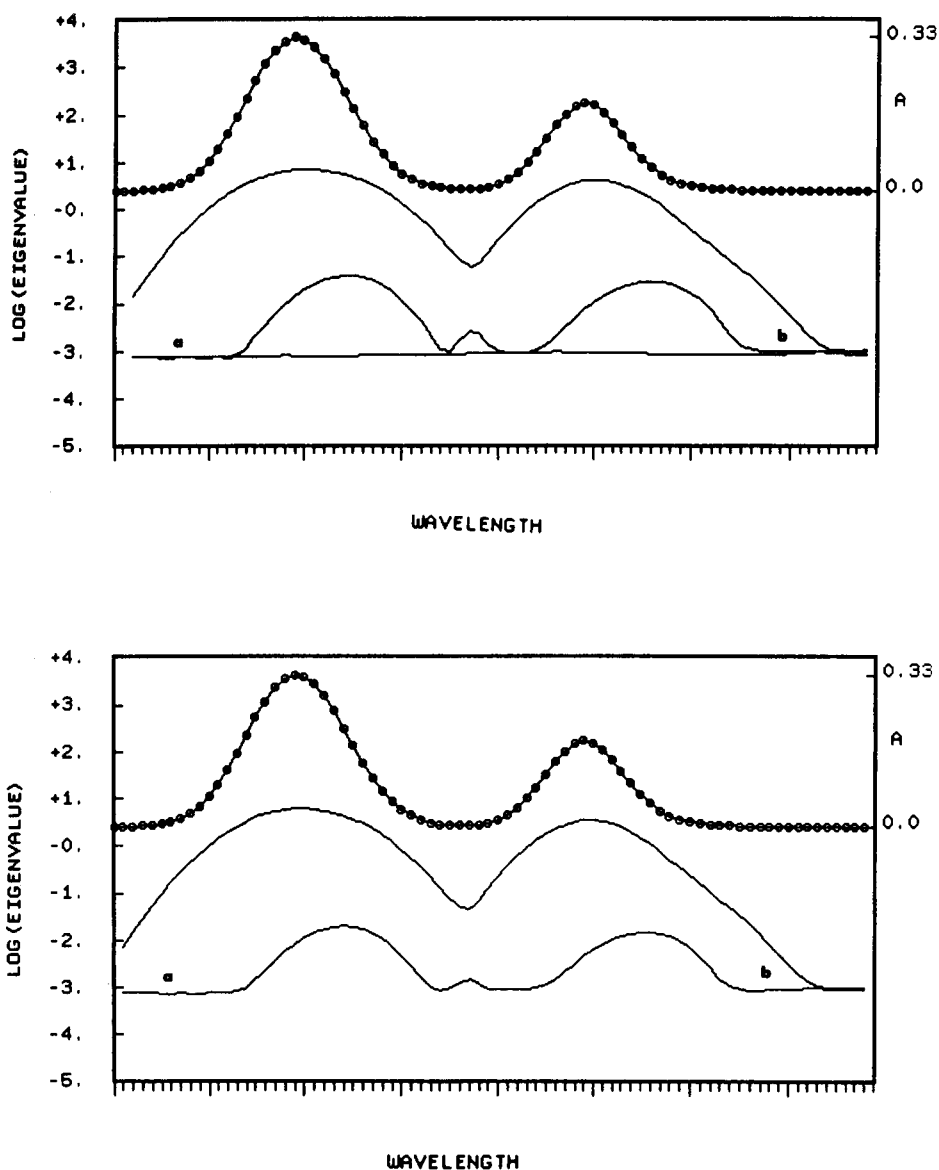


Fig. 5. Eigenstructure tracking analysis in wavelength direction for mixture A. Lower and upper part display the evolving eigenvalues when moving a window containing 2 and 3 neighbouring wavelengths, respectively, one wavelength at-the-time from the first until the last wavelength. The upper part (window size 3) reveals that system A is a two-analyte mixture with selective spectral regions a and b for the two analytes. Note that the third evolving eigenvalues (upper part) implies the noise level in the data.

projection of this line. The loop maps the chromatographic region where the two analytes coelute.

Although the analysis has revealed selective chromatographic regions for the major analyte, the system cannot be resolved using the procedure developed in HELP [1,2]. This is due to the lack of any zero-concentration region [12] for the major analyte. However, the latent-projective graph mapping the evolution in the spectral direction (right side), reveals straight-line segments, denoted (a) and (b) in plot, pointing towards origin. As shown previously [1], this pattern is indicative of selective wavelength regions. The results from ETA [2] where an evolving window is moved in either time or wavelength direction, support the same conclusion (Fig. 5). The figure

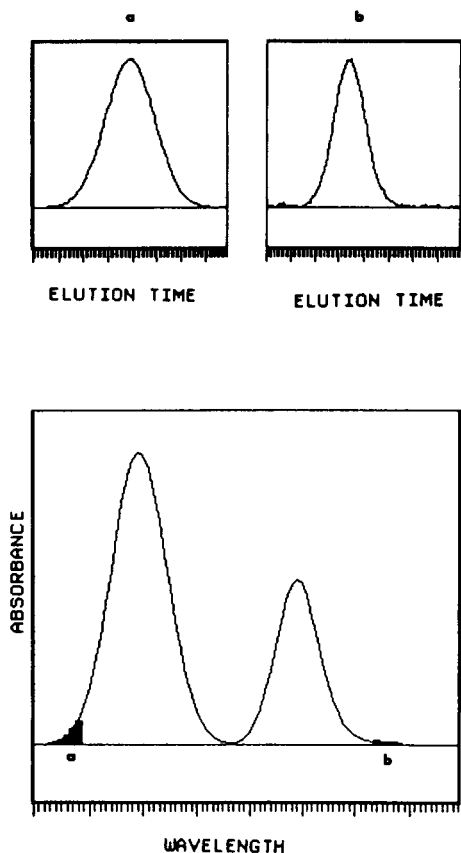


Fig. 6. The resolved elution profiles of the two analytes (upper part) estimated by principal component analysis of the selective spectral regions a and b (lower part).

shows the evolving eigenvalues in wavelength direction with window sizes of 2 (lower) and 3 (upper). This dynamic (and two-way) procedure is an extension of a window approach introduced by Keller and Massart [3]. The selective regions (a and b, Fig. 5) for the two eluting analytes are easily identified in the plots. Extracting the chromatographic profiles by principal component analysis on the two selective regions, provides the result shown in Fig. 6 for the two analytes, which should be compared with system A in Fig. 3. This result shows that if one can find selective information in spectral direction for both analytes, resolution becomes almost trivial.

Resolution of systems without selective spectral regions

We shall now turn our attention to the much more challenging resolution problem presented by the mixtures B and C (Fig. 3). Only the results for system B will be provided in detail since system C differs from system B only in a shift towards later elution times for the minor analyte. Figure 7 shows the two latent-projective graphs for system B. The latent-projective graph showing the evolution in chromatographic direction (Fig. 7, left side) suggests a similar chromatographic situation as for system A, namely a minor peak completely overlapped by a major one, but selective chromatographic regions for the major analyte at start and end of elution. The latent-projective graph mapping the spectral domain (Fig. 7, right side), however, reveals that the prospect for successful resolution and quantitation is worse for system B than for system A since no selective regions exist in the spectral domain. Apparently, there are two straight-line segments in the graph, but, unfortunately, they do not point to the origin of the coordinate system. As shown in previous work [1], this picture means that the spectra of the analytes overlap at all wavelengths.

Figure 8 shows the results of component analysis upon the selective chromatographic regions for the major analyte at start of elution as indicated by the latent-projective graph of the chromatographic domain (Fig. 7, left side). The loadings on the first principal component represent the pure spectrum of the major analyte, while the

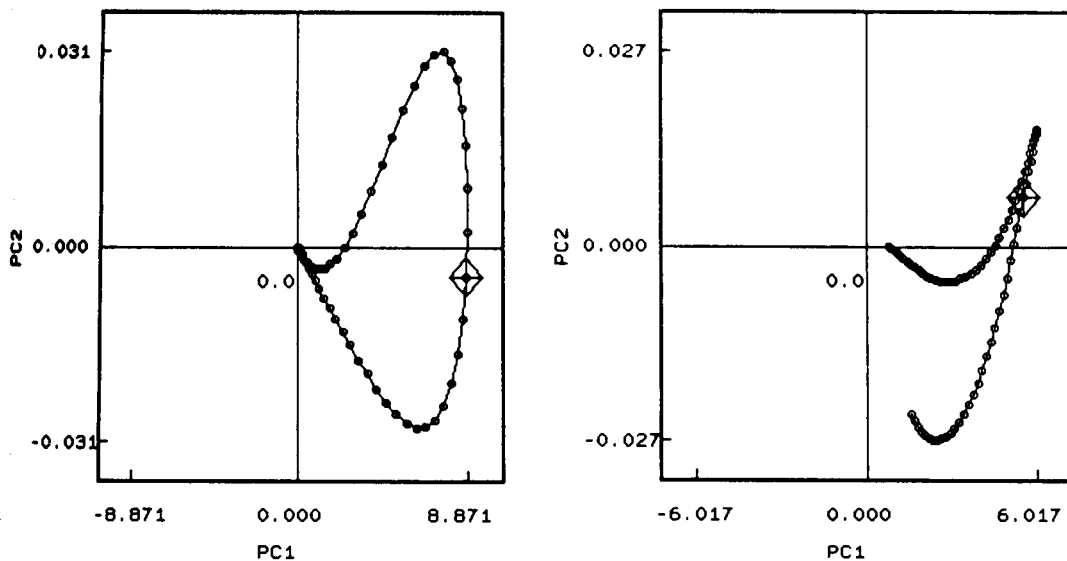


Fig. 7. Latent-projective graphs in time (left side) and wavelength (right side) domain for mixture B.

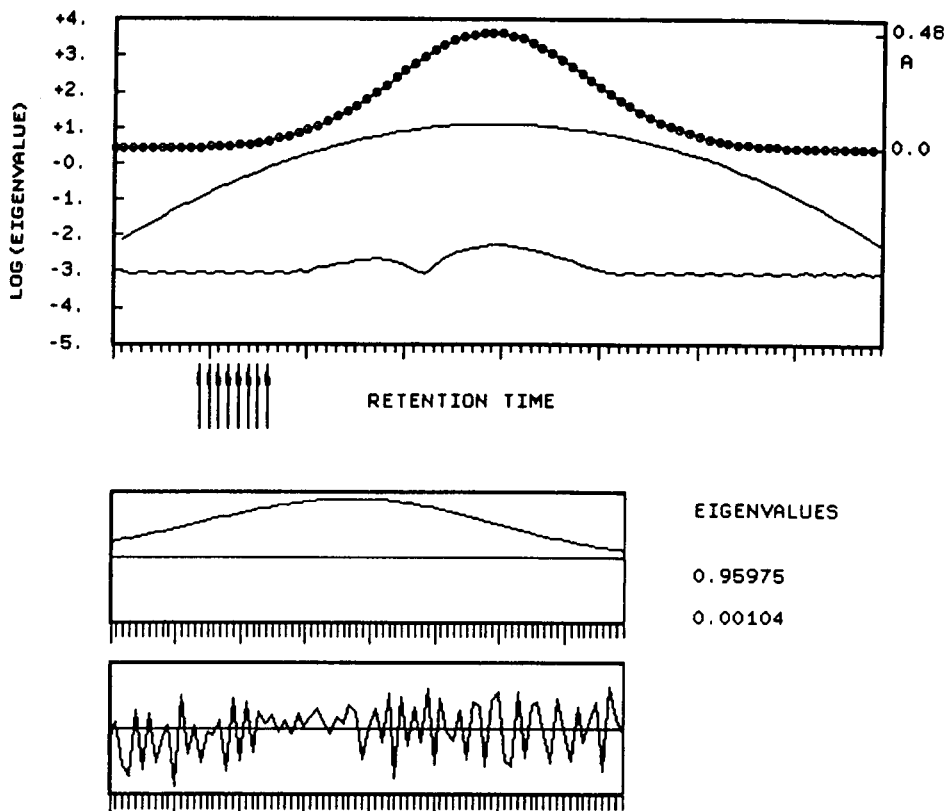


Fig. 8. Eigenstructure tracking analysis (upper part) of system B with window size 2 in the time direction. Local principal component analysis of the retention time interval marked with arrows (selective chromatographic regions for the major analyte) provide the loading patterns and the eigenvalues on the two first principal components shown in the lower part.

loadings on the second one displays a typical noise pattern. Principal component analysis upon the region at the end of elution showed the same picture: a single eluting analyte. As the spectra showed the same absorbances at all wavelengths, they definitely represent the same analyte.

In order to locate the maximum on the chromatographic profile of the major analyte, the original data matrix is differentiated in the time direction. Figure 9 shows the first-order derived spectra at the two crucial retention times, i.e., times 39 and 40, for the investigated system. These derived spectra imply that the chromatographic peak maximum of the major analyte is around retention time 40 (see also Fig. 2). The validity of this statement can readily be assessed by visual inspection of the derived spectra, which reveal that up to retention time 39 the spectra differentiated in the time detection are all positive or partially positive and that after time 40 the spectra in the derivative matrix are negative at all wavelengths. With this information, the chromatographic profiles and spectra of

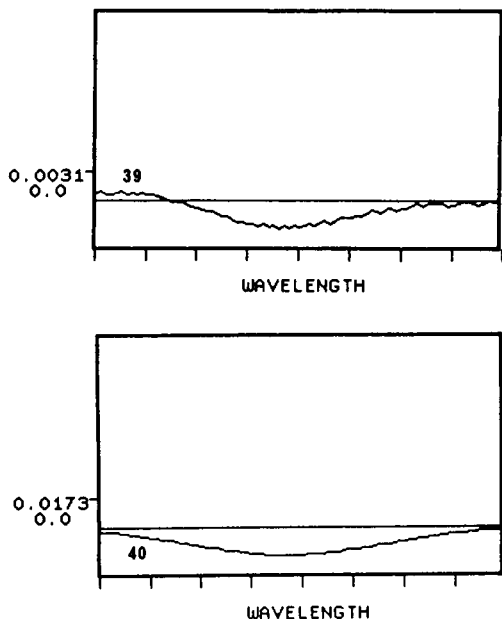


Fig. 9. The derived spectra at retention times just before (time 39) and after (time 40) peak maximum of the major analyte obtained by differentiation in the time direction for mixture B.

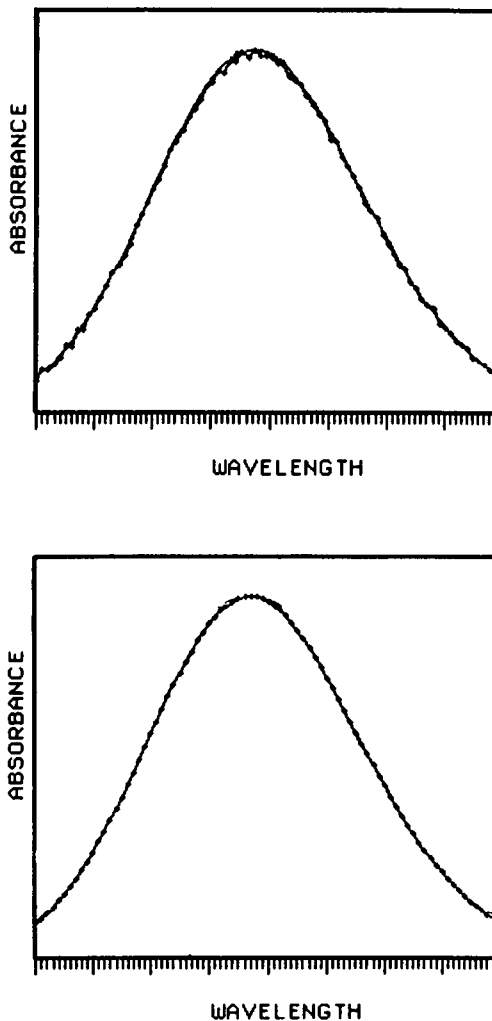


Fig. 10. Estimated spectrum of the minor analyte in mixture B. Upper part shows the first estimate, while the lower part shows the refined spectrum obtained by target transformation.

the analytes can be obtained by either of the two approaches derived in the theoretical section. The results obtained from the direct approach and the optimization approach, respectively, are shown in Fig. 10 and Fig. 11. In the direct approach, the pure spectrum of the minor analyte is first estimated. Figure 10, upper part, shows the first estimate of the minor analyte. The lower part shows the spectrum after refinement by using the target transformation technique. The agreement between the real one and calculated one is excellent.

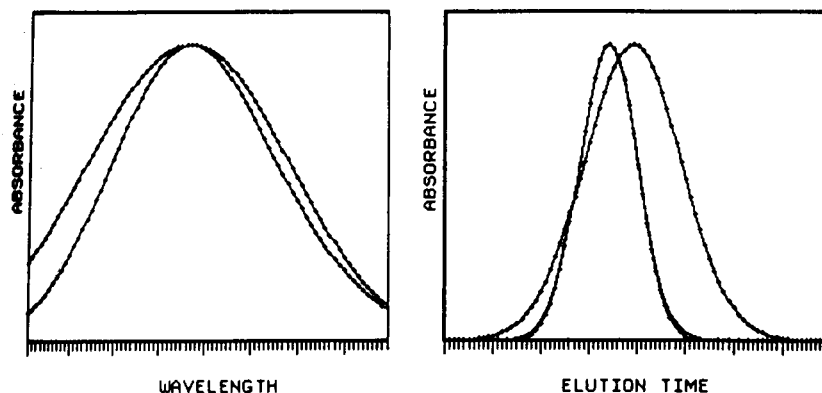


Fig. 11. The spectra (left side) and chromatographic profiles (right side) of the resolved analytes in mixture B using optimization with the retention time of peak maximum for the major analyte as objective function.

Figure 11 shows the estimates of both chromatographic profiles and spectra of the two analytes as calculated by the optimization approach described in the theoretical section. The chromatographic profile of the minor analyte was first estimated by orthogonal projections, then the chromatographic profile of the major one was obtained by optimization using the information

about the retention time for peak maximum of the major analyte. The pure spectra of the analytes were obtained by the least-squares procedure defined by Eqn. 17. Interpolation around the retention time of peak maximum of the major analyte was used as described in the theoretical section.

Figure 12 shows the first-order derivative spectra of system C at retention times 39 and 40. The difference observed between Fig. 12 obtained for system C and Fig. 9 obtained for system B is due to the fact that the peak maximum of the minor analyte for system C appears *after* the peak maximum for the major one. Thus, for system C the first-order derivative spectrum in time direction changes from positive at all wavelengths up to time 39 to partial positive after this time, since in the neighbourhood of peak maximum of the major analyte the chromatographic profile of the minor analyte is always increasing. It should be pointed out that by doing the differentiation in time direction backwards, i.e., starting from the last retention time, the reversed order of peak maximum in C can be handled in complete analogy with system B.

Conclusions

In this work, we have shown that chromatography with multiwavelength detection may enable resolution and quantitation of a minor analyte even for the case where the overlap is complete

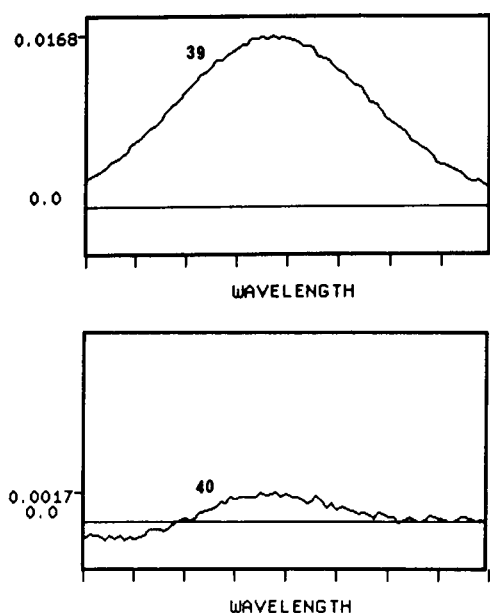


Fig. 12. The derived spectra at retention times 39 and 40 obtained by differentiation in the time direction for mixture C.

in both time and wavelength direction. By use of heuristic evolving latent projections [1] the diagnosis of such a case is readily made from visual inspection of the latent-projective graphs in the chromatographic and spectral domain. By utilizing the chromatographic selective regions, the spectrum of the major analyte can then be extracted by principal component analysis of the selective regions. With this information at hand, the problem is changed from one of resolving a "black" multicomponent system into one of resolving a "grey" system [13].

The key to successful resolution of the studied cases is the combination of projections and first-order differentiation. Thus, the present work represents a development and extension of the pioneering work of Milano et al. [4] and Fell et al. [5] on the use of derivatives in wavelength and time direction for resolution enhancement of seriously overlapping spectral and chromatographic profiles.

As the evaluation of the methods derived in this work is performed upon simulated systems, one may ask how the performance will be influenced by real noise. The answer to this is that correlated noise, represented by drifting baselines and systematic spectral background can be removed by analyzing the zero-component regions, i.e., the regions before elution starts and after elution is finished as shown in previous work [14]. This should leave us with random noise which seems to pose no major problem for the derived methods. However, the limit of resolution in the presence of real noise should be established for this case of systems and, indeed, suit-

able data are now generated in other laboratories [15].

Yi-zeng Liang thanks the Royal Norwegian Council for Scientific and Industrial Research (NTNF) for a postdoctoral fellowship. Several valuable discussions with R. Manne (University of Bergen) are also gratefully acknowledged.

REFERENCES

- 1 O.M. Kvalheim and Y.-z. Liang, *Anal. Chem.*, 64 (1992) 936.
- 2 Y.-z. Liang, O.M. Kvalheim, A. Rahmani and R.G. Brerton, *J. Chemom.*, 7 (1993) 15.
- 3 H.R. Keller and D.L. Massart, *Anal. Chim. Acta*, 246 (1991) 279.
- 4 M.J. Milano, S. Lam and E. Grushka, *J. Chromatogr.*, 125 (1976) 315.
- 5 A.F. Fell, H. Scott, R. Gill and A.C. Moffat, *J. Chromatogr.*, 273 (1983) 3.
- 6 A. Lorber, *Anal. Chem.*, 54 (1986) 1167.
- 7 T.V. Karstang and O.M. Kvalheim, *Anal. Chem.*, 63 (1991) 767.
- 8 G.R. Lindfield and J.E.T. Penny, Wiley, 1989, pp. 265–281.
- 9 E.R. Malinowski and D.G. Howery, *Factor Analysis in Chemistry*, Wiley, New York, 1980.
- 10 B.G.M. Vandeginste, W. Derks and G. Kateman, *Anal. Chim. Acta*, 173 (1985) 253.
- 11 O.M. Kvalheim, *Chemom. Intell. Lab. Syst.*, 2 (1987) 283.
- 12 M. Maeder, *Anal. Chem.*, 59 (1987) 527.
- 13 Y.-z. Liang, O.M. Kvalheim and R. Manne, *Chemom. Intell. Lab. Syst.*, in press.
- 14 Y.-z. Liang, O.M. Kvalheim, A. Rahmani and R.G. Brerton, *Chemom. Intell. Lab. Syst.*, in press;
- 15 H.R. Keller, D.L. Massart and J.O. De Beer, *Anal. Chem.*, submitted for publication.

Evaluation of stability constants from multi-wavelength absorbance data: program STAR

J.L. Beltrán, R. Codony and M.D. Prat

Departament de Química Analítica, Universitat de Barcelona, Diagonal 647, 08028 Barcelona (Spain)

(Received 12th May 1992; revised manuscript received 25th November 1992)

Abstract

The programs STAR and STAR/FA were developed for the study of ionic equilibria from spectrophotometric data. Both programs are written in Turbo-Pascal for use on personal computers. STAR is a non-linear regression program for the refinement of complex formation constants of systems that can be described by up to 5 components and 25 species $A_p B_q C_r D_s H_t$, where A, B, C and D can be either metal or ligand. The experimental data treated can contain up to 50 absorption spectra, measured at 50 wavelengths. Interaction with the user is provided by menu-driven operation and graphics presentation of data on the computer screen (or plotter). STAR/FA is a complementary program, used for the determination of the number of absorbing species by factor analysis of the absorbance data matrix. It can also be used for the smoothing of the experimental data. Two application examples are given: the interaction of boric acid with 2,3-dihydroxynitrobenzene (from literature data) and the dissociation and complex formation equilibria with Zn(II) ions of 8-hydroxyquinoline-5-sulphonic acid.

Keywords: UV-Visible spectrophotometry; Absorbance; Computer programs; Stability constants

Spectrophotometric methods have been widely used in the study of ionic equilibria [1,2]. Although in past years spectrophotometric measurements were less precise than potentiometric measurements in the determination of complex formation constants, absorbance data have been very useful in ascertaining the chemical model describing the ionic equilibria, provided that new absorbing species are formed. Otherwise, the spectrophotometric methods can be used when the experimental conditions do not allow the use of potentiometric measurements; this is the case when the ligand or the complexes formed are sparingly soluble.

Otherwise, the numerical and graphical methods used for the determination of formation con-

stants (continuous variations method [1,2], corresponding solutions [1], the Benesi-Hildebrand linearization method [3,4], etc.) are applicable only when relatively simple systems are studied. The use of general least-squares computer programs for the treatment of multi-wavelength absorbance data overcomes this problem, and fairly complicated equilibria (involving mixed-ligand, or hydroxo complexes) can be solved. The most commonly used programs in this way are SQUAD [3] and LETAGROP-SPEFO [5], although there are extensive revisions of least-squares programs for the study of ionic equilibria available [6,7].

The determination of stability constants from multi-wavelength absorbance data requires large amounts of computer memory, so, programs such SQUAD and LETAGROP-SPEFO were developed for use with mainframe computers. The use of microcomputers in studying these systems was allowed only with sophisticated mathematical

Correspondence to: J.L. Beltrán, Departament de Química Analítica, Universitat de Barcelona, Diagonal 647, 08028 Barcelona (Spain).

methods for data reduction by factor analysis [4] (SPECFIT program), or restricted to single-wavelength measurements [8,9].

At present, most common personal computers have the memory and speed needed to manage the data corresponding to equilibrium studies by multi-wavelength absorbance data (especially those based on i386 and i486 processors). With this aim, in this work the program STAR (STability constants by Absorbance Readings), written in Turbo-Pascal 5.0, was developed. Although this program can be used on an IBM-PC/XT or compatible computer with 512 kb RAM memory, it is highly recommended that at least an i80286-based computer with numeric co-processor is used.

Together with STAR, the program STAR/FA was also used to determine the number of absorbing species in solution by factor analysis of the absorbance data matrix.

The programs are described, together with their application in the determination of the equilibrium constants in the reaction of 2,3-dihydroxy-

nitrobenzene (H_2L) and boric acid (HM) (from literature data [7]) and the protonation and complex formation constants with Zn(II) ions of 8-hydroxyquinoline-5-sulphonic acid (QS^{2-} as free ligand).

STAR PROGRAM

This program was developed to be user-friendly and highly interactive in operation, taking into account the facilities provided by personal computers. In this way, their use is based on menu-driven selections, allowing the chemical model of the system studied to be modified. Moreover, the user has direct access to graphics routines for the presentation of data and results. These graphics are presented on the computer screen (provided that it has a CGA, Hercules, EGA or VGA graphics adapter). Also, an HP-GL plotting file (in ASCII code) can be created; in this case, the file can subsequently be dumped on an HP-GL compatible plotter, or it can be imported from

TABLE 1

Main menu of STAR, as displayed on the computer screen

| Species | Spec. ^a | Log β | Species | Spec. ^a | Log β |
|----------------|--------------------|-------------|--------------------|--------------------|-------------|
| 1 QS(1) | KS | 0.000 | 14 PO4(1)H(3) | NA | 19.460 |
| 2 QS(1)H(1) | KS | 8.358 | 15 Zn(1)PO4(1)H(1) | NA | 14.140 |
| 3 QS(1)H(2) | KS | 12.159 | 16 Zn(1)H(-1) | NA | -8.810 |
| 4 Zn(1) | NA | 0.000 | 17 Zn(1)H(-2) | NA | -16.610 |
| 5 QS(1)Zn(1) | US | 7.572 | 18 Zn(1)H(-3) | NA | -28.030 |
| 6 QS(2)Zn(1) | US | 14.423 | | | |
| 7 AcO(1) | NA | 0.000 | | | |
| 8 AcO(1)H(1) | NA | 4.560 | | | |
| 9 Zn(1)AcO(1) | NA | 1.100 | | | |
| 10 Zn(1)AcO(2) | NA | 1.900 | | | |
| 11 PO4(1) | NA | 0.000 | | | |
| 12 PO4(1)H(1) | NA | 11.740 | | | |
| 13 PO4(1)H(2) | NA | 17.460 | | | |

| | |
|---|--|
| Mean of absorbance values = 0.121864577 | Chi-squared test = 3.8091168 |
| Sum of squared residuals = 0.0080505 | Hamilton <i>R</i> factor (%) = 2.0170441 |
| Standard deviation of residuals = 0.002841606 | Skewness = 0.1371443 |
| Mean residual = 0.002169794 | Kurtosis = 3.1367840 |
| Residual mean = 0.000123074 | Spectral range: 270.0 to 400.0 nm |

| | | | |
|----------------|----------------|----------------|-----------------|
| PLOT EXP. DATA | RESIDUALS PLOT | PLOT MOL. ABS. | PLOT CALC. DATA |
| REFINE CONSTS. | CHANGE MODEL | SAVE DATA/RES. | END OF PROGRAM |

^a Spectral characteristics: KS, US and NA indicate known spectrum, unknown spectrum and non-absorbing species, respectively.

other programs that use these files (e.g., a WP 5.1 word processor).

In the present version, STAR can deal with up to 50 absorption spectra, measured at 50 wavelengths. The systems studied can be defined by 5 components, forming up to 25 species $A_p B_q C_r D_s H_t$, where A, B, C and D can be either ligand or metal. The program solves the mass balances for these four components, but the free concentration of the last component ($H =$ hydrogen ion in general) is measured directly from the solution.

The principal characteristics of STAR are described below.

Selection menu

The program starts by asking for a data file name. Once the data have been read, it calculates the mass balances and the theoretical spectra and the residuals after the given model. After these tasks, a selection menu (Table 1) is displayed on the computer screen. It contains the description of the system, goodness-of-fit test parameters (sum of squared residuals, standard deviation of residuals, etc.) and at the bottom the possible options. The selection between the different options is done by the cursor and ENTER keys. All these options are available without interrupting the program execution.

The first line indicates the plotting options (as 3D graphics): experimental data, residuals after the model given, molar absorbances or calculated spectra after the model.

The other options (bottom line) are as follows:

REFINE CONSTS.: in this option, the user selects the set of constants to refine (maximum ten). As in the principal menu of the program, the selection is made by the cursor and ENTER keys.

CHANGE MODEL: this option allows to change the model in several ways:

- Inclusion of new species.
- Removal of species.
- Change the values of the formation constants.
- Set fixed or variable the molar absorptivities of species.
- Select the wavelength range to take into account in the calculations.

SAVE DATA/RES: using this option, the user can obtain the following file types:

Results file, containing the model, molar absorbances of the species, last set of constants refined and the residuals after the given model.

Modified data file, which takes into account the changes made in the model. This file can be used directly as new input file for STAR and STAR/FA.

Molar absorptivities, containing only the wavelengths and the molar absorptivities of the species.

Concentration file, which contains the total concentration of the components, pH of the solutions and the calculated concentrations for each species.

Refinement method

The refinement of equilibrium constants is done by the procedure REFINE, using the Gauss–Newton non-linear least-squares algorithm [10] by numerical differentiation, until a minimum in the sum of squares residuals (U) is attained. This function is defined as

$$U = \sum_{i=1}^{n_s} \sum_{j=1}^{n_w} r_{i,j}^2 = \sum_{i=1}^{n_s} \sum_{j=1}^{n_w} (A_{i,j,\text{exp}} - A_{i,j,\text{calc}})^2$$

where n_s and n_w are the number of solutions and the number of wavelengths, respectively.

The minimization process is repeated until the relative change of U between two iterations is less than 0.01%. In the case of divergence in the refinement procedure, the method is modified to optimize the “shifts” of the constants [11].

The values of A_{calc} are obtained by Beer’s law in the procedure CALCABS, from the calculated concentrations of each species and their molar absorptivities. For the species which have unknown spectra, these are calculated by multilinear regression [12], damped to avoid negative values.

The mass balance equations of the system are solved in the COMPLEX procedure, from the given model, the total concentrations of the components and the pH of the solution. In this procedure, the COGS routine of the COMICS pro-

gram [13] and a damped Newton non-linear method [14] are used alternatively. This approach has been applied successfully to the simulation of complex equilibria in multi-metal–multi-ligand systems [14], and to the determination of equilibrium constants from liquid–liquid extraction distribution data [15].

Statistical tests

STAR gives several statistical characteristics to test the reliability of the regression process which are valuable when several chemical models are compared for a given system.

The most important parameter is the standard deviation of the absorbance, $S_{(A)}$:

$$S_{(A)} = \left[\frac{U}{n_w(n_s - n_u) - n_r} \right]^{1/2}$$

where n_r is the number of constants refined simultaneously and n_u the number of species that have unknown molar absorptivities. Usually $S_{(A)}$ is compared with the instrumental error of the spectrophotometer [$S_{\text{inst}(A)}$] or the standard deviation calculated by factor analysis [$S_{k(A)}$]. A fit is considered good [16] when $S_{(A)} \leq S_{\text{inst}(A)}$ or $S_{(A)} \leq S_{k(A)}$, but in most instances it can be considered acceptable if $S_{\text{inst}(A)} \leq S_{(A)} \leq 0.005$. Other parameters given are the residual mean ($\overline{r_{i,j}}$), which should be equal to zero, and the mean residual ($|\overline{r_{i,j}}|$).

The distribution of residuals is examined by the skewness, kurtosis and Pearson's χ^2 tests; for a Gaussian distribution, these values should be equal to 0, 3 and < 12.6 (for six degrees of freedom at the 95% confidence level), respectively.

STAR also calculates the Hamilton R factor (expressed as %), which indicate the relative fit (e.g., if $R \leq 1\%$, it can be considered as a good fit).

STAR/FA PROGRAM

This program was designed as a supplement to STAR. As noted before, it is used to determine the number of absorbing species in solution by

factor analysis of the absorbance data matrix (A) [17], as described by Kankare [7,18].

The program calculates the second moment matrix (M) from the product of the absorbance matrix and its transpose A^T as

$$M = (1/n_s)AA^T$$

The symmetrical matrix M ($n_s \times n_s$) can be expressed in terms of its eigenvalues (α_i) and eigenvectors (v_i). The mathematical rank of M (m_r) will be equal to the number of non-zero eigenvectors ($m_r = \min\{n_w, n_s\}$); however, taking into account that the elements of A are subject to experimental error, the number of independent components in the system (n_c , that is, the number of light-absorbing species) will be $n_c \leq m_r$.

To determine the number of absorbing species, the program calculates the standard deviation of the absorbance [$S_{k(A)}$] as a function of the number of independent components:

$$S_{k(A)} = \left\{ \left[\text{tr}(M) - \sum_{i=1}^k \alpha_i \right] / (n_w - k) \right\}^{1/2}$$

where $\text{tr}(M)$ is the trace of the M matrix (the sum of its diagonal elements). The values of $S_{k(A)}$ are calculated for k ranging from 1 to $m_r - 1$. By plotting $S_{k(A)}$ versus k , and by comparison with the instrumental error [$S_{\text{inst}(A)}$], the number of absorbing species can be deduced when $S_{k(A)} < S_{\text{inst}(A)}$ (see Figs. 2 and 7).

Factor analysis can be used also for data improvement. It must be considered that the experimental data matrix A is the sum of two matrices: a pure data matrix described by n_c eigenvalues and eigenvectors, and an error matrix [17] described by the remaining $m_r - n_c$ eigenvalues and eigenvectors. The pure data matrix (A') can be reproduced by

$$A' = GG^T A$$

where G is a matrix formed from the first n_c eigenvectors. This procedure can be applied to smooth the data matrix [18]. In this way, an experimental data point $A_{i,j}$ is replaced by the corresponding $A'_{i,j}$ when

$$|A_{i,j} - A'_{i,j}| \geq 3S_{nc(A)}$$

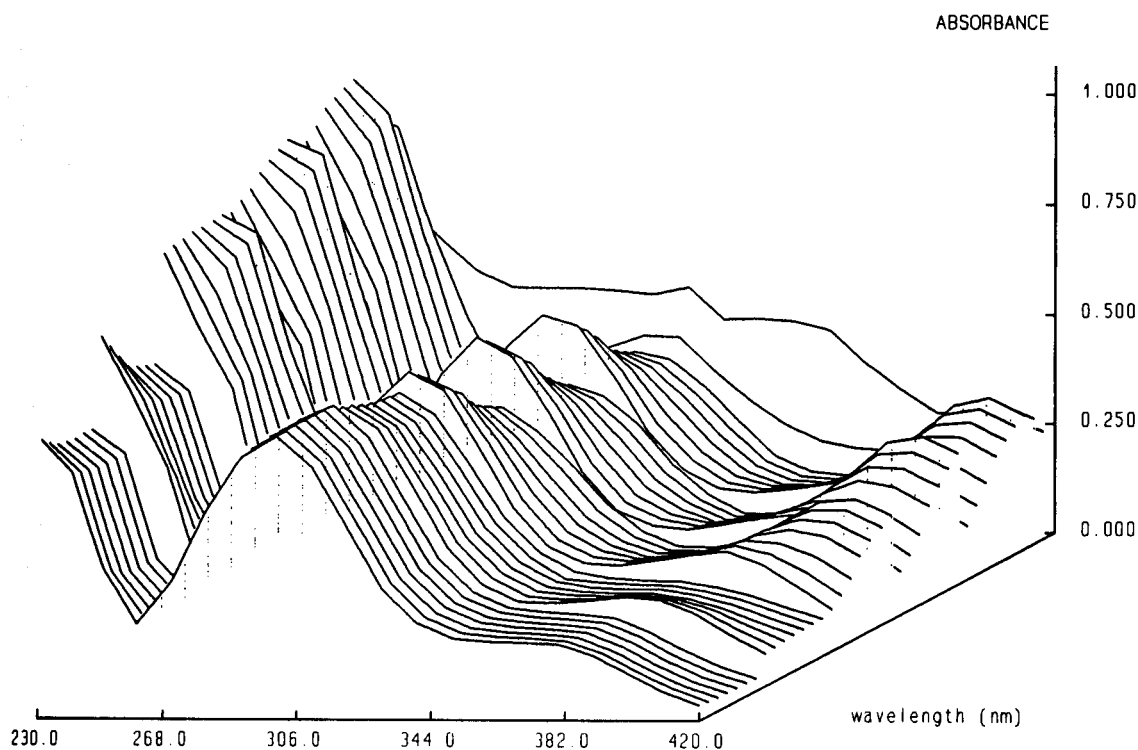


Fig. 1. Plot of experimental data for the 2,3-dihydroxynitrobenzene-boric acid system.

TABLE 2

Stability constants (β_{MLH}) and molar absorptivities (ϵ_{MLH}) for the 2,3-dihydroxynitrobenzene (H_2L)-boric acid (HM) system

| Parameter | Program | | | | |
|--|----------------------------|------------------------|------------------------|-----------------------|-----------------------|
| | FA608 + EY608 ^a | PSEQUAD ^a | SQUAD(84) ^a | STAR | STAR |
| Wavelength range (nm) | 230–420 | 230–420 | 230–420 | 230–420 | 280–420 |
| Log $\beta_{011} \pm \sigma_{\log \beta}$ ^b | 11.242 ± 0.007 | 11.172 ± 0.028 | 11.195 ± 0.024 | 11.193 ± 0.024 | 11.277 ± 0.017 |
| $\epsilon_{011(310,410)}$ ^c | 4487, 3425 | 4473, 3449 | 4477, 3442 | 4473, 3445 | 4488, 3416 |
| Log $\beta_{012} \pm \sigma_{\log \beta}$ ^b | 17.842 ± 0.027 | 17.838 ± 0.029 | 17.848 ± 0.024 | 17.844 ± 0.024 | 17.835 ± 0.018 |
| $\epsilon_{012(300)}$ ^c | 6482 | 6461 | 6466 | 6468 | 6501 |
| Log $\beta_{112} \pm \sigma_{\log \beta}$ ^b | 23.639 ± 0.010 | 23.353 ± 0.029 | 23.373 ± 0.025 | 23.379 ± 0.025 | 23.474 ± 0.018 |
| $\epsilon_{112(300)}$ ^c | 6665 | 6666 | 6669 | 6662 | 6637 |
| U_{MIN} | 0.01961 | 0.01966 | 0.01935 | 0.01962 | 0.00435 |
| Residual mean | 4.70×10^{-6} | -2.01×10^{-6} | -2.06×10^{-6} | 2.29×10^{-6} | 1.37×10^{-6} |
| Mean residual | 0.00350 | 0.00350 | 0.00350 | 0.00349 | 0.00217 |
| $S_{(A)}$ | 0.00563 | 0.00548 | 0.00546 | 0.00546 | 0.00297 |
| $S_{4(A)}$ | 0.00384 | 0.00384 | 0.00384 | 0.00387 | 0.00171 |
| Skewness (should be = 0) | 0.642 | -0.344 | -0.439 | 0.507 | -0.073 |
| Kurtosis (should be = 3) | 8.131 | 6.516 | 6.923 | 7.881 | 3.302 |
| R factor (%) | 1.262 | 1.206 | 1.203 | 1.217 | 0.823 |
| χ^2 (should be < 12.6) | - ^d | - ^d | - ^d | 95.78 | 7.782 |

^a After [7,16]. ^b Standard deviation of the constants as given by the programs. ^c Calculated molar absorptivities at the indicated wavelengths. ^d χ^2 not given.

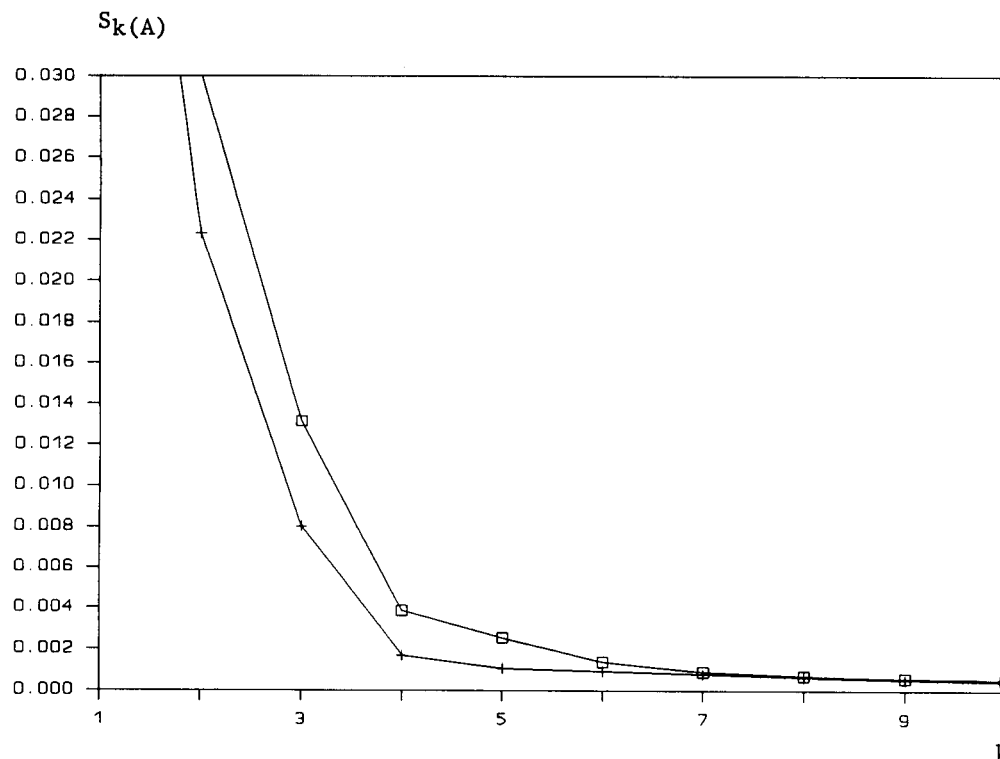


Fig. 2. Determination of the number of absorbing species in the 2,3-dihydroxynitrobenzene–boric acid system. $S_{k(A)}$ calculated from (□) the whole data set (230–420 nm) and (+) the data corresponding to the range 280–420 nm.

where $S_{nc(A)}$ is the estimated standard deviation for n_c selected number of eigenvalues and eigenvectors. STAR/FA uses this approach to replace only the data points that can be considered as outliers. To simplify their operation, this program uses the same data files as input to STAR. The smoothed data file is obtained also in this format.

EXAMPLES OF APPLICATION

Boric acid–2,3-dihydroxynitrobenzene system

In this example, STAR was applied to the reaction of 2,3-dihydroxynitrobenzene (H_2L) with boric acid (HM), in order to compare the results obtained with those given in the literature. The experimental data (taken from ref. 7, pp. 287–288) contain 37 spectra, measured at 20 wavelengths (from 230 to 420 nm, at 10-nm intervals), for several $[H_2L]/[HM]$ ratios, and pH ranging from

4.84 to 11.50. Figure 1 shows the experimental data as displayed by STAR. The number of absorbing species can be deduced by plotting $S_{k(A)}$ versus k (Figure 2); in this case, $n_c = 4$ and $S_{4(A)} = 0.00387$ are obtained.

The literature [7,16] gives the equilibrium constants for this system (dissociation of H_2L and formation of the species H_2ML), refined by the programs FA608 ± EY608 [18], PSEQUAD [6] and SQUAD(84) [16]; the dissociation constant for boric acid was kept constant in all calculations ($pK_a = 8.98$). These results, together with those obtained by using STAR, are summarized in Table 2, showing that the values of the equilibrium constants and molar absorptivities are nearly the same (within experimental error) when the programs are applied to the whole data set. The fitting parameters [$S_{(A)}$, $S_{4(A)}$, skewness, R factor, etc.] are also equivalent. Although the R factor and the standard deviation of the residuals indi-

cate a good fit, the high values obtained in the skewness, kurtosis and χ^2 tests show that they do not have a Gaussian distribution. Moreover, the residuals plot given by STAR (in Fig. 3A) shows that the residuals are significantly greater in the most UV region (between 230 and 270 nm). The STAR facility was applied to change the wavelength range used in the calculations, selecting the range 280–420 nm to recalculate the equilibrium constants, obtaining a significantly improved fit, as given in the last column of Table 2. Note that $S_{(A)}$ and $S_{4(A)}$ are about the half of the values obtained for the whole data set; the differences are more important in the skewness, kurtosis and χ^2 tests. The improvement of fit can also be noted in the better definition of the number of absorbing species (Fig. 2) and in the residuals plot after the recalculated constants for the range 280–420 nm (Fig. 3B). Otherwise, the set of equilibrium constants obtained from the reduced data set are very close to those obtained previously.

QS²⁻-Zn(II)-H⁺ system

8-Hydroxyquinoline-5-sulphonic acid has been used for the fluorimetric determination of metal ions, such as Al(III), Mg(II), Zn(II) and Cd(II) [19,20]. The complex formation constants for some of these metal ions are available in the literature [21].

Apart from the sulphonic group, this ligand has two dissociation constants, corresponding to the deprotonation of the heterocyclic nitrogen and the dissociation of the hydroxyl group. The complexes formed with Zn(II) ions are Zn(QS) and Zn(QS)₂²⁻.

The protonation constants of QS²⁻ and their complex formation constants with Zn(II) were determined spectrophotometrically at 25°C and ionic strength 0.1 M (NaCl). The experimental details are given below.

EXPERIMENTAL

Apparatus

The pH values were measured with a Radiometer PHM 84 pH meter, equipped with an Orion 81-02 combined glass electrode. Calibration of the electrode system was done with buffer

solutions at pH 4.008, 6.863 and 9.180, according to DIN 19266 (Merck Products Catalogue; see also Handbook of Chemistry and Physics, 72nd edn., 1991–1992, p. 8–34). The hydrogen ion concentration was obtained from the activity coefficient given by the Davies equation [22] (0.771 under the present experimental conditions).

The temperature of the solutions was kept constant to $25 \pm 0.2^\circ\text{C}$ with a Selecta Tectron thermostatic bath.

Absorbance data were recorded on a Beckman DU-7 single-beam spectrophotometer, connected to an IBM-PC via a serial interface. The data were acquired by using the DUMOD program [23].

Reagents

Sodium 8-hydroxyquinoline-5-sulphonate (Aldrich, analytical-reagent grade) was used without further purification.

A standard solution of Zn(II) (0.02 M) was prepared by dissolving pure metal (Merck) in hydrochloric acid, and standardized volumetrically with EDTA.

Sodium chloride solution (1.0 M) (Merck) was added to the solutions to maintain the ionic strength at 0.1 M.

Procedures

The experimental data were obtained by batch experiments by measuring the spectra of several series of solutions in which the metal and ligand concentrations were kept constant and the pH was varied by the addition of buffer solutions. In the determination of the dissociation constants of QS, two sets of batch experiments were carried out, at two concentration levels (corresponding to 36 spectra). In the determination of complex formation constants with Zn(II) ions, three series of experiments were carried out, at different metal concentrations and ligand to metal ratios, corresponding to 39 spectra (see Figs. 4 and 5 for experimental conditions).

Solutions containing QS and Zn(II) ion (when required), buffer (acetic acid, sodium dihydrogenphosphate, Tris, HCl and NaOH, depending on the pH range according to Perrin and Dempsey [22]) and NaCl were prepared in 50.0-ml volumet-

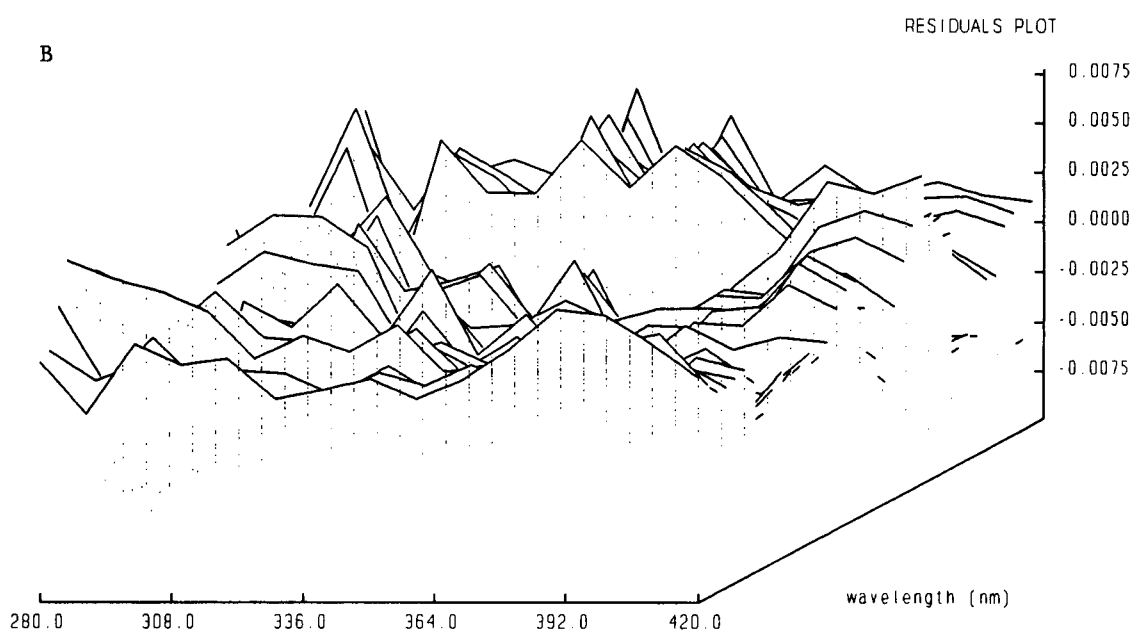
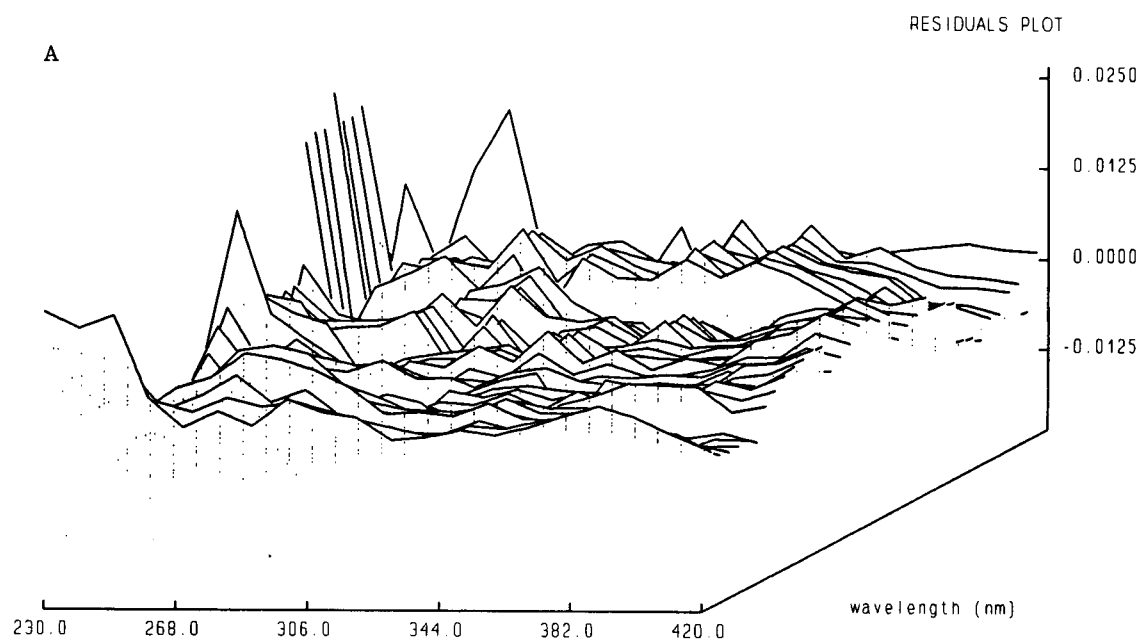


Fig. 3. Residuals plot after the refined constants (β_{011} , β_{012} and β_{112}), from the data corresponding to (A) 230–420 nm range and (B) 280–420 nm range.

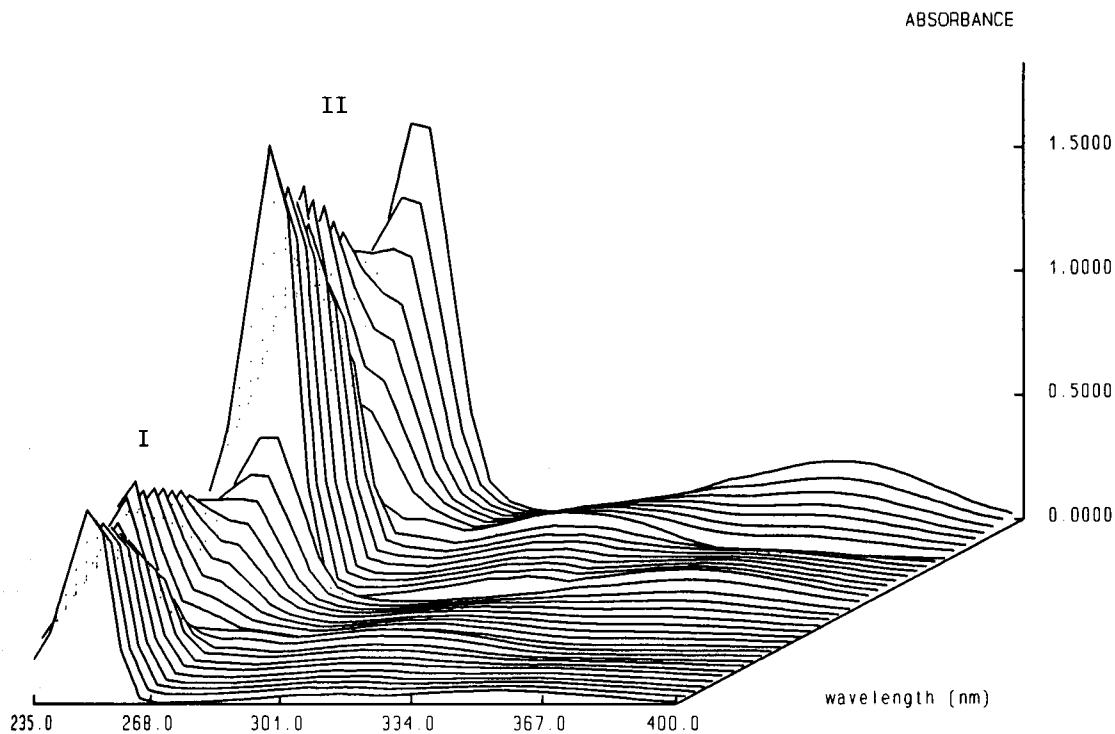


Fig. 4. Absorption spectra for the determination of dissociation constants of QS: (I) $C_{QS} = 2.07 \times 10^{-4}$ M (pH varied from 2.04 to 11.84); (II) $C_{QS} = 5.01 \times 10^{-4}$ M (pH varied from 2.02 to 11.81).

ric flasks. The concentrations of the buffers were about 0.003–0.004 M.

The solutions were thermostated in a water-bath at 25°C. The absorption spectra were

recorded at 5-nm increments from 220 to 450 nm, and the pH values of the solutions were measured.

The instrumental error of the spectrophotome-

TABLE 3

Dissociation constants of QS and complex formation constants with Zn(II) ions

| Parameter | This work | This work | This work | [25] ^a | [26] ^b |
|-----------------------------|-------------------|-------------------|--------------------|-------------------|-------------------|
| Wavelength range (nm) | 235–400 | 235–270 | 270–400 | | |
| pK_{a_1} | 3.801 ± 0.004 | 3.801 ± 0.007 | | 3.84 | 3.8 |
| pK_{a_2} | 8.358 ± 0.004 | 8.358 ± 0.007 | | 8.35 | 8.4 |
| $\text{Log } \beta_1$ | | | 7.572 ± 0.012 | 7.54 | |
| $\text{Log } \beta_2$ | | | 14.423 ± 0.022 | 14.32 | |
| Residual mean | 0.000361 | 0.001549 | 0.000123 | | |
| Mean residual | 0.00356 | 0.00727 | 0.00217 | | |
| $S_{(A)}$ | 0.00567 | 0.01033 | 0.00284 | | |
| $S_{3(A)}$ | 0.00277 | 0.00436 | 0.00111 | | |
| Skewness (should be = 0) | 0.968 | 0.512 | 0.137 | | |
| Kurtosis (should be = 3) | 9.089 | 3.860 | 3.137 | | |
| R factor (%) | 1.636 | 1.478 | 2.017 | | |
| χ^2 (should be < 12.6) | 221.48 | 13.11 | 3.809 | | |

^a Potentiometric. ^b Spectrophotometric.

ter [$S_{\text{inst}(A)}$] was 0.0023 absorbance units, as evaluated by the Wernimont's procedure [24].

Data treatment

Figure 4 plots the absorption spectra of QS at different pH, showing several bands, the most important between 235 and 270 nm, corresponding to the absorption maxima of the three different species (H_2QS , HQS^- and QS^{2-}). The dissociation constants were first determined from the data corresponding to the range 235–400 nm and then compared with the results obtained between 235 and 270 nm. As shown in Table 3, both results are in good agreement, and in accordance with the literature [25,26].

In the determination of complex formation constants between QS and Zn(II) ions, some of the most relevant features of the programs described were applied. Figure 5 plots the experi-

mental data for this system, showing several absorption bands, the most important between 230 and 270 nm. Although the variation in this band with change in the pH of solutions clearly indicates the formation of new species in solution, this band is not suitable for the computation of stability constants because of the high absorbance values (between 1 and 2). Instead of this band, the spectral range between 270 and 400 nm was used, where the absorbance of the ligand is lower, and the maximum absorbance values were about 0.3.

Figure 6A plots the data in this spectral range, showing two bands, the first centred at about 305 nm and the other about 360 nm. In the pH range studied (3.9–6.9), the first band decreases and the second increases. To demonstrate that the second band corresponds to the formation of Zn(II) complexes, Fig. 6B plots the calculated

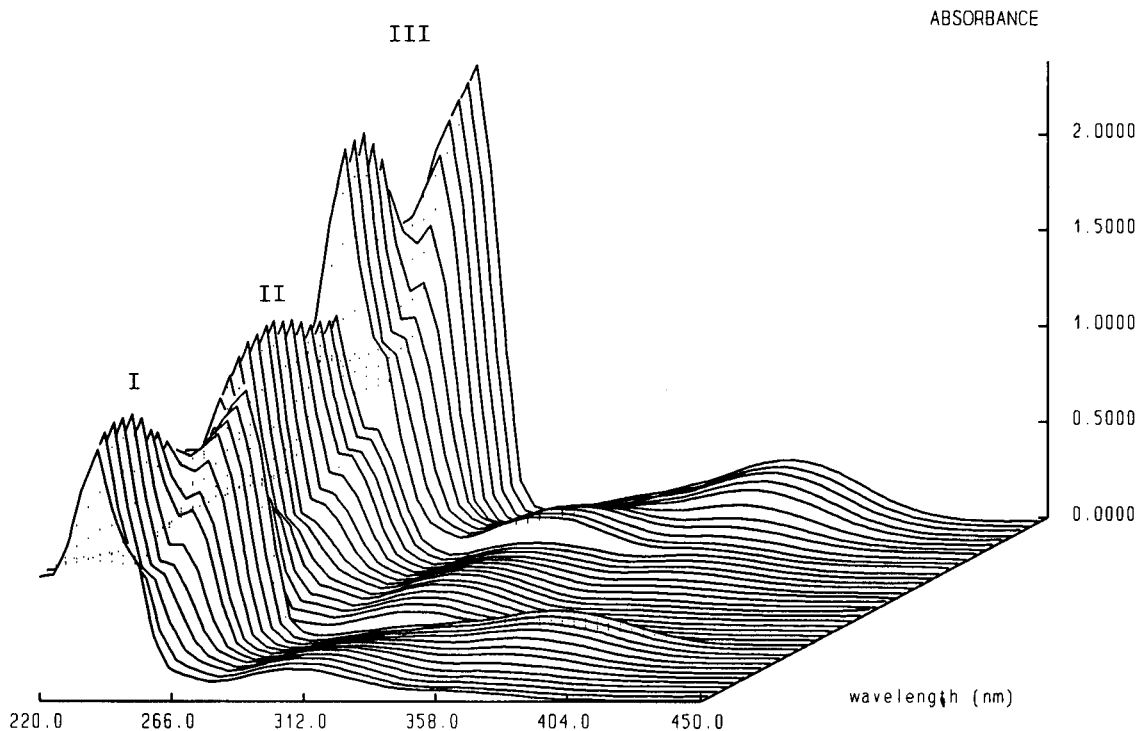


Fig. 5. Absorption spectra of the QS–Zn(II) system: (I) $C_{\text{QS}} = 5.01 \times 10^{-4}$ M, $C_{\text{Zn}} = 2.51 \times 10^{-4}$ M (pH from 4.27 to 6.95); (II) $C_{\text{QS}} = 5.02 \times 10^{-4}$ M, $C_{\text{Zn}} = 1.00 \times 10^{-4}$ M (pH from 3.81 to 6.95); (III) $C_{\text{QS}} = 8.04 \times 10^{-4}$ M, $C_{\text{Zn}} = 5.01 \times 10^{-4}$ M (pH from 4.44 to 6.91).

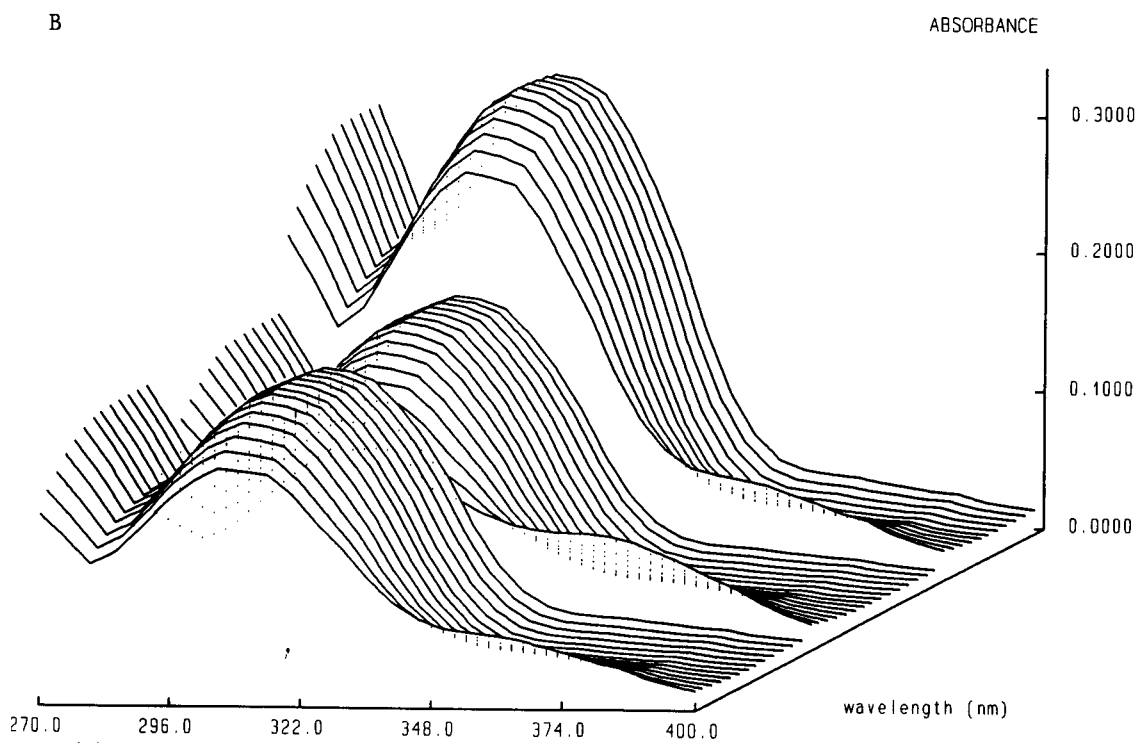
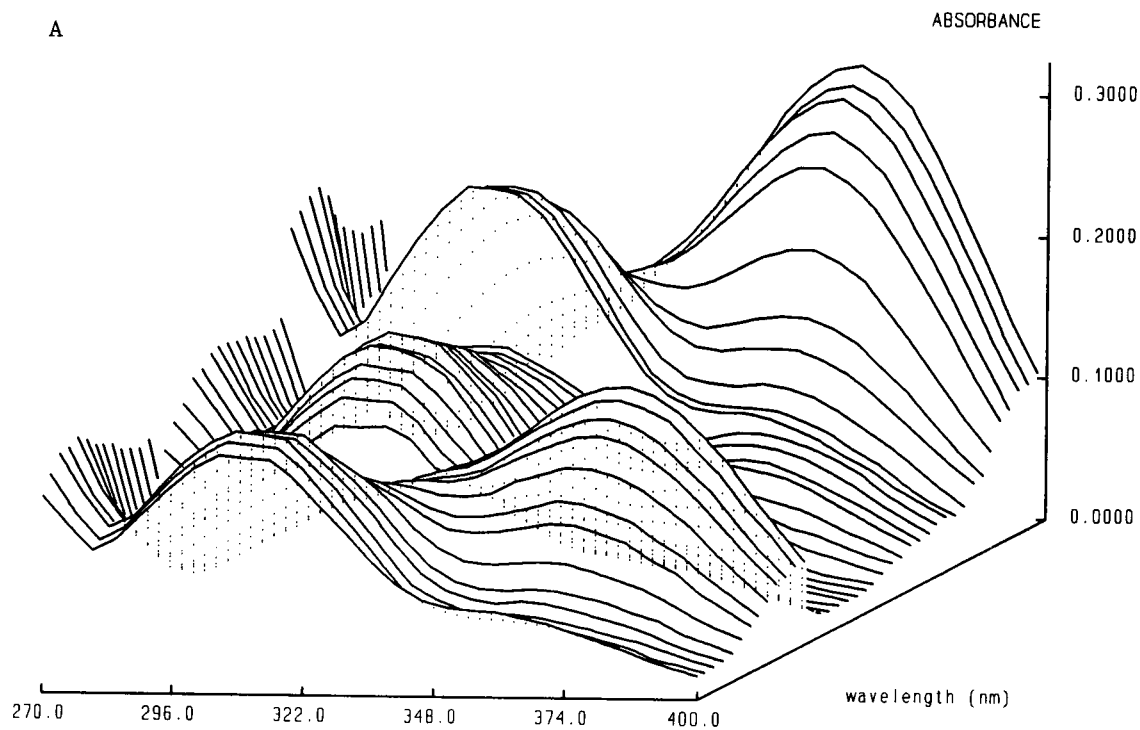


Fig. 6. (A) Experimental and (B) calculated spectra, obtained assuming no complex formation between Zn(II) and QS.

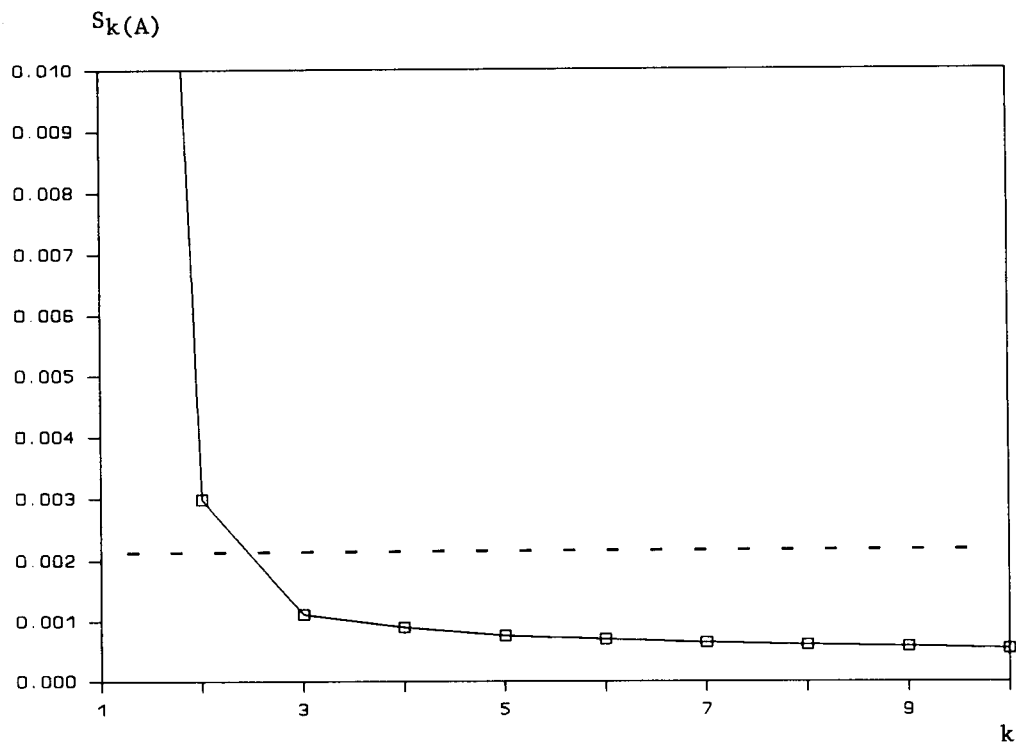


Fig. 7. Determination of the number of absorbing species in the Zn(II)-QS system after the data corresponding to Fig. 6A [dashed line indicates the instrumental error, $S_{inst(A)}$].

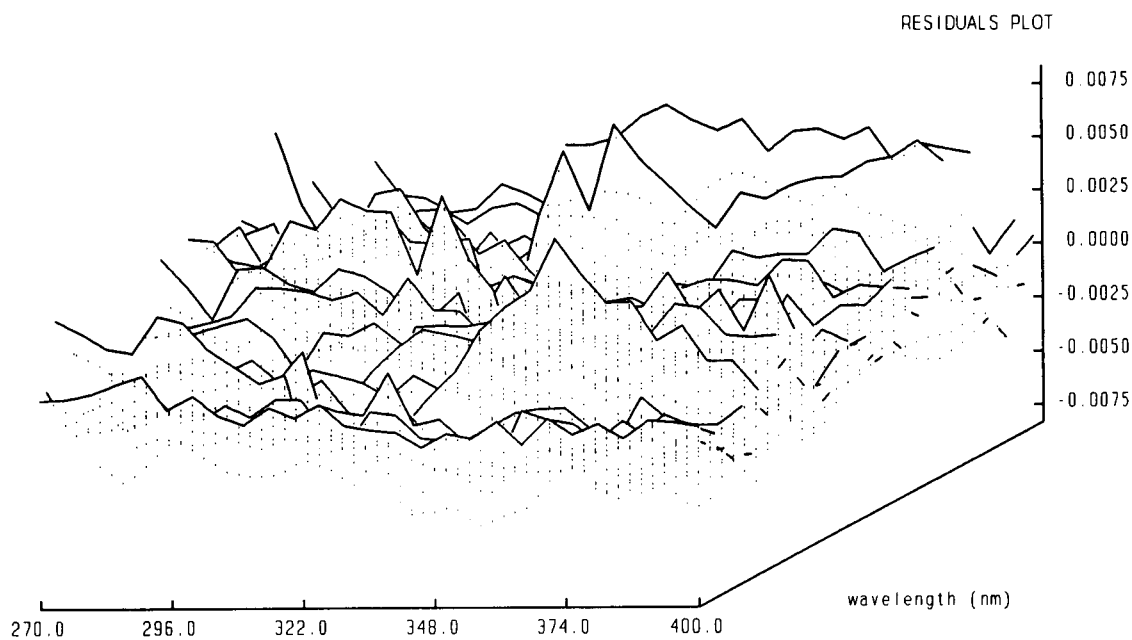


Fig. 8. Residuals plot after the refined formation constants in the Zn(II)-QS system.

spectra for QS under these experimental conditions. This task was done by deleting the species $Zn(QS)$ and $Zn(QS)_2$ from the model.

The experimental data were also treated by STAR/FA, in order to determine the number of absorbing species in solution. Figure 7 shows the plot of $S_{k(A)}$ versus k , the number of species, indicating that at least three absorbing species are needed to give a residual error comparable to the estimated instrumental error. Taking into account that the monoprotonated species of QS is predominant in the experimental pH range, it can be concluded that two complexes are formed.

The formation constants for the species $Zn(QS)$ and $Zn(QS)_2$ were refined by STAR, taking into account the complexes formed between Zn(II) and acetate and phosphate ions (the buffers used in this pH range) [21]. Starting values for $\log \beta_1$ and $\log \beta_2$ were taken as 8 and 15, respectively. The final values (7.572 and 14.423) were obtained after four iterations, giving a good fit to the experimental data. The standard deviation of the residuals was 0.00284 absorbance, close to the instrumental error of the spectrophotometer [$S_{inst(A)} = 0.0023$]. Figure 8 shows the residuals plot for this system after the refined constants.

Table 3 shows the results obtained, together with those given in the literature [25]. Although the formation constant for the complex $Zn(QS)$ agrees well with the literature, the difference in the logarithm of the formation constant for the complex $Zn(QS)_2$ is about 0.1 unit. Taking into account that both results were obtained at 25°C and 0.1 M ionic strength, this difference can be attributed to different experimental conditions, as it was reported [25] that some precipitation did occur at ca. pH 7, whereas in the present work, at lower concentrations of ligand and Zn(II) ions, no precipitation was observed.

DISCUSSION

The different routines implemented in STAR for the calculation of mass balances, refinement of constants and determination of molar absorbances are well known by the users of least-

squares programs for the determination of stability constants in complex equilibria. In this sense, STAR is a “classical” program. However, the aim in their development was not simply the refinement of equilibrium constants from absorbance data as a “black box”, but rather their use is dedicated to taking a closer look at experimental data.

The graphical information obtained directly on the computer screen (experimental and calculated data, together with the distribution of residuals) can be very useful in searching for possible errors in the experimental data and in planning new experimental designs when a system is studied. The possibilities of changing the model (by adding or deleting species) and with the selection of the wavelength range are also very valuable in searching for the “best” chemical model for a given system. In this way, the statistical tests given by the program are also a help for the user.

Otherwise, the results obtained by STAR are according to other programs when they are applied to the same data, but their advantages are the on-line plotting facilities and their interactive use.

The STAR and STAR/FA programs, together with sample data files, are available from the authors on request.

REFERENCES

- 1 W.A.E. McBryde, *Talanta*, 21 (1974) 979.
- 2 L. Sommer and M. Langová, *CRC Crit. Rev. Anal. Chem.*, 19 (1988) 225.
- 3 D.J. Leggett, S.L. Kelly, L.R. Shiue, Y.T. Wu, D. Chang and K.M. Kadish, *Talanta*, 30 (1983) 579.
- 4 H. Gampp, M. Maeder, C.J. Meyer and A.D. Zuberbühler, *Talanta*, 32 (1985) 257.
- 5 L.G. Sillén and B. Warnquist, *Ark. Kemi*, 31 (1968) 377.
- 6 D.J. Leggett (Ed.), *Computational Methods for the Determination of Formation Constants*, Plenum, New York, 1985.
- 7 M. Meloun, J. Havel and E. Högföldt, *Computation of Solution Equilibria: a Guide to Methods in Potentiometry, Extraction and Spectrophotometry*, Horwood, Chichester, 1988.
- 8 P.D. Taylor, I.E.G. Morrison and R.C. Hider, *Talanta*, 35 (1988) 507.
- 9 F. Gaizer and A. Puskás, *Talanta*, 28 (1981) 925.

- 10 E. Durand, *Solutions Numeriques des Equations Algébriques*, Tome II: Systèmes de Plusieurs Equations, Masson, Paris, 1972.
- 11 W.E. Wentworth, *J. Chem. Educ.*, 42 (1965) 96.
- 12 P.C. Wang, *Numerical Matrix Methods in Structural Mechanics*, Wiley, New York, 1966.
- 13 D.D. Perrin and I.G. Sayce, *Talanta*, 14 (1967) 833.
- 14 A. Izquierdo and J.L. Beltrán, *J. Chemometr.*, 3 (1988) 209.
- 15 J.L. Beltrán, R. Compañó, M. Granados, J. Guiteras and M.D. Prat, *An. Quim.*, 87 (1991) 593.
- 16 M. Meloun, M. Javurek and J. Havel, *Talanta*, 33 (1986) 513.
- 17 E.R. Malinowski and D.G. Howery, *Factor Analysis in Chemistry*, Wiley, New York, 1980.
- 18 J.J. Kankare, *Anal. Chem.*, 42 (1970) 1322.
- 19 W.R. Seitz, *CRC Crit. Rev. Anal. Chem.*, 8 (1980) 367.
- 20 Z. Zhujun and W.R. Seitz, *Anal. Chim. Acta*, 171 (1985) 251.
- 21 R.M. Smith and A.E. Martell, *Critical Stability Constants*, Vol. 2, Plenum, New York, 1975.
- 22 D.D. Perrin and B. Dempsey, *Buffers for pH and Metal Ion Control*, Chapman and Hall, London, 1974.
- 23 J.L. Beltrán, G. Centeno, A. Izquierdo and M.D. Prat, *Talanta*, 39 (1992) 981.
- 24 G. Wernimont, *Anal. Chem.*, 39 (1967) 554.
- 25 C.F. Richard, R.C. Gustafson and A.E. Martell, *J. Am. Chem. Soc.*, 81 (1959) 1033.
- 26 J.I. García Alonso, M.E. Díaz García and A. Sanz Medel, *Talanta*, 31 (1984) 361.

Identification of “grey” analytical systems with incomplete information

Yu-Long Xie, Yi-Zeng Liang and Ru-Qin Yu

Department of Chemistry and Chemical Engineering, Hunan University, Changsha 410082 (China)

(Received 21st November 1991; revised manuscript received 19th November 1992)

Abstract

For the calibration of “grey” analytical systems with a known range of components, the identification of truly co-existing species in a sample is of primary concern. Variance decomposition proportions (VDP), usually used as an indicator of the collinearities among regressors, were extended as a tool to judge the existence of any species among all possibly existing ones in a specific sample. The effect of the level of noise and the presence of spectral overlap was investigated by computer simulation, and some guidelines were developed. Experimental data for real analytical systems were interpreted by the proposed method with satisfactory results.

Keywords: Multivariate calibration; Grey analytical systems; Singular value decomposition; Variance decomposition proportion

An analyst often encounters analytical systems for which the range of possibly existing species are well known, but the really existing components are not exactly known. For example, the possible pollutants in certain environmental areas are usually well known, but the number and identities of truly existing species varies with the sampling location and time. Another example is the detection of additives in food samples. Usually limited identities of additives are permissible according to processing regulations and the range of additive species to be tested is known a priori.

Analytical systems of this sort belong to the so-called “grey” analytical systems [1]. The primary step in calibrating such a “grey” analytical system is to identify which components really exist in the sample. Target transformation factor analysis (TTFA) can be used in this situation [2],

but unfortunately a set of mixtures containing the same components with different concentrations necessary for TTFA is not always available. Using some concepts utilized in regression diagnostics [3], namely variance decomposition proportions (VDP), a method was developed to accomplish qualitative and quantitative analyses for a “grey” analytical system with only one sample mixture. The effect of noise and spectral overlap was investigated by computer simulation, and the interpretation of experimental data for real analytical samples was accomplished with satisfactory results.

THEORY

According to Beer’s law and the spectral additivity principle, the general calibration model of a “grey” analytical system in spectral analysis can be expressed as follows:

$$a = \sum s_i c_i + e = Sc + e \quad (1)$$

Correspondence to: Ru-Qin Yu, Department of Chemistry and Chemical Engineering, Hunan University, Changsha 410082 (China).

where \mathbf{a} is the mixture spectrum vector in n wavelengths, \mathbf{s}_i is the standard spectrum vector for species i ($i = 1, \dots, p$) in the same spectral range with n wavelengths, p is the number of possibly existing species, $\mathbf{S} = (\mathbf{s}_1, \dots, \mathbf{s}_p)$ is an $n \times p$ matrix of spectral sensitivities, c_i is the relative concentration of species i and c_i is zero when species i does not exist in the sample. The measurement error vector, \mathbf{e} , was assumed to obey a zero-mean, constant variance normal distribution, $N(0, \sigma^2)$. For one specific sample, \mathbf{a} is the linear combination of \mathbf{s}_k and $\mathbf{s}_k \{1 \leq k \leq p, \mathbf{s}_k \in \mathbf{S}\}$ is a subset of \mathbf{S} . The subscripts k are to be identified for the calibration of such a "grey" analytical system.

The singular value decomposition (SVD) of the matrix \mathbf{S} is defined as

$$\mathbf{S} = \mathbf{U}\mathbf{D}\mathbf{V}' \quad (2)$$

where \mathbf{U} is an $n \times p$ matrix, \mathbf{V} a $p \times p$ column orthogonal matrix and \mathbf{D} a $p \times p$ diagonal matrix with non-negative diagonal elements, d_i ($i = 1, \dots, p$), called the singular values of \mathbf{S} . The close relationship between the SVD and the eigen-decomposition is straightforward. Actually, \mathbf{U} is the matrix of eigenvectors for $\mathbf{S}\mathbf{S}'$ and \mathbf{V} for $\mathbf{S}'\mathbf{S}$. The squares of the singular values of \mathbf{S} are the eigenvalues of $\mathbf{S}'\mathbf{S}$ or $\mathbf{S}\mathbf{S}'$.

SVD (or eigen-decomposition) of matrices can be used to diagnose the extent of collinearity of \mathbf{S} [3]. Collinearity exists when variables in \mathbf{S} are not truly independent and display some multiple linear dependence. This is usually referred to as ill-conditioning and is due to the spectral overlap among the components present in the analytical sample. The nearness to zero of the smallest singular value is a measure of collinearity and the number of singular values close to zero indicates the number of near linear dependences among the variables. Some related criteria such as the condition number and condition index are defined as follows:

$$\text{Cond}(\mathbf{S}) = d_{\max}/d_{\min} \quad (3)$$

$$\eta_j = d_{\max}/d_j \quad (j = 1, \dots, p)$$

Generally, as a rule of thumb, values of Cond and η larger than 10 indicate a moderate

collinearity and larger than 30 suggest a very strong dependence between spectra of components. In spite of the fact that simultaneous appearance of several relatively large η_j implies the number of collinearities in a variable set, the identities of variables involved in these collinearity relationships remain unknown. The relevant information can be obtained by using the variance decomposition proportions (VDP) of regressor coefficients.

The variance of the estimation of regressor coefficients in Eqn. 1 can be expressed as

$$\text{Var}(\mathbf{c}) = \sigma^2(\mathbf{S}'\mathbf{S})^{-1} = \sigma^2(\mathbf{V}\mathbf{D}^{-2}\mathbf{V}') \quad (4)$$

and for the i th element of \mathbf{c}

$$\text{Var}(c_i) = \sigma^2 \sum v_{ij}^2/d_j^2 \quad (5)$$

Equation 5 shows that the variance of each regressor coefficient can be expressed through the summation of p separate terms, each corresponding to only one specific singular value. In each term, the d_j in the denominator reflects the extent of corresponding collinearity and the v_{ij} in the numerator is the weight of variable i in this near linear dependence. A very large value of $\text{Var}(c_i)$ would be expected when variable i involved a serious collinearity.

Belsley et al. [3] denoted the terms under the summation mark, v_{ij}^2/d_j^2 , as ϕ_{ji} and the sum, $\sum v_{ij}^2/d_j^2$ or $\sum \phi_{ji}$ as ϕ_i , and defined the ratio ϕ_{ji}/ϕ_i as VDP, denoted by π_{ji} :

$$\pi_{ji} = \phi_{ji}/\phi_i = (v_{ij}^2/d_j^2) / (\sum v_{ij}^2/d_j^2) \quad (i, j = 1, \dots, p) \quad (6)$$

The VDP can be used as a measure of collinearity among the variables of \mathbf{S} . Thus, a $p \times p$ matrix $\mathbf{\Pi}$ with π_{ji} as its elements was obtained, and the elements of each column of $\mathbf{\Pi}$ are the proportions of the variance for each c_i contributed by the j th singular value. Obviously, $0 \leq \pi_{ji} \leq 1$ and $\sum \pi_{ji} = 1$.

If relatively large values of π_{ji} for two or more columns i in the same row j are obtained, and the row is simultaneously associated with a large condition index η_j , a near linear dependence involving the variables corresponding to those columns i is present. In this way, the combination

of condition index and VDP can provide not only the number of collinearity among variables in S but also the variables involved in each near dependence.

Kalivas [4] used the variance decomposition proportion of pure component spectra as a measure of selectivity. The same concepts can be used for identification of components really present in an analytical sample among all possibly existing ones. This is the first step of calibration of a "grey" analytical system. Her the purpose is not to diagnose the collinearity among variables in S . Actually, one has to detect which variables in S have a linear dependence with mixture a .

If the experimental error is ignored, Eqn. (1) can be thought as a stringent linear relationship between a and s_k . Let $s_{p+1} = a$ and $S = (S|s_{p+1})$, the resulting $n \times (p+1)$ matrix S would be rank-deficient. Using SVD on S , a zero singular value d_{p+1} and the value of η_{p+1} approaching infinity would be expected. Thus, for the species with spectrum s_k which truly exist in the sample, the terms corresponding to d_{p+1} in Eqn. 5 will be dominate and $\pi_{p+1,k}$ will be equal to 1. So, picking out the columns in matrix II which have elements of value 1 in the $(p+1)$ th row will indicate the really existing components, i.e., the qualitative composition, in the mixture sample with recorded spectrum a .

In the presence of measurement errors, however, the stringent linear dependence between the mixture spectrum a and the spectra of its components, s_k , does not hold, and Eqn. 1 appears to be only a strong collinearity. Generally, under the condition of low noise level and weak collinearity in an analytical system itself as expressed by $\text{Cond}(S)$, the collinearity related to the mixture and its components is the strongest for matrix S . Hence we can still judge the composition of the mixture by observing the elements of the $(p+1)$ th row of matrix II . However, in this case, the value of $\pi_{p+1,k}$ related to the mixture and its components will not be equal to 1 but will have a smaller value near to 1.

It can be imagined that, as the measurement error, e , increases, the relationship between a and Sc will depart further from a stringent linear dependence, or the extent of the corresponding

collinearity will weaken and the value of $\pi_{p+1,k}$ and π_{p+1} will be lower than those for error-free systems. In this sense, the value of η_{p+1} can be taken as a measure of measurement error in recording the spectrum of the sample mixture, a .

Similarly, under the same noise level, the stronger the collinearity in the analytical system itself as expressed by $\text{Cond}(S)$, the smaller will be the difference between η_p and η_{p+1} . In this case, the corresponding $\pi_{p+1,k}$ will be much lower than 1, because there are two competing terms in Eqn. 5 in this situation. Hence the key point for the method to work successfully is to distinguish the effect of the linear relationship between a and s_k , and the effect of error and spectral overlap on the value of $\pi_{p+1,k}$. Here, the ratio of $\eta_{p+1}(S)$ and $\text{Cond}(S)$

$$R = \eta_{p+1}(S) / \text{Cond}(S) \quad (7)$$

is used for judgment of the effect of the aforementioned factors on the qualitative analysis based on $\pi_{p+1,k}$.

EXPERIMENTAL

The absorption spectra were measured on a Beckman DU-7 or Hitachi U-2000 UV-visible spectrophotometer and AQS-20 Fourier transform IR spectrophotometer. The spectra were processed with the proposed algorithm on a Macintosh II microcomputer.

The spectrum of a component was simulated by a Gaussian band generated over 140 points with a height of 1 and a bandwidth of 20 points. Differential components have Gaussian spectra with different band centres. Four groups each containing seven different components were formulated to study the effect of spectral overlapping. In each group seven mixtures were simulated by taking two or three components from this group by a linear combination of corresponding Gaussian bands. Mixture No. 4 in each group contained three components with the most seriously overlapping spectra. All mixture spectra were normalized to unit variance and normal distributed random noise with standard deviations 0.001, 0.002, 0.003, 0.004 and 0.005 was

added to them to simulate the experimental errors. The results of different simulated cases are shown in Table 1.

Up to fifteen mixture spectra consisting of 2–7 real chemical components were generated from the corresponding spectra of pure compounds taken arbitrarily from standard spectra of 21 amino acids (Table 2).

Standard solutions of Cu^{2+} , Co^{2+} , Cr^{3+} and Ni^{2+} were prepared with deionized water using reagents of analytical-reagent grade. Several two- and three-component mixtures were prepared with the standard solutions and the spectra were recorded every 10 nm from 350 to 800 nm.

Standard solutions of L-tyrosine, DL-histidine monohydrochloride, DL-tryptophan and DL- β -phenylalanine, and mixtures of three of them, were prepared with 0.1 mol l^{-1} HCl. The amino acids and other compounds used were of chromatographic purity (BDH, Poole). The UV absorption spectra were measured with 0.1 mol l^{-1} HCl as reference and the data were recorded in the range 200–300 nm at 1-nm intervals.

Several milligrams of pure amino acid were weighed accurately and mixed with KBr of analytical-reagent grade which had been dried for 6 h on 200°C , and the samples for IR analysis were prepared by pressing uniform mixtures of amino acids and KBr into a standard slice of 0.1. Four samples of two sets of three-component mixtures, first consisting of DL-alanine, L-glutamic acid and

L-leucine and the second consisting of 3-(3,4-dihydroxyphenyl)-DL-alanine, DL-serine and DL-threonine, were prepared according to the same procedure. The spectrum of a pure KBr slice was taken as reference and the spectra of all samples of pure and mixed amino acids were recorded from 459.0 to 804.9 cm^{-1} every 5 cm^{-1} after baseline correction. The amino acids used were DL-alanine (1), DL-2-amino-*n*-butyric acid (2), L-arginine monohydrochloride (3), L-cysteine hydrochloride (4), L-proline (5), L-glutamic acid (6), glycine (7), L-histidine monohydrochloride (8), L-hydroxyproline (9), L-leucine (10), DL-norleucine (11), L-lysine monohydrochloride (12), DL-methionine (13), L-ornithine monohydrochloride (14), DL- β -phenylalanine (15), 3-(3,4-dihydroxyphenyl)-DL-alanine (16), DL-serine (17), DL-threonine (18), DL-trptophan (19), L-tyrosine (20) and DL-valine (21).

Solutions of colouring matters, including amarant, new cocine, tartrazine, brilliant blue and erythrosine and twelve two- and three-component mixtures were prepared with analytical-reagent grade reagents and deionized water as solvent. The absorbance was measured at 2.5-nm intervals between 350 and 700 nm.

Solutions of drugs, including aminopyrine, antipyrine, barbital, aspirin, phenacetine and caffeine and fifteen mixtures of two sets of three-component mixtures consisting of three of these drugs were prepared with 0.1 mol l^{-1} NaOH.

TABLE 1

The smallest value of the $(p + 1)$ th variance decomposition proportion of existing components and corresponding R of simulated spectral systems with Gaussian bands

| Band centres ^a (1, 2, 3, 4, 5, 6, 7) | Cond(S) | Noise variance | | | | |
|--|-------------|--|-------------------------|-------------------------|-------------------------|-------------------------|
| | | 0.001 | 0.002 | 0.003 | 0.004 | 0.005 |
| 25, 35, 45, 65, 85, 95, 105 | 3.12 | 60.16 ^b (59.89) ^c 0.9979 ^d | 31.06 (28.24) 0.9903 | 20.38 (17.59) 0.9754 | 15.66 (15.31) 0.9688 | 12.25 (11.33) 0.9465 |
| 31, 38, 45, 65, 85, 92, 99 | 6.18 | 33.31 (32.39) 0.9923 | 16.48 (15.47) 0.9677 | 10.81 (9.60) 0.9204 | 8.35 (7.00) 0.8372 | 6.44 (6.85) 0.8357 |
| 35, 40, 45, 65, 85, 90, 95 | 12.34 | 16.45 (14.87) 0.9607 | 8.41 (7.38) 0.8458 | 5.79 (5.50) 0.7858 | 4.18 (4.06) 0.6340 | 3.34 (3.27) 0.4944 |
| 39, 42, 45, 65, 85, 88, 91 | 35.94 | 5.86 (5.74) 0.7564 | 3.05 (2.95) 0.4406 | 2.01 (1.82) 0.2746 | 1.61 (1.47) 0.2932 | 1.19 (1.16) – |

^a Composition of seven synthetic mixtures for each group: No. 1 (1, 2), No. 2 (1, 3), No. 3 (2, 3), No. 4 (1, 2, 3), No. 5 (1, 2, 4), No. 6 (1, 2, 6), No. 7 (1, 4, 6). ^b The mean of R values for all seven mixtures. ^c R value of mixture No. 4 (containing components 1, 2 and 3 of each group). ^d The smallest value of the $(p + 1)$ th variance decomposition proportion of existing components.

The spectra were recorded in the range 220–290 nm at 2-nm intervals.

A pharmaceutical sample of an injection ampoule with a lost label was taken and the identification and determination of the components were accomplished using the proposed method.

RESULTS AND DISCUSSION

Computer simulation was carried out to investigate the effect of the noise level and the collinearity of analytical signals due to spectral overlap. In order to take into account these effects, the ratio, R , of $\eta_{p+1}(\mathbf{S})$ and $\text{Cond}(\mathbf{S})$ (Eqn. 7) was used as a measure characterizing the given analytical system. The R values for all the mixtures for each noise level are listed in Tables 1 and 2 together with the smallest value of the $(p+1)$ th VDP of the existing components. The results for the case without noise added are not shown here, because all $\pi_{p+1,k}$ values for the existing species were 1 as expected. It can be seen from Tables 1 and 2 that the smallest value of $\pi_{p+1,k}$ of the existing species decreased with decrease in R . For the same simulation group, only

a minor difference was observed for mixtures with different numbers and identities of species. If one checks the smallest $\pi_{p+1,k}$ for existing species for all seven mixtures among each simulated spectral group (not shown in Table 1), then one can see that the lowest value for seven $\min(\pi_{p+1,k})$ happened to be always the $\min(\pi_{p+1,k})$ for the fourth sample with band centres 1, 2, 3 and the strongest spectral overlap. The value of R for the fourth mixture is given in parentheses in Table 1 together with the average R for all seven mixtures. For all cases except the last one in Table 1, the largest $\pi_{p+1,i}$ of non-existing species was lower than 0.1, with several exceptions which were near 0.2 (not shown in Table 1). Hence the difference between the two sorts of elements in the $(p+1)$ th row of \mathbf{II} is significant. In ideal situations, it seems that one can simply take the value 0.2 as a threshold and consider a species as really existing in a mixture as long as the corresponding $\pi_{p+1,k}$ is larger than 0.2, provided that the corresponding value of R is larger than 2. Unfortunately, however, for real systems the smallest $\pi_{p+1,k}$ of existing components could be lower and the largest $\pi_{p+1,i}$ of non-existing components could be much higher than 0.2 because of the failure of the normal

TABLE 2

The smallest value of the $(p+1)$ th variance decomposition proportion of existing components and corresponding R of simulated IR spectral system

| No. of species | Noise variance | | | | |
|----------------|---------------------|--------|--------|--------|--------|
| | 0.001 | 0.002 | 0.003 | 0.004 | 0.005 |
| 2 ^a | 34.79 ^c | 16.37 | 10.79 | 8.04 | 6.36 |
| | 0.9964 ^d | 0.9853 | 0.9661 | 0.9142 | 0.9120 |
| 3 ^b | 32.77 | 15.96 | 9.54 | 7.79 | 5.99 |
| | 0.9953 | 0.9849 | 0.9494 | 0.9324 | 0.8959 |
| 4 | 30.12 | 14.56 | 9.57 | 8.30 | 5.98 |
| | 0.9948 | 0.9781 | 0.9462 | 0.9349 | 0.8775 |
| 5 | 28.16 | 16.56 | 9.71 | 8.09 | 5.22 |
| | 0.9888 | 0.9606 | 0.8963 | 0.8478 | 0.6966 |
| 6 | 40.67 | 18.48 | 10.60 | 9.48 | 6.50 |
| | 0.9891 | 0.9502 | 0.8551 | 0.8488 | 0.7051 |
| 7 | 25.45 | 12.98 | 9.41 | 6.43 | 6.22 |
| | 0.9760 | 0.9134 | 0.8194 | 0.6322 | 0.7480 |

$\text{Cond}(\mathbf{S}) = 18.70$

^a Seven mixtures were simulated, average R values are shown. ^b Four mixtures were simulated, average R values are shown. ^c R values. ^d The smallest value of the $(p+1)$ th variance decomposition proportion of existing components.

TABLE 3

Metal ion solution mixtures: ions possibly existing are Cr³⁺, Ni²⁺, Co²⁺, and Cu²⁺

| No. | I ^a | II ^b | III ^c | Taken (mg ml ⁻¹) | | | | Found (mg ml ⁻¹) | | | | MRPE (%) |
|-----|----------------|-----------------|------------------|------------------------------|-------|-------|-------|------------------------------|-------|-------|----|----------|
| | | | | Cr | Ni | Co | Cu | Cr | Ni | Co | Cu | |
| 1 | 55.81 | 0.9984 | 0.5552 | 6.403 | 2.196 | 1.754 | 0.000 | 6.345 | 2.189 | 1.723 | – | 0.67 |
| 2 | 62.20 | 0.9967 | 0.5712 | 6.403 | 2.196 | 0.877 | 0.000 | 6.376 | 2.193 | 0.837 | – | 1.53 |
| 3 | 60.43 | 0.9864 | 0.5844 | 6.403 | 2.196 | 0.483 | 0.000 | 6.405 | 2.203 | 0.395 | – | 3.27 |
| 4 | 172.9 | 0.9997 | 0.0940 | 3.202 | 2.196 | 0.000 | 0.000 | 3.305 | 2.632 | – | – | 1.66 |
| 5 | 102.8 | 0.9989 | 0.6767 | 3.202 | 2.635 | 0.000 | 0.000 | 3.303 | 2.189 | – | – | 1.58 |
| 6 | 178.9 | 0.9995 | 0.2159 | 3.202 | 3.074 | 0.000 | 0.000 | 3.281 | 3.073 | – | – | 1.23 |
| 7 | 204.2 | 0.9995 | 0.2003 | 3.202 | 3.513 | 0.000 | 0.000 | 3.300 | 3.542 | – | – | 1.59 |
| 8 | 169.1 | 0.9990 | 0.1418 | 3.202 | 3.952 | 0.000 | 0.000 | 3.294 | 3.983 | – | – | 1.49 |
| 9 | 128.2 | 0.9985 | 0.1188 | 3.202 | 4.391 | 0.000 | 0.000 | 3.349 | 4.398 | – | – | 2.30 |
| 10 | 63.82 | 0.9992 | 0.5603 | 6.403 | 2.196 | 0.000 | 0.000 | 6.479 | 2.255 | – | – | 1.47 |

Cond(S) = 3.57

^a The value of R . ^b The smallest value of the $(p + 1)$ th variance decomposition proportion of the existing species in the mixture.^c The largest value of the $(p + 1)$ th variance decomposition proportion of non-existing species.

distribution assumption in real systems and the effect of experimental errors. This can be seen from Tables 3–6, where the spectral data for real systems are analysed. However, one can see the obvious difference between the two categories of elements in the $(p + 1)$ th row of the **II** matrix of a mixture and it is easy to find the existing components with the help of the value of $\pi_{p+1,i}$.

Based on a systematic analysis of the results of simulated and real analytical systems, some empirical regularities were formulated. It turned out that the critical values of $\pi_{p+1,i}$, denoted π_{crit} , varied with the value of R of the given analytical

system. With $R \geq 30$, a π_{crit} of 0.95 should be used, that is, components i corresponding to $\pi_{p+1,i} \geq 0.95$ could be identified as existing in the sample, otherwise the component should be considered as absent. This π_{crit} would decrease with decrease in R : for $30 > R \geq 10$, $\pi_{\text{crit}} = 0.80$, for $10 > R \geq 3$, $\pi_{\text{crit}} = 0.50$, and for $3 > R \geq 2$, $\pi_{\text{crit}} = 0.30$; undoubtedly, the higher the value of R , the more reliable is the identification result.

As the value of R approaches 1 (the lower right of Table 1), the reliability of identification cannot be assured, because in this case the extent of collinearities related to η_p and η_{p+1} becomes

TABLE 4

UV spectra system of amino acids: possibly existing species are L-tyrosine (1), L-histidine monohydrochloride (2), DL-tryptophan (3) and DL- β -phenylalanine (4)

| No. | I ^a | II ^b | III ^c | Taken ($\mu\text{g ml}^{-1}$) | | | | Found ($\mu\text{g ml}^{-1}$) | | | | MRPE (%) |
|-----|----------------|-----------------|------------------|---------------------------------|-------|------|------|---------------------------------|-------|------|---|----------|
| | | | | 1 | 2 | 3 | 4 | 1 | 2 | 3 | 4 | |
| 1 | 15.86 | 0.9776 | 0.0051 | 8.00 | 20.00 | 4.80 | 0.00 | 7.91 | 20.40 | 4.73 | – | 0.93 |
| 2 | 19.12 | 0.9760 | 0.0025 | 8.00 | 20.00 | 2.40 | 0.00 | 8.09 | 20.14 | 2.44 | – | 0.71 |
| 3 | 19.96 | 0.9731 | 0.1699 | 8.00 | 12.00 | 4.80 | 0.00 | 7.79 | 12.02 | 4.82 | – | 0.89 |
| 4 | 33.00 | 0.9946 | 0.6215 | 8.00 | 12.00 | 2.40 | 0.00 | 7.70 | 11.67 | 2.54 | – | 2.49 |
| 5 | 11.49 | 0.9332 | 0.0633 | 12.00 | 16.00 | 4.00 | 0.00 | 12.26 | 16.51 | 3.93 | – | 1.41 |
| 6 | 21.64 | 0.9728 | 0.0470 | 12.00 | 16.00 | 2.00 | 0.00 | 12.10 | 16.17 | 2.08 | – | 1.41 |
| 7 | 31.51 | 0.9791 | 0.4644 | 12.00 | 8.00 | 4.00 | 0.00 | 11.67 | 7.84 | 4.10 | – | 1.41 |
| 8 | 24.98 | 0.9772 | 0.2399 | 12.00 | 8.00 | 2.00 | 0.00 | 11.75 | 7.71 | 2.15 | – | 2.86 |

Cond(S) = 18.70

^{a-c} See Table 3.

TABLE 5

Coloring matter mixtures: possibly existing species are brilliant blue (1), tartrazine (2), erythrosine (3), amaranth (4) and coccine (5)

| No. | I ^a | II ^b | III ^c | Taken ($\mu\text{g ml}^{-1}$) | | | | | Found ($\mu\text{g ml}^{-1}$) | | | | | MRPE (%) |
|-----|----------------|-----------------|------------------|---------------------------------|-------|-------|-------|-------|---------------------------------|-------|-------|-------|-------|----------|
| | | | | 1 | 2 | 3 | 4 | 5 | 1 | 2 | 3 | 4 | 5 | |
| 1 | 63.10 | 1.0000 | 0.1177 | 10.00 | 22.00 | 0.00 | 0.00 | 0.00 | 9.99 | 21.88 | – | – | – | 0.28 |
| 2 | 37.40 | 0.9995 | 0.4422 | 10.00 | 0.00 | 14.04 | 0.00 | 0.00 | 10.02 | – | 14.17 | – | – | 0.47 |
| 3 | 61.60 | 0.9998 | 0.4205 | 10.00 | 0.00 | 0.00 | 38.00 | 0.00 | 10.03 | – | – | 37.30 | – | 0.93 |
| 4 | 97.60 | 0.9999 | 0.3534 | 10.00 | 0.00 | 0.00 | 0.00 | 42.00 | 10.01 | – | – | – | 41.50 | 0.60 |
| 5 | 74.30 | 1.0000 | 0.2506 | 0.00 | 22.0 | 14.04 | 0.00 | 0.00 | – | 21.92 | 14.18 | – | – | 0.53 |
| 6 | 114.4 | 0.9999 | 0.1914 | 0.00 | 22.00 | 0.00 | 38.00 | 0.00 | – | 22.13 | – | 37.65 | – | 0.55 |
| 7 | 119.1 | 0.9998 | 0.2743 | 0.00 | 22.00 | 0.00 | 0.00 | 42.00 | – | 21.67 | – | – | 40.97 | 1.44 |
| 8 | 82.00 | 0.9997 | 0.3120 | 0.00 | 0.00 | 6.84 | 19.00 | 0.00 | – | – | 6.84 | 18.74 | – | 0.68 |
| 9 | 31.20 | 0.9981 | 0.0691 | 9.60 | 22.00 | 14.04 | 0.00 | 0.00 | 9.52 | 21.81 | 13.88 | – | – | 0.55 |
| 10 | 42.10 | 0.9987 | 0.0095 | 9.60 | 22.00 | 0.00 | 38.00 | 0.00 | 9.54 | 21.84 | – | 38.04 | – | 0.32 |
| 11 | 38.30 | 0.9982 | 0.1003 | 4.80 | 0.000 | 6.84 | 18.00 | 0.00 | 4.87 | – | 6.74 | 18.00 | – | 0.69 |
| 12 | 67.60 | 0.9992 | 0.1156 | 0.00 | 11.0 | 6.84 | 18.00 | 0.00 | – | 10.97 | 6.75 | 18.21 | – | 0.59 |

Cond(S) = 11.17

^{a-c} See Table 3.

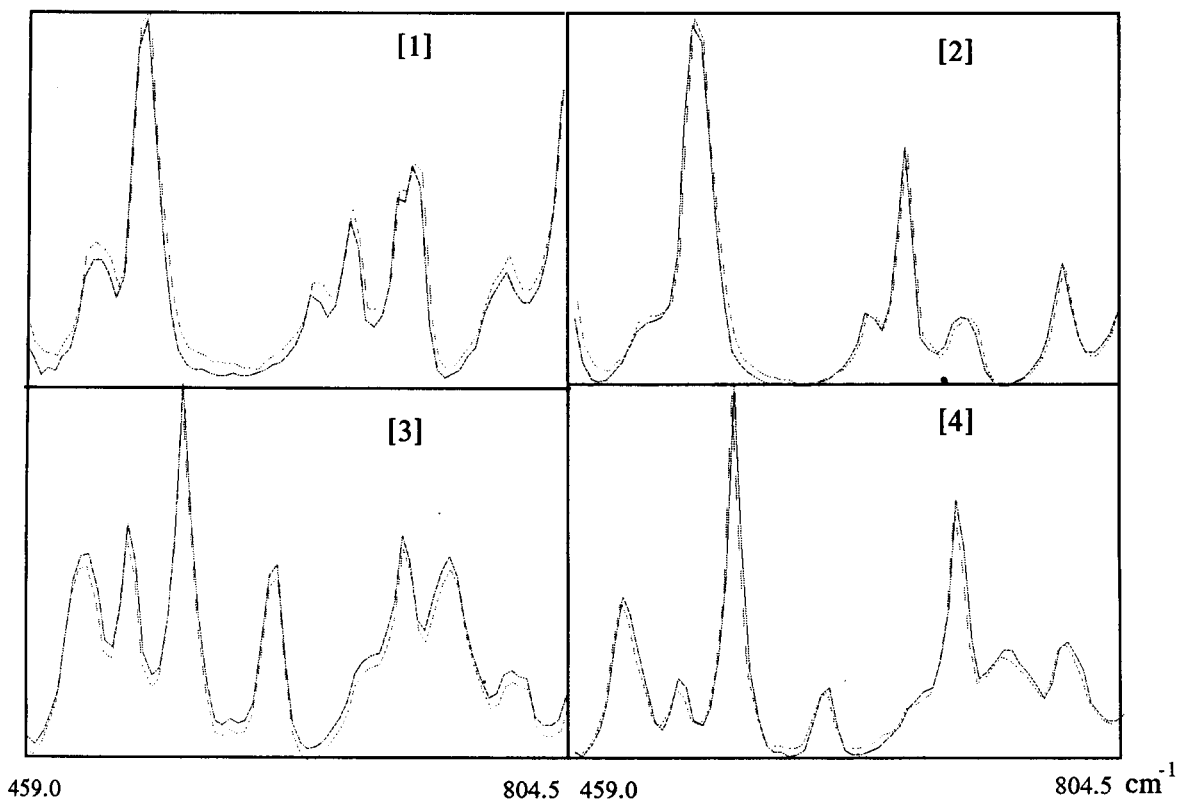


Fig. 1. Comparison between the actual IR spectra (solid lines) and the calculated IR spectra (dashed lines) of amino acid mixtures. (1) and (2) = three-component mixtures of Nos. 1, 6 and 10; (3) and (4) = three-component mixtures of Nos. 16, 17 and 18.

TABLE 6
Drug system: possibly existing species are aspirin (1), phenacetin (2), caffeine (3), aminopyrine (4), antipyrine (5) and barbital (6)

| No. | I ^a | II ^b | III ^c | Taken ($\mu\text{g ml}^{-1}$) | | | | | | Found ($\mu\text{g ml}^{-1}$) | | | | | | MRPE (%) | |
|-----|----------------|-----------------|------------------|---------------------------------|------|-------|-------|------|-------|---------------------------------|-------------------|-------------------|-------------------|-------|------|----------|-------------------|
| | | | | 1 | 2 | 3 | 4 | 5 | 6 | 1 | 2 | 3 | 4 | 5 | 6 | | |
| 1 | 37.60 | 0.9990 | 0.6150 | 7.48 | 7.54 | 7.51 | 0.00 | 0.00 | 0.00 | 0.00 | 7.34 | 7.52 | 7.60 | - | - | - | 0.75 |
| 2 | 11.50 | 0.9800 | 0.0301 | 4.98 | 2.51 | 10.01 | 0.00 | 0.00 | 0.00 | 0.00 | 4.96 | 2.59 | 9.89 | - | - | - | 1.15 |
| 3 | 18.40 | 0.9726 | 0.2212 | 12.46 | 5.02 | 2.50 | 0.00 | 0.00 | 0.00 | 0.00 | 12.25 | 5.09 | 2.51 | - | - | - | 0.74 |
| 4 | 3.20 | 0.3682 | 0.0261 | 9.97 | 5.02 | 1.00 | 0.00 | 0.00 | 0.00 | 0.00 | 10.27 | 5.36 | - | - | - | - | - |
| 5 | 14.10 | 0.9812 | 0.3433 | 9.97 | 7.54 | 5.00 | 0.00 | 0.00 | 0.00 | 0.00 | 9.83 ^d | 4.89 ^d | 1.17 ^d | - | - | - | 5.75 ^d |
| 6 | 26.20 | 0.9988 | 0.1574 | 4.98 | 5.02 | 10.01 | 0.00 | 0.00 | 0.00 | 0.00 | 4.98 | 7.53 | 4.91 | - | - | - | 0.72 |
| 7 | 10.60 | 0.9778 | 0.0542 | 12.46 | 5.02 | 5.00 | 0.00 | 0.00 | 0.00 | 0.00 | 12.21 | 4.82 | 4.93 | - | - | - | 0.47 |
| 8 | 21.80 | 0.9424 | 0.4441 | 10.96 | 7.54 | 1.75 | 0.00 | 0.00 | 0.00 | 0.00 | 10.89 | 7.62 | 1.81 | - | - | - | 1.56 |
| 9 | 5.70 | 0.9309 | 0.1872 | 0.00 | 0.00 | 0.00 | 7.48 | 5.00 | 5.00 | 2.53 | - | - | - | 7.58 | 4.97 | 2.40 | 1.78 |
| 10 | 5.20 | 0.9000 | 0.1833 | 0.00 | 0.00 | 0.00 | 12.47 | 5.00 | 2.53 | - | - | - | - | 12.24 | 5.05 | 2.48 | 0.96 |
| 11 | 4.90 | 0.7344 | 0.0470 | 0.00 | 0.00 | 0.00 | 4.99 | 7.51 | 5.06 | - | - | - | - | 4.99 | 7.50 | 4.95 | 0.73 |
| 12 | 4.20 | 0.7791 | 0.1351 | 0.00 | 0.00 | 0.00 | 7.48 | 7.51 | 7.58 | - | - | - | - | 7.58 | 7.44 | 7.42 | 0.89 |
| 13 | 4.40 | 0.7506 | 0.1148 | 0.00 | 0.00 | 0.00 | 4.99 | 2.50 | 10.11 | - | - | - | - | 5.15 | 2.39 | 9.92 | 1.92 |
| 14 | 4.00 | 0.8042 | 0.1383 | 0.00 | 0.00 | 0.00 | 9.98 | 5.00 | 10.11 | - | - | - | - | 10.08 | 4.91 | 9.90 | 0.98 |
| 15 | 4.50 | 0.9463 | 0.0840 | 0.00 | 0.00 | 0.00 | 2.49 | 5.00 | 10.11 | - | - | - | - | 2.63 | 4.97 | 9.93 | 1.98 |

Cond(S) = 156.42

^{a-c} See Table 3. ^d Analytical results for sample No. 4 calculated with correct number of components.

TABLE 7

Analysis of *Injectio antondin* samples and comparison with the unknown sample

| Sample | Aminopyrine (mg ml ⁻¹) | Antipyrine (mg ml ⁻¹) | Barbital (mg ml ⁻¹) |
|---|---------------------------------------|--------------------------------------|------------------------------------|
| Unknown ^a | 50.28 ± 0.60 | 19.53 ± 0.37 | 8.97 ± 0.25 |
| <i>Injectio antondin</i> ^b | 50.06 ± 0.55 | 19.55 ± 0.27 | 9.08 ± 0.28 |
| Nominal prescription of <i>Injectio antondin</i> | 50.00 | 20.00 | 9.00 |

^a Mean result of analysis of five unknown samples. ^b Mean result of analysis of five samples.

very close, that is, the collinearity between spectra of some possibly existing species is of the same order as or even stronger than the collinearity between S and a caused by coincidence of the components of the real analytical sample and spectral standards (one example is the lowest right case in Table 1). It is evident that in such cases identification based on spectral information is really impractical.

In Tables 3–6, the interpretation results for four real analytical systems using the critical value above are listed. The identification of components present in samples among the possibly existing ones was carried out by the proposed method, and quantitative analysis was carried out by using ordinary multivariate regression procedures. Satisfactory analytical results were obtained for all cases except mixture No. 4 of the drug samples (see Table 6), where only two of the three truly existing components were identified. The elements of the $(p + 1)$ th row of \mathbf{II} were 0.9976, 0.9603, 0.3682, 0.0267, 0.0013, 0.0042 and 0.9927, and the variable indices involved in this near dependence should be 1, 2, 3 and 7, but only 1 and 2 were picked out together with the index of the mixture itself, 7. This might result from the related large experimental error for this sample, with a mean relative predicted error (MRPE) up to 5.75% as calculated with the correct number of components, which was much higher than the error for other samples. Figure 1 shows the IR spectra of mixtures that contain some amino acids from 21 possibly identities. The spectra calculated by using the proposed procedure and actually recorded were in fair agreement.

In order to demonstrate the practical applicability of the proposed procedure, a pharmaceutical sample of an unknown injection sample was analysed by the proposed method. It was suspected that the injection preparation contained aminopyrine, aspirin, barbital, caffeine, antipyrine and phenacetin. The measured sample spectra were treated with the proposed procedure together with the measured standard spectra of the six suspected drugs and the composition of this injection preparation was identified as containing aminopyrine, antipyrine and barbital. Following the qualitative identification, the determination of aminopyrine, antipyrine and barbital was accomplished by least-squares regression and the results are given in Table 7. The results coincided with the composition of *Injectio antondin*. The analysis of known samples of *Injectio antondin* gave concordant results.

Hence for any unknown analytical sample, if one has information concerning the range of possibly existing components and the spectra of these pure components are available, it is simple to solve the problem of the identification and determination of the composition of such samples by using the proposed chemometric algorithm. The comparison of the calculated and measured spectra as shown in Fig. 1 could also serve as an indication of the successful chemical assay of a sample.

This work was supported by the National Natural Science Foundation of China and partly by the Electroanalytical Laboratory of Changchun Institute of Applied Chemistry, Chinese Academy of Sciences.

REFERENCES

- 1 Y.-Z. Liang, Y.-L. Xie and R.-Q. Yu, *Chemistry (Beijing)*, No. 8 (1989) 4.
- 2 E.R. Malinowski and D.G. Howery, *Factor Analysis in Chemistry*, Wiley, New York, 1980.
- 3 D.A. Belsley, E. Kuh and R.E. Welsch, *Regression Diagnostics: Identifying Influential Data and Sources of Collinearity*, Wiley, New York, 1980.
- 4 J.H. Kalivas, *J. Chemometr.*, 3 (1989) 409.

Direct cerimetric determination of tellurium(IV)

S.N. Dindi and V. Visweswara Reddy

Department of Inorganic Chemistry, Andhra University, Visakhapatnam 530 003 (India)

(Received 21st August 1992)

Abstract

A direct cerimetric determination of tellurium(IV) is reported. The determination can be accomplished either in hot 1–5 M sulphuric or 1–2 M nitric acid medium in the presence of ruthenium(III) as catalyst. Direct self-indicating end point titration can be carried out with standard solutions of ammonium cerium(IV) sulphate and ammonium cerium(IV) nitrate as oxidants in the sulphuric and nitric acid media, respectively. The method is also extended to the analysis of tellurium(VI)–tellurium(IV) mixtures.

Keywords: Catalytic methods; Titrimetry; Cerium; Tellurium; Ruthenium

Cerium(IV) is a versatile and powerful one-electron oxidant in acidic media and has definite advantages over other oxidants in redox titrimetry. It is readily available as ammonium cerium(IV) sulphate and ammonium cerium(IV) nitrate and standard solutions can easily be prepared from these compounds. The availability of these compounds in a high state of purity and their relatively large equivalent weights are of additional advantage in cerate oxidimetry. However, the application of cerium(IV) as an oxidant in the tellurium(IV) determination is limited only to two catalytic methods, viz., chromium(III) [1] and silver(I)–manganese(II) [2] catalysed oxidations, probably due to the relative slowness of the direct oxidation of tellurium(IV) by cerium(IV). Even these two methods, although being indirect, laborious and time consuming, demand careful control of high concentration of the catalysts. We have now developed the first direct cerimetric determination method for tellurium(IV) which

makes use of ruthenium catalysis and is free from the disadvantages mentioned earlier.

EXPERIMENTAL

Reagents

A 0.05 M cerium(IV) solution in 0.5 M sulphuric acid was prepared from G.R. grade ammonium cerium(IV) sulphate (Loba Chemie) and its cerium(IV) concentration checked [3]. A 0.05 M cerium(IV) solution in 1 M nitric acid was also prepared from G.R. grade ammonium cerium(IV) nitrate (Loba Chemie) and its cerium(IV) content verified with standard iron(II) solution following a potentiometric technique.

A 0.01–0.025 M tellurium(IV) solution was prepared by dissolving laboratory grade sodium tellurite, (BDH, Poole) in water and standardised [4]. About 250 mg of $\text{RuCl}_3 \cdot x\text{H}_2\text{O}$ (Johnson and Mathey, Royston) was subjected to repeated evaporation with sulphuric acid and finally diluted to 500 ml with water and the ruthenium(III) content determined [5]. The solution was further diluted to desired strength. All other reagents used were of analytical reagent grade.

Correspondence to: S.N. Dindi, Department of Inorganic and Analytical Chemistry, Andhra University, Visakhapatnam 530 003 (India).

Procedure

To an aliquot of tellurium(IV) solution (containing 10–100 mg of Te) taken in a 150-ml beaker sulphuric acid and ruthenium(III) were added until the overall concentration of sulphuric acid is 1–5 M when diluted to 50 ml and the mole ratio of tellurium(IV) to ruthenium is at least 800:1. The contents of the beaker was heated to ca. 100°C and titrated slowly with a standard solution of cerium(IV) using a microburette, while stirring the solution continuously with a magnetic stirrer. The appearance of first persistent pale yellow colour due to the presence of excess of cerium(IV) indicates the end point. A blank titration was carried out under identical conditions and a correction to the earlier titre was applied accordingly.

The same determination of tellurium(IV) can also be carried out with standard ammonium cerium(IV) nitrate in 1–2 M nitric acid medium (making use of nitrous acid free nitric acid [6]) keeping all other conditions the same as in the earlier procedure.

RESULTS AND DISCUSSION

Aliquots containing 10–100 mg of tellurium(IV) were analysed for tellurium content following the above procedure and some of the specific results obtained are shown in Table 1.

Precision and accuracy of the method were measured by analysing ten samples (in each

TABLE 1
Determination of tellurium(IV)

| Medium | Amount of tellurium(IV) (mg) | |
|--------------------------------|------------------------------|-------|
| | Taken | Found |
| H ₂ SO ₄ | 27.4 | 27.3 |
| | 47.0 | 47.0 |
| | 62.7 | 62.7 |
| | 86.2 | 86.3 |
| HNO ₃ | 10.6 | 10.6 |
| | 23.3 | 23.4 |
| | 53.8 | 53.7 |
| | 73.3 | 73.2 |

TABLE 2

Determination of tellurium(VI) and tellurium(IV) contents of a mixture

| Tellurium(VI) (mg) | | Tellurium(IV) (mg) | |
|--------------------|-------|--------------------|-------|
| Taken | Found | Taken | Found |
| 41.0 | 41.1 | 11.3 | 11.3 |
| 35.9 | 35.8 | 16.9 | 17.0 |
| 30.4 | 30.4 | 22.5 | 22.6 |
| 25.7 | 25.8 | 28.1 | 28.0 |
| 20.5 | 20.5 | 33.8 | 33.8 |
| 15.4 | 15.4 | 39.4 | 39.4 |

medium) containing the same amount of tellurium(IV) using the recommended procedure. The average and relative standard deviations (R.S.D.) in the two media were found to be: 14.0 mg, 0.21% (14.0 mg taken) in H₂SO₄ medium and 14.0 mg, 0.15% (14.0 mg taken) in HNO₃ medium.

Copper(II), silver(I) and chloride ions to overall concentrations of 0.0025, 0.06 and 0.01 M, respectively, do not interfere in either of the media whereas lead(II) does not interfere up to 0.05 M in nitric acid medium. All other ions which are oxidisable with cerium(IV) do interfere.

Analysis of tellurate–tellurite mixtures

Synthetic mixtures of tellurium(IV) and tellurium(VI) were prepared by mixing solutions of known concentrations of sodium tellurite and sodium tellurate in water. The amount of tellurium(IV) in each mixture was determined by taking an aliquot of the mixture in sulphuric acid medium and titrating with standard cerium(IV) by the procedure mentioned. An identical aliquot in each mixture was treated with concentrated hydrochloric acid and evaporated to dryness on a water bath [to convert all the tellurium(VI) to tellurium(IV)] and the residue obtained was finally heated with sulphuric acid to expel the chloride [4]. The total tellurium content was determined as before after suitably adjusting the sulphuric acid concentration. The amount of tellurium(IV) and tellurium(VI) present in each case

were calculated based on this titre and the earlier titre. Results obtained are shown in Table 2.

It has been experimentally found that ruthenium(VIII) in the form of RuO_4 is equally effective as catalyst in this determination. However, as RuO_4 is less stable in solution and has a high volatility, the use of ruthenium(III) is preferred. Our attempts to develop either a potentiometric or visual indicator end point method with indicators like nitroferroin were unsuccessful. Fleeting potentials were obtained in the former case while premature oxidation of the indicator took place in the latter.

REFERENCES

- 1 H.H. Willard and P. Young, *J. Am. Chem. Soc.*, 52 (1930) 553.
- 2 G.G. Guilbault and W.H. McCurdy, Jr., *Anal. Chim. Acta*, 24 (1961) 214.
- 3 K. Sriramam, B.S.R. Sarma and B.V.S. Sastry, *Analysis*, 10 (1982) 295.
- 4 N.P. Tikhomirova, *Metody Anal. Khim. Reakt. Prep.*, No. 12 (1966) 90; *Chem. Abstr.*, 68 (1968) 18448r.
- 5 F.E. Beamish and J.C. Van Loon, *Recent Advances in the Analytical Chemistry of Noble Metals*, Pergamon, Oxford, 1972, p. 465.
- 6 L.S.A. Dikshitulu and D. Satyanarayana, *Talanta*, 22 (1975) 313.

BOOK REVIEWS

G.E. Baiulescu, P. Dumitrescu and P.Gh. Zugravescu, *Sampling*, Ellis Horwood, Chichester, 1991 (ISBN 0-13-791021-5). 184 pp. Price US\$84.50.

The fast development of analytical chemistry and new analytical techniques is reflected in a continuous stream of textbooks and monographs. Although there is a growing awareness that the sampling process forms the first step to useful results (“no analysis is better than the sample itself”), a systematic approach to this domain is often missing and the number of books dedicated to sampling only is limited. Therefore it is an excellent idea to publish a monograph on this subject aimed at students in higher-education institutions.

In 4 chapters successively dealing with the history of the sample, homogeneity of the sample, chemical analysis of the sample and the influence of sampling on the analytical process, almost all aspects of analytical chemistry, of analytical techniques and all types of standard and exotic samples are discussed. The main impression is that a true analytical chemist should be familiar with all aspects of chemistry, geochemistry, cosmochemistry, physiology, environmental problems, etc.

A Dutch writer of a daily column in one of the newspapers once stated after reading a thesis in the area of social sciences that he had the impression of standing in a puddle of words. As a reviewer of this book I have to confess that I had the same feeling. The book gives the impression that the main aim of the authors was to avoid a systematic treatment of problems of sampling as discussed in other monographs in this field by Gy, the Warren Spring Group (Jepson et al.) and people in the field of chemometrics.

The statement of the present authors that the originality of their approach is the incorporation of separation methods in the sampling process seems only to be an excuse for giving an unstructured discussion of chemistry as a whole. This does not mean that it is not interesting to get

such a kaleidoscopic view; it is nice to be guided through the garden of analytical chemistry with an abundance of personal comments. However, it will be certainly very difficult for newcomers in the field of analytical chemistry to get a good and systematic impression of the problems of sampling.

In conclusion, the book can be recommended to those who are interested in the personal view of analytical chemistry by the authors, but it cannot be recommended for students to get even a glimpse of real sampling problems.

W.E. van der Linden

G. Beamson and D. Briggs, *High Resolution XPS of Organic Polymers. The Scientia Database*, Wiley, Chichester, 1992 (ISBN 0-471-93592-1). 295 pp. Price £65.00.

X-Ray photoelectron spectroscopy (XPS) is one of the most powerful methods in surface analysis, and is becoming more important every year. The following three reasons may account for this: (i) the method is able to supply information about the chemical status of a sample; (ii) the technical development allows the analysis of samples of diameters down to the μm -range, and (iii) poorly conductive or insulating materials provide no major hindrance for analysis.

The last is important for polymer surface analysis. Of course, charge-up of samples has to be compensated, especially if monochromatized x-rays are used.

The Scientia ESCA300 spectrometer (analysts call it sometimes the “jumbo”) is probably the most advanced ESCA (XPS) instrument in the world, providing not only very high sensitivity but also high energy resolution, therefore being extraordinarily suited for measuring the chemical shifts of organic material, e.g., polymers.

The authors have done a systematic reinvestigation of more than 100 standard polymers and

give full information about sample preparation, survey spectrum, multi-region scan with high spectral resolution, shake-up lines, Auger lines, and also valence band spectra, which are typically 20–200 times weaker than the ordinary core lines. For the first time also data on x-ray and heat-induced sample damage are presented, so that the analyst can choose an appropriate data acquisition time to minimize degradation.

Each measurement is documented very extensively showing the average XPS user what is possible today. It is the first time that a data handbook in the field of surface analysis has contained such a tremendous amount of collected information. This handbook is a "must" for every XPS laboratory, even if polymers are not the main field of interest.

H. Hantsche

Arnaldo D'Amico (Ed.), *Euroensors V. Proceedings of the Conference, Rome, 30 Sept.–2 Oct. 1991*, Elsevier, Amsterdam, 1992 (ISBN 0-444-89497-7). Vol. 1, xix + 808 pp.; Vol. 2, xi + 720 pp. Price Dfl.1250.00/US\$714.50.

The field of sensors is wide ranging, rapidly developing and relatively inexpensive in which to carry out research and development work. The rewards of success are high, but the frequency of achieving major advances is commensurately rare. These two large volumes, printed on high quality paper, and beautifully bound, contain the papers and posters delivered at the above conference, and as such give a snap-shot of current research into sensors, and an indication of how extensive are the areas being investigated and how numerous are the researchers. The papers are reprinted from the journal *Sensors and Actuators, A*, Vols. 31/32 and *B*, Vols. 6/7, and are divided into two volumes, Vol. 1 on chemical (and biochemical) sensors, Vol. 2 on physical sensors. All types of devices seem to be represented (ion sensors, gas sensors, humidity sensors, ISFETS, piezoelectric devices, sensor arrays, etc., etc.) including more unusual topics like plant-based sensors, lipid

monolayers prepared by Langmuir-Blodgett technology, organic-phase enzyme electrodes and silicon-integrated analysis systems. Three plenary lectures are included (Gross et al., Neuronal networks for biochemical sensing; Yamazoe, chemical sensors R & D in Japan; Collins, problems of bringing sensor technology to the market place). Each volume has its own subject index. Potential purchasers will have to decide whether they wish to pay for two such expensive volumes when the material they contain has already been published in primary research journals.

Alan Townshend

Lucia Banci, Ivano Bertini and Claudio Luchinat, *Nuclear and Electron Relaxation. The Magnetic Nucleus–Unpaired Electron Coupling in Solution*, VCH, Weinheim, 1991 (ISBN 3-527-28306-4). xvi + 208 pp. Price DM118.00.

Something the title may not suggest, even to a specialist in magnetic spectroscopy, is that this book is about NMR, ESR (and ENDOR), especially of paramagnetic compounds. As such, it is a very good book, and does a good job describing the theoretical background of these techniques as applied to appropriate compounds. The authors emphasize the similarity that should exist between the teaching of the properties of nuclear and electronic spins as is done in few other texts. As one who has always favoured this idea, it makes me more partial to the book.

When I noticed the book grew out of symposia held regularly in Italy, I feared it might be a disjointed symposium volume. However, it is nothing like that; in fact, the chapters are not claimed by different authors, and the links are seamless to form a readable, coherent book.

I recommend the book strongly to graduate students and researchers in the area. However, the book clearly does not aim to cover what the working analytical chemist would want to know.

E. Sinn

Francis M. Mirabella, Jr. (Ed.), *Internal Reflection Spectroscopy. Theory and Applications*, Marcel Dekker, New York, 1993 (ISBN 0-8247-8730-7). vii + 374 pp. Price US\$145.00.

This book comprises twelve chapters contributed by a number of authors, from Germany, Switzerland and the USA. The editor contributes the first two chapters, on historical aspects and principles and practice, as well as three other chapters on determination of molecular spatial orientation, on total internal reflection (TIR) Raman spectroscopy, surface-enhanced Raman scattering and TIR fluorescence spectroscopy, and on determination of optical constants (mainly refractive index). Other chapters cover industrial and process monitoring applications, biological applications, vibrational spectroscopy of adsorbates on semi-conductor surfaces, electrochemical applications, in situ IR spectroscopy of membranes (70 pp.), and matrix effects. This is a welcome text, that brings together a wide range of analytical and other applications of a technique that, in the opinion of the book's editor, "stands on the threshold of a resurgence".

G. Ganetsos and P.E. Barker (Eds.), *Preparative and Production Scale Chromatography (Chromatographic Science Series, Vol. 61)*, Marcel Dekker, New York, 1993 (ISBN 0-8247-8738-2). xiv + 786 pp. Price US\$195.00.

Large-scale chromatography is a logical extension of some indispensable analytical techniques. The technology and the directions in which the large scale processes have developed often contrast markedly with their analytical counterparts, aspects that are comprehensively discussed in this large text. The book contains 30 chapters, with 50 authors, covering cocurrent chromatography, continuous cross-current and counter-current chromatography, chromatographic reaction and separation, modelling of chromatographic processes, and applications in biochemistry (production of proteins, affinity chromatography reactor, and process-scale ion chromatography). This is a well-produced volume, except for the brief sub-

ject index, packed with information which will be of more than passing interest to the analytical chemist.

Biosensors'92, Proceedings of the Second World Congress on Biosensors, Elsevier Advanced Technology, Oxford, 1992 (ISBN 1-85617-161-2). xiv + 556 pp. Price US\$180.00/£90.00 (soft cover).

These are at the Proceedings of the International Conference held on 20–22 May, 1992, in Geneva, Switzerland, organised by A.P.F. Turner, W.R. Heineman, I. Karube and R.D. Schmid. It comprises more than 150 oral and poster presentations, organised into Symposia on enzyme-based sensors (much the biggest section), affinity sensors, biosensors and bioelectronics, and environmental monitoring and is presented in camera-ready format on A4 pages. The papers range in length from several pages to single page summaries. The volume's main contribution is as a demonstration of the tremendous research effort that is being put into biosensors, and the diversity of approaches that are being investigated. There is a table of contents, but a subject index would have been a useful addition.

C. Rappe, H.R. Buser, B. Dodet and I.K. O'Neill (Eds.), *Environmental Carcinogens. Methods of Analysis and Exposure Measurement*, Vol. 11, Polychlorinated Dioxins and Dibenzofurans, IARC, Lyon, 1991 (ISBN 92-832-2108-7). xvi + 426 pp. Price £45.00.

This book continues the series of useful IARC Manuals. It deals in considerable depth with the polychlorinated dioxins and dibenzofurans. It first discusses the toxicology and epidemiology of these chemicals and describes sources of human exposure. There follows a critical review of analytical procedures for these compounds, descriptions of the development of bioassays, quality assurance and control procedures for their determination, a chemometric study, and a useful article on dioxins in the analytical laboratory. The second half of the book provides ten detailed methods for

analysis of drinking water, air, milk and other environmental and biological matrices, mainly by GC-MS or isotope dilution MS.

Deutsche Forschungsgemeinschaft, *MAK- und BAT-Werte-Liste 1992. Maximale Arbeitsplatzkonzentrationen und Biologische Arbeitsstofftoleranzwerte*, VCH, Weinheim, 1992 (ISBN 3-527-27553-3). 123 + xii pp. Price DM27.00.

This annual update continues to expand its coverage to a wider range of compounds, and to provide more information on compounds already listed. In this instance, new entries include *m*- and *o*-phenylenediamines, *N*-methylolchloracetamide, chlorthalonil, 6-amino-2-ethoxynaphthalene (MAK), and 2-ethoxyethanol and 4-methylpentan-2-one (BAT). The basis and format of the presentation remains as before.

ANALYTICA CHIMICA ACTA, VOL. 276 (1993)

AUTHOR INDEX

- Aguilera-Del Real, A., see Valverde-Garcia, A. 15
- Akaiwa, H., see Tsunoda, K.-i. 133
- Alfassi, Z.B., see Sun, Y.C. 33
- Ansell, K., see Lai, E.P.C. 393
- Araújo, A.N., see Nogueira, A.R.A. 121
- Aruga, R.
—, Mirti, P. and Casoli, A.
Application of multivariate chemometric techniques to the study of Roman pottery (terra sigillata) 197
- Back, M.H., see Chakrabarti, C.L. 47
- Beltrán, J.L.
—, Codony, R. and Prat, M.D.
Evaluation of stability constants from multi-wavelength absorbance data: program STAR 441
- Bergveld, P., see Cobben, P.L.H.M. 347
- Bianco-Prevot, A., see De la Guardia, M. 173
- Birch, S.W., see Cardosi, M.F. 69
- Bomer, J.G., see Cobben, P.L.H.M. 347
- Bos, M., see Cobben, P.L.H.M. 347
- Bosch Mossi, F., see Gimeno Adelantado, J.V. 39
- Bosch Reig, F., see Gimeno Adelantado, J.V. 39
- Branica, M., see Komorsky-Lovrić, Š. 361
- Brienza, S.M.B., see Nogueira, A.R.A. 121
- Broekaert, J.A.C., see Bulska, E. 377
- Brzozka, Z., see Cobben, P.L.H.M. 347
- Bubernak, J.
Liquid scintillation applied to alpha counting of plutonium 205
- Bulska, E.
—, Broekaert, J.A.C., Tschöpel, P. and Tölg, G.
Comparative study of argon and helium plasmas in a TM₀₁₀ cavity and a surfatron and their use for hydride generation microwave-induced plasma atomic emission spectrometry 377
- Cai, Q.
— and Khoo, S.B.
Determination of trace aluminium by differential pulse adsorptive stripping voltammetry of aluminium(III)-8-hydroxyquinoline complex 99
- Camacho-Ferre, F., see Valverde-Garcia, A. 15
- Cardosi, M.F.
— and Birch, S.W.
Screen printed glucose electrodes based on platinised carbon particles and glucose oxidase 69
- Casoli, A., see Aruga, R. 197
- Chakrabarti, C.L.
—, Lu, Y., Cheng, J., Back, M.H. and Schroeder, W.H.
Studies on metal speciation in the natural environment 47
- Chen, G.-Z., see Guo, X.-Q. 151
- Cheng, J., see Chakrabarti, C.L. 47
- Chung, Y.S., see Sakai, T. 127
- Chwastowska, J.
—, Żmijewska, W. and Sterlińska, E.
Preparation and analytical properties of a chelating resin loaded with thionalide 265
- Cobben, P.L.H.M.
—, Egberink, R.J.M., Bomer, J.G., Schouwenaar, R., Brzozka, Z., Bos, M., Bergveld, P. and Reinhoudt, D.N.
Chemically modified ion-sensitive field-effect transistors: elimination of the liquid junction potential in a double sensor flow-injection analysis cell 347
- Codony, R., see Beltrán, J.L. 441
- Costa Lima, J.L.F., see Nogueira, A.R.A. 121
- Cruz, I., see Kelly, A.G. 3
- De la Guardia, M.
—, Peris-Cardells, E., Morales-Rubio, A., Bianco-Prevot, A. and Pramauro, E.
Preconcentration of aluminium by micellar-enhanced ultrafiltration 173
- Desai, M., see Higson, S.P.J. 335
- Diamond, D.
— and Forster, R.J.
Robust estimation of selectivity coefficients using multivariate calibration of ion-selective electrode arrays 75
- Dindi, S.N.
— and Reddy, V.V.
Direct cerimetric determination of tellurium(IV) 465
- Doménech Carbó, M.T., see Gimeno Adelantado, J.V. 39
- Egberink, R.J.M., see Cobben, P.L.H.M. 347
- Emnéus, J.
— and Gorton, L.
Comparison between different inorganic supports for the immobilization of amyloglucosidase and α -amylase to be used in enzyme reactors in flow-injection systems. Part I. Hydrolysis of maltose, maltooligosaccharides and soluble starch 303
- and Gorton, L.
Comparison between different inorganic supports for the immobilization of amyloglucosidase and α -amylase to be used in enzyme reactors in flow-injection systems. Part II. Hydrolysis of glycogen 319

- Espinosa-Mansilla, A.
—, Muñoz de la Peña, A., Salinas, F. and Martínez-Galera, M.
Simultaneous determination of 2-furfuraldehyde, 5-hydroxymethylfurfuraldehyde and malonaldehyde in mixtures by derivative spectrophotometry and partial least-squares analysis 141
- Fernández-Romero, J.M.
—, Luque de Castro, M.D. and Valcárcel, M.
Flow-injection spectrophotometric enzymatic and non-enzymatic methods for the determination of direct and total bilirubin in serum 271
- Forster, R.J., see Diamond, D. 75
- Fujiwara, K., see Takeda, K. 25
- Gallego, M., see Yebra, M.C. 385
- Georges, J.
— and Ghazarian, S.
Study of europium-sensitized fluorescence of tetracycline in a micellar solution of Triton X-100 by fluorescence and thermal lens spectrometry 401
- Ghazarian, S., see Georges, J. 401
- Jimeno Adelantado, J.V.
—, Peris Martínez, V., Bosch Reig, F., Doménech Carbó, M.T. and Bosch Mossi, F.
Analysis of toxic elements in plastic components for toys. Multi-elemental determination by x-ray fluorescence 39
- Gómez Benito, C., see Laredo Ortiz, S. 281
- Gonzalez-Pradas, E., see Valverde-Garcia, A. 15
- Gorton, L., see Emnéus, J. 303, 319
- Grätzel, M., see König, B. 329
- Guo, X.-Q.
—, Xu, J.-G., Wu, Y.-Z., Zhao, Y.-B., Huang, X.-Z. and Chen, G.-Z.
Determination of thiamine (vitamin B₁) by in situ sensitized photochemical spectrofluorimetry 151
- Guzowski, Jr., J.P., see Markelov, M. 235
- Hasebe, Y., see Uchiyama, S. 341
- He, R., see Wang, J. 419
- Higson, S.P.J.
—, Desai, M., Koochaki, Z. and Vadgama, P.M.
Glucose oxidase enzyme electrode: relation between inner membrane permeability and substrate response 335
- Huang, X.-Z., see Guo, X.-Q. 151
- Imai, O., see Takeuchi, T. 65
- Ishihara, H., see Uchiyama, S. 341
- Itabashi, H., see Tsunoda, K.-i. 133
- Karube, I., see Takeuchi, T. 65
- Katakya, R.
—, Parker, D. and Teasdale, A.
Comparative study of tripodal oxa-amides and oxa-esters as ionophores in potentiometric ion-selective electrodes for alkali and alkaline earth cations 353
- Katsu, T.
— and Yamanaka, K.
Potentiometric method for the determination of adenosine-5'-triphosphate 373
- Kelly, A.G.
—, Cruz, I. and Wells, D.E.
Polychlorobiphenyls and persistent organochlorine pesticides in sea water at the pg l⁻¹ level. Sampling apparatus and analytical methodology 3
- Khoo, S.B., see Cai, Q. 99
- Khots, M.S., see Vander Heyden, Y. 189
- Kobayashi, K., see Takeuchi, T. 65
- Komorsky-Lovrić, Š.
— and Branica, M.
Comparison of potentiometric stripping analysis and square-wave voltammetry with respect to the influence of Triton X-100 361
- König, B.
— and Grätzel, M.
Development of a piezoelectric immunosensor for the detection of human erythrocytes 329
- Koochaki, Z., see Higson, S.P.J. 335
- Kroon, H.
Determination of nitrogen in water: comparison of a continuous-flow method with on-line UV digestion with the original Kjeldahl method 287
- Kuang, W., see Xie, Q. 411
- Kubota, M., see Watanabe, T. 109
- Kvalheim, O.M., see Liang, Y.-z. 425
- Lai, E.P.C.
—, Statham, B.D. and Ansell, K.
Determination of beryllium(II) on solid substrates by photothermal spectrometry after selective complexation with Chrome Azurol S 393
- Laredo Ortiz, S.
—, Gómez Benito, C. and Martínez Calatayud, J.
Determination of fluphenazine hydrochloride in a flow assembly incorporating cerium(IV) arsenite as a solid-bed reactor 281
- Li, H.
— and Wolfbeis, O.S.
Determination of urease activity by flow-injection analysis using an ammonium-selective optrode as the detector 115
- Liang, Y.-z.
— and Kvalheim, O.M.
Unique resolution of hidden minor peaks in multidetection chromatography by first-order differentiation and orthogonal projections 425
- Liang, Y.-Z., see Xie, Y.-L. 455
- Ligon, Jr., W.V.
Azeotropic distillation as an enrichment strategy for determination of aromatic hydrocarbons 167
- Lin, Y.F., see Sun, Y.C. 33
- Lu, Y., see Chakrabarti, C.L. 47
- Luque de Castro, M.D., see Fernández-Romero, J.M. 271

- Markelov, M.**
— and Guzowski, Jr., J.P.
Matrix independent headspace gas chromatographic analysis. The full evaporation technique 235
- Martínez-Galera, M.**, see Espinosa-Mansilla, A. 141
- Martínez Calatayud, J.**, see Laredo Ortiz, S. 281
- Massart, D.L.**, see Vander Heyden, Y. 189
- Masuda, Y.**, see Takeuchi, T. 65
- Mirti, P.**, see Aruga, R. 197
- Miwa, T.**, see Xu, J. 261
- Mlakar, M.**
Square-wave voltammetry of uranyl-humate complex 367
- Morales-Rubio, A.**, see De la Guardia, M. 173
- Motomizu, S.**, see Sakai, T. 127
- Muñoz de la Peña, A.**, see Espinosa-Mansilla, A. 141
- Nie, L.**, see Xie, Q. 411
- Nie, L.H.**, see Shen, D.Z. 87
- Nogueira, A.R.A.**
—, Brienza, S.M.B., Zagatto, E.A.G., Costa Lima, J.L.F. and Araújo, A.N.
Multi-site detection in flow analysis. Part 2. Monosegmented systems with relocating detectors for the spectrophotometric determination of boron in plants 121
- Ohno, N.**, see Sakai, T. 127
- Ohta, H.**, see Seto, Y. 247
- Parker, D.**, see Katakya, R. 353
- Peris-Cardells, E.**, see De la Guardia, M. 173
- Peris Martinez, V.**, see Gimeno Adelantado, J.V. 39
- Pra Mauro, E.**, see De la Guardia, M. 173
- Prat, M.D.**, see Beltrán, J.L. 441
- Reddy, V.V.**, see Dindi, S.N. 465
- Reinhoudt, D.N.**, see Cobben, P.L.H.M. 347
- Rosés, M.**
Ionic equilibria in non-aqueous solvents. Part 1. General equations for calculation of pH, dissociation constants and reference potentials from potentiometric data 211
- Rosés, M.**
Ionic equilibria in non-aqueous solvents. Part 2. Computer programs for calculation of pH, dissociation constants and reference potentials from potentiometric data 223
- Saito, T.**
Determination by pyrolysis-gas chromatography of the phenolic resin concentration in particulate matter accumulated from traffic on roads 295
- Sakai, T.**
—, Chung, Y.S., Ohno, N. and Motomizu, S.
Double-membrane phase separator for liquid-liquid extraction in flow-injection analysis 127
- Salinas, F.**, see Espinosa-Mansilla, A. 141
- Sawant, S.R.**, see Shukla, J.P. 181
- Schouwenaar, R.**, see Cobben, P.L.H.M. 347
- Schroeder, W.H.**, see Chakrabarti, C.L. 47
- Seto, Y.**
—, Tsunoda, N., Ohta, H. and Shinohara, T.
Determination of blood cyanide by headspace gas chromatography with nitrogen-phosphorus detection and using a megabore capillary column 247
- Shen, D.Z.**
—, Zhu, W.H., Nie, L.H. and Yao, S.Z.
Behaviour of a series piezoelectric sensor in electrolyte solution. Part I. Theory 87
- Shimizu, H.**, see Uchiyama, S. 341
- Shinohara, T.**, see Seto, Y. 247
- Shukla, J.P.**
—, Singh, R.K., Sawant, S.R. and Varadarajan, N.
Liquid-liquid extraction of palladium(II) from nitric acid by bis(2-ethylhexyl) sulphoxide 181
- Singh, R.K.**, see Shukla, J.P. 181
- Statham, B.D.**, see Lai, E.P.C. 393
- Sterlińska, E.**, see Chwastowska, J. 265
- Sun, Y.C.**
—, Yang, J.Y., Lin, Y.F., Yang, M.H. and Alfassi, Z.B.
Determination of antimony(III,V) in natural waters by coprecipitation and neutron activation analysis 33
- Suzuki, M.**, see Takeuchi, T. 65
- Takeda, K.**
— and Fujiwara, K.
Determination of nitrate in natural waters with the photo-induced conversion of nitrate to nitrite 25
- Takeuchi, T.**
—, Yokoyama, K., Kobayashi, K., Suzuki, M., Tamiya, E., Karube, I., Utsunomiya, K., Imai, O. and Masuda, Y.
Photosynthetic activity sensor for microalgae based on an oxygen electrode integrated with optical fibres 65
- Takeuchi, T.**, see Xu, J. 261
- Tamiya, E.**, see Takeuchi, T. 65
- Teasdale, A.**, see Katakya, R. 353
- Terajima, K.**, see Watanabe, T. 109
- Tölg, G.**, see Bulska, E. 377
- Tschöpel, P.**, see Bulska, E. 377
- Tsunoda, K.-i.**
—, Itabashi, H. and Akaiwa, H.
Characteristics of potassium ion-doped glass slab optical waveguide as an absorption cell and its application to the spectrophotometric detection of Methylene Blue 133
- Tsunoda, N.**, see Seto, Y. 247
- Uchida, H.**
Determination of major and minor elements in sintered fine ceramics by inductively coupled plasma emission spectrometry utilizing a sputtering technique 161
- Uchiumi, A.**, see Watanabe, T. 109
- Uchiyama, S.**
—, Hasebe, Y., Shimizu, H. and Ishihara, H.
Enzyme-based catechol sensor based on the cyclic reaction between catechol and 1,2-benzoquinone, using L-ascorbate and tyrosinase 341
- Ureña-Amate, M.D.**, see Valverde-García, A. 15
- Utsunomiya, K.**, see Takeuchi, T. 65

- Vadgama, P.M., see Higson, S.P.J. 335
 Valcárcel, M., see Fernández-Romero, J.M. 271
 Valcárcel, M., see Yebra, M.C. 385
 Valverde-García, A.
 —, Gonzalez-Pradas, E., Aguilera-Del Real, A., Ureña-Amate, M.D. and Camacho-Ferre, F.
 Determination and degradation study of chlorothalonil residues in cucumbers, peppers and cherry tomatoes 15
 Vander Heyden, Y.
 —, Khots, M.S. and Massart, D.L.
 Three-level screening designs for the optimisation or the ruggedness testing of analytical procedures 189
 Varadarajan, N., see Shukla, J.P. 181
- Wang, J.
 — and He, R.
 Stopped-flow kinetic spectrophotometric method for the simultaneous determination of iron, titanium and vanadium 419
 Watanabe, T.
 —, Terajima, K., Kubota, M. and Uchiumi, A.
 Electrostatic effect of chelation with metal ions on streaming potentials in chelating resins containing formazan derivatives 109
 Wells, D.E., see Kelly, A.G. 3
 Wolfbeis, O.S., see Li, H. 115
 Wu, Y.-Z., see Guo, X.-Q. 151
- Xie, Q.
 —, Kuang, W., Nie, L. and Yao, S.
 Determination of traces of iron by thin-layer spectroelectrochemistry 411
 Xie, Y.-L.
 —, Liang, Y.-Z. and Yu, R.-Q.
 Identification of "grey" analytical systems with incomplete information 455
 Xin, M., see Xu, J. 261
 Xu, J.
 —, Xin, M., Takeuchi, T. and Miwa, T.
 Determination of oxidizable inorganic anions by reversed-phase ion-pair chromatography with amperometric detection 261
 Xu, J.-G., see Guo, X.-Q. 151
- Yamanaka, K., see Katsu, T. 373
 Yang, J.Y., see Sun, Y.C. 33
 Yang, M.H., see Sun, Y.C. 33
 Yao, S., see Xie, Q. 411
 Yao, S.Z., see Shen, D.Z. 87
 Yebra, M.C.
 —, Gallego, M. and Valcárcel, M.
 Automatic determination of reducing sugars by atomic absorption spectrometry 385
 Yokoyama, K., see Takeuchi, T. 65
 Yu, R.-Q., see Xie, Y.-L. 455
- Zagatto, E.A.G., see Nogueira, A.R.A. 121
 Zhao, Y.-B., see Guo, X.-Q. 151
 Zhu, W.H., see Shen, D.Z. 87
 Żmijewska, W., see Chwastowska, J. 265

Erratum

Anal. Chim. Acta, 273 (1992) 27–34

p. 33, 2nd column, 4th line:

$$(I_p/\mu A) = 8.8 \times 10^6 (C_{Ni(II)}/\text{mol l}^{-1}) + 0.14$$

should read

$$(I_p/\mu A) = 4.4 \times 10^7 (C_{Ni(II)}/\text{mol l}^{-1}) + 0.14$$

Announcing...

International Ion Chromatography Symposium 1993

September 12-15, 1993
Hyatt Regency Inner Harbor
Baltimore, Maryland USA

PROGRAM CHAIRMAN:

Richard M. Cassidy

Chemistry Department

University of Saskatchewan

Saskatoon, SK Canada S7N 0W0

Telephone: 306/966-4668

Fax: 306/966-4730

SESSION TOPICS

- Separation Selectivity and Column Technology
- Developments in Separation Methodology
- Advances in Detection
- Special Sample Treatment Procedures
- Novel Applications
- Carbohydrate Separations
- Process Monitoring and Control
- Separation of Metal Ions
- Pharmaceutical Applications
- Environmental Applications
- Ion Analysis in the Electrical Generating Industry
- Interactions at the Capillary/Wall Interface and Ion Separations
- Standard Methods and Data Processing

Poster Abstracts will be accepted until **June 1, 1993.**

For program details and registration information, write or call:

Century International, Inc.
P.O. Box 493 • 25 Lee Road
Medfield, MA 02052 USA
508/359-8777 • 508/359-8778 (FAX)

Journal of Chromatography Library

Volume 53

Hyphenated Techniques in Supercritical Fluid Chromatography and Extraction

edited by K. Jinno

This is the first book to focus on the latest developments in hyphenated techniques using supercritical fluids. The advantages of SFC in hyphenation with various detection modes, such as, FTIR, MS, MPD and ICP and others are clearly featured throughout the book. Special attention is paid to coupling of SFE with GC or SFC.

1992 x + 334 pages

Price: US \$ 157.25 / Dfl. 275.00

ISBN 0-444-88794-6

Volume 52

Capillary Electrophoresis

Principles, Practice and Applications
by S.F.Y. LI

All aspects of CE, from the principles and technical aspects to the most important applications are covered in this volume. It is intended to meet the growing need for a thorough and balanced treatment of CE. The book will serve as a comprehensive reference work and can also be used as a textbook for advanced undergraduate and graduate courses. Both the experienced analyst and the newcomer will find the text useful.

1992 xxvi + 582 pages

Price: US \$ 225.75 / Dfl. 395.00

ISBN 0-444-89433-0

"...anybody wanting to write a book on CE after this would look like a fool. Everything seems to be there, any detection system you have ever dreamed of, any capillary coating, enough electrolyte systems to saturate your wits, and more, and more.

...by far the most thorough book in the field yet to appear."

P.G. Righetti

Volume 51

Chromatography, 5th edition

Fundamentals and Applications of Chromatography and Related Differential Migration Methods

edited by E. Heftmann

Part A: Fundamentals and Techniques

Part A covers the theory and fundamentals of such methods as column and planar chromatography, countercurrent chromatography, field-flow fractionation, and electrophoresis. Affinity chromatography and supercritical-fluid chromatography are covered for the first time.

1992 xxxvi + 552 pages

Price: US \$ 200.00 / Dfl. 350.00

ISBN 0-444-88236-7

Part B: Applications

Part B presents various applications of these methods. New developments in the analysis and separation of inorganic compounds, amino acids, peptides, proteins, lipids, carbohydrates, nucleic acids, their constituents and analogs, porphyrins, phenols, drugs and pesticides are reviewed and summarized. Important topics such as environmental analysis and the determination of synthetic polymers and fossil fuels, are covered for the first time.

1992 xxxii + 630 pages

Price: US \$ 211.50 / Dfl. 370.00

ISBN 0-444-88237-5

Parts A & B

Set price: US \$ 371.50 / Dfl. 650.00

ISBN 0-444-88404-1

Volume 50

Liquid Chromatography in Biomedical Analysis

edited by T. Hanal

This book presents a guide for the analysis of biomedically important compounds using modern liquid chromatographic techniques. After a brief summary of basic liquid chromatographic methods and optimization strategies, the main part of the book focuses on the various classes of biomedically important compounds: amino acids, catecholamines, carbohydrates, fatty acids, nucleotides, porphyrins, prostaglandins and steroid hormones.

1991 xii + 296 pages

Price: US \$ 154.25 / Dfl. 270.00

ISBN 0-444-87451-8

"...will be valuable for anyone involved in liquid chromatography. It is timely and highlights throughout the techniques that are most successful. This is not so much a book to put on the shelf of the specialist for reference purposes, but instead it is a book which is meant to be read by the general reader to obtain perspective and insights into this general area."

Trends in Analytical Chemistry

ORDER INFORMATION

For USA and Canada

ELSEVIER SCIENCE PUBLISHERS

Judy Weislogel

P.O. Box 945

Madison Square Station,
New York, NY 10160-0757

Tel: (212) 989 5800

Fax: (212) 633 3880

In all other countries

ELSEVIER SCIENCE PUBLISHERS

P.O. Box 211

1000 AE Amsterdam

The Netherlands

Tel: (+31-20) 5803 753

Fax: (+31-20) 5803 705

US\$ prices are valid only for the USA & Canada and are subject to exchange rate fluctuations; in all other countries the Dutch guilder price (Dfl.) is definitive. Customers in the European Community should add the appropriate VAT rate applicable in their country to the price(s). Books are sent postfree if prepaid.



ELSEVIER
SCIENCE PUBLISHERS

Analytical Voltammetry

edited by **M.R. Smyth** and **J.G. Vos**, School of Chemical Sciences, Dublin City University, Dublin, Ireland

Series editor: **G. Svehla**, University College, Cork, Ireland

The aim of this volume is to review the state-of-the-art in analytical voltammetry with regard to theory and instrumentation, and show how these relate to the analysis of inorganic, organometallic, organic and biological molecules. Modern voltammetric techniques have practical applications in biological, pharmaceutical and environmental chemistry. The growing importance of voltammetry in the development of modified electrodes and biological electrodes and chemical and biological sensors is also highlighted.

Contents:

1. Theory of Analytical Voltammetry (J.F. Cassidy). Introduction to analytical voltammetry. Classical techniques. Modern techniques. Electroanalysis in flowing streams. Microelectrodes, microelectrode arrays and hydrodynamically modulated rotating disc electrochemistry. Mathematical, coulometric and reflectance methods applied to voltammetry. Conclusions. **2. Instrumentation** (J.N. Barisci, P.J. Riley, G.G. Wallace). Introduction. The electrochemical cell. The working electrode. The reference electrode. The auxiliary electrode. Electronics. **3. Analytical Voltammetry of Biological Molecules** (J.M. Séquaris). In vivo voltammetry in neurochemistry. Electrochemical immunoassay. Voltammetric analysis of biological macromolecules: proteins and nucleic acids. **4. Analytical Voltammetry in Pharmacy** (P.M. Bersier, J. Bercier). Introduction. Polarographic and voltammetric techniques applied to drug analysis. Practical applications of polarography, voltammetry and hybrid techniques in drug analysis. **5. Analytical Voltammetry in**

Environmental Science. I. Inorganic Species (J.M. Fernandez, P.J. Hayes, M.R. Smyth). Introduction. General aspects of trace analysis. Polarography and voltammetric methods. Trace metals. Application of polarographic and voltammetric methods to trace metal analysis. **6. Analytical Voltammetry in Environmental Science. II. Organic and Organometallic Species** (P.M. Bersier, J. Bercier). Introduction. Use of advanced polarographic, voltammetric and hybrid techniques for the determination of organometallic and organic pollutants. Polarographic and voltammetric determination of organometallic and organic pollutants in air. Polarographic and voltammetric determination of organometallic and organic pollutants in aqueous environment. Determination of organic pollutants in soils. Determination of organometallic and organic pollutants in foodstuffs- and biological matrices. **7. Theory and Analytical Applications of Modified Electrodes** (R.J. Forster, J.G. Vos). Introduction. Preparation of modified electrode surfaces. Characterisation of modified electrodes. Theoretical aspects of mediation processes at modified electrodes. Analytical applications of modified electrodes. Conclusion. **8. Amperometric Biosensors** (J. Rodriguez Flores, E. Lorenzo). Introduction. Principles of biosensors. Fundamentals of amperometric biosensors. Classification. Applications. **Subject Index.**

1992 xxvi + 578 pages

Price: US \$ 254.00 / Dfl. 495.00

Subscription price: US \$ 228.00 / Dfl. 445.00

ISBN 0-444-88938-8



Elsevier Science Publishers

P.O. Box 211, 1000 AE Amsterdam, The Netherlands

P.O. Box 882, Madison Square Station, New York, NY 10159, USA

Vibrational Spectra and Structure

A Series of Advances

Volume 20

edited by J.R. Durlig, College of Science and Mathematics,
University of South Carolina, Columbia, SC, USA

The current volume comprises five chapters, three of which address recent advances in experimental techniques for providing information on biomolecular reaction paths, for determining linewidth and small frequency shifts, and for applying the microwave Fourier transform technique to experiments of static gases in waveguide cells. Chapters 4 and 5 consider *ab initio* calculations for both inorganic and organic systems.

Contents:

1. Applications of Matrix Infrared Spectroscopy to Mapping of Bimolecular Reaction Paths (*H. Frei*). Introduction. Oxygen Transfer Reactions. Hydrogen Transfer Reactions. Concluding Remarks.

2. Vibrational Line Profile and Frequency Shift Studies by Raman Spectroscopy (*B.P. Asthana, W. Kiefer*). Introduction. Deconvolution of Raman Line Profile. Determination of Frequency Shifts by Raman Difference Spectroscopy (RDS). Study of Linewidth Changes by RDS. Experimental Techniques. Applications. Summary.

3. Microwave Fourier Transform Spectroscopy (*A. Bauder*). Introduction.

Experimental. Rotational Spectra.

4. *Ab Initio* Quality of SCMEH-MO Calculations of Complex Inorganic Systems (*E.A. Boudreaux*).

Introduction. Theoretical Foundation. Applications and Results. Comments, Conclusions and Acknowledgments.

5. Calculated and Experimental Vibrational Spectra and Force Fields of Isolated Pyrimidine Bases (*W.B. Person, K. Szczepaniak*).

Introduction. Methods for Study of Isolated Molecules. Stabilities, Structures, and Dipole Moments of Isolated Pyrimidine Bases. Comparison of Experimental and Calculated Infrared Spectra for Pyrimidine Bases. Basis Set Dependence of Calculated Infrared Spectra and Vibrational Parameters for Uracil. Comparison of Spectra Calculated for Uracil, Thymine, Cytosine, and 1-Methylcytosine. Comparison

and Transferability of Bond Force Constants from Thymine, Uracil, Cytosine, and 1-Methylcytosine. Comparison and Transferability of Bond Dipole Derivatives from Uracil, Thymine, Cytosine, and 1-Methylcytosine. Concluding Remarks. Author Index. Subject Index.

"Each volume in this excellent series is eagerly awaited and the general reader is never disappointed."

**Journal of Molecular
Structure**

1993 xx + 352 pages
Price: US \$ 231.50 / Dfl. 370.00
ISBN 0-444-89865-4

ORDER INFORMATION

For USA and Canada
**ELSEVIER SCIENCE
PUBLISHERS**
Judy Weislogel
P.O. Box 945
Madison Square Station,
New York, NY 10160-0757
Tel: (212) 989 5800
Fax: (212) 633 3880

In all other countries
**ELSEVIER SCIENCE
PUBLISHERS**
P.O. Box 211
1000 AE Amsterdam
The Netherlands
Tel: (+31-20) 5803 753
Fax: (+31-20) 5803 705

US\$ prices are valid only for the USA & Canada and are subject to exchange rate fluctuations; in all other countries the Dutch guilder price (Dfl.) is definitive. Books are sent postfree if prepaid.



ELSEVIER
SCIENCE PUBLISHERS

PUBLICATION SCHEDULE FOR 1993

| | S'92 | O'92 | N'92 | D'92 | J | F | M | A | M | J | J | A |
|------------------------------|----------------|----------------|----------------|----------------|----------------|---------------------------|----------------|---------------------------|----------------|----------------|----------------|----------------|
| Analytica Chimica Acta | 267/1 267/2 | 268/1 268/2 | 269/1 269/2 | 270/1 270/2 | 271/1 271/2 | 272/1 272/2 273/1-2 | 274/1 274/2 | 275/1-2 276/1 276/2 | 277/1 277/2 | 278/1 278/2 | 279/1 279/2 | 280/1 280/2 |
| Vibrational Spectroscopy | | 4/1 | | | 4/2 | | 4/3 | 5/1 | | 5/2 | | 5/3 |

INFORMATION FOR AUTHORS

Manuscripts. The language of the journal is English. English linguistic improvement is provided as part of the normal editorial processing. Authors should submit three copies of the manuscript in clear double-spaced typing on one side of the paper only. *Vibrational Spectroscopy* also accepts papers in English only.

Abstract. All papers and reviews begin with an Abstract (50–250 words) which should comprise a factual account of the contents of the paper, with emphasis on new information.

Figures. Figures should be prepared in black waterproof drawing ink on drawing or tracing paper of the same size as that on which the manuscript is typed. One original (or sharp glossy print) and two photostat (or other) copies are required. Attention should be given to line thickness, lettering (which should be kept to a minimum) and spacing on axes of graphs, to ensure suitability for reduction in size on printing. Axes of a graph should be clearly labelled, along the axes, outside the graph itself. All figures should be numbered with Arabic numerals, and require descriptive legends which should be typed on a separate sheet of paper. Simple straight-line graphs are not acceptable, because they can readily be described in the text by means of an equation or a sentence. Claims of linearity should be supported by regression data that include slope, intercept, standard deviations of the slope and intercept, standard error and the number of data points; correlation coefficients are optional. Photographs should be glossy prints and be as rich in contrast as possible; colour photographs cannot be accepted. Line diagrams are generally preferred to photographs of equipment. Computer outputs for reproduction as figures must be good quality on blank paper, and should preferably be submitted as glossy prints.

Nomenclature, abbreviations and symbols. In general, the recommendations of the International Union of Pure and Applied Chemistry (IUPAC) should be followed, and attention should be given to the recommendations of the Analytical Chemistry Division in the journal *Pure and Applied Chemistry* (see also *IUPAC Compendium of Analytical Nomenclature, Definitive Rules*, 1987).

References. The references should be collected at the end of the paper, numbered in the order of their appearance in the text (not alphabetically) and typed on a separate sheet.

Reprints. Fifty reprints will be supplied free of charge. Additional reprints (minimum 100) can be ordered. An order form containing price quotations will be sent to the authors together with the proofs of their article.

Papers dealing with vibrational spectroscopy should be sent to: Dr J.G. Grasselli, 150 Greentree Road, Chagrin Falls, OH 44022, U.S.A. Telefax: (+ 1-216) 2473360 (Americas, Canada, Australia and New Zealand) or Dr J.H. van der Maas, Department of Analytical Molecule Spectrometry, Faculty of Chemistry, University of Utrecht, P.O. Box 80083, 3508 TB Utrecht, The Netherlands. Telefax: (+ 31-30) 518219 (all other countries).

Multivariate Pattern Recognition in Chemometrics, Illustrated by Case Studies

edited by R.G. Brereton, University of Bristol, Bristol, UK

Data Handling in Science and Technology Volume 9

Chemometrics originated from multivariate statistics in chemistry, and this field is still the core of the subject. The increasing availability of user-friendly software in the laboratory has prompted the need to optimize it safely. This work comprises material presented in courses organized from 1987-1992, aimed mainly at professionals in industry.

The book covers approaches for pattern recognition as applied, primarily, to multivariate chemical data. These include data reduction and display techniques, principal components analysis and methods for classification and clustering. Comprehensive case studies illustrate the book, including numerical examples, and extensive problems are interspersed throughout the text. The book contains extensive cross-referencing between various chapters, comparing different notations and approaches, enabling readers from different backgrounds to benefit from it and to move around chapters at will. Worked examples and exercises are given, making the volume valuable for courses.

Tutorial versions of SPECTRAMAP and SIRIUS are optionally available as a Software Supplement, at a low price, to accompany the text.

Contents:

- Introduction (*R.G. Brereton*).
1. Introduction to Multivariate Space (*P.J. Lewi*).
 2. Multivariate Data Display (*P.J. Lewi*).
 3. Vectors and Matrices: Basic Matrix Algebra (*N. Bratchell*).
 4. The Mathematics of Pattern Recognition (*N. Bratchell*).
 5. Data Reduction Using Principal Components Analysis (*J.M. Deane*).
 6. Cluster Analysis (*N. Bratchell*).
 7. SIMCA - Classification by Means of Disjoint Cross Validated Principal Components Models (*O.M. Kvalheim, T.V. Karstang*).
 8. Hard Modelling in Supervised Pattern Recognition (*D. Coomans, D.L. Massart*).
- Software Appendices:
SPECTRAMAP (*P.J. Lewi*),
SIRIUS (*O.M. Kvalheim, T.V. Karstang*).
- Index.

1992 xii + 326 pages

Hardbound

Price: US \$ 174.50 / Dfl. 305.00
ISBN 0-444-89783-6

Paperback

Price: US \$ 85.50 / Dfl. 150.00
ISBN 0-444-89784-4

5 Pack Paperback + Software Supplement

Price: US \$ 428.50 / Dfl. 750.00
ISBN 0-444-89786-0

Software Supplement

Price: US \$ 100.00 / Dfl. 175.00
ISBN 0-444-89785-2

TO ORDER

Contact your regular supplier or:

ELSEVIER SCIENCE PUBLISHERS

P.O. Box 211
1000 AE Amsterdam
The Netherlands

Customers in the USA & Canada:

ELSEVIER SCIENCE PUBLISHERS

Attn. Judy Weislogel
P.O. Box 945

Madison Square Station
New York, NY 10160-0757, USA

No postage will be added to prepaid book orders. US \$ book prices are valid only in the USA and Canada. In all other countries the Dutch guilder (Dfl.) price is definitive. Customers in The Netherlands please add 6% BTW. In New York State please add applicable sales tax. All prices are subject to change without prior notice.



ELSEVIER
SCIENCE PUBLISHERS



0003-2670(19930430)276:2;1-A